D2.3 Scaling up: risk reduction as a function of active/passive restoration scale in the Pilots

30/09/24

WP2

Lead beneficiary: Deltares

Author/s: Marijnissen, R.J.C., van Maren, D.S., Garrote, L., Santillán, D., Iglesias, A., Subbiah, B., Sánchez Artús, X., Gracia, V., Espino, M., Sanchez-Arcilla, A.,Villa Castrillon, L, Jacob, B., Pein, J., Chen, W., Staneva, J., Dissanayake, P., Oberrecht, D., Wurpts, A., Schrijvershof, R.A., van Weerdenburg, R.J.A., Zennaro, F., Horneman, F., Furlan, E., Torresan, S., Critto, A., Brière, C., Fornasari, J., Caillibotte, R., Mahe, S., Beudin, A. Musumeci, R.E., Marino, M., Nasca, S., Alkharoubi, A., Cavallaro, L., Foti, E., Valchev, N., Eftimova, P., Hineva, E., Andreeva, N., Różyński, G., Jolivet, M., Faraon, T., Boutron, O., Cathala M.

REST-COAST

Large Scale RESToration of COASTal Ecosystems through Rivers to Sea Connectivity

Prepared under contract from the European Commission
Grant agreement No. 101037097
EU Horizon 2020 Coordination and Support Action

Project acronym:	**REST-COAST**
Project full title:	**Large Scale RESToration of COASTal Ecosystems through Rivers to Sea Connectivity**
Start of the project:	01.10.2021
Duration:	54 months
Project coordinator:	Prof. Agustín Sánchez-Arcilla, Universitat Politècnica De Catalunya (UPC)
Type:	Restoring biodiversity and ecosystem services
Call:	H2020-LC-GD-2020-3
Deliverable title	Portfolio of restoration interventions for coastal risk reduction, based on the selected ESS and as a function of restoration type/scale and stakeholder/policy-maker criteria at the Pilots
Deliverable n°	D2.3
Nature of the deliverable:	Report
Dissemination level:	Public
WP responsible:	WP2.3
Lead beneficiary:	Deltares
Citation:	Marijnissen, R.J.C., van Maren, D.S., Garrote, L., Santillán, D., Iglesias, A., Subbiah, B., Sánchez Artús, X., Gracia, V., Espino, M., Sanchez-Arcilla, A.,Villa Castrillon, L,Jacob, B., Pein, J., Chen, W., Staneva, J., Dissanayake, P., Oberrecht, D., Wurpts, A., Schrijvershof, R.A., van Weerdenburg, R.J.A., Zennaro, F., Horneman, F., Furlan, E., Torresan, S., Critto, A., Brière, C., Fornasari, J., Caillibotte, R., Mahe, S., Beudin, A. Musumeci, R.E., Marino, M., Nasca, S., Alkharoubi, A., Cavallaro, L., Foti, E., Valchev, N., Eftimova, P., Hineva, E., Andreeva, N., Różyński, G., Jolivet, M., Faraon, T., Boutron, O. & Cathala M. (2024). *Restoration interventions - Portfolio of restoration interventions for coastal risk reduction*. Deliverable D2.3. EU Horizon 2020 REST-COAST Project, Grant agreement No 101037097
Due date of deliverable:	Month n° 36
Actual submission date:	Month n° 36

Deliverable status:

Version	Status	Date	Author(s)
0.1	Template	21 August 2024	R.J.C. Marijnissen
1.0	Draft Ch. 11	26 August 2024	Różyński, G.
1.1	Draft Ch. 5	29 August 2024	Dissanayake, P., Oberrecht, D. & Wurpts, A.
1.2	Draft Ch. 7	4 September 2024	Zennaro, F., Horneman, F., Furlan, E., Torresan, S., Critto, A.
1.3	Draft Ch. 12	8 September 2024	Jolivet, M., Faraon, T., Boutron, O., Cathala M.
1.4	Draft Ch. 4	10 September 2024	Villa Castrillon, L., Jacob, B., Pein, J., Chen, W. & Staneva, J.
1.5	Draft Ch. 2	12 September 2024	Garrote, L., Santillán, D. & Iglesias, A.
1.6	First draft Ch. 10	17 September 2024	Valchev, N., Eftimova, P., Hineva, E., Andreeva N.
1.7	Draft Ch. 6	18 September 2024	R.J.C. Marijnissen, D.S. van Maren, R.A. Schrijvershof, R.J.A. van Weerdenburg
1.8	Draft Ch. 8	19 September 2024	Brière C., Fornasari J., Caillibotte R., Mahe, S. & Beudin A.
1.9	Draft Ch. 3	20 September 2024	Subbiah, B., Sánchez-Artús, X., Gracia, V., Espino, M., Sanchez-Arcilla, A.
1.10	Draft Ch 9.	20 September 2024	Musumeci, R.E., Marino, M., Nasca, S., Alkharoubi, A., Cavallaro, L., Foti, E.
1.11	Revision Ch. 4	20 September	Villa Castrillon, L.
1.12	Draft Ch 1 and summary	23 September 2024	R.J.C. Marijnissen
1.13	Draft Ch. 13	23 September 2024	D.S. van Maren, R.J.C. Marijnissen
1.14	Revision Ch.10	24 September 2024	Valchev, N., Eftimova, P., Hineva, E., Andreeva, N.
1.15	Revision Ch. 12	26 September 2024	Jolivet, M., Faraon, T., Boutron, O., Cathala M.
2.0	Finalized draft	26 September 2024	R.J.C. Marijnissen
2.1	Final revision	14 October 2024	A. Sanchez-Arcilla, R.J.C.Marijnissen

Table of Contents

Preface

The Rest-Coast Project (Large scale RESToration of COASTal ecosystems through rivers to sea connectivity) is an EU Horizon 2020 research project (Grant agreement No. 101037097) whose overall goal is to address with effective and innovative tools the key challenges faced by coastal ecosystem restoration across Europe. The approach chosen for this project will deliver a highly interdisciplinary contribution, with the demonstration of improved practices and techniques for hands-on ecosystem restoration across several pilot sites, supported by the co-design of innovative governance and financial arrangements, as well as an effective strategy for the dissemination of results.

Summary

Within this portfolio of restoration interventions, we present a range of model-based projections assessing the impact of large-scale Nature-based Solutions (NbS) on enhancing Eco System Services (ESS) in various coastal systems. This deliverable applies these models to detail how these systems respond to climate change and nature-based interventions intended to mitigate climate change impacts under different Sea Level Rise (SLR) scenarios. The models range from hydro-morphological simulations of future conditions to a machine-learning approach, all aimed at demonstrating the ESS provided by restoration in the future.

The most widely applied restoration strategy is seagrass restoration, which involves the replanting and protection of seagrass beds to enhance marine biodiversity, improve water quality, and stabilize sediments. Modelling suggests the sea grass can reduce the bed shear stress and limit erosion (ch. 4, ch. 10), reduce turbidity and maintenance dredging (ch. 8), and contribute to mitigating flooding (ch. 10).

The second most widely applied restoration strategy is sediment management. This approach focuses on the strategic placement and stabilization of sediments to combat erosion, support coastal resilience, and maintain healthy ecosystems. Nourishing sediment underwater or on land as dunes can alleviate historical sediment deficits while reducing coastal erosion and flood risk (ch. 2 and 3). On the other hand, strategically removing sediment from a hyper-turbid system (e.g. by extracting dredge spoil from harbours) is possible to limit increasing turbidity, but the effect is highly conditional on the sediment supply trends of the region and may negatively influence ESS like flood risk reduction and carbon sequestration (ch.6).

Salt marsh restoration was investigated across the Wadden Sea and Venice Lagoon pilot sites. This strategy involves promoting the growth of salt marshes, which are vital for flood protection, water filtration, and providing habitat for a variety of wildlife. Salt marshes stabilize the bed (ch. 5) and locally reduce flood risk (ch. 5, 6), and act as a potential nutrient sink to prevent hypoxia (ch. 7).

Restoring hydraulic connectivity was investigated for the Rhone and Venice pilots. This strategy seeks to re-establish the natural flow of water between rivers, wetlands, and coastal areas, with the aim to improve water quality, support fish migration, and enhance the resilience of these areas to climate change. The removal of (dyke) infrastructure restores the variations in salinity and improve water quality favourably for fish populations (ch. 7, 12), but may result in short term erosion and greater dynamics along the coastline (ch. 12).

Various pilots have explored how the shifts in local ecotopes, units representing homogeneity in hydro- and morphological conditions such that similar types of biota can be expected, affect the provisioning of ecosystem services (ch. 4, 6, 9, 10). The Vistula Lagoon pilot has demonstrated how targeted habitat can be created using engineering and hydrodynamic insights (ch. 11). These insights give an indication for future biodiversity trends as well as estimate effects of ESS that can be expected from the gain/loss of ecotopes.

List of abbreviations

BAS	Institute of Oeanology in Varna
CMCC.	Centro Euro-Mediterraneo sui Cambiamenti Climatici
COR.	Consorzio coordinamento delle ricerche al Sistema lagunare di Venezia (CORILA)
CORE-PLAT.	COastal REstoration PLATform
D.	Deliverable
DEL.	Deltares
EGIS.	EGIS Water and Maritime
ESS.	Ecosystem services
EU.	European Union
FSK.	NLWKN-Forschungsstelle Küste
HZG.	Helmholtz-Zentrum Geesthacht
INR.	Institut national de recherche pour l´agriculture, l´alimentation et l´environnement INRAE
M.	Milestone
NbS.	Nature-Based Solutions
NN.	NetworkNature
T.	Task
TDV.	Tour du Valat
UC	Università degli Studi di Catania
UPC.	Universitat Politècnica de Catalunya
UPM.	Universidad Politécnica de Madrid
WP.	Work Package

1. Introducing the portfolio of interventions

1.1. Approach

REST_COAST / WP2 has developed suites of numerical models to quantify the impact of climate change and Nature-based Solutions (NbS) on EcoSystem Services (ESS). Earlier deliverables provided details on the developed models including ecosystem services (D2.1) and parameterizations of climate change (D2.2). The current deliverable provides an application of these models, detailing how the various systems respond to climate change and to nature-based interventions aimed at mitigating the impact of climate change. The aim is to demonstrate to what extent restoration reduces coastal risks as a function of restoration interventions and to prepare a portfolio of restoration interventions suited to future climates (business-as-usual SSP2-RCP4.5 and pessimistic SSP5-RCP8.5) and horizons (up to 2100). Pilots may deviate from these scenarios when data for a projection is not available (e.g. the Ebro Delta in ch. 2), or comply with stakeholder requirements and compatibility with previous administration plans (Rhone Delta in ch. 12).

In this contribution we aim to demonstrate the role of numerical models in predicting the effect of various NbS on ESS in the context of climate change. In order to generate an accessible portfolio, we focus within this report on the most relevant outcome of the various pilots. We deliberately restrained from synthesizing all model results, believing that such a product dilutes our main message (focusing on which NbS work and which not, and how NbS may serve in mitigating adverse effects of climate change). Through this framework, we also facilitate the conversion of this product into a set of papers to be published in a scientific journal.

1.2. The pilots: tools, NbS and ESS

Each pilot site in REST_COAST is exploring various types of Nature-based Solutions (NbS) to address coastal hazards under the commonly agreed climate scenarios and Pilot restoration scenarios (M2.3). NbS address

Figure 1-1 Overview of pilot sites in this deliverable

coastal challenges by the provisioning of ecosystem services (ESS) while improving the local biodiversity (BDV). Within the REST_COAST project five ESS are defined: Reduction Flood Risk (RFR), Reduction Coastal Erosion (RCE), Water Purification (WP), Climate Change Regulation (CCR), and Food Provisioning (FP). Depending on the specific challenges at each pilot site (Figure 1-1), a different portfolio of NbS is considered to enhance the necessary ESS. As shown in Table 1-1, a wide range of NbS restoration interventions is explored across pilots, covering all five ESS in REST_COAST. While the same NbS may be considered at various sites, each pilot site offers its own ESS evaluation based on the needs of local stakeholders. For example, sea grass restoration is considered at various pilot sites like in the Wadden Sea, and at Archachon Bay. The Wadden Sea pilot offers an estuary-scale exploration of large-scale sea grass restoration on coastal erosion, while the Arcachon pilots offers a local perspective on effects on channels, flats, and water quality within a bay.

To arrive at ESS assessments per pilot per NbS measure each pilot has employed various types of models. Models vary per pilot depending on the stakeholder needs, but may also build on validated models accepted by the stakeholder of the pilot site. The models in this "tool box" have been described in D2.1 and D2.2 and are refined further for the ESS assessment of the NbS portfolio in this deliverable. The main tools used across pilots are hydro-morphological models (e.g. SCHISM, Delft3D, XBeach, SWAN) simulating flows and/or waves that erode or expand the coastal zone. Recent additions to the toolbox for D2.3 are the Machine Learning application to predict hypoxia in the Venice Lagoon, and the application of ecological rules to assess biotopes with DEco-Impact (Wadden Sea pilot and Foros Bay). Each of the tools produces a range of indicators (e.g. renewal time, carbon sequestration rate, wave height reduction) describing the performance of their portfolio of NbS measure under future conditions. From these indicators, each pilot demonstrates the effectiveness of their portfolio of restoration interventions.

Table 1-1 Overview of chapters as a portfolio of restoration measure(s), ecosystem services, and type of modelling used

Pilot	Chapter(s)	NbS portfolio	ESS and /or BDV demonstrated*	Type of model(s) used**
Ebro Delta	2, 3	• River flow management • Dune restoration	RFR, RCE	H, M
Wadden Sea	4, 5, 6	• Sea grass restoration • Salt marsh restoration • Wetland creation • Sediment management	RFR, RCE, WP, CCR, BDV	H, M, E
Venice lagoon	7	• Riparian buffers • Transplantation of seagrasses • Saltmarsh restoration • Restoration hydraulic connectivity	WP	H, ML
Arcachon Bay	8	• Sea grass restoration		H, M, E
Sicily Lagoon	9	• Seagrass restoration • Dune revegetation • Beach nourishment		H, M
Foros Bay	10	• Sea grass restoration	RFR, RCE, BDV	H, M, E
Vistula lagoon	11	• Bird island	-***	H, M
Rhone Delta	12	• Restoration hydraulic connectivity	FP, RFR, RCE	H, M
Nahal Dalia	*Not in WP2*			

* RFR = Reduction Flood Risk, RCE = Reduction Coastal Erosion, WP= Water Purification, CCR = Climate Change Regulation, FP = Food provisioning

** H = Hydrological, M = Morphological, E = Ecological, ML = Machine Learning

*** This pilot is not linked directly to ESS, but instead demonstrates the feasibility of constructing the NbS measure

2. Estimation of the current and future potential sediment transport capacity of the Ebro River

Garrote, L.[1], Santillán, D. [1] & Iglesias, A.[2]

[1] *Department of Civil Engineering: Hydraulics, Energy and Environment, Universidad Politécnica de Madrid*
[2] *IDepartment of Agricultural Economics, Statistics and Business Managment, Universidad Politécnica de Madrid*

ABSTRACT: The natural flow of sediment in the Ebro River has been altered by a variety of factors, which have impacted the geomorphic and ecological balance of the Delta. Ongoing restoration efforts in the Delta would benefit if the flow of sediments in the river could be increased. Understanding the dynamics of sediment flow in the Ebro River is an important component to devise effective management strategies for the Ebro Delta. This study estimates the sediment transport potential of the Ebro River under current and future conditions through numerical simulation. Historical data from the late 19th century indicates that the river once transported up to 28.1 million tons of sediment per year. However, due to water abstractions and flow regulations, current sediment transport is limited to 9 million tons annually—a 67% reduction. Future projections suggest further decreases in flow and sediment transport potential, with reductions of up to 30% by 2060 and 50% by 2100, depending on climate conditions and water management practices. The findings underscore the need for integrated management strategies to mitigate the impacts of reduced sediment flow, emphasizing the importance of restoring sediment transport as a crucial component of the Delta restoration efforts.

2.1. Introduction

The Ebro Basin is in the NE of the Iberian Peninsula and occupies a total area of 85,534 km^2, where approximately 3.2 million inhabitants live. In addition to supplying the population with freshwater, the Ebro's water resources support numerous socioeconomic activities: industry, irrigation, livestock, hydroelectricity, refrigeration, aquaculture, navigation, and other recreational uses. Today, the Lower Ebro River is regulated by a complex of three reservoirs. The Mequinenza Reservoir, with a storage capacity of 1500 hm^3, regulates the Ebro flow. The Ribarroja Reservoir, of 210 hm^3, regulates the flow of the Cinca and Segre rivers. The relatively smaller Flix reservoir, 11 hm^3, is located downstream of the previous one and about 100 km upstream of the Ebro Delta (Figure 2-1).

During recent decades, anthropogenic activities, such as dam construction, channelization, and land use changes, have altered natural sediment flow in the Ebro River, triggering cascading effects on the ecological and geomorphic equilibrium of the Ebro River and Delta systems. The consequences of these alterations are multiple, impacting ecosystem health, reducing sediment delivery to the Delta, and increasing the vulnerability of the coastal area to erosion and sea level rise. Against this backdrop, understanding the intricate dynamics of sediment flow in the Ebro River becomes imperative for devising informed management strategies aimed at restoring sediment flow in the Ebro River.

The work of the Ebro pilot case is focused on analysing the options for mobilising the sediment accumulated in the three reservoirs of the lower Ebro. The increase in the flow of sediment in the river, however small, has been identified as a critical aspect to facilitate the environmental restoration tasks of the Ebro Delta, which are described in a separate chapter. The alteration of the hydrological regime and the movement of sediments is a consequence of all water uses of the Ebro Basin, but the three lower Ebro reservoirs are the closest to the Delta and offer the best options for sediment mobilisation. This section presents the analyses

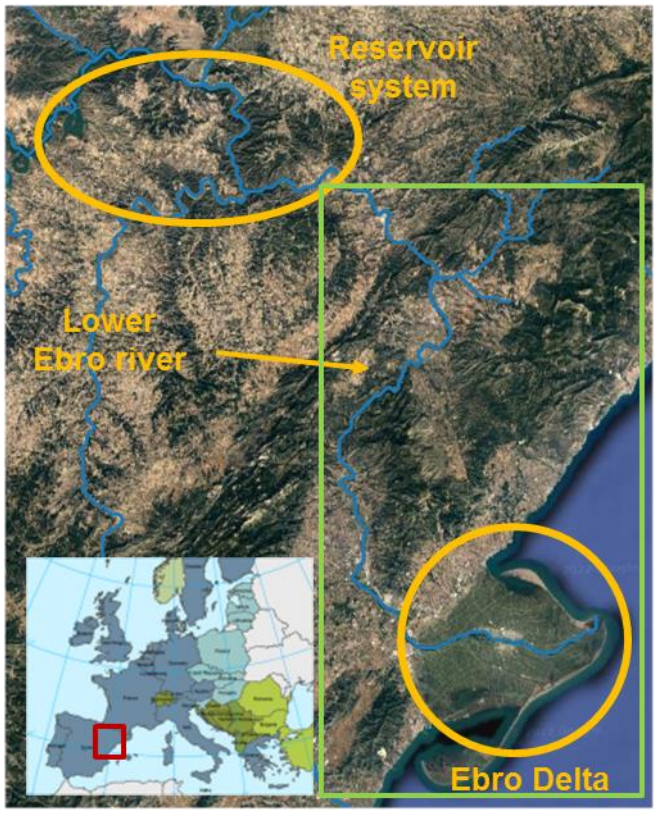

Figure 2-1 Lower Ebro River and Delta

performed to estimate the potential for increasing sediment flow in the lower Ebro as a critical component in the restoration efforts.

2.1.1. Description of problems

This section presents two main problems: the loss of sediment flow in the Ebro River and the accumulation of sediment in the reservoirs.

The reduction of sediment flow in the Lower Ebro River

Sediment transport in the Lower Ebro River has been extensively studied in the literature and is well characterized. One of the main drivers of sediment flow alteration in the Ebro River is the construction of reservoirs. Reservoir construction occurred mainly in the twentieth century, when more than 7000 hm^3 of reservoir storage was developed. More than 4000 hm^3 entered operation in the decade between 1955 and 1965 alone, including the Mequinenza Reservoir, the largest reservoir in the basin with more than 1500 hm^3 of storage capacity. Data on sediment transport before the construction of reservoirs in the basin are scarce. The mean annual sediment transport before reservoir construction was estimated by Ibàñez et al. (1996) at 28.1 Mton/yr, based on data compiled by Gorría in 1877. The figure reported by Catalán (1969), between 2 Mton/yr and 3 Mton/yr, is taken from direct intermittent measurements, but it corresponds to a period (1962-63) when there was already a significant reservoir capacity. Several researchers recently conducted field campaigns specifically designed to measure sedimentary transit, either through direct measurements (Vericat and Batalla,2006; Batalla and Vericat, 2011; Batalla et al., 2014) or through estimates from turbidity (Tena et al., 2011, Tena et al., 2012). These campaigns are the most reliable, due to their methodological approach, their spatial representativeness, and their duration. From them, it can be estimated that the sediment flow upstream of the Mequinenza reservoir ranges between 0.6 Mton/yr and 1.6 Mton/yr. The estimate after Ribarroja has been decreasing over time, from the 0.4 Mton/yr estimated in the campaigns of the late twentieth century to figures lower than 0.1 Mton/yr deducted in the most recent campaigns. This

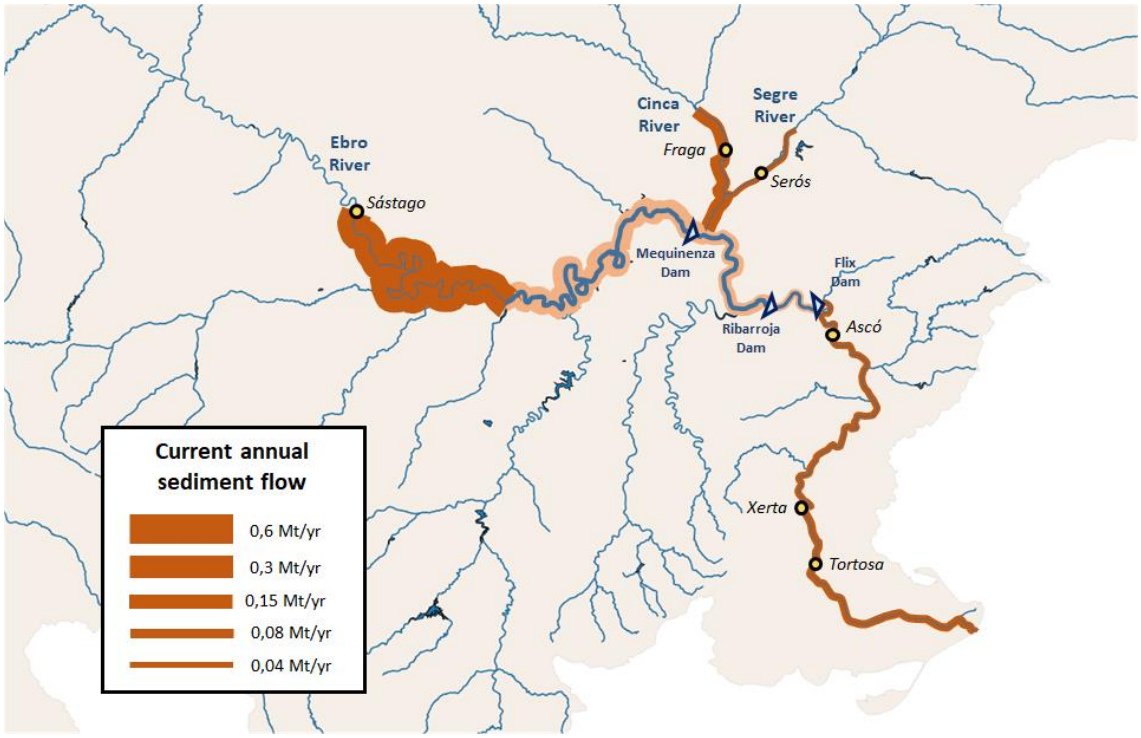

Figure 2-2 Current sediment flow in the lower Ebro River

figure is increasing downstream (Figure 2-2). Researchers agree that a significant part of the sediment transport to the mouth comes from the riverbed material itself and is carried out as bedload transport.

The release of water from reservoirs with very low sediment load also alters the morphology of the river. It leads to incision of the river channel and alters the channel morphology with bank erosion. The remaining sediment on the riverbed is being flushed out by high flows, leading to degradation and armoring of the riverbed. Vericat et al. (2006) described the process of breaking and re-establishing the armor layer of the bed observed during floods in the Lower Ebro in the period 2002-2004. Sediment from the riverbed was sampled on several exposed bars with sparse vegetation. Samples of the bedload were also taken during high flows. An alternation was observed between the armoring layer of the bed with low flow rates and high flow situations, where the armoring broke and the material was dragged, causing an incision.

Sediment accumulation in reservoirs

Sediment transport can also be estimated from sediment accumulation in reservoirs, although this estimate is highly uncertain because of the difficulty of matching the true datum of different surveys. Several bathymetric surveys are available for Mequinenza (1961, 1982 and 2012) and Ribarroja (1967, 1982 and 2007). A screening of sediment accumulation in Spanish reservoirs carried out by CEDEX (Avendaño et al, 1997), includes an estimate of capacity loss of 92.8 hm^3 for Mequinenza in 1982, 16 years after the commissioning of the dam. This corresponds to an average of 5.8 hm^3/yr. The estimation of capacity loss in Ribarroja was 12.24 hm^3 in 1982, 13 years after dam construction, leading to an accumulation rate of 0.94 hm^3/yr. The Ebro River Basin Authority (Confederación Hidrográfica del Ebro) carried out several studies to estimate the sediment accumulation in the reservoirs. The sediment accumulation in Mequinenza was analyzed in three studies carried out in 2011-2012. During this period, the water level in Mequinenza was the lowest in the record, thus facilitating accurate field surveys. In these studies, field visits were made and the reservoir basin, described by the original cartography developed for the construction of the dam, was compared with cross-sectional profiles taken in the emergent zone and the bathymetric reconstruction of the submerged zone. The first study carried out was limited to the last 35 km of the tail of the reservoir,

where a sediment accumulation of 4.91 hm^3 was estimated. The two studies carried out in the entire reservoir in the period 2011-2012 estimated sediment accumulation volumes of 133 hm^3 in 2008 and 76.9 hm^3 in 2011. Garrote (2018) compared the three studies, analyzing their discrepancies, and obtained a combined estimate between 75 hm^3 and 100 hm^3, which implies an average annual retention between 1.5 hm^3/yr and 2 hm^3/yr in the 48 years that had elapsed since the Mequinenza reservoir was put into operation. In Ribarroja, two studies were carried out by the Flumen group (Dolz et al. 2009; Dolz et al. 2010), which analyzed data from the period 1997-1999 and performed a bathymetric survey of the reservoir. The sedimentation accumulated in Ribarroja in 2007 was estimated at 13.1 hm^3, which corresponds to an average rate of 0.34 hm^3/yr since its inception in 1968. López Gómez et al. (2022) analyzed available bathymetric surveys compared to flow rate and obtained an estimate of the time evolution of sediment transport upstream of the reservoirs. During the 1960s and 1970s of the twentieth century, the average sediment transport upstream of the reservoirs was about 8 Mton/yr. Due to changes in land use and climate change over the last three decades, this contribution would have been reduced to about 5 Mton/yr. The sediment trapping efficiency of Mequinenza is close to 100%, due to its large storage volume and its length, which exceeds 100 km. The trapping efficiency of Ribarroja Reservoir was estimated at 40% from direct measurements (Dolz et al., 2009). These figures are consistent with an estimated sediment accumulation of 320 Mt in Mequinenza and 64 Mt in Ribarroja.

2.1.2. Description of restoration efforts

The current restoration efforts in the lower course of the Ebro River focus on two main lines of action: the mobilisation of the sediments accumulated in the reservoirs and the actions to facilitate the transit of sediments along the river.

Feasible technical options for reservoir bypass

There is a wide range of techniques for sediment management in reservoirs. They can be classified into three broad groups (Kondolf 2018): protective measures, which reduce sediment entry into the reservoir, evacuation measures, which conduct sediments through or around the reservoir, and recovery measures, which remove sediment from the reservoir. Garrote (2018) analyzed the options for sediment mobilization in the Mequinenza-Ribarroja-Flix system and concluded that the only real possibilities for sediment mobilization are hydrodynamic removal by flushing or sluicing and mechanical removal by excavation or dredging. He analyzed the flushing by applying the Tsinghua model, which is an empirical procedure that allows one to estimate the result of the flushing operation based on the geometric characteristics of the reservoir. The method is based on the compilation of a set of experiences in China where washing had been practiced successfully (Atkinson 1996). The conditions of the Mequinenza reservoir are not favorable to flushing, because the basin is very long and the capacity of the bottom outlets (160 m^3/s) is very limited. Although the Tsinghua method provides acceptable rates of sediment mobilization, the reservoir levels that can be reached to enable the flushing flows mean that a large amount of water would still remain impounded in the reservoir during the flushing operation, from 100 hm^3 to 200 hm^3. The sediment mobilized at the tail of the reservoir would have to travel distances between 35 and 40 km to reach the bottom outlet. A large fraction of the mobilized sediment would be deposited in the reservoir before being evacuated through the bottom outlet. Consequently, it can be concluded that flushing is not technically feasible in the Mequinenza reservoir. The empirical formulas of the Tsinghua method give better results for the case of Ribarroja and Flix. For example, with a washing flow rate of 200 m^3/s in Ribarroja, a sediment concentration of about 60 kg/m^3 could be expected, which would allow 1 Mton to be evacuated in one day. As a result of the analysis carried out, it can be concluded that, in principle, the flushing operation is technically possible in both reservoirs. However, there are concerns about the environmental, economic, and social impacts of the flushing operation. The flushing operation requires practically total emptying of the reservoir, followed by a period of sediment evacuation and a period in which the initial reservoir volume is recovered. These three processes can produce significant environmental effects in the reservoir and downstream. The water

released during the emptying of the reservoir comes from the lower layers, which are usually of less quality than the surface water. It is also common that the material settled at the bottom of the reservoir is active from a biochemical point of view, so the water in the lower layers is exposed to the resuspension of this material. The emptying of the reservoir also has negative effects. The reduction in stored volume and flooded area produces substantial changes in biological communities. The flushing process evacuates water with a very high concentration of sediment into the river. This would undoubtedly produce environmental effects of great importance. From an economic point of view, the main effect corresponds to hydroelectric production. Important social impacts can also be identified since there are many interests related to the management of the lower Ebro reservoirs. The uses of downstream water would be altered by the high concentration of suspended solids and by the possible mobilization of toxic substances accumulated in the reservoir sludge. The water supply intakes of the Lower Ebro, recreational uses, or the cooling of the Ascó nuclear power plant are the most obvious problems. In summary, there are a wide variety of environmental, economic, and social impacts that must be considered when planning flushing operations.

Mechanical removal procedures are always technically feasible, and their only limitation is cost. Data collected from world experiences, which can be assumed to correspond to favorable situations where the procedure has been put into practice, show relatively high costs, but hydraulic dredging seems to be the only feasible alternative for bulk sediment removal from the reservoirs.

Planned activities for sediment mobilization

The Ebro Basin Management Plan for the period 2021-2027 includes a wide range of initiatives to characterize sediment transport in the Lower Ebro and explore alternatives for sediment mobilization. The global objective for this period is to study the current situation of sediment transport in the lower course of the river and to analyze the most appropriate corrective measures to increase sediment delivery to the Delta. The first step was to conduct new bathymetric surveys of the Mequinenza and Ribarroja reservoirs and to develop field campaigns to characterize their sediments. A detailed bathymetry of the lower course of the Ebro River from the reservoirs to the outlet was also obtained. Sediment samples confirmed the high degree of armoring of the lower course between Flix and Tortosa, where more than 80% of the sampled material was coarse-grained gravel. Sand only appears in significant amounts after Tortosa. The information obtained in these studies is essential to develop a correct numerical model of sediment transport in the Ebro River that can provide support to evaluate the effectiveness of the alternative measures proposed.

The strategy contemplated in the River Basin Management Plan also enables funds to carry out, in coordination with all affected stakeholders, a series of pilot tests for the mobilization of retained sediment, with the necessary safeguards for the environment, security, and economy of the population. Pilot tests are planned to be carried out in the regatta area of the town of Mequinenza, at the tail end of the Ribarroja reservoir. Sediment mobilization techniques will be analyzed by mechanical means and by hydraulic dredging. The planned operation consists of lowering the water level of the Ribarroja reservoir in coincidence with flood flows in the Segre River to enhance the hydraulic gradient in the tail of the reservoir and facilitate erosion of the deposited material. Another test will analyze the viability of extracting sediments that the Matarraña River deposits when it joins the Ebro River in the Ribarroja reservoir. This test aims to analyze the technical feasibility and profitability of a system that allows the material deposited at the bottom of the reservoir to be sucked and transported by pumping, through floating pipes, to the downstream face of the Ribarroja dam. The plan also considers the possibility of sediment flushing in the Ribarroja reservoir by partially lowering the water level in the reservoir during high flows. It is also planned to produce direct sediment that feeds the Ebro River with material taken from the mouth of the Ciurana River. During recent Storm Gloria, a significant volume of material accumulated near the confluence with the Ebro River and is currently limiting the conveyance of the bridges across the Ciurana River. It is planned to deposit this material on the Ebro riverbed, monitoring sediment particles through isotopic tracers or electromagnetic transmitters

to track their movement and obtain useful data for the calibration of numerical models. Numerical analyses proved that, to facilitate sediment drag, it is more efficient to deposit the material forming a transverse dike than in a longitudinal arrangement. Other alternative tests are being considered, such as mobilizing sediment retained in the Xerta Dam. These tests will provide valuable information for evaluating the effectiveness of alternative actions proposed in the future.

2.2. Methods

The methodological approach of the work is presented in this section. The strategy for restoring sedimentary flow in the river is based on two components: the mobilization of sediments accumulated in the reservoirs and their transport to the Delta. The mobilization of sediments in reservoirs is fundamentally an economic problem that will be solved by carrying out a series of pilot tests that will allow the identification of the best technology. It is planned to use the transport capacity of the Ebro River itself for the second component. However, there are doubts about the amount of sediment that can be transported through the river, since the hydrological regime of the basin has been strongly altered by water abstractions and regulation. The aim of the analysis is to answer a critical question for the approach to the Delta's restoration efforts: what is the potential sediment transport capacity of the Ebro River under current and future conditions? To answer this question, the hydrodynamic model of the Ebro River has been used.

The processes of erosion, sediment transport, and sediment deposition in the Ebro River are analyzed through numerical simulations. River simulations were performed with the Iber code (Cea et al. 2007; Bladé et al. 2014). Iber is a two-dimensional (2-D) freely available code that solves the 2-D hydrodynamic equations coupled to the sediment transport equations, among others. The hydrodynamic equations and the erosion model are described in the following section. The model setup is described next, in terms of model configuration data: topography, hydrodynamic parameters, and boundary conditions. Calibration of the hydrodynamic numerical model with controlled flood observations is described in the last section.

2.2.1. Description of the hydrodynamic model

Iber solves the 2-D Depth-Integrated Shallow-Water Equations (SWE) using a finite volume scheme. This scheme can manage unstructured meshes, irregular topographies, friction losses, and wet-dry fronts (Cea et al. 2007). The 2D SWEs are derived from the Navier–Stokes equations by assuming quasi-hydrostatic flow and incompressibility of water. The 2D mass conservation equation in a Cartesian coordinate system is given by:

$$\frac{\partial \mathrm{h}}{\partial \mathrm{t}} + \frac{\partial \mathrm{hU_x}}{\partial \mathrm{x}} + \frac{\partial \mathrm{hU_y}}{\partial \mathrm{y}} = 0, \tag{1}$$

The momentum balance equations in conservative form with source terms in a Cartesian coordinate system are:

$$\frac{\partial}{\partial \mathrm{t}}(\mathrm{hU_x}) + \frac{\partial}{\partial \mathrm{x}}\left(\mathrm{hU_x^2} + \mathrm{g}\frac{\mathrm{h}^2}{2}\right) + \frac{\partial}{\partial \mathrm{y}}(\mathrm{hU_xU_y}) = -\mathrm{gh}\frac{\partial \mathrm{z_b}}{\partial \mathrm{x}} + \frac{\tau_{\mathrm{s,x}}}{\rho} - \frac{\tau_{\mathrm{b,x}}}{\rho} + \frac{\partial}{\partial \mathrm{x}}\left(\nu_\mathrm{t}\mathrm{h}\frac{\partial \mathrm{U_x}}{\partial \mathrm{x}}\right) + \frac{\partial}{\partial \mathrm{y}}\left(\nu_\mathrm{t}\mathrm{h}\frac{\partial \mathrm{U_x}}{\partial \mathrm{y}}\right), \tag{2}$$

and

$$\frac{\partial}{\partial \mathrm{t}}(\mathrm{hU_y}) + \frac{\partial}{\partial \mathrm{y}}\left(\mathrm{hU_y^2} + \mathrm{g}\frac{\mathrm{h}^2}{2}\right) + \frac{\partial}{\partial \mathrm{x}}(\mathrm{hU_yU_x}) = -\mathrm{gh}\frac{\partial \mathrm{z_b}}{\partial \mathrm{y}} + \frac{\tau_{\mathrm{s,y}}}{\rho} - \frac{\tau_{\mathrm{b,y}}}{\rho} + \frac{\partial}{\partial \mathrm{x}}\left(\nu_\mathrm{t}\mathrm{h}\frac{\partial \mathrm{U_y}}{\partial \mathrm{x}}\right) + \frac{\partial}{\partial \mathrm{y}}\left(\nu_\mathrm{t}\mathrm{h}\frac{\partial \mathrm{U_y}}{\partial \mathrm{y}}\right). \tag{3}$$

In the previous equations, h is the water depth, $\mathrm{U_i}$ is the depth-averaged velocity along the i direction, ρ is the density of the water, $\mathrm{z_b}$ is the channel-bottom elevation, g is the acceleration of gravity, $\tau_{\mathrm{b,i}}$ is the bed friction along the i direction, $\tau_{s,\mathrm{i}}$ is the free-water surface friction along the i direction (i.e., wind traction),

and ν_t is the turbulent eddy viscosity. Molecular and eddy viscosities, wind traction and Coriolis acceleration were neglected in the simulations performed.

The bed friction terms, $\tau_{b,i}$, read:

$$\tau_{b,i} = \rho g h \frac{n^2 U_i^2}{h^{4/3}} = 0, \quad (4)$$

where j = x, y, and n is the Manning's coefficient.

Iber erosion and sediment transport module solves the non-cohesive sediment transport equations with uniform granulometries, in a non-stationary regime. The hydrodynamics, sediment transport processes, and river morphology interplay at mobile-bed simulations. Iber software couples these three processes. Iber simulates sediment transport as bedload and suspended load.

The sediment transport process is simulated through the 2D Exner equation (Anderson 2002; Mudd & Furbish 2004; Paola & Voller 2005). The equation provides the bed elevation evolution in response to the erosion and sedimentation and is given in the form of bedload and suspended load. It reads:

$$(1-\phi)\frac{\partial z_b}{\partial t} + \frac{\partial q_{b,x}}{\partial x} + \frac{\partial q_{b,y}}{\partial y} + (E - D) = 0, \quad (5)$$

where ϕ is the porosity, $q_{b,i}$ is the bedload discharge along the i direction, E is the entrainment deposition term of suspended sediment on the bed, and D is the deposition term of suspended sediment on the bed.

The bedload solid flow rate due to the bedload transport is simulated using the van Rijn equation (van Rijn 1984a), as it provides satisfactory results compared with laboratory experiments (Santillán et al. 2020). The equation reads:

$$q_b^* = \frac{0.053}{D^{*0.3}} \left(\frac{\tau^*}{\tau_{crit}^*} - 1 \right)^{2.1}, \quad (6)$$

where q_b^* is the dimensionless bedload solid volumetric flow rate, D^* is the dimensionless diameter of solid particles, τ^* is the dimensionless shear stress acting on the particles, and τ_{crit}^* is the dimensionless critical shear stress. The dimensionless bedload solid volumetric flow rate, q_b^*, reads:

$$q_b^* = \frac{q_b}{\sqrt{(s-1) g D^3}}, \quad (7)$$

where q_b is the bedload solid volumetric flow rate, s is the ratio between the densities of the particles and water, $s = \rho_S / \rho$, and D is the characteristic diameter of sediments, usually taken as the median diameter $D = D_{50}$.

The dimensionless diameter of solid particles is given by:

$$D^* = D \left(\frac{g(s-1)}{\nu^2} \right)^{1/3}, \quad (8)$$

being ν the kinematic viscosity of water, and the dimensionless shear stress reads:

$$\tau^* = \frac{\tau_b}{\rho (s-1) g D}, \quad (9)$$

being τ_b the bed friction shear stress, given by Eq. (4).

The dimensionless critical shear stress τ_{crit}^* is given by the Soulsby-Whitehouse equation (Soulsby & Whitehouse 1997), based on the experiments of Shields (1936). It is given by:

$$\tau_{crit}^* = \frac{0.3}{1 + 1.2 D^*} + 0.055 \left(1 - e^{-0.02 D^*} \right). \quad (10)$$

Iber simulates the suspended sediment transport with the depth-averaged convection-diffusion equation for the sediment concentration. The model accounts for the turbulent diffusion and the equilibrium suspended concentration, and is given by:

$$\frac{\partial \mathrm{hC}}{\partial \mathrm{t}}+\frac{\partial \mathrm{hU_x C}}{\partial \mathrm{x}}+\frac{\partial \mathrm{hU_y C}}{\partial \mathrm{y}}=\frac{\partial}{\partial \mathrm{x}}\left(\left(\Gamma+\frac{\nu_\mathrm{t}}{\mathrm{S_c}}\right)\mathrm{h}\frac{\partial \mathrm{C}}{\partial \mathrm{x}}\right)+\frac{\partial}{\partial \mathrm{y}}\left(\left(\Gamma+\frac{\nu_\mathrm{t}}{\mathrm{S_c}}\right)\mathrm{h}\frac{\partial \mathrm{C}}{\partial \mathrm{y}}\right)+\frac{\partial \mathrm{D_{s,x}}}{\partial \mathrm{x}}+\frac{\partial \mathrm{D_{s,y}}}{\partial \mathrm{y}}+(\mathrm{E}-\mathrm{D}), \quad (11)$$

where C is the depth-averaged concentration of suspended solids, Γ is the molecular diffusion coefficient for suspended solids, $\mathrm{S_c}$ is the Schmidt number, which relates the moment turbulent diffusion coefficient with the suspended turbulent diffusion coefficient, and $\mathrm{D_{s,i}}$ is the suspended sediment dispersion along the i direction due to the non-homogeneous vertical velocity profile and sediment concentration.

The Entrainment/ Deposition term, $(\mathrm{E}-\mathrm{D})$, models the bedload grains that become suspended (entrainment) and deposited from suspended sediments to the bed layer. We simulate the Entrainment/ Deposition term with the Van Rijn formula (van Rijn, 1987), given by:

$$\mathrm{E}-\mathrm{D}=\alpha\omega_\mathrm{s}(\mathrm{C}^*-\mathrm{C}), \quad (12)$$

where α is a coefficient that relates the mean suspended particle concentration and the river bedload concentration, ω_s is the fall velocity of the suspended sediments, C^* is the depth-averaged suspended load concentration at equilibrium conditions, and C is the depth-averaged suspended load concentration.

The fall velocity of the suspended sediments for sand particles is computed using van Rijn (1984b) recommendations. For particles smaller than about 0.1 mm, ω_s is given by:

$$\omega_\mathrm{s}=\frac{(\mathrm{s}-1)\mathrm{g}\mathrm{D}_{50}^2}{18\nu}, \quad (13)$$

for suspended sand particles in the range 0.1 to 1 mm, the fall velocity is:

$$\omega_\mathrm{s}=10\frac{\nu}{\mathrm{D}_{50}}\left\{\left(1+\frac{0.01(\mathrm{s}-1)\mathrm{g}\mathrm{D}_{50}^3}{\nu^2}\right)^{0.5}-1\right\}, \quad (14)$$

and for particles larger than 1 mm, the following equation is used:

$$\omega_\mathrm{s}=1.1[(\mathrm{s}-1)\mathrm{g}\mathrm{D}_{50}]^{0.5}. \quad (15)$$

The depth-averaged suspended load concentration at equilibrium conditions, C^*, reads (van Rijn 1984b):

$$\mathrm{C}^*=\frac{1}{\alpha}0.005\frac{\mathrm{T}^{1.5}}{\mathrm{D}^{*0.3}}, \quad (16)$$

where T is the transport stage parameter given by:

$$\mathrm{T}=\frac{(\mathrm{U}^*)^2-(\mathrm{U}^*_{\mathrm{crit}})^2}{\left(\mathrm{U}^*_{\mathrm{crit}}\right)^2}, \quad (17)$$

in which $\mathrm{U}^*_{\mathrm{crit}}$ is the critical bed-shear velocity, that according to Shields (1936) reads:

$$\mathrm{U}^*_{\mathrm{crit}}=\sqrt{\frac{\tau^*_{\mathrm{crit}}}{\rho}}, \quad (18)$$

and bed-shear velocity, U^*, reads (van Rijn 1984b):

$$\mathrm{U}^*=\frac{\sqrt{\mathrm{g}}}{\mathrm{C}'}\overline{\mathrm{U}}, \quad (19)$$

in which $\mathrm{C}'=18\log(12\mathrm{R_b}/3\mathrm{D}_{90})$ is the Chézy-coefficient related to grains, $\mathrm{R_b}$ is the hydraulic radius related to the bed according to Vanoni-Brooks (1957), and $\overline{\mathrm{U}}$ is the mean flow velocity.

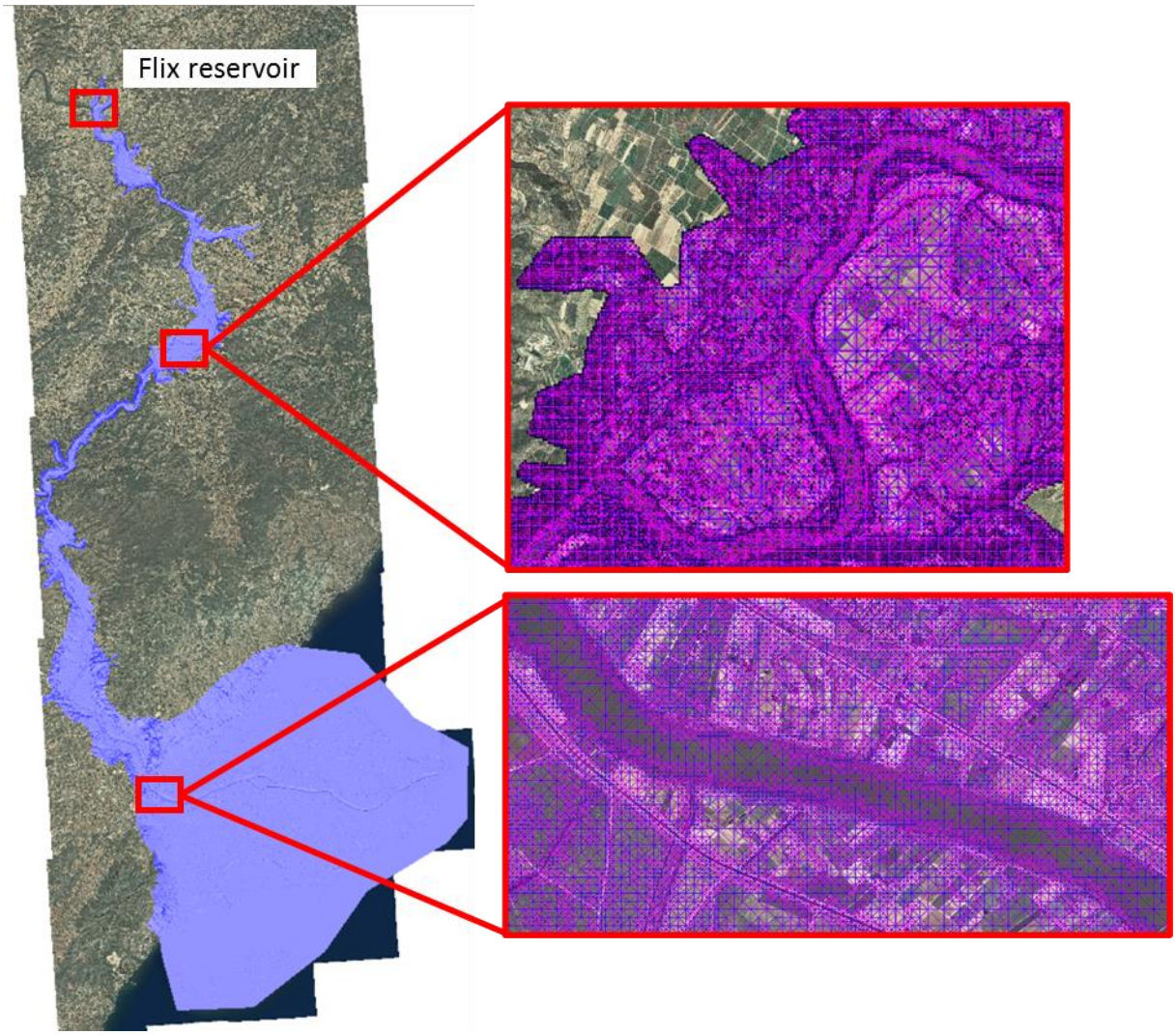

Figure 2-3 Domain of the numerical simulations in the Ebro River

The system of Partial Differential Equations is solved using a first-order finite volume scheme based on the Monotonic Upwind Scheme for Conservation Laws (van Leer 1979).

2.2.2. Model setup

The domain of the numerical simulations to model the sediment transport to the Ebro Delta includes the river reach between the reservoir system and the Delta. The modelling objectives are: (1) to study the alternatives to restore, at least in part, the sediment flow, (2) to estimate the quantity of sediments that can be mobilized, (3) to determine how long the sediments would take to reach the Delta site, and (4) to know how the sediment would be delivered to the Delta system.

The topography of the simulated reach is shown in Figure 2-3. Fluid flow and sediment transport are simulated from the Flix reservoir, located in Tarragona province at 41.1 meters above sea level, down to the Delta site, located in the river mouth at 0 meters above mean sea level. The Flix dam is the last sediment barrier on the Ebro River and is located about 100 km from the river mouth. The domain topography was obtained from a high-resolution Digital Terrain Model (DTM) with a 0.5 m resolution of the Ebro River that includes river bathymetry. A Triangulated Irregular Network (TIN) model of the river was built using this DTM, with 0.1-meter tolerance, maximum side of 2000 meters, and minimum side of 12 m. The model includes about 100 km of the Ebro River topography and it is composed of approximately 4,923,448 triangles. An

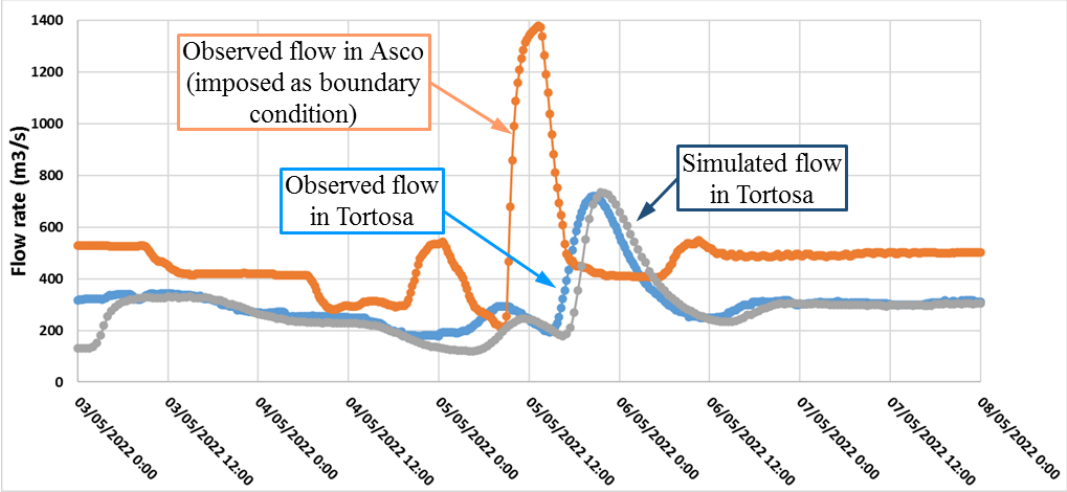

Figure 2-4 Observed and simulated flow rate in Tortosa.

unstructured computational mesh was generated from the TIN, composed of about 2,489,643 triangles; each triangle of the TIN model is one finite volume in the numerical model, i.e. the TIN model is coincident with the computational mesh. The picture on the left in Figure 2-3 depicts the coverage of the TIN model of the Ebro topography in blue. Two detailed snapshots of the computational mesh are shown on the right.

2.2.3. Model calibration

The riverbed roughness, given by Manning coefficient, was calibrated with the observed flood event on May 5th, 2022. This event also allowed testing the performance of the hydrodynamic model. The Ebro Automatic Hydrological Information System (SAIH) provided 30-minute flow rate observations at two points of the river: Asco and Tortosa (see Figure 2-2). A set of numerical simulations with several values of Manning coefficient was run. The best agreement between the simulated and the observed flow rate in Tortosa were obtained with Manning coefficient equal to 0.03. The results are shown in Figure 2-4. The model can capture the flood-wave propagation along the river in terms of time and flood peak downstream of the inlet.

2.3. Results and discussion

This section describes the results of the analysis carried out. First, a rating curve of sediment transport in the river was obtained from the available information on sediment transport under natural conditions. The rating curve was used to calculate the potential transport capacity under natural conditions and with the current flow regime. Finally, it was analyzed how it is expected that the transport capacity will evolve in the future, taking into account climate projections and the possible evolution of water use in the basin.

2.3.1. Rating curve for sediment transport

A rating curve for sediment transport was built in the Lower Ebro River with the aid of the numerical model described above. The sediment transport part was calibrated using data compiled by Ibàñez et al. (1996). They provided estimates of the annual transport of suspended sediments for several flow ranges in the Ebro. Data were obtained from Gorria's experiments, conducted in 1877, well before the dam construction period. They identified two representative regimes: normal flow, between 300 m^3/s and 1500 m^3/s, with an estimated mean flow of 710 m^3/s and a duration of 256 days and an average sediment concentration of 0.9 g/L, and annual flood, for discharge larger than 1500 m^3/s, with a mean flow of 1764 m^3/s, a mean duration of 11 days and an estimated sediment concentration of 7.2 g/L. Sediment transport was estimated to be 14.1 Mton/yr for normal flow and 12.1 Mton/yr for annual flood. They added a contribution to the mean sediment transport of 1.7 Mton/yr from exceptional floods. The remaining 0.2 Mton/yr correspond to flows of less

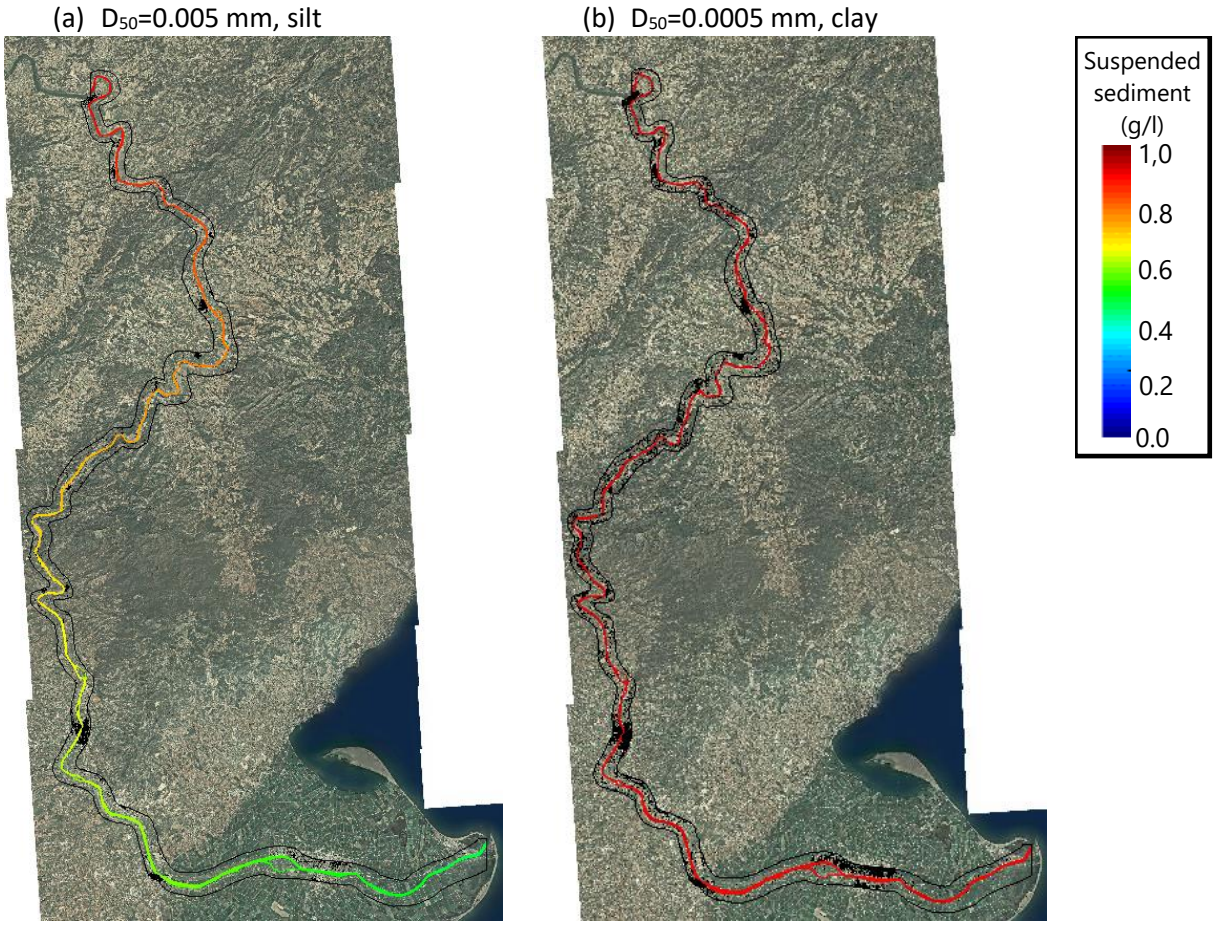

Figure 2-5 Suspended sediment concentration for the normal flow regime of the Ebro River after 1,5 days. Water flow is 710 m³/s and the sediment concentration at the inlet is 0.9 g/L. Plot (a) shows sediment concentration for $D50$ equal to 0.005 mm. Plot (b) shows sediment concentration for $D50$ equal to 0.0005 mm, ten times smaller.

than 300 m³/s. These values imply a total annual volume of 17.38 km³/yr and sediment transport of 28.1 Mton/yr.

Numerical simulations were run for the two identified flow regimes, estimating sediment transport parameters to fit the observed data until good agreement was obtained. In the numerical experiments, the suspended sediment concentration corresponding to the flow regimes was specified at the upstream boundary condition. The numerical simulations are aimed at analyzing whether the Ebro River can transport those sediment concentrations down to the Ebro. The analysis focused on the size of the suspended particles, characterized in the model with the median diameter, $D50$. The parameter $D50$ was estimated with a calibration process for the two representative regimes. A set of simulations was run varying the value of $D50$, checking for the evolution of suspended sediment concentration along the river. The adopted value for for $D50$ was the maximum diameter that does not produce substantial sedimentation in the river and is able to carry the suspened load to the Delta. The following features were adopted for the sediment: relative density is 2.65, friction angle is 30 degrees, suspended sediment dispersion coefficient is 0.001 m²/s, and the Schmidt number is 1.1. The best performance was obtained for a $D50$-value equal to 0.0005 mm, clay.

A sample of the results obtained in simulations run during the calibration process is presented in Figure 2-5. The figure shows two contour plots of the suspended sediment concentration for two $D50$-values: 0.005 mm –silt–, and 0.0005 mm –clay– after 1,5 days of simulation. The flow is 710 m³/s in both cases. The flow cannot

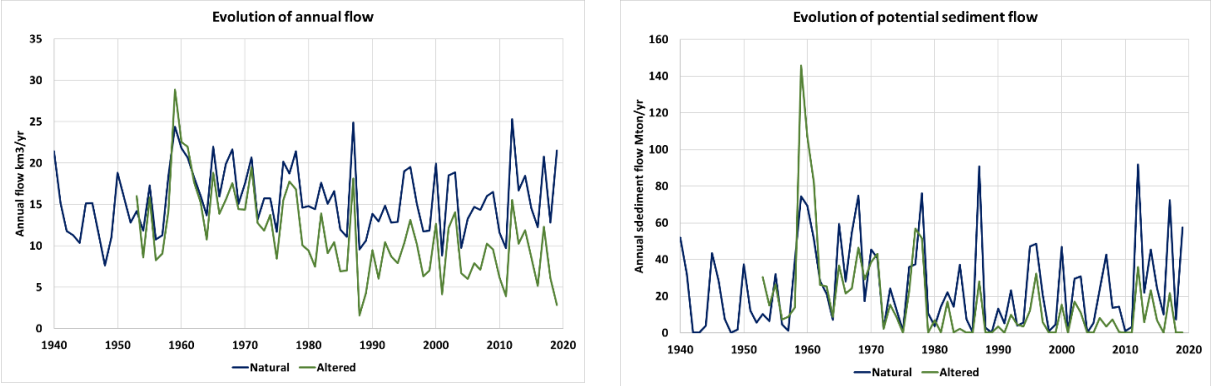

Figure 2-6 Evolution of annual flow and potential sediment transport in the Lower Ebro River under natural and altered conditions. Left: annual flow. Right: sediment transport

convey the silt suspended load, and sedimentation occurs during the transport process. The silt concentration decreases down to about 0.5 g/L in the Delta, as depicted in Figure 2-5a. However, the flow can convey the clay suspended load with the given concentration, 0.9 g/L, down to the Delta without sedimentation, as shown in Figure 2-5b. The model was then used to simulate other flows to build a sediment rating curve for the lower Ebro River.

2.3.2. Current potential sediment delivery under natural and altered conditions.

The low transport rate currently observed in the Lower Ebro River is due to the lack of availability of sediments. The potential sediment transport that would be available was estimated based on observed flow data and on the sediment transport rating curve derived from numerical simulations. Flow data under actual conditions is obtained from the Tortosa gauging station. Data are available from 1913, but there are several small gaps and a larger one from 1936 to 1951. The period when data are continuously available spans from the hydrological year 1953-34 to 2019-20. Potential sediment transport was estimated for that period by applying the sediment transport rating curve to daily flows measured in the Tortosa station. The average potential sediment transport is 11.11 Mton/yr, much larger than the currently observed sediment flow.

This figure can be compared to the potential sediment transport under natural hydrologic regime, without flow alteration produced by regulation and water abstractions. Flow data under natural conditions are obtained from the results of the SIMPA model, Spanish acronym for Integrated System for Precipitation-Runoff Modelling. SIMPA is a conceptual distributed hydrological model that simulates the average monthly flows in the natural regime at any point of the hydrographic network of Spain. The available simulated period is between the hydrological year 1940-41 and the year 2019-20. Monthly time series of the flow corresponding to the entire Ebro basin were obtained. The values of naturalized and observed flows begin to diverge in the 1960s decade, when reservoir constructions in the Ebro basin allowed the development of irrigation and the corresponding water extraction. Although some irrigation is still being developed in the basin, the large irrigation districts were finished in the 1980s. The average flow measured in Tortosa in the last 40 years with data is 9.09 km^3/yr, while the estimate under natural conditions from the SIMPA model is 15.13 km^3/yr. The difference, 6.04 km^3/yr, can be mainly attributed to irrigation abstractions. The Ebro River Basin Management Plan for the cycle 2021-2027 considers 924,400 ha of irrigated land with an annual demand of 8.141 km^3/yr. The difference between natural and measured flow would correspond to a net loss of water to evapotranspiration of 75% of the bulk abstraction, which is a reasonable figure.

The results obtained under natural and altered conditions are summarized in Figure 2-6, which shows the evolution of annual flow and potential sediment transport in the Lower Ebro River under the two situations. The impact of water abstractions on potential sediment transport is much greater than that of annual flow.

Potential sediment transport was estimated by applying the sediment transport rating curve to monthly flows. The average value in the last 40 years is 22.39 Mton/yr under natural conditions and 6.93 Mton/yr under actual altered conditions, a 70% reduction versus 42% for annual flow. It should be noted that the application of the rating curve produces different results for daily and for monthly flows due to its nonlinearity. The rating curve shows that sediment transport requires a minimum flow of approximately 575 m^3/s. This threshold was exceeded in 146 months in the last 40 years under natural conditions (30% of the time) and only 59 months under altered conditions (12% of the time).

2.3.3. Potential sediment transport under climate projections.

This section studies how the transport capacity of the Ebro River is expected to evolve in the future using climate projections. First, the source of climate projections used in the analysis is described. Below are the results under natural conditions. Finally, the results are shown under altered conditions under the hypothesis of maximum water use in the basin.

Climate projections

Estimates of potential sediment transport for future scenarios can be obtained using climate projections. The climate projections were taken from a report produced in the AgWaMed project, where climate projections were analyzed for all Mediterranean basins (Garrote et al. 2023). The scenarios considered were taken from IPCC AR6: SSP1-2.6, SSP3-7.0 and SSP5-8.5 scenarios. The required data was obtained from the ISIMIP repository. The ISIMIP (Inter-Sectoral Impact Model Intercomparison Project) initiative is a collaborative research effort that aims to assess the impacts of climate change on various sectors of society and the environment. The hydrological regime of the Ebro basin was taken from the results of global hydrological models H08 and CWatM, available in the ISIMIP repository. Two sets of climate scenarios were used: historical scenarios, for past times and future scenarios, for future times. Selected historical scenarios from ISIMIP are of two types: obsclim and historical. The denomination obsclim corresponds to impact models forced with observed climate in the actual time sequence. They are based on reanalysis data. This option was selected to validate the runoff obtained with the two global climate models against the results of the SIMPA model in the historical period. The denomination historical corresponds to impact models forced with results from climate models. This option was selected as a control reference to estimate changes of potential sediment transport in the future. Future scenarios correspond to the three emission scenarios of AR6 selected: SSP1-2.6, SSP3-7.0 and SSP5-8.5. In these options, climate models were forced with the emission patterns expected in each emission scenario. The simulations for future time periods start in 2015 and end in 2100. The hydrological models were forced with climate drivers in the corresponding scenarios. There are two types of climate drivers: based on observations and based on climate models. The climate driver based on observations is gswp3 and is used in the obsclim scenario. The climate drivers based on models are gfdl-esm4, mri-esm2, ipsl-cm6a-1r, mpi-esm1-2hr and ukesm1-0-11. They are used in the historical and future scenarios.

Sediment transport under natural conditions

The results produced by SIMPA model and ISIMIP hydrologic models for mean annual flow in all scenarios analyzed are presented in Table 2-1. The values correspond to averages taken over 40-year periods. The time period for SIMPA and the obsclim scenario spans from 1979-80 to 2018-19. The time series of the historical scenario only cover up to year 2014, so the time period selected for this scenario is 1974-75 to 2013-2014. Two time periods were selected for the climate projections: 2020-21 to 2059-60 and 2060-61 to 2099-2100. The table presents the values of mean annual flow obtained for the SIMPA and the average values obtained with all climate drivers in each ISIMIP model and scenario.

The results show a significant difference between the mean annual flow estimated with the two global hydrologic models. For the obsclim scenario, H08 provides a mean annual flow for the Ebro River of 12.63

Table 2-1 Mean annual flow obtained under the hypothesis of maximum use of water resources in the Ebro basin, in km³/yr

Scenario	obsclim	obsclim	historical	ssp126	ssp370	ssp585	ssp126	ssp370	ssp585
	80-19	*75-14*	*75-14*	*20-59*	*20-59*	*20-59*	*60-99*	*60-99*	*60-99*
SIMPA	14.97	15.19							
Mean H08	12.63	13.19	13.49	11.59	10.46	10.86	11.68	9.24	8.57
Mean CWatM	15.17	15.63	15.62	14.80	13.93	14.11	14.98	13.03	12.11

Table 2-2 Mean annual flow obtained in the simulations of the scenarios for the Ebro basin, in km³/yr

Scenario	obsclim	obsclim	historical	ssp126	ssp370	ssp585	ssp126	ssp370	ssp585
	80-19	*75-14*	*75-14*	*20-59*	*20-59*	*20-59*	*60-99*	*60-99*	*60-99*
Observed in Tortosa	8.91	11.26							
SIMPA	6.26	6.01							
Mean H08	2.58	4.28	5.97	4.21	3.21	5.37	4.66	2.68	2.13
Mean CWatM	6.63	7.28	8.98	9.19	7.16	9.39	10.18	7.37	6.86

km³/yr, while the estimate of CWatM is 15.17 km³/yr. The estimate of the SIMPA model, 14.97 km³/yr, is almost coincident with that of the CWatM model. The values for the average over the five climate drivers of the historical scenario are 13.49 km³/yr for the H08 model and 15.62 km³/yr for the CWatM model. The corresponding values of the obsclim scenario for the historical period, 1974-75 to 2013-2014, are 13.19 km³/yr for the H08 model and 15.63 km³/yr for the CWatM model, which means that there is an excellent agreement between the obsclim and the average of the results obtained with the five climate drivers used in the historical scenario. The projections for future scenarios show some sensitivity to the climate drivers used, but they provide a consistent picture of the expected evolution of mean annual flow in the Ebro basin. Mean annual flow is expected to decrease in the Ebro basin for most scenarios.

The time series produced by SIMPA model and ISIMIP hydrologic models in all scenarios analyzed were processed using the sediment transport rating curve to obtain projections of potential sediment transport in natural conditions. The analysis was performed on the bias-corrected series. The results are presented in Table 2-2. The values correspond to the same periods shown in Table 2-1. Table 2-2 presents the values of mean annual potential sediment transport obtained for the SIMPA and the average values obtained with all climate drivers in each ISIMIP model and scenario.

The results show a significant difference between the mean potential sediment transport estimated with the SIMPA model and those estimated with the two global hydrologic models, despite the bias correction. For the obsclim scenario, the estimate of the SIMPA model is 22.68 Mton/yr. H08 provides a mean sediment transport for the Ebro River of 15.61 Mton/yr (31% less than SIMPA), while the estimate of CWatM is 31.01 Mton/yr (36% more than SIMPA). These estimations are, therefore, highly uncertain. The values for the average over the five climate drivers of the historical scenario are 23.24 Mton/yr for the H08 model and 38.11 Mton/yr for the CWatM model. The corresponding values of the obsclim scenario for the historical period, 1974-75 to 2013-2014, are 19.06 Mton/yr for the H08 model and 34.48 Mton/yr for the CWatM model. The projections for future scenarios show more variability than in the case of annual flows. The potential for sediment transport under natural conditions is expected to decrease dramatically in some scenarios.

Figure 2-7 shows a summary of projected changes of mean annual flow and sediment transport under normal conditions. The projected reductions in mean annual flow will dramatically reduce the sediment transport

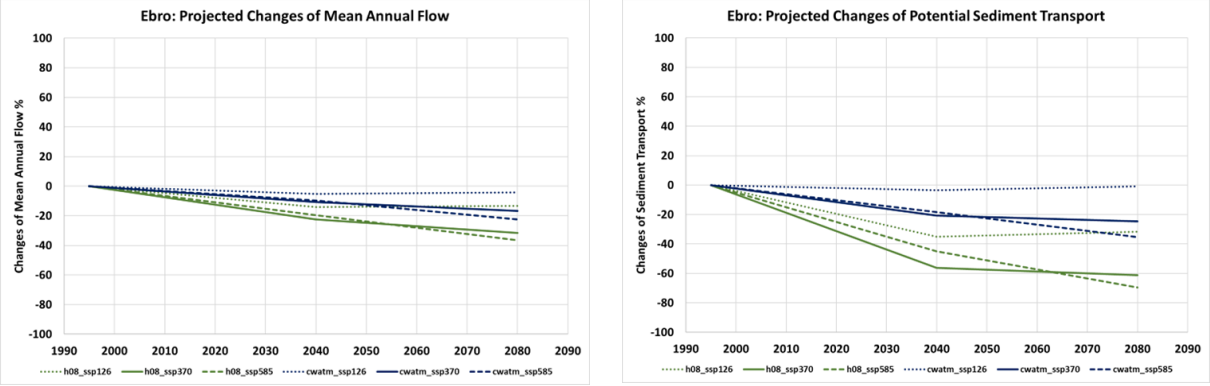

Figure 2-7 Projected changes of mean annual flow and potential sediment transport in the Ebro River under ISIMIP climate scenarios. Left: Changes of mean annual flow. Right: Changes of potential sediment transport

capacity of the Ebro River under natural conditions, due to the nonlinearity of the sediment transport rating curve. Although the H08 and CWatM models produce different absolute figures, the relative projected evolution is similar in both models. In the most likely scenario, SSP37.0, the expected reduction in the first time period, 2020-2059, ranges between 10% and 22% for mean annual flow and between 23% and 57% for sediment transport.

Sediment transport under altered conditions

The impact of projected reductions on the potential sediment transport capacity of the Ebro River under altered conditions will depend on how the Ebro River is managed in the future. Under the current management strategy, roughly 6 km^3/yr are abstracted from the 15 km^3/yr of natural flow, leaving 9 km^3/yr in Tortosa. This reduces the potential sediment transport capacity from 22 Mton/yr under natural conditions to 7 Mton/yr, but this figure is still enough to convey the sediment required by the Delta. The projected reductions suggest a future mean annual flow between 12 km^3/yr and 13.5 km^3/yr. The potential sediment transport capacity for the natural regime is expected to be reduced to between 10 Mton/yr and 17 Mton/yr. If the potential sediment transport under altered conditions was similarly reduced, it would fall to a range between 3.5 km^3/yr and 5 km^3/yr and some carrying capacity would still remain in the river. However, if current abstractions of 6 km^3/yr were maintained in the future, available flow would be reduced to a range between 6 km^3/yr and 7.5 km^3/yr, which represents a larger reduction than that of natural flow. Therefore, it is very likely that the potential for sediment transport under altered conditions will be reduced more than that under natural conditions.

It is possible to obtain an estimate of the expected future flow of water in the Ebro River under altered conditions by taking the results of the AgWaMed project (Garrote et al. 2023). In this project, the potential availability of water in the Ebro basin was evaluated in the different climate scenarios. To this end, a simulation model of the management of water resources in the basin was built, in which the maximum demand that could potentially be met at each point was considered. The flow of water circulating through the lower Ebro in this hypothesis allows us to estimate a lower level of the river's transport capacity, since it assumes the maximum use of the water resources available in each climate scenario.

The results produced by the AgWaMed project for mean annual flow under the hypothesis of maximum use of water resources under each climate scenario are presented in Table 2-3. It should be noted that the water demand is different in each of the scenarios, since it has been assumed that the water resources corresponding to each scenario are used to the maximum.

Table 2-3 Mean annual flow obtained under the hypothesis of maximum use of water resources in the Ebro basin, in km³/yr

Scenario	obsclim	obsclim	historical	ssp126	ssp370	ssp585	ssp126	ssp370	ssp585
	80-19	*75-14*	*75-14*	*20-59*	*20-59*	*20-59*	*60-99*	*60-99*	*60-99*
Observed in Tortosa	8.96	9.66							
SIMPA	6.57	6.75							
Mean H08	6.21	6.72	6.95	5.84	5.98	6.92	5.85	4.90	4.83
Mean CWatM	8.91	9.35	9.15	8.88	8.48	9.49	8.99	7.64	7.64

Table 2-4 Mean potential sediment transport obtained under the hypothesis of maximum use of water resources in the Ebro basin, in Mton/yr

Scenario	obsclim	obsclim	historical	ssp126	ssp370	ssp585	ssp126	ssp370	ssp585
	80-19	*75-14*	*75-14*	*20-59*	*20-59*	*20-59*	*60-99*	*60-99*	*60-99*
Observed in Tortosa	8.91	11.26							
SIMPA	6.26	6.01							
Mean H08	2.58	4.28	5.97	4.21	3.21	5.37	4.66	2.68	2.13
Mean CWatM	6.63	7.28	8.98	9.19	7.16	9.39	10.18	7.37	6.86

The results show that the estimate of CWatM model fits the observed flow in Tortosa better than that of the H08 model, but H08 is closer to the results provided by the SIMPA model. For the obsclim scenario, H08 provides a mean annual flow for the Ebro River of 6.21 km³/yr, while the estimate of CWatM is 8.91 km³/yr. The estimate of the SIMPA model, 6.57 km³/yr, is similar to that of the H08 model, while the observed flow in Tortosa, 8.96 km³/yr is almost coincident with that of the CWatM model. The values for the average over the five climate drivers of the historical scenario are 6.72 km³/yr for the H08 model and 9.35 km³/yr for the CWatM model.

The time series produced by the water resources simulation model in all scenarios analyzed were processed using the sediment transport rating curve to obtain projections of potential sediment transport in altered conditions. The results are shown in Table 2-4, which presents the values of mean annual potential sediment transport obtained for each scenario.

The results show a significant difference between the mean potential sediment transport estimated with the results of the water resources model under the hypotheisis of maximum water use and those estimated with

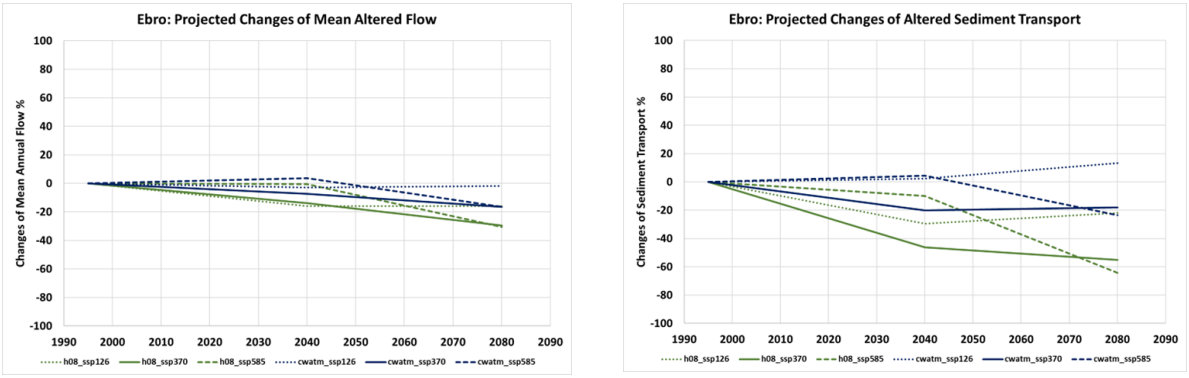

Figure 2-8 Projected changes of mean annual flow and potential sediment transport in the Ebro River under altered conditions in future climate scenarios. Left: Changes of mean annual flow. Right: Changes of potential sediment transport

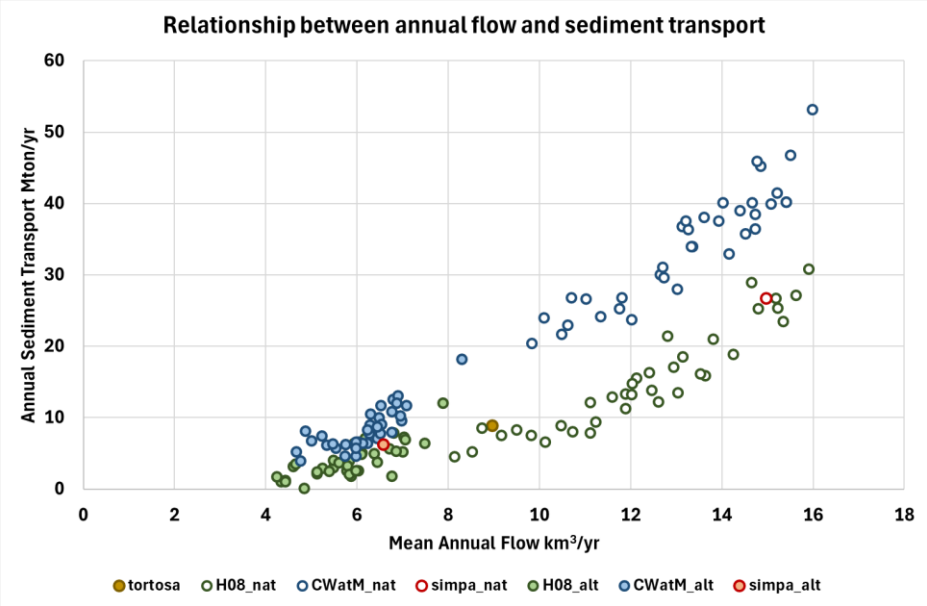

Figure 2-9 Relationship between mean annual flow and potential sediment transport for all scenarios examined

the observed flow in Tortosa. The differences are due to uncertainty in modelling and also to the fact that current water use in the Ebro basin is not maximum.

The results obtained in the analysis of altered flow in future projections are summarized in Figure 2-8. The effects are similar to those shown in Figure 2-7, but with larger spread between hydrologic models and climate scenarios. In the most likely scenario, SSP37.0, the expected reductions projected by H08 model for the first time period, 2020-2059, are 13.9% for mean annual flow and 46.3% for sediment transport. The reductions projected by the CWatM model are 7.9% for mean annual flow and 20.3% for sediment transport

2.3.4. Relationship between annual flow and sediment transport

The analyses carried out in this study allow us to characterize the relationship between average annual flow and potential sediment transport capacity. Figure 2-9 shows the overall result of all the analyses carried out, representing the value of the potential sediment transport capacity as a function of the value of the average annual flow for each of the scenarios and models examined. The figure clearly shows that each of the two global hydrological models has a distintct behavior. The CWatM model provides a higher sediment transport capacity than the H08 model. This is due to the different monthly distribution of the flow. In the CWatM model, the flow is concentrated in a few months of the year, while in the H08 model it is more evenly distributed throughout the year. Since sediment transport occurs in the months of greatest flow, the net result is that the potential sediment transport capacity is greater for the CWatM model than for the H08 model, although both have similar average annual flows.

The most reliable data are those corresponding to the flow observed in Tortosa and the results obtained with the natural and altered flows computed with the SIMPA model. These three points seem to be better aligned with the results of the H08 model, which is also more conservative. It is therefore appropriate to base the analyses on the results of the latter model.

2.4. Conclusion

The analysis carried out has made it possible to estimate the effect of the hydrological regime of the Ebro River on the potential capacity of sediment transport. It was based on the historical reference of the late

nineteenth century, in which an average annual flow of 17.38 km^3/yr and an annual sediment transport capacity of 28.1 Mton/yr were estimated. This reference was used to estimate a rating curve for potential sediment trasport that was applied to the current and future flow regimes under natural and altered conditions. The current observed flow in the lower Ebro River would be able to transport up to 9 Mton/yr of sediment to the Delta. This is a strong reduction compared to the estimated potential capacity of 27 Mton/yr under natural conditions. Currently, water abstractions and flow regulation in the Ebro basin have reduced mean annual flow by 40% and this has translated in a reduction of the potential sediment transport capacity of 67%.

Future projections show a highly uncertain scenario. The main sources of uncertainty of the analysis carried out are the variations between the emission scenarios and between the climate models, the limitations of the hydrological models to capture the real hydrology of the basin and the non-linearity of the relationship between flow and sediment transport capacity. For the first time window, between 2020 and 2060, natural flow is projected to decrase between 10% and 15%. This would imply a reduction of the potential sediment transport capacity between 15% and 30%. If the Ebro basin is managed to maximize water supply, the current altered flow would be reduced up to an additional 10%, which would imply a reduction of sediment transport potential under altered condition of up to 30%. Reductions are larger in the secont time window, 2060-2100: between 10% and 30% for natural flow, between 15% and 50% for sediment transport potential, between 10% and 40% for altered flow and up to 40% for sediment transport potential under altered conditions.

2.5. References

Anderson, R.S.(2002) Modeling the tor-dotted crests, bedrock edges, and parabolic profiles of high alpine surfaces of the Wind River Range, Wyoming. Geomorphology 46, 35–58.

Atkinson E (1996): The feasibility of Flushing Sediment from Reservoirs. HR Wallingford Technical Report OD 137.

Avendaño Salas, C.; Cobo Rayán, R.; Sanz Montero, E.; Gómez Montaña, J.L (1997): Capacity situation in Spanish reservoirs. Proceedings XIX ICOLD World Congress, Q 74, R.53, pp 849-862.

Batalla R.J., Vericat D. (2011) Hydrology and Sediment Transport. The Ebro River Basin. Handbook of Environmental Chemistry 13, 21–46, D. Barcelo and M. Petrovic (eds.)

Batalla RJ, Vericat D, Tena A (2014): The fluvial geomorphology of the lower Ebro (2002-2013): Bridging gaps between management and research. Cuadernos de Investigación Geográfica 40(1): 29-51

Cea, L., Puertas, J., Vázquez-Cendón, M.E. (2007) Depth Averaged Modelling of Turbulent Shallow Water Flow with Wet-Dry Fronts. Arch. Comput. Methods Eng., 14, 303–341.

Bladé, E., Cea, L., Corestein, G., Escolano, E., Puertas, J., Vázquez-Cendón, E., Dolz, J., Coll, A. (2014) Iber: Herramienta de simulación numérica del flujo en ríos. Rev. Int. Métodos Numér. Cálc. Diseño Ing., 30, 1–10.

Catalán (1969): Química del agua. Ed Blume.

Dolz, J., Armengol, J., Roura, M., De Pourcq, K., Arbat, M., López, P. (2009): Estudio de la dinámica sedimentaria y batimetría de precisión del embalse de Ribarroja. Grupo FLUMEN.

Dolz, J., Bladé, E., Arbat, M. (2010): Estudio de hidrodinámica del Segre. Annex 7 of the work: "Recuperación del Lecho y Mejora del Estado Ecológico del Río Segre en la Confluencia con el Ebro. T.M. De Mequinenza (Zaragoza)". Confederación Hidrográfica del Ebro.

Garrote, L. (2018): Evaluación preliminar sobre las posibilidades de restauración del tránsito sedimentario en los embalses de Mequinenza-Ribarroja-Flix. Confederación Hidrográfica del Ebro.

Garrote, L.; Sordo-Ward, A.; Iglesias, A.; Bianucci, P.; Javandel, N. Martin-Carrasco, F. (2023): Assessment of blue and green water availability for agriculture in the Mediterranean. AgWaMed Deliverable 5.1.

Gorría, H. (1877) Desecación de las marismas y terrenos pantanosos denominados de Los Alfaques. Tech. Rep., Ministerio de Agricultura. Madrid

Ibàñez C., Prat N., Canicio A. (1996) Changes in the hydrology and sediment transport produced by large dams on the lower Ebro river and its estuary. Regulated Rivers: Research and Management, 12, 51-62.

Kondolf GM, Farahani A (2018): Sustainably Managing Reservoir Storage: Ancient Roots of a Modern Challenge. Water, 10, 117.

López-Gómez, D.; Balairón, L.; García-Vera, M.A.; Galván, R.; Arrazola, C.; Polanco,L: Sánchez-Martínez, F.J. (2022): Estudios para la mejora de la gestión de los sedimentos en el curso bajo del río Ebro. XXX Latin-American Congress. IAHR.

Mudd, S.M., Furbish, D.J. (2004) Influence of chemical denudation on hillslope morphology. J. Geophys. Res. Earth Surf., 109. doi:10.1029/2003JF000087.

Paola, C., Voller, V.R. (2005) A generalized Exner equation for sediment mass balance. J. Geophys. Res. Earth Surf., 110. doi:10.1029/2004JF000274.

Santillán, D., Cueto-Felgueroso, L., Sordo-Ward, A., Garrote, L. (2020) Influence of Erodible Beds on Shallow Water Hydrodynamics during Flood Events. Water, 12, 3340, doi:10.3390/w12123340

Shields, A. (1936). Anwendung der Aehnlichkeitsmechanik und der Turbulenzforschung auf dieGeschiebebewegung. Mitteilung der Preussischen Versuchsanstalt fur Wasserbau und Schiffbau, Heft 26, Berlin.

Soulsby, R.L., Whitehouse, R.J.S. (1997) Threshold of Sediment Motion in Coastal Environments. Pacific Coasts and Ports '97: Proceedings of the 13th Australasian Coastal and Ocean Engineering Conference and the 6th Australasian Port and Harbour Conference, Volume 1

Tena A., Batalla R.J., Vericat D., Lopez–Tarazón J.A. (2011) Suspended sediment dynamics in a large regulated river over a 10-year period (the lower Ebro, NE Iberian Peninsula). Geomorphology, 125, 73–84.

Tena A, Batalla RJ, Vericat D (2012): Reach-scale suspended sediment balance downstream from dams in a large Mediterranean river. Hydrological Sciences Journal 57, pp 1–19

van Leer, B. (1979) Towards the Ultimate Conservative Difference Scheme, V. A Second Order Sequel to Godunov's Method. J. Comput. Phys., 32, 101–136.

van Rijn, L.C. (1987). Mathematical modelling of morphological processes in the case of suspended sediment transport. Delft: Delft Hydraulics Communications #382.

van Rijn, L.C. (1984a) Sediment Transport, Part I: Bed Load Transport. J. Hydraul. Eng., 110, 1431–1456.

van Rijn, L.C. (1984b) Sediment Transport, Part II: Suspended Load Transport. J. Hydraul. Eng., 110, 1613–1641.

Vanoni V. A., Brooks N. H. (1957) Laboratory studies of the roughness and suspended load of alluvial streams. Sedimentation Laboratory, California Institute of Technology, Pasadena, Calif.

Vericat D, Batalla RJ (2006): Sediment transport in a large impounded river: The lower Ebro, NE Iberian Peninsula. Geomorphology 79: 72–92

Vericat D, Batalla RJ, Garcia C (2006) Breakup and reestablishment of the armour layer in a large gravel-bed river below dams: the lower Ebro. Geomorphology 76: 122–136

3. Barrier beach management under climate change scenarios. The Ebro Delta study case

Subbiah, B.[1,2], Sánchez-Artús, X.[1], Gracia, V.[1], Espino, M.[1], Sanchez-Arcilla, A.[1]

[1] *Universitat Politècnica de Catalunya - BarcelonaTech (UPC), Laboratori d'Enginyeria Marítima (LIM), C/Jordi Girona, 31, 08034, Barcelona, Spain*

[2] *IH Cantabria - Instituto de Hidráulica Ambiental, Universidad de Cantabria, Santander, Spain*

ABSTRACT: Barrier beaches, such as the Trabucador beach in the Ebro Delta, Spain, play a critical role in coastal protection but are increasingly vulnerable to the impacts of climate change, particularly sea level rise. This study examines the morphodynamic evolution of the Trabucador barrier beach (NW Mediterranean Sea) under varying sea level rise scenarios, considering the effectiveness of nature-based solutions strategies in form of embryonic alternating dunes and comparing it against classical nourishment. Using a calibrated XBeach model, the study simulates the impact of three significant storms - Gloria, Filomena, and Isaak - under SLR projections for 2050 (+0.27 m), 2075 (+0.57 m), and 2100 (+0.75 m). Results demonstrate that while classical nourishment and embryonic alternating dunes provide considerable protection against storm-induced breaching at lower SLR levels (+0.27 m), their effectiveness diminishes significantly at higher SLR conditions. Under the most severe scenarios (+0.57 m and +0.75 m), widespread breaching occurs across all management strategies, indicating a critical threshold where these approaches fail to withstand storm impacts. The findings suggest an urgent need for adaptive, scalable coastal management solutions to mitigate the increasing risk of erosion, flooding, and breaching due to climate change. This study contributes to the knowledge on barrier beach management by emphasizing the limitations of current protective measures under future climate conditions and highlighting the necessity for ongoing research and innovation in coastal defence strategies.

3.1. Introduction

Barrier beaches, in the form of barrier islands or spits, are coastal landforms that play a crucial role in protecting the coastline from the direct impact of ocean waves and storms (Stéphan et al. 2024). These elongated, narrow landforms are typically formed by the accumulation of sand and sediment transported by littoral processes. Acting as natural barriers, they shield the inland areas from storm surges and high-energy wave action, thereby reducing coastal erosion and flooding. The dynamic nature of barrier beaches is characterized by continuous changes due to natural processes like tides, waves, and sediment transport. These landforms are also highly sensitive to changes in sea level and weather patterns, making them particularly vulnerable to the impacts of climate change (Hoagland et al. 2024, Moore and Murray 2018). Human activities such as the construction of dams and coastal development further exacerbate these vulnerabilities by disrupting natural sediment supply and altering hydrodynamic conditions. The barrier beaches are found in various regions across the globe, each exhibiting unique environmental conditions and management challenges (Cueto Fonseca et al. 2021). Examples include the Outer Banks in the USA, Fraser Island in Australia, the Wadden Sea in Europe, Rio Formosa in Portugal, Dniester in Ukraine, Kakinada and Pentha barrier beaches in India and the barrier islands of the Chesapeake Bay. These sites highlight the diverse nature of barrier beaches and the common challenges they face in terms of erosion, habitat loss, and the need for sustainable management practices.

Sea level rise (SLR) will become one of the main problems for barrier beaches in future (Passeri et al. 2018) due to several reasons. Firstly, higher sea levels can lead to more frequent and severe flooding, especially during storm events. This increased inundation can cause significant erosion, overwash, and even permanent

loss of parts of the barrier beach. Secondly, SLR can alter the sediment dynamics of these coastal systems. For instance, the increased water depth can reduce the effectiveness of wave energy dissipation over the beach, leading to greater erosion. Moreover, SLR can submerge the back-barrier marshes and wetlands, which are crucial for the stability and resilience of barrier beaches. While long-term evolution of barrier beach itself is a complex phenomenon driven by complex processes, rising sea levels will exacerbate the potential problems, enhancing sediment transport and deposition, potentially causing beach retreat (Mariotti and Hein 2022). This will also increase the frequency and intensity of overwash events, destabilizing the coastal features. Morphodynamic responses include landward migration and alterations in beach profiles, with subsidence further increasing vulnerability. Besides, climate change will not only affect SLR, but alter the storminess. For Mediterranean Sea in general, it is predicted that climate change will lead to increased storm intensities and frequencies with increased storm surges. The Catalan part of Mediterranean coast will likely experience reduction in storm intensities though frequency will be increasing, while level of storm surges also is expected to increase up to 7% by the end of the century.

Case studies from Nova Scotia and the UK's Chesil Beach and Hurst Spit highlight the delicate balance between natural processes and adaptive management strategies, such as beach nourishment and dune restoration, emphasizing the need for continuous monitoring to effectively preserve these dynamic coastal systems. In order to complement the information gathered from monitoring, many studies have been focused on describing the storm impacts on the barrier beaches using numerical modelling for different sea level rise scenarios by increasing total water level. These studies have described that this increased water level led to enhanced erosion and breaching events. Therefore, there are no major studies focused on the potential role of additional protection measures like nature-based solutions in resultant morphodynamics due to the increased water levels.

In this study, we analyse the morphodynamic behaviour of the Trabucador barrier beach under various SLR scenarios, focusing on the effectiveness of embryonic alternating dunes as nature-based solution and comparing it to classical nourishment in mitigating storm impacts. The suitability of these interventions to enhance the resilience of the beach during extreme events is evaluated using the calibrated XBeach model (Roelvink et al., 2009), with simulations for historical storms such as Gloria, Filomena, and Isaak. These scenarios are compared against a baseline condition with no protective measures. To further assess the efficiency of the proposed strategies, their performance is tested under future SLR projections for the years 2050, 2075, and 2100, revealing critical thresholds where traditional mitigation efforts become less effective. This study is the continuation of Sánchez-Artús et al (2024), focused predominantly on the effectiveness of the proposed mitigation action for present conditions, and the validation of the XBeach model in the study area.

This work is organised as follows: Section 3.2 presents the study area, the model used, and the different coastal mitigation strategies and scenarios proposed. Section 3.3 shows the results for all the studied cases. Finally, Section 3.4 shows the discussion of the work and Section 3.5 the final conclusions.

3.2. Methods

3.2.1. Study area

The Ebro Delta, situated in the north-western Mediterranean Sea about 200 km south of Barcelona, spans an area of around 320 km², including a 7,802 hectares Natural Park, and boasts a 50 km coastline (Figure 3-1). The region is ecologically rich, with a variety of habitats such as freshwater bodies, lagoons, and salt marshes that support a wide diversity of species. This biodiversity not only enhances the ecological value of the area but also supports key economic activities such as tourism, hunting, fishing, aquaculture, and rice cultivation (Valdemoro et al. 2007, Rovira et al. 2007). However, the construction of dams along the Ebro

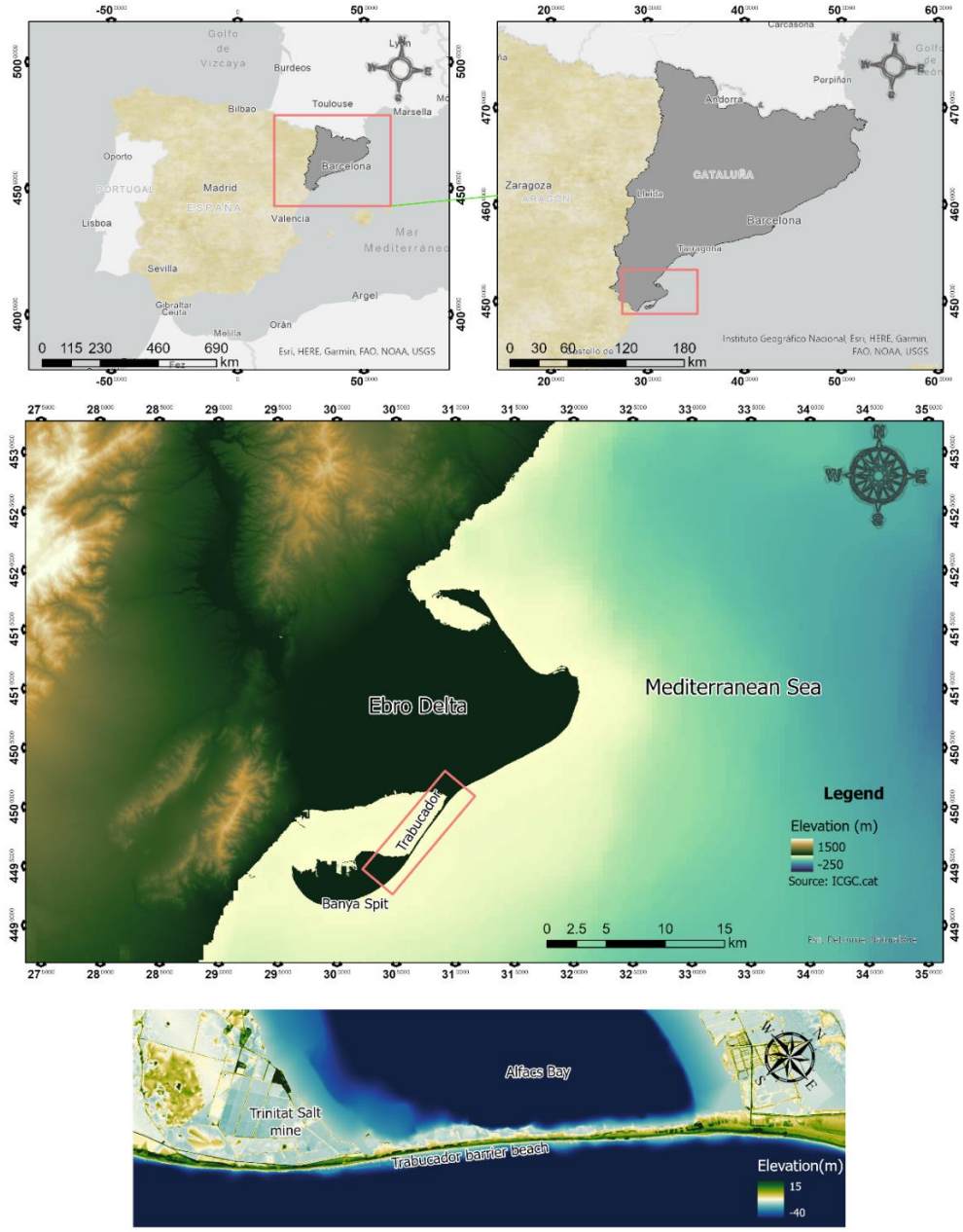

Figure 3-1 Study Area. Close-up from Spain to Ebro Delta, with red rectangles showing Barcelona, Ebro Delta and Trabucador barrier beach respectively. Bottom image shows an elevation map of the studied region.

River has significantly reduced the river's sediment discharge, leading to notable issues of erosion and subsidence in the region. The delta features two prominent spits: Fangar to the northwest and Banya to the southwest, with the latter connected to the mainland by the Trabucador barrier beach.

This barrier, the focal point of this study, lies between the Mediterranean Sea and the semi-enclosed Alfacs Bay (Grifoll et al. 2019). The beach is approximately 5.5 km long, 100 to 150 m wide, and reaches a maximum elevation of 1.5 m. Despite its environmental significance, the beach is highly vulnerable to breaching, particularly during winter storms, as seen with the severe impacts of Storm Gloria in 2020 and Storm Filomena in 2021, both of which caused substantial damage that took nearly a year to repair. The Trabucador beach, formed only four centuries ago through littoral transport, is now threatened by the very processes

that created it. A sediment deficit, exacerbated by these upstream dams, has accelerated beach depletion and retreat. Historically, the barrier beach has played a crucial role in protecting Alfacs Bay's vulnerable ecosystem, which species such as *Pinna nobilis* and seagrasses. The beach also supports the local economy by providing access to a salt mine located on Banya Spit.

3.2.2. Numerical model

XBeach model (version 1.23) is employed in this study to simulate the coastal response of the Trabucador barrier beach. XBeach is a 2DH (depth-averaged) model widely used for modelling wave energy, flow dynamics, infragravity wave propagation, and sediment transport, including processes like dune avalanching (Roelvink et al. 2009, McCall et al, 2010). Its robust numerical framework effectively captures flooding events, such as overwash and breaching on sandy beaches. Previous studies have demonstrated XBeach's capability to accurately represent the behaviour of deltaic and barrier beaches (Grases et al. 2020., Elsayed and Oumeraci 2016, Harter and Figlus 2017, Schambach et al. 2018). Specifically, Garcia et. al (2013) explored the breaching of the storm events from the years 2001, 2003 and 2009 in the Ebro Delta. Sánchez-Artús et al. (2024) focused on calibrate the model for the Trabucador barrier beach, and also assessed the impact of storm Gloria, Filomena and Isaak in the barrier beach. Further, it also assesses the role of protection measures like continuous dune system, alternating dune system and shoreface nourishment on mitigating these breaching processes.

For this research, XBeach is operated in its two-dimensional hydrostatic surfbeat mode, which accounts for temporal variations in wave height, crucial for modelling long-wave motions that influence swash waves impacting or overflowing the front beach. This feature enables the model to predict beach response according to Sallenger's storm impact regimes (Sallenger Jr., 2000). The model has been also used in studying storm impacts on barrier beaches specific to SLR but some of these past studies are made in an uncalibrated state given the difficulty to obtain post storm information. The current model setup used for this study have been deeply calibrated using a novel Goodness of fit approach utilizing post storm images of breaching shape (Sánchez-Artús et al., 2024).

3.2.3. Mitigation strategy approaches

In response to these growing threats, an embryonic alternating dune system was implemented as a Nature-based Solution (NbS) in 2022 to mitigate flooding and breaching hazards. This intervention is part of broader efforts to manage the Trabucador barrier, which has been continuously studied and restored following major storm events. It involves the placement of dunes at strategic intervals along the coast, potentially enhancing the resilience of certain areas while allowing natural processes to occur in others. Previous research has documented storm impacts, including long-term evolution and critical thresholds for beach survival under sea-level rise, emphasizing the need for both immediate and sustainable protective measures (Cooper et al. 2020, Lepesant 2024). To complement the results obtained from this novel approach, a digital generation of classical nourishment approach was done. This strategy refers to periodic addition of sediment to the beach system to maintain its width and height, counteracting the effects of erosion. Finally, a final state of the barrier beach representing a baseline or control scenario where no defensive measures are taken against coastal processes is considered and named as no protection. More details about the final meshes containing the mitigation strategies and the no protection can be found at Sánchez-Artús et al. (2024).

3.2.4. Storm and scenarios description

For the study, three different SLR scenarios were studied representing the conditions for the years 2050, 2075 and 2100. Following IPCC (Parmesan et al. 2022) and NASA Sea Level Projection tool predictions, the simulated levels were +0.27 m, +0.57 m and +0.75 m respectively. While IPCC provides different confidence of projections and different scenarios, for the above years the water level coinciding with multiple scenarios is chosen instead of particular RCP or SSP scenarios.

These scenarios are tested for three storms of the past in order to see differences with current sea level conditions. First, Gloria was tested as the biggest storm ever registered on Catalonia, in January 2020. This storm persisted for 204 hours and reached a maximum wave height of 7.8 m with an associated peak period of 11 s. Then, in January 2021 the storm Filomena hit the coast for nearly 140 h, with a maximum wave height of 5.15 m and a peak period of 11 s. Finally, in February 2023, storm Isaak affected the Trabucador beach while the embryonic alternating dune system was placed. The storm remained during 56 hours reaching a wave height of 4.67 m and a peak period of 12.11 s.

The simulations shown in this study are done for each of the three different beach states under the presented storms and for each of the sea level rise scenarios, leading to a complete analysis of the possible problems associated with both storms and SLR if no interventions are done.

3.3. Results

The section will be organized showing the storm effects in terms of breaching (Appendix A) and long-shore profile changes for each of the SLR scenarios. Then, a subsection specifically presenting the breaching volumes and areas for all the scenarios will be included. The described results about present conditions and current sea levels are described in Sánchez-Artús et al. (2024).

3.3.1. SLR projection for 2050 (+0.27 m)

For this scenario, during storm Filomena, more severe impacts than those at current sea levels were observed. The degree of breaching was comparable to that caused by storm Gloria under conditions without sea level rise. Each of the three scenarios—no protection, alternating dunes, and classical nourishment—experienced widespread breaching, particularly in the central section of Trabucador beach, indicating a high vulnerability in this area. Despite the overall breaching, the alternating dunes in the southern part of Trabucador beach remained intact, and the formation of a swash zone bar was also evident, suggesting some localized resilience in this configuration (Appendices Figure A-1).

During storm Gloria, the barrier was completely breached in all three management scenarios, demonstrating a similar pattern to the extensive breach observed in the middle part of the beach over a span of more than two kilometers. Smaller breaches were also noted in the southern part of the beach, while a wide breach occurred in the northern part. This indicates that none of the protection measures could withstand the increased water levels brought by storm Gloria, leading to significant overwash across the rest of the beach (Appendices Figure A-2). Finally, storm Isaak caused breaching with patterns entirely similar to those of storm Filomena at current water levels. In the no protection scenario, the storm resulted in the formation of six distinct crescentic islands along with a shore-parallel swash-zone bar, a feature also seen under current conditions with storm Filomena. In the scenario with alternating dunes, there were multiple smaller breaches along the barrier beach, including between the alternating dunes in the southern part of Trabucador, again mimicking the impact patterns observed with storm Filomena under present sea levels. The classical nourishment scenario produced smaller breaches primarily in the middle part of Trabucador and overwash depositions along the length of the beach (Appendices Figure A-3).

In terms of long-shore profile changes, storm Gloria caused significant breaches ranging from 1 m to 1.5 m deep, while storm Filomena resulted in a 0.5 m deep breach without protection but negligible effects under classical nourishment, highlighting its effectiveness in mitigating erosion. Interestingly, the breach depths during storm Filomena were greater in the southern part of Trabucador beach than those during storm Gloria, indicating localized variability in storm impact and the effectiveness of protective measures. This illustrates the importance of considering both generalized and specific responses of coastal defences to different storm intensities under elevated sea level conditions (Figure 3-2).

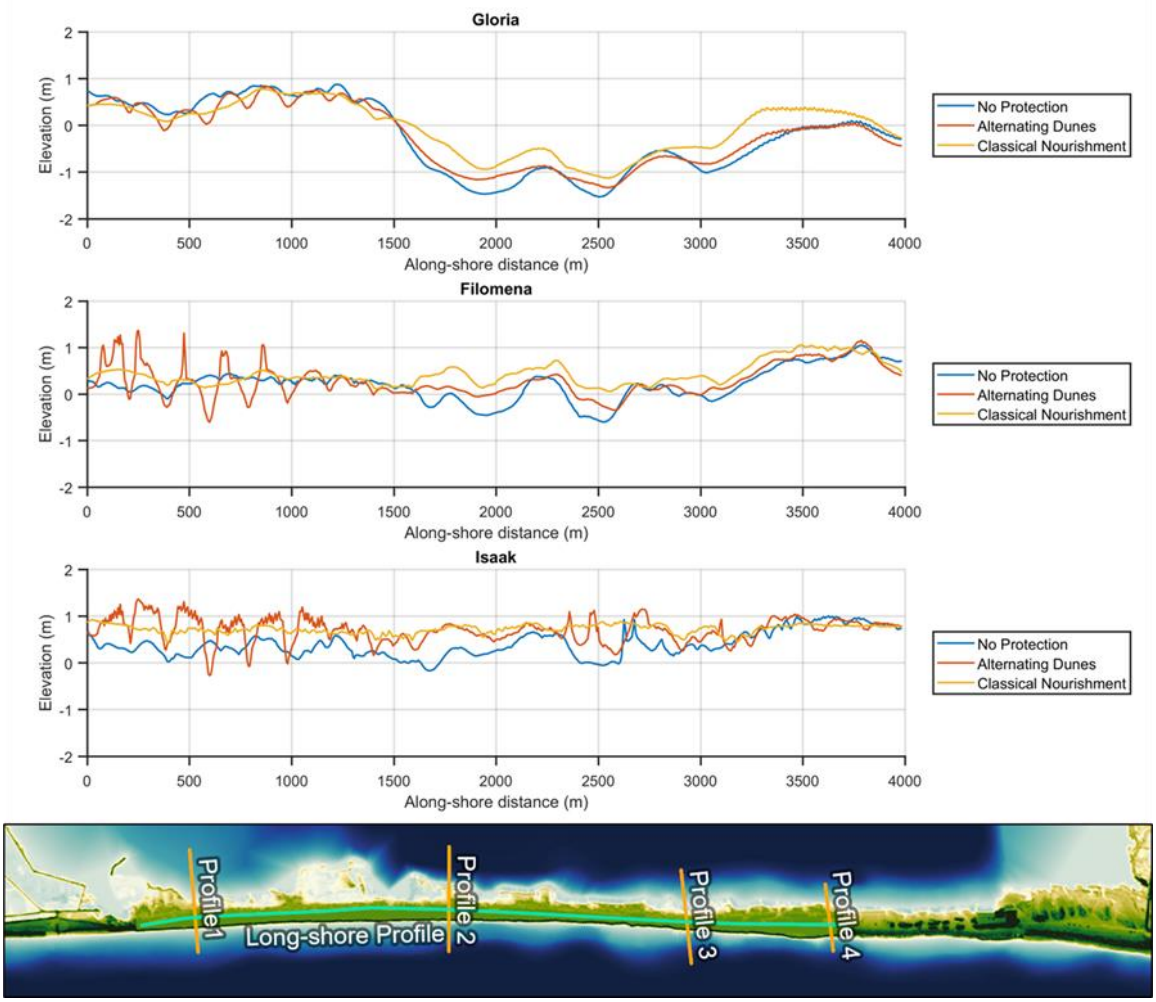

Figure 3-2 Cross-shore variations of beach profiles along the Trabucador barrier beach for each of the mitigation strategies and with the +0.27 m SLR scenario

3.3.2. SLR projection for 2075 (+0.57 m)

Under a 0.57 m rise in water levels, storm Filomena managed to entirely breach the barrier system, with two notable islands emerging within a four-kilometer stretch of the coast. This significant breaching manifested similarly across all management scenarios—no protection, alternating dunes, and classical nourishment—highlighting a major vulnerability in the central part of the Trabucador beach, along with smaller breaches to the north and south. The protective measures in place proved ineffective at this increased water level, as erosion extended over the beach and nearshore areas, while sedimentation occurred on the bay side. Notably, the formation of a swash zone bar was less apparent compared to previous conditions (Appendices Figure A-4). For Storm Gloria, the landscape changed drastically from previous scenarios, with the destruction of previously observed crescentic islands in the middle part of the beach. Breaching was comprehensive and similar across all topo-bathymetric conditions. A singular crescentic island was observed in the southern part of Trabucador. The entire beach shifted towards the bay, with almost no formation of swash zone bars, indicating a profound reshaping of the coastal landscape. This suggests that the coastal barrier system is reaching a critical threshold under such elevated SLR conditions (Appendices Figure A-5). In contrast to the lesser impacts observed in the +0.27 m SLR scenario, storm Isaak with +0.57 m SLR induced significant breaches across all management scenarios. In the no-protection case, major breaches were noted particularly in the middle of Trabucador, with a crescentic island positioned between them. The alternating dunes scenario showed wider breaches in the middle and small breaches between the dunes in the southern

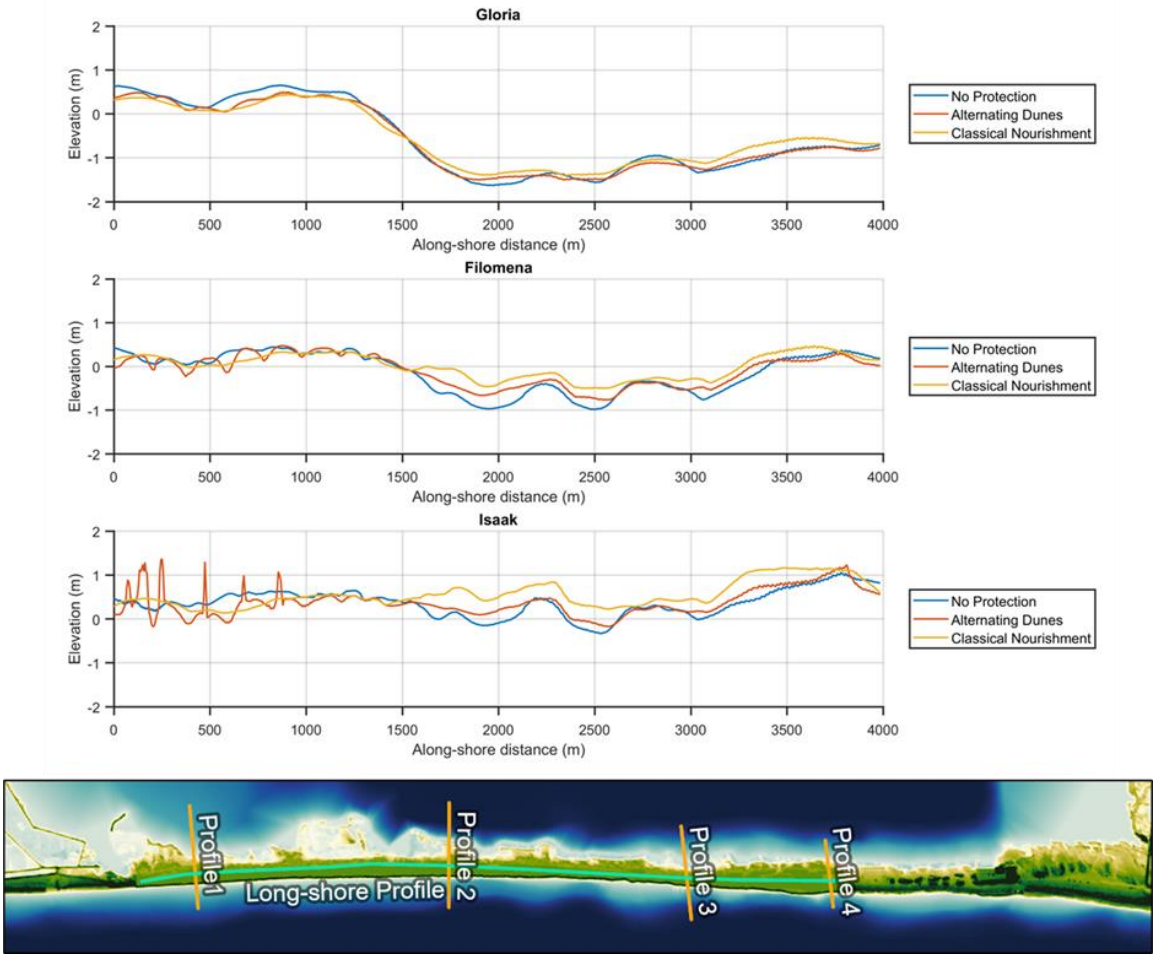

Figure 3-3 Cross-shore variations of beach profiles along the Trabucador barrier beach for each of the mitigation strategies and with the +0.57 m SLR scenario

part, while the classical nourishment scenario experienced multiple breaches along the entire beach. The presence of strong overwash throughout the beach and notable formation of a swash zone bar in the southern part further demonstrated the intensified geomorphological changes (Appendices Figure A-6).

Long-shore profile changes showed that during storm Gloria, breaching depths reached up to 1.5 m across all scenarios, indicating a severe uniformity in the degradation of the beach profile. The lack of variability in long-shore changes among different scenarios underscores a tipping point in the resilience of the coastal system. For storm Filomena, breaching depths increased significantly compared to the +0.27 m SLR condition, while for Storm Isaak, the largest breaches were observed in the no protection case, though parts of the alternating dunes remained intact, highlighting some residual effectiveness of this management strategy (Figure 3-3).

3.3.3. SLR projection for 2100 (+0.75 m)

With a 0.75 m SLR, storm Filomena led to complete breaching of the Trabucador beach across all management scenarios, essentially washing away the beach along its entire length, with only negligible patches remaining above the increased water level. The results depict a beach landscape that has reached a tipping point under these conditions, with significant erosion across the beach and sediment displacement into the bay area. The formation of swash-zone bars, previously noted, was largely absent under these severe conditions, indicating a substantial morphological transformation of the coastal zone (Appendices Figure A-7). Similarly, storm Gloria replicated the severe impacts seen with Filomena under the same SLR conditions,

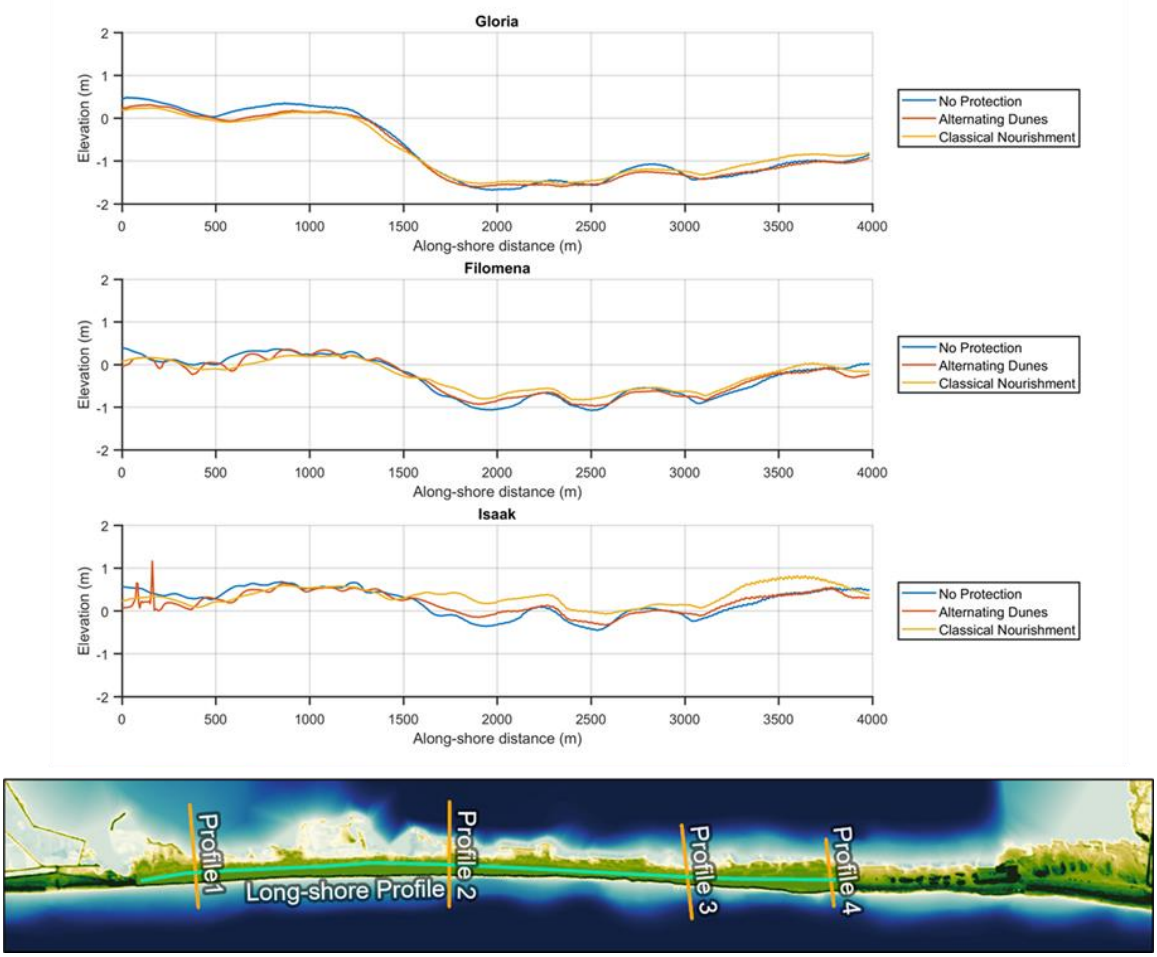

Figure 3-4 Cross-shore variations of beach profiles along the Trabucador barrier beach for each of the mitigation strategies and with the +0.75 m SLR scenario

confirming the beach's vulnerability at this elevated sea level. The entire beach experienced a complete breach, with minor patches marginally above the current water level. The absence of swash-zone shore parallel bars, which are indicative of sediment redistribution processes, points to a drastic displacement of the beach into the bay, emphasizing the failure of protection measures to mitigate such extreme impacts (Appendices Figure A-9). Storm Isaak, while causing widespread breaching across all management scenarios, did not completely breach the barrier beach as seen in the other storms. The no protection scenario showed complete breaching in the middle with significant overwash extending to the northern and southern stretches. In the alternating dunes scenario, a wider breach occurred in the middle with smaller breaches at the southern and northern ends, marking the first time these structures have failed under such conditions. The classical nourishment scenario also experienced strong breaching, particularly in the southern and middle sections of the beach.

The long-shore profile changes during storms Gloria and Filomena showed a near-uniform depth of breaches across all scenarios, reaching depths just above 1.5 m for Gloria and about 1 m for Filomena, similar to the breaches in previous SLR conditions. Despite widespread breaching during Storm Isaak, the depth of these breaches was relatively shallow compared to other storms, indicating varied impacts based on storm characteristics and perhaps some residual effects of the coastal defences, although the alternating dunes were notably destroyed (Figure 3-4).

3.3.4. Breaching volume and area

In the context of varying SLR scenarios, a detailed examination of breaching volumes and areas highlights the increasing vulnerability of coastal defences under escalating sea levels. The collected data delineates how breaching dynamics evolve across different management strategies and storm conditions. At the current sea level, the no protection scenario records the highest breaching volumes, with Gloria leading at 121,881 m^3, followed by Filomena at 41,252 m^3, and Isaak at 13,574 m^3. Alternating dunes and classical nourishment show significantly reduced volumes, emphasizing their initial effectiveness. Under a +0.27 m SLR, there is a marked increase in breaching volumes. For instance, under no protection, Gloria's breaching volume escalates to 311,506 m^3. Despite the application of protective measures, similar increases are noted, with classical nourishment and alternating dunes reaching 300,902 m^3 and 317,149 m^3 respectively for Gloria, underscoring the limited scalability of these defences against rising sea levels. At a +0.57 m SLR, the breaching volumes continue to rise, with no protection reaching 500,599 m^3 for Gloria and classical nourishment peaking at 595,621 m^3, indicating a reduced protective benefit at this higher SLR. With a +0.75 m SLR, the volumes under no protection for Gloria are at 583,575 m^3, with classical nourishment reaching an even higher 732,359 m^3 (Figure 3-5). This illustrates a further decline in defence effectiveness, as even the most robust measures fail to significantly mitigate breaching impacts.

Regarding breaching areas, the trend also indicates increasing susceptibility, where at current sea levels, the areas affected are relatively modest, with no protection yielding 0.20 km^2 for Gloria and 0.22 km^2 for Filomena. With a +0.27 m SLR, these areas expand, reaching 0.45 km^2 for Gloria under no protection, and classical nourishment results in an area of 0.51 km^2. At +0.57 m SLR scenario, the area for Gloria under no

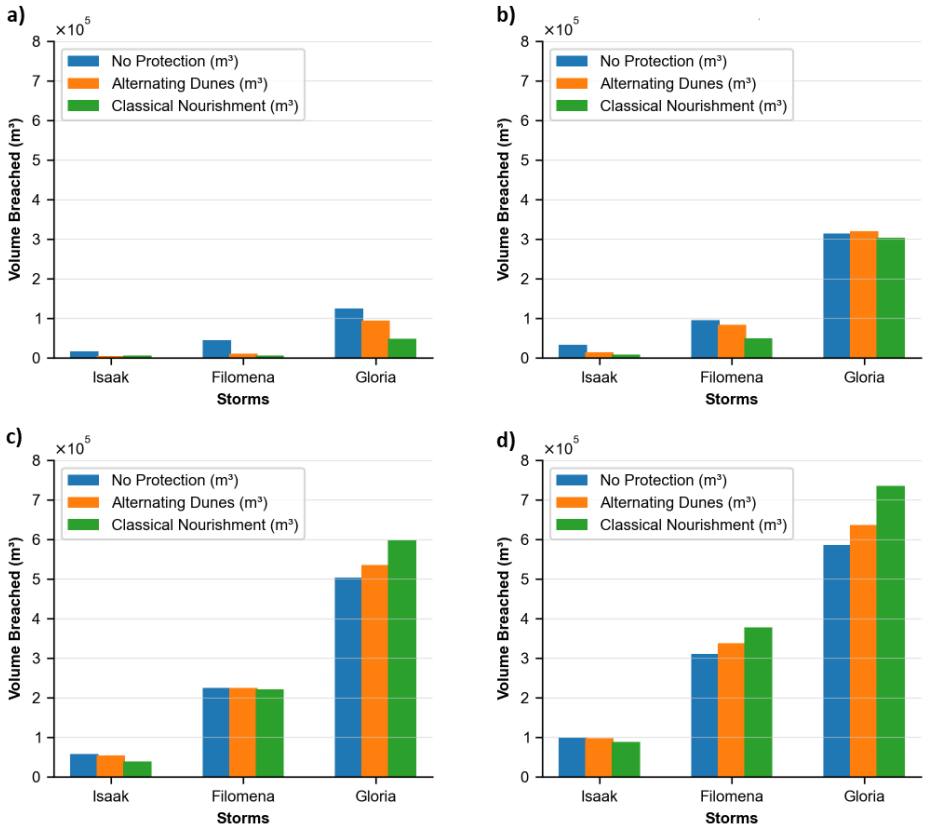

Figure 3-5 Breaching volume, a) Current, b) SLR 0.27m, c) SLR 0.57m, and SLR 0.75m

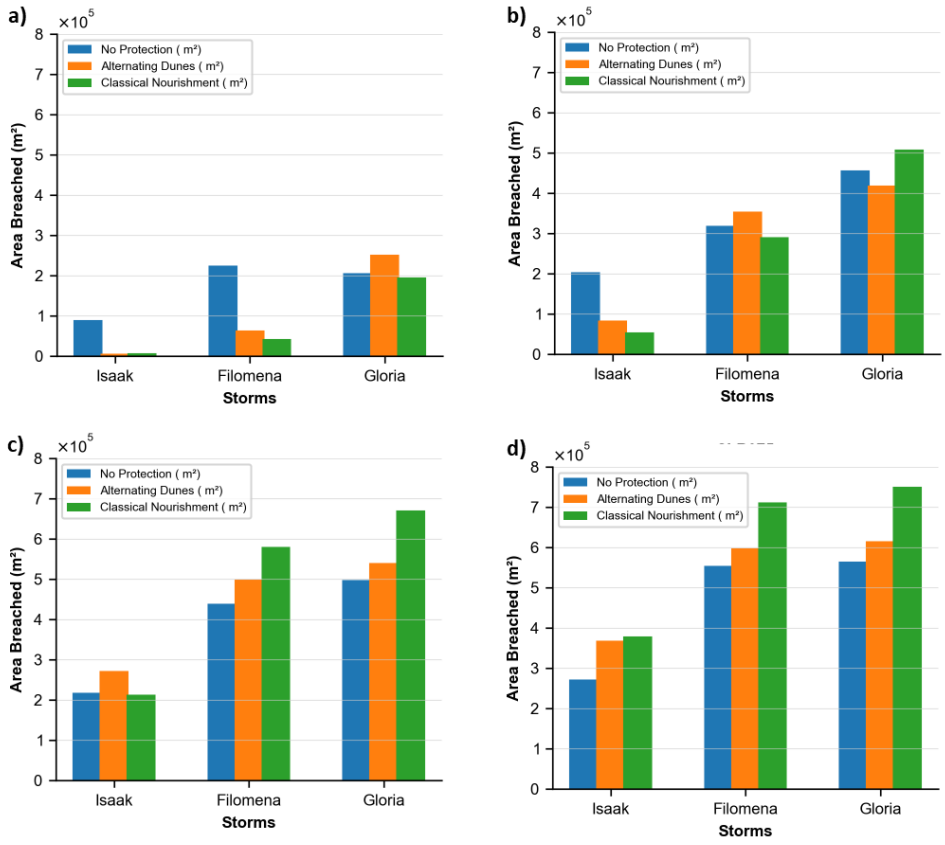

Figure 3-6 Breaching area, a) Current, b) SLR 0.27m, c) SLR 0.57m, and SLR 0.75m

protection increases to 0.49 km², and under classical nourishment, it reaches 0.67 km². Finally, under +0.75m SLR, the breaching area for Gloria extends to 0.56 km² under no protection and to 0.75 km² under classical nourishment, marking the highest recorded area (Figure 3-6).

3.4. Discussion

The results show that while the proposed protective measures may reduce breaching volumes and areas at scenarios with low SLR, their efficacy diminishes as SLR increases, reaching a point where traditional coastal defences are overwhelmed (Cooper et al. 2020), suggesting the need for more advanced or adaptive strategies in coastal management to handle the impacts of higher sea levels and more severe storm scenarios, in concordance with Lepesant (2024). The analysis of coastal protection measures efficiency under varying Sea Level Rise (SLR) scenarios shows a clear trend of diminishing effectiveness as sea levels increase. The performance of classical nourishment and embryonic alternating dune system is evaluated against the benchmark of no protection under different storm and water level conditions. At the current water level, both protection measures are highly effective. For Storm Isaak, the measures completely prevent breaching. In the case of Storm Filomena, breaching is reduced by 80%, and for Storm Gloria, classical nourishment reduces breaching by 65 % while alternating dunes achieve a 30% reduction, as seen in Figure 3-7. Under a +0.27 m SLR, the protection measures still function effectively for milder storms like Isaak and Filomena, with classical nourishment providing more substantial reductions in breaching compared to embryonic alternating dunes. However, for Storm Gloria, both protection strategies only reduce breaching by about 10 %, indicating a significant decrease in their effectiveness. With +0.57 m SLR, the reduction in breaching efficiency becomes more pronounced. Classical nourishment results in a 40 % reduction for Storm Isaak, significantly less effective than at lower sea levels, and alternating dunes only reduce breaching by 15 %. For Storm Filomena, both strategies reduce breaching by just 9 %, and for Storm Gloria, the measures fail almost completely, with

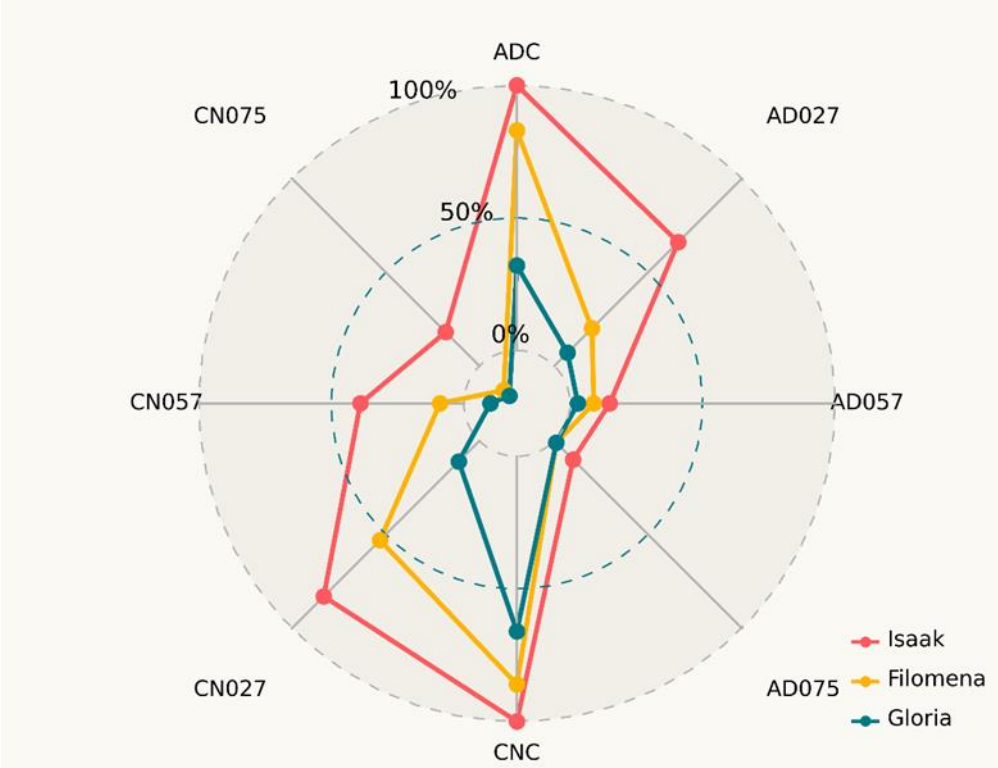

Figure 3-7 Efficiency of the mitigation strategies. CN stands for classical nourishment and AD for alternating dunes. The numbers within the description of each case refers to the climate change scenario with current water level, +0.27 m, +0.57 m and +0.75 m.

alternating dunes providing a mere 2.7 % reduction, and classical nourishment actually resulting in a 10 % increase in breaching compared to no protection. In the scenario of a +0.75 m SLR, the protection measures struggle to prevent breaching effectively. Classical nourishment reduces breaching by 17.5 % for Storm Isaak, while alternating dunes manage only a 10 % reduction. For storms Gloria and Filomena, the measures are almost ineffective, with breaching volumes similar to scenarios without any protection, indicating a near-total failure of the coastal defences (Figure 3-7).

As commented previously, with +0.27 m SLR, both classical nourishment and embryonic alternating dunes demonstrate a considerable capacity to reduce the impacts of storm-induced breaching. This SLR level represents conditions likely to be encountered around mid-century, based on current climate projections. In these scenarios, the protection measures are able to mitigate not just the frequency of breaching but also maintain more controlled breach characteristics, such as location and morphology. The effectiveness of these measures under a +0.27 m SLR is not uniform across the entire beach but is more pronounced in certain areas by targeted breaching especially in alternative dune condition. This indicates that the strategic placement and design of protection measures can enhance their overall effectiveness, particularly in guarding critical or vulnerable sections of the coastline. The success of these protective measures at +0.27 m SLR suggests that they are sustainable options for managing coastal risks associated with moderate increases in sea levels. This is significant for coastal planning and management, as it provides a viable timeframe during which these measures can be expected to perform effectively, allowing for planning and adaptation before conditions worsen.

As SLR increases beyond +0.27 m, the effectiveness of both classical nourishment and alternating dunes rapidly declines. This was particularly evident in scenarios simulating SLRs of +0.57 m and +0.75 m, where these measures failed to significantly mitigate the effects of storm-induced breaching. This threshold

behaviour highlights a critical limit in the current design and implementation of such measures. The failure of traditional protection measures at higher SLRs underscores the necessity for developing scalable and adaptable coastal defences strategies. As SLR projections for later this century exceed the +0.27 m mark, it becomes imperative to explore more innovative, flexible, and robust solutions that can accommodate more severe changes in sea level and associated storm dynamics. The analysis from the Trabucador beach case study starkly illustrates the significant role that beach level and width play in determining the impact of storms under different SLR scenarios compared to current conditions. The beach's inherent characteristics, particularly its width and elevation, are pivotal in moderating storm-driven morphodynamical changes. Under current conditions, the beach's configuration, especially width, is a critical factor in mitigating storm impacts. For instance, in the no protection scenario, the beach width is notably narrower in the middle sections (ranging from 35 m to 60 m), making these areas more susceptible to breaching. The classical nourishment strategy, which increases the beach width to 120 m and stabilizes the crest level at 0.7 m, shows a substantial reduction in breaching, as it enhances the beach's capacity to absorb and dissipate storm energy more effectively. However, as SLR scenarios intensify, the dynamics shift considerably. The observations indicate that while beach width and initial elevation are significant in current conditions, their importance is overshadowed by the elevation factor as SLR increases. With higher SLRs, the waves begin to break directly over the barrier beach, effectively negating the benefits of increased width. This behaviour was also observed by Anarde et al. (2024a, 2024b). The protective measures fail to prevent significant breaching, highlighting a need for adaptive strategies that consider not just width but also the elevation and resilience of the beach profile in response to rising sea levels and more potent storm surges, as discussed by Bongarts et al. (2021). The near uniformity of storm impacts across different management scenarios at higher SLRs underscores the pressing challenge of developing coastal defences that can withstand the effects of climate change-driven sea level increases.

3.5. Conclusions

The study of Trabucador barrier beach and the Ebro Delta under various SLR scenarios reveals the critical need for adaptive and innovative coastal defence strategies, particularly emphasizing the effectiveness of NbS such as embryonic alternating dunes at moderate SLR levels (+0.27 m). These measures are shown to significantly reduce breaching impacts and maintain beach resilience, highlighting their potential applicability to similar coastal systems facing moderate SLR. However, the effectiveness of these NbS and other classical approaches declines sharply at higher SLR levels (+0.57 m and +0.75 m), suggesting that while they provide substantial protection in the near term, additional or enhanced measures will be needed for long-term sustainability. The long-term evolution of barrier beach systems, including Trabucador, is highly debated with considerable uncertainties, and the projected SLR impacts might not precisely represent future conditions but offer valuable insights into potential responses to higher water levels. The study also indirectly addresses the influence of additional storm surges on storm impacts by examining different increased water levels aligned with SLR scenarios. Climate change projections indicate a potential minor increase in storm intensities and surge levels in the Mediterranean, underscoring the urgency for innovative, adaptable NbS to protect coastal areas. These findings suggest that while current NbS are effective for moderate SLR, ongoing research, monitoring, and adaptive management will be essential for addressing the complex and evolving challenges posed by climate change to coastal systems like the Trabucador barrier beach and similar environments globally.

3.6. References

Anarde, K. A., Moore, L. J., Murray, A. B., & Reeves, I. R. (2024a). The future of developed barrier systems: 1. Pathways toward uninhabitability, drowning, and rebound. Earth's Future, 12(4), e2023EF003672.

Anarde, K. A., Moore, L. J., Murray, A., & Reeves, I. (2024b). The future of developed barrier systems: 2. Alongshore complexities and emergent climate change dynamics. Earth's Future, 12(4), e2023EF004200.

Bongarts Lebbe, T., Rey-Valette, H., Chaumillon, É., Camus, G., Almar, R., Cazenave, A., ... & Euzen, A. (2021). Designing coastal adaptation strategies to tackle sea level rise. Frontiers in Marine Science, 8, 740602.

Cueto Fonseca, J. E., Otero Díaz, L. J., Ospino Ortiz, S. R., & Torres-Freyermuth, A. (2021). The role of morphodynamics in predicting coastal flooding from storms on a dissipative microtidal beach with SLR conditions: Cartagena de Indias (Colombia). Natural Hazards and Earth System Sciences Discussions, 2021, 1-25.

Cooper, J. A. G., Masselink, G., Coco, G., Short, A. D., Castelle, B., Rogers, K., ... & Jackson, D. W. (2020). Sandy beaches can survive sea-level rise. Nature Climate Change, 10(11), 993-995.

Elsayed, S. M., & Oumeraci, H. (2016). Combined modelling of coastal barrier breaching and induced flood propagation using XBeach. Hydrology, 3(4), 32.

Gracia, V., García, M., Grifoll, M., & Sánchez-Arcilla, A. (2013). Breaching of a barrier under extreme events. The role of morphodynamic simulations. Journal of Coastal Research, (65), 951-956.

Grases, A., Gracia, V., García-León, M., Lin-Ye, J., & Sierra, J. P. (2020). Coastal flooding and erosion under a changing climate: implications at a low-lying coast (Ebro Delta). Water, 12(2), 346.

Grifoll, M., Cerralbo, P., Guillén, J., Espino, M., Hansen, L. B., & Sánchez-Arcilla, A. (2019). Characterization of bottom sediment resuspension events observed in a micro-tidal bay. Ocean Science, 15(2), 307-319.

Harter, C., & Figlus, J. (2017). Numerical modeling of the morphodynamic response of a low-lying barrier island beach and foredune system inundated during Hurricane Ike using XBeach and CSHORE. Coastal Engineering, 120, 64-74.

Hoagland, S. W., Irish, J. L., & Weiss, R. (2024). Morphodynamic and modeling insights from global sensitivity analysis of a barrier island evolution model. Geomorphology, 451, 109087.

Lepesant, G. (2024). Between hard protection measures, nature-based solutions, and managed retreat: Adapting coastal areas to sea level rise in the Netherlands and France. Zeitschrift für Vergleichende Politikwissenschaft, 1-16.

Mariotti, G., & Hein, C. J. (2022). Lag in response of coastal barrier-island retreat to sea-level rise. Nature Geoscience, 15(8), 633-638.

McCall, R. T., De Vries, J. V. T., Plant, N. G., Van Dongeren, A. R., Roelvink, J. A., Thompson, D. M., & Reniers, A. J. H. M. (2010). Two-dimensional time dependent hurricane overwash and erosion modeling at Santa Rosa Island. Coastal Engineering, 57(7), 668-683.

Moore, L. J., & Murray, A. B. (Eds.). (2018). Barrier dynamics and response to changing climate. Springer.

Parmesan, C., Morecroft, M. D., & Trisurat, Y. (2022). Climate change 2022: Impacts, adaptation and vulnerability (Doctoral dissertation, GIEC).

Passeri, D. L., Bilskie, M. V., Plant, N. G., Long, J. W., & Hagen, S. C. (2018). Dynamic modeling of barrier island response to hurricane storm surge under future sea level rise. Climatic Change, 149, 413-425.

Roelvink, D., Reniers, A., Van Dongeren, A. P., De Vries, J. V. T., McCall, R., & Lescinski, J. (2009). Modelling storm impacts on beaches, dunes and barrier islands. Coastal engineering, 56(11-12), 1133-1152.

Rovira, A., & Ibàñez, C. (2007). Sediment management options for the lower Ebro River and its delta. Journal of Soils and Sediments, 7, 285-295.

Sallenger Jr, A. H. (2000). Storm impact scale for barrier islands. Journal of coastal research, 890-895.

Sánchez-Artús, X., Subbiah, B., Gracia, V., Espino, M., Grifoll, M., Espanya, A., & Sánchez-Arcilla, A. (2024). Evaluating barrier beach protection with numerical modelling. A practical case. Coastal Engineering, 191, 104522.

Schambach, L., Grilli, A. R., Grilli, S. T., Hashemi, M. R., & King, J. W. (2018). Assessing the impact of extreme storms on barrier beaches along the Atlantic coastline: Application to the southern Rhode Island coast. Coastal Engineering, 133, 26-42.

Stéphan, P., Suanez, S., Guérin, T., Rivier, A., Leballeur, L., Waeles, B., ... & Houron, J. (2024). Breaching of the Sillon de Talbert gravel spit (North Brittany, France) and coastal flooding risk assessment. Geomorphology, 109302.

Valdemoro, H. I., Sánchez-Arcilla, A., & Jiménez, J. A. (2007). Coastal dynamics and wetlands stability. The Ebro delta case. Hydrobiologia, 577, 17-29.

4. Seagrass as a Nature-Based-Solution (NbS) for coastal protection under future climate projections

Villa Castrillon, L.[1], Jacob, B.[1], Pein, J.[1], Chen, W.[1]& Staneva, J.[1]

[1] *Institute of Coastal Systems - Analysis and Modeling, Helmholtz-Zentrum Hereon, Geesthacht, Germany*

ABSTRACT: The Wadden Sea is a coastal region of significant ecological and economic importance. Climate change-driven sea level rise (SLR) and intensified storms heighten the risks of coastal flooding and erosion, necessitating the integration of nature-based solutions into management practices for long-term sustainability. This study examines the role of seagrass in reducing coastal risks in the German Bight, focusing on Jade Bay located in the southern Wadden Sea. Historical and end-of-century SLR scenarios were simulated using the SCHISM model, which couples hydrodynamics, waves, sediments, and a seagrass module. Simulations with and without seagrass were analyzed to assess habitat and ecosystem service changes due to SLR, based on the EUNIS habitat classification system using the D-ECO impact tool. Ecosystem services (ESS) evaluated included provisioning, carbon sequestration, water quality regulation, natural hazard regulation, and coastal erosion prevention. The findings indicate that seagrass meadows reduce current velocities and wave heights by approximately 45%, leading to a 45% reduction in bottom shear stress and an 80% decrease in erosion flux. Although seagrass remains effective at reducing erosion under elevated sea levels, its efficiency slightly declines compared to current conditions. Future climate scenarios suggest a potential expansion of sublittoral habitats and a 30-50% reduction in salt marshes, which provide among the highest ecological value in terms of ESS score. This shift could result in a 30% decrease in erosion protection and a 3% decline in carbon sequestration capacity.

4.1. Introduction

4.1.1. Coastal vulnerability

Coastal areas are among the most dynamic and vulnerable environments on Earth, subject to the influences of natural processes and human activities. These regions are of critical importance for their ecological value, economic importance, and social significance. However, these areas are also facing significant challenges because of climate change, which is expected to exacerbate existing issues such as erosion, flooding, and habitat loss. To ensure the effective management and protection of coastal zones, it is imperative to gain an understanding of how these areas respond to varying climatic conditions and anthropogenic pressures (UNEP, 2017).

Climate change scenarios, as delineated by the Intergovernmental Panel on Climate Change (IPCC), provide a framework for projecting future conditions. The Representative Concentration Pathways (RCPs) present a range of potential trajectories for greenhouse gas concentrations and their associated impacts on the global climate. This study concentrates on the high-emission RCP8.5 scenario, which represents a future characterized by sustained high levels of greenhouse gas emissions and minimal mitigation efforts. Global temperatures could rise by 3.2 to 5.4°C by the end of the century under RCP8.5, leading to significant increases in sea levels, more extreme weather events, and profound impacts on coastal systems. By examining the 5th, 50th, and 95th percentiles within this scenario, it is possible to gain insight into a range of potential environmental conditions, from moderate to extreme (Masson-Delmotte, et al., 2021).

The Wadden Sea, located in the southeastern region of the North Sea, is becoming increasingly exposed to flooding and coastal erosion due to the rising frequency and intensity of extreme weather events driven by global climate change. These threats endanger the coastal communities and ecosystems of the region, underscoring the need to develop alternative mitigation strategies. As a UNESCO World Heritage Site, the Wadden Sea faces the distinctive challenge of balancing the preservation of its ecological integrity with the necessity for adaptive measures. Consequently, conventional hard engineering solutions, such as dams and breakwaters, are less favored. This has led to an increased focus on innovative nature-based solutions (NbS) in recent years.

4.1.2. Restoration efforts

As part of the REST-COAST project, Hereon explores the theoretical benefits of seagrass restoration in the German Wadden Sea. While we are not involved in hands-on restoration activities and no active seagrass restoration projects are currently permitted in our study area, we focus on modelling potential outcomes. Our "What-if" scenarios for the East Frisian Wadden Sea are motivated by two factors: the observed recovery of seagrass in the North Frisian Wadden Sea, attributed to improved water quality from reduced eutrophication via rivers, and the growing body of scientific evidence supporting seagrass as an effective nature-based solution with multiple ecological benefits: Seagrass restoration as a NbS and coastal protection measure offers significant benefits, including the attenuation of wave energy, reduction of near-shore currents, and stabilization of the seabed. Recent studies have documented a positive trend in the natural recovery of seagrass meadows in the Wadden Sea area over the past two decades (van Katwijk, et al., 2024).

Recognizing the crucial role of coastal vegetation, particularly seagrass, in modulating coastal dynamics, we incorporate what-if scenarios into our modeling efforts to evaluate and assess the impact of seagrass under historical (1999-2003) and future (2090-2093) climate conditions. Moreover, the impact of seagrass on the hydrodynamic forces and sediment transport processes will be evaluated to gain insights into its role as a natural adaptation strategy. Therefore, within D 2.3 we expand further upon the works initialized within D2.2 addressing future climate projections and integrate the habitat and ESS approach illustrated in D 4.1.

4.2. Methods

The future risk projections are based on the RCP8.5 scenario, which assumes a continuous rise in greenhouse gas emissions throughout the 21st century. Despite ongoing debates about the likelihood of this emissions pathway (Hausfather, & Peters, 2020), the RCP8.5 scenario is of significant scientific importance due to its high signal-to-noise ratio. This characteristic makes it particularly effective for identifying emerging climate change signals. Under this scenario, the global mean sea level is expected to increase by approximately 40 cm, with regional rises potentially reaching up to 1 meter in the German Wadden Sea by 2100 (Pein et al., 2023).

4.2.1. Downscaling: initialization and forcing

The boundary forcing is derived from downscaled regional projections of mean sea level (MSL) and outputs from coupled Remo climate scenario simulations (Pein et al.,2023). The principal dynamic factors under consideration in our study are changes in the global mean sea level and coupled ocean-atmosphere variability. The increase in global mean sea level is attributable to several factors, including thermosteric expansion, the melting of polar ice caps and glaciers, and gravitational responses resulting from the conversion of ice masses to liquid (Church et al., 2013; Golledge, 2020). Regional variations in global MSL rise may be influenced by vertical land movements, including postglacial isostatic rebound. Probabilistic estimates for MSL rise under the RCP8.5 scenario from the UKCP18 project are used to prescribe these changes (Palmer et al.,2018 & Palmer et al.,2020).

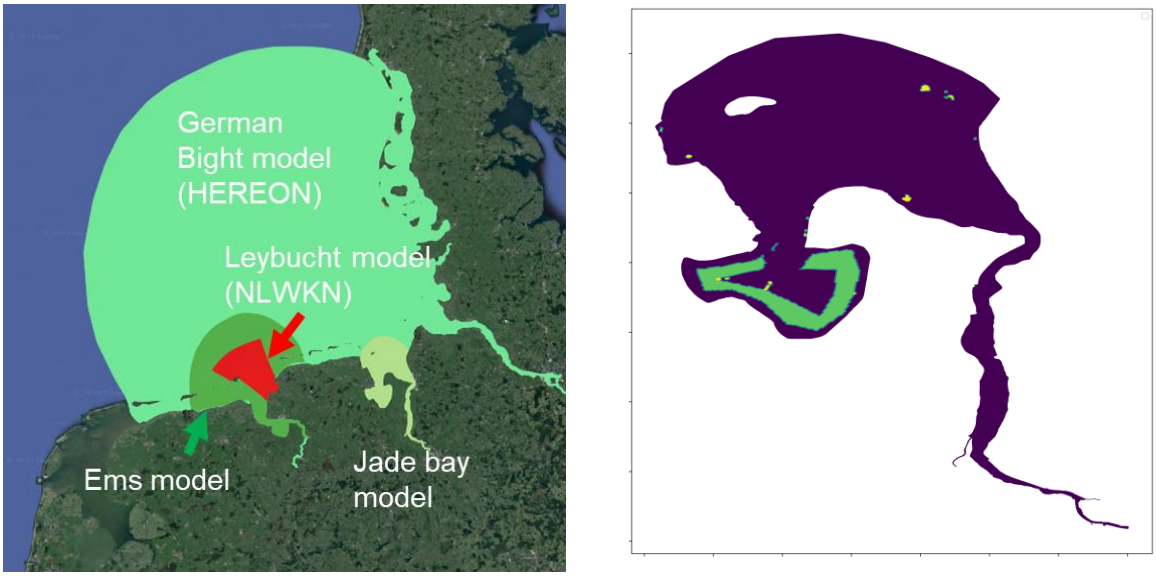

Figure 4-1 Model domains for Hereon and NLWKN and Seagrass implementation (Left) and seagrass scenario for Jade Bay experiments (right)

The regionalized simulations from the Max Planck Institute Earth System Model Low Resolution (MPI-ESM-LR) ensemble, conducted under the RCP8.5 scenario, were employed to analyze the coupled ocean-atmosphere dynamics. The global climate ensemble was downscaled using a regionally coupled climate system model with a nominal resolution of 5 km in the Southern North Sea (MPI-OM, as described by (Mayer et al., 2022; Mikolajewicz et al.,2005; Mathis, & Mikolajewicz 2020). The REMO atmospheric module, with a resolution of approximately 7 km, not only includes atmospheric variables but also predicts daily surface runoff, which contributes to river input. The ensemble simulation dataset captures the variations in ocean density and currents, as well as the meteorological conditions, including atmospheric water transport, which are driven by the increased radiative forcing due to climate change.

The ensemble was generated by initializing the global model with various historical states from the years 1950-1959, based on three previous simulations using the same model system (Mathis, & Mikolajewicz 2020). The 6-hourly outputs from these global simulations were employed to drive the MPI-OM-REMO regional climate modeling framework, which subsequently provided boundary forcing for the Semi-implicit Cross-scale Hydroscience Integrated System Model (SCHISM) simulations for the Southern North Sea setup analyzed in Pein et al.,2023. Subsequently, the initial forcing for the German Bight and Jade Bay setups (Figure 4-1) was downscaled from the southern North Sea setup. The ensemble approach permits the examination of the internal variability of the climate system by varying the initial states across the 30 ensemble members. However, it does not account for MSL rise, which is therefore incorporated here using probabilistic estimates along with the forcing data (Palmer et al., 2018 & Palmer et al., 2020).

4.2.2. SCHISM model and sub-modules

The hydrodynamic impact of seagrass then is evaluated through numerical simulations using SCHISM (Zhang et al., 2016; Zhang et al., 2020). This model employs the Reynolds-averaged Navier-Stokes equations, utilizing unstructured grids, with the hydrostatic and Boussinesq approximations. The Eulerian-Lagrangian Method (ELM) facilitates enhanced momentum advection, while the salinity and heat transfer equations are solved with a second-order total variation diminishing (TVD) approach.

The SCHISM model was integrated with the wind wave model WWMIII (Roland et al., 2012) and the sediment transport model SED3D. SED3D is an adaptation of the Community Sediment Transport Model (Warner et al., 2008), which has been further documented by Pinto et al., 2012. The turbulence model accounts for

sediment-induced stratification, which is essential for accurately simulating hydrodynamics and sediment dynamics in highly turbid environments. The sediments are divided into classes, each of which is defined by specific parameters, including grain size, density, settling velocity, erosion rate, and critical shear stress for erosion. The model differentiates between cohesive and non-cohesive sediments and calculates erosion, deposition, bedload transport, and suspended sediment transport across eight sediment classes with median grain sizes (d50) ranging from 0.06 mm to 2.0 mm.

In addition to the wave and sediment model, the study also incorporated vegetation in some experiments. The impact of seagrass is accounted for by introducing an additional drag term in the Reynolds-averaged Navier-Stokes equations, along with an extra source term for turbulent kinetic energy and mixing length, as detailed by Zhang et al., 2020. (See Jacob et al., 2023 for more information).

4.2.3. Experiments

The study comprises a series of simulations conducted for both historical (1999-2002) and future (2090-2092) periods, focusing on different forcings (r212-median, r217-lower, and r219-upper) with respect to the variability of atmospheric forcing under the RCP8.5 scenario median of regionalised global MSL rise (Table 4-1). Each period includes two sets: one with vegetation and one as a reference without vegetation. This setup allows for a comprehensive assessment of how different forcing conditions and the presence of seagrass influence hydrodynamic and sediment transport. The experiments aim to provide insights into the role of seagrass as a natural adaptation strategy across varying climatic conditions.

Due to the high computational costs and limitations of running the German Bight setup for multiple years, the experiment was limited to a comparison between historic and future conditions in 2090, based on the ensemble median RCP scenario (r212) presented in D 2.2 (adding further analysis within 2.3). In contrast, the Jade Bay setup includes multi-annual, multi-ensemble member simulations, as outlined in Table 4-1. For the German Bight the seagrass restoration is realized as a maximally upscaled seagrass restoration filling the entire inter-tidal area within the Wadden Sea, while for the Jade Bay vegetation is introduced in the intertidal Jade Bay for the area highlighted in Figure 4-2(right): The location of the seagrass in this restoration scenario was based on observations, and previous measurements campaigns, where we identified potential areas where seagrass had previously grown and simulated different scenarios, placing the seagrass in various locations, to assess its potential as a NbS (see Dolch, et al., 2017).

Table 4-1 Simulation overview for Historical (1999-2002) and Future (2090-2092) periods for the different scenarios, with the reference scenario without seagrass (ref) and the vegetation one with seagrass (veg)

Period	Forcing	Scenario
Historical	212-median	historical-median-ref/veg
	217-lower	historical-lower-ref/veg
	219-upper	historical-lower-ref/veg
Future	212-median	future-median-ref/veg
	217-lower	future-low-ref/veg
	219-upper	future-upper-ref/veg

4.2.4. Habitat Postprocessing via the D-Eco Impact tool

The model simulations are classified using the European Nature Information System (EUNIS), which categorizes habitats based on species composition, abiotic conditions, and geographic location utilizing habitat codes (Olenin et al.,2006; Baptist et al.,2019, see also Deliverable 4.1 Table 5). The methodology was detailed in Deliverable 4.1, that further introduced a scoring system for ecosystem services and biodiversity indicators, assigning each habitat an ESS score for functions like Food Provisioning (FP), Carbon Sequestration

Table 4-2 Overview of ESS measures quantified from model output

ESS	Model parameter	Indicator system specific
Reduction coastal erosion	Erosion volumes	Annual mean erosion volume (flux) / bottom stress for a user-defined area
	Vegetation/biotope cover on foreshore	Area (in m2) per EUNIS ecotope in a user-defined area at the end of a time horizon
Reduction flood risk	Water levels during extreme/storm conditions	mean during storm
	Waves during extreme/storm conditions	mean during storm

(CCR), Water Quality Regulation (WP), Natural Hazard Regulation (RFR), and Coastal Erosion Prevention (RCE).

The EUNIS classification is applied to the SCHISM model output through D-Eco Impact, an impact assessment tool that supports the creation of resilient, healthy water systems for both people and nature (Weeber et al., 2024). This tool enables scenario analysis, habitat suitability studies, and explores the relationship between abiotic conditions and species composition. It operates using user-defined knowledge rules, such as EUNIS-defined abiotic ranges, specified in YAML configuration files.

4.2.5. Direct Quantification of ESS

-For the present deliverable report D.2.3, the focus is on risk reduction related to flooding and erosion. As part of the risk projection strategy, the evaluated measures for NbS are explored under the aforementioned (2.3) environmental and climatic conditions quantifying the ESS FP and RCE based on statistical measures for the model output according to Table 4-2.

4.3. Results

4.3.1. Validation

In D 2.2, the German Bight model was shown to be an effective means of replicating the observed water and wave levels. Likewise, the Jade Bay model here shows close agreement with the observations, for the tide gauges located in the model domain, giving a mean standard deviation about 1.03 a mean correlation of 0.9, and a relatively low mean RMSE of 0.3 m meaning there is a good consistency between simulated tidal maximums and minimums and the observed ones (Figure 4-2).

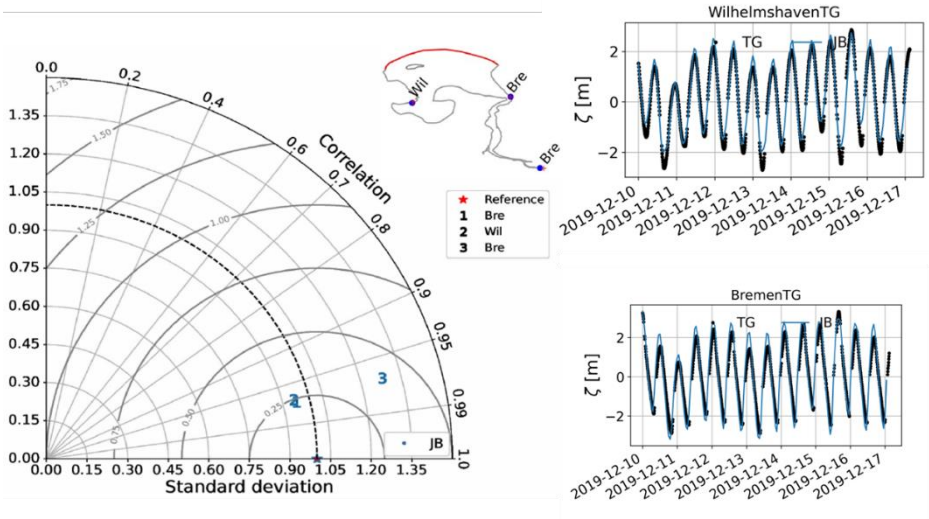

Figure 4-2 Taylor diagram with map of the 3 TG stations used for the validation (Left) and Time series comparison for the stations Bremen and Wilhelmshaven (right)

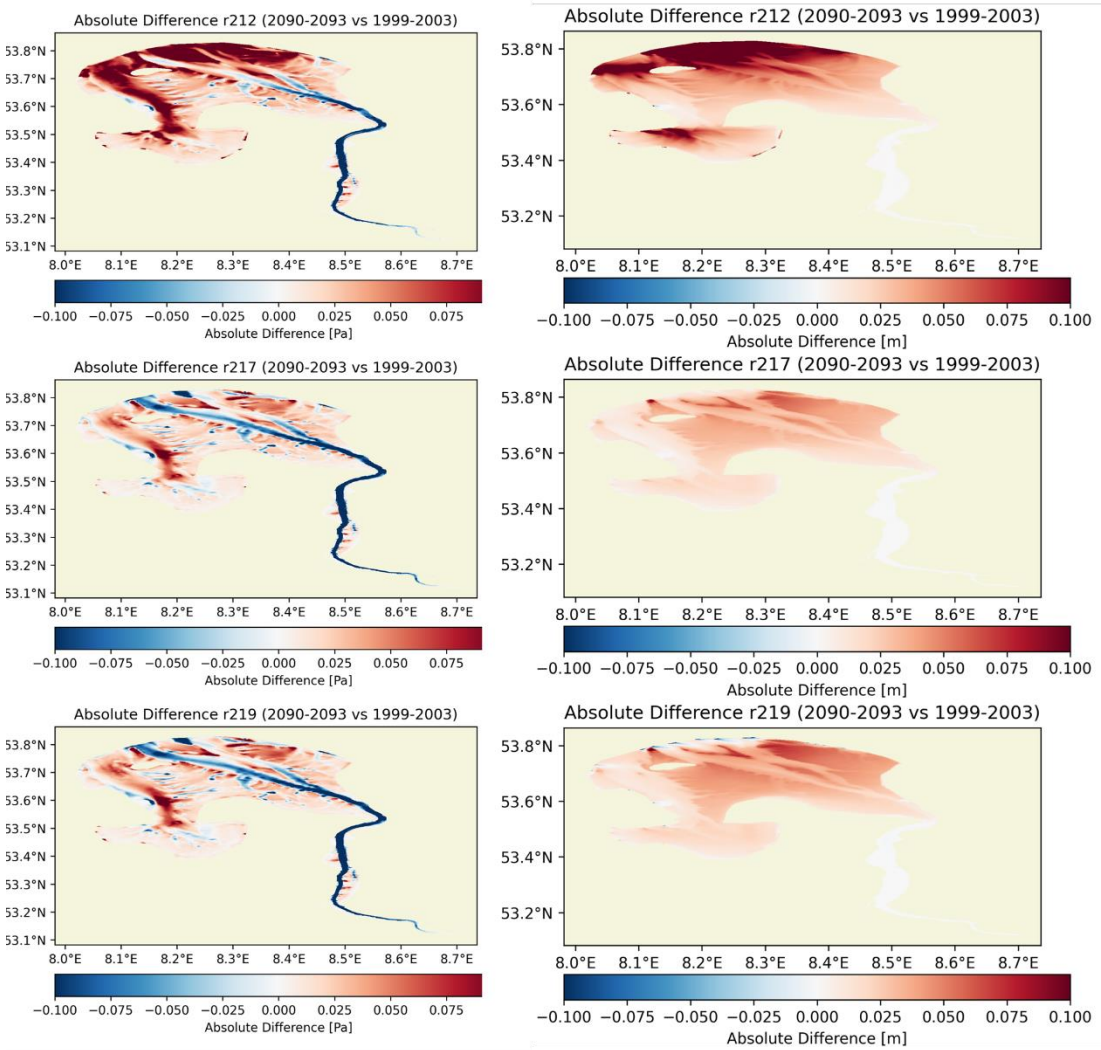

Figure 4-3 Change in multi annual average of Left side: bed Stress; Right side: significant wave height (Hs)

4.3.2. Effect of Sea level rise

-To assess the impact of future sea level rise on the hydrodynamics of the region, a series of numerical simulations were conducted, comparing the projected future period (2090-2093) against the historical baseline (1999-2003) for the various forcing scenarios. Figure 4-3 indicates that regions depicted in red will be at an elevated risk of erosion due to rising sea levels. The enhanced currents and elevated bed stress in these regions will likely mobilize a greater volume of sediment, potentially resulting in coastal retreat and alterations in seabed morphology. The r212 scenario indicates that moderate future changes are likely to occur, with localized increases in velocity, bed stress, and significant wave height (Hs). These interrelated factors suggest that while some areas will experience stronger currents, more energetic waves, and increased erosion, other areas may stabilize or accumulate sediment as a result of reduced bed stress and lower velocities.

In contrast, the r219 scenario highlights the most extreme future changes, with extensive areas of increased velocity, bed stress, and significant wave height. The significant future increases in these areas underscore their increased vulnerability to erosion and other dynamic coastal processes. The stronger currents, combined with higher bed stress and more intense wave conditions, suggest that sediment mobilization and coastal erosion will be particularly severe under this scenario, resulting in significant shoreline reshaping.

4.3.3. Effect of restoration in combination with sea-level rise

Initial exploration on the effect of SLR was started in D.2.2 utilizing the GB model, for end of the century simulations (2.2), exploring the ensemble median SLR for the 2090 ensemble projection under the ensemble median atmospheric variability. This overall demonstrated that for the same seagrass restoration scenarios, the overall efficiency of kinematic reduction is reduced and in particular the extended effect of how the flats affect the adjacent channels is reduced. Nevertheless, it remains an effective solution, especially in terms of reducing bottom stress and sediment mobilization.

The different percentiles of atmospheric variability affecting the future climate model were explored via the Jade Bay model. The following analysis examines the impact of sea level rise and the potential role of seagrass restoration in mitigating its effects on coastal dynamics. It considers bed stress, erosion flux, significant wave height, and depth-averaged velocity under the r212-median scenario (Figure 4-4).

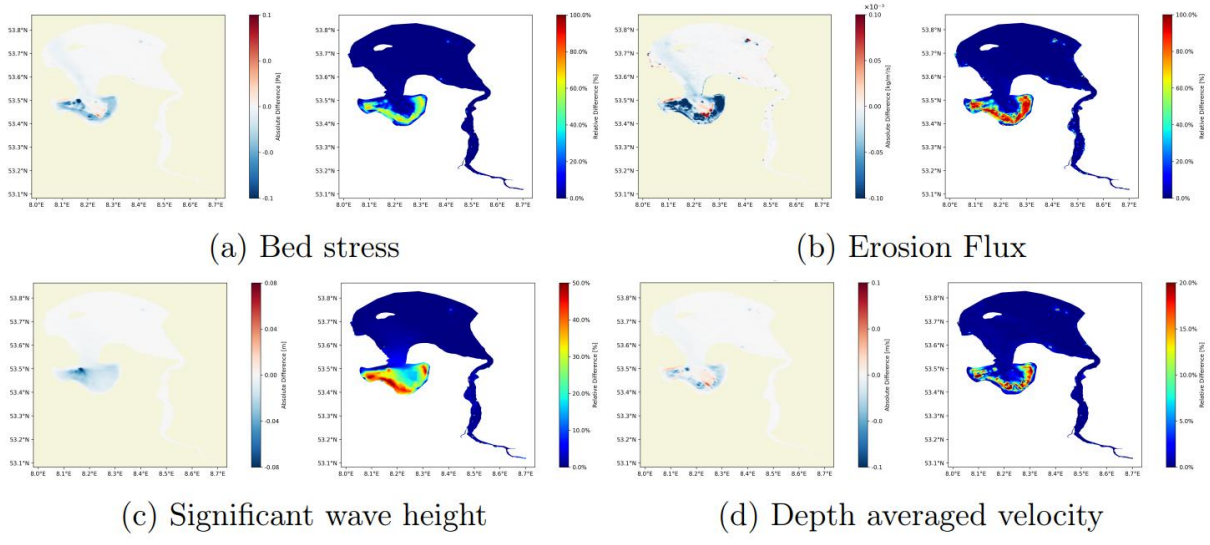

Figure 4-4 Restoration for 212-median scenario; (a) Bed Stress; (b) Erosion Flux; (c) Significant Wave Height; (d) Depth-Averaged Velocity

The analysis illustrates that seagrass restoration represents a key strategy for mitigating the adverse impacts of sea level rise on coastal dynamics. By reducing bed stress by 45%, erosion flux by 80%, significant wave height by 50%, and depth-averaged velocity by 20%, seagrass provides a natural buffer that helps to protect the coastline from the increased risks posed by rising sea levels. Seagrass plays an instrumental role in stabilizing sediments, reducing the energy of waves and currents, and mitigating the forces that contribute to erosion. This stabilizing effect is of great consequence in the preservation of coastal integrity, particularly in light of the rising sea levels and the concomitant increase in the frequency and intensity of storm events.

4.3.4. Risk Analysis

To provide a comprehensive spatial assessment of seagrass effectiveness under storm-induced stress conditions, erosion risk maps were generated for the two periods, the preceding and during the storm. These maps categorize erosion risk from No-risk (green) to High-risk (red), allowing for a visual comparison of erosion risk before and during the storm (Figure 4-5). The storm, which occurred from September 17-22, 2090 (days 263-265), was identified within the future climate projections by analyzing the wind speed in the region. The period before the storm occurred from September 15-17, 2090 (days 260-263).

The erosion risk is quantified by comparing the bottom shear stress to the critical shear stress necessary for sediment mobilization. Initially, a spatially distributed mean critical shear stress is computed for each node in the model domain, considering the characteristics of the sediment types present at those nodes. This mean

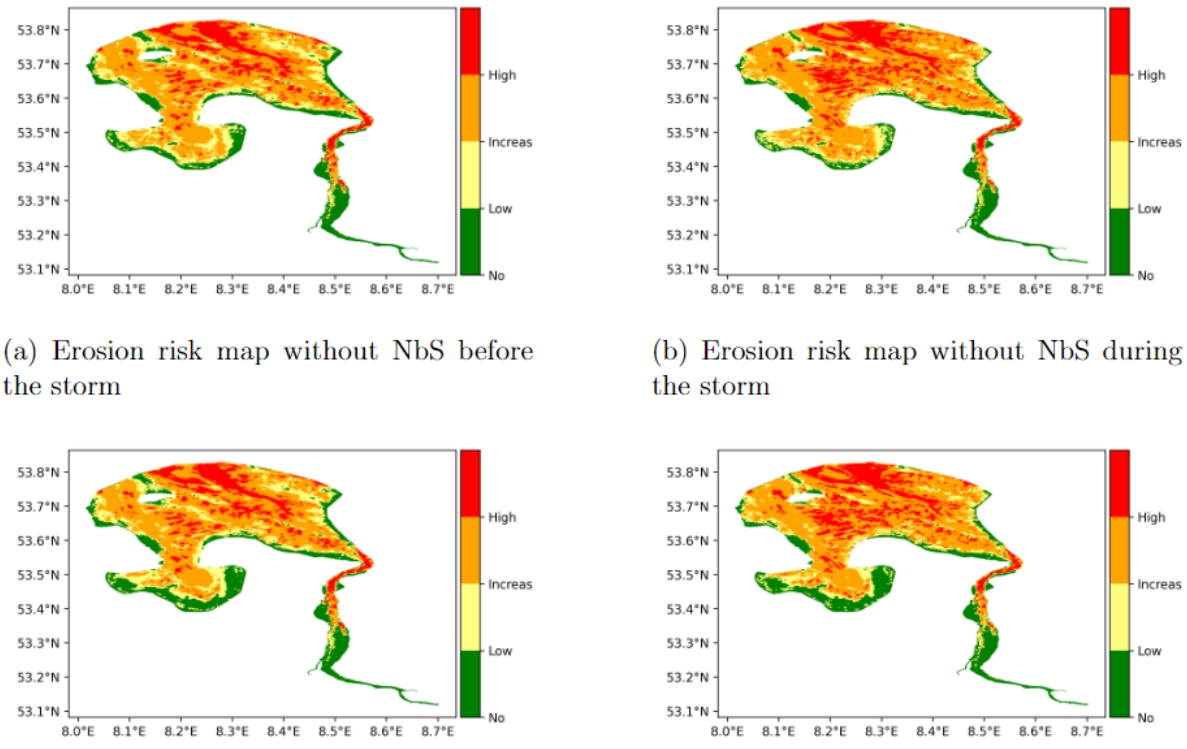

(a) Erosion risk map without NbS before the storm

(b) Erosion risk map without NbS during the storm

(c) Erosion risk map with NbS before the storm

(d) Erosion risk map with NbS during the storm

Figure 4-5 Erosion risk maps from No-risk (green) to High-risk (red) for two different periods: before the storm for (a) and (c) and during the storm for (b) and (d); (a) and (b) represent the maps without Nature based Solutions (NbS); (c) and (d) include the NbS

value represents the average stress required to mobilize the sediments at each node, based on their composition.

This approach allows the model to assess erosion risk accurately by incorporating the specific sediment characteristics at each location. We calculate an exceeding factor to quantify the erosion risk by dividing the modeled bottom shear stress by the mean critical shear stress. A value greater than 1 in this ratio indicates that the actual shear stress is sufficient to cause erosion potentially. This exceeding factor is computed for scenarios with and without vegetation, allowing for comparing erosion risks and illustrating the protective effects of vegetation cover. The frequency of exceeding events is then statistically analyzed by calculating the proportion of time steps where the critical shear stress is exceeded. This provides a measure to assess and visually compare erosion risk across the model domain.

Figure 4-5a and Figure 4-5b show the erosion risk maps without the restoration. The risk maps before the storm indicate the existence of extensive Increased-risk to High-risk areas along the coastlines, thereby suggesting an elevated level of vulnerability. During the storm, these Increased-risk zones intensified to High-risk zones.

--For the maps with the restoration, a notable reduction in Increased-risk to High-risk zones is observed before the storm, particularly in the central and southern sections close to the bay (see Figure 4-5c). This reduction suggests that the seagrass plays a role in stabilizing sediment, which may result in less sediment mobilization in the absence of a storm. During the storm, however, the Increased-risk to High-risk areas expanded (see Figure 4-5d). This indicates that while the seagrass helps distribute the stress more evenly across the region, its protective effect is challenged by the storm's intensity. Nevertheless, the seagrass within the bay continues to serve as an effective buffer and dissipater of storm energy, thereby providing localized protection.

4.3.5. Ecotope maps

Ecotope maps had been created applying D-Eco Impact to the scenario simulations conducted with the German Bight and Jade Bay models, identifying habitats according to Table 4-3. The potential salt marsh area is displayed in the green tones, while the infra and circalittoral areas are colour coded in blue, and the mud areas in reddish-brown colours (Figure 4-6 and Figure 4-8).

The habitat maps produced by the model generally exhibit a good correspondence with the observation- and survey-based maps provided in D 4.1. Sub-littoral and coastal salt marsh areas, such as those in Jade Bay, align reasonably well with D 4.1 Fig. 8. Muddy littoral habitats (MA6) are also present in the SCHISM D-Eco Impact post-processed output, though they appear slightly reduced in extent and are shifted towards a more saline environment. The interpolated background maps of grain sizes in the model seem too coarse, resulting in a shift toward a coarser sediment classification resulting in MA32 where the sandy MA52 was expected based on observations.

Projections of future sea level scenarios suggest an expansion of infralittoral and circalittoral zones, extending from the tidal channel network and transitioning to deeper littoral types (Figure 4-6 and Figure 4-8). In the nearshore zone, there is a projected loss of valuable potential salt marsh areas (Table 4-3) as these zones are pushed back by an expanding littoral area and the associated increase in flooding frequency. Introducing small seagrass meadow areas does not much alter the outcome of the habitat maps, thus they are omitted in the Jade Bay experiments. Applying the ESS scoring approach (4.2.3, Table 4-3) initially developed under D.41 for the different habitats, it becomes evident that the SLR-induced habitat shift results in a decrease across all ESS (Figure 4-7 d, Figure 4-8f), except for food provisioning which enhances as the increasing littoral areas provide suitable fish grounds and benthic habitats, and the expanded infra- and circa-

littoral sand areas score higher for this particular ESS compared to the lost littoral mud areas. The Carbon Sequestration score remains relatively unchanged, with a minor increase (Jade Bay) or decrease (Waden Sea) depending on the total area considered. The largest relative change occurred with respect to the Natural Hazard Regulation (12-14 %) and Coastal Erosion Prevention (~ 30 %) scores, which is a direct consequence of the marsh land loss, which is the top provider of these ESS and the reason why we apply coastal vegetation as NbS (in our case seagrass).

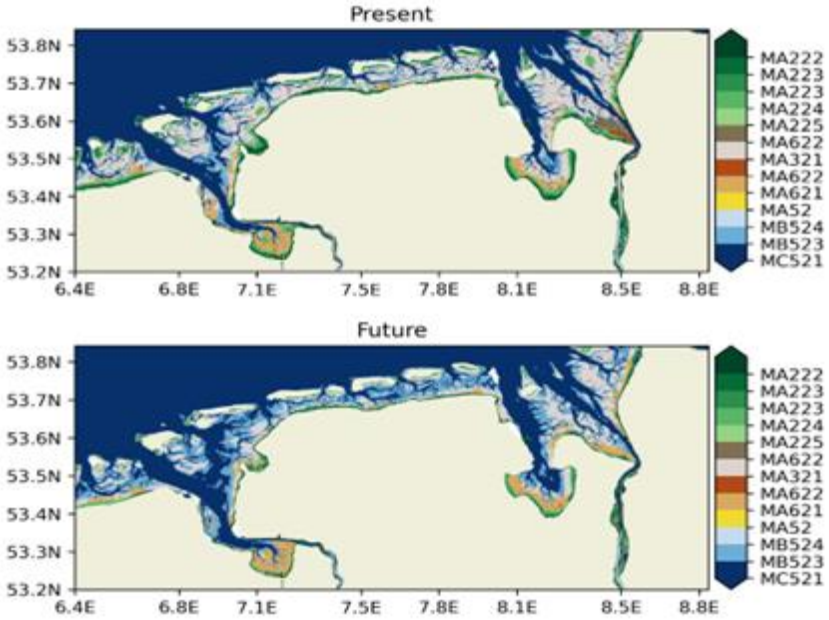

Figure 4-6 EUNIS map of the Wadden Sea are for present and future sea level

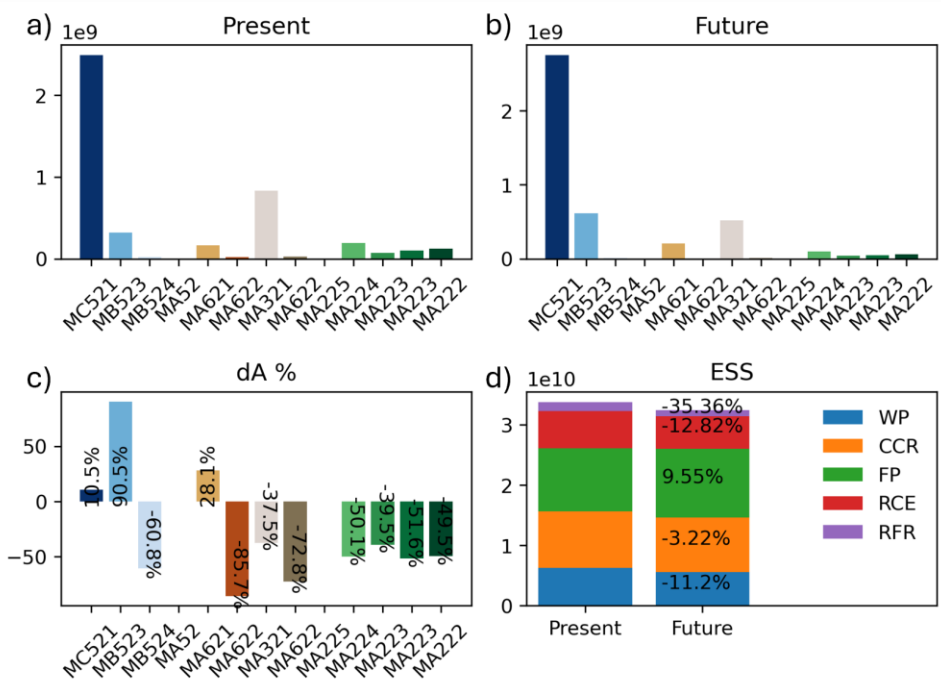

Figure 4-7 Area (m²) by habitat under present day and end of the century sea levels (a, b), relative changes due to SLR (c) for EUNIS map of the Wadden Sea displayed in 4-5. d) shows the area multiplied habitat scores according to Table 4-1, the %-numbers indicate the percentage change with respect to the default area in the vegetation less 1997 reference scenario

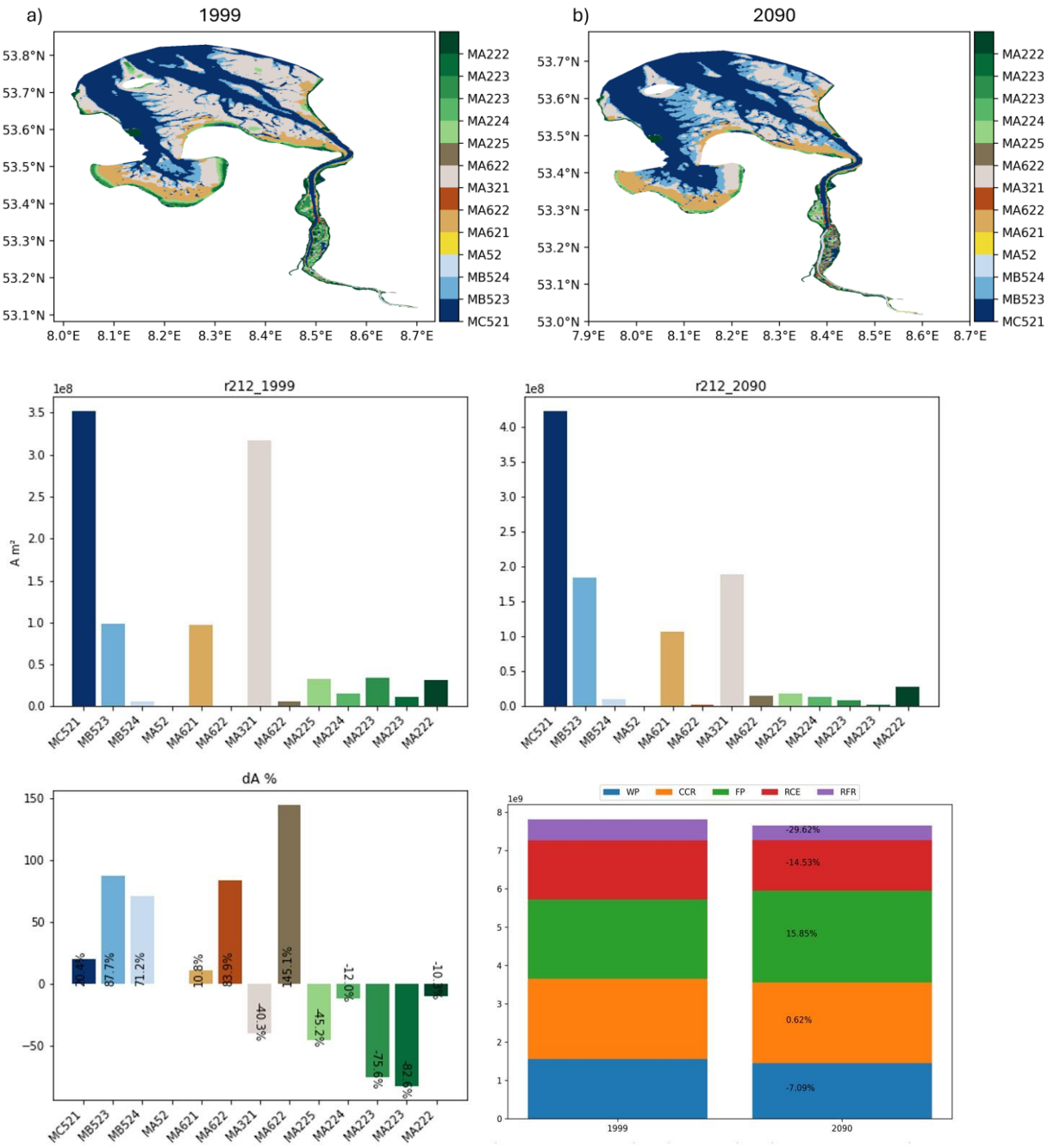

Figure 4-8 EUNIS map of the Jade Bay for the median scenario for both a) historical and b) future. Area (m²) by habitat in the different scenarios (c,d) and e) relative changes due to SLR (row-wise differences). j) shows the area multiplied habitat scores according to Table 4-3, the %-numbers indicate the percentage change with respect to the default area in 1999

Table 4-3 EUNIS habitat overview and ESS scores applying the Ems Dollart scale (D4.4) for the Wadden Sea. Habitat scores are indicated for Food provisioning (FP), Carbon Sequestration (CCR), Water Quality Regulation (WP), Natural Hazard Regulation (RFR), and Coastal Erosion Prevention (RCE). The table was enhanced by the MA32 entry.

Code	EUNIS Name	WP	CCR	FP	RCE	RFR	SUM
MA22	*Atlantic littoral biogenic habitat*	2	2	3	2	1	10
MA222	*High marsh*	4	5	1	3	1	14
MA223	*Brackish marsh*	4	5	1	3	1	14
MA224	*Atlantic mid-low saltmarshes*	4	4	2	3	1	14
MA225	*Atlantic pioneer saltmarshes*	3	3	2	2	1	11
MA52	*Atlantic littoral sand*	2	2	1	1	1	7
MA523	*Barren or amphipod-dominated Atlantic littoral sand*	2	2	1	1	1	7
MA525	*Polychaete/bivalve-dominated Atlantic littoral muddy sand*	2	2	1	1	1	7
MA621	*Faunal communities of full salinity Atlantic littoral mud*	3	3	2	1	1	10
MA622	*Faunal communities of variable salinity Atlantic littoral mud*	3	3	2	1	1	10
MB12	*Atlantic infralittoral rock*	0	0	4	3	2	9
MB52	*Atlantic infralittoral sand*	1	2	3	1	0	7
MC52	*Atlantic circalittoral sand*	1	2	3	1	0	7
	Dikes	0	0	0	5	5	10
MA32	*Atlantic littoral coarse sediment*	1	1	1	2	1	6

4.4. Discussion

We explored the potential of seagrass for mitigating flooding and erosion under both historical and end-of-century climate projections. In response to sea level rise (SLR), significant changes were observed in bed stress and significant wave height (Hs). The increased water column height reduces friction, diminishing wave attenuation and breaking in the back-barrier Wadden Sea and Bays. Consequently, the average wave height increases across the area, contributing to an elevated risk of flooding and overtopping, compounded by the higher sea levels.

The increased water volume alters the tidal prism and reduces friction, potentially strengthening tidal currents and affecting the entire amphidromic system. Leading to enhanced bottom shear stresses, especially in shallow areas and the Jade Channel. However, the Weser River and channel experience reduced bottom

friction, likely contributed by decreased river discharge in the future projection and, more importantly, due to complex changes in tidal resonance and river volume, which need further study.

Statistical analysis of physical fields and erosion risk during storms under SLR conditions confirmed our earlier findings: seagrass effectively dissipates local ocean energy, but its impact is spatially limited. Restoration primarily protects the directly restored areas and, to some extent, adjacent coastal zones shielded by larger seagrass meadows. Even under elevated sea levels, seagrass maintained its capacity to attenuate coastal erosion, reducing local erosion rates by up to 80%. However, its overall efficiency is reduced compared to present-day conditions.

The habitat maps for the present day, generated from the model output, largely align with observation-based maps. Deviations, such as a shift towards more saline mud areas, suggest limitations related to model sensitivities, like river runoff. Part of the Wadden Sea area being attributed with more coarse sediment compared to the survey-based habitat might denote a need for higher-resolution grain size distribution data. For the overlapping scenario the German Bight and Jade Bay models resulted in comparable habitat maps. Future climate scenario maps plausibly indicate an expansion of sublittoral habitats and a narrowing of salt marshes, as rising sea levels and amplified tides increase littoral areas. As a result, habitats with the highest overall ecological scores (Table 4-3), particularly those with strong erosion protection and Natural Hazard Regulation capacities (i.e. the saltmarshes), are diminished.

Based on this background, seagrass restoration scenarios, which demonstrated effective erosion protection in direct simulation assessments, could help compensate for some lost salt marsh functions in these areas. Additionally, seagrass restoration may indirectly support Wadden Sea growth by accumulating sediment, potentially reducing salt marsh loss. However, our calculations are based on morphostatic time slices, of reduced temporal extent (1-3 years) each in the present and in the future, rather than a continuous simulation until the end of the century. Simulating long-term bathymetric changes would be computationally too expensive and likely inaccurate. Thus, we only model without sediment changes for these limited intervals. Therefore, while we have an implicit indication of positive impacts of seagrass NbS on salt marsh conservation, further research is needed to obtain numerically quantifiable results.

4.5. References

Baptist, M. J., van der Wal, J. T., Folmer, E. O., Gräwe, U., & Elschot, K. (2019). An ecotope map of the trilateral Wadden Sea. Journal of Sea Research, 152, 101761. https://doi.org/10.1016/j.seares.2019.05.003

Church, J. A., Clark, P. U., Cazenave, A., Gregory, J. M., Jevrejeva, S., Levermann, A., Merrifield, M. A., Milne, G. A., Nerem, R. S., Nunn, P. D., & others. (2013). Sea level change. PM Cambridge University Press.

Dolch, T., Folmer, E. O., Frederiksen, M. S., Herlyn, M., van Katwijk, M. M., Kolbe, K., Westerbeek, E. P. (2017). Seagrass. In The Wadden Sea Quality Status Report

Golledge, N. R. (2020). Long-term projections of sea-level rise from ice sheets. Wiley Interdisciplinary Reviews: Climate Change, 11(2), e634. https://doi.org/10.1002/wcc.634

Hausfather, Z., & Peters, G. P. (2020). Emissions—the 'business as usual' story is misleading. Nature Publishing Group.

Jacob, B., Dolch, T., Wurpts, A., & Staneva, J. (2023). Evaluation of seagrass as a nature-based solution for coastal protection in the German Wadden Sea. Ocean Dynamics, 73(11), 699-727. https://doi.org/10.1007/s10236-023-01577-5

Masson-Delmotte, V. P., Zhai, P., Pirani, S. L., Connors, C., Péan, S., Berger, N., Caud, Y., Chen, L., Goldfarb, M. I., & Scheel Monteiro, P. M. (2021). Summary for policymakers. In Climate change 2021: The physical science basis. Contribution of working group I to the sixth assessment report of the

intergovernmental panel on climate change. Cambridge University Press, Cambridge, United Kingdom and New York, NY, USA.

Mathis, M., & Mikolajewicz, U. (2020). The impact of meltwater discharge from the Greenland ice sheet on the Atlantic nutrient supply to the northwest European shelf. Ocean Science, 16(1), 167-193. https://doi.org/10.5194/os-16-167-2020

Mayer, B., Mathis, M., Mikolajewicz, U., & Pohlmann, T. (2022). RCP8.5-projected changes in German Bight storm surge characteristics from regionalized ensemble simulations for the end of the twenty-first century. Frontiers in Climate, 4, 992119. https://doi.org/10.3389/fclim.2022.992119

Mikolajewicz, U., Sein, D. V., Jacob, D., Königk, T., Podzun, R., & Semmler, T. (2005). Simulating Arctic sea ice variability with a coupled regional atmosphere-ocean-sea ice model. Meteorologische Zeitschrift, 14(6), 793-800. https://doi.org/10.1127/0941-2948/2005/0083

Olenin, S., & Ducrotoy, J.-P. (2006). The concept of biotope in marine ecology and coastal management. Marine Pollution Bulletin, 53(1-4), 20-29. https://doi.org/10.1016/j.marpolbul.2006.01.003

Palmer, M. D., Gregory, J. M., Bagge, M., Calvert, D., Hagedoorn, J. M., Howard, T., Klemann, V., Lowe, J. A., Roberts, C. D., Slangen, A. B. A., & Spada, G. (2020). Exploring the drivers of global and local sea-level change over the 21st century and beyond. Earth's Future, 8(9), e2019EF001413. https://doi.org/10.1029/2019EF001413

Palmer, M. D., Howard, T., Tinker, J., Lowe, J., Bricheno, L., Calvert, D., Edwards, T., Gregory, J., Harris, G., Krijnen, J., Pickering, M., Roberts, C., & Wolf, J. (2018). UKCP18 marine report. Met Office Hadley Centre.

Pein, J., Staneva, J., Mayer, B., Palmer, M. D., & Schrum, C. (2023). A framework for estuarine future sea-level scenarios: Response of the industrialized Elbe estuary to projected mean sea level rise and internal variability. Frontiers in Marine Science, 10, 1102485. https://doi.org/10.3389/fmars.2023.1102485

Pinto, L., Fortunato, A. B., Zhang, Y., Oliveira, A., & Sancho, F. E. P. (2012). Development and validation of a three-dimensional morphodynamic modelling system for non-cohesive sediments. Ocean Modelling, 57-58, 1-14. https://doi.org/10.1016/j.ocemod.2012.08.005

Roland, A., Zhang, Y. J., Wang, H. V., Meng, Y., Teng, Y.-C., Maderich, V., Brovchenko, I., Dutour-Sikiric, M., & Zanke, U. (2012). A fully coupled 3D wave-current interaction model on unstructured grids. Journal of Geophysical Research: Oceans, 117(C11). https://doi.org/10.1029/2012JC007952

UNEP. (2017). Frontiers 2017: Emerging issues of environmental concern. United Nations Environment Programme, Nairobi.

UNESCO. (2009). Wadden Sea. Retrieved January 31, 2024, from http://whc.unesco.org/en/list/1314/.

van Katwijk, M. M., van Beusekom, J. E., Folmer, E. O., Kolbe, K., de Jong, D. J., & Dolch, T. (2024). Seagrass recovery trajectories and recovery potential in relation to nutrient reduction. *Journal of Applied Ecology*.

Warner, J. C., Sherwood, C. R., Signell, R. P., Harris, C. K., & Arango, H. G. (2008). Development of a three-dimensional, regional, coupled wave, current, and sediment-transport model. Computers & Geosciences, 34(10), 1284-1306. https://doi.org/10.1016/j.cageo.2008.02.012

Weeber, M., Elzinga, H., Schoonveld, W., Van de Vries, C., Klapwijk, M., Mischa, I., Rodriguez Aguilera, D., Farrag, M., Ye, Q., Markus, A., Van Oorschot, M., & Saager, P. (2024). D-Eco Impact (v0.3.0) Zenodo. https://doi.org/10.5281/zenodo.10941913 (Downloaded: August 27, 2024)

Zhang, Y. J., Gerdts, N., Ateljevich, E., & Nam, K. (2020). Simulating vegetation effects on flows in 3D using an unstructured grid model: Model development and validation. Ocean Dynamics, 70, 213-230. https://doi.org/10.1007/s10236-019-01333-8

Zhang, Y. J., Ye, F., Stanev, E. V., & Grashorn, S. (2016). Seamless cross-scale modeling with SCHISM. Ocean Modelling, 102, 64-81. https://doi.org/10.1016/j.ocemod.2016.05.002

5. Potential application of saltmarsh as a Nature-Based Solution (NbS) for coastal protection

Dissanayake, P.[1], Oberrecht, D.[1] & Wurpts, A.[1]

[1] *State of Lower Saxony Agency of Water Management, Coastal Defence and Nature Conservation, Jahnstrasse 1, 26506 Norden, Germany.*

ABSTRACT: The Wadden Sea area has a rich biodiversity and a high socio-economic value, providing numerous benefits for the local communities. These functionalities however mainly depend on the interaction between the Wadden Sea and the marine forcing, which is expected to aggravate in the future. Nature-Based-Solutions (NbS) are increasingly adapted for the sustainable use of this system. Application of saltmarsh as NbS for coastal protection was investigated using numerical experiments (Delft3D/SWAN) based on the Ley Bay in the east Frisian Wadden Sea. The focused ecosystem-services (ESS) are expected to improve by mitigating hydrodynamics and increasing sedimentation. The constant sea level rise (SLR) scenarios indicated that there is a non-linearity in how water level, wave height and velocity in the Ley Bay area are affected, with the highest SLR (MSL+0.78 m) showing the largest impacts. In the SLR from 2090 to 2100, the NbS application caused sedimentation indicating that the saltmarsh decreases the risk of erosion and enhances ESS. Implementing wave dissipation by saltmarsh in the Delft3D-WAVE resulted in about two order of magnitudes higher dissipation by vegetation than bottom friction and breaking and decrease the susceptibility of the wave attack at the dyke front. Mitigation of wave heights and velocities are about 60% and 80% respectively in the saltmarsh area. Water quality improves due to a significant decrease in sediment concentration. Almost no erosion occurred with the NbS and sediment import into the saltmarsh area was achieved. Therefore, the selected NbS can be used as an effective tool for coastal protection in response to SLR by mitigating adverse impacts and enhancing ESS.

5.1. Introduction

5.1.1. Coastal vulnerability

The Wadden Sea area has a rich biodiversity and a high socio-economic value, and therefore is a unique dynamic environment providing numerous benefits for the local communities. Due to these functionalities, this area has been declared a UNESCO World Heritage site and embedded in a number of EU Directives (www.waddensea-worldheritage.org). The Wadden Sea is however continuously shaped by the marine forcing exerted in different spatiotemporal scales (Dissanayake et al., 2012).

The existence of this system and its functionalities mainly depend on the dynamics resulting from the interaction among the marine forcing, land drain and the exposure of the bed topography. The marine forcing, like wave climate, nowadays occurs in clustered-pattern (Dissanayake et al., 2015) and also with high severity (e.g., storm *Xaver* with a return level of 125 years, see previous report D 2.2) causing strong velocities resulting into significant physical impacts of the system (e.g., erosion at the supratidal area, hinterland flooding). These forcing are expected to be aggravated due to future sea level rise (SLR) and climate change scenarios, which will certainly worsen the impacts. The land drain is expected to increase during events (i.e., intensity and duration) in the future, though the total precipitation decreases (Trenberth, 2011). The exposure of the bed topography (e.g., availability of saltmarsh, seagrass, and mussel beds) has a large contribution to damping incoming waves, and thus velocities mitigating the coastal vulnerability and enhancing the systems behaviour (Bouteiller and Venditti, 2015; De Oude, 2010).

For example, the tidal basin between Borkum and Juist barrier islands (East-Frisian Wadden Sea – Germany) indicates the importance of the salt marsh existence in damping velocities (Figure 5-1). Saltmarsh is populated at (A) in the Ley Bay area, whereas (B) has a bare bottom. Our sensitivity analyses using different wind approaches always resulted in higher velocities at (B) than (A). Within the REST-COAST project, NLWKN investigates to understand these situations quantitatively, which can support the coastal managers to restore or implement saltmarsh areas to decrease the coastal vulnerability and increase coastal protection.

5.1.2. Restoration efforts

Under the framework of REST-COAST, NLWKN has no direct engagement in any application of restoration efforts. We perform numerical experiments under different scenarios to quantitatively understand the system response to the saltmarsh presence. Such information is very relevant to identify preferable conditions and suitable areas for the saltmarsh restoration/implementation, and the importance of saltmarsh in the context of coastal protection.

5.1.3. Scenarios

Sea Level Rise (SLR) is selected as the same scenario as Hereon (Chapter 4) to compare hydrodynamics, sediment transport and morphodynamics between WT – NbS (No Saltmarsh) and NbS (with Saltmarsh) experiments. Application of SLR is twofold: a constant increase of mean sea level by 0.07 m, 0.12 m, 0.26 m and 0.78 m referring to the 50th percentile of the years 2020, 2030, 2050, and 2100 respectively, and the forecasted increase of mean sea level from 2090 to 2100 (Pein et al., 2023). Both these are based on RCP 8.5 (Garner et al., 2021). Each scenario was simulated with WT- NbS and NbS to compare and contrast the saltmarsh effects on the hydrodynamics and the morphological evolution.

5.1.4. Objectives

The main objective of our numerical experiments is to investigate the potential use of saltmarsh as a nature-based-solution (NbS) for coastal protection. The focused Ecosystem Services (ESS) are enhanced by controlling two physical processes, 1) Decrease of hydrodynamics (i.e., wave heights and flow velocities) – decrease turbidity and increase water quality, and 2) Increase of sedimentation (or decrease of erosion) – minimise vulnerability to the biotic and abiotic systems. Preliminary results were presented in D 2.2, which covers the results of saltmarsh simulations during extreme events, namely *Herwert* and *Xaver* from October 2017 and December 2013 respectively.

Our scientific objective is to quantify the response of hydrodynamics and morphological evolution under the presence of saltmarsh for different rates of SLR in the Ley Bay area. Our hypothesis is that the effectiveness of saltmarsh decreases as the rate of SLR increases.

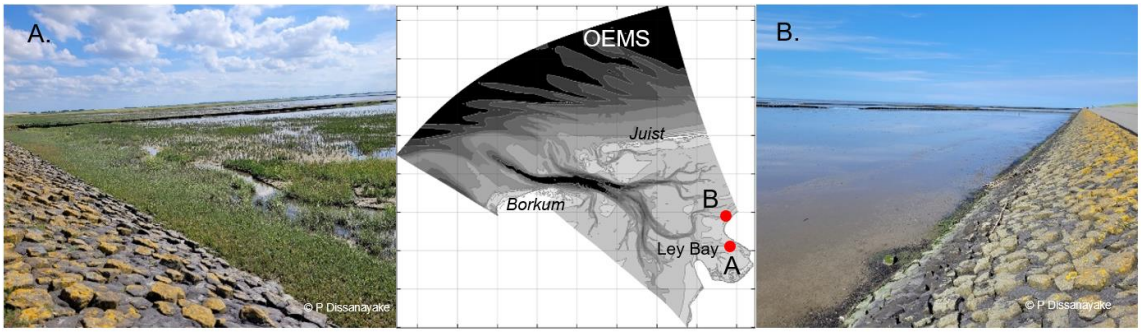

Figure 5-1 Example of Saltmarsh population in the Ley Bay area located behind Borkum and Juist barrier islands; Area with scattered saltmarhses (A) and a bare area without saltmarshes (B). The middle figure indicates the respective locations on the OEMS domain use

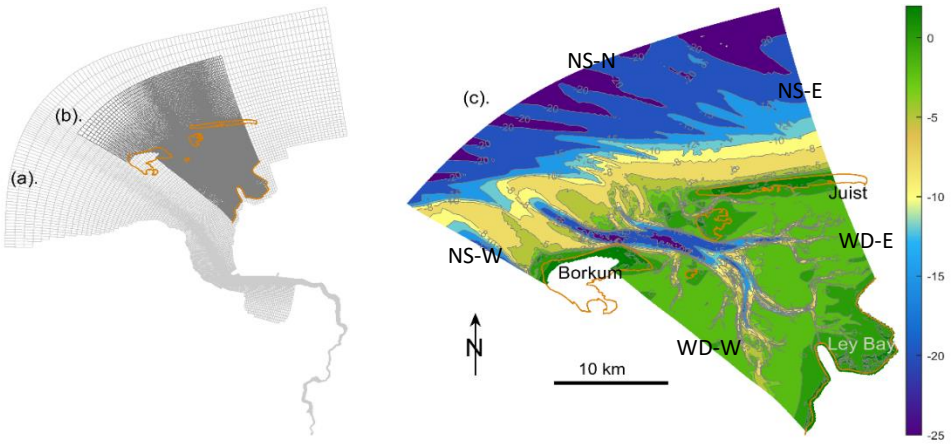

Figure 5-2 EMS-grid (a), OEMS-grid (b) and OEMS-bathymetry (c). For clarity, only every other gird is shown. The orange-line indicates the land boundary, and the investigation area is Ley Bay. Colour bar indicates water dephts with respect to NHN (Normalhöhennull: equivalent to Mean Sea Level - MSL). The OEMS has 5 open boundaries: 2 at Wadden Sea, East (WD-E) and West (WD-W), and 3 at North Sea, East (NS-E), North (NS-N) and West (NS-W).

5.2. Approach

5.2.1. Model setup

Ley Bay is located at the landward end of the tidal basin between Borkum and Juist barrier islands and spans an area of about 5 km x 5 km. A high resolution grid (OEMS: Figure 5-2b) and bathymetry (Figure 5-2c) were developed within the present project to investigate the potential effect of NbS on hydrodynamics and morphological evolution (ESS). The OEMS domain consists of parts from both the North Sea and the Wadden Sea to provide good interactions between the physical processes therein. The calibration and validation of this model are referred to in the D 2.2 report.

Bed sediment composition was implemented using spatial varying six sediment fractions based on the NLWKN measured data covering littoral and eulittoral areas (e.g., grab sampling, sediment cores) (Mascioli et al., 2021). Initially, a quasi-equilibrium sediment distribution of each fraction was established by simulating the model for the sediment distribution without bed level change following the approach of Dissanayake and Wurpts (2013). These sediment maps were then used as the initial bed sediment composition of the model to simulate the scenarios.

The models were simulated in the 2DH-mode (depth-averaged). Therefore, the presence of saltmarsh was implemented using a Trachytope approach (Delft3D, 2023), which has been developed following the formulas by Baptist (2005) to estimate the drag force exerted by submerged and non-submerged plants.

SLR driven boundary conditions for the Ley Bay model (OEMS) were developed using a model consisting of three nested domains. These experiments were separately carried out applying five scenarios of constant increase of mean sea level (0 m, 0.07 m, 0.12 m, 0.26 m and 0.78 m, see section 5.1.3). First, a North Sea scale model (Hartsuiker, 2008), which has astronomical boundary forcing, was simulated by applying SLR as a correction to the mean value of each tidal constituents and forcing with spatiotemporal wind fields from German Weather Service (DWD, 2023). Using the predicted water levels, the EMS-Dollard model (EMS: Oberrecht and Wurpts, 2023) was next simulated to extract the water level and current boundary forcing for the OEMS model (see report D 2.2 for the boundary setup). This approach provides the effect of SLR on the tidal wave propagation in the North Sea, and thus the accurate forcing for the OEMS model, rather constant increase of the mean water level at the boundaries of the OEMS model itself. The simulation period of the OEMS model is two years in which noticeable effects of SLR on hydrodynamics, sediment transport and morphology are expected. For the simulation from 2090 to 2100, the boundary forcing for the EMS model was obtained from the project partner HEREON.

The standard Delft3D modelling suite does not include the effect of saltmarsh on the wave energy dissipation. Therefore, while investigating the scenarios, the Delft3D-WAVE code was extended and tested for the wave dissipation due to saltmarsh. Some investigations presented in D 2.2 were repeated to explore the improvements of the Delft3D-WAVE code.

5.2.2. Schematisation of wave and wind climate

The state-of-the-art long-term morphodynamic simulations are based on morphological acceleration (Roelvink et al., 2006), in which schematisation of forcing is a pre-requisite. Both wave and wind are herein schematised using the long-term measured data.

Long-term wave and wind data are available at the Fino 1 research platform (Location of FINO1), which is located about 20 km North of the EMS-Model domain seaward boundary. These data from 2015 to 2021 were obtained from the Federal Agency for Hydrography and Navigation (www.bsh.de; Fachhochschule Kiel GmbH). All parameters were separately binned in 18 wave directional sectors from 0^o to 360^o and 10 wave height classes from 0 to 9 following the approach of Dissanayake and Wurpts (2013). As the Fino 1 is located about 20 km away from the EMS domain, these schematised conditions were first transformed up to the EMS-Model seaward boundary using Delft3D-WAVE. Then, each wave condition was separately simulated for a period of 1.5 days and the resulting erosion and sedimentation pattern within the last 24 hours was used for a statistical analysis, which determines the contribution of each wave condition for the morphodynamics. Using the respective probability and bed evolution of each wave condition, the overall bed level change was first estimated. An iterative process was then adopted, in which the wave condition with the least contribution to the overall bed level change was removed each iteration. This enables to select a few numbers of conditions based on the statistical values and decreases the computational cost.

To investigate the future forcing effects on the selected NbS and the respective ESSs, the period from 2090 to 2100 was selected based on the predicted wind fields from the ensemble, which demonstrates the fairly similar sea level rise as of the averaged of 3 considered ensemble scenarios (Pein et al., 2023). For the numerical experiments, a representative one-year period was therein selected analysing the forecasted wind data at the OEMS domain (see the approach in Dissanayake et al., 2024) and simulated with a morphological acceleration factor (*mf*) of 10 to generalise the evolution within the 2090 – 2100 period.

5.2.3. Improving modelling code

The standard Delft3D-WAVE does not include the effect of vegetation on wave propagation and dissipation. Therefore, the communication between Delft3D-WAVE and SWAN was improved to facilitate the vegetation effects on waves. For these experiments, an additional high-resolution domain (Grid size ~10 m, VEG) was developed covering the saltmarsh area (Figure 5-3). Nested wave computation runs in the sequence of EMS→OEMS→VEG.

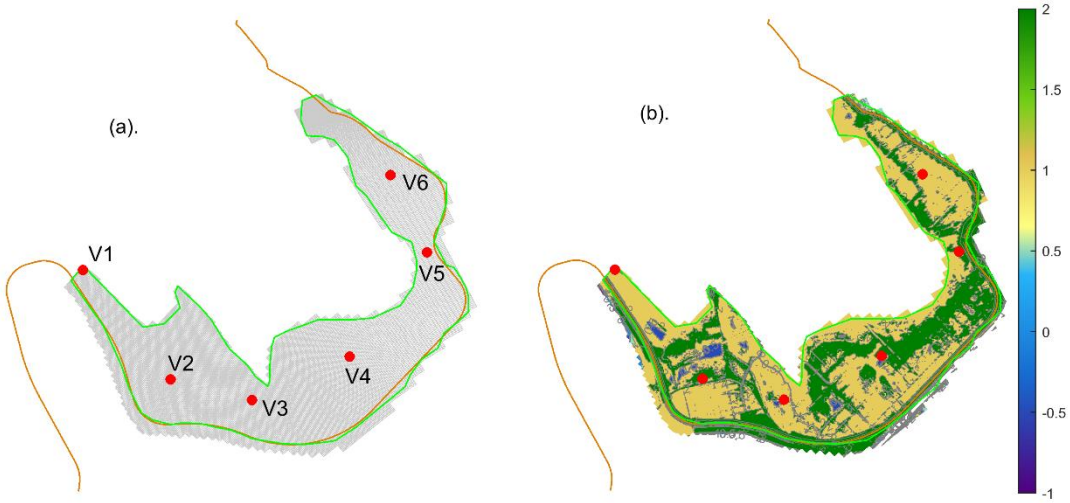

Figure 5-3 Additional high-resolution wave domain (VEG) prepared to simulate saltmarsh effects on waves, (a) grid area and (b) bathymetry covering the saltmarsh area (green-polygon). V1 – V6 indicate monitoring locations in the domain

5.2.4. Numerical experiments

The performed numerical experiments to investigate the effect of NbS and therein ESS are summarised in Table 5-1. Wave boundary was implemented using a nesting approach EMS→OEMS (scenarios 1) and EMS→OEMS→VEG (scenario 2 and 3) consisting of the schematised 3 wave conditions (Table 5-2), and the mean water level was increased according to SLR. Each wave condition is forced during multiple tidal cycles corresponding to its probability of concurrence to avoid a sediment imbalance from the applied morphological acceleration (see Dissanayake and Wurpts, 2013). All other model conditions are similar to the setup explained in the D 2.2 report (e.g., spatially varying bed sediment composition of 6 fractions). Each scenario simulation is simulated twice; once without the saltmarsh area (WT-NbS) and once after implementing the saltmarsh area (NbS).

Table 5-1 Model simulations performed with different scenarios to investigate the effect of NBS and therein ESSs

Scenarios	Description
1. Synthetic increase of MSL	MSL was increased by 0, 0.07, 0.12, 0.26 and 0.78 m (Garner et al., 2021), and simulated for a 2-year period with *mf* = 20 using measured wind and schematised waves for a hydrodynamic period of 36 days starting from 02 Oct 2015.
2. Future forcing from 2090 to 2100	Model predicted MSL variation, wind and wave forcing corresponding to Ensemble 2 in Pein et al. (2023), and simulated the representative year with *mf* = 10.
3. Storm event *Xaver*	Measured forcing during the storm to test the improved wave dissipation due to vegetation in Delft3D-WAVE with *mf* = 1

5.2.5. Quantification of ESS

The first ESS, the effects on hydrodynamics (1), was quantified by analysing water level, wave height and currents, while the second ESS, the effects on sedimentation (2), was estimated by sediment transport, and erosion/sedimentation patterns and volumes.

5.3. Results

5.3.1. Schematisation of model forcing

The last three wave conditions of the iterative analysis were selected as the representative waves of the overall wave climate (R^2 >0.99 and RMSE <0.002). A qualitative comparison of the resulting erosion and sedimentation pattern from the overall wave climate and the three selected wave conditions show a good agreement (Figure 5-4). At the North Sea side, a strong pattern is found on the ebb-tidal delta. At the Juist island, shore-oblique alternative erosion and sedimentation ridges are evident in both applications. At the Wadden Sea side, erosion and sedimentation are mainly limited in the channels. In summary, the predicted bed evolution of the selected 3 wave conditions has a good resemble with that of the entire wave climate. However, it should be noted that the pattern in the overall climate is relatively stronger than that of the selected 3 waves.

Sea level variations of the 3 ensembles for the period 2090 – 2100 indicate that the mean sea level of the ensemble 2 has a fairly similar increase as in the averaged of all 3 ensembles (Figure 5-5). Therefore, the forcing of the ensemble 2 was selected for the numerical experiments.

A representative wind year, which has similar characteristics in wind speed and direction to the overall data, was selected based on the values of three statistical parameters (Figure 5-6a-c). The optimum values are found for the wind year 01 October 2093 to 30 September 2094 (μ = -0.01, *rmsd* = 0.47 m/s, *skill* = 0.78). This agreement is further supported by the wind roses (d and e), though the representative year has higher occurrences in some directional sectors than the overall data.

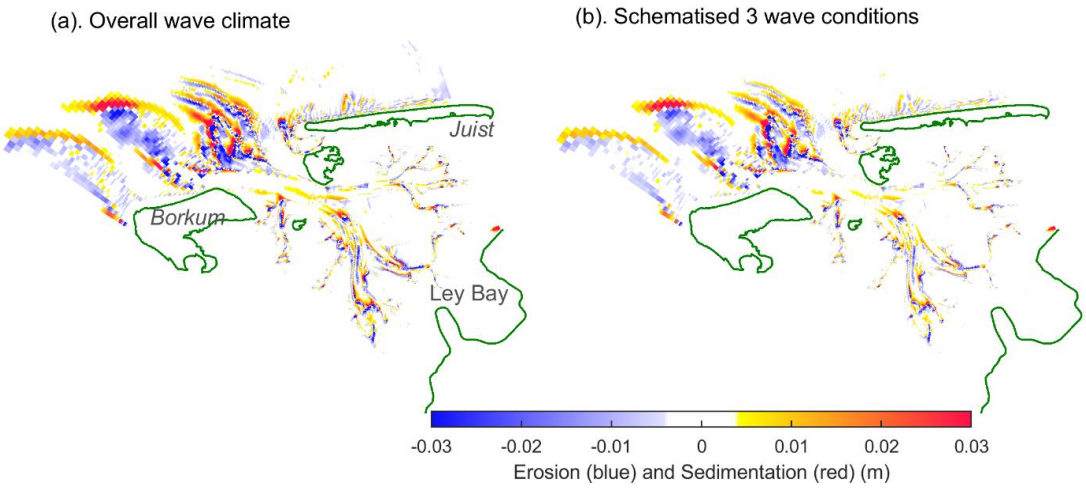

Figure 5-4 Erosion and Sedimentation pattern resulting from the overall wave climate (a) and from the schematised 3 wave conditions (b).

Table 5-2 Characteristics of the selected 3 wave and wind conditions and the respective wind parameters

Wave ID	Hs (m)	Tp (m)	Dir. (°)	Probability	Wind speed (m/s)	Wind Dir. (°)
48	0.5	2.7	176	0.21	6.2	172
93	0.7	10.7	324	0.57	3.8	172
95	2.4	8.3	321	0.22	8.7	271

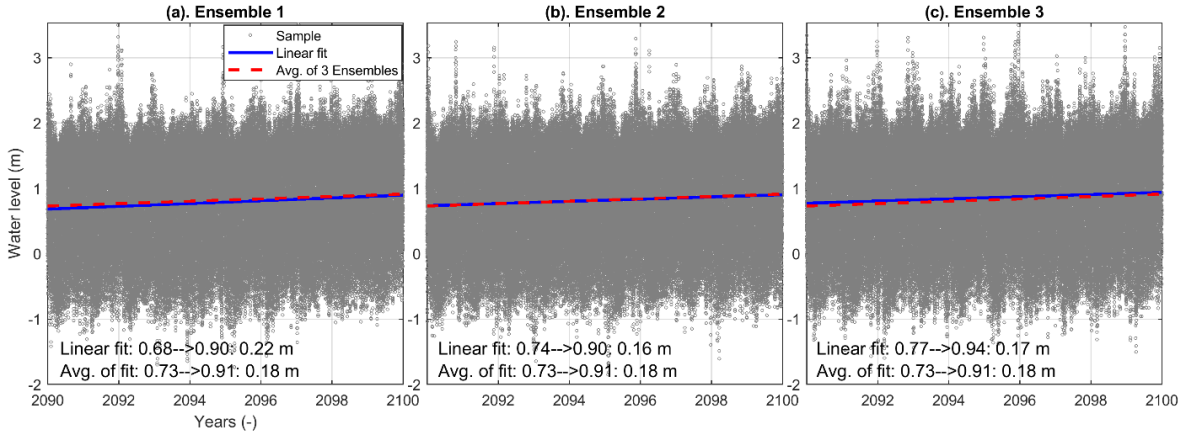

Figure 5-5 Sea level variation from 2090 to 2100 of three ensemble scenarios according to Pein et al. (2023). Blue-line indicates the linear fit and dash-red-line is the averaged linear fit of all three ensembles.

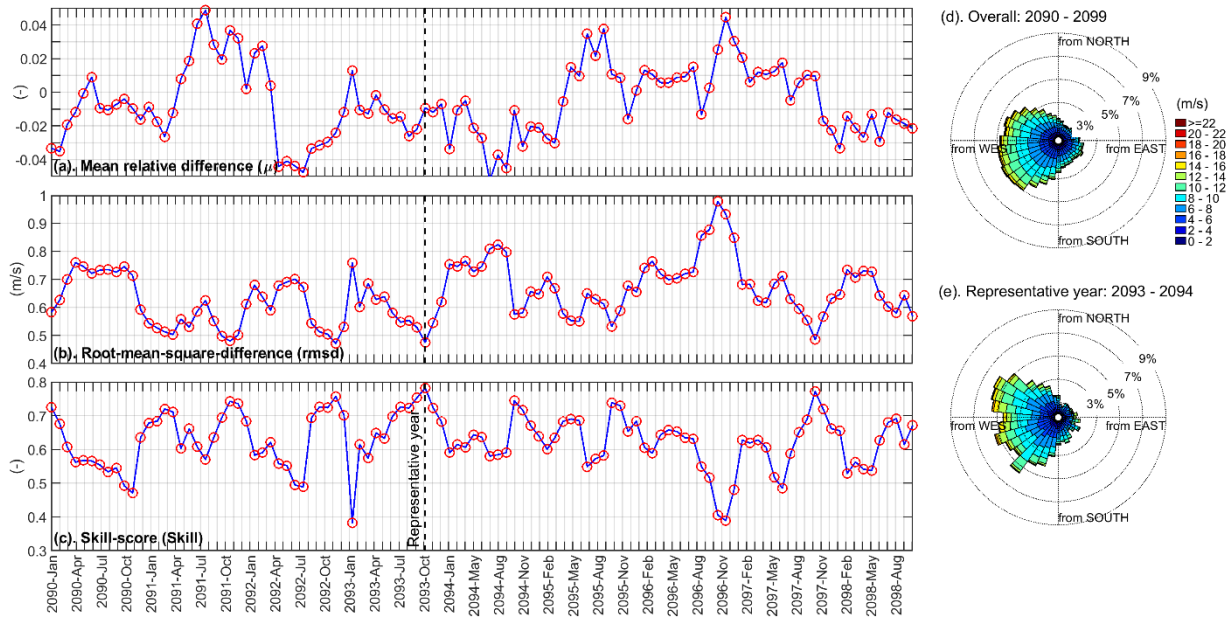

Figure 5-6 Statistical analysis to define a representative year: Mean relative difference (a), Root-mean-square-difference (b), Skill-score (c). Only the starting month of each wind year is indicated. Dash-line shows the occurrence of the representative year. Wind rose of overall wind data from 2090 to 2099 (d) and Wind rose of the selected representative wind year from 01 October 2093 to 30 September 2094 (e).

5.3.2. Effects of NbS on ESS due to constant increase of mean sea level

Exemplary hydrodynamic pattern

A one-day period during spring-tide (13 October 2015) was selected to demonstrate the impacts of constant SLR on the hydrodynamics in Ley Bay, during which the monitoring location has a depth of about 1 m. It should be noted that the saltmarsh area is located at around 1.25 m above NHN, which will be submerged for a few hours during high water spring.

The water level in Ley Bay does not increase by the exact amount of SLR for the different scenarios (Figure 5-7a). Under No SLR, the monitoring location emerges about 2 hours during low water. This period decreases as the SLR increases. However, there is no proportionality of this decrease to the amount of SLR. Only under

the highest SLR, the location remains submerged. It is generally found that the higher the SLR, the higher the increase of high-water peak than the amount of applied SLR. With respect to No SLR, the average increase of water level during the entire period accounts for 5.3% for 0.07 m SLR, 9.3% for 0.12 m SLR, 20% for 0.26 m SLR and 60% for 0.78 m SLR. These indicate that SLR has different influences on the high-water and the low-water phases.

Wave height variations are sensitive to to water levels as well as wind (Figure 5-7b). The stepwise pattern occurs due to the larger coupling interval (30 min.) between flow and wave modules than the monitoring interval (10 min.). The existence of waves depends on the prevailing wind. For example, the highest SLR keeps the location always submerged, however no waves during the entire low-water period (see around 04 and 17 hour). Over the simulated period, the average wave height of the SLR scenarios increases up to 3.5%, 4.9%, 11.9% and 35.9% with respect to No SLR.

Variations of velocity magnitude indicate not only increase but also phase shift as the SLR increases (Figure 5-7c). As in the water level, the highest SLR resulted in non-zero velocity throughout the period. All scenarios indicate the lowest velocity at the low-water slack, and the difference between the highest SLR and the others is considerable at both high- and low-slack waters. The phase difference with respect to No SLR increases as the SLR increases. During the flood phase, the velocity increase is faster than No SLR, while during the ebb phase, the velocity decrease is delayed as the SLR increases (i.e., faster-rise and slower-fall due to SLR). Therefore, the period with significant flow velocity increases with SLR (i.e., area under the curve). The average increase of velocity for the SLR scenarios is 2.7%, 3.9%, 10.6% and 22.2% respectively during the entire analysis period. These results indicate that the SLR effects on the hydrodynamics are non-linear processes, and therefore the influence of a specific SLR scenario on the hydro-morphodynamics needs to be separately investigated.

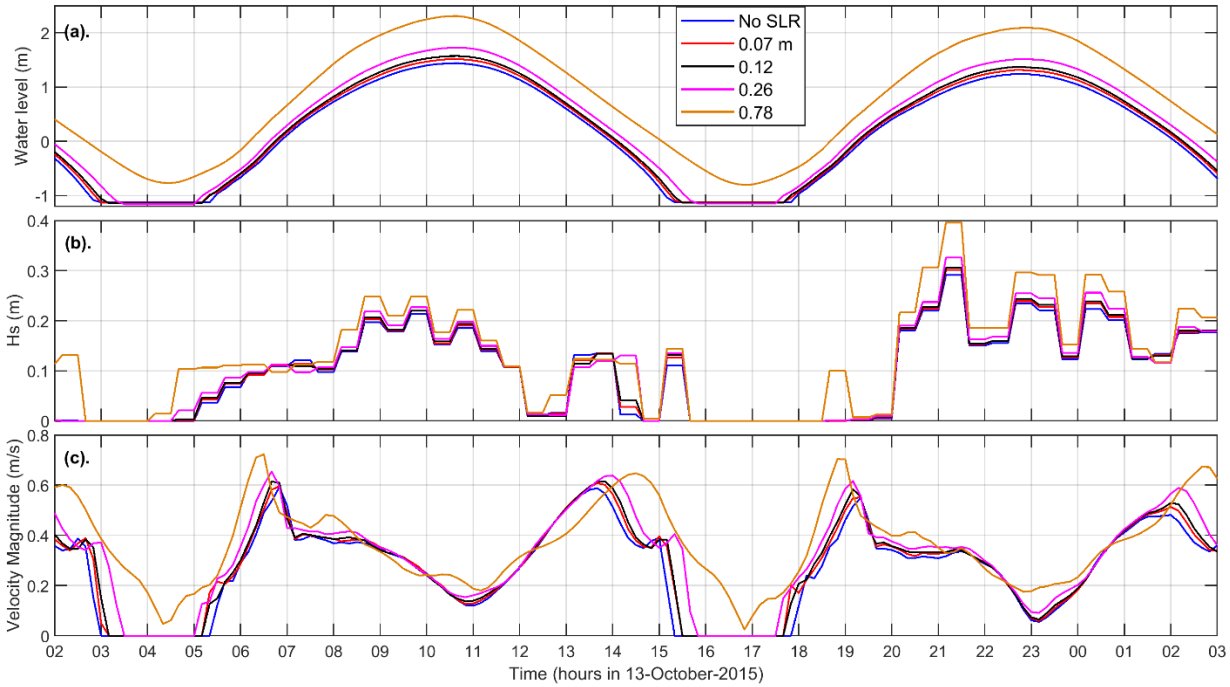

Figure 5-7 Variation of Water level (a), Wave height (b) and Velocity magnitude (c) in Ley Bay for No SLR (blue-), 0.07 m (2020: RCP 8.5 50% - Garner et al., 2021, red-), 0.12 m (2030: RCP 8.5 50%, black-), 0.26 m (2050: RCP 8.5 50%, magenta-) and 0.78 m (2100: RCP 8.5 50%, orange-line). For clarity, only one-day period during spring-tide is shown.

Maximum velocity distribution

The moment of maximum velocity in the Ley Bay was estimated by selecting the maximum velocity at each grid cell during the entire analysis period (Figure 5-8). The green-polygon indicates the extent of the saltmarsh area.

SLR causes an increase in the velocity as well as the flood extent in the Ley Bay. The spatial patterns of the first three scenarios (see a, b, and c in WT-NbS) hardly demonstrate any increment as the SLRs are relatively small (as found previously in Figure 5-7c). However, the patterns of the last two (particularly e) show clear distinct compared with that of the No SLR (a). Only with the highest SLR scenario (e), the saltmarsh area (green polygon) experienced high velocities. It should be noted that for the clarity, the colour bar is white close to zero. Therefore, very small velocities might not be distinguishable. After implementing the saltmarsh (NbS), the velocity patterns of the first 4 scenarios are fairly similar to that of the WT-NbS. In these scenarios, the saltmarsh area is not fully submerged due to the low water levels. However, the velocity reduction of the highest SLR is apparent by comparing WT-NbS and NbS, in which the NbS application decreases the magnitudes down to about zero.

These velocity patterns imply that the saltmarsh area remains partly exposed depending on the maximum water level experienced during the analysis period. The NbS application significantly dampens the velocities in the saltmarsh area. The largest effect on the velocity mitigation is found with the highest SLR, which results in a complete submergence of the saltmarsh area.

Maximum sediment transport distribution

Similar to the velocity, the maximum sediment transport at each grid cell was estimated for suspended (colour) and total transport (vectors) separately (Figure 5-9). The resulting patterns indicate that the higher the amount of SLR, the higher the rate of sediment transport. Differences among a, b and c are not clearly visible being minor increases. However, in the last two scenarios, both vectors and colours show distinct patterns compared with the No SLR (a).

These patterns indicate that the difference between the WT-NbS and NbS applications is very marginal for the scenarios in a, b, c and d. However, noticeable difference is found with the highest SLR (e). For example,

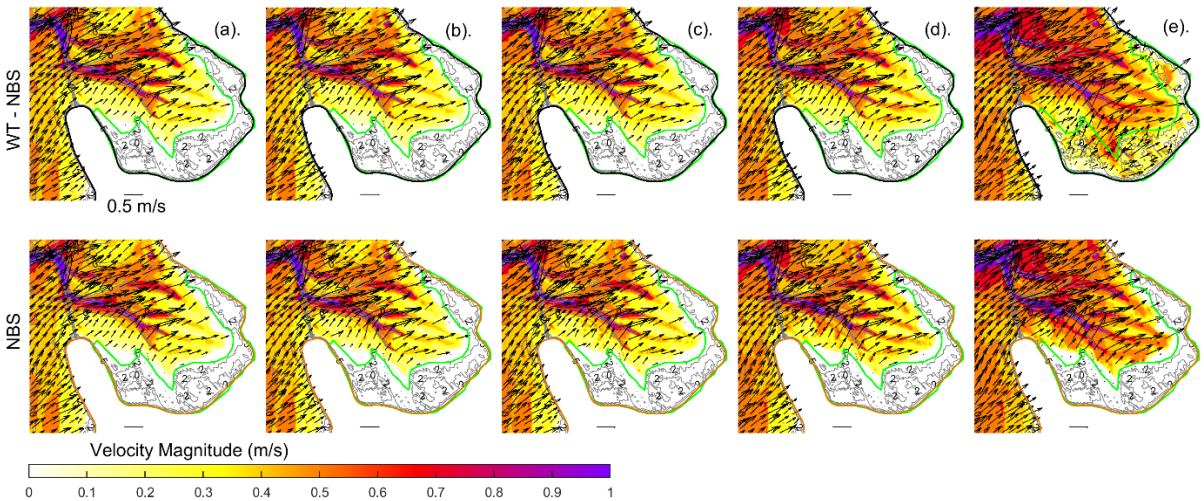

Figure 5-8 Maximum velocity, magnitude (colour), and magnitude and direction (vectors), in Ley Bay for No SLR (a), 0.07 m (2020: RCP 8.5 50% - Garner et al., 2021, b), 0.12 m (2030, c), 0.26 m (2050, d) and 0.78 m (2100, e) in the applications of without the saltmarsh area (WT – NBS) and after implementing the saltmarsh area (NBS). Contours show the bed topography.

the vectors and colour close to the saltmarsh edge decreased in the NbS compared with the WT-NbS. Therefore, the NbS can provide a significant influence on decreasing the sediment transport rate for the high SLR scenarios.

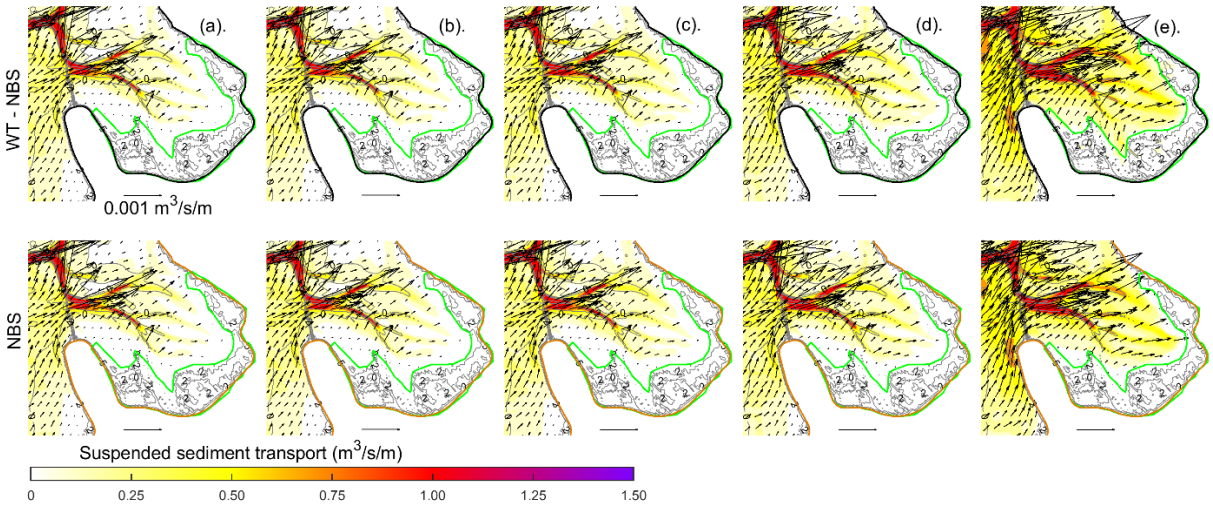

Figure 5-9 Maximum suspended sediment transport (colour) and total sediment transport (vectors), in Ley Bay for No SLR (a), 0.07 m (2020: RCP 8.5 50% - Garner et al., 2021, b), 0.12 m (2030, c), 0.26 m (2050, d) and 0.78 m (2100, e) in the applications of without the saltmarsh area (WT – NBS) and after implementing the saltmarsh area (NBS). Contours show the bed topography.

Bed evolution pattern

A qualitative comparison of the bed evolution patterns clearly indicates both erosion and sedimentation areas gradually increase as the SLR increases (Figure 5-10). All scenarios generally resulted in deepening of channels (i.e., erosion) and shallowing of the shoal areas (i.e., sedimentation). As found earlier, the noticeable difference between the WT-NbS and the NbS applications is shown only with the highest SLR (e). The saltmarsh area in the WT-NbS shows erosion and sedimentation patterns, and these are hardly visible in the case of the NbS application. Therefore, the results suggest, both erosion and sedimentation processes are hindered by the effects of the saltmarsh.

The absolute values of the erosion and sedimentation volumes within the saltmarsh area contrast between the highest SLR scenario and the others, i.e., volumes are two orders of magnitude higher in the highest SLR than the others (Figure 5-11a, zoom-view). These indicate that the increase of MSL of the latter scenarios is not adequate to strongly influence the bed evolution within the saltmarsh area. Of the highest SLR, both erosion and sedimentation volumes are larger in the WT-NbS than in the NbS. Therefore, the saltmarsh significantly decreases both erosion and sedimentation. This counter-intuitive result suggest the modelling tool may omit relevant physical processes or SLR changes the system behaviour. Furthermore, the erosion volume is higher than that of the sedimentation in both applications, in which the eroded sediment from the saltmarsh area partly escapes seaward.

The relative volumes were separately estimated for erosion and sedimentation with respect to the WT-NbS application (Figure 5-11b). Positive values indicate higher volumes in the WT-NbS than the NbS, and vice versa. Volumes of the No SLR show erosion decreased by 100% (i.e., no erosion in NbS) and sedimentation increased by 100% (i.e., twice of sedimentation in NbS than WT-NbS), which can partly be expected in the nature. However, this trend changes with the increase of SLR. It is generally found that the percentages of both erosion and sedimentation positively increase as the SLR increases. For erosion, this means, the higher the SLR the lower the erosion within the saltmash area. The amount of sedimentation in the NbS is lower

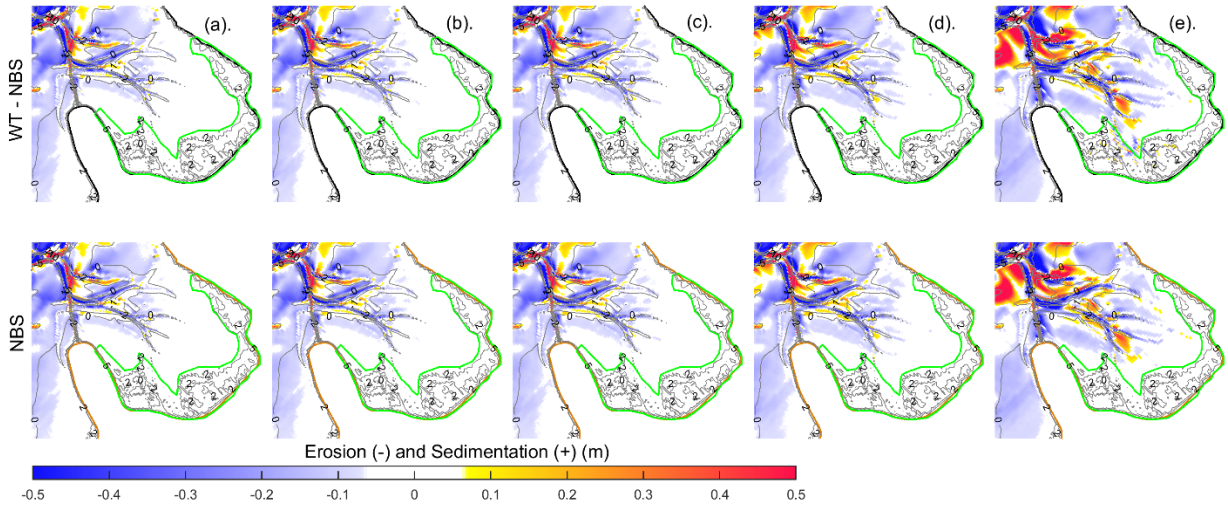

Figure 5-10 Erosion and sedimentation patterns in Ley Bay for No SLR (a), 0.07 m (2020: RCP 8.5 50% - Garner et al., 2021, b), 0.12 m (2030, c), 0.26 m (2050, d) and 0.78 m (2100, e) in the applications of without the saltmarsh area (WT – NBS) and after implementing the saltmarsh area (NBS). Contours show the bed topography.

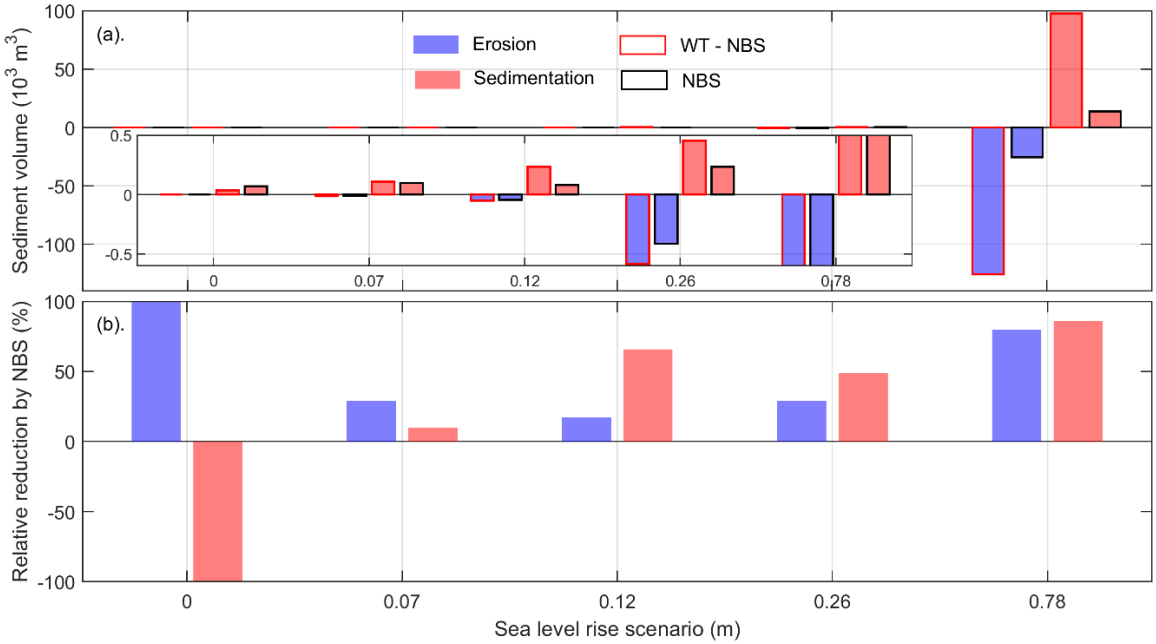

Figure 5-11 Change of erosion and sedimentation volume (a) and relative reduction by NBS (([WT - NBS] – [NBS])/[WT-NBS]×100%) within the Saltmarsh area for 0 m (No SLR), 0.07 m (2020: RCP 8.5 50% - Garner et al., 2021, b), 0.12 m (2030, c), 0.26 m (2050, d) and 0.78 m (2100, e) in the applications of without the saltmarsh area (WT – NBS) and after implementing the saltmarsh area (NBS).

than the WT-NbS in these scenarios (i.e., positive values). This difference increases as the SLR increases. It should be however noted that the adaptiaion of the system for the applied SLR might not have succeeded within the simulated 2-year period.

5.3.3. Evolution from 2090 to 2100

For the simulation from 2090 to 2100, the improved Delft3D-WAVE approach was used (see section 5.3.4), in which the wave computation is performed within three domains, EMS→OEMS→VEG, and additional wave energy dissipation occurs by the saltmarsh. Only the first 5 years from the period 2090 to 2100 were able to simulate due to a technical failure. It should be noted that repeating these runs costs more than one month due to the nesting of 3 domains with high resolutions (i.e., VEG ~10 m).

Erosion and sedimentation pattern, and volume change were estimated to explore the effect of saltmarsh presence on the bed evolution in the phase of SLR from 2090 to 2100. In the WT -NbS application (Figure 5-12a), strong erosion is shown along the edge and inside the saltmarsh area, while the sedimentation mainly occurred inside. The maximum erosion and sedimentation heights are -0.8 m and 1.2 m respectively. In contrast, the NbS application (Figure 5-12b) resulted in only sedimentation along the saltmarsh edge extending landward (maximum ~ 0.1 m). These results are further evident in the sediment volume analysis within the saltmarsh area (Figure 5-12c). A large volume was eroded only with WT-NbS, while fairly similar sedimentation occurred in both applications. The relative reduction in volume (Figure 5-12d) has 100% in erosion (i.e., no erosion in NbS) and 20% reduction of volume in sedimentation. If the simulation is conducted over a 10-year period (2090 - 2100 more erosion and more sedimentation in WT-NbS might be expected, while only landward sedimentation is increased in the NbS.

These results indicate that NbS causes sedimentation within the saltmarsh area, and this sediment amount is imported from the seaward of the saltmarsh area. More than 50% of the eroded sediment in WT-NbS is escaped from the saltmarsh area causing therein net erosion. Therefore, applying the selected NbS can support to mitigate the erosion due to future SLR scenarios, and act as a successful coastal protection measure.

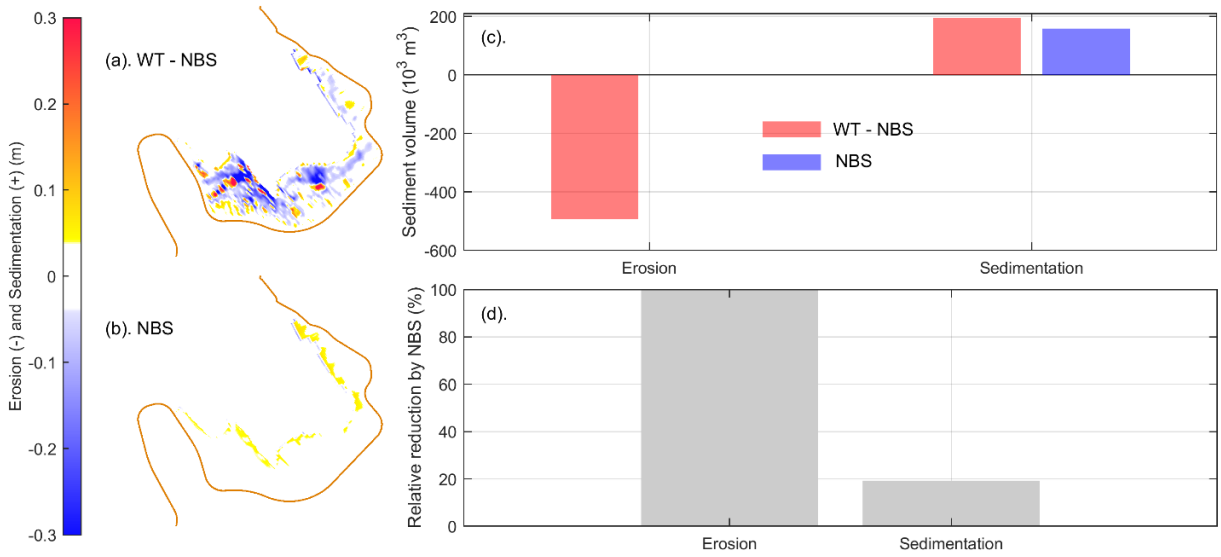

Figure 5-12 Predicted erosion and sedimentation patterns during the first 5-year of the 2090 – 2100 period for WT - NBS (a) and NBS (b). Erosion and sedimentation volumes within the saltmarsh area without NBS (WT - NBS) and with NBS (NBS) applications (c), and the relative reduction of volume in erosion and sedimentation with respect to the WT - NBS application: (([WT - NBS] – [NBS])/[WT- NBS]×100%) (d).

5.3.4. NbS effects on ESS with the improved-wave application

The improved Delft3D-WAVE (i.e., including wave energy dissipation by vegetation) was tested for the storm event Xaver (see D 2.2 report for the classification of this event). Resulting hydrodynamics and bed evolution between WT-NbS and NbS were compared to explore the enhancement to the ESSs.

Wave energy dissipation

Wave dissipation in the WT-NbS is driven by bottom friction and breaking (Figure 5-13). However, the dissipations by these two processes are two orders of magnitude lower in the NbS than in the WT-NbS (note: not visible according to the colour scale). Therefore, the main dissipation driver in the NbS is vegetation. Both applications show high dissipation along the dyke. This is dominated by wave breaking in the WT-NbS, and it is clearly higher than in the NbS scenario. These results indicate that the susceptibility of the wave attack at the dyke front decreases by implementing the saltmarsh in the foreland. However, the occurrence of high dissipation along the dyke in the NbS could be related to the plant density (i.e., only 50×50 per m^2 hereon tested) and needs further investigations.

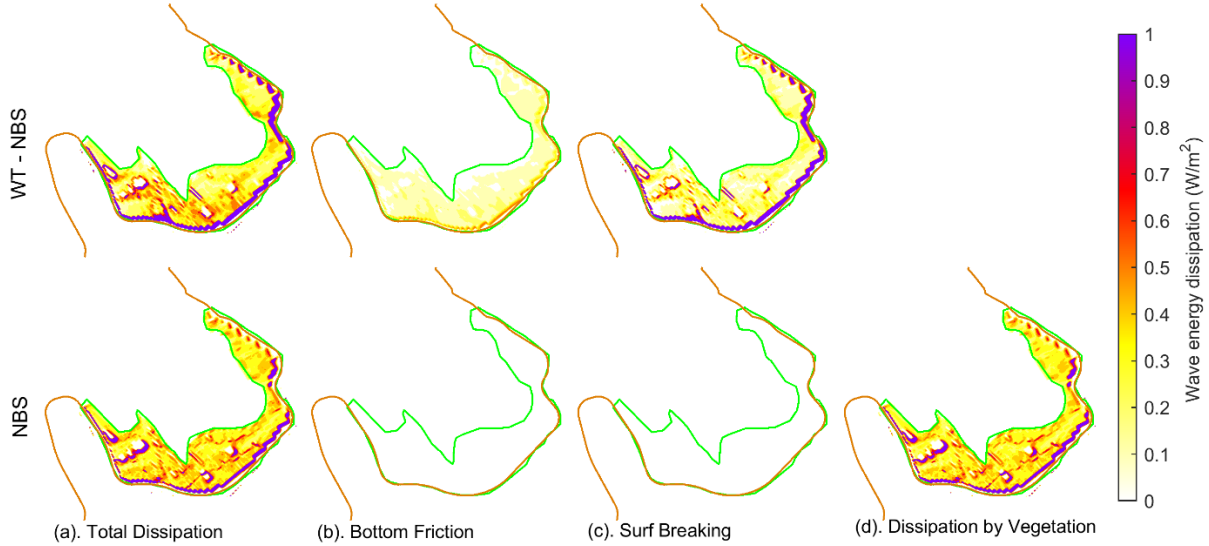

Figure 5-13 Comparison of the maximum wave energy dissipation during the event Xaver in the WT-NBS and the NBS applications: (a) Total wave energy dissipation, (b). Dissipation by bottom friction, (c). Dissipation by surf breaking and (d). Dissipation by vegetation

Hydrodynamics and Sediment concentration

Significant wave height (Hs), velocity and sediment concentration at three locations (V2, V4 and V5) within the saltmarsh area were analysed to demonstrate the effect of NbS on hydrodynamics by comparing the WT-NbS and NbS applications (Figure 5-14). For clarity, the variations of water level, Hs, velocity and sediment concentration in the Ley Bay (LB) are shown with the right y-axis. At V2, V4 and V5, the peaks of Hs correspond to the water level peaks. The NbS causes a strong decrease in Hs depending on the location within the saltmarsh area and the exposure to the incoming waves (i.e., 64% at V2, 40% at V4 and 65% at V5). This is further evident by the decrease of velocity at these locations 82%, 71% and 90% respectively, which can be expected because the wave-driven currents dominate the velocity during a storm event. The sediment concentration is almost decreased by 100% at all locations by the application of saltmarsh. This is a good proxy to claim that water quality certainly increases by implementing the NbS.

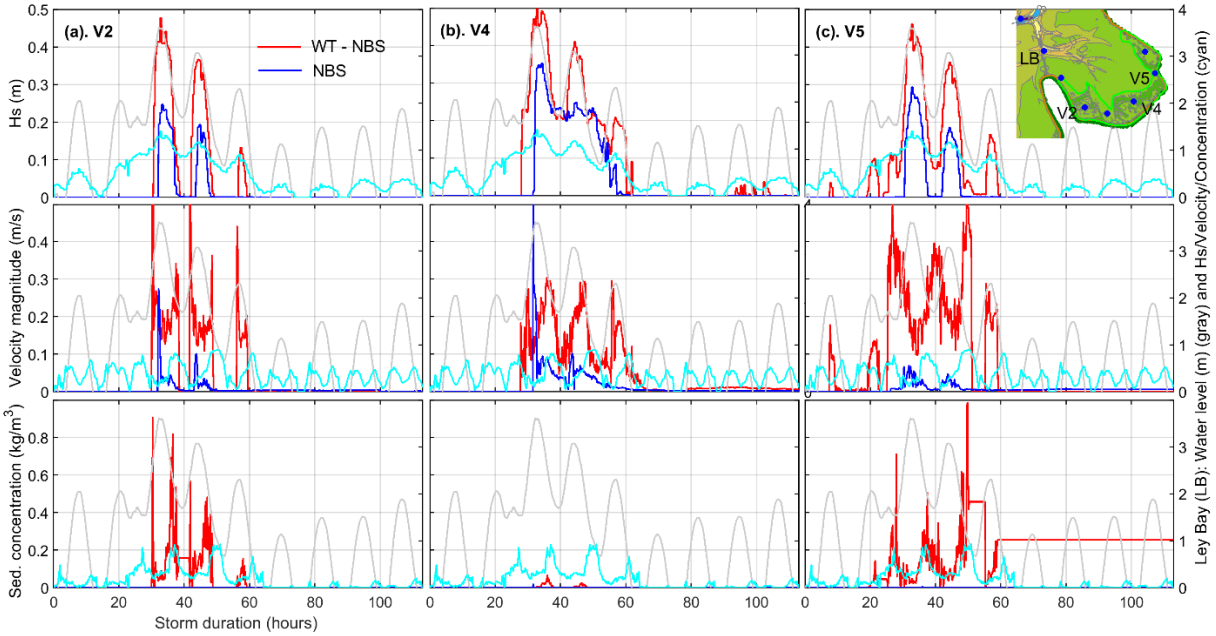

Figure 5-14 Comparison of wave height (Hs), Velocity magnitude and Sediment concentration at the selected locations V2, V4 and V5 (see on Ley Bay bathymetry: insert view), without NBS (WT- NBS) and with NBS (NBS) during the event Xaver. Respective water level (gray), and Hs/Velocity magnitude/Sediment concentration (cyan) variations at Ley Bay (LB) are indicated on the right-y axis.

Erosion and sedimentation

The effect of NbS on the bed evolution was investigated by comparing the erosion and sedimentation between the WT-NbS and NbS applications (Figure 5-15). The saltmarsh area of the WT-NbS shows that erosion occurs almost everywhere and sedimentation is limited to some locations inside and along the saltmarsh edge (a). No such erosion areas are found in the NbS, whereas the sedimentation at the edge is pronounced (b). This is clearly evident with the volume change (c), in which the NbS caused almost no

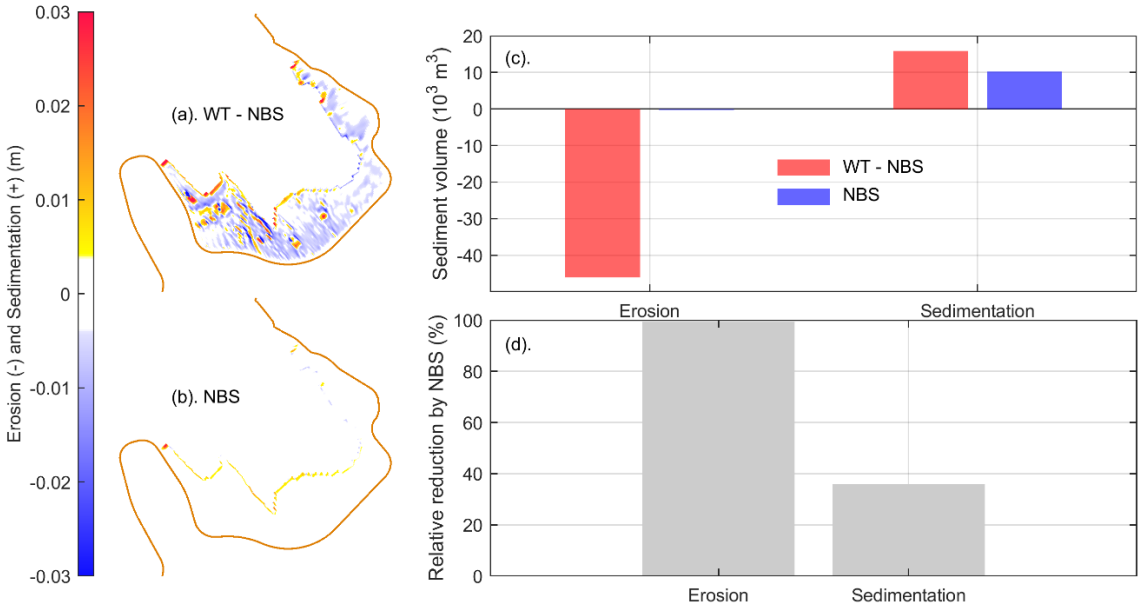

Figure 5-15 Predicted erosion and sedimentation patterns for WT - NBS (a) and NBS (b). Erosion and sedimentation volumes within the saltmarsh area without NBS (WT - NBS) and with NBS (NBS) applications (c), and the relative reduction of volume in erosion and sedimentation with respect to the WT - NBS application: (([WT - NBS] – [NBS])/[WT- NBS]×100%) (d).

erosion, however sedimentation was found within the saltmarsh area (36% in d). These imply, the WT-NbS loses sediment from the saltmarsh area, while gaining sediment in the NbS application. The focused ESSs are positively improved by the NbS (i.e., decrease hydrodynamics and increase sedimentation) in the improved Delft3D-WAVE, which can support to mitigate the adverse effects of marine forcing enhancing the coastal protection.

5.4. Discussion

5.4.1. Effectiveness of the NbS under the SLR scenarios

Only the highest SLR scenario (0.78 m + MSL) indicated contrasting impacts on the hydro- morphodynamics due to the implementation of the NbS. The nested models were simulated with an astronomical tide with increasing MSL according to the SLR scenarios. Therefore, the model forced water levels excluding storm surges, which can lead to submergence of the saltmarsh area and changes the morphodynamic setup. With the No SLR scenario, the saltmarsh area is submerged only a few hours during spring-high water with weak velocities (see Figure 5-7). This period slightly increases as the SLR increases. Under such conditions, no significant change in the saltmarsh area can be expected even under the WT-NbS. Therefore, the effectiveness of NbS is only observed under the highest SLR. The velocity pattern indicated strong decrease with the NbS (Figure 5-8e). However, the corresponding sediment transport (Figure 5-9e) and bed evolution (Figure 5-10e) are not clearly visible as these are relatively small compared to the rest of Ley Bay.

The erosion and sedimentation volumes within the saltmarsh area appear to be good indicators to demonstrate the NbS impacts. The absolute volume of NbS is always smaller than WT-NbS (Figure 5-9a). The higher the SLR the larger the volume changes. A decrease of sedimentation with NbS however suggests some physical processes may be missing in the model (see Suzuki, 2011). These trends are further supported by the relative change (Figure 5-9b), in which the impact of NbS on the sedimentation appears to be generally higher than on the erosion for each scenario. Furthermore, the higher the SLR the higher the NbS impacts. Therefore, the effectiveness of NbS increases for high SLR during the selected simulation period. This is plausible as the interaction of hydrodynamics and thus morphodynamics within the saltmarsh area increases with SLR. Our hypothesis of decreasing effectiveness with SLR deviates for the selected scenarios. However, the effectiveness decreases after flattening the saltmarsh by exposing to extreme forcing (Möller, 2014). The gradual increase of SLR from 2090 to 2100 in NbS caused only strong sedimentation along the saltmarsh edge extending landward. In WT-NbS, strong erosion occurred inside the saltmarsh area. Therefore, the application of saltmarsh supports to mitigate the risk of SLR induced erosion and potential hinterland flooding, and acts as an effective tool for coastal protection (see also in Langley et al., 2009).

5.4.2. Wave dissipation by the NbS needs to be considered

With the improved communication between Delft3D-WAVE and SWAN, the saltmarsh contributes to about 100% of the wave energy dissipation (Figure 5-13), while the model is computing sediment transport and bed evolution. The early numerical studies using SWAN have focused only on hydrodynamics (e.g., Suzuki, 2011; De Oude, 2010). For example, we found a reduction of Hs of more than 60% with the NbS (Figure 5-14). This agrees with De Oude (2010); a wave reduction of 60% to 75% was found using SWAN-VEG (no sediment transport) to simulate the vegetation induced wave dissipation. SWAN-VEG has embedded physical processes to simulate the vegetation effect on wave attenuation (SWAN, 2023), though the communication with Delft3D-WAVE lags. Furthermore, Suzuki (2011) investigated the impact of vegetation on wave dissipation for different laboratory and field cases, and showed about 70% of dissipation. Such a reduction leads to weak wave driven velocities, and in turn lower sediment transport and slower bed evolution. By the interaction of the NbS, the erosion volume decreased by almost 100%, while sedimentation increased by 35% during the simulated storm event Xaver, which has a return level of 125 years (see D 2.2 report for the analysis of return period). In the constant SLR analysis, the NbS caused a decrease in sedimentation without the wave dissipation by saltmarsh. For the SLR simulation 2090 – 2100, an increase in sedimentation was

found even without erosion after applying the dissipation by saltmarsh. Therefore, the adopted improvement of Delft3D-WAVE is of utmost importance in investigating the saltmarsh contribution for coastal protection.

These results indicate that the selected NbS (application of saltmarsh) serves to improve the focused ESS (decrease the severity of hydrodynamics and increase sedimentation), and therefore is a potential agent for coastal protection, which enables the resistance against the adverse impacts during the extreme events (i.e., SLR, storms). Furthermore, a previous project of NLWKN, A-KUEST (Niemeyer et al., 2014; Kaiser et al., 2010), revealed that increased sedimentation in the saltmarsh areas of the Ems-Dollard estuary improves the system adaptation to SLR. Also, the higher the saltmarsh the lower the wave heights during storm surges resulting to a significant reduction of wave runup and overwash.

5.4.3. Drawbacks and recommendations

Long-period with respective forcing needs to be simulated to investigate the NbS in the phase of SLR

The SLR effects on the morphodynamic changes are simulated focusing on decadal time scales, in which a more realistic increase of MSL over the time can be implemented (e.g., Dissanayake et al., 2012). In this study, constant increases of MSL were however adopted representing the 50^{th} percentile of the years 2020, 2030, 2050, and 2100 based on RCP 8.5 (Garner et al., 2021) to simulate over a 2-year period. This selection is twofold: marginal change of MSL over a 2-year period and to get the first impression on the ESS behaviour for different SLRs by optimising the available project time. Therefore, a future study should focus on applying decadal scales (e.g., 2020-2030, 2030-2050) with realistic MSL increases to investigate the NbS effects on the selected ESS.

Only SLR is not enough to represent the future forcing. Besides SLR, changes in the wind fields as well as wave climates can be expected due to the future scenarios (Pein et al., 2023; Dreier and Fröhle, 2020). Therefore, applying only SLR provides preliminary insights on the NbS effects, which need to be repeated with the full-spectrum of forcing enhancement. For the period 2090-2100, we followed a such approach based on the predictions from Pein et al. (2023).

Configuration of the saltmarsh

The saltmarsh area in the Ley Bay was determined based on the bathymetry measurements, i.e., the area above 1.25 m + NHN and below 2.20 + NHN, which encompasses the lowest wind setup limit at the surrounded dyke. Accordingly, the saltmarsh covers about 35% of the Ley Bay area. This classification might be different to the actual saltmarsh presence due to some zonation effects. Furthermore, the present approach used uniform plant characteristics (i.e., density, height, diameter and species), and there is no variation of the vertical plant structure, which are simplifications. Our sensitivity analyses and also previous studies (e.g., Bouteiller and Venditti, 2015; Suzuki, 2011; De Oude, 2010) show wave attenuation and the subsequent hydrodynamics depend on the plant configuration. The flexibility of stems was not considered in this analysis, though the saltmarsh substrate remains stable resisting to erosion even after flattening due to extreme conditions (Möller, 2014). Furthermore, growth and decay of saltmarshes plays an important role in the long-time scales, which should be incorporated in the model. Therefore, the configuration of the saltmarsh needs to be improved as much as possible by comparing with additional field data for more realistic predictions.

Implementation of vegetation

The discussed model results are based on the 2DH simulations in Delft3D, which has a unform vertical structure for plants. This implementation uses the Trachytope 154 (Delft3D, 2023) following Baptist (2005), to estimate the vegetation exerted drag force to the flow. To avoid increasing bed roughness causing increased bed shear stress and then sediment transport, the bed roughness is split into two components in Delft3D: background roughness and flow resistance of the vegetation. Only the first component contributes

to the sediment transport estimation. On the other hand, in a 3D model, the vertical bifurcation of plants can be implemented. The influence of vegetation on momentum is estimated by the vertical distribution of friction force, similar to the effect of cylindrical elements in oblique flow (Winterwerp and Uittenbogaard, 1997; Oberez, 2001). The results of our initial 3D tests indicated numerical instabilities demanding further investigations.

In the SWAN version 41.31, wave damping from vegetation is included by expanding the Mendez and Losada (2004) approach, which describes the mean rate of wave energy dissipation per unit horizontal area for irregular waves (Suzuki, 2011). We activated this process by improving the communication between Delft3D-WAVE and SWAN, which is not available with the standard Delft3D.

The performances of 2DH, 3D and wave attenuation by vegetation in SWAN are required to compare with the field data to understand the capability of the model physics and the processes need further improvements.

5.5. Conclusions

The potential application of saltmarsh as a nature-based-solution (NbS) for coastal protection was investigated using numerical experiments (Delft3D/SWAN) based on the Ley Bay in the east Frisian Wadden Sea. The ecosystem-services (ESS) are expected to enhance by mitigating hydrodynamics and increasing sedimentation.

Schematized wave and wind forcing were developed using the measured data, which is a pre-requisite in a long-term morphological simulation. The SLR scenarios with constant increases in MSL showed that there is a non-linearity in the effects of water levels, wave height and velocity in the Ley Bay area (Figure 5-8). Only the highest SLR caused significant mitigation of hydrodynamics and reduction of both erosion and sedimentation within the saltmarsh area. In the SLR from 2090 to 2100, the NbS application caused only sedimentation along the saltmarsh edge indicating that the saltmarsh decreases the risk of erosion and enhances ESS. The improved Delft3D-WAVE (i.e., communication between Delft3D and SWAN) resulted in about two order of magnitudes higher dissipation by vegetation than bottom friction and breaking, and decrease the susceptibility of the wave attack at the dyke front. Mitigation of wave heights and velocities are about 60% and 80% respectively in the saltmarsh area. Water quality increases in the NbS due to significant decrease of sediment concentration (almost 100%). Furthermore, the NbS enables almost no erosion while importing sediment into the saltmarsh area. Therefore, the selected NbS can be used as an effective tool for coastal protection in the phase of sea level rise by mitigating adverse impacts and enhancing the ESS functionalities.

Further numerical experiments together with the field data collected in the saltmarsh areas can support the credibility of the model predictions by improving the modelled physical processes, as well as to optimize the saltmarsh restoration efforts.

5.6. References

Baptist, M., 2005. Modelling floodplain biogeomorphology, PhD Dissertation, TU Delft library, http://resolver.tudelft.nl/uuid:b2739720-e2f6-40e2-b55f-1560f434cbee.

Bouteiller C.L., Venditti, J.G., 2015. Sediment transport and shear stress partitioning in a vegetated flow, Water Resources Research 51, 2901-2922.

De Oude, R., 2010. Modelling wave attenuation by vegetation with SWAN-VEG, Master Thesis, University of Twente, the Netherlands.

Dissanayake, P., Amft, J., Sibbertsen, P., 2024. Defining an exposure index along the Schleswig-Holstein Baltic Sea coast, Marine Geology 46, 107382.

Dissanayake, P., Brown., J., Wisse, P. and Karunarathna, H., 2015. Comparison of storm cluster vs isolated event impacts on beach/dune morphodynamics, Estuarine, Coastal and Shelf Science 164, 301-312.

Dissanayake, D.M.P.K., Ranasinghe, R. and Roelvink, J.A., 2012. The morphological response of large tidal inlet/basin systems to relative sea level rise, Climatic Change 113, 253-276.

Dissanayake, P. and Wurpts, A., 2013. Modelling an anthropogenic effect of a tidal basin evolution applying tidal and wave boundary forcing: Ley Bay, East Frisian Wadden Sea, Coastal Engineering 82, 9-24.

Dreier, N., Fröhle, P., 2020. Long-term changes of waves at the German Baltic Sea coast: are there trends from past, Jpournal of coastal research 95, 1416.

Delft3D, 2023. Delft3D-Flow User Manual: Delft3D-FLOW User Manual (deltares.nl), p. 252-261 and 627-630.

DWD, 2023. German Weather Service Open Data Portal:
Index of /climate_environment/CDC/observations_germany/climate/ (dwd.de).

Garner, G. G., T. Hermans, R. E. Kopp, A. B. A. Slangen, T. L. Edwards, A. Levermann, S. Nowikci, M. D. Palmer, C. Smith, B. Fox-Kemper, H. T. Hewitt, C. Xiao, G. Aðalgeirsdóttir, S. S. Drijfhout, T. L. Edwards, N. R. Golledge, M. Hemer, R. E. Kopp, G. Krinner, A. Mix, D. Notz, S. Nowicki, I. S. Nurhati, L. Ruiz, J-B. Sallée, Y. Yu, L. Hua, T. Palmer, B. Pearson, 2021. IPCC AR6 Sea-Level Rise Projections. Version 20210809. PO.DAAC, CA, USA. Dataset accessed [2023-11-26] at https://podaac.jpl.nasa.gov/announcements/2021-08-09-Sea-level-projections-from-the-IPCC-6th-Assessment-Report.

Hartsuiker, G., 2008. German Bight model suite, grid generation and set-up of tidal flow models, Report, Prepared by Alkyon-Hydraulic Consultancy & Research for Niedersächsisches Landesamt für Ökologie, Forschungstelle Küste, Norderney.

Kaiser, R.; Knaack, H.; Miani, M.; Niemeyer, H.D., 2010. Examination of Climate Change adaptation strategies for Coastal Protection. In: MCKEE SMITH, J. and LYNETT, P. (ed.): Proceedings of the 32nd International Conference on Coastal Engineering, 2010, Shanghai. http://journals.tdl.org/icce/index.php/icce/issue/view/154/showToc

Langley, J. A., McKee, K. L., Cahoon, D. R., Cherry, J. A., Megonigal, J. P., 2009. Elevated CO2 stimulates marsh elevation gain, counterbalancing sea-level rise. Proceedings of the National Academy of Sciences U. S. A., 106, 6182–6186

Le Bouteiller, C. and Venditti, J.G., 2015. Sediment transport and shear stress partitioning in a vegetated flow, Water Resources Research 51, 2901-2922.

Mascioli, F., Piattelli, V., Cerrone, F., Gasprino, D., Kunde, T., Miccadei, E., 2021. Feasibility of objective seabed mapping techniques in a coastal tidal environment (Wadden Sea, Germany), *Geosciences*, *11*(2), 49.

Mendez, F.J. and I.J. Losada, 2004: An empirical model to estimate the propagation of random breaking and nonbreaking waves over vegeation fields, Coastal Engineering 51, 103-118.

Möller. I., Kudella, M., Rupprecht, F., Spencer, T., Paul, M., Wesenbeeck, B, K., Wolters, G., Jensen, K., Bouma, T.J., Mirinda-Lange, M., Schmmels, S., 2014. Wave attenuation over coastal salt marshes under storm surge conditions, Nature Geoscience 7, 727-731.

Niemeyer, H. D., Berkenbrink, C., Ritzmann, A., Knaack, H., Wurpts, A., Kaiser, R., 2014. Evaluation of Coastal Protection Strategies in Respect of Climate Change Impacts. In: Die Küste 81. Karlsruhe: Bundesanstalt für Wasserbau. S. 565-577.

Oberez, A., 2001. Turbulence modeling of hydraulic roughness of submerged vegetation. Master's thesis, UNESCO IHE, Delft. H.E.100.

Oberrecht, D. and Wurpts. A., 2023. Hydromorphologische Untersuchungen zur geplanten flexiblen Tidesteuerung mit dem Emssperrwerk – hydromorphodynamische Modellvalidierung Version 1.3, NLWKN-Forschungsstelle Küste, Norden, Bericht 02/2023.

Pein, J., Staneva, J., Mayer, B., Palmer, M.D., Schrum, C., 2023. A framework for estuarine future sea-level scenarios: Response of the industrialised Elbe estuary to projected mean sea level rise and internal variability, Frontires in Marine Science, doi: 10.3389/fmars.2023.1102485.

Roelvink, J., 2006. Coastal morphodynamic evolution techniques, Coastal Engineering 53 (2-3), 277-287.

SWAN, 2023. SWAN User Manual, SWAN Cycle III version 41.45A.

Suzuki, T., 2011. Wave dissipation over vegetation fields, PhD Dissertation, Technical University of Delft.

Trenberth, K.E., 2011. Changes in precipitation with climate change, Climate Research, Vol. 47, 123-138.
Winterwerp, J. C. and R. E. Uittenbogaard, 1997. Sediment transport and fluid mud flow. Tech. Rep. Z2005, WL | Delft Hydraulics, Delft, The Netherlands.

6. Role of morphological feedbacks on the effectiveness of Nature-based Solutions in the Ems Estuary

Marijnissen, R.J.C.[1], van Maren, D.S.[1,2], Schrijvershof, R.A.[1,3], & van Weerdenburg, R.J.A.[1,2]

1 Department of Marine and Coastal Systems, Deltares, Delft, The Netherlands
2 Faculty of Civil Engineering and Geosciences, Delft University of Technology, Delft, The Netherlands
3 Department of Environmental Sciences, Wageningen University and Research, Wageningen, The Netherlands

ABSTRACT: We studied the effectiveness of Nature-based Solutions (NbS) as an adaptation strategy for the Ems estuary, a turbid estuary within the Wadden Sea at the border between the Netherlands and Germany. Challenged by both sea-level rise and a high turbidity, we develop and apply a numerical hydro-morphological model to study how morphological feedbacks influence the effectiveness of three types of NbS measures for the Ems estuary: 1) converting a polder to wetland, 2) facilitating salt marsh growth with brushwood groynes, and 3) the dredging of sediment from harbours for re-use in climate adaptation. The model projects a strong autonomous development towards a higher turbidity in the Dollard Bay. This trend is amplified by sea-level rise through a combination of factors: an increase in sediment import, higher availability of weakly consolidated sediment, and a higher exposure of flats promoting the resuspension and recirculation of sediment within the Dollard Bay. The predicted increase is probably an overestimate because sediment availability will probably become more limiting than accounted for in the present model-setup, but it does suggest that (1) the up-estuary sediment transport capacity will increase as the sea level rises and (2) at a certain moment large-scale sediment availability becomes a limiting factor. The autonomous trend of increasing up-estuary sediment transport results in a growth of salt marsh because the increase in turbidity leads to accretion rates exceeding the rate of sea-level rise. The NbS measures can provide benefits in reducing turbidity on the short-term and promoting the growth of salt marsh on a local scale but are limited in effectiveness compared to the long-term trends.

6.1. Introduction

The Ems-Dollard estuary is a heavily engineered system on the Dutch-German border. A major challenge for the estuary is the increasing turbidity, which is the result of land reclamations and maintenance dredging (van Maren et al., 2016). This increase of fine particles in the water column has caused a decline in primary production in the estuary (Brinkman & Jacobs, 2023), the base of the food chain. Climate change induced sea-level rise increases the risk of flooding and of saltwater intrusion to the surrounding low-lying subsiding polders.

To overcome these challenges, mitigating measures were developed as part of the so-called EmsDollard2050 programme (ED2050). The objective of the program is to create an ecologically sustainable estuary focusing on three objectives: 1) reducing turbidity; 2) strengthening natural habitats; and 3) mitigating climate change. Various pilot measures are explored that are expected to restore natural ecosystems in the region while enhancing local ecosystem services (e.g. salt marshes attenuating waves). As the abundance of sediment in the Ems estuary is hindering biodiversity and a resource for climate adaption, the ED2050 concepts have a large focus on the management of sediment in the estuary and include:

1. Convert polder areas to wetlands to create nature and capture fine sediment
2. Enhancing sedimentation on the estuary's intertidal areas s and reinforcing nature

3. Re-using dredge spill from local harbours as a local resource

While ambitions and targets are clear, the effectiveness of these strategies (both short- and long-term) is unclear. One major uncertainty is the amount of sediment that is available for deposition in the Wadden Sea. Benninghoff & Winter (2019) concluded there is a sediment surplus in the German Wadden Sea including the Ems estuary, causing an accumulation of sediment on the intertidal flats equal or higher than the rate of sea-level rise. However, more recently Colina Alonso et al. (2024) concluded the sediment budget for the Wadden Sea is already closed, with a sediment deficit already present in the down drift regions, suggesting drowning of these areas as a result. The Ems estuary itself is a morphologically complex system. An interplay of many processes contribute and have contributed in shaping the estuary into its turbid state, such as enhanced tidal asymmetry in relation to dredging of harbours and channels (Winterwerp, 2011), a lack of intertidal area for deposition of fine material due to land reclamation in the past (van Maren et al., 2016), mud particle interactions such as hindered settling and flocculation (Dijkstra et al., 2019; van Leusden, 2011), and biological processes like the role of algal mats in reinforcing mud flats (van Duyl et al., 2000).

Earlier work describing the response of the Ems estuary to different sediment management strategies covered relatively short time scales (2050 or earlier). A framework for linking interventions, morphology, and biodiversity has previously been proposed by Spiteri et al. (2011), who suggest an effect chain from hydrodynamics, to sediment, to water quality, and to ecology. This framework was applied in van Maren et al. (2015a) and followed-up in 2017 (Van Maren et al., 2017) to explore the effects of interventions on sediment concentrations including sediment extraction from harbours, facilitating sediment deposition along marshes, and new wetland. In summary, these studies suggest that the estuary will deepen as a result of sea-level rise. The intertidal flats are expected to accrete, although not enough to compensate for sea-level rise. Under autonomous development this deepening is expected to enhance estuarine circulation but also further increase turbidity. The most effective reduction in turbidity (up to 50%) can be achieved through the extraction of mud from dredging, while a short-term reduction can be achieved through the construction of additional accommodation space. Measures to reduce turbidity in the estuary are expected to increase the primary production by phytoplankton by roughly the same order of magnitude as the reduction in turbidity. Benthic production is more complex as growth and production on the tidal flats is limited by nutrients. We are now increasingly realising that the expected acceleration of Sea Level Rise (SLR) further challenges sediment management. Although we may presently experience a sediment surplus (resulting in maintenance dredging and increasing turbidity), on the longer timescale (decades to centuries) SLR will likely create a sediment deficit. As a consequence, sustainable sediment management requires evaluation of restoration efforts on longer timescales. Therefore, our current understanding of how the ecosystem services in the estuary are changing on the long term (towards 2100) is limited.

We aim to advance our knowledge on the long-term impact of restoration efforts on ecosystem services by developing a numerical model that captures the sediment dynamics needed for the assessment on the effects of proposed NbS, while maintaining feasible computational times for simulations up to 2100. The main goal of the modelling of the Ems estuary is to predict how the proposed sediment management strategies in the EmsDollard2050 programme will contribute to biodiversity and ecosystem services in the estuary on the long-term.

6.2. Methods

6.2.1. Model

General approach

Many estuarine systems are expected to keep pace with sea level rise until a certain critical value after which they drown. Herin fine sediments deposit on the intertidal flats, which become supratidal marshes when sedimentation rates are sufficiently high. With our focus on NbS to restore muddy intertidal flats and reduce

turbidity, we only model muddy sediments. Ignoring the morphological contribution of sand prevents unpredictable and often erroneous development of sand-dominated tidal channels, hampering our prediction of the tidal flats. For this study it is assumed that major features governed by sand transport like tidal channels will not change significantly up to 2100, which is reasonable for a highly regulated estuary like the Ems.

Typically tides transport fine-grained sediments to the intertidal flats whereas waves occasionally erode sediments. A tide-only model therefore overpredicts sedimentation on the tidal flats. In order quantify both the natural balance between erosion and sedimentation, but also the effect of restoration efforts on wave damping and therefore sedimentation of mud, the hydrodynamics of the model is driven by tides, waves, and storm setup. Vegetation can establish during the simulation according to simple rules (see section Vegetation schematization) and influence the flows and wave action on the flats.

Computational domain

A Delft3D – Flexible Mesh model was developed to predict the impact of sediment management strategies and sea-level rise (small Ems in Figure 6-1). Boundary conditions for this smaller model were extracted from an intermediate-sized model developed by Schrijvershof et al. (2023) (Ems Large in Figure 6-1) using procedures described in greater detail hereafter. The hydrodynamic forcing of the large Ems model, i.e. tides and storm surges, was derived from the Dutch Continental Shelf Model (DCSM) (Zijl, Groenenboom, Laan & Zijlker, 2022). Wave forcing (i.e. wave height, period, and direction) was derived from a nearby observation buoy located at ~20 m water depth. The model covers the Ems estuary and includes the Wadden Sea from the island of Norderney (Germany) to the east to Ameland (Netherlands) to the west (Figure 6-1).
A smaller model is nested inside the estuary, with a seaward boundary at Eemshaven and a landward boundary at the lock near Herbrum (Germany) (Figure 6-1). This smaller model is forced with the tides and waves propagating through the Ems estuary mouth with the large model. The smaller model simulates the morphological response of muddy sediments under different measures (e.g. clay extraction) and sea-level rise scenarios.

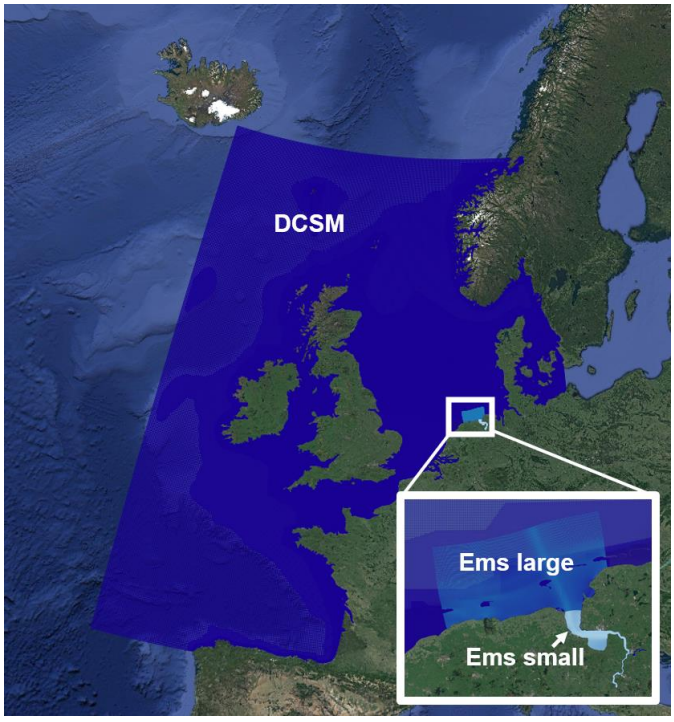

Figure 6-1 Modelling domains for the Ems model

Hydrodynamic schematization

Long-term simulations require idealised hydrodynamic forcing that can be repeated until 2100. The first simplification is to accelerate bed level changes. An efficient way to speed up the computational time of morphological models is by multiplying the change in bed level with a so-called morphological acceleration factor. As part of this study, we use a morphological acceleration factor of 24. This morphological acceleration influences the definition of the model boundaries, as evaluated below.

A synthetic spring-neap tidal cycle was constructed at the boundaries of the large Ems model from the DCSM model hindcast of the year 2018, following the procedure of Schrijvershof et al. (2023). The wave- wind climate was schematised into 12 representative wave-wind classes, following the procedure described by Walstra (2013). For each wave climate class a non-tidal residual is added to the model boundary in the smaller Ems model by correlating the wave and wind conditions to the observed storm surges in the past 10 years. Each spring-neap cycle each wave-wind class is applied in a random order to mimic natural variability in storm events. The discharge time-series of the Ems is compressed to fit within 14 days, to represent the annual discharge variation within a simulated morphological year. There is an intentional offset between the compressed discharge time series and the spring-neap cycle to avoid a systematic phase-relationship between peak discharge and the spring-neap cycle. The large Ems model was validated on the tidal movement, and the progression of surges and waves from local observation stations (see Schrijvershof, et al. (2023)).

Vegetation schematization

The effect of vegetation (such as salt marshes) is computed within the hydrodynamic and wave modules. According to the ecotope delineations in Bouma et al. (2005) areas with a maximum flow speed below 0.8 m/s and 300 or fewer inundations per year are considered low marsh, and less than 150 inundations per year characterize mid- to upper marshes. Every five morphological years (or five spring neap cycles in the model) the cells are updated with vegetation based on these rules. To avoid the large variance in estimating inundation times on a limited time series at low resolution, only mid- to upper marshes are schematised with vegetation during the morphological simulation. To determine the full ecotope maps that are used for determining the ESS in 2030, 2050 and 2100 separate hydrodynamic simulations were run to compute the number of inundations annually. Vegetation is modelled as trachytopes in the hydrodynamic module according to Baptist et al. (2007) while the interaction between vegetation and waves is schematised by the method of Mendez & Losada (2004).

Typical vegetation parameters for salt marshes are assumed as: stem density of 250 stems/m^2, stem diameter of 2.5 mm and stem height of 0.5 m. For the computiation of ESS in 2030, 2050, and 2100 where ectope maps are computded we refined these paremeters to better reflect the ecotopes present These from Vuik (2017) as measured at the end of the growing season when storms are most likely to occur. The vegetation parameters used are presented in Table 6-1.

Table 6-1 Schematisation of vegetation per EUNIS ecotope

EUNIS Code	Representative species	Vegetation height (cm)	Stem diameter (mm)	Stem density (n. of stems /m2)
MA225	Spartina anglica	47	3.3	232
MA224	Suaeda maritima	57	2.7	274
MA223 & MA222	Elymus athericus & repens	50	1.3	405

Mud transport and morphology

Long-term morphological simulations are executed with the small Ems model (Figure 6-1). Along the model boundary at the Wadden Sea near Eemshaven a constant sediment concentration is assumed (C_{in}) where mud flows in and out of the model. The mud dynamics are modelled by the approach presented by van Kessel *et. al* (2011), which is an extension of the classic Krone-Partheniades approach by simulating two, rather than a single, bed layers. The top layer (S_1) represents the fluffy unconsolidated top-layer of mud, which is easily resuspended on each tide. Beneath the fluff layer is a buffer layer (S_2) of more consolidated mud. Erosion fluxes of these layers (E_1, E_2) are modelled by:

$$E_1 = \min(M_0, m_1 M_1)\left(\frac{\tau}{\tau_{cr,1}} - 1\right) \quad (6.1)$$

$$E_2 = p_2 M_2 \left(\frac{\tau}{\tau_{cr,2}} - 1\right)^{1.5} \quad (6.2)$$

The parameters controlling erosion for layer S_1 are the mass of mud (m_1), the zeroth- and first-order erosion parameters (M_0, M_1), the critical bed shear stress ($\tau_{cr,1}$) and the applied bed shear stress (τ). The parameters controlling erosion for layer S_2 are the fraction of fines in the layer (p_2), the erosion rate parameter (M_2), the critical bed shear stress ($\tau_{cr,2}$).

The burial flux (B) from the fluff layer (S_1) to the buffer layer (S_2) is modelled as:

$$B = \min(B_0, m_1 B_1) \quad (6.3)$$

The mud deposition flux (D) to the fluff layer S_1 is modelled with the classical approach by Krone as:

$$D = \alpha w_s C \quad (6.4)$$

Here w_s is the sediment settling velocity, C is the sediment concentration, and α is a deposition efficiency factor. This efficiency factor parameterizes turbulence effects on floc size and therefore settling velocity which are not computed with a 2D model which does not compute turbulence nor flocculation. It effectively reduces the sediment settling velocity to account for the break-up of flocs in the shallow intertidal area as well as the greater importance of turbulence from wave and wind action at the surface when averaged across the water depth. The deposition is modulated with a sigmoid function from the water depth (h) and parameters k and h_0:

$$\alpha = \frac{1}{1 + e^{-k(h-h_0)}} \quad (6.5)$$

We used the calibration values of Smolders et al., (2020) developed for the Upper Scheldt ($k = 5$ and $h_0 = 1.5$), a system with comparable tidal dynamics, dimension, and sediments.

Another parameter compensating for processes not directly modelled is the wave stress reduction factor f_{τ_w}. The current model is only limited to a fluff and a buffered layer. However, mud consolidates further over time resulting in a build-up of strength and greater erosion resistance over depth. During storm events waves can erode enough mud to reach deeper consolidated mud layers. The effect of an increasing erosion resistance can be mimicked by reducing the effect of waves on the bed shear stress instead.

6.2.2. NbS measures and sea-level rise scenarios

Sea-level rise scenarios

The sea-level rise scenarios are adopted from the latest IPCC shared social economic pathways (ssp's) at the location of Delfzijl up to 2100 (Garner et al., 2021). The selected scenarios are a null sea-level rise scenario as a reference (ssp000), a moderate sea-level rise scenario (ssp245) representing business as usual, and a high-end sea-level rise scenario (ssp585) (Table 6-2).

Table 6-2 Median Sea-Level Rise Projections per shared social-economic pathway from Garner et al. (2021) for the location of Delfzijl, with 2020 as the year of reference and excluding vertical land motion.

Year	Sea-level rise scenario		
	ssp000	**ssp245**	**ssp585**
2020	+0.00 m	+0.00 m	+0.00 m
2030	+0.00 m	+0.12 m	+0.12 m
2050	+0.00 m	+0.24 m	+0.26 m
2100	+0.00 m	+0.58 m	+0.78 m

Implementation of measures

The measures modelled are: 1) the conversion of protected polder (Groote Polder) to 300 ha of intertidal area , 2) the construction of brushwood groynes to stimulate sediment deposition in the Dollard, and 3) the extraction of mud dredged from a) Delfzijl or b) the port of Emden and its approach channel (Figure 6-2). In addition, a reference scenario was modelled where no measures are implemented. Each measure is discussed in more detail below.

Table 6-3 Parameters used for simulating the mud dynamics in the DFM model of the Ems estuary.

Parameter	Description	Sediment fraction		
		Mud1	**Mud2**	**Mud3**
General:				
d_{sand,S_2}	Thickness of sand in layer S_2 $[m]$		0.3	
f_{τ_w}	Wave shear stress reduction factor [-]		0.4	
B_0	Zeroth order burial rate $[kgm^{-2}s^{-1}]$		$1.0*10^{-5}$	
B_1	First order burial rate $[s^{-1}]$		$1.5*10^{-7}$	
Mud specific:				
w_s	Sediment setling velocity $[mm/s]$	1.5	0.4	0.1
$\tau_{cr,1}$	Critical bed shear stress of layer S_1 $[Pa]$	0.2	0.2	0.2
$\tau_{cr,2}$	Critical bed shear stress of layer S_2 $[Pa]$	0.6	0.6	0.6
M_0	Zeroth order erosion parameter of layer S_1 $[kgm^{-2}s^{-1}]$	$3.0*10^{-3}$	$3.0*10^{-3}$	$3.0*10^{-3}$
M_1	First order erosion parameter of layer S_1 $[s^{-1}]$	$1.0*10^{-4}$	$1.0*10^{-4}$	$1.0*10^{-4}$
M_2	Erosion parameter of layer S_2 $[kgm^{-2}s^{-1}]$	$7.5*10^{-4}$	$7.5*10^{-4}$	$7.5*10^{-4}$
C_{in}	Sediment concentration at inflow boundary with Wadden Sea $[kg/m^3]$	$5*10^{-2}$	$5*10^{-2}$	$5*10^{-2}$

Groote Polder:

Groote Polder is 300 ha of polder that is in consideration to be reconnected to the estuary through a culvert in the existing dike. Plans with different extents of the polder being reconnected at different phases, with varying levels of tidal exchange, are still being explored. For this study we opted for the variant with the maximum extent (i.e. 300 ha) connected by the largest culvert considered (80 m wide) to facilitate tidal

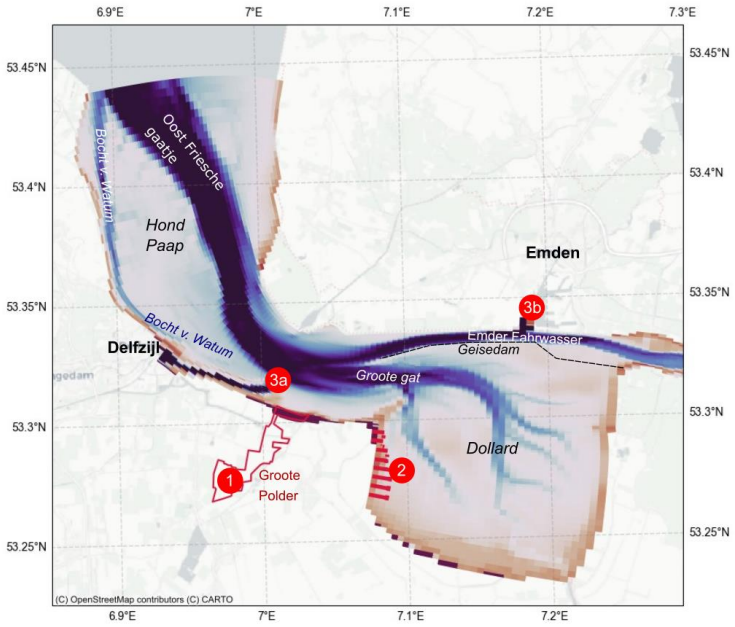

Figure 6-2 The Ems Dollard estuary including the 3 modelled measures: 1) a new intertidal area for inland sediment capture, 2) promoting local marsh accretion 3) re-use dredged mud from harbours at a) Delfzijl, and b) from Emden.

exchange. In doing so, the maximum potential of the measure is explored. To avoid abrupt morphological changes in the simulation, five years of initial development in Groote polder and the area adjacent to the culvert were simulated separately with only a sandy bottom to allow channels to form within the area. This new bathymetry was used in the subsequent long-term morphological simulations.

Brushwood groynes
Brushwood groynes are implemented as a grid of 400 x 400 m long groynes at the western side of the Dollard following the traditional way these groyne fields have been constructed in the past centuries to reclaim large parts of the North of the Netherlands (Dijkema et al., 2001). As such, this intervention is expected to promote expansion of salt marsh. These groynes are assumed to be permiable (no effect on flow), but these do act as obstacles for incoming waves (similar to the implentation by Siemes et al. (2020)).

Sediment extraction from Delfzijl and Emden
In the reference case sediment that is dredged from Delfzijl harbour is disposed outside of the harbour entrance. Sediment dredged form the Port of Emden is disposed in the nearby tidal channel (Oost Friesche gaatje, see Figure 6-2). For the sediment extraction scenarios this sediment is not disposed in the areas above but removed.

6.2.3. ESS quantification

The effect of each NbS measure is assessed for the short-term (2030), mid-term (2050) and long-term (2100) using ecosystem service delivery (ESS) metrics (Table 6-4). These metrics are either computed directly from the morphological model results or obtained from an additional hydrodynamic model simulation, where historic storm events are modelled concurrently with the risen sea-level per period (2030, 2050, or 2100).

Reduction flood risk
A reduction in flood risk is explored for the Ems-Dollard pilot site as a reduction in wave height during two sample storms: storm Xaver from December 2013 and storm Herwart from October 2017. Both these storms were simulated with the morphological changes and higher sea level belonging to the year and sea-level rise scenario of interest. The change in wave height relative to 2020 near the flood defences is used as the indicator for changes in flood risk.

Reduction coastal erosion

The pilot site of the Ems estuary comprises of channels, intertidal flats, and marshes. In such an area, where many square kilometres can be exposed or inundated depending on the tide, it is not insightful to consider the position of a single coastline as is customary for sandy beaches. Instead, for this pilot site we explore coastal erosion by comparing the vertical elevation change of an area to the change in mean sea level. For this we define four categories:

1. *eroding*:
   there is a net loss of sediment and a decrease in mean elevation,
2. *drowning*:
   there is a net gain of sediment but the increase in mean elevation is smaller than the increase in sea-level rise,
3. *stable*:
   there is a net gain of sediment and the increase in mean elevation is about equal (± 5 cm) to the increase in sea-level rise,
4. *accreting*:
   there is a net gain of sediment and the increase in mean elevation is greater than the increase in sea-level rise.

Climate change regulation

The carbon sequestration ecosystem service is assessed using an empirical relation between observed accretion rate and carbon sequestration. The relation, derived with data from Elschot et al. *(in prep*) is (see Figure 6-3):

Table 6-4 Overview of ecosystem services assessed in the Ems estuary

Ecosystem service	**Assessment**	
	Metric	**Method**
Reduction flood risk (RFR)	Wave height reduction by NbS compared to no NbS [m]	Storm simulation of storms Xaver (2013) and Herwart (2017)
Reduction coastal erosion (RCE)	Additional deposition with respect to sea-level rise compared to no NbS [m]	Morphological simulation
Climate change regulation (CCR)	Additional sequestered carbon by NbS [$kg/m^2/y$]	Morphological simulation + field data (Elschot, Willemsen, van Wesenbeeck, *in prep*)
Water purification (WP)	Reduction in mean suspended sediment concentration with NbS [mg/L]	Morphological simulation

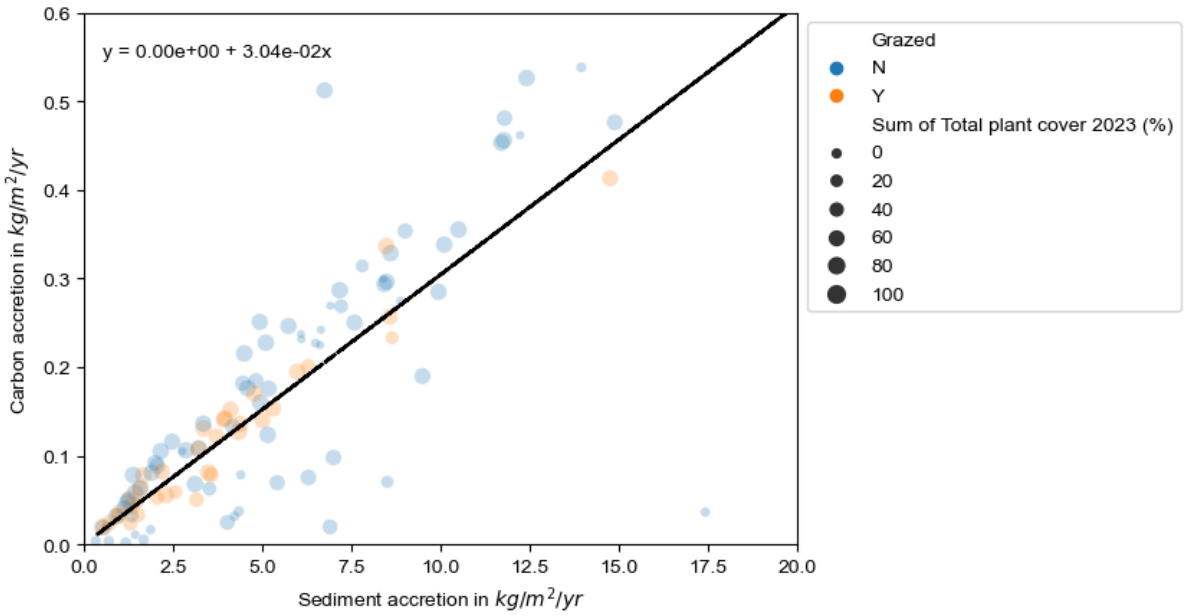

Figure 6-3 Relation between average sediment accretion and carbon accretion, including a linear regression used to convert computed sediment accretion to carbon sequestration.

$$S_{carbon} = 3.04 * 10^{-2} * S_{sed} \quad (6.6)$$

where S_{carbon} is the carbon accumulation rate and S_{sed} the sediment deposition rate.

A qualitative assessment of biodiversity was made by classifying the results of the morphological model into habitats based on the European Nature Information System (EUNIS), as described in Baptist et al. (2024) using the software D-Eco Impact (Weeber et al., 2024).

Water purification

The ecosystem service water purification has been interpreted as the change in average suspended sediment concentration at the study site. The measures aim to reduce turbidity by removing sediment from the water either by promoting natural deposition of sediment out of the water in dedicated areas (measures 1 and 2) or by active extraction of dredged sediment (measure 3). The sediment concentration is a direct result of the model. To account for variations and the morphological acceleration (one spring-neap tide represents one year), sediment concentrations are averaged for a period of five years (or five spring-neap cycles).

6.3. Results

6.3.1. Model calibration

Bed sediment composition

The model was calibrated against observed SSC, bed level changes, residual sediment fluxes and grain size distribution, with model settings of the calibrated model provided in Table 6-3. The model was run for one and a half years starting from a bed sediment composition consisting of 30 cm of sand, while mud supplied at the model boundaries. After about 36 years of morphological simulation, the model had reached a near-equilibrium between major import and export fluxes and thus the model does no longer produce significant

changes in areas with high or low mud content. At this point the computed mud distribution shows good agreement with the observed mud distribution (McLaren et al., 1998) – see Figure 6-4. The model reproduces areas of high and low mud content reasonably well; on the island of Hond-Paap the north-east to south-west gradient from sandy to muddy is reproduced, and there is high mud content (40 to 80%) along the edges of the of the Dollard.

The model does not capture the high mud content near the tidal channels in the centre of the Dollard and at the Geise dam. These are areas of pronounced resuspension by tides (channel) or waves (Geise Dam). Mud builds up during calm conditions and is eroded from the tidal flats during events with higher wind speeds and waves, releasing sediment into the water and contributing to high spikes in turbidity (Ridderinkhof et al., 2000). As reported by Elias *et al.* (2022), there is no trend for either erosion or deposition on the flats of the Dollard with elevation changes varying between erosion and deposition across periods. Owing to the schematisation of compressing a yearly wave climate within a spring-neap cycle (see Methods), mud deposited at flats exposed to waves is more regularly eroded and resuspended with limited time for mud to accumulate. In reality, storminess in the Dollard is seasonal leaving more time in between storms for mud to consolidate and build up. While the model approximates consolidation through the burial rate of mud from the weak fluff to the stronger buffer layer underneath, the randomly distributed storms forced each spring-neap cycle in the model make periods of sustained calm conditions with mud build-up and consolidation impossible, thereby resulting in no net accumulation of mud. Thus, when starting the model without initial mud, there is only a limited increase in the mud fraction at wave-exposed areas. Even though the model may be limited in reproducing the mud fraction on the tidal flats, the alternating build-up and release mud from the flats with limited net elevation changes matches the behaviour of the system.

Suspended sediment concentration

To validate the suspended sediment concentration (SSC) the (year-representative) concentrations predicted by the model the results are compared to field observations from Imares (Brinkman et al., 2014) and the EDoM campaign (van Maren et al., 2023). Suspended sediment observations from Imares consist of water samples taken at various dates from a vessel that were analysed in in a laboratory. In total samples were taken during 14 days in summer and 5 days in winter. During the EDoM campaign SSC was measured using various instruments such as a from a stationary boat, mooring chain, and fixed frames for 13 hours in January

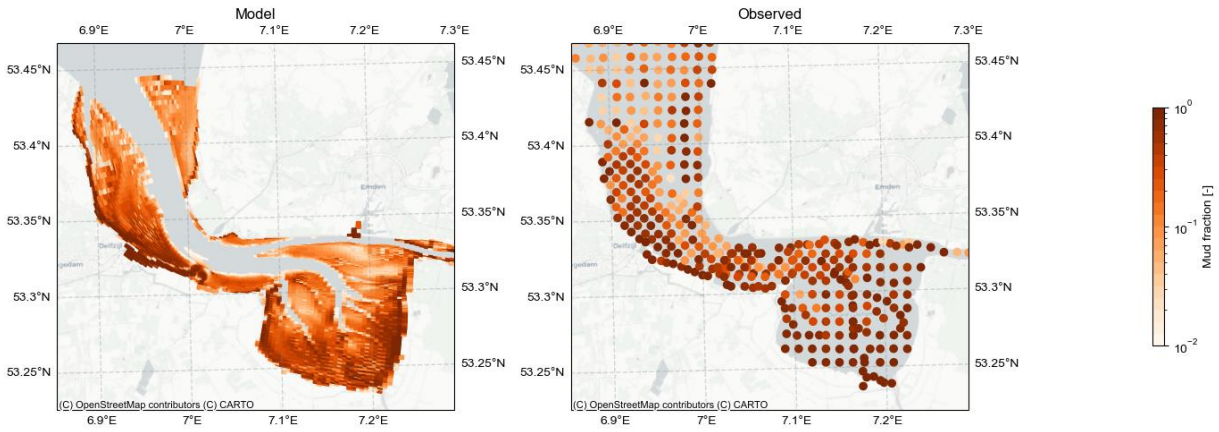

Figure 6-4 Distribution of the mud fraction, defined as defined as the volume fraction with a grain size smaller than 63 µm, modelled (left) and observed (McLaren et al., 1998) in the Dollard

and August. At the locations SB_EFW and SB_EMD SSC was measured during both periods at both the water surface and the bottom.

After calibration the model is able to reproduce the general pattern in suspended sediment concentration within the Ems estuary and Dollard (Figure 6-5). From the model boundary near Eemshaven the suspended sediment concentration is increasing towards lower Ems. The model is nevertheless able to reproduce average SSC within a range consistent with observations. Large spikes in SSC as observed in winter at SB_EMD cannot be reproduced within the model as the instantaneous SSC is highly influenced by processes not implemented in the 2D model such as flocculation, hindered settling, and the formation of a fluid mud layer near the bottom. A more extensive validation on SSC is not possible due the limited observations available.

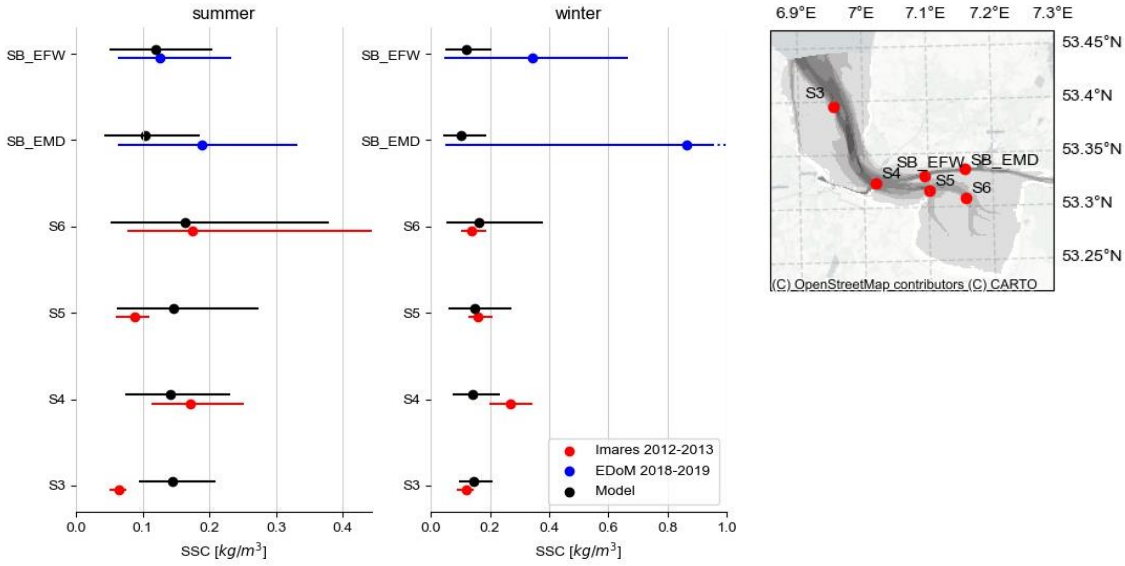

Figure 6-5 Comparison of suspended sediment concentration (SSC) as measured by Imares from 2012 and 2013 (red), the EDoM campaign from 2018-2019 (blue) in summer and winter, compared to the concentration in the model. The lines represent the 5% to 95% interval of observations during the days of the summer/winter campaign or values in the model, and the dots represent the average of the (modelled) period.

Sediment transport fluxes and sinks

Sediment fluxes predicted by the model are generally lower than those reported in literature (Figure 6-6 and Table 6-5). Most notable is the amount of sediment transported upstream the lower Ems River where the model predicts 0.1 million tons per year, strongly underestimating the actual up-estuary flux (Vroom et al. (2021) estimate this flux to be 1.0 to 1.5 million tons annually). However, the up-estuary flux in the lower Ems River is very difficult to reproduce – also with more complex 3D sediment transport models as developed by can Maren et al. (2015b). Major sediment pathways such the circulation of suspended sediment across the Geise dam (arrows 5 and 6 in Figure 6-6) observed in the EDoM campgain (van Maren, 2023) are reproduced by the model. Sediment accumulation in the marshes is captured remarkably well given the modelling limitations and the fact that deposition in these regions is primarily event driven. The Bocht van

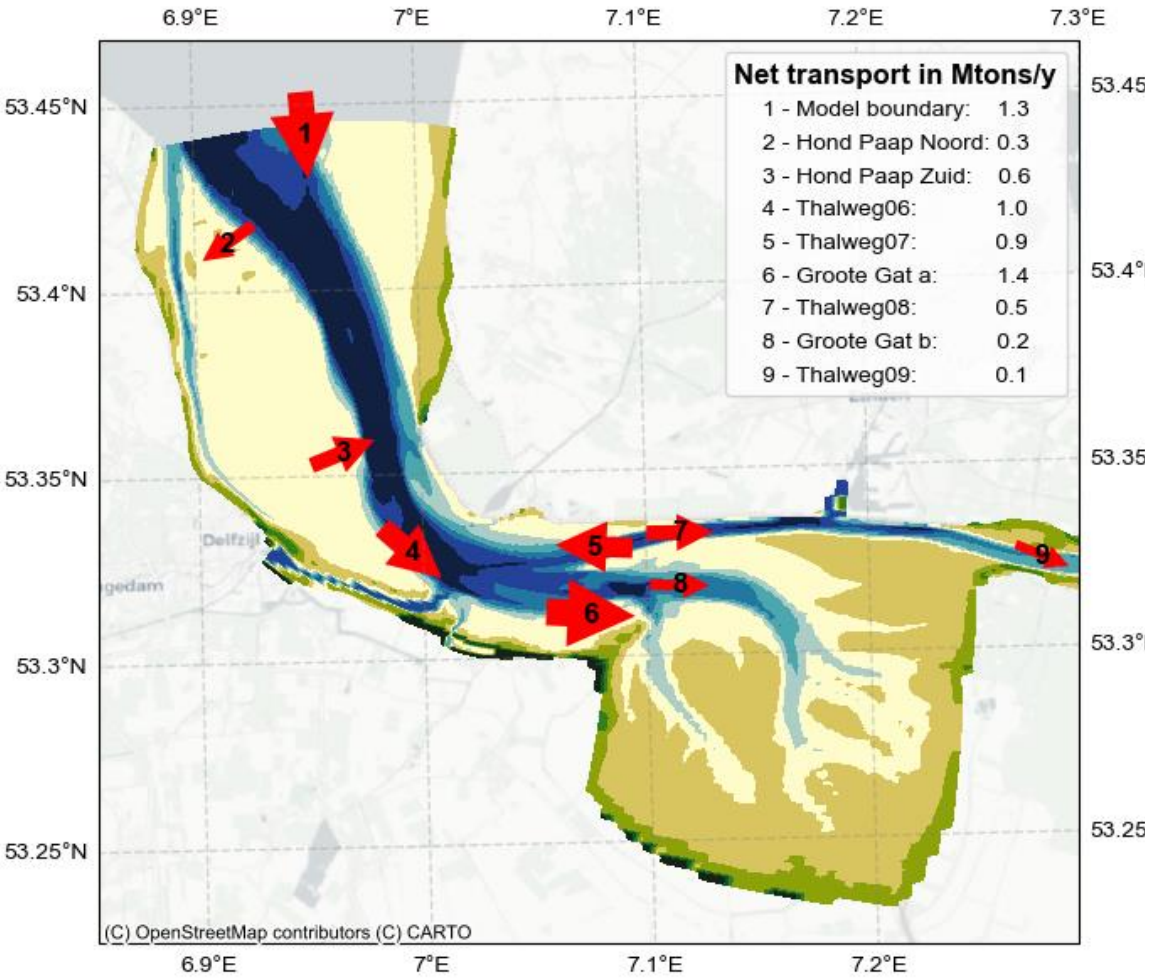

Figure 6-6 Net annual sediment fluxes computed by the model

Watum acts as a sediment sink in agreement with observations, although the net deposition is underestimated similarly to the amount of sediment dredged from the port of Delfzijl.

The general tendency of the model to underpredict fluxes and deposition may be the result of the schematisation of storms. Year-representative storm events are randomly distributed for each spring-neap cycle. Because of this, there is no prolonged (summer) period for sediment to accumulate in the (consolidated) underlayer. This may have also influenced the net fluxes as the seasonal interaction between net deposition in summer, and net erosion, is influenced by the seasonal river discharge of the Ems. Furthermore, it is known that net sediment fluxes differ across the water depth, with most of the upstream sediment transport occurring near the bottom. These vertical transport gradients are not captured in a depth-averaged model as used in this study. Yet, for morphological models (and especially simplified depth-averaged models) the modelled fluxes are within the right order of magnitude.

Table 6-5 Fluxes and sinks computed in the model compared with those reported in literature in million tons per year.

	Model	Reported	Source
Fluxes:			
Thalweg 06	1.0	≈4.0	van Maren (2023)
Thalweg 07	0.9	≈5.0	van Maren (2023)
Groote Gat (a)	1.4	≈6.0	van Maren (2023)
Thalweg 09	0.1	≈1.0-1.5	Vroom (2021)
Sinks:			
Bocht van Watum	0.38	≈0.6-1.0	van Maren (2023)
Dollard marshes (NL)	0.06	≈0.02-0.05	Cleveringa (2008)
Dollard marshes (GE)	0.09	≈0.004	Cleveringa (2008)
Dredging:			
Dredged at Delfzijl	0.3	≈0.8	Mulder (2013)

6.3.2. Autonomous development

The model predicts major changes as a result of sea-level rise by 2100 (Figure 6-7). The following major developments are projected in the absence of any restoration measures:

- The Bocht van Watum west of the island Hond-Paap is projected to fill in, continuing the trend observed in the past centuries (van Maren et al., 2016; Schrijvershof et al., 2024). This will eventually connect the southern part of the island to the mainland and facilitate salt marsh development. In contrast, the northern side of the island Hond-Paap is projected to become increasingly exposed resulting in net erosion.
- Within the model, at the current low level of sea-level rise, marshes are projected to expand slightly. However, with increasing SLR the marsh in the Dollard is paradoxically projected to expand rather than drown. This is related to the next point:
- Turbidity is projected to increase further towards 2100. The computed turbidity is increasing with sea-level rise, potentially doubling the average sediment concentration within the Dollard (Figure 6-9). This surplus of sediment translates into enhanced deposition within the model and the ability of marsh to grow in elevation beyond the rate of sea-level rise.

Aside from the second bullet, the autonomous changes reflect trends already observed for the Ems estuary. Turbidity levels have been steadily increasing during the past decades (van Maren et al., 2015b). One explanation for the rising turbidity has been the continued dredging of the main channels. The current modelling supports this hypothesis, although the mechanism is sea-level rise driven increase of the water depth. The larger water depth enhances the incoming flood tide from Eemshaven to Delfzijl, amplifying the tide and promoting sediment transport into the Dollard. This is further exacerbated by a growing tidal prism, as the shallow Dollard tidal flats inundate, increasing intertidal storage, necessitating an increased water (and sediment) exchange at the model boundary near Eemshaven. Within the model, fine sediment deposited on the flats remains easily erodible until sufficient time has passed for it to be buried and consolidate (modelled as a burial flux). Furthermore, the comparatively larger water depths on the flats with sea-level rise enable more wave action on the flats. The combination of these factors (increasing import of fine sediment, greater availability of fine erodible sediment, increasing wave action on tidal flats) results in a system where an increasing amount of fine sediment is recirculating within the Dollard as sea-level rise accelerates, thus increasing the turbidity.

The expansion of salt marshes in the Dollard is not in agreement with observations -most of the salt marshes are static. However, the conditions in most of the higher intertidal areas in the Dollard appear to be suitable for salt marsh colonization. Why the Dollard remains a mudflat rather than being partly converted to salt

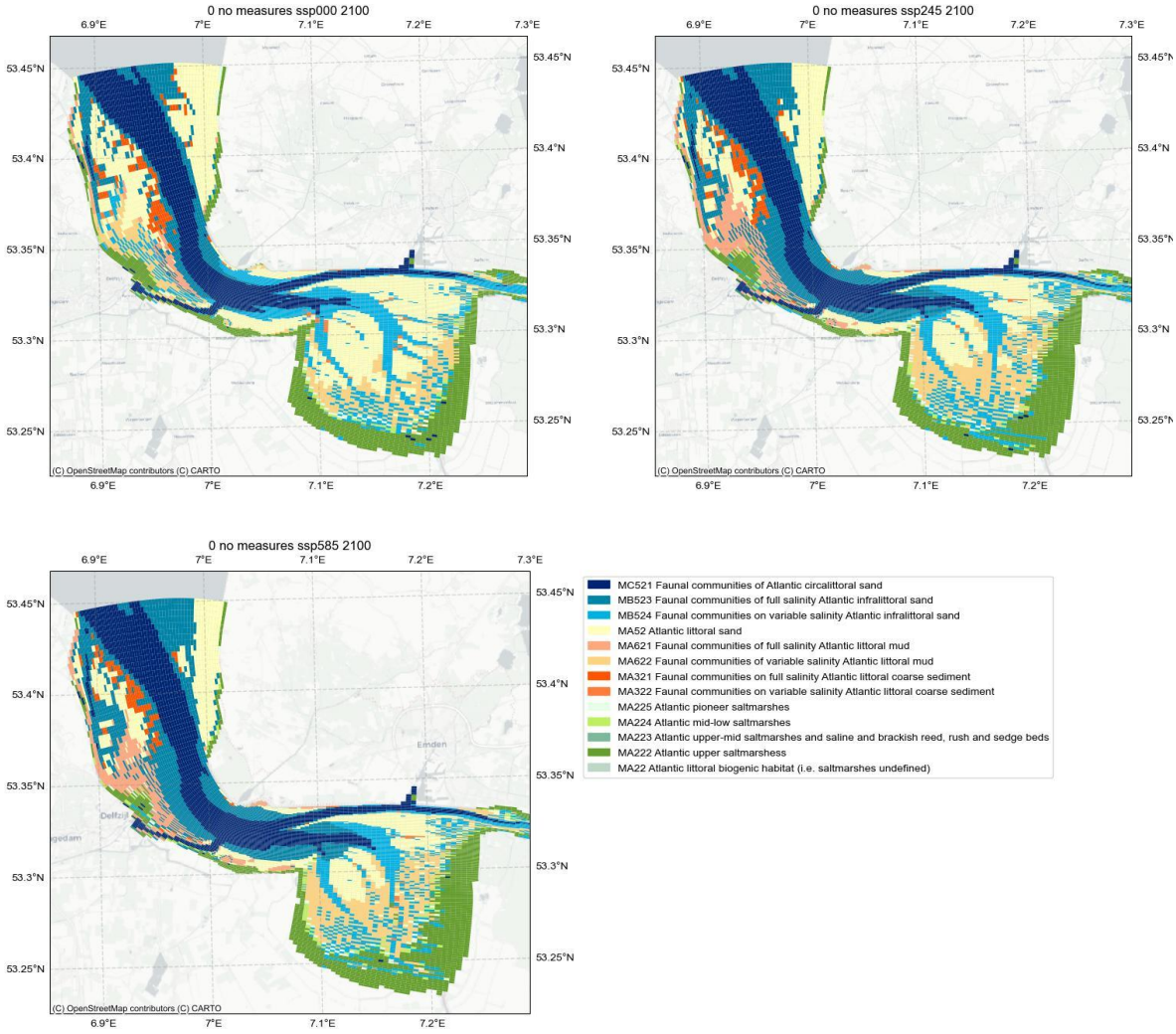

Figure 6-7 Projections of the development of ecotopes in Ems estuary by 2100, for projections without sea-level rise (ssp000), the middle sea-level rise scenario (ssp245) and the high sea-level rise scenario (ssp585).

marsh is presently not known. The tendency of the model to expand salt marsh area is therefore partly in line with expectations (though not observed in reality).

The only areas that facilitate deposition are the edges of the Dollard where salt marshes are present, as well as the infilling Bocht van Watum. The model projects that the marsh accretion facilitated by the increasing turbidity exceeds the rate of SLR. Therefore, for this particular site sea-level rise is projected to aid salt marsh development, rather than hinder it. This comes, however, with the caveat that the turbidity, which is already hampering the marine life at present levels, is increasing even further.

6.3.3. Reduction coastal erosion (RCE) with NbS measures

We apply categories for coastal erosion (eroding •, drowning •, stable •, and accreting • to geographic areas in the Ems estuary with roughly similar characteristics in accretion/erosion rate and cover (tidal flat or marsh) for the short-term (2030), mid-term (2050) and long-term (2100) developments with and without the implementation of the four NbS measures considered. These results are presented in Figure 6-8.

Measures that extract sediment from the estuary (measure 1 and 3) result in sediment losses. Without sea-level rise only the flats in the middle of the Dollard are affected by extraction. With sealevel rise extraction measures affect the south of Hond-Paap, the flats in the Dollard, and the southern salt marshes in the Dollard, which switch to a drowning or eroding state on the short and mid-term with sea-level rise. Surprisingly, the model projects an increase in turbidity on the long-term (with and without measures). The increase in turbidity compensates the effects of SLR on coastal erosion through an increase in available sediment. In contrast, extraction from Emden (measure 4) is projected to have no effect on the erosion state, presumably because too little sediment deposits in (and is therefore dredged from) from the port of Emden.

The measure promoting deposition (measure 2: brushwood groynes along the marshes in the western Dollard) increases the overall resilience to coastal erosion, specifically in the area where these NbS measured are applied. The effect is most pronounced on the short-term. As mentioned before, the autonomous development promotes expansion of salt marsh within the Dollard. Hence, on the mid- and long-term the benefits of the brushwood groynes become less pronounced.

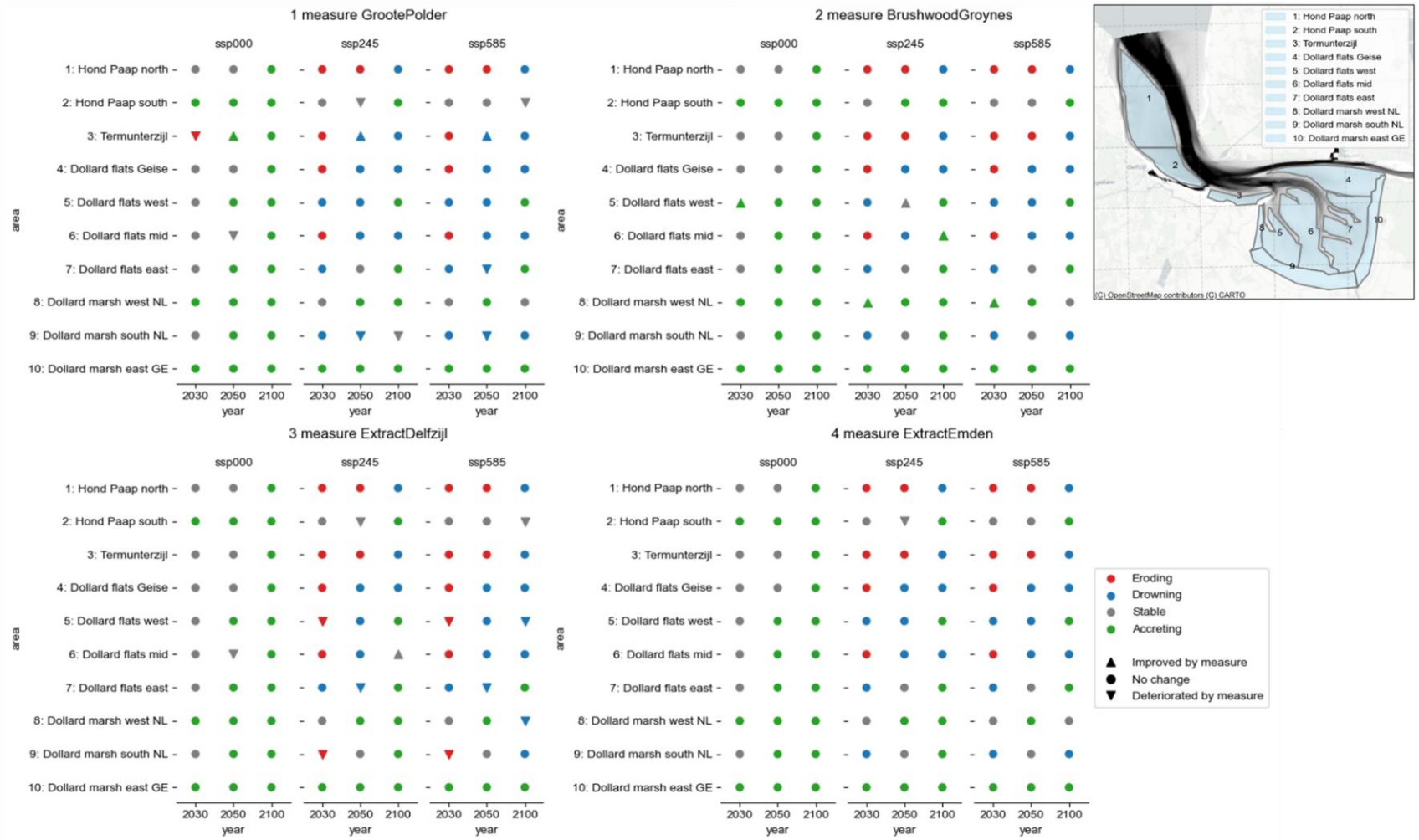

Figure 6-8 Effect of measures on coastal erosion for different areas in the Ems estuary, organised per year and climate scenario.

6.3.4. Water purification (WP) with NbS measures

The model predicts a strong rising turbidity trend, amplified by sea-level rise. A first glance at Figure 6-9 reveals that the magnitude of this process exceeds the capacity of all measures tested to regulate turbidity on the scale of the estuary. Trends across all measures show an increase in turbidity by 2100. Without sea-level rise (ssp000) the suspended sediment concentration within the Dollard is expected to increase by 25%, in scenario ssp585 the sediment concentration could almost double according to the model in 2100.

The NbS measures, however, do influence turbidity. Particularly the extraction of sediment from Delfzijl results in a decrease of suspended sediment between 10 and 20 km of the plotted transect in Figure 6-9 in 2030 compared to 2020. Similarly, the Groote Polder is a sufficient sediment sink in its initial years to prevent an increase in sediment concentrations up to 12.5 km of the transect. The other NbS measures (brushwood groynes in the western Dollard and extraction of sediment dredged at Emden) do not show a noticeable effect on suspended sediment concentrations.

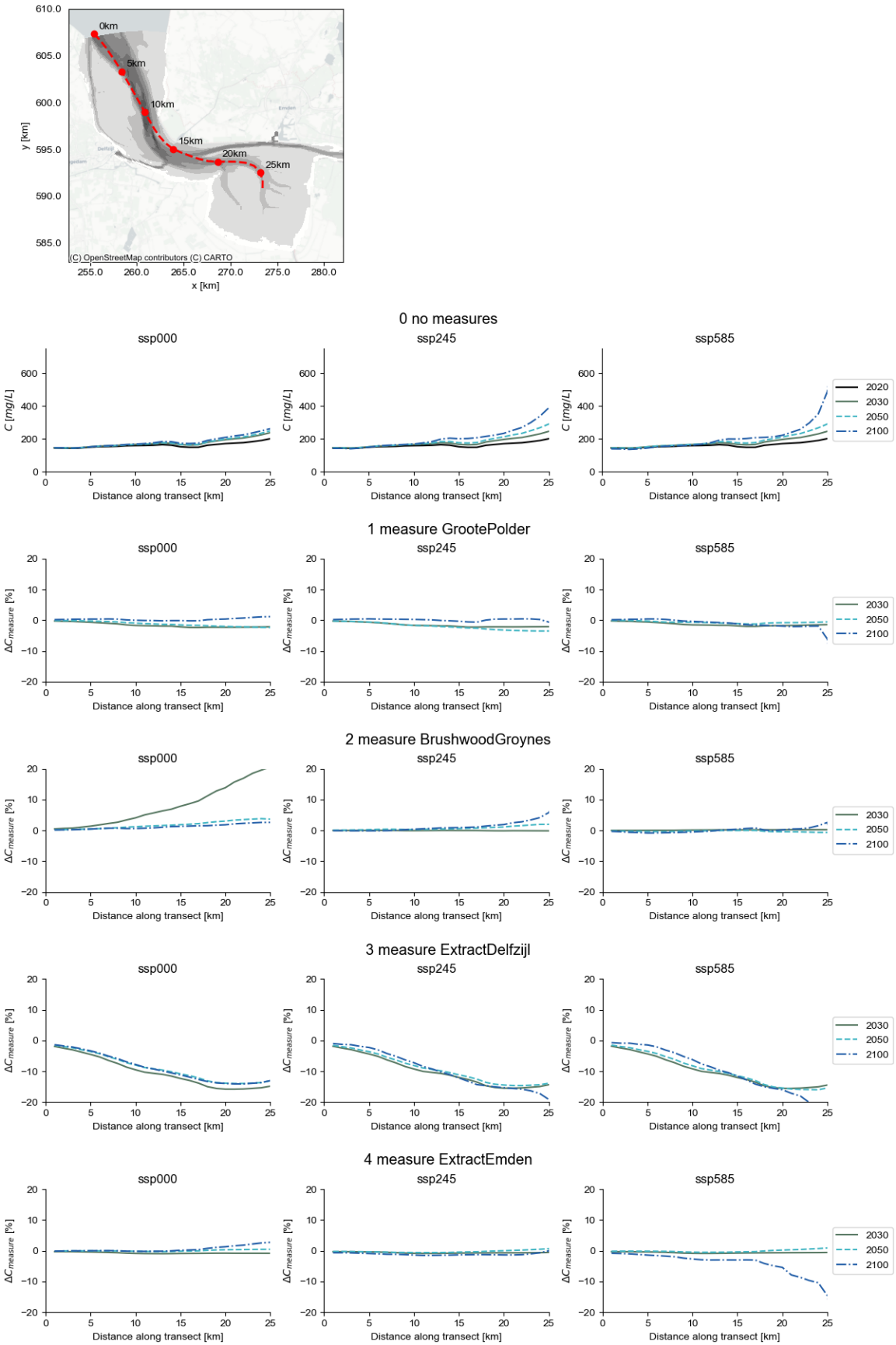

Figure 6-9 Along-estuary average suspended sediment concentration without measures, and the relative change in concentration due to each measure (ΔC) in 2030, 2050, and 2100 for three sea-level rise scenarios.

6.3.5. Climate change regulation (CCR) with NbS measures

The amount of carbon sequestration is inversely linked to the coastal erosion indicators (Figure 6-10) as both depend on bed level changes. However, the analysis of carbon sequestration is confined to the upper tidal zone where effects appear to be more local. For example, both the new intertidal area (Groote Polder) and the extraction of sediment at Delfzijl reduce carbon sequestration rates on the mid-term at the area "Delfzijl & Marconi" but the effect tapers down towards 2100. Similarly, applying brushwood groynes in the western Dollard enhances carbon sequestration on the short and mid-term across the Dollard, but only has a lasting positive effect near the brushwood groynes. The only measure with long term effects is sediment extraction at Delfzijl, resulting in a projected decrease in carbon sequestration within the Dollard of approximately 50 g/m^2/year.

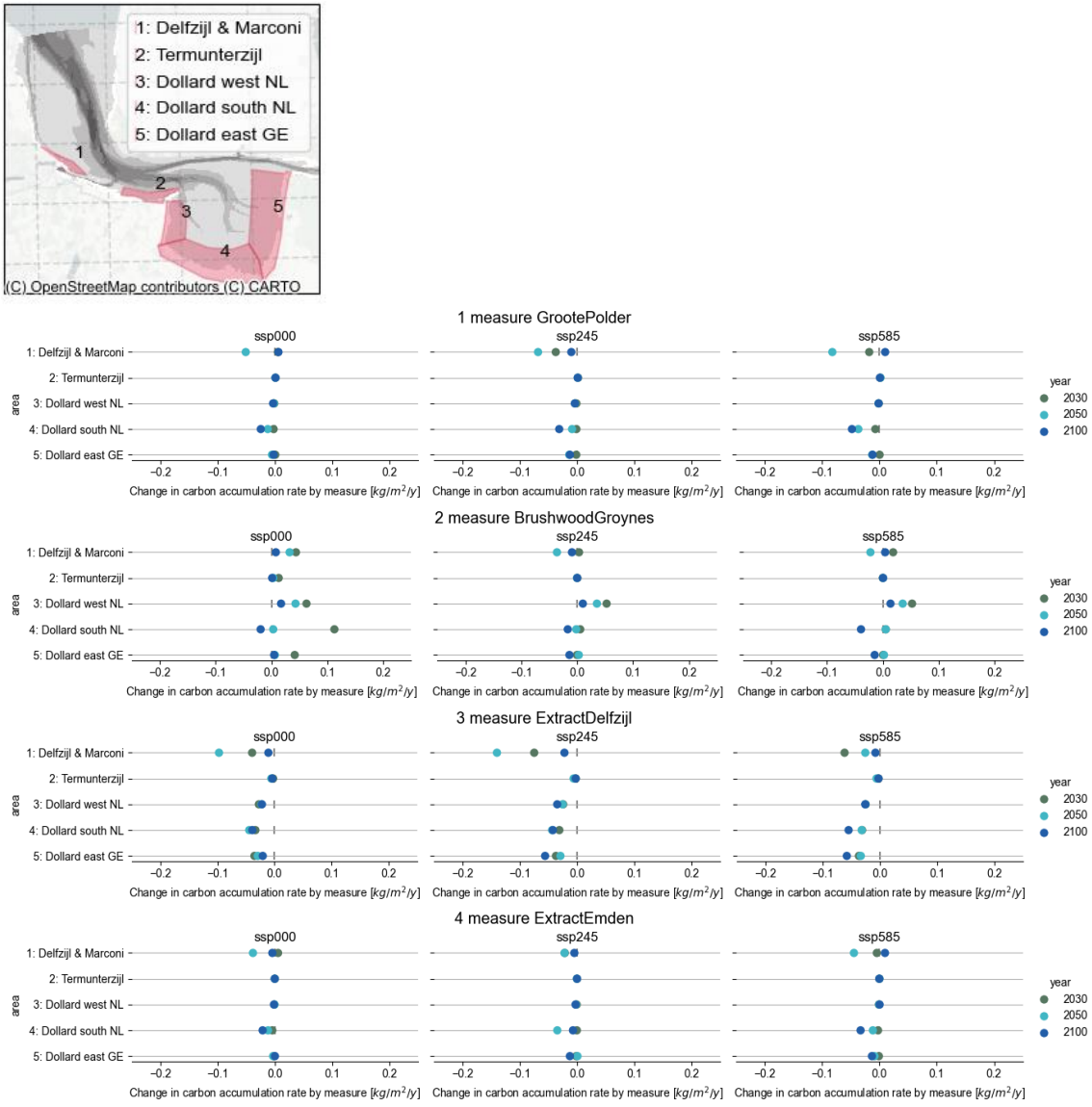

Figure 6-10 Relative change in carbon accretion rates between simulations without and without NbS measure, for 2030, 2050, and 2100 with no sea-level rise (ssp000), mid-sea-level rise (ssp245) and high sea-level rise (ssp585).

6.3.6. Reduction flood risk (RFR) by NbS measures

For brevity only the predicted flood risk reduction for 2100 during storm Herwart is discussed (shown in Figure 6-11), because the changes on the long term are most pronounced.

In the absence of sea-level rise (storm) wave heights are projected to decrease up up to 25 cm during storm Hewart as a result of autonomous morphological changes. These reductions result from the projected expansion of the salt marsh and the infilling of the Bocht van Watum. With sea-level rise, a consistent trend emerges across all scenarios. In general, the wave height is projected to increase most near Delfzijl, followed by the marshes in the south of the Dollard. The wave height decreases near areas with substantial salt marsh development (the eastern side of the Dollard and near the Bocht van Watum).

In addition to these general trends, several effects are uniquely tied to specific interventions. The new channel connecting the Groote polder with the Ems greatly increases wave exposure locally. In contrast, the brushwood groynes in the western Dollard contribute, as expected, to substantial reductions in wave heights in the western Dollard.

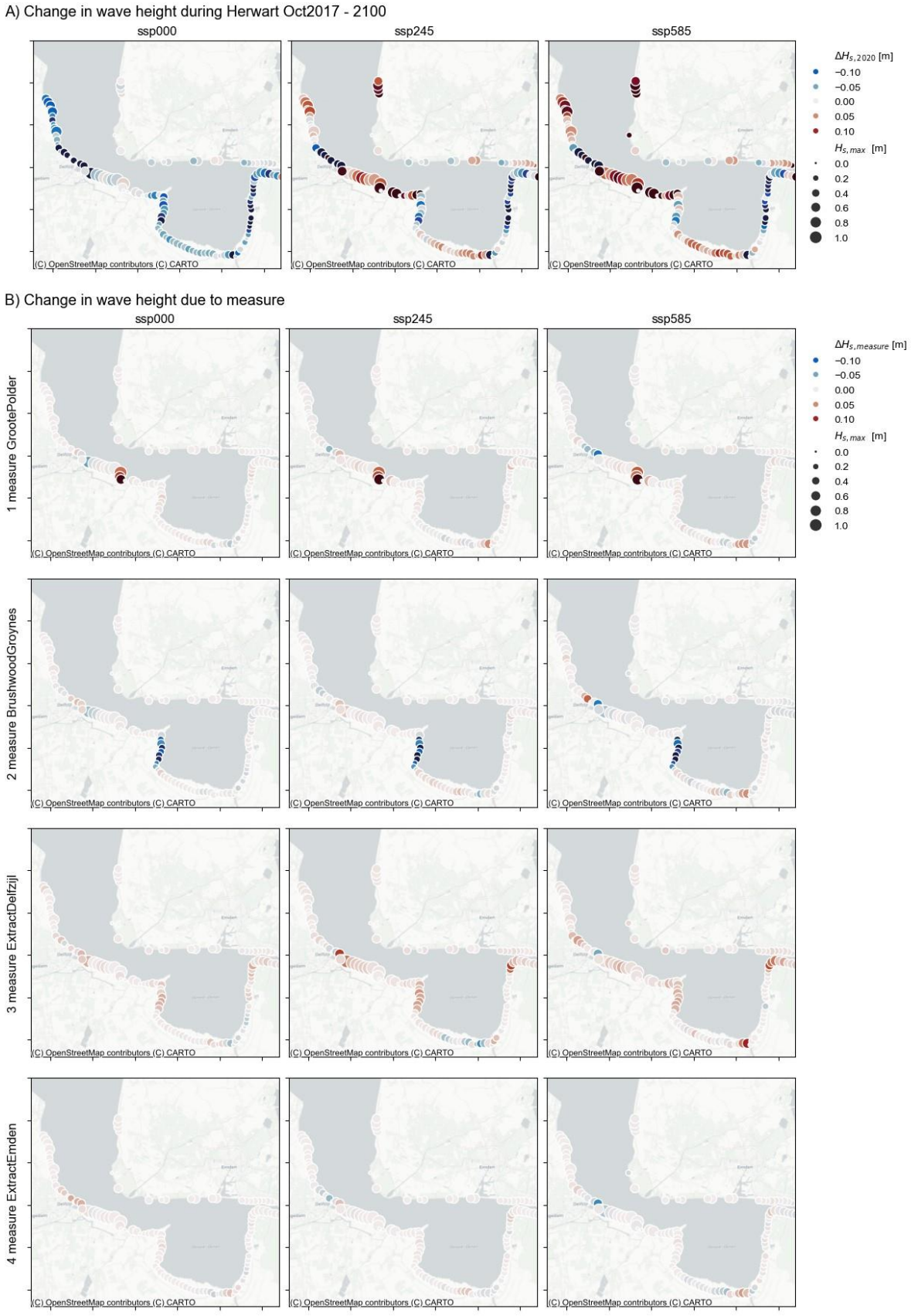

Figure 6-11 A) Change in wave height in 2100 compared to 2020 during storm Hewart at various sea-level rise scenarios and B) Change in wave height due to implemented measures in each sea level rise scenario

6.3.7. Changes in ecotopes with NbS measures

In general, the model predicts an overall steepening of the slopes within the Ems estuary, with expansion of the marsh and infralittoral zone at the expense of the littoral zone, even without sea-level rise (Figure 6-12). This trend of steepening becomes even more pronounced with sea-level rise. As expected, the Groote Polder measure adds new marsh area. More interesting is the fact that the with the brushwood groynes a noticeable expansion of marsh like in Groote Polder is projected. For the other measures (extraction at Delfzijl and Emden) no noticeable difference was found between ecotope distribution with and without these measures.

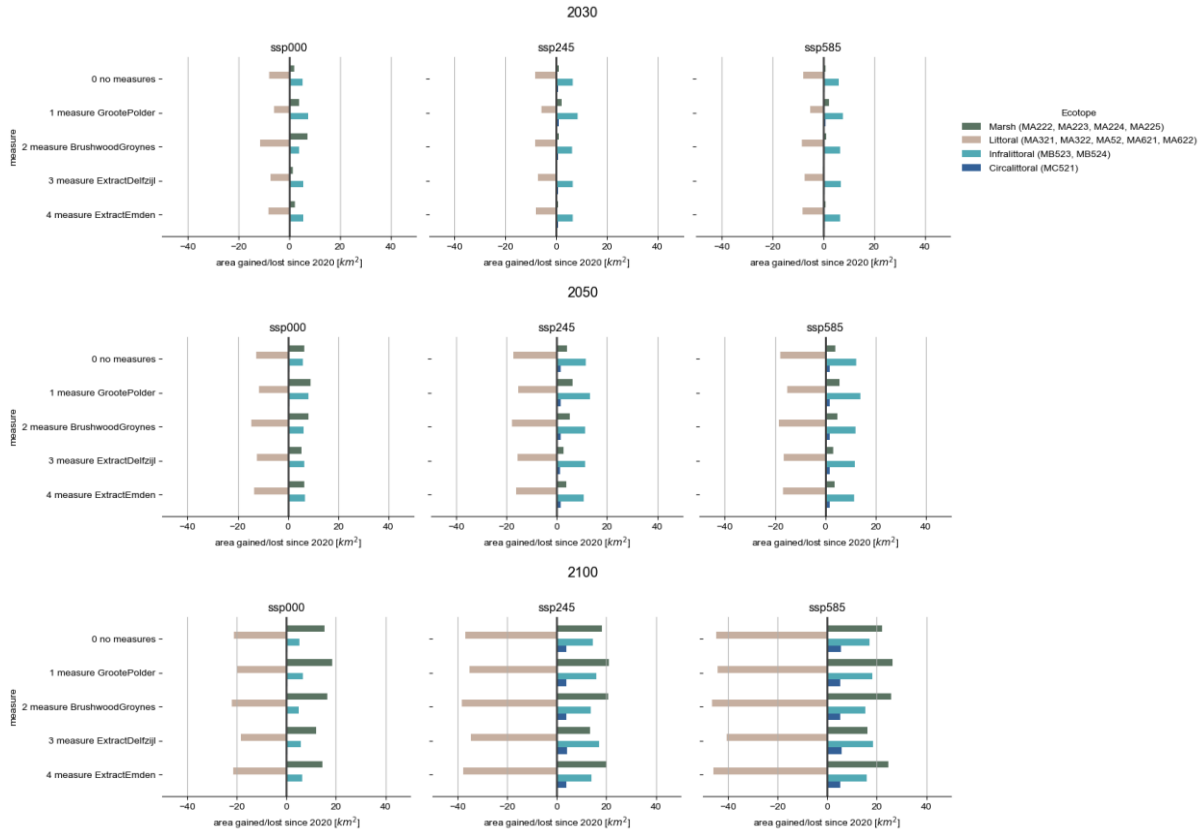

Figure 6-12 Changes in aggregated ecotopes per sea-level rise scenario and measure

6.4. Discussion

6.4.1. Limitations and uncertainties

The morphological Ems estuary model includes many relevant processes that shape the estuary (tides, waves, vegetation), but is at the same time constrained by the long duration of the required predictions (preventing the use of e.g. consolidation models or 3D hydrodynamics and restrict the model domain and numerical grid cell size). An important limitation herein is the limited model domain. The boundary for the morphological model is located near Eemshaven and assumes a constant sediment concentration of 150 mg/l. It was further assumed that this concentration will not change within the modelled period. As a result, there is no limitation to the amount of sediment that enters the model domain through this boundary. The computed sediment import increased from roughly 1 Mton / year to 5 Mton / year by 2100 for a scenario with high sea-level rise (ssp585). This amount is, most likely, (much) more than the Wadden Sea can provide. Around 15 million ton is estimated to annually deposit in the entire Dutch – German – Danish Wadden Sea (Colina Alonso et al.,

2024). It is unlikely that 1/3 of the total amount of available mud would deposit in the Ems Estuary. Even more, as this study suggests that the trapping of mud increases with SLR, the amount of mud depositing on the updrift tidal areas of the Dutch Wadden Sea may also increase. This could then lead to a reduction in fine sediment availability. What our model does suggest, is that the up-estuary transport capacity of the model will strongly increase as sea levels rise. Further study on the sediment fluxes in the Wadden Sea in conjunction with the effects of sea-level rise is required to corroborate the findings in this study.

Another source of uncertainty are the processes linked to the erosion, consolidation, and suspension of sediment within the Dollard. These processes determine how much sediment remains in the bed, and how much is recirculated contributing to the turbidity. In this study, a 2-layer bed-fluff model was implemented (Van Kessel et al., 2011), with the burial from weak fluff to the underlayer acting as both burial and a form of consolidation. Scaling of the wave-induced bed shear stress acted as a correction factor for mass-erosion by waves in deeper consolidated layers versus shallower surface erosion by tides. Ideally a more sophisticated model should be used to capture the strengthening of the bed by consolidation, thereby fixating sediment in the bottom, and resuspension by tides and waves. However, such algorithms (e.g. by Winterwerp et al. (2018)) are computationally intensive for long-term morphodynamic simulations.

6.4.2. Projection of coastal hazards and ecosystem services

The simulated projections of ESS change allow to re-evaluate the hazards faced in the project area. Contrary to expectations from earlier 1D-modelling studies (Kirwan et al., 2016; Marijnissen et al., 2020; Elschot et al., 2023), this 2D model projects increasing seaward marsh expansion for scenarios with higher sea-level rise, rather than degradation or eventual drowning in extreme sea-level rise scenarios. The reason for these counter-intuitive results is a strong increase in turbidity and sediment availability with sea-level rise projected by the model, to a degree that was not considered in earlier studies. The strong increase in sediment availability for marshes in the Dollard arises from a combination of factors: 1) a projected increase in sediment import arising from (a) the relative deepening of the main channels amplifying tides up to Delfzijl as well as (b) an increased tidal prism of the Dollard, 2) an enhanced deposition of fine unconsolidated material on the tidal flats and 3) a lowering of the flats relative to the mean sea-level resulting in more wave exposure and resuspension of these accumulated fines. Consequently, hazards such as flooding and coastal erosion are mitigated by the projected increase in deposition leading to increased marsh expansion with sea-level rise. The downside is a continued trend of deteriorating water quality due to the increase in turbidity. Previous studies have already found that the turbidity at present levels is limiting the primary production in the waters of the estuary (Brinkman et al., 2014; Brinkman & Jacobs, 2023). Hence, turbidity may become an even greater hazard in the future according to the model projections.

6.4.3. Effectiveness of NbS restoration measures

The model projects that the impact of the simulated NbS measures is limited compared to the autonomous long-term trends, especially in scenarios with sea-level rise. The Dollard is projected to increase in turbidity even without sea level rise, albeit at a slower rate than with sea-level rise. This result is in line with previous studies suggesting the system is still adapting to past interventions such as the loss of intertidal flats and the structural deepening of channels by dredging van (van Maren et al., 2016). The limited effectiveness of the NbS tested in this study is therefore not necessarily related to the measures themselves but reflect the strong autonomous morphological trends in the Dollard and Ems Estuary.

Despite the strong autonomous trends, some benefits from the simulated measures can still be observed. The measure Groote polder, which creates new wetland by reconnecting a polder back to the sea, is the measure with the most additional biotopes compared to the other simulations. Furthermore, it does reduce turbidity slightly on the short- and midterm by a couple of percent compared to the situation without the

measure. The limitation of the measure is that it does not prevent the increased import of sediment, nor does it prevent sediment from being recirculated within the Dollard, which are the main drivers of the rising turbidity within the model.

The brushwood groynes measure is highly effective facilitating marsh growth locally. From 2030 to 2050 the area enclosed by the groynes has been converted to salt marsh, boosting local carbon sequestration and reducing flood risk. However, the effect of the brushwood groynes on a large scale is relatively small and so it has a only a limited effect on the long-term trends in the estuary.

The effect of extraction of sediment was found to be highly area specific. Extraction from Delfzijl is effective in reducing turbidity compared to the autonomous trends, reducing turbidity by upwards of 25%. However, extraction of sediment dredged near Emden was found to have no substantial effect of turbidity levels. Presumably less sediment deposits in the harbour of Emden compared to Delfzijl and material currently dumped outside of the harbour of Delfzijl has a high likelihood of being transported into the Dollard.

6.4.4. Implications for adaptation strategies

The results show ESS are highly dependent on the local context. Many studies on ESS from NbS are available where different measures (e.g. salt marsh restoration) are quantified for their ecosystem services outside of the context of drastic long-term morphological shifts, e.g. Barbier et al. (2011); Van Coppenolle et al. (2018); Vuik et al. (2019). This is important to understand the mechanisms through which NbS measures provide ESS, such as flood risk reduction. However, when also accounting for sea-level rise in morphologically dynamic areas such as the Ems estuary, morphological adaptation needs to be included.

The predicted impact of restoration efforts is useful for developing adaptation strategies for areas where morphological feedbacks are important. A major factor controlling turbidity in the model is the circulation of mud depositing on the tidal flats during calm conditions, followed by erosion and channel deposition during more energetic periods wave resuspension. Calm areas where prolonged deposition of this mobile sediment may settle (e.g. the marshes) are only limitedly present in the Ems estuary. The adaptation measures considered in this study aim at limiting the suspended sediment concentration through sediment extraction from harbours or facilitating additional deposition. This study provides quantitative insights into the longevity of such measures, with Groote polder and brushwood groynes obviously becoming less effective in time as they fill up with sediments. As such trapping scenarios are effective on the short- and mid-term but require maintenance on the long term. On the long term, the predicted effect of SLR is a substantial increase of SSC, to the point that even with sediment extraction strategies the SSC may increase.

Our model results suggest the following adaptation strategies for the Ems Estuary. 1) The Dollard is allowed to continue its natural trend of rising turbidity, infilling of the remaining calm areas, and salt marsh expansion with additional ESS in flood risk reduction and carbon sequestration at the expense of water quality. Such a strategy may be facilitated with brushwood groyne structures. Or, 2) the alternative would be to actively create new calm areas such as Groote Polder on a larger scale than currently considered.

6.5. Conclusion

We have developed a model to compute the autonomous morphological trends in the Ems Estuary with and without SLR, and with measures primarily mitigating the high SSC in the estuary. The model projects a pronounced increase in the turbidity of the Ems estuary, and Dollard in particular, by the year 2100. This increase results from sea-level rise due to an increasing tidal prism (and therefore sediment import), an increased availability of readily erodible sediment on the flats, and increased exposure of the flats to waves. Under these developments water quality may deteriorate. The salt marshes are, however, expected to benefit from the rise in turbidity, expanding further into the Dollard with higher rates of sea-level rise. A

weakness of the model herein is that it assumes a larger transport of mud from the Wadden than realistically available. Therefore, the effect of SLR is that the up-estuary transport capacity will increase, but not necessarily the actual turbidity (at least not in quantities predicted by the model).

The NbS measures prove useful on the short- to mid-term. Extraction of sediment from the harbour at Delfzijl limits the increase in turbidity, the brushwood groynes locally enhance the development of salt marshes, and Groote Polder becomes a new wetland. The predicted long-term effects are small relative to the predicted autonomous trend, but this autonomous trend is probably flawed by overestimation of sediment availability. Further study is required into especially the projected future availability of fine-grained sediments and impact thereof on the effectiveness of restoration efforts.

6.6. References

Baptist, M. J., Babovic, V., Rodríguez Uthurburu, J., Keijzer, M., Uittenbogaard, R. E., Mynett, A., & Verwey, A. (2007). On inducing equations for vegetation resistance. *Journal of Hydraulic Research*, *45*(4), 435–450. https://doi.org/10.1080/00221686.2007.9521778

Baptist, M., Marijnissen, R., Różyński, G., Musumeci, R. E., Marino, M., Borzi, L., Stefano, A. di, Jolivet, M., Stocco, A., Horneman, F., Rova, S., Torresan, S., Furlan, E., Dabalà, C., Coccon, F., Critto, A., Pranovi, F., Bertomeu, F., Ibáñez, C., … Cognat, M. (2024). D4.1 Scorecard methodology (tool) for coastal system restoration effects on ESS and BDV. *ARPHA Preprints, 5*, e128550. https://doi.org/10.3897/arphapreprints.e128550

Barbier, E. B., Hacker, S. D., Kennedy, C., Koch, E. W., Stier, A. C., & Silliman, B. R. (2011). The value of estuarine and coastal ecosystem services. *Ecological Monographs*, *81*(2), 169–193. https://doi.org/10.1890/10-1510.1

Benninghoff, M., & Winter, C. (2019). Recent morphologic evolution of the German Wadden Sea. *Scientific Reports*, *9*(1), 9293. https://doi.org/10.1038/s41598-019-45683-1

Brinkman, A. G., & Jacobs, P. (2023). Gross pelagic primary production in the Ems-Dollard estuary. *Journal of Sea Research*, *192*, 102362. https://doi.org/10.1016/j.seares.2023.102362

Brinkman, A. G., Riegman, R., Jacobs, P., Kuhn, S., & Meijboom, A. (2014). *Ems Dollard primary production research, full data report* (IMARES Report C160/14; p. 2080). IMARES Wageningen UR.

Cleveringa, J. (2008). *Ontwikkeling sedimentvolume Eems-Dollard en het Groninger wad, Overzicht van de beschikbare kennis en gegevens* (A2269). Alkyon.

Colina Alonso, A., van Maren, D. S., Oost, A. P., Esselink, P., Lepper, R., Kösters, F., Bartholdy, J., Bijleveld, A. I., & Wang, Z. B. (2024). A mud budget of the Wadden Sea and its implications for sediment management. *Communications Earth & Environment*, *5*(1), 1–9. https://doi.org/10.1038/s43247-024-01315-9

Dijkema, K., Nicolai, A., de Vlas, J., Smit, C., Jongerius, H., & Nauta, H. (2001). Van landaanwinning naar kwelderwerken. *ISBN 9036935830*. https://repository.tudelft.nl/islandora/object/uuid%3Af4f2b66d-4164-48da-87e7-e79c7619b6ce

Dijkstra, Y. M., Schuttelaars, Henk. M., & Schramkowski, G. P. (2019). A Regime Shift From Low to High Sediment Concentrations in a Tide-Dominated Estuary. *Geophysical Research Letters*, *46*(8), 4338–4345. https://doi.org/10.1029/2019GL082302

Elias, E., Alonso, A. C., & van Maren, B. (2022). *Morfologische veranderingen Eems-Dollard en Groninger Wad* (11203742-000-ZKS-0003,; p. 144). Deltares.

Elschot, K., Baptist, M. J., & van Puijenbroek, M. E. B. (2023). Biocompacting livestock accelerate drowning of tidal salt marshes with sea level rise. *Frontiers in Marine Science*, *10*. https://doi.org/10.3389/fmars.2023.1129811

Elschot, K., Willemsen, P., & van Wesenbeeck, B. (*in prep*). *In situ Carbon measurements in the Wadden Sea pilot*.

Garner, G. G., Hermans, T., Kopp, R. E., Slangen, A. B. A., Edwards, T. L., Levermann, A., Nowicki, S., Palmer, M. D., Smith, C., Fox-Kemper, B., Hewitt, H. T., Xiao, C., Aðalgeirsdóttir, G., Drijfhout, S. S., Golledge, N. R., Hemer, M., Krinner, G., Mix, A., Notz, D., … Pearson, B. (2021). *IPCC AR6 Sea Level Projections* (Version 20210809) [Dataset]. Zenodo. https://doi.org/10.5281/zenodo.6382554

Kirwan, M. L., Temmerman, S., Skeehan, E. E., Guntenspergen, G. R., & Fagherazzi, S. (2016). Overestimation of marsh vulnerability to sea level rise. *Nature Climate Change*, *6*(3), 253–260. https://doi.org/10.1038/nclimate2909

Marijnissen, R., Esselink, P., Kok, M., Kroeze, C., & van Loon-Steensma, J. M. (2020). How natural processes contribute to flood protection—A sustainable adaptation scheme for a wide green dike. *Science of The Total Environment*, *739*, 139698. https://doi.org/10.1016/j.scitotenv.2020.139698

McLaren, P., Steyaert, F., & Powys, R. (1998). Sediment transport studies in the tidal basins of the Dutch Waddenzee. *Senckenbergiana Maritima*, *29*(1), 53–61. https://doi.org/10.1007/BF03043943

Mendez, F. J., & Losada, I. J. (2004). An empirical model to estimate the propagation of random breaking and nonbreaking waves over vegetation fields. *Coastal Engineering*, *51*(2), 103–118. https://doi.org/10.1016/j.coastaleng.2003.11.003

Mulder, H. P. J. (2013). *Dredging volumes in the Ems-Dollard estuary for the period 1960-2011* (Unpublished report). Dutch Ministry of Public Works.

Provincie Groningen, & Ministerie van Infrastructuur en Milieu. (2018). *Programma Eems-Dollard 2050*. Provincie Groningen.

Ridderinkhof, H., van der Ham, R., & van der Lee, W. (2000). Temporal variations in concentration and transport of suspended sediments in a channel–flat system in the Ems-Dollard estuary. *Continental Shelf Research*, *20*(12), 1479–1493. https://doi.org/10.1016/S0278-4343(00)00033-9

Schrijvershof, R. A., van Maren, D. S., Torfs, P. J. J. F., & Hoitink, A. J. F. (2023). A Synthetic Spring-Neap Tidal Cycle for Long-Term Morphodynamic Models. *Journal of Geophysical Research: Earth Surface*, *128*(3), e2022JF006799. https://doi.org/10.1029/2022JF006799

Schrijvershof, R., Maren, D. S. V., Wegen, M. V. D., & Hoitink, A. J. F. (Ton). (2024). Land Reclamation Controls on Multi-Centennial Estuarine Evolution. https://doi.org/10.22541/essoar.171405335.56595430/v1

Siemes, R. W. A., Borsje, B. W., Daggenvoorde, R. J., & Hulscher, S. J. M. H. (2020). Artificial Structures Steer Morphological Development of Salt Marshes: A Model Study. *Journal of Marine Science and Engineering*, *8*(5), Article 5. https://doi.org/10.3390/jmse8050326

Smolders, S., Bi, Q., Vanlede, J., De Maerschalck, B., Plancke, Y., & Mostaert, F. (2020). Integraal plan Boven-Zeeschelde: Sub report 6. Scaldis mud: a mud transport model for the Scheldt estuary. *FHR Reports*. https://www.waterbouwkundiglaboratorium.be/nl/publicaties/open-wl-archief-owa

Spiteri, C., Maren, B. van, Kessel, T. van, & Dijkstra, J. (2011). Effect Chain Modelling to Support Ems-Dollard Management. *Journal of Coastal Research*, *61 (10061)*, 226–233. https://doi.org/10.2112/SI61-001.19

van Duyl, F. C., Winder, B. de, Kop, A. J., & Wollenzien, U. (2000). Consequences of diatom mat erosion for carbohydrate concentrations and heterotrophic bacterial activities in intertidal sediments of the Ems-Dollard estuary. *Continental Shelf Research*, *20*(10), 1335–1349. https://doi.org/10.1016/S0278-4343(00)00026-1

Van Coppenolle, R., Schwarz, C., & Temmerman, S. (2018). Contribution of Mangroves and Salt Marshes to Nature-Based Mitigation of Coastal Flood Risks in Major Deltas of the World. *Estuaries and Coasts*, *41*(6), 1699–1711. https://doi.org/10.1007/s12237-018-0394-7

Van Kessel, T., Winterwerp, H., Van Prooijen, B., Van Ledden, M., & Borst, W. (2011). Modelling the seasonal dynamics of SPM with a simple algorithm for the buffering of fines in a sandy seabed. *Continental Shelf Research*, *31*(10, Supplement), S124–S134. https://doi.org/10.1016/j.csr.2010.04.008

van Leussen, W. (2011). Macroflocs, fine-grained sediment transports, and their longitudinal variations in the Ems Estuary. *Ocean Dynamics*, *61*(2), 387–401. https://doi.org/10.1007/s10236-011-0384-9

van Maren, B., Stolte, W., Sittoni, L., Vroom, J., Arents, L., & de Kluijver, A. (2015a). *Mud dynamics in the Ems-Dollard, phase 2* (1205711–001). https://publications.deltares.nl/1205711_001b.pdf

van Maren, D.S., van Kessel, T., Cronin, K., Sittoni, L. (2015b). The impact of channel deepening and dredging on estuarine sediment concentration. Continental Shelf Research 95, p. 1-14 http://dx.doi.org/10.1016/j.csr.2014.12.010.

van Maren, D. S., Maushake, C., Mol, J.-W., van Keulen, D., Jürges, J., Vroom, J., Schuttelaars, H., Gerkema, T., Schulz, K., Badewien, T. H., Gerriets, M., Engels, A., Wurpts, A., Oberrecht, D., Manning, A. J., Bailey, T., Ross, L., Mohrholz, V., Horemans, D. M. L., … Dankers, P. J. T. (2023). Synoptic observations of sediment transport and exchange mechanisms in the turbid Ems Estuary: The EDoM campaign. *Earth System Science Data*, *15*(1), 53–73. https://doi.org/10.5194/essd-15-53-2023

van Maren, D. S., Oost, A. P., Wang, Z. B., & Vos, P. C. (2016). The effect of land reclamations and sediment extraction on the suspended sediment concentration in the Ems Estuary. *Marine Geology*, *376*, 147–157. https://doi.org/10.1016/j.margeo.2016.03.007https://doi.org/10.1016/j.margeo.2016.03.007

Van Maren, D. S., Schrijvershof, R., Smits, B., Cronin, K., & van der Wegen, M. (2017). *Hydromorfologische verbetering ED2050, eerste beoordeling maatregelrichtingen* (11200116–000). Deltares.

Vuik, V., Borsje, B. W., Willemsen, P. W. J. M., & Jonkman, S. N. (2019). Salt marshes for flood risk reduction: Quantifying long-term effectiveness and life-cycle costs. *Ocean & Coastal Management*, *171*, 96–110. https://doi.org/10.1016/j.ocecoaman.2019.01.010

Vuik, V. (2017). POV Waddenzeedijken; effectiviteit voorlanden HR - Stabiliteit van vegetatie. HKV memo PR3365.30.

Walstra, D. J. R., Hoekstra, R., Tonnon, P. K., & Ruessink, B. G. (2013). Input reduction for long-term morphodynamic simulations in wave-dominated coastal settings. Coastal Engineering, 77, 57–70. https://doi.org/10.1016/j.coastaleng.2013.02.001

Weeber, M., Elzinga, H., Schoonveld, W., van de Vries, C., Klapwijk, M., Mischa, I., Rodriguez Aguilera, D., Farrag, M., Ye, Q., van Oorschot, M., Sager, P., & Icke, J. (2024). *D-Eco Impact (v0.3.0)*. Stichting Deltares. https://doi.org/10.5281/zenodo.10941913

Winterwerp, J. C. (2011). Fine sediment transport by tidal asymmetry in the high-concentrated Ems River: Indications for a regime shift in response to channel deepening. *Ocean Dynamics*, *61*(2), 203–215. https://doi.org/10.1007/s10236-010-0332-0

Winterwerp, J. C., Zhou, Z., Battista, G., Van Kessel, T., Jagers, H. R. A., Van Maren, D. S., & Van Der Wegen, M. (2018). Efficient Consolidation Model for Morphodynamic Simulations in Low-SPM Environments. *Journal of Hydraulic Engineering*, *144*(8), 04018055. https://doi.org/10.1061/(ASCE)HY.1943-7900.0001477

Zijl, F., Groenenboom, J., Laan, S. & Zijlker, T. (2022). DCSM-FM 100m: a sixth-generation model for the NW European Shelf: 2022 release. Deltares rapport 11208054-004-ZKS-0002.

7. Matching restoration interventions with NbS upscaling for climate adaptation in the Venice lagoon based on hypoxia risk under present and future climate scenarios

Zennaro, F.[1,2], Horneman, F.[2,1], Furlan, E.[1,2], Torresan, S.[1,2], Critto, A.[2,1]

[1] *RAAS division, CMCC Foundation - Euro-Mediterranean Center on Climate Change, 30175, Marghera, Italy*

[2] *Department of Environmental Sciences, Informatics and Statistics, Ca'Foscari University of Venice, 30172 Mestre, Italy*

ABSTRACT: Coastal and marine ecosystems, such as the Venice Lagoon, face significant threats from both anthropogenic and natural pressures, further intensified by climate change. While previous modelling efforts, including SHYFEM for hydrodynamics, have examined erosion and flood risks and the impact of saltmarsh restoration, the issue of hypoxia remains sparsely studied. Hypoxia, indicative of adverse water quality, requires more precise predictions and projections to inform adaptation strategies. This study introduces a hybrid Biogeochemical-Machine Learning (BGC-ML) model to enhance the accuracy of future hypoxia predictions under the RCP8.5 scenario. Results indicate an increase in hypoxia events from 3.5% in the reference period to 8.8% in the long term, with significant rises expected during summer, projecting a 15.3% increase by 2050 and a doubling by 2100. The hypoxia-prone season is also extending, with more occurrences in June and autumn. In response to these increases, coastal habitat restoration may mitigate hypoxia through processes such as nutrient loading reduction, eutrophication control, and oxygenation. Effective interventions include riparian buffer zones, seagrass transplantation, and saltmarsh restoration. These measures, tested in the Venice Lagoon, may influence water quality by nutrient retention, oxygen release, and restoring natural gradients, thereby reducing hypoxia risk. Comprehensive adaptation strategies must therefore explore synergies between various restoration measures, including NbS upscaling, to maximise ecosystem service provisioning and cumulative risk reduction.

7.1. Introduction

About 60% of the global marine and coastal environments have been degraded or are unsustainably used (Buonocore et al. 2021), this degradation can occur through numerous natural and anthropogenic processes (Nichols et al. 2019). At the same time climate change is exacerbating climate extremes (e.g., floods, heat waves, droughts), and is breaking long-standing records by large margins (Fisher et al., 2021). Coastal and marine environments are on the frontline of climate change, sensitive to sea level rise, ocean acidification, and rising temperatures, thus increasingly experiencing adverse impacts (Mallette et al., 2021). A variety of modelling activities exploring these extremes have been implemented by the REST-COAST consortium, in particular focusing on the risk reduction in relation to flooding and erosion during current and future hydrodynamics and extreme wave conditions. Less widely known but equally impactful and dangerous are extreme events that undermine water quality in water bodies such as marine heat waves, eutrophication, and hypoxia (Gruber et al., 2021). Hypoxia, defined by low oxygen availability, is one of the most critical phenomena in aquatic ecosystems, driven by both climate change and human activities through elevated temperatures, increasing CO2 levels, heightened nutrient inputs, and shifts in marine species abundance and distribution (Breitburg et al., 2018). Natural causes commonly attributed to hypoxia include diurnal oscillations in algal respiration, seasonal flooding, and stratification. Nevertheless, the current seascape reveals a heightened frequency and intensity of hypoxic events (Sampaio et al., 2021); this trend can be traced back to diminishing oxygen concentrations since the mid-20th century due to climate change (Baxter, 2019) and is likely to be exacerbated in the future (Du et al., 2018). Dissolved oxygen (DO) is identified as a

key indicator for assessing progress towards improved water quality in line with EU policy objectives such as the Water Framework Directive and the Marine Strategy Framework Directive (EEA, 2024; Best et al., 2007); and relates to the EU Mission Starfish 2030 goals to regenerate marine and coastal ecosystems (European Commission, Directorate-General for Research and Innovation).

Transitional environments, such as the Venice Lagoon, are particularly at high risk of hypoxia due to their delicate interface between land and sea. In the last years, the Lagoon has faced several hypoxic crises (Facca et al., 2014; Sfriso & Facca, 2007; Brigolin et al., 2021) that often resulted in mass fish and benthic invertebrate mortalities (Vaquer-Sunyer & Duarte, 2008). Furthermore, the increasing frequency of summer heat waves and drought could lead to an increased occurrence and extent of hypoxic events (Brigolin et al., 2021). Moreover, hypoxia can alter or interrupt ecosystem services like nutrient cycling and biodiversity (Rabalais et al. 2010). Nutrient cycling is important to maintain because it can affect the rate of marine plant and algal growth, which are critical to keep in balance (Diaz and Rosenberg 2008). This ecosystem service can be affected through a positive feedback where low DO concentrations inhibit both nitrification, denitrification, and phosphorus burial, which in turn promotes benthic recycling of N and P that stimulates phytoplankton growth and thereby bottom water DO depletion (Zhang et al., 2010). Moreover, biodiversity is essential to the existence and proper functioning of all ecosystems and provides a variety of ecosystem services such as maintaining global temperatures, habitat for species, and food supply (NOAA 2007). These ecosystem services are interconnected, with nutrient cycling and biodiversity jointly contributing to the health of marine environments, supporting fisheries, carbon sequestration, and coastal protection, thereby ensuring the resilience and sustainability of both natural and human systems.

Preventing the risk and recovery of coastal and marine ecosystems from hypoxia is possible (Caballero-Alfonso et al., 2015), but since responses to hypoxia and their subsequent pathways to recovery are nonlinear (Friedrich et al., 2014; Zhang et al., 2010) there is a need to understand the spatial and temporal variability of hypoxia events in order to design local and regional adaptation pathways (Low et al, 2021). This is particularly relevant given that some aspects of the current Venetian climate adaptation strategy for protecting the Lagoon and the city from sea level rise in this area could exacerbate hypoxia events in the future (Zanchettin et al., 2021). This in particular regards the construction of the Mo.S.E.[1] which through its activation prevents the exchange of sea water with the lagoon at the inlets to avoid flooding. A side effect of the activation is the interruption of the water circulation (i.e., prolonged residence time), which can influence the water quality of the entire lagoon. In fact, as the barriers are expected to be continuously closed for long tidal periods (multiple, and more days) due to sea level rise and extreme storms, very low DO concentrations and other harmful effects are likely to occur more invasively (Umgiesser, 2020; Canu et al., 2001).

Extending those restorations already present and introducing nature-based solutions (NbS) to address hypoxia is crucial, especially since future projections indicate an increase in hypoxic events, undermining the ecological health, biodiversity, and the ecosystem services of the Venice Lagoon, while also enhancing its resilience and capacity to adapt to changing climate conditions. At the same time, to avoid maladaptation, there is the need to develop a reliable method able to disentangle emerging patterns from the complex interactions between hypoxia events, water quality and climate drivers, and to predict their future patterns in order to obtain robust hypoxia scenarios under future climate change conditions. Yet, most studies focus on the evaluation of past hypoxia events and their consequences on the ecosystem (Brigolin et al., 2021; Munari & Mistri, 2011; Solidoro et al., 2010). The few case studies that handle future scenarios of hypoxia in coastal ecosystems have a common aspect which is the development of the scenarios using deterministic models, such as physical models rather than biogeochemical or hydro-ecological (e.g. Lehrter et al., 2017; Meier et al., 2021; Duvall et al., 2022). However, as a deterministic model, it has a limited capability to capture the entire range of natural variability, reproducing fluctuations and extremes, especially when

[1] Mo.S.E. = Modulo Sperimentale Elettromeccanico

biological dynamics are involved (Kwiatkowski et al., 2020). Furthermore, the model's capability to reproduce extreme events is reduced by the lack of high variability in the external forcings (i.e., rivers input), which is filtered off by the (low) frequency of the forcing monitoring systems (Zennaro et al., 2023). For this reason, in this methodology it was chosen to combine the deterministic model with the emerging Machine Learning (ML) approach, including various algorithms as well as their ensemble versions. This decision leverages recent advancements in ML, that has strong predictive capabilities and capitalises on the synergies between these capabilities and the strengths of deterministic simulations. However, as with all extreme events, detecting hypoxia in large datasets presents a significant challenge due to its infrequent occurrence.

The present work represents the first attempt to address hypoxia and climate change in the Venice Lagoon, a transitional system particularly exposed and vulnerable due to its land-to-sea interface. Specifically, the methodology attempts to improve the evaluation of hypoxia events in the Venice Lagoon over ten years (2008-2019) and the prediction of potential changes in the mid (2050) and far (2100) future, considering RCP 8.5 scenario (Intergovernmental Panel on Climate Change, 2014). Through this approach, this deliverable will bring together risk predictions and projections to estimate the spatial risk evolution of water quality through hypoxia occurrence, while at the same time considering the relation of various restoration interventions from the Venetian restoration portfolio with the processes influencing the occurrence of hypoxia in the future.

7.2. Data & Methods for the assessment of water quality through hypoxia

Past modelling inquiries within REST-COAST have focused on the evolution and future potential of erosion and flood risk for the Venice lagoon both with and without restoration interventions, however, water quality as ecosystem service has not been explored thoroughly. Considering hypoxia a negative expression of water quality, driven by biological, physical, and meteorological processes, the indicators affecting this process are remarkably similar to those used to evaluate the water quality purification service including nutrient availability, dissolved oxygen, and turbidity (STAP, 2011). Through the development of a coupled BGC-ML model, this work evaluates the water quality purification service of the Venice Lagoon, considering hypoxia in particular in the present and future as a proxy for water quality. The modelling framework presented in this deliverable proposes to create future risk profiles including the estimated impacts, and map hypoxia risk

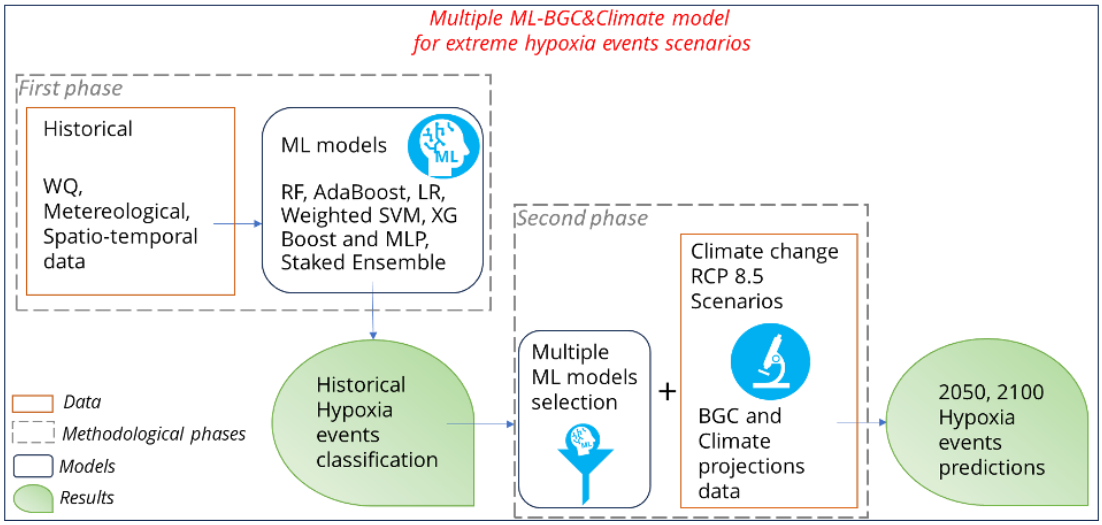

Figure 7-1 Overall methodology behind hypoxia extreme events analysis and predictions, including various machine learning (ML) algorithms[1].

---

[1] **RF = random forest, LR = linear regression, SVM = support vector machine, MLP = multilayer perceptron, BGC = Biogeochemical-.**

hotspots, and support adaptation and restoration actions by evaluating the role of interventions included in the Venetian restoration portfolio such as riparian buffers, seagrass transplantation, and saltmarsh restoration to reduce the occurrence and intensity of future hypoxia. This research involves the ML models fine-tuning using a suite of biogeochemical and meteorological response variables to classify extreme hypoxia events, and follows two consecutive phases (Figure 7-1), subsequently described in section 7.2.1 and 7.2.2.

7.2.1. Defining the Case Study: The Venice Lagoon, feature selection and climate projections

Venice Lagoon, the largest transitional environment of the Mediterranean sea covering ~550 km^2, is located in the northern part of the Adriatic Sea (Figure 7-2) and is characterised by a tide dominated hydro-dynamic regime. The tidal sea-water exchange through the three inlets (Lido, Malamocco, and Chioggia) is approximately 1.46 x 10^9 m^3 at each tidal cycle (12 hours), which is more than half of the entire water loading, although the water renewal in the inner areas may take ca. 10-20 days (Sfriso et al., 2009). As a result of hydrodynamic and morphological heterogeneity, accompanied by differences in the proximity of water bodies to anthropogenic pressures, there is high spatial variability in the water quality (water quality) of the Lagoon, e.g., salinity gradients (Solidoro et al., 2004), concentration of nutrients and Chl-a (Berti et al., 2022; Facca, et al., 2014; Micheletti et al., 2011; Solidoro et al., 2004). In addition to the intensive anthropogenic activities in and around the Lagoon, the prevalence of several climate-related pressures, including variations in precipitation and consequent river flooding (e.g. Pesce et al., 2018), variations in wind regimes (Solidoro et al., 2010), storm events (Lionello et al., 2021), as well as drought in the Mediterranean region (Tramblay et al., 2020) may alter the hydro-morphodynamic processes that determine the water quality and ecological status of the lagoon. In particular, they can affect the release, transport and redistribution of nutrients and/or pollutants, and alter water quality parameters such as temperature, salinity, turbidity, pH, and DO, with consequent effects on primary productivity and higher trophic levels.

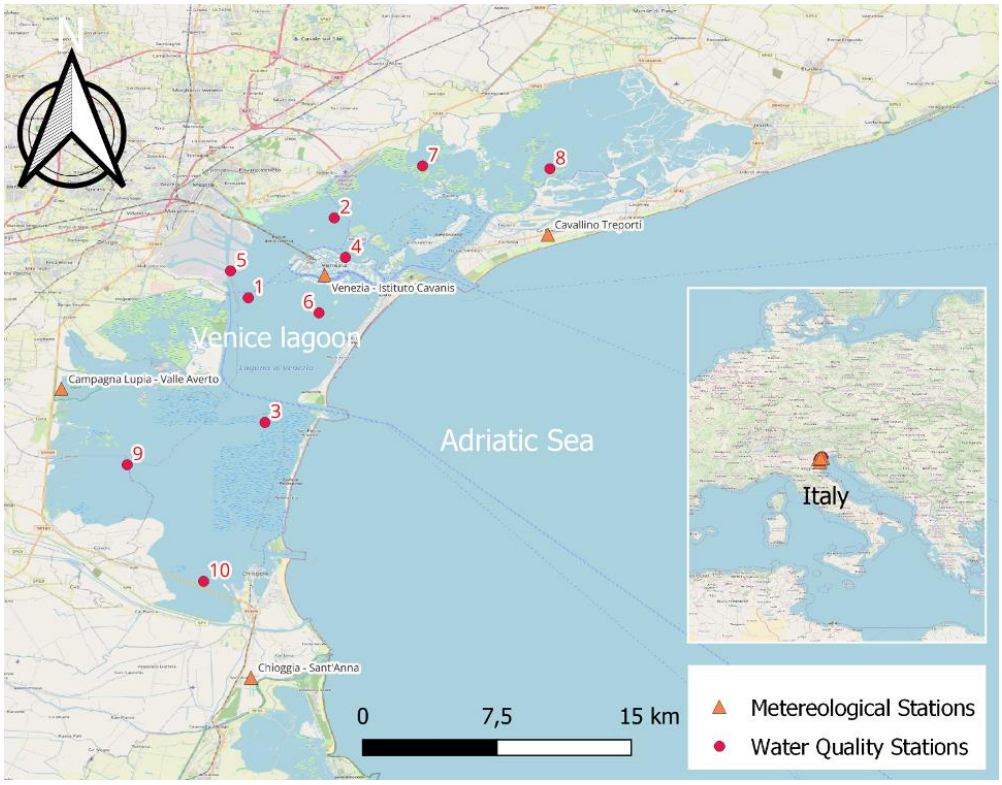

Figure 7-2 Map showing the 10 sampling probes sites investigated (red dots) within the Venice Lagoon case study and the 4 meteorological stations (orange triangles).

Features selections and historical data for ML development

The choice of the input variables for the ML models are connected to the processes driving hypoxia, description included in Appendix B-I, and accordingly related variables were selected (Table 7-1). The dataset comprises variables from two sources: 1) water quality data from the ten SAMANET stations located at a depth of 1 m managed by Provveditorato for the Public Works of Veneto, Trentino Alto Adige, and Friuli Venezia Giulia (hereafter Provv.OO.PP.); 2) Meteorological data from four stations located across the Venice Lagoon, provided by the Regional Agency for Environmental Prevention and Protection of Veneto (ARPAV). Since the spatial distribution of meteorological stations does not match all ten water quality stations (refer to Figure 2), they have been interpolated using the Inverse Distance Weighting (IDW) method. All the features are aligned as a daily mean, except precipitation, which is presented as daily cumulative precipitation. As the occurrence of hypoxic events is not an instantaneous process, the indicators representing cumulatively the previous three days are calculated from daily variables. Particularly since hypoxia events at a given time may be partially defined by environmental conditions in previous time periods (Lee et al., 2013); as such the concept of time lag has been previously adopted in ML modelling for predicting DO (Politikos et al., 2021; Khani and Rajaee, 2017). Accordingly, within the present methodology both the daily variables and their three-day cumulative indicator for each variable are taken into account, and the more influencing ones are chosen.

Table 7-1 Variables used as input in the ML models and general statistics of the historical period (2008-2009).

				2008 - 2019	
Variables	**Type**	**Temporal resolution**	**Source**	**Range**	**Mean**
DO (mmol/m^3)	water quality	daily mean, 3 days cumulative	SAMANET	0.00 - 671.95	263.30
water temperature (°C)	water quality	daily mean, 3 days cumulative	SAMANET	-1.55 - 32.24	16.66
salinity (PSU)	water quality	daily mean, 3 days cumulative	SAMANET	1.85 - 37.62	29.25
Chl-a (µg/L)	water quality	daily mean, 3 days cumulative	SAMANET	0.02 - 60.93	2.43
precipitation (mm)	Climate	daily mean, 3 days cumulative	ARPAV	0.00 - 159.82	2.27
solar radiation (W/m3)	Climate	daily mean, 3 days cumulative	ARPAV	0.00 - 823.34	160.22
relative humidity (%)	Climate	daily mean, 3 days cumulative	ARPAV	12.79 - 100.00	77.58

Future water quality and climate projections derrived from deterministic models

The development of climate change scenarios is based on projections from two models: the SHYFEM-BFM for water quality variables and the COSMO-CLM for meteorological variables respectively (Table 7-2; model details included in Appendix B-II). Both these two deterministic models are forced with the RCP 8.5 and provide, as output, the projections until the far future (2100). In this study, all future projections are incorporated into the ML model as values derived from the BGC and climate models, with the exception of DO due to a bias between model and observation in the historical data. Specifically, the DO min-max range of the 2019 baseline extends from 190.86 to 342.01 mmol/m3. In contrast, the DO min-max range of the historical data spans from 0.00 to 671.95 mmol/m3 (see Table 7-1 and Table 7-2). This disparity has necessitated the recalculation of the DO variable to ensure its alignment with historical trends (Appendix B-II).

Table 7-2 BGC and climate projections obtained from the deterministic models.*Rescaled DO future projections aligned with historical values.

		2019		2050		2100	
Variables	**Source**	**Range**	**Mean**	**Range**	**Mean**	**Range**	**Mean**
DO (mmol/m^3)	SHYFEM-BFM	190.86 – 342.01	258.02	182.33 - 556.48	265.20	168.71 - 511.97	243.37
				*60.29 – 452.32	*246.90	*49.69 – 410.63	*222.03
water temperature (°C)	SHYFEM-BFM	2.38 – 32.88	16.83	4.06 – 34.01	19.65	8.83 – 38.98	22.69
salinity (PSU)	SHYFEM-BFM	21.38 – 36.71	31.38	24.86 – 37.27	32.85	25.49 – 38.47	33.64
Chl-a (µg/L)	SHYFEM-BFM	0.30 – 6.93	1.41	0.09 – 13.27	1.20	0.05 – 7.43	1.00
precipitation (mm)	COSMO-CLM	0.00 – 40.30	0.97	0.00 – 35.42	0.91	0.00 – 27.84	1.11
solar radiation (W/m3)	COSMO-CLM	2.28 – 294.30	132.11	2.16 – 294.71	132.19	1.78 – 290.03	133.46
relative humidity (%)	COSMO-CLM	34.72 – 97.27	72.59	35.13 – 94.78	72.17	23.69 – 96.67	68.42

7.2.2. Methodology: ML for modelling hypoxia in the Venice Lagoon

Past deliverables described the deterministic modelling of the risk evolution in relation to the ecosystem services reduction of flood and erosion risk, while this deliverable works to complement the past knowledge by considering water quality purification. This expansion of work was deemed necessary in order to inform future upscaling, since it is necessary to better understand the relation between climate change and hypoxia, as well as the processes underlying the occurrence of hypoxia so that adaptation can be designed to address the root issues. This section provides the basis for the modelling of hypoxia through the delineation of hypoxia extreme events, the ML methodology, and the scenario development.

Defining hypoxia events and threshold

Hypoxia is defined in terms of measurable consequences reflected in the ecosystem, such as the oxygen concentration at which fisheries collapse (Renaud, 1986) or a particular biological function is impaired (Diaz and Rosenberg, 1995). Regarding the threshold chosen in this methodology, it is important to consider that hypoxia thresholds proposed in the literature range from 2 mgO2/l (Diaz and Rosenberg, 2008) to 4 mgO2/l (Paerl et al., 2006). 2 mgO2/l refers to the oxygen level for fisheries mortality, but there is ample experimental evidence that 2 mgO2/l may be insufficient to describe the onset of hypoxia for many organisms that experience hypoxic effects at higher oxygen concentrations, i.e. up to 4 mgO2/l (Pezner et al., 2023; Tellier et al., 2022; Vaquer-Sunyer & Duarte, 2008). Accordingly, 4 mgO2/l is the selected threshold within this methodology, as more representative of the ecosystem depletion. Moreover, consideration of event duration is extremely relevant in the case study because as defined by Tellier et al. (2022) diel hypoxia is a natural phenomenon that can develop in highly productive, shallow, aquatic habitats, such the Venice Lagoon is, during the warmer months. Hypoxia events are here specifically defined as the occurrence wherein the DO concentration remains below the established limit of 125 mmol/m³ (equivalent to 4 mgO2/l) (Paerl et al., 2006; Politikos et al., 2021) for a duration of at least 8 hours within a single day even if not continuous (e.g. DO < 125 mmol/m³ from 00:00 to 05:00 am and from 08:00 am to 11:00 am of a given day). Furthermore, in order to account for situations where data are missing for specific days, a proportion equivalent to 8/24, i.e. the 33.3%, of the total hours in which the DO concentrations stay within the predefined threshold level is taken into consideration. This approach aims to compensate for data gaps, without having to remove days with missing data from the dataset, thus avoiding its reduction. This systematic approach ensures consistent identification and accurate characterization of hypoxia events, even in scenarios with incomplete data coverage.

ML models and skill metrics

ML models are well suited to problems with various interactions between inputs and outputs being able to disentangle complex non-linear relationships between variables. The choice of the present methodology is related to the considerations of the available water quality and meteorological datasets; characterised by

high complexity and non-linear distribution and by a short available time frame, i.e. 2008-2019 (historical) and 2050, 2100 (future). Due to their AI-power, ML models can be an ideal tool for classifying hypoxia events, but since extreme events are characterised by an unbalanced dataset this method can face some issues. The unbalanced dataset is a special case of the classification problem, where the distribution between classes is uneven and it is difficult to classify the data accurately (Zhou et al., 2023). This implies that when a dataset is biased towards one class, an algorithm trained on the same data will be biased towards the same class. The outcome could be a scenario where the model assumes that all the data belongs to the majority class. As a result, the model will appear naive in its predictions, regardless of the high accuracy it achieves. Accordingly with the complexity of hypoxia events unbalanced dataset (~3:100 ratio), an ensemble-based strategy is used to ensure the robustness of the analyses. Among all the response variables involved (comprehensive of daily mean and time-lagged indicators), the most influential indicators are selected through ML future importance, by applying permutation importance and the Gini index. According to the feature importance procedure, the final set of response variables comprehend: daily DO, water temperature, and precipitation, and 3 cumulative days Chl-a, salinity, solar radiation and humidity.

The MLs task involves the binary classification of the hypoxia event (class 0) versus the normal condition (class 1) of each day of the historical period. The multiple approach combines the performance and results of many classifiers to improve the performance of a single classifier and try to achieve the highest possible prediction accuracy in the final model. The multiple ML modelling is intended here in the training of six separate well-known ML models: Random Forest (RF) (Liaw and Wiener, 2002), AdaBoost (Freund & Schapire, 1997), Linear Regression (LR) (Bisong 2019), Weighted Support Vector Machine (SVM), XG Boost (Chen & Guestrin, 2016) and Multi-Layer Perceptron (MLP) (Ahmed et al., 2019). In addition the Staking ensemble technique is used to test whether multiple learning methods are more effective than a single one. Each proposed algorithm is fine-tuned in the present methodology using the most suited settings to weight the classes (e.g. class_weight). In contrast to single algorithms, the design of the Staking ensemble is more complex. Stacking is an ensemble learning technique to combine multiple classification models via a meta-classifier.

All the presented algorithms are validated with the cross-validation technique, necessary to assess models' performance and generalizability (Pedregosa et al., 2011). Finally, to evaluate the predictive performance of the multiple ML algorithms on the testing set, accuracy and ROC-AUC metrics are reported. Accuracy, the ratio of correctly predicted instances to the total instances, is easy to interpret but can be misleading with unbalanced datasets. In such cases, ROC-AUC is a better alternative, quantifying the model's ability to discriminate between classes at different thresholds. Precision, recall, and F1 score are also calculated for a detailed performance assessment. Confusion matrices provide insights into true positives, false positives, true negatives, and false negatives. Additionally, sensitivity analysis, specifically using the Morris method, is performed to understand the influence of input variations on model predictions, ensuring robustness and precision in the results.

Future climate change scenarios design

After selecting the suit of ML models that best perform on the test sets, the ML-BGC&Climate model is implemented. This process implies integrating in the ML models the reference (20° percentile of the historical period 2008-2019) data and future (2050 and 2100) BGC and climate projections. As presented in the dataset section, the projections are estimated by SHYFEM-BFM model for water temperature, DO, Chl-a, salinity, and by COSMO-CLM for solar radiation, humidity, and precipitation variables. The results consist of daily hypoxia event predictions and relative model uncertainty for the years 2050 and 2100, as well as for the reference period. In order to present as robust scenarios as possible, the calculation of the number of hypoxia events is based on the average values obtained from the results of the multiple ML model selection (i.e. the average of the Adaboost, RF and Staked ensemble predictions). Furthermore, estimated variability of the possible

min-max prediction of the whole range of selected models is given to express the uncertainty. An in-depth seasonal analysis (i.e. winter, spring, summer and autumn) is also carried out with a focus on summer (i.e. June, July and August) temporal variability. Furthermore, a station-based analysis is undertaken, accounting for the geographical locations of monitoring stations (Figure 7-1), thereby incorporating the spatial dimension.

7.3. Results

Through the ML model it is possible to establish a risk profile for the Venice Lagoon, displaying the evolution of hypoxia events both in space and time, thereby elaborating the historical and future risk influencing the decisions surrounding NbS upscaling of interventions in the Venetian restoration portfolio.

7.3.1. Historical hypoxia events

Hypoxic conditions can frequently occur in lagoon areas subject to reduced water exchange, in the warmer season, and mainly at night, especially in the layers close to the sediment (Diaz et al., 2008). Here, an in-depth analysis of historical hypoxia events in the Venice Lagoon for the period 2008 - 2019 is provided to understand whether past events were natural conditions (diel hypoxia) or dangerous extreme events. Looking at the events given the threshold defined in Section 7.2.2, it is evidenced that only 16% of hypoxia events ended before 10:00 am while the remaining 84% continued during the daytime. These results indicate that the great majority of events are not natural temporary hypoxia but effectively dangerous events. Considering spatial variability, the stations in which more events occurred (1, 5, 7 and 10) are the landward stations where the residence time of the water is higher (Cucco & Umgiesser, 2006). A further explanatory analysis of hypoxia events characteristics shows that, when looking at the DO daily mean, a significant proportion, 40%, of the recorded events remain within the established threshold of 125 mmol/m^3 (Figure

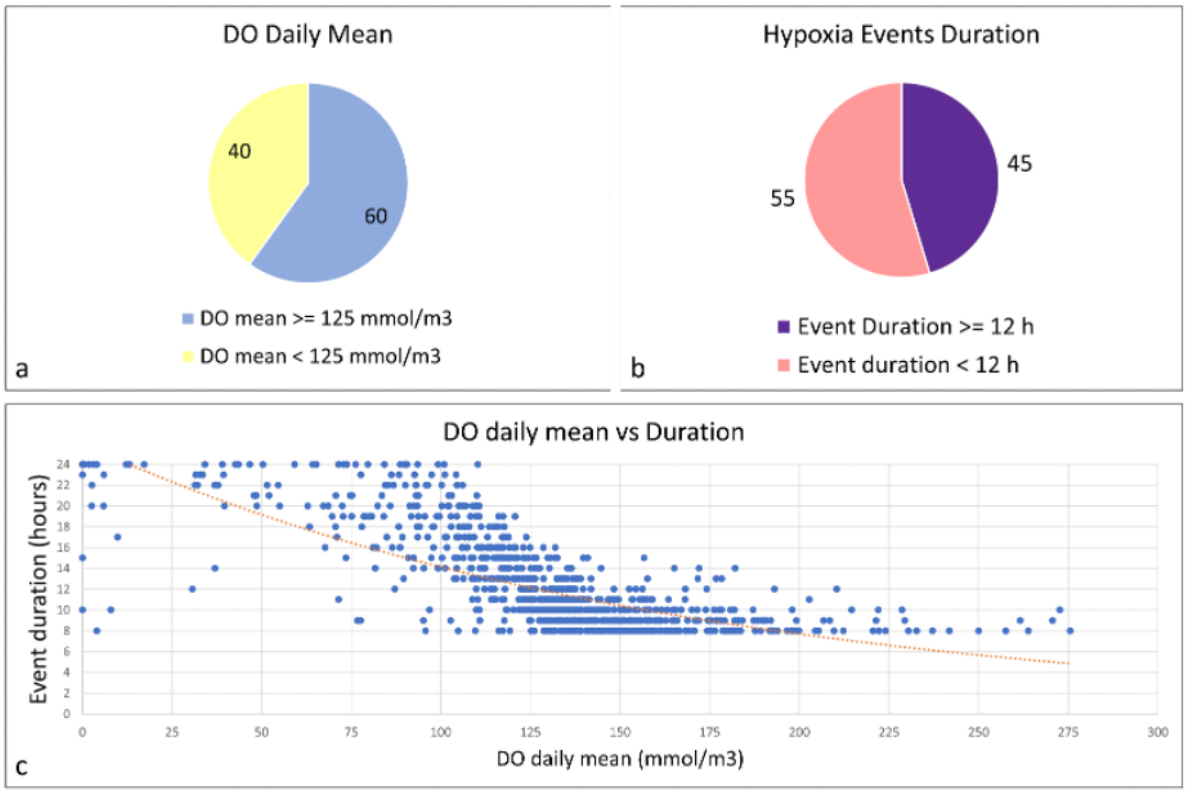

Figure 7-3 General statistics of historical monitored (2008-2019) hypoxia events across the ten Venice Lagoon stations. a) Percentage of DO daily mean below or above the 125 mmol/m3. b) Percentage of hypoxia events with a duration of less than or more than 12 hours. c) Relation between the DO daily mean and the duration of the hypoxia event expressed in hours.

7-3a). This emphasises that there is a high frequency of events that are either more intense, e.g. with very low hourly DO peaks, or that have a duration of more than 8 hours. Then, looking at the duration of the events (Figure 7-3b) it is noteworthy that a substantial portion, 45%, of the investigated events display durations that extend beyond 12 hours in a day. This prolonged temporal extent of events highlights the persistence of hypoxic conditions below the 125 mmol/m^3 threshold for a time span that can threaten the wellness and survival of sessile organisms, unable to move toward better-oxygenated water. Finally, the duration of the events compared with the daily DO mean values (Figure 7-3c) shows that the longer the events, the lower the DO mean is. When the event lasts more than 16 hours, the daily average is always below 125 mmol/m^3.

7.3.2. ML models performances

The binary classification of hypoxia events or normal conditions are performed by six separate ML models, i.e., RF, AdaBoost, LR, Weighted SVM, XG Boost, and MLP, and a Staking ensemble model. The models are trained, validated and tested with daily water quality and meteorological data monitored in the Venice Lagoon during the period 2008-2019. Their accuracy, ROC-AUC score, precision, recall, and F1 score metrics calculated on the two classes, are presented in Appendix B-III. The results indicate that RF, AdaBoost, MLP, and the Stacking ensemble models achieve the highest accuracy (0.99). Among them, RF, AdaBoost, and the Stacking ensemble also demonstrate the highest F1 score for class 0 (i.e. hypoxia event occurrence), while MLP exhibit a lower F1 score for this class, as indicated by its very high precision (0.94) but lower recall (0.61), suggesting that it may miss various positive cases. When comparing the AUC-ROC scores, Weighted SVM and XG Boost score the highest. Nevertheless, their precision and accuracy scores in class 0 are weak (e.g., 0.34 and 0.67 for precision, respectively), indicating that these algorithms are not suitable for describing this particular problem of an unbalanced dataset (more detailed results are reported in Appendix BIII).

7.3.3. Future hypoxia events

The hypoxia events under the RCP 8.5 climate change scenario are determined by averaging the simulated events generated by each selected ML model using projections of water quality and climate variables from deterministic models as input data. Results show a notable upward trend in the annual frequency of hypoxia events over time (Figure 7-4a), with the days affected by hypoxia increasing from 3.5% of the reference period (20° percentile of the 2008-2019 timeframe) to 4.1% in the mid-future and 8.8% in the far future, which corresponds to a relative increase with respect to the reference period of +1.7% and +4.3% for the mid- and far- future respectively. However, a notable increase in inter-model variability also occurs, causing a rise in uncertainty to 29 days in the mid-future and 67 days in the far future.

The seasonal analysis (Figure 7-4b) confirms the prevalence of hypoxia events in summer, which is in line with the natural processes associated with such events. However, a smaller proportion of events also occur during the autumn season. For both seasons, an increasing trend of events is predicted for 2050 and 2100 compared to the reference period. In summer, the model predicts 136 hypoxia events in 2050 and 265 in 2100, compared to 118 events observed in the reference period (indicating an average increase of 15.3% between the reference scenario and the mid-future, followed by a further increase of 94.9% from mid to the far-future). In autumn, 15 events are projected in 2050 and 27 in 2100, an increase of more than two and four times compared to the 6 events in the reference period. Notably, no events are predicted for winter, even in the far future. However, the model predicts a small number of events (4) during spring in 2100, indicating a possible seasonal anticipation of hypoxic events.

Focusing on summertime only, Figure 7-4c shows that in the reference period, the months with the highest estimated number of hypoxia events are July and August, with 50 events in each month. In future simulations, there is a notable increase in occurrences, particularly in July (71 events in the mid future and 110 in the far future), while August experiences a more moderate increase, remaining nearly unchanged in the mid future

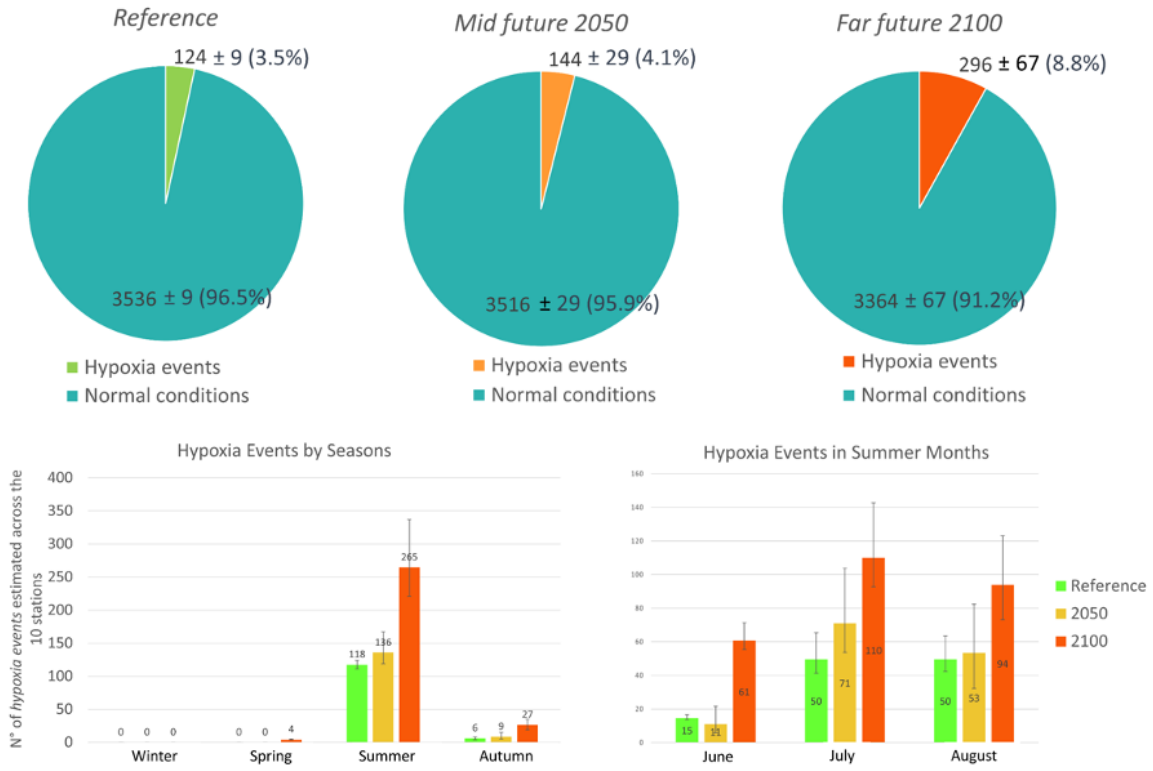

Figure 7-4 Temporal dimension of hypoxia scenarios designed by the ML-BGC&Climate model, across the reference period and the mid and far future in the ten Venice Lagoon stations. a) Pie charts indicating the count and the relative percentage of hypoxia events over the entire period. B) Bar plots indicating the number of hypoxia events estimated in each season. c) Bar plots indicating the number of hypoxia events estimated in each summer month. The error bars represent the predictions variability given by the whole range of the selected models.

(53 events) and rising to 94 events in the far future. Conversely, estimates for June show a different trend, with a decrease in events occurring in the mid future (from 15 in the reference period to 11) and a significant rise in the far future (61 events). Accordingly, the hypoxia event period in the far future is expected to expand from the historical two-month period to a three-month duration, and to become a larger challenge for aquatic life.

The maps in Figure 7-5 depict a comparison of hypoxia event percentages across the ten Venice Lagoon stations during the three analysed periods: the reference, 2050, and 2100. Notably, stations 1, 5, and 7, located landward, i.e. the area with the longest water residence time (Cucco & Umgiesser, 2006), consistently exhibit the highest number of hypoxia events in all the three scenarios (Figure 7-5a,b,c) and the largest increase in the number of hypoxia events over the far future. Specifically, as illustrated in Figure 7-5d, the number of events rises from 29 in the reference period to 55 in the far future at station 1, 50 to 78 at station 5, and from 32 to 69 at station 7. Looking at stations 8, 9, and 10, where hypoxic events are rare or nonexistent during the reference period, there is a noticeable increase in events, with a discernible upward trend extending from the mid to the far future. The slow circulation of water at the landward stations coupled with the changes in biogeochemical and meteorological conditions (e.g. in the present study, maximum water temperatures increase from a historical value of 32°C to 39°C by 2100, see Table 7-1 and Table 7-2), mean that these areas of the Venice Lagoon are expected to be at risk of frequent extreme hypoxia. Stations 2 and 4 similarly display an increasing trend, although the overall number of events at these stations remains relatively low (maximum of 14 events) even by 2100. Lastly, stations 3 and 6, situated seaward, closest to the Malamocco inlet and channel (the largest channel of the Lagoon with a depth of 14 metres (Ghezzo et al., 2010)), remain in a well-oxygenated state, with no hypoxic events expected for the mid and far future.

Figure 7-5 Spatial dimension of hypoxia scenarios designed by the ML-BGC&Climate model. Pie charts visualizing the a) reference, b) mid future and c) far future scenarios across the ten Venice Lagoon stations. d) Bar plots indicating the number of hypoxia events across the reference period and the mid and far future in the ten Venice Lagoon stations. The error bars represent the predictions variability given by the whole range of the selected models.

The uncertainty bars in Figure 7-5d, depicting variability in predictions among the selected ML models, emphasise stations 1, 9, and 10 as particularly susceptible to high variability. These bars illustrate a wide min-max range of potential hypoxia events. For instance, at station 1, events in 2100 could vary from as high as 90 to as low as 36. Despite these ML model-related fluctuations, all the results suggest that the Venice Lagoon will be more prone to hypoxic events in the mid and especially in the far future, under climatic conditions induced by the RCP8.5 scenario. Among all the environmental changes considered in climate projections, the temperature is undoubtedly a key factor driving these changes. Indeed, increasing temperatures contribute to a reduction in the solubility of oxygen in seawater (Garcia and Gordon, 1992) and stimulate the metabolic activity of aquatic organisms (Hsieh et al., 2021) leading to heightened oxygen biological demand (Sokolova and Lannig, 2008).

The estimation of an increased risk of hypoxia can also be aggravated by other factors not included in this methodology: firstly, it is likely that some areas of the Venice Lagoon could experience hypoxia events in a more massive way in the deeper waters immediately above the sediments. It should be considered that shallow coastal lagoons often exhibit a significant decrease in oxygen concentration with depth (Brigolin et al., 2021; Hsieh et al., 2021), coupled with intense dynamics of the daily cycle of oxygen concentration. Moreover, higher sea surface temperatures also lead to density stratification, which can greatly reduce vertical mixing and thus restricts the transport of oxygen to deeper layers (Howarth et al., 2011). Secondly, it's plausible that the Mo.S.E. could potentially heighten the risk of hypoxia by impeding the exchange of seawater with the Lagoon. With the projected sea level rise in the mid and far future, the Mo.S.E. barriers might be activated for more extended periods (for example, 4 or 5 consecutive days), leading to a disruption of seawater inflow. However, more targeted studies are necessary to examine these aspects in detail, particularly since the Mo.S.E. system has only been operational since 2020 and the available data are not enough for robust analysis. Thirdly, it is possible that future scenarios of land use change, urbanisation, and population growth could also negatively affect the occurrence of hypoxia events. Indeed, in a business-as-

usual scenario, high levels of nutrients discharged into the lagoon during both dry and wet periods can trigger microbial growth. During dry periods, phytoplankton can produce large amounts of particulate organic carbon and consume nutrients and oxygen in the water column. Oxygen depletion is more pronounced during wet periods, when heavy rainfall, which brings turbid water with high concentrations of nitrogenous nutrients, can stimulate phytoplankton growth, and increase the discharge of particulate organic carbon and dissolved organic carbon into the lagoon. Indeed, negative correlations between DO and dissolved organic carbon and DO and particulate organic carbon can be observed in both seasons, suggesting that heterotrophic bacteria may largely use dissolved oxygen in the water column (Hsieh et al., 2021).

7.4. Discussion

Having understood the risk prediction and risk projection of coastal erosion and flood risk in the Venice Lagoon, as well as the influence of pilot scale saltmarsh restoration on these particular ecosystem services in past deliverables (most notably D2.1. and D2.2.), this deliverable has aimed to widen the scope to include the water quality purification service. The need to develop new tools and models to biogeochemical dynamics and ecosystem behaviour will improve the confidence in remediation strategies for coastal hypoxia (Friedrich et al., 2014). The present work introduces a first step towards the exploration of sequenced restoration and adaptation measures for the Venice Lagoon, highlighting in particular the risks associated with water quality through the projections for hypoxia occurrence. In particular, it details the spatial and temporal variability of hypoxia in the Venice lagoon and in the following sections the implications (section 7.4.1), and possible guidance for local adaptation (section 7.4.2).

7.4.1. Hypoxia risk scenario evaluations and implications for the future

Considering the vulnerability of the Venice Lagoon to both natural and anthropogenic pressures, this work delved deeper into the evaluation of water quality considering in particular the risk of hypoxia. Uncovering the physical and biogeochemical processes at work to drive the occurrence of hypoxia is a necessary step to abate its negative effects (Dai et al., 2023). Through the hybrid BGC-ML model it is possible to advance the accuracy of future predictions, which in turn can help design mitigation and adaptation actions such as restoration to inform transformative pathways for the Venice Lagoon (Zennaro et al., 2023). The hybrid model envisages more frequent and longer-lasting hypoxia periods in the RCP8.5 scenario. In particular, the annual frequency of hypoxia events shows a significant upward trend over time. The events will predominantly occur in summer, consistent with natural processes, but also some events are expected in autumn in the future. July and August currently see the most hypoxia events, with future projections indicating substantial increases, particularly in July. Concerning June, it is expected to see a significant rise in the far future, so, the hypoxia event period is expected to extend from two months to three months, posing a greater risk for aquatic life.

Spatially, areas located landward, with the longest water residence time, show the highest number of hypoxia events and the largest increases over time. This can partially be attributed to the slow water circulation and the temperature, which is projected to increase from 32°C in the historical period to 39°C in 2100. Moreover, in the future there are some emerging hypoxias in previously unaffected areas: Stations 8, 9, and 10 (located at the landward boundaries of the lagoon), which had few or no hypoxic events during the reference period, are projected to see a noticeable increase in events by 2100. On the contrary, there are some persistently well-oxygenated areas, the ones located seaward near the Malamocco inlet and channel, that are expected to remain well-oxygenated with no hypoxic events in the mid and far future. It should be noted that hypoxia is not only coupled to the physical and biogeochemical processes, but is also intimately related to human activities (Dai et al., 2023). Which is supported by the fact that the pattern for hypoxia has also been observed for other water quality variables in the historical timeframe (e.g., Solidoro et al., 2004; Berti et al., 2022; Facca, et al., 2014; Micheletti et al., 2011; Solidoro et al., 2004). Facca, et al. (2014) observed a clear gradient in total nitrogen between the northern and southern Lagoon, with decreasing concentrations seaward and

higher concentrations of total phosphorus, total carbon, and inorganic carbon in the central basin. Similarly, Solidoro et al. (2004) reported high nutrient and Chl-a concentrations in the central Lagoon, with less bloom in areas with greater sea influence. In general, higher concentrations of nutrients and other contaminants are found in areas close to urban canals (e.g. Venice city centre), industrial canals affected by effluents, confined areas with limited hydrodynamics (longer residence time) and landward areas affected by tributary discharges, fish farm outfalls and runoff from the mainland (e.g. Berti et al., 2022). As the landward areas of the Lagoon receive most of the inputs from the catchment, higher concentrations of pollutants exceeding the environmental quality standards (DM 23/04/1998, DM 367/2003) were also found there by Micheletti et al. (2011).

These evaluations run counter to the goals outlined in for instance the EU reference Mission, particularly the Starfish 2030 initiative titled 'Restore our Ocean and Waters Report of the Mission Board – Healthy Oceans, Seas, Coastal and Inland Waters'. More specifically, these estimations depict a scenario for the Venice Lagoon that departs from one of the main goals of Starfish 2030: to attain zero pollution of our oceans and waters by 2030, which entails, among others, cutting down hypoxia by at least 50%. Moreover, hypoxia causes a deterioration of a variety of characteristics important to the sustainability of marine and coastal ecosystems (Zhang et al., 2010), including an inference with biogeochemical processes. Since the generation of ecosystem services depends on the physical, chemical, and biological processes that underpin ecosystem functioning and maintain ecosystem structures (Buonocore et al. 2021) a decrease in those can be expected. Ecosystem responses to hypoxia and pathways of recovery from hypoxia are typically nonlinear (Caballero-Alfonso et al., 2015; Friedrich et al., 2014). However, recovery is possible through a combination of measures tackling the drivers of hypoxia including nutrient loading, oxygen availability and eutrophication.

7.4.2. Portfolio of restoration activities for water quality purification and upscaling potential

Adaptation strategies now focus on nature-based solutions (NbS), such as preserving or restoring ecosystems like marshes and seagrass beds, which offer crucial coastal protection (Rivadeneyra et al 2024). Introducing and expanding already present NbS in the Venice Lagoon to address hypoxia is crucial, especially since future projections indicate an increase in hypoxic events, undermining the ecological health, biodiversity, and the ecosystem services, while also enhancing its resilience and capacity to adapt to changing climate conditions. The most commonly used assumption in developing management strategies for hypoxia in estuarine and semi-enclosed seas has been that decreasing nutrient loads will lead to reduced eutrophication and as such reduce or eliminate hypoxia (STAP, 2011). By leveraging the natural processes and functions of ecosystems, such as nutrient filtration and uptake, sediment trapping and water clarity improvement, and enhancement of oxygen levels, NbS can provide sustainable and cost-effective ways to improve water quality and address hypoxia. A variety of NbS can be identified, already implemented in the Venice Lagoon by the PROVVV.OO.PP. and other stakeholders, that have the possibility to influence water quality, through DO and nutrients, including: i) riparian buffer zones; ii) seagrass and phragmites transplantation; iii) saltmarsh restoration and/or creation; and iv) restore hydrology; and might be expanded to address future hypoxia risk by affecting the processes determining their occurrence.

Riparian buffer along the banks of aquatic systems/rivers to reduce nutrient loading

The most important indicator for stress reduction is the annual load entering the system via riverine inputs (STAP, 2011). Ecosystems can provide a purification service by retaining or degrading pollutants before they enter the system. The ability of riparian buffers in retaining nitrogen has been studied since the early 80s, and depends primarily on the conditions conducive to high denitrification rates as well as the maintenance of a stable vegetation structure (Gumiero et al., 2009). Appropriately managed riparian areas offer multiple functions related to improving water quality, biodiversity, and climate adaptation (Stutter et al., 2019). Plants in these zones can uptake nutrients, but also provide other ecosystem services such as stabilisation of the soil, reducing erosion and sedimentation. Implementing riparian buffer strips along rivers and streams that

feed into the lagoon can significantly reduce nutrient loading. These strips, planted with native vegetation, help filter out nutrients from agricultural runoff before they reach the lagoon. Establishing vegetated buffer zones along the lagoon's shoreline can reduce runoff containing nutrients and pollutants from entering the water. The vegetation can absorb nutrients and pollutants through assimilation by the roots and storing them in their tissue. The annual absorption capacity per hectare of surface area of the terrestrial macrophytes assumes typical values of 200 - 10000 kg of N and 30 - 150 kg of P (Borin et al., 2014). The spatial distribution of riparian buffer zones relative to sources of excess nutrients, like agricultural fields, is likely to affect their functioning and performance in controlling nitrogen fluxes (Gumiero et al., 2009). Moreover, the efficiency of the buffer zone is a function of the hydrological length of contact between the riparian zone and the upland drainage basin (Gumiero et al., 2009). This knowledge can be used to inform possible upscaling of riparian buffers along the Venice Lagoon, as such this measure would support improvements along the river-to-sea continuum and could help suppress the possibility of future hypoxia events by reducing the variables related to hypoxia.

Transplantation of seagrasses for improved water quality

Seagrass beds are crucial for maintaining healthy coastal ecosystems, however they have been experiencing a global decline. In the Venice Lagoon, a variety of measures were introduced by PROVV.OO.PP. to limit the negative impacts on meadows, and encourage the establishment of seagrasses, including limiting the turbidity, loss of sediments and wind waves. Human-mediated seagrass restoration can be employed as a form of compensatory mitigation by creating new seagrass meadows in areas that appear to be suitable for their growth in order to balance their destruction and recession from other areas due to anthropogenic activities (Sfriso et al., 2023). Aquatic angiosperms were reintroduced into the Lagoon by the City of Venice between 1992 and 1997, various transplantations by the Provv. OO. PP. as part of the Piano Morfologico, in saltmarsh ponds by IUAV and Consorzio Thetis in 1994, explanting sods between 1996 and 1997 (Tagliapietra et al., 2018); as well as through the Life SeResto project between 2012 and 2017 that transplanted more than 75,000 rhizomes resulting in roughly 15 km^2 of new meadows (Sfriso et al., 2022). These transplantations focused on Zostera marina, Zostera noltei, Rupppia cirrhosa, and Cymodocea nodosa (Sfriso et al., 2021), primarily in areas where natural recolonisation was limited, including the Northern Lagoon and aim to contribute to achieving a good ecological status. Widespread manual transplantations of small sods or single rhizomes of aquatic angiosperms are the simplest, rapid and least expensive tool to favour the recolonisation and establishment of meadows. Results from past transplantation actions indicate that seagrasses are an excellent tool to accelerate a quick recovery of ecological conditions, and subsequently limit the hypoxia risk (Sfriso et al., 2022). Seagrasses act as a nutrient filter by taking up nitrogen and phosphorus from the water column and sediments and by mediating bacterial processes that impact nutrient retention (Reynolds et al., 2016). The presence of seagrasses affects the total nitrogen pool by retaining it as plant biomass and altering sediment conditions that influence microbially mediated biogeochemical processes (Reynolds et al., 2016); thus reducing the nutrient concentrations in the water column and the potential for hypoxic events. Moreover, through photosynthesis oxygen is released, since aquatic plants in the presence of adequate supplies of carbon dioxide and light, oxygen is released as a by-product (Best et al., 2007). Aware of the possible future hypoxia-prone areas, an upscaling of seagrass transplantation can be considered, taking into account the suitable areas encompassing the environmental conditions for their growth and survival in a longer timeframe such as depth (m), seabed slope (%), substrate type (Ozkiper, in prep).

Saltmarsh restoration or creation as nutrient sink

Wetlands and marshes have been restored in the Venice Lagoon by the Venice Water Authority since the 1970s to fulfil a variety of functions including the recovery of morphological balance, wave attenuation, biodiversity, and ecological functionality such as filtering out excess nutrients. Additional LIFE projects aiming to reduce erosion and enhance ecosystem service provisioning including carbon sequestration, sediment retention and water purification, fish productivity; namely LIFE VIMINE and LIFE Vital have been implemented

in the Lagoon. The results of the restoration interventions are significant for the saltmarshes, equal to 27% of the natural marshes and recovering 30% of the marshes lost since the 1930s (Tagliapietra et al., 2018). The selection of restoration sites, and sites for possible upscaling, should be based on the suitability of the area to ensure long-term success (Pétillon et al 2023). The restoration and creation of saltmarshes is occurring by learning from history, focusing on locations where salt marshes have been present and aiming to recover their functioning. As such their restoration is focused primarily on the water bodies further away from the sea, these overlap with the stations where hypoxia risk is higher, and restoring marshes here might help mitigate their impact. The purification capacity of intertidal ecosystems could play an important role in the mitigation of nutrient inputs, acting as a buffer zone between watersheds and coastal waters, especially in relation to climate change and the increase in impulsive extreme events (Bonometto et al., 2019). Through this function, restored and created saltmarshes in the Venice Lagoon could help reduce the risk of hypoxia in the future. These areas act as natural buffers, absorbing and transforming nutrients through plant uptake and microbial processes (EPA, 2021). These engineered systems mimic natural wetlands and are effective at removing nutrients through sedimentation, plant uptake, and microbial activity. The core of the tidal flat's purification capacity is the ability of microorganisms to remove organic matters and nutrients introduced to the tidal flat. Tidal flats provide sedimentary layers with oxygen through disturbance, submergence, and exposure of the surface sediments from water, enabling the more effective aerobic decomposition process (Kim et al., 2020). Bioturbation of sediment through marine organism movement increases oxygen content in the sediment-water interface, and could cause an increase in the purification of nutrients through denitrification (Kim et al., 2020).

Re-establishment of the Lagoon's hydrology to improve the water quality

The creation of a transition strip at the lagoon edge must be accompanied by interventions aimed at restoring the natural transition morphology between the mainland and the lagoon. The areas, located in correspondence with fresh water inlets, must be separated from the surrounding lagoon areas via saltmarshes, mudflats, and other structures; without hindering high tides, and increasing the residence time of the incoming freshwater. One such project implemented in the past in the Venice Lagoon was LIFE Lagoon Refresh, in which actions such as the diversion of freshwater flow in the Northern lagoon from the Sile reintroduced freshwater into the lagoon, intertidal morphology was restored, reeds and aquatic angiosperms were transplanted with the support of local fishermen and hunters, and pressures from hunting and fishing were reduced (Feola et al., 2018). The low salinity and morphological variations would make the environment more suitable for the growing of reedbeds and it could provide valuable and diversified ecosystem services, such as the purification of the water by reducing the degree of eutrophication with, consequently, the improvement of benthic biocenosis (Boscolo Brusà et al., 2022). This pilot site indicates the capacity to reestablish the physical, chemical, and biological processes, and whilst NbS such as this one can take a minimum of 15 to 25 years to attain the original biotic composition and diversity, some ecological improvements can already be observed including the restoration of the salinity gradient (Boscolo Brusà et al., 2022). The potential of the restoration of these processes highlights the possibility to mitigate the load of nutrients and suspended substances and subsequently affect the occurrence of hypoxia. Upscaling of these types of measures could be in similar areas to those of the LIFE Lagoon Refresh project, where in past centuries river diversions adversely affected the hydrology of the lagoon.

7.5. Conclusion

Coastal and marine ecosystems are at risk, such as the Venice Lagoon, vulnerable both to anthropogenic and natural pressures, exacerbated by climate change. Past modelling exercises, including the application of the SHYFEM model for hydrodynamics have explored erosion and flood risk for Venice and aimed to evaluate the impact of saltmarsh restoration on flood and erosion risk. However, hypoxia, as an expression of adverse impacts on water quality, is one such hazard with only limited predictions and projections of its future occurrence. Understanding the behaviour of hypoxia in coastal areas, to complement the knowledge already

attained for erosion and flood risk, is essential to inform adaptation strategies. This work elaborated the development of a hybrid BGC-ML model to advance the accuracy of future predictions by evaluating the historical, mid- and long-term RCP8.5 scenario. Based on the results it should be noted that hypoxia is projected to increase, with more frequent and longer lasting hypoxic episodes. Moreover, the hypoxia-prone summer season seems to be expanding, with increased hypoxia occurrence in June and autumn. Restoration of coastal habitats may help abate hypoxia through its influence on other associated processes, including nutrient loading, eutrophication and oxygenation. Designing transformative adaptation to safeguard the Venice Lagoon will need to dive deeper into the different restoration interventions and NbS, considering their potential for risk reduction through ecosystem service provisioning, the exploration of synergies between various measures and their cumulative risk reduction. When narrowing the focus on water quality, the long history of restoration interventions and NbS aiming to safeguard the lagoon provides a portfolio, of which four specific measures have been highlighted in relation to hypoxia in particular the establishment of riparian buffer zones, seagrass transplantation, saltmarsh restoration and/or creation, and the re-establishment of lagoon's hydrology. Each of these measures have been tested, and effectively influence water quality through nutrient retention or storage, the release of oxygen, or the restoration of natural gradients. Thereby, through the integration of these measures as part of the extensive Venetian NbS portfolio, implemented as building blocks both in space and time, restoration has the potential to reduce hypoxia occurrence and subsequently reduce its risk.

7.6. References

Ahmed, U., Mumtaz, R., Anwar, H., Shah, A. A., Irfan, R., & García-Nieto, J. (2019). Efficient water quality prediction using supervised machine learning. *Water*, *11*(11), 2210.

Baxter, J. M. (2019). Ocean deoxygenation: everyone's problem. Causes, impacts, consequences and solutions. In Ocean deoxygenation: everyone's problem. Causes, impacts, consequences and solutions. https://doi.org/10.2305/iucn.ch.2019.13.en.

Berti, M., Scardia, F., Carrer, C., & Sorrentino, F. (2022). Analysis of a comprehensive monthly dataset on nitrogen, phosphorus and organic carbon in the Venice lagoon waters (Italy). EQA-International Journal of Environmental Quality, 49, 1–11. https://doi.org/110.6092/issn.2281-4485/14871

Best, M. A., Wither, A. W., & Coates, S. (2007). Dissolved oxygen as a physico-chemical supporting element in the Water Framework Directive. *Marine pollution bulletin*, *55*(1-6), 53-64.

Bisong, E. (2019). Logistic regression. Building machine learning and deep learning models on google cloud platform: A comprehensive guide for beginners, 243-250.

Bonometto, L. (2003). *ECOLOGIA APPLICATA E RIPRISTINO AMBIENTALE NELLA LAGUNA DI VENEZIA: ANALISI E CLASSIFICAZIONE FUNZIONALE DELLE "BARENE" E DELLE TIPOLOGIE DI INTERVENTO SULLE BARENE*. 1–235.

Borin, M., Maucieri, C., Mietto, A., Pavan, F., Politeo, M., Salvato, M., ... & Tocchetto, D. (2014). La fitodepurazione per il trattamento di acque di origine agricola e di reflui zootecnici. Quaderno progetto AQUA, Veneto Agricoltura, ISBN 978-88-6337-107-9, 44 p.

Boscolo Brusà, R., Feola, A., Cacciatore, F., Ponis, E., Sfriso, A., Franzoi, P., ... & Bonometto, A. (2022). Conservation actions for restoring the coastal lagoon habitats: Strategy and multidisciplinary approach of LIFE Lagoon Refresh. *Frontiers in Ecology and Evolution*, *10*, 979415.

Breitburg, D., Levin, L. A., Oschlies, A., Grégoire, M., Chavez, F. P., Conley, D. J., ... & Zhang, J. (2018). Declining oxygen in the global ocean and coastal waters. *Science*, *359*(6371), eaam7240.

Brigolin, D., Rabouille, C., Demasy, C., Bombled, B., Monvoisin, G., & Pastres, R. (2021). Early Diagenesis in Sediments of the Venice Lagoon (Italy) and Its Relationship to Hypoxia. Frontiers in Marine Science, 7(January), 1–15. https://doi.org/10.3389/fmars.2020.575547

Buonocore, E., Grande, U., Franzese, P. P., & Russo, G. F. (2021). Trends and evolution in the concept of marine ecosystem services: an overview. *Water*, *13*(15), 2060.

Caballero-Alfonso, A. M., Carstensen, J., & Conley, D. J. (2015). Biogeochemical and environmental drivers of coastal hypoxia. *Journal of Marine Systems*, *141*, 190-199.

Canu, D. M., Aveytua-Alcazar, L., Laurent, C., Rosati, G., & Solidoro, C. (2023). Is the future given? Cumulative impact of Climate change and MOSE closures on Venice and its lagoon.

Canu, D., Umgiesser, G., & Solidoro, C. (2001). Short-term simulations under winter conditions in the lagoon of Venice: a contribution to the environmental impact assessment of temporary closure of the inlets. In Ecological Modelling (Vol. 138). http://www.salve.it/uk/attivita/OPERE/

Chen, T., & Guestrin, C. (2016, August). Xgboost: A scalable tree boosting system. In *Proceedings of the 22nd acm sigkdd international conference on knowledge discovery and data mining* (pp. 785-794).

Cucco, A., & Umgiesser, G. (2006). Modeling the Venice Lagoon residence time. *Ecological modelling*, *193*(1-2), 34-51.

Diaz, R. J., & Rosenberg, R. (1995). Marine benthic hypoxia: a review of its ecological effects and the behavioural responses of benthic macrofauna. *Oceanography and marine biology. An annual review*, *33*(245), 03.

Diaz, R. J., & Rosenberg, R. (2008). Spreading dead zones and consequences for marine ecosystems. *science*, *321*(5891), 926-929.

Du, J., Shen, J., Park, K., Wang, Y. P., & Yu, X. (2018). Worsened physical condition due to climate change contributes to the increasing hypoxia in Chesapeake Bay. Science of the Total Environment, 630, 707–717. https://doi.org/10.1016/j.scitotenv.2018.02.265

Duvall, M. S., Jarvis, B. M., & Wan, Y. (2022). Impacts of climate change on estuarine stratification and implications for hypoxia within a shallow subtropical system. Estuarine, Coastal and Shelf Science, 279. https://doi.org/10.1016/j.ecss.2022.108146

Facca, C., Bilaničovà, D., Pojana, G., Sfriso, A., & Marcomini, A. (2014). Harmful algae records in venice lagoon and in Po river delta (northern adriatic sea, Italy). *The Scientific World Journal*, *2014*(1), 806032.

Feola, A., Bonometto, A., Ponis, E., Cacciatore, F., Oselladore, F., Matticchio, B., ... & Boscolo Brusà, R. (2018). LIFE LAGOON REFRESH. Ecological restoration in Venice Lagoon (Italy): concrete actions supported by numerical modeling and stakeholder involvement.

Fisher, M. C., Moore, S. K., Jardine, S. L., Watson, J. R., & Samhouri, J. F. (2021). Climate shock effects and mediation in fisheries. Proceedings of the National Academy of Sciences, 118(2), e2014379117.

Freund Yoav, Schapire Robert E , A Decision-Theoretic Generalization of On-Line Learning and an Application to Boosting, Journal of Computer and System Sciences, Volume 55, Issue 1, 1997, Pages 119-139, ISSN 0022-0000, https://doi.org/10.1006/jcss.1997.1504.

Garcia Herncin E. , Gordon Louis I. , (1992), Oxygen solubility in seawater: Better fitting equations, *Limnology and Oceanography*, 37, doi: 10.4319/lo.1992.37.6.1307.

Ghezzo, M., Guerzoni, S., Cucco, A., & Umgiesser, G. (2010). Changes in Venice Lagoon dynamics due to construction of mobile barriers. Coastal Engineering, 57(7), 694–708. https://doi.org/10.1016/j.coastaleng.2010.02.009

Gruber, N., Boyd, P. W., Frölicher, T. L., & Vogt, M. (2021). Biogeochemical extremes and compound events in the ocean. In Nature (Vol. 600, Issue 7889, pp. 395–407). Nature Research. https://doi.org/10.1038/s41586-021-03981-7

Gumiero, B., Boz, B., & Cornelio, P. (2009). River restoration and sustainable agriculture in the Venice Lagoon Basin: the Nicolas project. *Sustainable Use of Water in Agriculture. Water Civilization International Centre, Marie Curie actions, Treviso Italy*, 43-52.

Howarth, R., Chan, F., Conley, D. J., Garnier, J., Doney, S. C., Marino, R., & Billen, G. (2011). Coupled biogeochemical cycles: eutrophication and hypoxia in temperate estuaries and coastal marine ecosystems. *Frontiers in Ecology and the Environment*, *9*(1), 18-26.

Hsieh, H. H., Chuang, M. H., Shih, Y. Y., Weerakkody, W. S., Huang, W. J., Hung, C. C., Muller, F. L. L., Ranatunga, R. R. M. K. P., & Wijethunga, D. S. (2021). Eutrophication and Hypoxia in Tropical Negombo Lagoon, Sri Lanka. Frontiers in Marine Science, 8. https://doi.org/10.3389/fmars.2021.678832

Intergovernmental Panel on Climate Change (2014) Climate Change 2014: Synthesis Report. Contribution of Working Groups 646 I. *II and III to the Fifth Assessment Report of the Intergovernmental Panel on Climate Change*, 151.

Khani, S., & Rajaee, T. (2017). Modeling of dissolved oxygen concentration and its hysteresis behavior in rivers using wavelet transform-based hybrid models. *CLEAN–Soil, Air, Water*, *45*(2).

Kim, T., Noh, J., Kwon, B. O., Lee, C., Kim, B., Kwon, I., ... & Khim, J. S. (2020). Natural purification capacity of tidal flats for organic matters and nutrients: A mesocosm study. *Marine Pollution Bulletin*, *154*, 111046.

Kwiatkowski, L., Torres, O., Bopp, L., Aumont, O., Chamberlain, M., Christian, J. R., ... & Ziehn, T. (2020). Twenty-first century ocean warming, acidification, deoxygenation, and upper-ocean nutrient and primary production decline from CMIP6 model projections. Biogeosciences, 17(13), 3439-3470.

Lee, H. H., Chang, C. C., Shieh, M. J., Wang, J. P., Chen, Y. T., Young, T. H., & Hung, S. C. (2013). Hypoxia enhances chondrogenesis and prevents terminal differentiation through PI3K/Akt/FoxO dependent anti-apoptotic effect. Scientific reports, 3(1), 2683.

Lehrter, J., Ko, D., Lowe, L., & Penta, B. (2017). Predicted Effects of Climate Change on Northern Gulf of Mexico Hypoxia. In Modeling Coastal Hypoxia: Numerical Simulations of Patterns, Controls and Effects of Dissolved Oxygen Dynamics (pp. 173–214). https://doi.org/10.1007/978-3-319-54571-4_8

Liaw, A., & Wiener, M. (2002). Classification and regression by randomForest. R news, 2(3), 18-22.

Lionello, P., Nicholls, R. J., Umgiesser, G., & Zanchettin, D. (2021). Venice flooding and sea level: past evolution, present issues, and future projections (introduction to the special issue). *Natural Hazards and Earth System Sciences*, *21*(8), 2633-2641.

Low, N. H., Micheli, F., Aguilar, J. D., Arce, D. R., Boch, C. A., Bonilla, J. C., ... & Woodson, C. B. (2021). Variable coastal hypoxia exposure and drivers across the southern California Current. *Scientific reports*, *11*(1), 10929.

Mallette, A., Smith, T. F., Elrick-Barr, C., Blythe, J., & Plummer, R. (2021). Understanding preferences for coastal climate change adaptation: a systematic literature review. Sustainability, 13(15), 8594.

Markus Meier, H. E., Dieterich, C., & Gröger, M. (2021). Natural variability is a large source of uncertainty in future projections of hypoxia in the Baltic Sea. *Communications Earth & Environment*, *2*(1), 50.

Micheletti, C., Gottardo, S., Critto, A., Chiarato, S., & Marcomini, A. (2011). Environmental quality of transitional waters: The lagoon of Venice case study. Environment International, 37(1), 31–41. https://doi.org/https://doi.org/10.1016/j.envint.2010.06.009

Munari, C., & Mistri, M. (2011). Short-term hypoxia modulates Rapana venosa (Muricidae) prey preference in Adriatic lagoons. Journal of Experimental Marine Biology and Ecology, 407(2), 166–170. https://doi.org/10.1016/j.jembe.2011.06.003

Nichols, C. R., Zinnert, J., & Young, D. R. (2019). Degradation of coastal ecosystems: causes, impacts and mitigation efforts. *Tomorrow's Coasts: Complex and Impermanent*, 119-136.

Ozkiper, O., Allegrie, E., Bianconi, A., Pham, H.V., Furlan, E., Simide R., van der Geest, M., Critto, A. (in prep). A GIS-MCDA approach to map environmental suitability of Posidonia oceanica meadows as blue nature-based solutions in the Mediterranean eco-region. STOTEN

NOAA (National Oceanic and Atmospheric Administration). 2007. Marine Biodiversity. https://oceanexplorer.noaa.gov/explorations/07twilightzone/background/biodiversity/biodiversity.html.

Paerl, H. W. (2006). Assessing and managing nutrient-enhanced eutrophication in estuarine and coastal waters: Interactive effects of human and climatic perturbations. Ecological Engineering, 26(1), 40–54. https://doi.org/10.1016/j.ecoleng.2005.09.006

Pedregosa, F., Varoquaux, G., Gramfort, A., Michel, V., Thirion, B., Grisel, O., ... & Duchesnay, É. (2011). Scikit-learn: Machine learning in Python. the Journal of machine Learning research, 12, 2825-2830.

Pesce, M., Critto, A., Torresan, S., Giubilato, E., Santini, M., Zirino, A., Ouyang, W., & Marcomini, A. (2018). Modelling climate change impacts on nutrients and primary production in coastal waters. Science of the Total Environment, 628–629, 919–937. https://doi.org/10.1016/j.scitotenv.2018.02.131

Pezner, A.K., Courtney, T.A., Barkley, H.C. *et al.* Increasing hypoxia on global coral reefs under ocean warming. *Nat. Clim. Chang.* **13**, 403–409 (2023). https://doi.org/10.1038/s41558-023-01619-2

Politikos, D. V., Petasis, G., & Katselis, G. (2021). Interpretable machine learning to forecast hypoxia in a lagoon. *Ecological Informatics*, *66*, 101480.

Renaud, M. L. (1986). Detecting and avoiding oxygen deficient sea water by brown shrimp, Penaeus aztecus (Ives), and white shrimp Penaeus setiferus (Linnaeus). *Journal of Experimental Marine Biology and Ecology*, *98*(3), 283-292.

Reynolds, L. K., Waycott, M., McGlathery, K. J., & Orth, R. J. (2016). Ecosystem services returned through seagrass restoration. Restoration Ecology, 24(5), 583-588.

Rivadeneyra, P., Cornacchia, F., Martinez, A., Bidoia, M., & Giupponi, C. (2024). Multi-platform assessment of coastal protection and carbon sequestration in the Venice Lagoon under future scenarios.

Sampaio, E., Santos, C., Rosa, I. C., Ferreira, V., Pörtner, H.-O., Duarte, C. M., Levin, L. A., & Rosa, R. (2021). Impacts of hypoxic events surpass those of future ocean warming and acidification. Nature Ecology & Evolution, 5(3), 311–321. https://doi.org/10.1038/s41559-020-01370-3

Sfriso, A. A., Sciuto, K., Mistri, M., Munari, C., Juhmani, A. S., Buosi, A., ... & Sfriso, A. (2023). Where, when, how and what seagrass to transplant for long lasting results in transitional water systems: the cases of Cymodocea nodosa, Zostera marina, Zostera noltei and Ruppia cirrhosa. *Frontiers in Marine Science*, *10*, 1299428.

Sfriso, A., Buosi, A., Facca, C., Sfriso, A. A., Tomio, Y., Juhmani, A. S., ... & Bonometto, A. (2021). Environmental restoration by aquatic angiosperm transplants in transitional water systems: The Venice Lagoon as a case study. *Science of the Total Environment*, *795*, 148859.

Sfriso, A., Buosi, A., Sciuto, K., Wolf, M., Tomio, Y., Juhmani, A. S., & Sfriso, A. A. (2022). Effect of ecological recovery on macrophyte dominance and production in the venice lagoon. *Frontiers in Marine Science*, *9*, 882463.

Sfriso, A., Facca, C., & Ghetti, P. F. (2009). Validation of the Macrophyte Quality Index (MaQI) set up to assess the ecological status of Italian marine transitional environments. *Hydrobiologia*, *617*, 117-141.

Sfriso, A., & Facca, C. (2007). Distribution and production of macrophytes and phytoplankton in the lagoon of Venice: comparison of actual and past situation. In *Lagoons and Coastal Wetlands in the Global Change Context: Impacts and Management Issues: Selected papers of the International Conference "CoastWetChange", Venice, 26–28 April 2004* (pp. 71-85). Springer Netherlands.

Sokolova, I. M., & Lannig, G. (2008). Interactive effects of metal pollution and temperature on metabolism in aquatic ectotherms: implications of global climate change. *Climate research*, *37*(2-3), 181-201.

Solidoro, C., Bandelj, V., Bernardi, F. A., Camatti, E., Ciavatta, S., Cossarini, G., ... & Torricelli, P. (2010). Response of the Venice Lagoon ecosystem to natural and anthropogenic pressures over the last 50 years. *Coastal lagoons: Critical habitats of environmental change*, *8*, 483-511.

Solidoro, C., Pastres, R., Cossarini, G., & Ciavatta, S. (2004). Seasonal and spatial variability of water quality parameters in the lagoon of Venice. *Journal of Marine Systems*, *51*(1-4), 7-18.

STAP. (2011). Hypoxia and Nutrient Reduction in the Coastal Zone. Advice for Prevention, Remediation and Research. A STAP Advisory Document. Global Environment Facility, Washington, DC.

Stutter, M., Kronvang, B., Ó hUallacháin, D., & Rozemeijer, J. (2019). Current insights into the effectiveness of riparian management, attainment of multiple benefits, and potential technical enhancements. Journal of Environmental Quality, 48(2), 236-247.

Tagliapietra, D., Baldan, D., Barausse, A., Buosi, A., Curiel, D., Guarneri, I., ... & Ghirardini, A. V. (2018). Protecting and restoring the salt marshes and seagrasses in the lagoon of Venice. *Management and Restoration of Mediterranean Coastal Lagoons in Europe. Included in the Project "LIFE Pletera (LIFE13 NAT/ES/001001)*, 39-65.

Tellier, J. M., Kalejs, N. I., Leonhardt, B. S., Cannon, D., Höök, T. O., & Collingsworth, P. D. (2022). Widespread prevalence of hypoxia and the classification of hypoxic conditions in the Laurentian Great Lakes. In Journal of Great Lakes Research (Vol. 48, Issue 1, pp. 13–23). International Association of Great Lakes Research. https://doi.org/10.1016/j.jglr.2021.11.004

Tramblay, Y., Koutroulis, A., Samaniego, L., Vicente-Serrano, S. M., Volaire, F., Boone, A., Le Page, M., Llasat, M. C., Albergel, C., Burak, S., Cailleret, M., Kalin, K. C., Davi, H., Dupuy, J. L., Greve, P., Grillakis, M., Hanich, L., Jarlan, L., Martin-StPaul, N., … Polcher, J. (2020). Challenges for drought assessment in the Mediterranean region under future climate scenarios. In Earth-Science Reviews (Vol. 210). Elsevier B.V. https://doi.org/10.1016/j.earscirev.2020.103348

Umgiesser, G. (2020). The impact of operating the mobile barriers in Venice (MOSE) under climate change. Journal for Nature Conservation, 54. https://doi.org/10.1016/j.jnc.2019.125783

Vaquer-Sunyer, R., & Duarte, C. M. (2008). Thresholds of hypoxia for marine biodiversity. *Proceedings of the National Academy of Sciences*, *105*(40), 15452-15457.

Zanchettin, D., Bruni, S., Raicich, F., Lionello, P., Adloff, F., Androsov, A., Antonioli, F., Artale, V., Carminati, E., Ferrarin, C., Fofonova, V., Nicholls, R. J., Rubinetti, S., Rubino, A., Sannino, G., Spada, G., Thiéblemont, R., Tsimplis, M., Umgiesser, G., … Zerbini, S. (2021). Review article: Sea-level rise in Venice: historic and future trends, Nat. Hazards Earth Syst. Sci. Discuss. Natural Hazards and Earth System Science. https://doi.org/https://doi.org/10.5194/nhess-2020-351

Zennaro, F., Furlan, E., Canu, D., Alcazar, L. A., Rosati, G., Solidoro, C., ... & Critto, A. (2023). Venice lagoon chlorophyll-a evaluation under climate change conditions: A hybrid water quality machine learning and biogeochemical-based framework. *Ecological Indicators*, *157*, 111245.

Zhang, J., Gilbert, D., Gooday, A. J., Levin, L., Naqvi, S. W. A., Middelburg, J. J., Scranton, M., Ekau, W., Peña, A., Dewitte, B., Oguz, T., Monteiro, P. M. S., Urban, E., Rabalais, N. N., Ittekkot, V., Kemp, W. M., Ulloa, O., Elmgren, R., Escobar-Briones, E., and Van der Plas, A. K.: Natural and human-induced hypoxia and consequences for coastal areas: synthesis and future development, Biogeosciences, 7, 1443–1467, https://doi.org/10.5194/bg-7-1443-2010, 2010.

Zhou, Q., Qi, Y., Tang, H., & Wu, P. (2023). Machine learning-based processing of unbalanced data sets for computer algorithms. Open Computer Science, 13(1). https://doi.org/10.1515/comp-2022-0273.

8. Ecosystem services provision as a function of restoration scale in Arcachon Bay

Brière, C.[1], Fornasari, J.[1], Caillibotte, R.[1], Mahe, S.[1] & Beudin, A.[1]

[1] *EGIS WATER & MARITIME, France*

ABSTRACT: Arcachon Bay, located in the Nouvelle-Aquitaine region of France, hosts Europe's largest Zostera seagrass bed, which has experienced significant decline over recent decades. Though restoration efforts are being considered, they currently operate on a small to medium scale. The study aims to demonstrate the benefits of upscaling Zostera seagrass restoration to enhance key services for disaster risk reduction and climate adaptation, while also enhancing biodiversity. To do so, the study emphasizes the connection between the natural system and the socio-economic system, addressing technical challenges related to data metrics availability, and proposes a three-layer systemic modelling approach to evaluate the achievement of ecosystems goals as a function of the restoration scale. The first layer involves an eco-morphodynamic modelling system to simulate natural system dynamics, including hydrodynamics and morphological changes. The second layer is a conceptual socio-economic system model that links socio-economic activities to ecosystem services provided by seagrass beds. The third layer evaluates the impact of restoration actions on ecosystem services, considering different restoration scales and climate change scenarios. Results indicate that large-scale restoration generally improves sediment dynamics control, reduces turbidity, and positively impacts water renewal times, particularly in the northern and eastern parts of the bay. However, partial restoration may yield better outcomes for certain ecosystem goals, such as water quality improvement and sediment control dynamics in the innermost parts of the bay. The study underscores the importance of considering both physical and socio-economic drivers to achieve successful large-scale restoration. Sea-level rise is identified as a key physical driver influencing the system's response, while socio-economic factors such as land use, urbanization, and navigation activities also play significant roles. The findings highlight the potential of large-scale seagrass restoration to enhance biodiversity, improve ecosystem services, and contribute to climate adaptation and disaster risk reduction. The study provides a framework for evaluating restoration interventions and emphasizes the need for integrated approaches that consider both natural system dynamics and socio-economic factors.

8.1. Introduction

Human activities and settlements have long been drawn to coastal regions. Historically, these areas have been used extensively, but the 20th century saw a marked increase in human-induced pressures (Neumann, 2015). These growing pressures have had detrimental effects on biological communities, resulting in reduced biodiversity and compromised ecosystem services (Barbier, 2011). Among the affected habitats are seagrass meadows, which consist of submerged flowering plants located in coastal and estuarine systems. Seagrasses, encompassing 72 species within 14 different genera (Short, 2017), flourish in the soft substrates of both subtidal and intertidal areas, and are found along all European coastlines. As noted in the latest IPBES report (2019), these key habitats are rapidly declining worldwide, including in Europe.

Moreover, seagrass has been recognized for its contribution to blue carbon and coastal habitat provision (Vierros, 2017). For instance, the EU Biodiversity Strategy for 2030 specifically mentions these habitats as key carbon-rich ecosystems to be protected and the need to anticipate climate impacts that will trigger spatial shifts. For this reason, seagrass restoration and transplantation projects are being implemented globally in

order to offset carbon emissions and preserve coastal wildlife. Additionally, some studies have more recently explored how seagrass could be used for coastal protection by influencing hydro-morphodynamics at the coast (Orth, 2020). Seagrass meadows is now recognized has a key ecosystem providing many critical ecological functions and ecosystem services, including coastal inundation mitigation, erosion control and coastal stabilisation, water quality improvement, habitats for a high diversity of marine species and support for coastal fisheries, carbon capture and storage.

As part of the Horizon 2020 research and innovation programme, the REST-COAST EU research project (https://rest-coast.eu/https://rest-coast.eu/) has the main objective of demonstrating to what extent coastal restoration upscaling is required to provide a low Carbon (C) solution to climate adaptation and disaster risk reduction for threatened low-lying coastal systems, combined with gains in their biodiversity status. Pilot restoration cases are selected representing coastal vulnerability hotspots in Europe, including the Arcachon Bay Pilot, being the home to the largest seagrass bed of Zostera *noltei* in Europe, and where the protection of tidal flats via Zostera seagrass recovery is targeted using naturalistic engineering techniques.

As indicated by (Sánchez-Arcilla, 2022), the transition from local restoration to large-scale implementation is hampered by a range of technical, financial and governance barriers. Moreover, it is emphasized that these barriers are difficult to overcome without large enough interventions that demonstrate the potential of restoration for enhancing biodiversity and ecosystem service delivery. Technical barriers in the metrics for coastal biodiversity and ecosystem services have more especially exerted a negative effect on socio-economic engagement towards large-scale restoration. This is compounded by the wide range of scales for assessing restoration performance. As illustration, the establishment of some coastal vegetation may require months, while decades may be needed to achieve fully developed wetlands. Further technical barriers are introduced by the effect of meteo-oceanographic extremes such as wave storms, whose impact is hard to predict on the mid- to long-term scales.

In line with the REST-COAST objectives, this study aims at addressing the technical barrier related to data-metrics availability, while investigating the benefits of the large-scale recolonisation of Zostera in the Arcachon Bay Pilot. To that end a system modelling approach is developed using a suite of hydrodynamic and morphological simulations and associated responses as input data, to assess the impact on a selection of ecosystem services as a function of restoration scale and climatic conditions, taking also into account the socio-economic environment of the Arcachon Bay.

The methodology follows (Slinger, 2000) and (Slinger, 2023) by introducing a three-layer systemic modelling approach. The first layer corresponds to the study of the natural system dynamics, using an eco-morphodynamic modelling approach. The second layer consists of a conceptual socio-economic system modelling. The third layer finally addresses the evaluation of restoration actions in terms of their impact on ecosystem services using indicators representative of the natural and socio-economic systems components and for two future horizons. Ecosystem goals are evaluated as a function of projection horizon and restoration scale, in the context of climate change.

The publication is structured as follows. Section 8.2 presents the case study area from its natural perspective and socio-economic activities. After a short introduction about the three-layer systemic modelling approach, section 8.3 focusses on the natural and socio-economic systems description and on the evaluation framework. Section 8.4, 8.5, and 8.6 provide results, discussion points and concluding remarks respectively.

8.2. Case study area

8.2.1. The Arcachon Bay natural system

The Arcachon Bay lies along the southwest coast of France, situated within the Nouvelle-Aquitaine region (Figure 8-1). The bay opens to the sea between Cap Ferret and Arcachon and is a complex system made of primary and secondary channels, surrounding tidal flats.

Arcachon Bay covers approximately 174 km² at high tide, with about 65% of this area exposed at low tide. The tidal cycle is semi-diurnal with minimal diurnal inequality, and tidal amplitude ranges from 0.8 m during neap tides to 4.6 m during spring tides. The mean depth is 4.6 m (Ganthy et al. 2013). Wind-generated waves are the second primary hydrodynamic force in the bay, following tidal forcing (Parisot et al. 2008). The entry of offshore waves into the bay is restricted by the bay's geometry and bathymetry. Inside the bay, wind-induced wave generation is significantly influenced by the tide, which affects both water height and fetch length.

The bay communicates with the sea through two main channels, separated by the Arguin Bank. Many small streams flow into the lagoon, but the two main rivers, the Eyre and the Porges Canal, contribute more than 95% (73% and 24%, respectively) of the total annual freshwater inflows (Plus et al. 2009). The mean monthly flows range from 8.4 to 38.6 $m^3.s^{-1}$ for the Eyre and from 1.8 to 12.9 $m^3.s^{-1}$ for the Porges canal, with maxima occurring in February and minima in August.

At the main entrance and in the channels, medium sand (between 320 and 500 µm) and gravels are predominantly found. The secondary channels mainly consist of sand and muddy sand (a mix between 175 and 365 µm). The intertidal flats are composed of sandy mud and muddy sands (Cayocca, 1996; Bouchet et al. 1997).

Human well-being is intrinsically linked to ecosystems, a relationship that can be articulated through the concept of ecosystem services (e.g. Costanza and Kubiszewski, 2012). Seagrass beds, for instance, offer a range of ecosystem services (ESS) including coastal erosion control, reduction of coastal flooding, water quality improvement, provision of natural habitats for coastal marine species, and carbon sequestration (e.g. Balle-Beganton et al. 2015).

Arcachon Bay hosts the largest Zostera seagrass bed in Europe (PNMBA), where two species of Zostera coexist: Zostera noltii, primarily found in intertidal areas, and Zostera marina, located in submerged zones along the channel edges (Auby et al., 2011). Additionally, the bay is rich in biodiversity with more than 500 different species identified (PNMBA).

The Millenium Ecosystem Assessment (MA, 2005) revealed that more than 60% of ecosystem services are being degraded or transformed, posing a threat to future human well-being. Specifically, in Arcachon Bay, a significant decline in the spatial extent of seagrass beds was observed between 1989 and 2012, with a 38% reduction for Zostera noltii and an 85% reduction for Zostera marina (Cognat, 2019). This decline may be attributed to heat waves, the adverse effects of pollutants, and amplification loops that exacerbate the phenomenon.

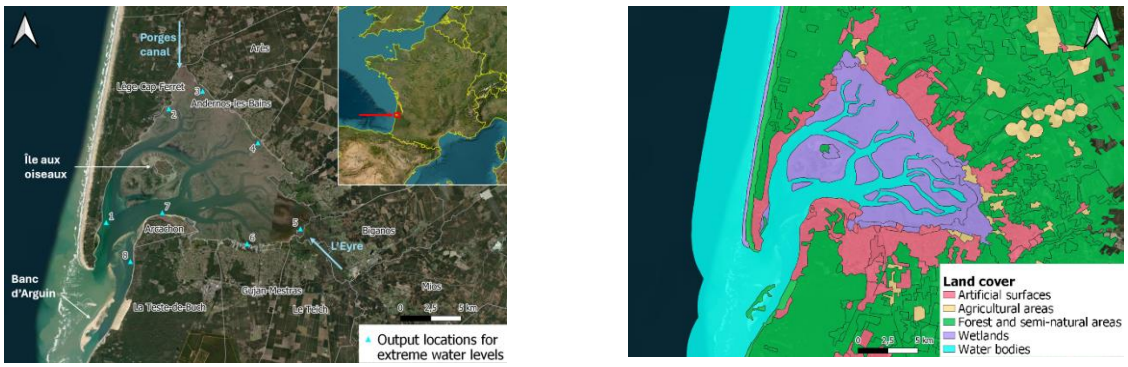

Figure 8-1 General situation of Arcachon Bay and main freshwater inputs (left), land cover around the bay (CORINE Land Cover)

8.2.2. The Arcachon Bay socio-economic system

The socio-economic system of Arcachon Bay is a dynamic and multifaceted network that balances economic development with environmental sustainability and social well-being. The region's natural resources and cultural heritage are central to its identity and economic vitality. Prevalent economic activities are tourist-driven marine activities, fishing and oyster farming.

Arcachon Bay is a tourist destination, attracting approximately 1 million visitors annually (Arcachon Tourist Office website). Tourism drives local businesses, including hotels, restaurants, and services, including recreational fishing, pleasure boating, visits to popular sites such as the Banc d'Arguin and Île aux Oiseaux. Tourism generates significant revenue for the local economy, estimated at around €500 million annually (INSEE website).

The bay supports a vibrant fishing industry, particularly known for its oyster farming, producing around 10,000 tons of oysters annually, and contributing approximately €50 million to the local economy each year. (CRCAA website). The fishing industry, although smaller than oyster farming, is also significant. The bay supports a variety of fisheries, including shellfish, finfish, and crustaceans. The total annual catch from fishing activities in Arcachon Bay is estimated to be around 2,000 tons (Ifremer website).

Land cover analysis of the Arcachon Bay territory (Figure 8-1) reveals that within the first 200 meters from the coastline (excluding wetlands), approximately 75% consists of artificial zones, 20% is covered by forests and semi-natural areas, and 5% is agricultural land.

From a social perspective, the bay area is home to a mix of permanent residents and seasonal visitors. The population swells during the summer months due to tourism. The tourism sector provides employment for approximately 5,000 people in the region, including seasonal jobs (Arcachon Tourist Office website), while oyster farming and related activities provide employment for around 1,000 people in the region (CRCAA website).

8.2.3. On-going and planned restoration activities

At Arcachon Bay, the influx of tourists and the growth of local industries place demands on infrastructure, including transportation, waste management, and public services. Issues such as pollution, habitat loss, and climate change pose significant threats to the bay's ecosystem. These environmental challenges can have socio-economic repercussions, affecting industries like fishing and tourism.

There are ongoing efforts to preserve the natural environment at Arcachon Bay, including its seagrass beds and diverse marine life. Conservation initiatives are supported by local, regional, and national agencies. The marine park management plan adopted in 2017 for a 15-year period (PNMBA, 2017) provides a framework for other actions in addition to Zostera restoration. Restoration should be supported by raising awareness among users, alerting them to the impacts and providing information on best practices. In addition, the quality and quantity of freshwater must be ensured, 'excellent' bathing quality must be achieved for all beaches, and 75% of the oyster-farming wasteland must be rehabilitated. Local memories and maritime heritage must be preserved.

The Parc Naturel Marin du Bassin d'Arcachon (PNMBA) is actively involved in several restoration efforts to ensure the health and sustainability of seagrass beds. A Seagrass Bed Monitoring and Mapping project aims at regularly monitoring and mapping the extent and health of seagrass beds, particularly Zostera noltii and Zostera marina. Additionally, recurrent Habitat Restoration Projects aim at actively restoring degraded seagrass habitats through transplantation and other techniques. Proposed technical innovations to stimulate seagrass re-growth include a hybrid solution centered around a tidal current attenuation device known as La Roselière (Sánchez-Arcilla, 2022). This biomimetic device mimics the sheltering effects of grass and algae and consists of ropes of adjustable length with attached coconut wicks. The grey infrastructure component provides the hydro-morphodynamic damping necessary for seagrass to develop under a broader range of hydrodynamic conditions, including those influenced by climate change or human activities (e.g., sea-level

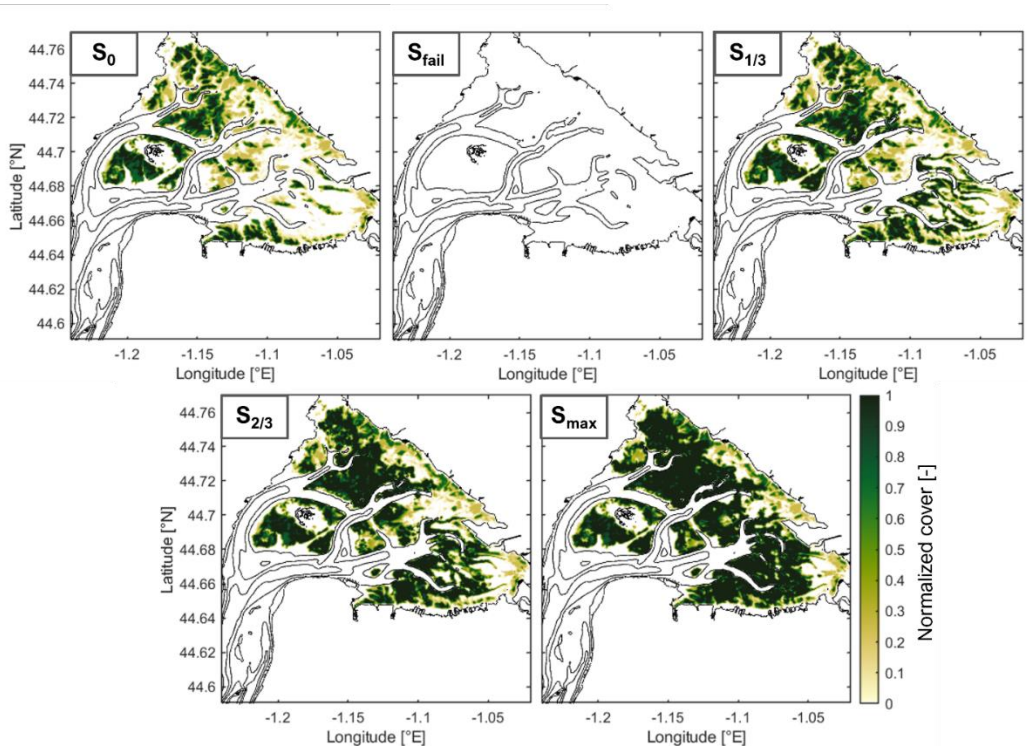

Figure 8-2 Normalized seagrass cover for each of the studied restoration scenarios: S_0, S_fail, S_1/3, S_2/3 and S_max.

rise or increased tidal currents due to dredging). The Nature-based Solution aspect of this intervention promotes seagrass development, which in turn further dampens hydrodynamic forces and enhances the system resilience to future disturbances, a growing concern for coastal lagoons worldwide.

The current restoration efforts using La Roselière modules follow a three-phase scaling-up method. The first phase involves a small-scale experiment to calibrate the La Roselière modules. This is followed by a medium-scale deployment aimed at supporting the recovery of Zostera over a 1-hectare area. The final phase will involve a large-scale restoration plan at the basin level.

In this study, the following five restoration scenarios have been considered (Figure 8-2):

- **S_fail**: restoration failure corresponding to the disappearance of all seagrass beds.
- **S_0**: current vegetation condition that will be maintained in the long term (0% further restoration).
- **S_1/3**: 1/3 of the full restoration potential.
- **S_2/3**: 2/3 of the full restoration potential.
- **S_max**: maximum restoration potential (100%) based on the pre-regression state of 1989

8.3. Methods

8.3.1. Three-layer systemic modelling approach

To characterize the substantive connection between the eco-morphology and socio-economics, a hybrid three-layer approach (Figure 8-3) is designed to connect numerical hydro-eco-morphological model simulations through the socio-economic model to the ecosystem goals. The first level of the three-layer systemic modelling approach uses morphological simulations of bed topography and associated hydrodynamic responses as input data. These simulations are transformed to relevant natural system indicators, such as bed level changes, inundation extent, turbidity levels and water renewal times. The second level consists of describing a conceptual socio-economic system with system variables or actions that can be

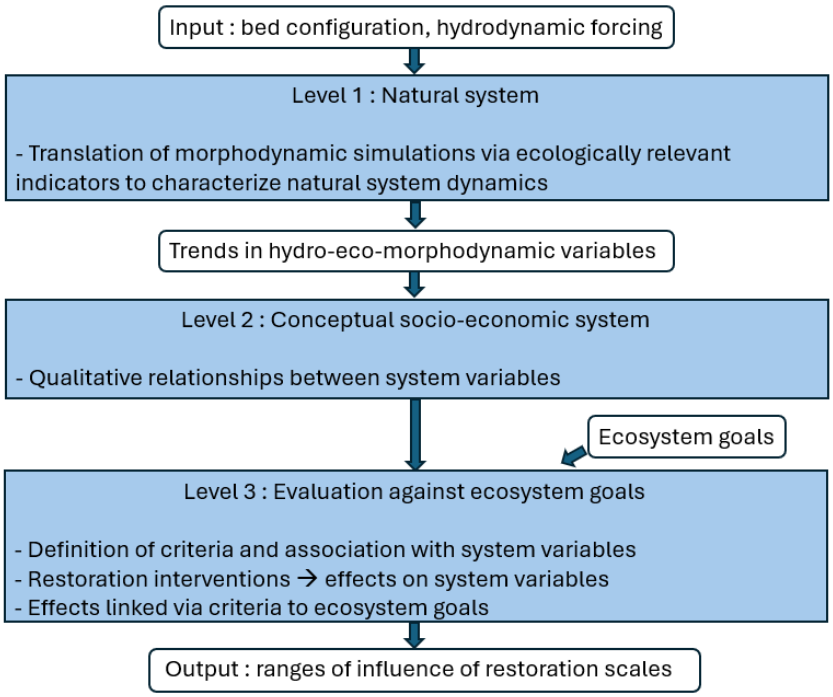

Figure 8-3 Integrated three-level hybrid modelling system that translates hydro-eco-morphological simulations via ecologically relevant indicators, which are linked to the conceptual socio-economic model variables for evaluation of ecosystem goals as a function of restoration scales. Adapted from (Slinger, 2000) and (Slinger, 2023).

associated to the natural system indicators. In level 3, the criteria for evaluating the achievement of ecosystem goals are identified and systematically linked to the system variables. The impacts of seagrass restoration interventions are assessed qualitatively by initially determining the strength and direction of their effects on individual system variables. Subsequently, the outcomes are evaluated as these effects ripple through the ecosystem.

8.3.2. Natural system dynamics

Modelling approach and configuration

The D-FM numerical modelling suite (Delft3D, 2023) has been chosen to simulate the hydrodynamics and morphodynamics in Arcachon Bay due to its computational efficiency and widespread use within the coastal community for modelling morphological evolutions. This model solves non-linear shallow water equations, derived from the three-dimensional Navier-Stokes equations for the flow of incompressible fluids.

The model is implemented on a 2D curvilinear grid that covers Arcachon Bay and the adjacent coastal area on the ocean side. The grid resolution ranges from 100m within the bay to 300m at the offshore boundaries. The model bathymetry (Figure 8-4) is based on bathymetric surveys processed by Ifremer in 2016.

The effect of seagrass meadows is incorporated using the formulations of Baptist (2005), which distinguish between the impact of vegetation on flow resistance and bed roughness. In some conventional formulations, flow resistance is calculated by increasing bed roughness (James et al. 2004). However, this approach results in higher bed shear stress and greater sediment transport rates when modelling morphological changes. To address this, a $-(\lambda u^2)/2$ term is included in the momentum equation (where λ represents the flow resistance of the vegetation and u is the flow velocity) to account for reduced bed shear stress and lower sediment transport rates. To better understand the influence of vegetation on hydrodynamic components, various vegetation configurations are employed. Specifically, Mütterlein et al. (2016) proposed parameter values for coverage, leaf length, leaf width, and leaf density that are representative of Arcachon Bay, which were used in the MARS3D model developed by Ifremer (Kambiadou et al. 2014; Cognat, 2019). They suggested different

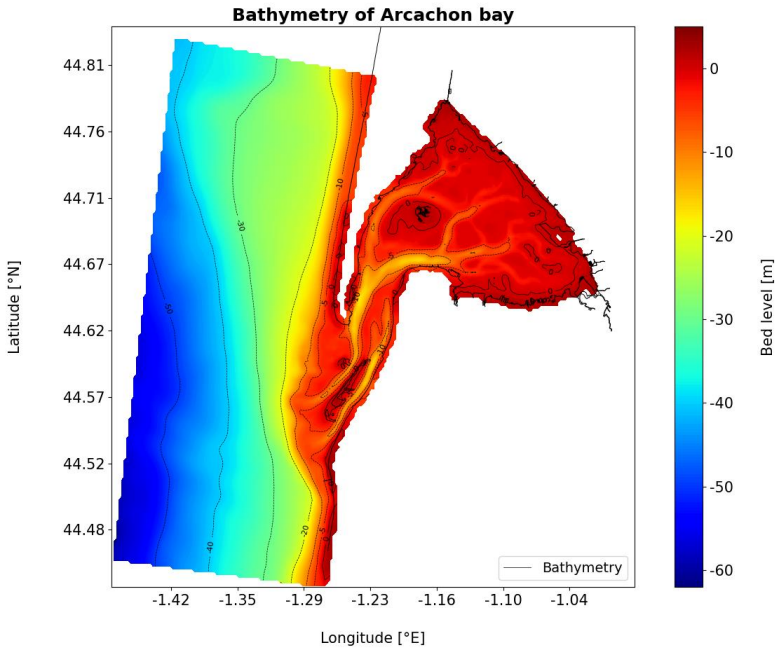

Figure 8-4 Initial bathymetry applied in the model (m with respect to current MSL).

configurations depending on the season, as these parameters have higher values in summer than in winter. For the purpose of evaluating the effectiveness of restoration scenarios, only the summer configuration is considered.

Given that the modelling application aims to ultimately assess the influence of restoration scales on the three main ecosystem services provided by seagrass at Arcachon Bay—namely flooding reduction, sediment dynamics control, and water quality improvement (see also section on the conceptual socio-economic system)—distinct models are implemented:

- an eco-wave-hydro model (model 1) for computing wave characteristics and water levels, accounting for storm surges, at various nearshore locations, and for different extreme events (stationary model),
- an eco-wave-hydro model (model 2) for computing water renewal times and turbidity levels, over a spring-neap time cycle,
- an eco-hydro-morpho model (model 3) for representing morphological evolutions of tidal flats and channels within the bay.

Model boundary conditions

The hydrodynamic model is driven by meteorological data from the ERA5 reanalysis model by ECMWF, tidal harmonic components derived from tidal gauge time series located in Arcachon harbor (REFMAR, SHOM), freshwater inputs from the Leyre River (site S2242510, HydroPortail), and offshore waves from the IOWAGA database (products from the large-scale model by (Ardhuin, et al., 2014).

Extreme water levels in Arcachon Bay are influenced by tidal processes, wind-induced waves, and meteorological factors like atmospheric pressure during storms. Therefore, flooding scenarios, to be studied with model 1, are primarily defined by analyzing wind forcings rather than offshore waves (Parisot et al. 2008). An extreme values analysis uses a 1-year block maxima approach to determine extreme wind speeds linked to return periods, fitted with the Gumbel distribution. The same method is applied to water levels measured by SHOM at the Eyrac station in Arcachon harbor. A multivariate analysis considers the co-occurrence of extreme water levels and extreme wind conditions (speed and direction). Following the JOIN-SEA approach by Mugica et al. (2014), a 100-year return period for such concomitant events is assessed. The

results, presented in Table 8-1, align with Mugica et al.'s findings, identifying the most unfavorable wind directions for coastal flooding.

Table 8-1 Definition of flooding events for different return periods, based on joint analysis of water levels and wind characteristics.

Return period (year)	Water level (m MSL)	Wind speed (m.s-1)	Wind direction (°N)
1	1.92	10.6	[270°, 215°]
5	2.18	12.4	[270°, 215°]
10	2.42	16.6	[270°, 215°]
100	2.65	22.6	[270°, 215°]

For morphodynamic simulations carried out with model 3, the hydrodynamic module calculates water levels and vertically averaged currents, initiating sediment movement. The morphodynamic module is then applied to represent sediment dynamics and morphological evolutions. It accounts for both bedload and suspended load transport of cohesive and non-cohesive sediments and calculates bed level changes using the concept of the morphological acceleration factor (Lesser, 2004). A schematic representation of tidal forcing, indicative of long-term morphological bed evolutions, is based on the method by Schrijvershof et al. (2023). To account for the complex sand-mud mixtures within the bay, the formulation by van Ledden (2003) is used, in conjunction with the van Rijn (1993) transport formula for sand.

The coupled hydro-eco-morphodynamic model is validated using bathymetric surveys from 2016 and 2019, proving its accuracy in assessing morphological changes over a three-year span in a complex coastal estuarine environment (see following section). However, this validation period is too brief for predicting changes over multiple decades, raising questions about the existence and nature of a morphological equilibrium. Achieving such equilibrium is challenging due to constantly evolving external conditions, making reliable long-term predictions uncertain (Dam et al., 2016). Given these challenges, various methodologies have been explored to evaluate morphological projections for the bay, including considerations regarding the tidal asymmetry modification due to the presence of seagrass (not detailed here). Due to inherent uncertainties, a more straightforward approach is adopted. The current methodology involves shorter, three-year simulations using a morphological acceleration factor. The initial bathymetry remains constant for each scenario, and the effects of different restoration scenarios are analysed by assessing various bio-physical indicators such as erosion/sedimentation rates on the tidal flats and in the channels.

Model calibration and validation

In-situ observations from various sampling stations within Arcachon Bay are used for model calibration and validation. These stations measured water levels (m; 9 sampling stations), wave characteristics (Hs in m, Tp in s, Direction in °N, etc.; 3 stations), and sediment characteristics and concentrations (11 stations) during the 2015-2016 period. Data collected in 2015 are used to calibrate all models. Subsequently, models 1 and 2 are validated against data collected in 2016. Model 3 is validated against sediment concentration data from 2016 and morphological changes occurring between 2016 and 2019, based on bathymetric surveys conducted by SIBA (Syndicat Intercommunal du Bassin d'Arcachon).

The model results show good agreement with in-situ water level data, despite a slight overestimation (about 10 cm) at stations near the coastline. For wave characteristics, comparisons with observations at three sampling stations indicate that significant wave heights (H_s), peak wave period (T_p), and spectra align well with model results (Figure 8-5). Since waves in the Arcachon Bay are primarily wind-induced, accurate meteorological forcing is crucial. The model uses hourly ERA5 meteorological data, which tend to overestimate wind velocities (Molina et al. 2021), leading to some discrepancies in wave characteristics. Despite uncertainties in spectral wave component analysis, the model's performance is satisfactory. The determination coefficient is 0.6 at the GARR station, near intertidal areas. Although the model

underestimates wave heights, particularly for higher H_s values, it reasonably captures the overall wave dynamics. The hourly wind forcing may miss some peak values, which should be considered when assessing coastal flooding hazards.

No in situ observations of current velocities are available for the studied period. However, the validated MARS3D modeling platform by Ifremer provides current velocity estimates for 2015-2016. Comparisons between the MARS3D and D-FM model results obtained over a tidal cycle show good agreement in terms of Root Mean Square Error (m/s) and correlation coefficient. D-FM currents in the Arcachon Bay closely match MARS3D calculations, with the largest discrepancies near the bay entrance where MARS3D is less calibrated.

For sediment characteristics, bi-monthly sediment concentration measurements from 2015-2016 are available. Model results, shown in Figure 8-6 are generally in the same order of magnitude as in situ observations. However, the model tends to underestimate low sediment concentrations. The determination coefficient is satisfactory at 0.44 for the Girouasse station.

The validated coupled model allows for the following capabilities: (1) simulating wave generation and propagation driven by wind forcing; (2) accurately representing hydrodynamics influenced by meteorological forcing, tidal processes, and wave interactions; (3) effectively modeling sediment transport and resuspension, encompassing three sediment types; and (4) incorporating the impact of vegetation on waves, hydrodynamics, and erosion/sedimentation patterns.

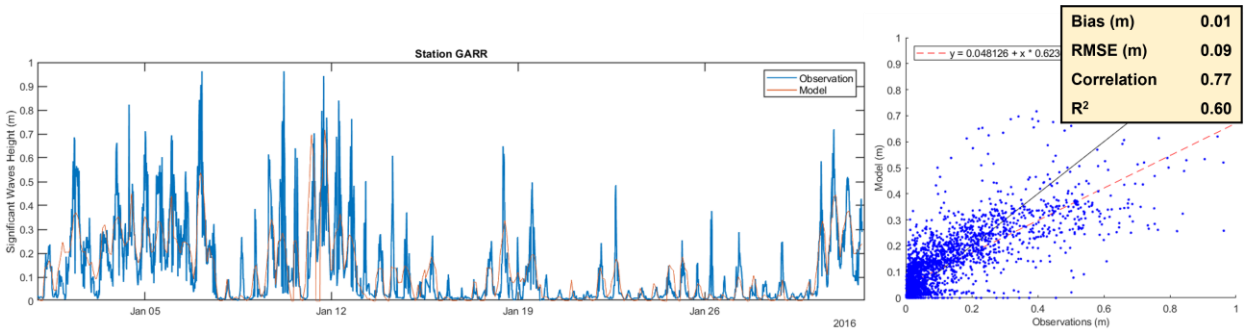

Figure 8-5 Significant waves height (m) for GARR station over the period 2015-2016. Regression diagram for the entire period of simulation (right). The equation of the linear regression is indicated.

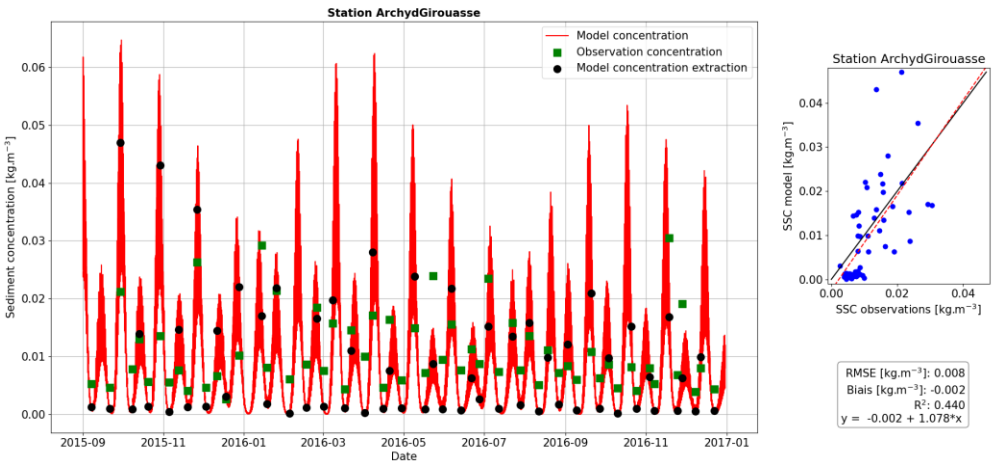

Figure 8-6 Suspended sediment concentration (kg.m-3) for Girouasse station over 2015-2016 period. Regression diagram for the entire period of simulation (right). The equation of the linear regression is indicated.

Climate change scenarios

To evaluate future climate projections, conditions are defined based on IPCC projections. Sea level rise is considered for scenarios SSP2-4.5 and SSP5-8.5, targeting the years 2050, 2070, and 2100. Table 8-2 presents the regional projections of water level rise for the North-European Atlantic coast, as reported by IPCC AR6 (Garner et al. 2021). These projections compare future sea levels to the current mean level (1995-2014) for the two selected climate scenarios (SSP2-4.5 and SSP5-8.5).

Table 8-2 Sea level rise projections (m), median and likely range, for two climate scenarios: SSP2-4.5 and SSP5-8.5. Extracted from "https://sealevel.nasa.gov".

Horizon \ Climate Scenario	SSP2-4.5	SSP5-8.5
2050	0.21	0.23
2070	0.34	0.39
2100	0.53	0.74

IPCC projections for wind magnitude suggest a decrease in mean surface wind (-2.6% by 2100 for scenario SSP5-8.5). After examination of extreme wind events from the Meteo-France station in Cap Ferret, dating back to 1985, no significant trend in the frequency or duration of these events can be detected. On the contrary, a minor uptick in the intensity of maximum wind speeds can be observed. Despite these observations, the extreme values as detailed in Table 8-1 are used for future climate scenarios.

8.3.3. Conceptual socio-economic system

The socio-economic system of Arcachon Bay is characterized by a complex interplay between its natural resources, economic activities, and social dynamics. The key economic components encompass tourist-driven marine activities, including pleasure boating and other water-based recreational activities, as well as fishing.

The population of Arcachon Bay was 138,983 in 2020, reflecting a 9.2% increase over six years (INSEE). During the summer, the population swells to 400,000 (SIBA). Projections indicate a 21% population increase by 2040 (SCoT, sybarval.fr). In 2022, tourism in the bay generated €760 million (SIBA, 2023), with €300 million from restaurants and the food sector, €200 million from accommodation, and the remainder from leisure activities (SIBA, 2023). Tourism can alter water quality through the release of wastewater, increasing the nutrient runoff leading to eutrophication and potentially damaging the seagrass beds (UICN France, 2014), but it can also benefit from the aesthetic appeal of improving water clarity and quality through seagrass beds.

The bay serves as a hub for recreational boating, encompassing both shuttle services and pleasure boating. The shuttle boats primarily connect Arcachon with Moulleau-Cap-Ferret and Andernos (Figure 8-7). The navigation sector comprises 120 companies, provides 450 direct jobs, and generates an annual turnover of €127 million (SIBA, 2023), which also accounts for a portion of the fishing activities. Navigation can alter the water quality and the food provisioning by exerting pressure on the biosphere through noise pollution and introduction of hazardous substances (affecting water quality and subsequently, food supply) (UICN France, 2014; Auby et al., 2011). Potential uprooting/crushing of seagrass may also occur. On the other hand, seagrass beds provide a food reservoir for fish.

Mooring within the bay is regulated and prohibited in Zostera areas. Approximately 5,000 moorings are available, primarily located on the foreshore (mainly in Cap-Ferret and Arcachon) and in the river Eyre (parc-marin-bassin-arcachon.fr, prefectorial decree (Le Corre et al., 2015)). Mooring conditions could be enhanced by reducing both current and wave activity downstream of seagrass beds.

Commercial and recreational fishing activities generate an annual income of €23 million for the port of Arcachon alone ((UICN France, 2014), geoimage.cnes.fr), which hosts 400 professional fishermen. Fishing activities are primarily concentrated in the harbours and navigation channels, but also extend to the mudflats

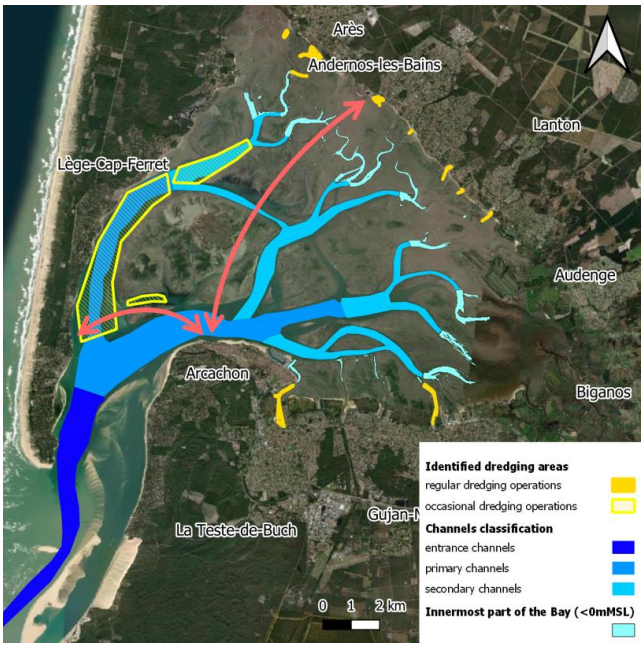

Figure 8-7 Location of identified dredging works (SMPBA 2023), main boating lines (red arrows) and channels classification

Figure 8-8 Location of oyster farms and main beaches and corresponding zoning for modelling post-processing

and beaches for foot and creel fishing, although these are less common. The ports of Arcachon and Lège-Cap-Ferret are the most significantly impacted.

Oyster farming in the Arcachon Bay generates an annual turnover of €35 million (UICN France, 2014) and accounts for 8% of the French oyster production. It spans 780 ha in the bay (Figure 8-8). Beyond its economic significance, oyster farming represents a valuable cultural heritage. Oyster farming can impact the availability of light and sediment stability, which are crucial for the growth and health of seagrass beds (Maxwell, P. et al., 2016). Conversely, the health and productivity of oyster beds are supported by the water filtration and sediment stabilization provided by seagrass beds.

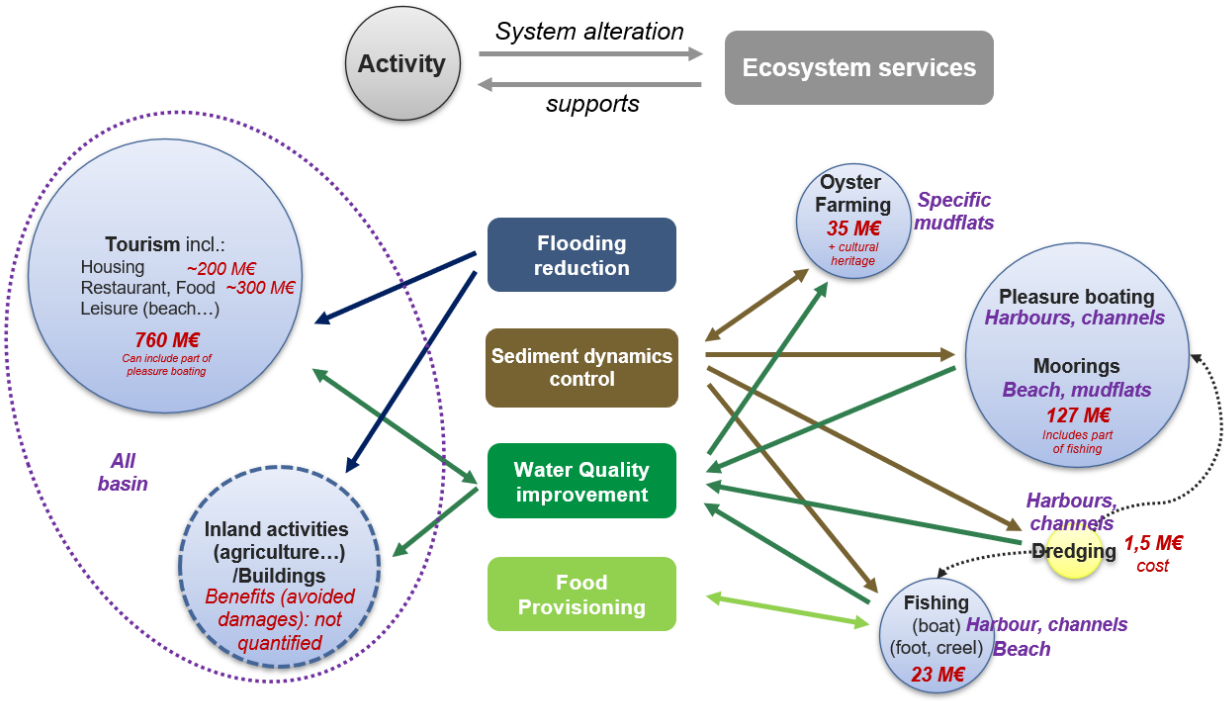

Figure 8-9: Conceptual synthesis of interactions between socio-economic components of the system and provided ESS by seagrass beds.

Dredging in Arcachon Bay is crucial to maintain navigability for all water-related activities. Major dredging operations are conducted approximately every ten years at the bay entrance channels (Gironde.gouv.fr). More regular dredging is planned at the entrances to the ports and in some mooring areas (smpba.fr) and involves an average volume of 30,000 m³ per year and costs €1.5 million annually (smpba.fr). Major dredging projects in the 2000s (SIBA) in the main and secondary channels (Courbey, Arès, Piquey) handled volumes up to 1 million m³. Dredged material can be recycled and used as backfill for sewage treatment plants, to construct forest roads, and as topsoil for landscaping.

Dredging can impact water quality by increasing turbidity and remobilizing tributyltin (TBT), a former antifouling agent banned since 1982 and buried in the substrate (UICN France, 2014), which is hazardous to the biosphere, particularly oysters. Any dredging operation can potentially affect the surrounding environment through habitat degradation, noise pollution, and the remobilization of other contaminants. Conversely, the erosion control provided by Zostera seagrass can help reduce dredging volumes. Seagrass meadows contribute to increased sedimentation by slowing down the water flow in their vicinity (Maxwell et al., 2016).

The conceptual diagram in Figure 8-9 illustrates the interactions between the ecosystem services provided by seagrass and various activities. The size of each circle represents the economic significance of each socio-economic component but does not depict their interdependencies or cultural importance. Considering the interrelationships between the system components, the sediment dynamics control, the flooding reduction and water quality improvement are selected as key ecosystem services provided by the Zostera seagrass at the Arcachon Bay.

8.3.4. Evaluation framework

Ecosystem goals

Restoration at Arcachon Bay aims at providing services for addressing several ecosystem goals, namely: (i) reducing sedimentation in channels where dredging operations take place for ensuring navigation conditions,

(ii) improving conditions for seagrass growth by damping current velocities and reducing sedimentation on mudflats, (iii) sustaining coastal uses, by limiting wave action or flooding extent in coastal areas, (iv) creating favourable conditions for oyster farming through turbidity level reduction and water quality improvement in dedicated areas, and (v) creating favourable conditions for tourism, through turbidity level reduction and water quality improvement in the innermost part of the bay.

Definition of criteria and association with system variables

An evaluation framework is set, where criteria are defined for evaluating the achievement of the ecosystem goals (Table 8-3). Based on the set criteria, the impacts of seagrass restoration interventions are then assessed qualitatively by initially determining the strength and direction of their effects on individual system variables, and as a function of the scale of the restoration. The criteria are evaluated qualitatively using a seven-point scale ranging from strongly positive (+++), through positive (++), weakly positive (+), no effect (0), weakly negative (-), negative (–) to strongly negative (—).

Table 8-3 Set of criteria for evaluation of the achievement of ecosystem goals at Arcachon Bay

ID	System variables	Criteria
1	Reduce sedimentation / dredging operations	Sedimentation rate in primary channels
2	Reduce sedimentation / dredging operations	Sedimentation rate in secondary channels
3	Reduce sedimentation / dredging operations	Sedimentation rate near ports
4	Improve conditions for seagrass growth	Sedimentation rate on mudflats
5	Protection of coastal uses / flooding reduction	Storm surge levels
6	Protection of coastal uses / wave damping	Maximum wave height
7	Conditions for tourism / water quality	Renewal times – beaches (Lège)
8	Conditions for tourism / water quality	Renewal times – beaches (Arcachon to Gujan)
9	Conditions for tourism / water quality	Renewal times – beaches (Arès/Andernos)
10	Conditions for tourism / water quality	Renewal times – beaches (Lanton/Audenge)
11	Improve conditions for seagrass growth	Turbidity level on mudflats

Effects (magnitude and direction) on system variables

The Table 8-4 sums up the evaluation laws for determining the strength and direction of the effects of restoration interventions on individual system variables.

Annual average sedimentation rates are calculated for each restoration intervention and climate scenario across areas, with classification shown in Figure 8-7. This classification includes entrance channels, primary channels (approximately 500 to 1000 meters wide), secondary channels (approximately 100 to 200 meters wide), and channels near the ports, situated in the innermost part of the Bay (defined as deeper than +0.6m LAT and used for harbour access). Erosion is identified when the evolution rate is less than -1 mm/year, while sedimentation is noted when it exceeds +1 mm/year. A reduction in sedimentation within channels is considered a positive impact (+). For mudflats (defined as higher that 0mLAT), increased sedimentation is deemed positive (+) as it fosters favourable conditions for seagrass growth.

Extreme water levels are retrieved from hydrodynamic simulations at six output locations along the coastline. Reductions in storm surge levels and wave heights are considered positive impacts.

Renewal times and turbidity levels are calculated for various areas depicted in Figure 8-8, including beaches (divided into four sectors), oyster farms (near Bird Island and at the edges of the mudflats), and the mudflats. Water renewal time is defined as the duration required for the concentration of a theoretical passive tracer, initially introduced throughout the bay, to decrease below 37% (i.e., e^-1) of its initial concentration,

Table 8-4 Evaluation laws for determining the strength and direction of the effects on individual system variables associated to restoration interventions.

	Criteria	Magnitude	Direction
Sediment dynamics control	Sedimentation rate in primary channels Sedimentation rate in secondary channels Sedimentation rate near ports	Change in sedimentation rates (+++)/(---): >50% change (++)/(--): 25% to 50% change (+)/(-): 5% to 25% change (0): <5% change	(+) less sedimentation
	Sedimentation rate on mudflats		(+) more sedimentatio
Flooding reduction	Storm surge levels	Level or height change (+++)/(---) : >20% change (++)/(--) : 5% to 20% change (+)/(-) : 2% to 5% change (0) : < 2% change	(+) smaller storm surge
	Maximum wave height		(+) smaller wave heigh
Water quality improvement	Renewal times – beaches (Lège) Renewal times – beaches (Arcachon to Gujan) Renewal times – beaches (Arès/Andernos) Renewal times – beaches (Lanton/Audenge)	(+++): >90% of the area renewed faster (++): >75% of the area renewed faster (+): >60% of the area renewed faster (0): >40% of the area renewed faster (-): >25% of the area renewed faster (--): >10% of the area renewed faster (---): <10% of the area renewed faster	(+) faster renewal
	Turbidity level on mudflats	(+++): >90% of the area is less turbid (++): >75% of the area is less turbid (+): >60% of the area is less turbid (0): >40% of the area is less turbid (-): >25% of the area is less turbid (--): >10% of the area is less turbid (---): <10% of the area is less turbid	(+) less turbidity

following the method of Plus et al. (2009). A reduction in water renewal time is considered an improvement (+). For mudflats, a decrease in turbidity is regarded as a positive effect.

For the beaches, a reduction in renewal time is considered positive as it allows bacteria, chemicals, and pollutants to be removed more quickly. However, for the oyster farms, the relationship between turbidity, water renewal, and oyster growth is complex. A reduction in renewal time does not necessarily result in a change in oyster growth in controlled basins (Baud et al., 2002). If the renewal time is shorter than the clearance time (the time it takes for the bivalves to filter the water body), it suggests that oysters have limited control over the ecosystem (Venier et al., 2019). While sufficient turbidity could provide oysters with necessary nutrients, the precise relationship remains unclear and site-specific. Consequently, the study does not provide conclusive insights regarding the potential positive or negative impacts on oyster farms. It is recommended to establish a biochemical model that includes phytoplankton, oxygen, pollutants, bacteria, and viruses. Additionally, temperature is a crucial element influencing oyster growth. When temperatures are elevated, oysters allocate a greater proportion of their energy towards reproduction (Haure et al., 2003).

8.4. Results

The study aims at assessing the impact of large-scale seagrass restoration in Arcachon Bay on ecosystem services. The results are based on a three-layer systemic modelling approach that integrates natural system dynamics, socio-economic factors, and evaluation criteria. The Arcachon Bay system's response to various restoration scenarios is evaluated against eleven predefined criteria, utilizing the classification detailed in chapter 8.3.4.

8.4.1. Flooding reduction

A comparative analysis of indicators representative of wave damping, and flood reduction is performed across four restoration scenarios (*S_fail, S_1/3, S_2/3*, and *S_max*) and compared with the current state (*S_0*). The differences in water levels at the shoreline across all scenarios and all horizons are estimated less than 1 cm, which is negligible. However, the scenario without vegetation (S_fail) exhibits slightly higher water levels compared to the current state, while *S_1/3, S_2/3*, and *S_max* show equal or lower water levels. This pattern is also observed for wave height, with no significant differences (up to a maximum of 2 cm, equating to a 1.2% difference). The no-vegetation scenario (*S_fail*) displays identical or slightly increased wave heights (+0 to +1cm), whereas the restored scenarios show either identical or slightly reduced wave heights (-0 to -1cm).

When considering changes in water levels due to vegetation, it is crucial to account for soil subsidence and sea level rise. A recent study, using vertical ground motion data from Sentinel-1 satellite imagery, suggests that subsidence in the Bay of Arcachon could reach rates of up to -1.6mm/yr (Thiéblemont et al., 2024). The impact of subsidence will depend on land use and human activities. By 2100, sea level rise, projected to increase by +74 cm, will be the main cause of coastal flooding, with subsidence contributing around 10 cm. The effect of seagrass restoration on water levels remains therefore minimal. Still, the flooding hazard model does not consider bathymetric changes, so these results should be interpreted cautiously.

8.4.2. Water quality improvement

Potential changes in renewal times are investigated more especially with respect to enhancing tourism conditions. For the current vegetation state (*S_0*), the renewal times are the shortest in the vicinity of the birds' island (averaging 6.3 days) and increase towards the innermost part of the bay (14.1 days for the beaches of Lège, 18.8 days for Arès/Andernos, 20.4 days for Arcachon to Gujan, and 24.3 days for Lanton/Audenge), as shown in Figure 8-10 (left panel).

The restoration of seagrass shows a positive or strongly positive effect on the renewal times at three out of the four zones under study. The most significant impact is observed on the beaches of Lège and Lanton/Audenge. Conversely, the effect on the southern beaches, from Arcachon to Gujan, is strongly negative. In these areas, renewal times increase with vegetation, and turbidity decreases, indicating reduced water movement and less suspended matter. Interestingly, the model suggests that *S_1/3* has a more favourable impact than *S_2/3* and *S_max*, even though *S_max* corresponds to a fully restored state. The reason for this is not clear and may warrant investigation into a potential hydrodynamic threshold caused by denser vegetation.

Under a specific restoration scenario, renewal time does not uniformly decrease with increasing sea level rise (SLR), as might be expected with enhanced hydrodynamics. Instead, it decreases with SLR in the southern and eastern parts of the bay while increasing in the western and northern parts (Figure 8-10, right panel).

On mudflats, turbidity considerably decreases as the restoration scale increases, aligning with the reduced hydrodynamics within seagrass patches. This effect is more pronounced with higher sea-level rise (SLR). The sensitivity of renewal times to sea-level rise and restoration scale within the bay is of a similar magnitude, from -6% to +6% change.

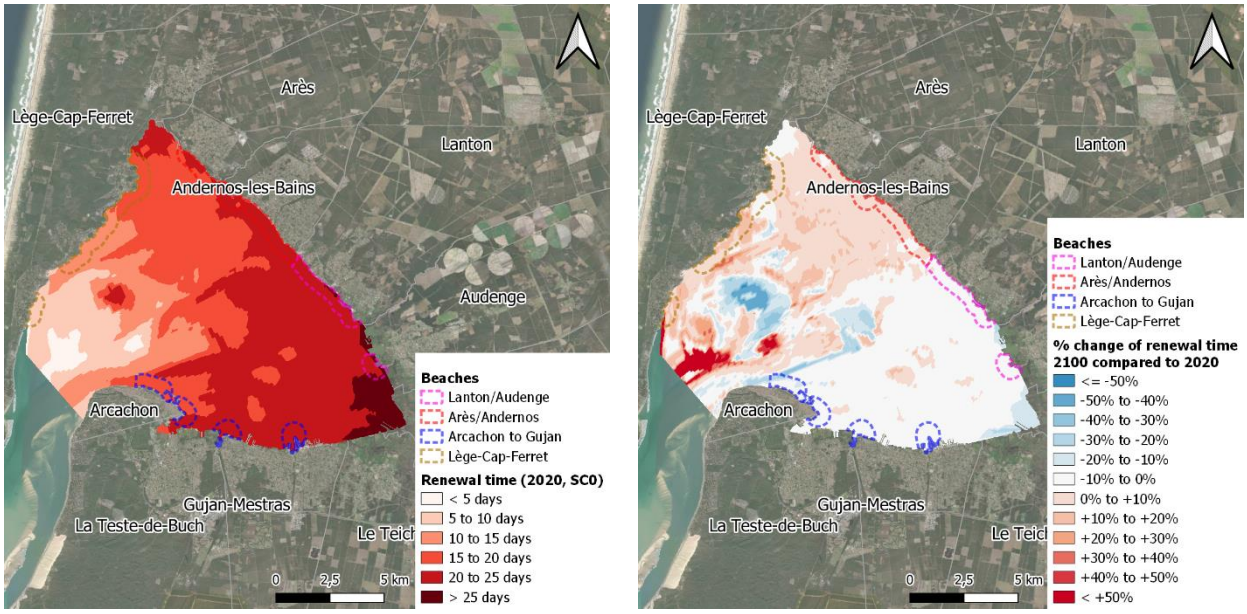

Figure 8-10 Simulated renewal time for current vegetation state S_0 at horizon 2020 (left) and evolution of renewal time from horizon 2020 to 2100 in % for current vegetation state (right)

If restoration fails, renewal times could substantially increase. Restoration failure would result in strongly degrading conditions for tourism in the coastal recreation zones (ecosystem goal (v)). With increasing the seagrass cover, achievement of this specific ecosystem goal varies across different beaches: it is achieved for beaches in the western and eastern parts of the bay but not in the southern part. Partial restoration yields better outcomes.

8.4.3. Sediment dynamics control

Sediment dynamics is analysed to understand the processes of sedimentation and erosion in channels where dredging operations are conducted to maintain navigation conditions. In the current vegetation state (*S_0*), erosion/sedimentation rates are estimated in average to be -16 cm/year in primary channels, -4.5 cm/year in secondary channels, and in the order of -1 cm/year in the innermost bay channels, for the 2020 horizon.

With seagrass restoration, sediment is redirected from intermediate and small channels towards mudflats and primary channels, resulting in the channelling of the bay. Figure 8-11 illustrates this effect: bed changes are more confined to channels in the fully vegetated state. The intensity of these processes however varies spatially. Erosion/sedimentation rates for scenario *S_max* are estimated at -12 cm/year in primary channels, -7.7 cm/year in secondary channels, -0.6 cm/year in the innermost bay channels, and +0.6 cm/year on mudflats.

Seagrass restoration leads to an increase of the erosion rate in the secondary channels (ranked from (++) to (+++)), suggesting a potential reduction in the need for dredging. In the innermost parts of the bay, erosion is more pronounced with partial restoration (*S_1/3*) but lessens with larger-scale restoration (ranked as (++) for *S_1/3* and (-) for *S_2/3* and *S_max*). Conversely, sedimentation on mudflats tends to increase with restoration (ranked from (++) to (+++)), while erosion rate decreases in primary channels (ranked as (-)).

The sedimentation rate trend aligns closely with the restoration scale for secondary channels and mudflats, indicating that larger restoration efforts enhance sediment dynamics control. However, partial restoration yields better outcomes for channels near harbours. Primary channels continue to experience erosion, with no change in dredging requirements.

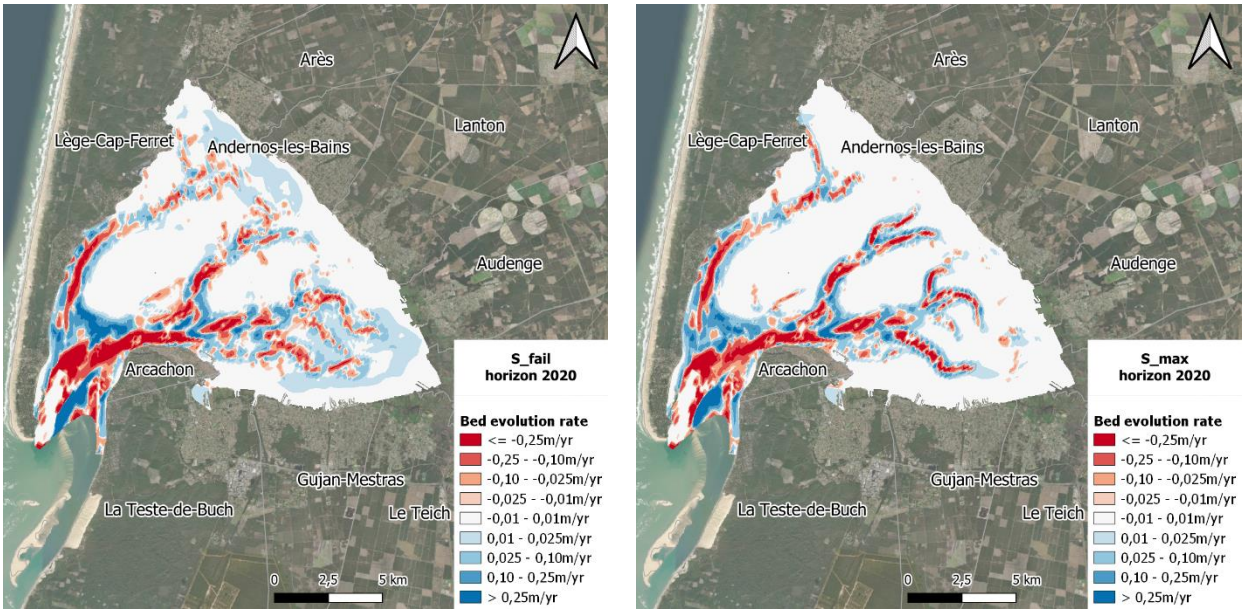

Figure 8-11 Bed evolution rate (m/yr) for the no-vegetation case (S_fail) and fully restored scenario (S_max)

In all restoration scenarios and all zones except primary channels, results indicate that sedimentation increases, or erosion decreases with rising sea levels. In the context of climate change, sediments from deeper and larger channels appear to be redistributed to smaller channels and mudflats. Note that the model assumes unchanged initial bathymetry across all climate horizons and anticipates seabed changes with gradual sea level rise. Additionally, wave forcing is not considered in the model. Waves can, however, trigger material suspension, especially in shallow areas. Thus, results for mudflats and the innermost part of the bay should be nuanced.

8.5. Discussion

Balancing the achievement of ecosystem objectives through seagrass restoration with the organizational demands of large-scale restoration in Arcachon Bay is essential. The required technical and financial investments may not increase proportionally to the restoration's potential. Furthermore, the extent of restoration that can be achieved grows with the amount of restoration undertaken. As such, a fully restored scenario is not feasible in the coming decades.

The eco-morphological model is useful for assessing ecosystem goals against specific criteria but does not capture all the interrelationships that define the biophysical dynamics of the system. Restoring seagrass meadows affects sedimentation, influencing sediment size and seabed stabilization both within the meadows and in channels. Limiting sedimentation in channels impacts positively dredging requirements, which in turn affects water quality due to the potential remobilization of tributyltin and the increased presence of toxic substances as navigation increases (UICN France, 2014). Additionally, sediment control aims to reduce flood risk by stabilizing the shoreline. However, this aspect is not explored here due to the separate application of hydro- and morphodynamic models.

Moreover, the three-layer model could benefit from an additional layer to account for inherent feedback mechanisms. For instance, improved water quality can result from shorter renewal times and the absorption of toxic substances (like irgarol) by seagrass beds (UICN France, 2014). The 7-point rating system used here may initiate positive or negative feedback that are currently not considered.

Finally, the system’s reaction to graduated restoration highlights various tipping points and key drivers for future adaptation. A tipping point is a critical threshold that marks a change in the system's response to

different forcing agents (Haasnoot et al., 2018). The first potential threshold is associated with vegetation cover, density, and channeling. The findings suggest that partial restoration may be more effective than complete restoration in achieving ecosystem goals such as water quality and sediment control dynamics in the innermost part of the Bay. The system's response is expected to change partially upon reaching this restoration scale. Regarding water quality, further research is needed on the biological response of oysters to changes in water renewal times and turbidity, as an optimal point might be reached, constituting a tipping point for oyster development.

The findings also help identify physical and socio-economic drivers that might lead to a tipping point. The main physical drivers are climatic forces. Sea-level rise appears to be a key driver of the system's response. Sea-level rise affects several aspects, such as flooding risk, water quality regulation, and sediment dynamics control. Tidal asymmetry can change with sea-level rise due to differences in tidal duration and range (e.g., Mütterlein et al. 2016; Mahavadi et al. 2024). Morphological changes with sea-level rise could also lead to tidal asymmetry changes (van Maanen et al. 2013; Yang et al. 2022). Additionally, the bay's bed level will reach a new equilibrium with the new water levels, introducing some uncertainty. Socio-economic drivers will also influence how tipping points are reached. Changes in land use, urbanization, and coastal recreation zone management are key socio-economic drivers for reducing flooding risk. Wastewater management and navigation activities significantly impact water quality. Regarding sediment dynamics control, dredging is a major socio-economic force that modifies the system.

Following the evaluation of the criteria specified in Table 8-5, the Arcachon Bay system's response is represented as a function of restoration scale in the conceptual sketch of Figure 8-12; see also Table 8-5.

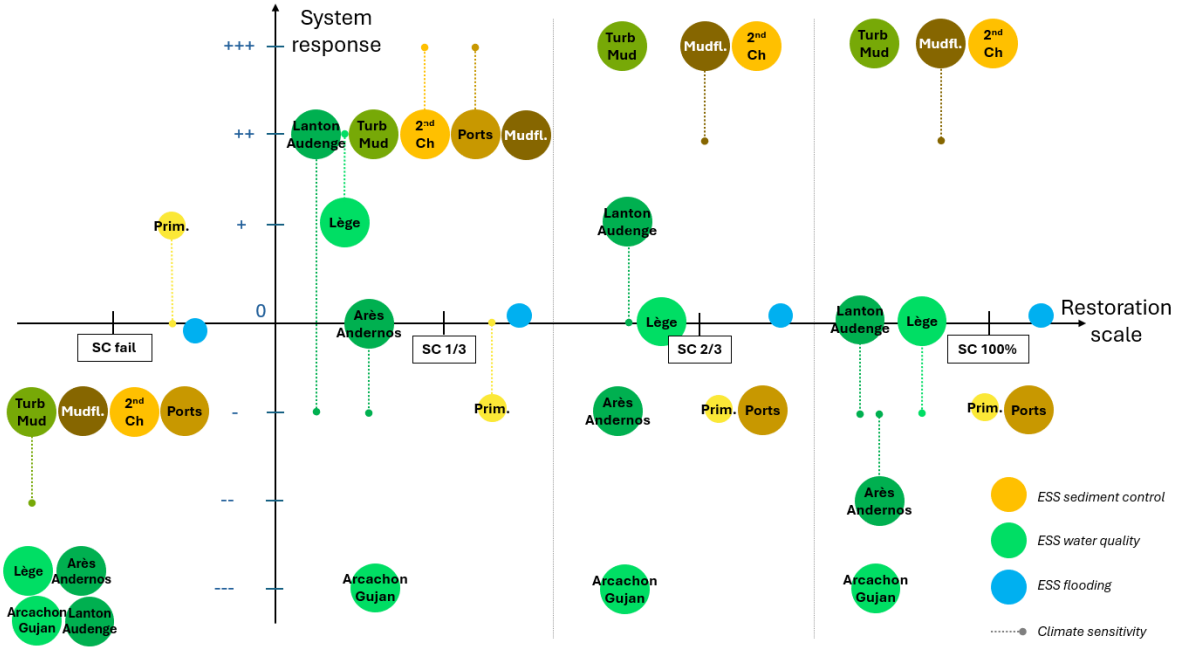

Figure 8-12 Graduated response from the system variables to restoration scenarios and failure case. The primary channel disc is smaller as erosion is modelled in any case.

Table 8-5 System response to restoration scenarios for each climate horizon, for each criteria and corresponding ecosystem goals.

Criteria	S_fail 2020 / 2050 / 2100	S_1/3 2020 / 2050 / 2100	S_2/3 2020 / 2050 / 2100	S_max 2020 / 2050 / 2100	*ecosystem goal*
Sedimentation in channels – primary	+ / 0 / 0	- / - / 0	- / - / -	- / - / -	*i*
Sedimentation in channels – secondary	- / - / -	++ / ++ / +++	+++ / +++ / +++	+++ / +++ / +++	*i*
Sedimentation – innermost part of the Bay close to ports	- / - / -	++ / ++ / +++	- / - / -	- / - / -	*i*
Sedimentation – mudflats	- / - / -	++ / ++ / ++	+++ / +++ / ++	+++ / +++ / ++	*ii*
Storm surge levels – along the coastline	0 / 0 / 0	0 / 0 / 0	0 / 0 / 0	0 / 0 / 0	*iii*
Maximum wave height - along the coastline	0 / 0 / 0	0 / 0 / 0	0 / 0 / 0	0 / 0 / 0	*iii*
Water renewal times – beaches intermediary west	--- / --- / ---	+ / + / ++	0 / 0 / 0	0 / - / 0	*v*
Water renewal times – beaches intermediary south	--- / --- / ---	--- / --- / ---	--- / --- / ---	--- / --- / ---	*v*
Water renewal times – beaches innermost part north	--- / --- / ---	0 / - / -	- / - / -	-- / -- / -	*v*
Water renewal times – beaches innermost part east	--- / --- / ---	++ / ++ / -	+ / 0 / 0	0 / - / -	*v*
Turbidity level – mudlfats	- / - / --	++ / ++ / ++	+++ / +++ / +++	+++ / +++ / +++	*ii*

8.6. Conclusion

Arcachon Bay is home to Europe's largest Zostera seagrass bed, where two species, Zostera noltii and Zostera marina, coexist. Zostera noltii predominates in intertidal zones, while Zostera marina is found in submerged areas along channel edges. Between 1989 and 2012, the bay experienced a significant reduction in seagrass beds, with Zostera noltii decreasing by 38% and Zostera marina by 85%. Conservation efforts in Arcachon Bay, supported by various agencies, focus more especially on preserving seagrass beds. Scaling up these local restoration efforts faces however several challenges, including technical, financial, and governance barriers. The technical challenges, particularly in the definition of metrics for coastal biodiversity and ecosystem services, have hindered socio-economic engagement in large-scale restoration.

To overcome these limitations, a three-layer systemic modelling approach is proposed to assess the benefits and impacts of large-scale seagrass restoration in Arcachon Bay, while integration natural system dynamics, socio-economic factors, and evaluation criteria. An eco-morphodynamic modelling system, integrating the effect of seagrass meadows, aims at investigating the natural system dynamics and constitutes the first layer. The morphological evolution of tidal flats and channels is modelled using an eco-hydro-morpho model, while an eco-wave-hydro model is employed to calculate water renewal times and turbidity levels. The second layer is a conceptual socio-economic system model that emphasises the interactions between the socio-economic components of the system and the provision of ecosystem services by seagrass beds. The importance of activities linked to any form of navigation and tourism is significant, and they have interrelationships with flooding reduction potential, sediment dynamics control and water quality

improvement. Finally, the third layer assesses the impacts of larger restoration on ecosystem services provided by seagrass in the context of climate change at horizons 2050 and 2100.

Modelling indicates that the control of sediment dynamics is likely to improve with restoration scale, except for channels in close proximity to ports. The hydrodynamic and morphodynamic models are consistent in their representation of the mudflats, indicating a decrease in turbidity and an increase in sedimentation with larger restoration. Impacts on water quality are projected to be positive or strongly positive regarding renewal times in the northern and eastern parts of the bay. Climatic factors, mainly sea-level-rise, appear to have an influence on how seagrass provide ecosystem services, though this influence is of a lesser extent than the influence of large-scale restoration.

By analysing the socio-economic benefits associated to scaling-up seagrass restoration, the study underscores the potential for such larger-scale interventions to enhance biodiversity, improve ecosystem services, and contribute to climate adaptation and disaster risk reduction. The demonstration of the potential of large-scale restoration should ideally result in the preparation of a portfolio of restoration interventions. In Arcachon, a framework already exists in the marine park management plan (PNBMA, 2017), and could be further elaborated in the context of climate change.

8.7. References

Ardhuin, F., Accensi, M., Roland, A., Girard, F., Filipot, J. F., Leckler, F., & Le Roux, J. F. (2014). Numerical wave modeling in PREVIMER: multi-scale and multi-parameter demonstrations. Editorial–Apr 2014–The Pre-operational PREVIMER system.

Auby, I., Bost, C.-A., Budzinski, H., Dalloyau, S., Desternes, A., Belles, A., Trut, G., Plus, M., Pere, C., Couzi, L., Feigne, C., & Steinmetz, J. (2011). *Régression des herbiers de zostères dans le Bassin d'Arcachon: État des lieux et recherche des causes*. https://archimer.ifremer.fr/doc/00054/16507/

Ballé-Béganton J., J. Herry, M. Philippe, R. Pasco, B. Angst, M. Urien, D. Bailly, M. Cassé (2015). Les services écosystémiques en soutien à la gestion des herbiers de zostères du golfe du Morbihan, Projet Interreg IVA Manche VALMER, 14p.

Banzo, M., Cazals, C., & André-Lamat, V. (2018). *Le bassin d'Arcachon entre attractivité et protection. Avant-propos* (Issue 45). Presses universitaires du Mirail.

Baptist, M. (2005). Modelling floodplain biogeomorphology, PhD Dissertation, TU Delft library, http://resolver.tudelft.nl/uuid:b2739720-e2f6-40e2-b55f-1560f434cbee.

Barbier, E. B., Hacker, S. D., Kennedy, C., Koch, E. W., Stier, A. C., & Silliman, B. R. (2011). The value of estuarine and coastal ecosystem services. *Ecological Monographs*, *81*(2), 169–193. https://doi.org/10.1890/10-1510.1

Baud, J.-P., Palvadeau, H., & Nourry, M. (2002). *Influence du taux de renouvellement et de la qualité de l'eau sur l'affinage contrôlé de Crassostrea gigas*.

Bouchet J.-M., J.-P. Deltreil, F. Manaud, D. Maurer, and G. Trut (1997). Etude intégrée du bassin d'arcachon.

Braat L.C., de Groot, R (2012). The ecosystem services agenda: bridging the worlds of natural science and economics conservation and development, and public and private policy. Ecosyst. Serv. 1, 4–15.

CASAGEC INGENIERIE. (2021). *Actualisation du fonctionnement hydrosédimentaire du littoral intra-bassin de Lège-Cap-Ferret - Programme de rechargement.*

Cayocca F. (1996). Modélisation morphodynamique d'une embouchure tidale: Application aux passes d'entrée du Bassin d'Arcachon. PhD thesis, Bordeaux 1.

CGDD. (2018). *Analyse multicritère des projets de prévention des inondations : Guide méthodologique.*

Cognat M. (2019). Rôles des facteurs environnementaux et des interactions biomorphodynamiques sur l'évolution spatio-temporelle des herbiers de zostères dans une lagune mésotidale. PhD thesis, Université de Bordeaux.

Cognat, M. (2019). *Decline of Seagrass Beds in Arcachon Bay: Causes and Conservation Strategies.* Marine Ecology Progress Series.

Costanza R., Kubiszewski, I (2012). The authorship structure of ecosystem services as a transdisciplinary field of scholarship. Ecosyst. Serv. 1, 16–25, 2012.

Delft3D (2023). Delft3D-Flow User Manual: Delft3D-FLOW User Manual (deltares.nl), p. 252-261 and 627-630.

Dam, G., M. van der Wegen, R. J. Labeur, and D. Roelvink (2016). Modeling centuries of estuarine morphodynamics in the Western Scheldt estuary. Geophys. Res. Lett., 43, 3839-3847.

Dinu, I., Monclús i Bori, A., Gràcia, V., García-León, M., Lin-Ye, J., Stănică, A., & Sánchez-Arcilla, A. (2023). Assessing the coastal protection role of seagrass meadows along a barrier beach, southern Romanian coast. *Journal of Sea Research*, *191*, 102329. https://doi.org/10.1016/j.seares.2022.102329

Donatelli, C., Ganju, N. K., Fagherazzi, S., & Leonardi, N. (2018). Seagrass Impact on Sediment Exchange Between Tidal Flats and Salt Marsh, and The Sediment Budget of Shallow Bays. *Geophysical Research Letters*, *45*(10), 4933–4943. https://doi.org/10.1029/2018GL078056

Ganthy, Sottolichio and Verney (2013): Seasonal modification of tidal flat sediment dynamics by seagrass meadows of Zostera noltii (Bassin d'Arcachon, France), Journal of Marine Systems, ELSEVIER, vol. 109-110, pp. s233-s244.

Garner, G. G., T. Hermans, R. E. Kopp, A. B. A. Slangen, T. L. Edwards, A. Levermann, S. Nowikci, M. D. Palmer, C. Smith, B. Fox-Kemper, H. T. Hewitt, C. Xiao, G. Aðalgeirsdóttir, S. S. Drijfhout, T. L. Edwards, N. R. Golledge, M. Hemer, R. E. Kopp, G. Krinner, A. Mix, D. Notz, S. Nowicki, I. S. Nurhati, L. Ruiz, J-B. Sallée, Y. Yu, L. Hua, T. Palmer, B. Pearson, 2021. IPCC AR6 Sea-Level Rise Projections. Version 20210809. PO.DAAC, CA, USA.

Haasnoot, M., van 't Klooster, S., & van Alphen, J. (2018). Designing a monitoring system to detect signals to adapt to uncertain climate change. *Global Environmental Change*, *52*, 273–285. https://doi.org/10.1016/j.gloenvcha.2018.08.003

Haure, J., Durin, O., Palvadeau, H., Papin, M., Nourry, M., Penisson, C., & Martin, J.-L. (2003). *L'amélioration de la qualité des huîtres à échelle professionnelle: Intégration de l'eau salée souterraine traitée comme milieu d'élevage*. *Ifremer*.

IPBES (2019). Global assessment report on biodiversity and ecosystem services of the Intergovernmental Science-Policy Platform on Biodiversity and Ecosystem Services (Version 1).

James C. S., A. L. Birkhead, A. A. Jordanova & J. J. O'Sullivan. Flow resistance of emergent vegetation, Journal of Hydraulic Research, 42:4, 390-398, 2004.

Kambiadou K., Ganthy F., Verney R., Plus M., Sottolichio A. Modelling the effects of Zostera noltei meadows on sediment dynamics: application to the Arcachon lagoon. Ocean Dynamics 64, pp. 1499-1516, 2014.

Le Corre, N., Le Berre, S., Peuziat, I., Brigand, L., & Courtel, J. (2015). Approche des espaces de la pratique nautique par l'analyse de la fréquentation: L'exemple du bassin de navigation arcachonnais. *VertigO - la revue électronique en sciences de l'environnement*, *Volume 15 Numéro 3*, Article Volume 15 Numéro 3. https://doi.org/10.4000/vertigo.16817

Lesser, G., Roelvink, J.A., Van Kester, J.A.T.M., Stelling, G.S. (2004). Development and validation of a three-dimensional morphological model. Coastal Engineering, 51, 883–915.

MA. Millennium Ecosystem Assessment (2005). World Resources Institute, Washington, DC.

Maxwell, P. S., Eklöf, J. S., van Katwijk, M. M., O'Brien, K. R., de la Torre-Castro, M., Boström, C., Bouma, T. J., Krause-Jensen, D., Unsworth, R. K. F., van Tussenbroek, B. I., & van der Heide, T. (2017). The fundamental role of ecological feedback mechanisms for the adaptive management of seagrass ecosystems – a review. *Biological Reviews*, *92*(3), 1521–1538. https://doi.org/10.1111/brv.12294

Mahavadi T.F., Seiffert R., Kelln J., and Fröhle P. (2024). Effects of sea level rise and tidal flat growth on tidal dynamics and geometry of the Elbe estuary. *Ocean Sciences*, 20, 369-388.

Molina, M. O., Gutiérrez, C., & Sánchez, E. (2021). Comparison of ERA5 surface wind speed climatologies over Europe with observations from the HadISD dataset. *Int. J. Climatol*, *41*(10), 4864-4878.

Mugica J., Bulteau T., Paris F. et Pedreros R., and Delvallee E (2014). Caractérisation de l'aléa submersion marine dans le cadre des PPRL du Bassin d'Arcachon (Gironde), Détermination de l'évènement naturel de référence. Rapport intermédiaire BRGM/RP-61408-FR, 73 p.

Mütterlein S., Ganthy F., Sottolichio A (2016). Effect of small seagrass Zostera noltei on tidal asymmetry in a semi-enclosed shallow lagoon: the Arcachon Bay (SW France). International Coastal Symposium, 6-11 March 2016.

Neumann B., V. A. (2015). Future coastal population growth and exposure to sea-level rise and coastal flooding - a global assessment. *PLoS ONE 10(3):e0118571*.

Orth, R. L. (2020). Applied ecology restoration of seagrass habitat leads to rapid recovery of coastal ecosystem services. *Sci. Adv. 6.*

Parisot J.-P., J. Diet-Davancens, A. Sottolichio, E. Crosland, C. Drillon, and R. Verney (2008). Modélisation des agitations dans le bassin d'arcachon. Xèmes Journées Sophia Antip, pages 435–444.

Plus M., Dumas F., Stanisière J.-Y. and Maurer D. (2009). Hydrodynamic characterization of the Arcachon Bay, using model-derived descriptors. Continental Shelf Research 29, 1008-1013.

PNMBA. (2017). *Plan de gestion du Parc Naturel Marin du Bassin d'Arcachon 2017-2032.*

Reeves, I. R. B., Moore, L. J., Goldstein, E. B., Murray, A. B., Carr, J. A., & Kirwan, M. L. (2020). Impacts of Seagrass Dynamics on the Coupled Long-Term Evolution of Barrier-Marsh-Bay Systems. *Journal of Geophysical Research: Biogeosciences*, *125*(2), e2019JG005416. https://doi.org/10.1029/2019JG005416

Sánchez-Arcilla, A., Cáceres, I., Roux, X. L., Hinkel, J., Schuerch, M., Nicholls, R. J., Otero, del M., Staneva, J., de Vries, M., Pernice, U., Briere, C., Caiola, N., Gracia, V., Ibáñez, C., & Torresan, S. (2022). Barriers and enablers for upscaling coastal restoration. *Nature-Based Solutions*, *2*, 100032. https://doi.org/10.1016/j.nbsj.2022.100032

Schrijvershof, R. A., van Maren, D. S., Torfs, P. J., & Hoitink, A. J. F. (2023). A Synthetic Spring-Neap Tidal Cycle for Long-Term Morphodynamic Models. Journal of Geophysical Research: Earth Surface, 128(3), e2022JF006799.

Short, F., Short, C., & Novak, A. (2016). Seagrasses. In C.M. Finlayson, G.R. Milton, R.C. Prentice and N.C. Davidson (eds.) *The Wetland Book: II: Distribution, Description and Conservation*. Springer Science. https://doi.org/10.1007/978-94-007-6173-5_262-1

Slinger, J. (2000). The link between morphology and ecology in the Long Term Vision for the Schelde Estuary - A conceptual framework and preliminary results.

Slinger, J. (2023). Developing the transboundary Long Term Vision of the Scheldt Estuary - an untold story. *Water international*. doi:10.1080/02508060.2023.2264668.

Thiéblemont, R., Le Cozannet, G., Nicholls, R. J., Rohmer, J., Wöppelmann, G., Raucoules, D., de Michele, M., Toimil, A., & Lincke, D. (2024). Assessing Current Coastal Subsidence at Continental Scale: Insights From Europe Using the European Ground Motion Service. *Earth's Future*, *12*(8), e2024EF004523. https://doi.org/10.1029/2024EF004523

UICN France. (2014). *Panorama des services écologiques fournis par les écosystèmes français - étude de cas : les écosystèmes marins et côtiers d'Aquitaine.* Paris, France.

van Ledden (2003). Sand-mud segregation in estuaries and tidal basins. PhD, Delft University of Technology, 248 pages.

van Maanen B., Coco G., Bryan K.R., and Friedrichs C.T. (2013). Modeling the morphodynamic response of tidal embayments to sea-level rise. *Ocean Dynamics*, 63, 1249-1262.

van Rijn, L. C., & Kroon, A. (1993). Sediment transport by currents and waves. *Coastal Engineering*, ASCE, pp. 2613-2628.

Venier, P., Gerdol, M., Domeneghetti, S., Sharma, N., Pallavicini, A., & Rosani, U. (2019). Biotechnologies from marine bivalves. *Goods and Services of Marine Bivalves*, 95–112.

Vierros, M. (2017). Communities and blue carbon: the role of traditional management systems in providing benefits for carbon storage, biodiversity conservation and livelihoods. *Clim. Chang.* 140 (1), 89–100. https://doi.org/10.1007/s10584-013-0920-3.

Yang Q., Hu S., Fu L., Zhang P., Chu N., Liu F., and Cai H. (2022). Responses of tidal duration asymmetry to morphological changes in Lingding Bay of the Pearl River Estuary. *Frontiers in Marine Sciences*, Coastal Ocean Processes, 9. https://doi.org/10.3389/fmars.2022.983182.

9. Catalogue of Nature-based Solutions to reduce storm-driven coastal flooding and erosion along the Sicily coast

Musumeci, R.E.[1], Marino, M.[1], Nasca, S.[1], Alkharoubi, A.[1], Cavallaro, L.[1] & Foti, E.[1]

[1] *Department of Civil Engineering and Architecture, University of Catania*

ABSTRACT: In the present contribution, a catalogue of Nature-based Solutions (NbS) to reduce storm-driven coastal flooding and erosion are assessed by means of a modelling study within a case study along the Sicily coast (Italy). An hydro-morphodynamic modelling chain (SWAN and XBeach) is setup to evaluate the effectiveness of four interventions—a dune revegetation, two upscaling options of seagrass meadow reconstruction and a beach nourishment—to reduce coastal inundation and eroded volumes. The study investigates present and future *what-if* scenarios, by simulating storm conditions based on present, 4.5, and 8.5 W/m^2 radiative forcing scenarios. Habitat maps were built for both current state and NbS to evaluate dissipative effects of vegetation. The latter are modelled by providing morphological and hydrodynamic characteristics as well as spatial distribution of different plant species. Simple flooding and erosion reduction efficiency indicators are computed to support the assessment. Moreover, a scorecard methodology-based assessment is carried out to investigate habitat and ESS provisioning change due to sea level rise, both in absence and presence of NbS. Results reveal that the vulnerability of the area to flooding is predominantly driven by sea level rise rather than by increase in significant wave height. In this regard, beach nourishment and large-scale seagrass reconstruction perform best in reducing flooded areas across all investigated scenarios. Their efficacy however is less significant for 2100-time horizon scenarios, under which the dune revegetation intervention resulted the most resilient. The habitat change analysis revealed that sea level rise determines a permanent connection between sea and lagoons, reducing their natural capabilities of flooding risk reduction.

9.1. Introduction

The combination of urban development, marine resource exploitation, and other human activities has led to widespread degradation of coastal habitats, affecting both their ecological quality and spatial extent on a global scale (Geijzendorffer et al., 2018; Salinas et al., 2020; Waltham et al., 2020). These habitats are crucial not only for their ecological and aesthetic value but also for the ecosystem services they provide (Barbier et al., 2011). Coastal vegetation plays a key role in climate regulation, being significantly more effective than forests in carbon sequestration (Mossman et al., 2022). Salt marshes serve as efficient pollutant filters, greatly contributing to nutrient cycling (Sousa et al., 2010). In terms of coastal protection, these habitats are well-documented for their ability to mitigate coastal hazards. Dune belts act as natural barriers against storm surges (van Slobbe et al., 2013; Bryant et al., 2019; Feagin et al., 2019; Grases et al., 2020), while seagrass meadows effectively reduce wave energy (Ondiviela et al., 2014; Leonardi et al., 2018; Maza et al., 2022; Pillai et al., 2022), and salt marshes help diminish storm surge impacts (Barbier et al., 2013; Möller et al., 2014; Vuik et al., 2016).

There is an increasing demand for implementing Nature-based Solutions (NbS) in coastal zones. Using a "Building with Nature" approach (van Slobbe et al., 2013; de Vriend et al., 2015), NbS are emerging as promising strategies for both restoring biodiversity and mitigating the negative effects of climate change (van Zelst et al., 2021; Sánchez-Arcilla et al., 2022; Jacob et al., 2023; Chen et al., 2024). Research indicates that these solutions might offer benefits that outweigh their costs and, in some cases, could be more cost-

effective than traditional engineering approaches (Sutton-Grier et al., 2015; Morris et al., 2018; Reguero et al., 2018).

Despite their growing recognition as sustainable alternatives, the effectiveness and adaptability of NbS under climate change conditions remain significantly under-researched (Seddon et al., 2020). Existing modeling efforts have primarily assessed NbS performance based on past extreme events or probabilistic approaches using historical data (Guannel et al., 2016; James et al., 2021; Unguendoli et al., 2023), with few exceptions (Grases et al., 2020; Forrester et al., 2024). While these studies are valuable, they often do not account for future climate projections, which is essential for dynamic adaptive planning (Werners et al., 2021; Sánchez-Arcilla et al., 2022). Adaptive planning emphasizes flexibility and resilience to changing conditions, unlike traditional methods that rely on static predictions and fixed plans.

To address this gap, this contribution applies a modelling framework to evaluate the performance of Nature-based coastal defense measures by testing it on a Mediterranean transitional coastal case study in Sicily (Italy), a region characterized by significant natural value and high levels of urbanization. The framework utilizes a hydro-morphodynamic modelling chain, incorporating SWAN and XBeach models, to assess the effectiveness of four interventions: dune revegetation, beach nourishment and two seagrass reconstruction interventions with two upscaling options. These measures are analyzed under current conditions and future scenarios, including sea level rise and marine climate projections corresponding to radiative forcing scenarios of 4.5 and 8.5 W/m². The model includes vegetation characteristics and spatial distribution to account for the effects of vegetation. The model's outputs—such as flooded areas, eroded volumes, and shoreline changes—are used to calculate efficiency indicators that measure the NbS performance in reducing storm-induced inundation and beach erosion. Moreover, an Ecosystem Services (ESS) assessment is conducted using semi-quantitative biotope scores to evaluate changes in key services like water quality purification and coastal risk reduction. The study is organized as follows: Section 9.2 describes the modelling framework, study area, input data, model setup and validation, Methodology for scoring ecosystem services, and the formulation of flooding/erosion efficiency indicators. Section 9.3 presents the modelling results. The study concludes with a final chapter summarizing the findings (Section 9.4).

9.2. Methods

9.2.1. Study area

The "Pantani della Sicilia Sud-Orientale" (South-East Sicily lagoons, Figure 9-1a) is a saline lagoon and wetland system closely connected to the adjacent coastal environment. The area supports important breeding populations of rare and endangered species and is a crucial migration hotspot for birds along the central Mediterranean migration flyway. Due to its ecological and biodiversity significance, the region is included in international environmental protection frameworks, such as RAMSAR and Natura 2000, and is designated as a Special Protection Area and a regional nature reserve.

The Cuba-Longarini lagoons form the largest wetland complex in the area (Figure 9-1b), covering approximately 240 hectares. These lagoons are separated from the sea by a narrow coastal fringe, consisting of a dune strip and sandy beach, and are intermittently connected to the sea through a small estuary channel, depending on the lagoon's water level. The lagoons are characterized by shallow waters, generally less than one meter deep.

The construction of the small town of Granelli in the 1970s, on the narrow fringe between the sea and the lagoons, has reduced the hydraulic connectivity between the wetlands and the sea and degraded the coastal dune belt, over which the urbanized area is located. As a result, the region is prone to flooding from intense runoff from the lagoon and wave storms from the sea. To mitigate coastal risks and restore biodiversity, a

Figure 9-1 The "Pantani della Sicilia Sud-Orientale" coastal wetlands and lagoon system in Sicily (a and b), the study area of Cuba and Longarini lagoons (c), coastal erosion at the beach town of Granelli (d), artificial islands and channels for birds nesting/breeding of birds at the Cuba-Longarini site (e).

range of Nature-based Solutions (NbS) are being investigated, considering both the current state (with active restoration measures) and proposed additional measures.

As mentioned, Granelli was built over a coastal dune strip, reducing sediment connectivity and the natural protective capacity of the environment. While full dune reconstruction may not be feasible due to the limited space between the beach and the urbanized area, revegetation to stabilize the dune and enhance wave dissipation is proposed. The endemic species Ammophila arenaria, already marginally present on-site, has been selected for this purpose. The intervention involves expanding the dune habitat over an area of approximately 4.3 hectares, stretching along the shoreline for 3.3 km with an average width of 13 meters. Furthermore, a replantation of the seagrass meadow in front of the town is also investigated. Specifically, an extension of the existing meadow of *Posidonia oceanica*, which is a protected marine plant, is designed to evaluate its capabilities to dissipate wave energy and reduce storm-induced erosion. The proposed replantation plan includes two hypothetical scenarios. The first scenario involves expanding the existing seagrass meadow by an additional 10.82 ha, bringing the total area to 87.62 ha. The second scenario involves

a further expansion to a total area of 180.52 ha, which represents an increase of 103.72 ha from the current meadow area.

The coastline where the town of Granelli is located is particularly susceptible to significant coastal erosion. Since 1955, variations in the coastline have been observed, with a substantial retreat in the beach width from the initial 99 meters to the current 11 meters. This phenomenon is more pronounced in the central part of the coastline, along a stretch of approximately 2 km, and is accompanied by a regression of the coastal dunes. In order to restore this stretch of coastline, mitigate the risk of erosion, and protect the surrounding urban and natural areas, a beach nourishment project has been planned. The project involves the use of fine sand, compatible with that found at Granelli, which may be sourced from an underwater deposit located off the coast of Sicily, between Capo San Marco and Punta Molinazzo, west of the port of Mazara del Vallo (TP). Based on the site's grain size, with a median diameter (D_{50}) of 0.27 mm, sediment from the offshore quarry area with a median diameter D_{50} of 0.45 mm was selected.

Considering the coastal morphology and the possibility to carry out the intervention in a way that it is naturally protected by the eastern promontory, the nourishment project involves a beach advancement of 20 meters along a 3.3 km stretch of coastline, from the beginning of the town to the eastern promontory (Punta Mici). The berm was designed considering the gentle slopes of the site, with a height of 0.50 m. It is estimated that approximately 120,000 m³ of sand will be required for the project. For simplicity sake, here no additional coastal protection infrastructures are considered in this NbS scenario.

9.2.2. Input data description

In order to build the SWAN numerical grid, bathymetric contours were taken from nautical charts (Istituto Idrografico della Marina, 2019). In order to build the Xbeach numerical grid, a Digital Elevation Model (DEM) of the study area was obtained from the Regional Geographic Information System of Sicilia Region. The DEM was recovered through LiDAR flights in 2013 and has an horizontal resolution of 2x2 m and vertical resolution of 0.01 m. The DEM was combined with bathymetric data obtained through a multi-beam survey, previously carried out by the University of Catania, that covered the entire nearshore part of the domain in 2019. The dataset is integrated with data obtained by means of satellite images, drone data and field surveys, to include small artificial islands and channels built as wetland restoration measures in 2023 to improve biodiversity value of the site.

The shoreline was obtained through PlanetScope satellite imagery (having 3x3 m resolution) by tracking the wet/dry boundary. Elevations from DEM, bathimetry and shoreline position were combined to assign elevation at the XBeach grid nodes through linear interpolation. The beach is made up by fine sand, with d_{50}=0.27mm, estimated based on several field samples collected at the Granelli beach.

Present wave conditions were obtained from the MEDSEA MULTIYEAR WAV 006 012 reanalysis dataset (Korres et al., 2021) provided by the Copernicus Marine Service. The dataset spans the years 1993-2022 and includes hourly time series of marine climate, with a spatial resolution 4.66 × 4.66 km (Figure 9-2). Climate change projected wave conditions were taken from *Ocean surface wave time series for the European coast from 1976 to 2100 derived from climate projections* dataset (Caires et al., 2020). The dataset provides hourly time series of the marine wave climate derived from ocean surface wave parameters calculated across a European-wide domain.The year timespan of the dataset is 2041-2100, with hourly temporal resolution and a spatial resolution of 30 x 30 km.The dataset includes projected wave conditions for two IPCC AR5 Representative Concentration Pathway (RCP) scenarios: one aligns with a more optimistic emission trajectory, wherein emissions begin to decline beyond 2040 (RCP4.5), and the other represents a pessimistic scenario where emissions persistently increase throughout the century, often referred to as the business-as-usual scenario (RCP8.5).

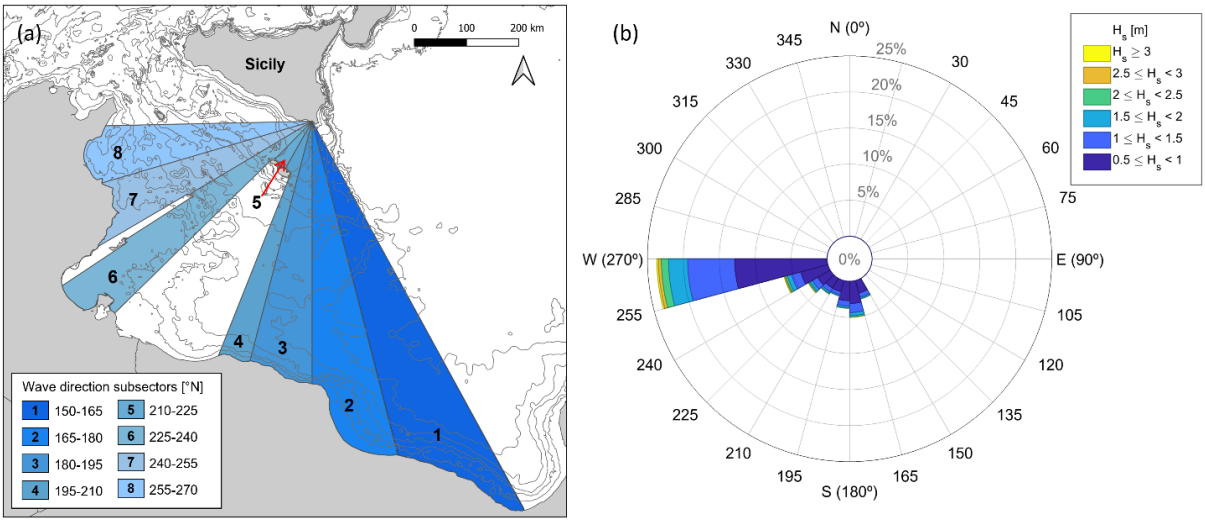

Figure 9-2 Geographical fetch and wave direction subsectors for the directional extreme value analysis (a); Wave rose of significant wave height classes (b).

For both present and future projection datasets, significant wave height H_s, peak period T_p and mean wave direction ϑ were extracted for present, RCP4.5 and RCP8.5 scenarios. The data were extracted in the correspondence of the grid point closest to our model offshore boundary (latitude 36.69°N, longitude 15.00°E - EPSG 32633).The categorization of events based on their H_s and ϑ was also carried out to identify the prevailing direction and the direction associated with the most energetic sea states. Considering the geographical fetch of the site under investigation, the directional sector for wave propagation spans from 150°N to 270°N, covering a total width of 120°. Therefore, the whole sector was subdivided into eight sub-sectors, each spanning 15° (Figure 9-2).

For each sub-sector, an extreme value analysis was conducted to obtain H_s associated with storms with given return period T_r. In order be consistent among the present and future scenarios, the extreme value analysis was conducted considering the same length of for the time window of analysis. For the hystorical timeseries the time window correspond to the actual extension of the dataset time series, namely 1993-2022 (present condition). For the RCP scenarios two year windows were considered instead, namely the 2041-2070 and the 2071-2100. Thus doing, the extreme value analysis is carried out considering a dataset 30 years long, for each scenario. Extreme value analysis was conducted as follows. First, a Peak-Over Threshold method was used to identify peaks associated with storms within the extracted H_s timeseries, given an H_s threshold of 2.0 m and a minimum temporal distance between independent events equal to 12 hours (Boccotti, 2004). Then, a range of probability distributions (Weibull, Gumbel, LogNormal and Generalised Pareto) were tested against the storm H_s timeseries to check which one best-fits with the sample. The goodness-of-fit was tested by means of the Kolmogorov-Smirnov test. The Generalised Pareto distribution was identified as the best-fitting one for the extreme values of H_s for each one of the directional sub-sectors. Finally, for each subsector H_s values for a return period T_r of 5, 50, 100 years were extracted from the adapted Pareto distribution. From a preliminary analysis of both the storms per each subsector and the geographical fetch, it was noted that a predominant occurrence of events came from the western directions. Consequently, the subsequent analysis was focused on the eight-th subsector corresponding to the West (ϑ = 262.5°N).

Local sea level rise medium confidence projections based on IPCC AR6 for the years 2020-2100 were obtained from the NASA Sea Level Change projection tool at the closest geographical coordinates to the study site

Table 9-1 Present and future hydrodynamic scenarios investigated for the Sicily pilot site.

Return Period [years]	Hydrodyamic scenario	Year window	H_S [m]	T_P [s]	SLR [m]
5	Present (SP)	1993 - 2022	4.26	9.65	0.00
	S4.5-2070	2041 - 2070	5.68	10.42	0.37
	S4.5-2100	2071 - 2100	5.16	10.14	0.57
	S8.5-2070	2041 - 2070	5.22	10.20	0.48
	S8.5-2100	2071 - 2100	5.48	10.34	0.78
50	Present (SP)	1993 - 2022	5.61	10.37	0.00
	S4.5-2070	2041 - 2070	8.06	11.52	0.37
	S4.5-2100	2071 - 2100	7.21	11.16	0.57
	S8.5-2070	2041 - 2070	6.67	10.95	0.48
	S8.5-2100	2071 - 2100	8.36	11.68	0.78
100	Present (SP)	1993 - 2022	6.01	10.56	0.00
	S4.5-2070	2041 - 2070	8.70	11.77	0.37
	S4.5-2100	2071 - 2100	7.75	11.39	0.57
	S8.5-2070	2041 - 2070	6.97	11.09	0.48
	S8.5-2100	2071 - 2100	9.18	12.00	0.78

(latitude 36.00° and longitude 14.00°). In IPCC AR6, the RCP scenarios have been replaced with Socioeconomic Pathways (SSP). Since there is no direct one-to-one correspondence between specific RCP and SSP scenarios, a combinations of RCP and SSP scenarios can be chosen depending on the projected storyline to be investigated. Since considerations about future socio-economic projections at our study case are not available, we decided to combine RCP and SSP scenarios based on the same radiative forcing value. Therefore, wave conditions for RCP4.5 scenarios were matched with sea level rise projections for SSP2-4.5 scenario (radiative forcing equal to 4.5 W/m^2). Similarly, data projected for RCP8.5 wave scenarios are associated with sea level rise corresponding to SSP5-8.5 scenario (radiative forcing equal to 8.5 W/m^2). The sea level rise projection is the one corresponding to the last year of the examined year window, i.e. 2070 and 2100, for the 2041-2070 and 2071-2100 windows respectively.

In the end, we investigated 5 climatic scenarios, a present scenario (SP) based on the analysis of the hystorical re-analysis dataset, two climate change projection scenarios associated with a radiative forcings equal to 4.5 W/m^2 with 2070 and 2100 time horizons (S4.5-2070 and S4.5-2100 respectively), and two scenarios for radiative forcing equal to 8.5 W/m^2 scenarios (S8.5-2070 and S8.5-2100). Considering the abovementioned, a range of hydrodynamic scenarios were investigated, based on combination of sea level rise and wave conditions at different return period (Table 9-1).

The XBeach model allows to simulate the wave dissipation due to the presence of vegetation. To do so, characteristics of vegetation and spatial distribution of the vegetation must be given as input to the model. The spatial distribution of vegetation was obtained by EUNIS2019 habitat maps (Chytrý et al., 2020) integrated with field surveys.

A detailed EUNIS map of the Sicily lagoon system was created by integrating the Corine Biotopes map (1:10,000 scale) and the Corine Coastal Zones Land Cover/Land Use 2018 dataset. The Corine Biotopes

classification was converted to EUNIS 2012 using the Italian Interpretation Manual of the 92/43/EEC Directive. Semi-natural and artificial habitats were cross-referenced using EUNIS 2012 and Corine Land Cover classifications. Conversion to EUNIS 2021 was completed with available crosswalks, though some codes (e.g., J1 – Buildings) lacked conversion systems. The final EUNIS map was validated through field surveys and satellite imagery.

XBeach also simulates sediment transport by using a depth-averaged advection-diffusion scheme to model sediment concentration in the water column, based on equilibrium sediment concentration (Galappatti et al., 1983).

In our model, morphodynamic processes were considered, so simulations were carried out with a variable seabed, as the area is subject to erosion. A granulometric analysis was conducted on the sediments of Granelli's emerged beach, yielding D15, D50, and D90 values of 0.22 mm, 0.27 mm, and 0.30 mm, respectively, which indicate the presence of medium-fine sand, characterised by a standard deviation of 0.35. The sediment for nourishment was selected from the finest available in the offshore quarry, based on ten samples collected at different depths. It was decided to use the sediment from the surface layer of the first section (within the first half meter), having a median diameter of 0.45 mm. A subsequent granulometric analysis provided D15 and D90 values of 0.41 mm and 0.48 mm, respectively, with a standard deviation of 0.35 mm.

Since the native sediment diameter (0.27 mm) and the nourishment sediment diameter (0.45 mm) are different, the width of the emerged beach will be calculated using the "equilibrium profile concept." This approach is based on the depth as a function of the distance y from the shoreline and considers the relationship between sediment characteristics and beach shape. The parameter A, known as the profile scale factor, reflects this relationship and depends on the grain size of the sediment used. The simplest form of the equilibrium profile is given by the following equation:

$$h = Ay^{2/3} \tag{9.1}$$

where h represents the depth and y the distance from the shore (Bruun, 1954). By applying the specific morphological data of the site, an intersecting beach profile can be achieved, ensuring an optimal configuration for nourishment. This method is essential for predicting how the beach will respond to the

Table 9-2 Semi-quantitative rank scores for three of the five selected REST-COAST ecosystem services applied to Sicily Lagoons EUNIS biotopes through an expert approeach.

Code	EUNIS Name	WP	RCE	RFR
D5.1	Reedbeds normally without free-standing water	5	5	4
MA25	Mediterranean littoral biogenic habitat	3	4	3
MA2515	Mediterranean *Sarcocornia perennis* mats	4	4	4
N12	Mediterranean and Black Sea sand beach	1	4	4
N14	Mediterranean, Macaronesian and Black Sea shifting coastal dune	2	5	4
J1	Buildings of cities, towns and villages	0	0	0
R1E	Mediterranean tall perennial dry grassland	3	4	3
V13	Arable land with unmixed crops grown by low-intensity agricultural methods	0	1	1
V61	Broadleaved fruit and nut tree orchards	1	2	2
MB252	Biocenosis of Posidonia oceanica	5	2	3
MB55	Meditrerranean Infralittoral sand	1	1	0

added sediments and for maintaining a long-term balance between the coastline and the sea, minimizing the risk of future erosion.

To conduct the ESS assessment, accurate biotope scores, as shown in Table 3, are essential (Potts et al., 2014, Baptist et al., 2024). These scores for the Sicily Lagoon were derived from expert evaluations of terrestrial EUNIS biotopes, with each expert independently rating their contribution to Ecosystem Services like Water Quality Purification (WP), Coastal Erosion Risk Reduction (RCE), and Coastal Flooding Risk Reduction (RFR) on a scale 0 to 5, with 5 being the highest score indicating the larger contribution of the biotope to a given ecosystem service.

9.2.3. Model setup

The SWAN computational domain extends for 2068 km^2, encompassing approximately 90 km of coastline (Figure 9-3a). The numerical grid consists of 17141 nodes. The unstructured grid resolution (i.e. distance

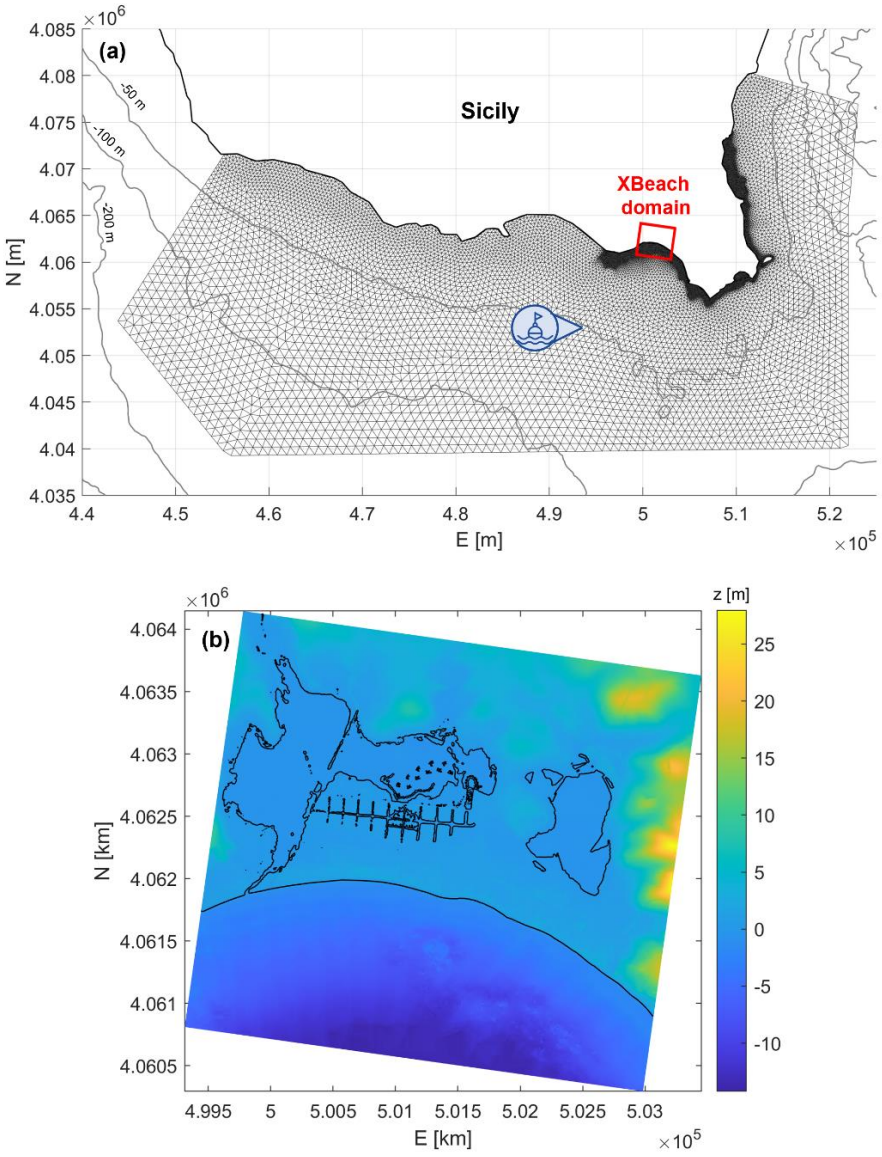

Figure 9-3 a) SWAN numerical grid. The red rectangle shows the nested Xbeach domain. b) XBeach numerical grid with associated elevation values in color scale.

between nodes) is variable and bathymetry-dependant. For depths greater than 100 m, the elements have a side of 1 km. For depths between 100 m and 30 m, the size gradually changes from 1 km to 400 m. For depth less than 30 m, the elements maintain a size of 400 m. A higher resolution (100 m) was adopted in the proximity of the XBeach domain.

The XBeach computational domain (Figure 9-3b) is nested within the SWAN domain and consists of a 3.36 km cross-shore and 3.69 km long-shore tile, consisting of a total surface of 12398 km^2, enclosing the Cuba-Longarini lagoon system, Granelli town and beach. A structured grid with variable resolution was built within the domain, ranging 2.5 - 10 m cross-shore and 5 - 10 m longshore. The grid is made up by 1150 (cross-shore) x 544 (long-shore) cells, for a total of 625,600 nodes. To each cell node, an elevation value is associated based on the topographical data mentioned in Section 9.2.1.

In order to investigate the performance of the beach nourishment soultion, a second XBeach computational domain was developed (Figure 9-4), also nested within the SWAN domain. This domain spans 16 km² and includes, in addition to the lagoon system, the urban area, and the beach, the two promontories located to the east (Punta Mici) and to the west (Punta Castellazzo). The numerical grid, with a variable resolution between 2.5 and 10 m, consists of 1,219 cross-shore cells and 655 long-shore cells, for a total of 798,445 nodes.

For each habitat within the study area, a representative vegetation species is assigned based on a cross-comparison between EUNIS habitat mapping and field surveys. The pertinent characteristics of the vegetation, such as the number of vertical sections (n_v), vertical section height (αh), drag coefficient ($\widetilde{C_d}$), stem diameter (b_v), and vegetation density (N) were sourced from relevant literature (Knutson et al., 1982; Van Loon-Steensma et al., 2016; Garzon et al., 2019; Fernández-Montblanc et al., 2020) and local expert approach. The specific values employed in the study are presented in Table 9-3. Vegetation maps for current state (including already performed restoration), dune revegetation, and seagrass revegetaion used in Xbeach are shown in Figure 9-5.a,b, and c respectively.

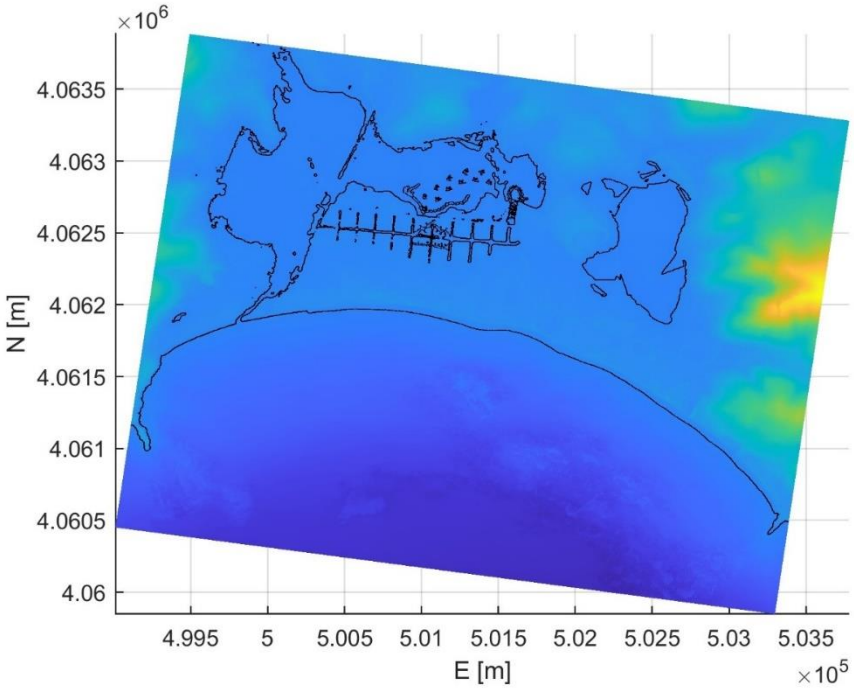

Figure 9-4 Second XBeach computational domain that includes beach nourishment intervention.

Table 9-3 Vegetation characteristics associated with EUNIS habitat codes

Species	Associated habitat (EUNIS code)	n_{sec}	αh [m]	$\widetilde{C_d}$ [-]	b_v [m]	N_v
Ammophila arenaria	Shifting coastal dunes (N14)	1	1	0.7	0.0025	260
Spartina alterniflora	Coastal saltmarshes and saline reedbeds (MA25)	1	0.625	1	0.003	400
Phragmites australis	Reedbeds normally without free-standing water (Q51)	2	0.25 2	0.86 0.86	0.006 0.026	110 110
Posidonia oceanica	Biocenosis of Posidonia oceanica (MB252)	1	0.50	1	0.01	280

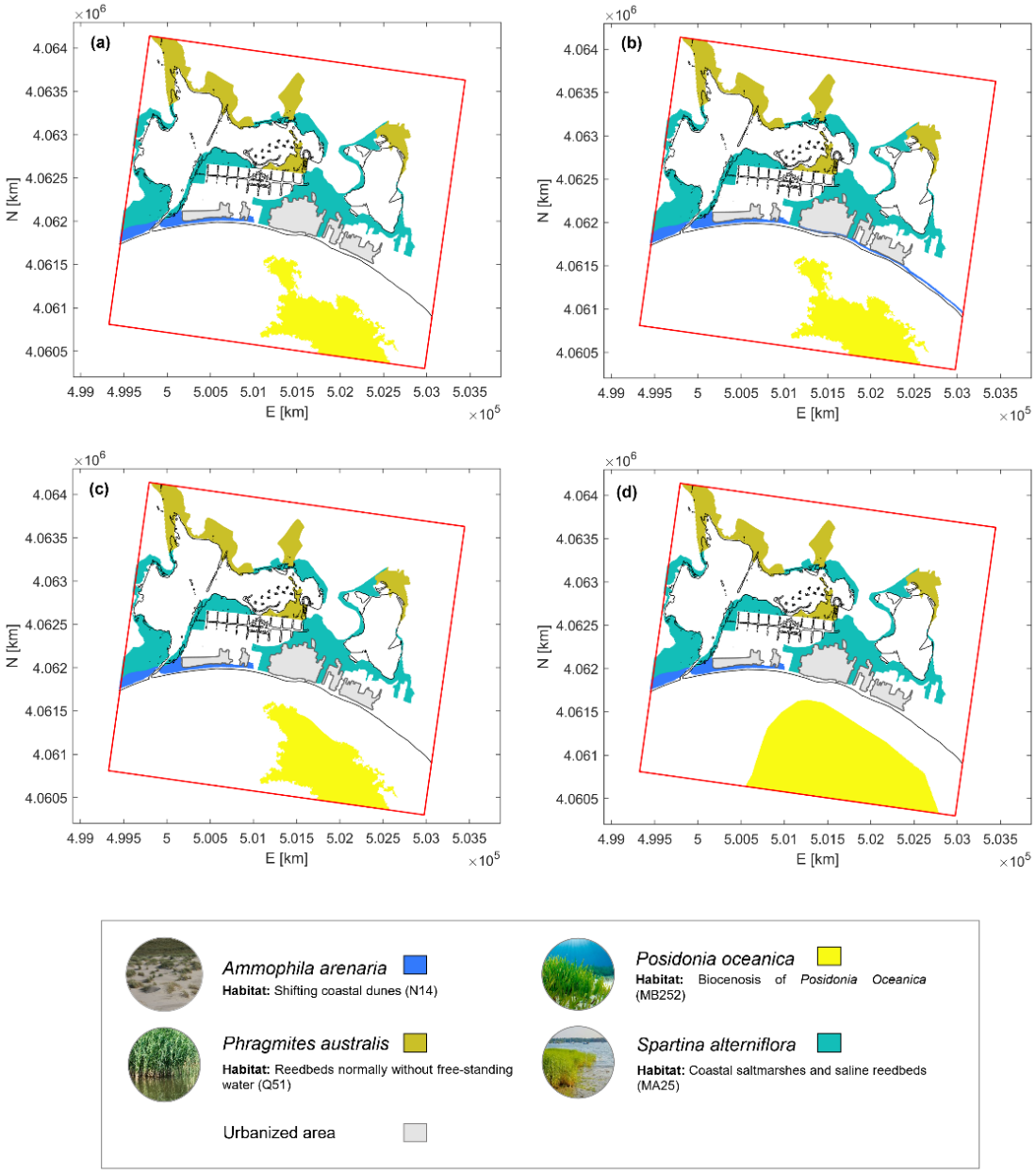

Figure 9-5 Vegetation maps used as inputs in Xbeach for: (a) current state, (b) dune revegetation, (c), seagrass reconstruction, (d) seagrass reconstruction upscaling. For the beach nourishment case, the habitat map of the current state (a) was used.

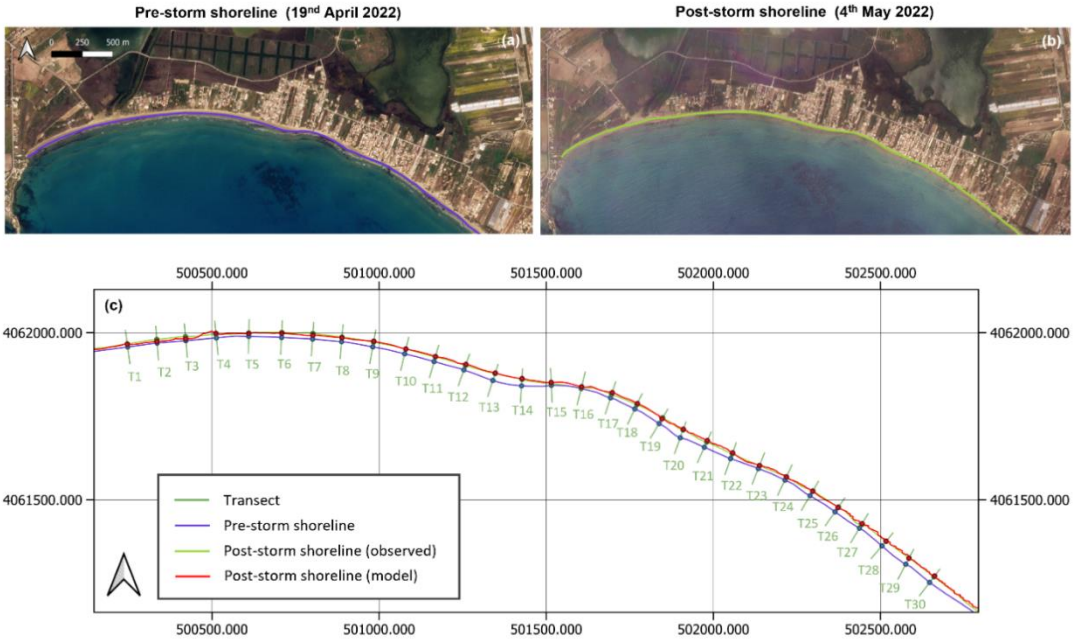

Figure 9-6 Pre-storm (blue line), post-storm (green line) shorelines obtained from satellite imagery and post-storm shoreline predicted by our model (red line). The figure shows the position of the 30 transects along which shoreline observed and predicted shoreline retreat is computed.

9.2.4. Model validation

The validation of the SWAN and XBeach models involved assessing their accuracy in predicting hydrodynamic and morphodynamic changes during a storm from April 21 to April 22, 2022. The storm had a significant impact on the shoreline, and the models' predictions were compared with post-storm satellite imagery from May 4, 2022. Hourly wave data from April 20 to April 25, 2022, were used to drive the SWAN model, with performance metrics showing a high level of agreement between model predictions and observations (Bias: 0.02 m, RMSE: 0.37 m, Willmott Skillscore: 0.95).

For XBeach, the validation focused on its ability to predict storm-induced morphodynamics. The procedure involved five sea states selected from the storm, each 5 hours apart, with XBeach simulating 0.5 hours of hydrodynamic time and 5 hours of morphodynamic time, using a morphodynamic acceleration factor of 10. The final bed elevation from each simulation was used as input for the subsequent one, and the predicted shoreline after the final simulation was compared with the observed post-storm shoreline from May 4, 2022. Figure 9-6.c shows the pre-storm (blue line), post-storm (green line) shorelines obtained from satellite imagery and post-storm shoreline predicted by the model (red line). Model performance was assessed using 30 transects to measure distances between the observed and modeled shorelines, with Bias, RMSE, and BSS metrics used to evaluate the prediction skill.

9.2.5. Plan of simulations

Appendix C shows the plan of the numerical simulations, which have been obtained by combining all hydrodynamic scenarios, and the three restoration scenarios No-NbS (NN), dune revegetation (DR), seagrass reconstruction (SR1), seagrass reconstruction – upscale (SR 2) and beach nourishment (BN).

9.2.6. General methodology for ESS evaluation

For evaluating the ecosystem service change, methodology from Baptist et al. (2024) is employed. Scores for three chosen services (water purification, WP; erosion risk reduction, RE; and flood risk reduction, RF) is

determined by calculating the weighted contribution of each EUNIS habitat. The overall score for each of the five ecosystem services (ESS) is calculated by summing up the product of each EUNIS habitat's area and its rank score for the ESS.

$$ESS_{tot} = \sum_{i=1}^{n} Area_i \times ESS_i \tag{9.2}$$

where ESS_{tot} is the total score for a (one of five) ESS in a pilot area, n is the number of EUNIS (sub)habitats, $Area_i$ is the surface area (m^2) of EUNIS habitat i and ESS_i is the rank score (0 to 5) of the ecosystem service for EUNIS habitat i.

Any variation in the surface area of EUNIS (sub)habitats due to future conditions, such as climate change or restoration efforts, results in a change in the overall ESS score (ESStot). This change is quantified as a relative difference:

$$ESS_{rel,2} = \frac{ESS_{tot,2} - ESS_{tot,1}}{ESS_{tot,1}} \tag{9.3}$$

Where $ESS_{rel,2}$ is the relative change in the ESS-score at time 2 with respect to time 1, $ESS_{tot,1}$ is the total ESS score at the (initial) time 1 and $ESS_{tot,2}$ is the total ESS score at the (next) time 2. The relative change in the ESS score ranges from -1 to +1, reflecting the degree of improvement (+) or decline (-) in the provision of the ecosystem service. To address the issue of comparing small changes (a few percent) with large changes (tens of percent) in total ESS scores, a transfer function is applied. This function uses a sigmoid curve that outputs values between -5 and +5, corresponding to relative changes between -1 and +1.

$$\sigma(x) = \frac{10}{1 + e^{-kx}} - 5 \tag{9.4}$$

here, σ is the sigma-score (ranging from -5 to 5), and x represents the relative change in the ESS score (between -1 and +1). The sigma-scores are then grouped into eleven categories (as shown in Table 9-4) to express the relative change in ESS in a consistent, uniform metric for both gains and losses.

Table 9-4 Transformation of sigma-scores to rounded classes, their meaning in terms of magnitude of change and the relative change in percentage for the considered ecosystem services.

σ-score	rounded	meaning		%change
-5 to -4	-5	very large	decrease	-100 to -22
-4 to -3	-4	large	decrease	-22 to -13.9
-3 to -2	-3	medium	decrease	-13.9 to -8. 5
-2 to -1	-2	small	decrease	-8.5 to -4.1
-1 to 0	-1	very small	decrease	-4.1 to 0
0	0	No	change	0
0 to 1	1	very small	increase	0 to 4.1
1 to 2	2	small	increase	4.1 to 8.5
2 to 3	3	medium	increase	8.5 to 13.9
3 to 4	4	large	increase	13.9 to 22
4 to 5	5	very high	increase	22 to 100

9.2.7. Efficacy Indicators for evaluating NbSs in Coastal Flooding and Erosion Reduction

The performance of the investigated NbSs in reducing coastal flooding and erosion is quantified using efficiency indicators. To evaluate the effectiveness of the proposed intervention in reducing flood risk, the flooding reduction efficiency E_f is calculated as:

$$E_f = \frac{A_{f,NN} - A_{f,NbS}}{A_{f,NN}} \cdot 100 \quad (9.5)$$

where $A_{f,NN}$ represents the flooded area in the scenario no-NbS NN (NN, Figure 7a) , and $A_{f,NbS}$ represents the flooded area considering the interventions of DR or SR. An additional efficiency indicator, E_{fc} , is computed to assess the flooding reduction specifically within the city area. This indicator is calculated similarly to E_f, but only considers the flooded areas within the city.

$$E_{fc} = \frac{A_{fc,NN} - A_{fc,NbS}}{A_{fc,NN}} \cdot 100 \quad (9.6)$$

where $A_{fc,NN}$ and $A_{fc,NbS}$ represent the flooded city area in the no-NbS (Figure 7a) and NbS (Figure 7b)scenarios, respectively.

Regarding the NbS's ability to reduce erosion caused by wave storms, two erosion reduction efficiency indicators are calculated. To evaluate the NbS performance in reducing the eroded volumes of the beach foreshore, the eroded volume reduction efficiency indicator is computed as:

$$E_{eV} = \frac{V_{e,NN} - V_{e,NbS}}{\max(V_{e,NN})} \cdot 100 \quad (9.7)$$

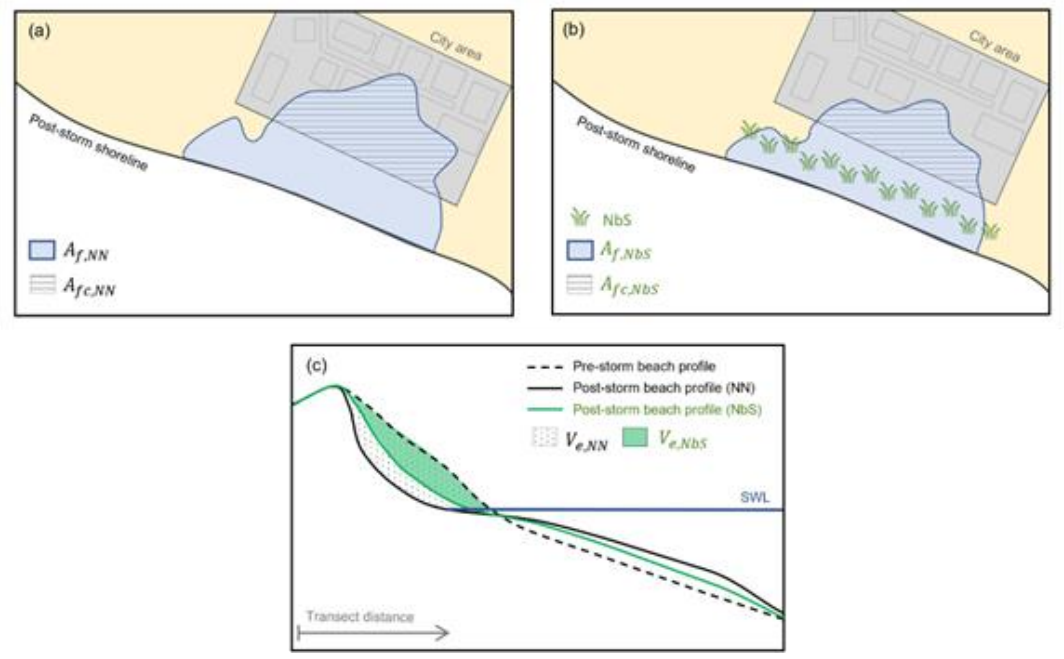

Figure 9-7 Schematization of the terms used within the efficiency indicators: Flooded areas without or with NbS (a and b respectively); eroded volumes (c).

where $V_{e,NN}$ and $V_{e,NbS}$ represent the eroded volumes of the initially emerged beach profile at t = 1800 s for the no-NbS and NbS scenarios, respectively (Figure 9-7c). Here, $\max(V_{e,NN})$ refers to the maximum eroded volume across all transects in that specific simulation defined in Figure 9-6c.

9.3. Results

9.3.1. Evaluation of NbS flooding reduction efficacy

To evaluate the efficiency of the NbS interventions studied, Figure 9-8 present bar graphs showing flooded urban areas and the percentage reduction in these flooded areas for each return period analysed (5 and 100 years).

Specifically, considering 5 and 100-year return period and the scenario without NbS (NN), the flooded urban areas range from 0.013 km² (SP) to 0.218 km² (S8.5-2100); implementing the dune revegetation intervention reduces the flooded urban areas to values between 0.011 km² (SP) and 0.163 km² (S8.5-2100). When the seagrass revegetation intervention covers 87 hectares, the flooded urban area slightly increases, ranging between 0.013 km² (SP) and 0.200 km² (S8.5-2100). Therefore, it was decided to increase the existing seagrass area by about 100 hectares, reaching approximately 190 hectares; as a result, the flooded urban area decreases, with values between 0.004 km² (SP) and 0.090 km² (S8.5-2100). Considering the last sand nourishment intervention, a substantial reduction in the flooded urban area is observed, with values reaching zero for the SP scenario and up to 0.0496 km² (S8.5-2100).

Examining the reduction efficiency for this return period (Figure 9-8b), a significant percentage reduction in flooded urban areas is evident due to the sand nourishment intervention across all five hydrodynamic scenarios analysed, with up to 100% reduction in flooding for the SP scenario, and reductions of 75% for the scenario with the highest wave height (HS = 8.70 m, S4.5-2070) and 78% for the scenario with the highest sea level rise (SLR = 0.78 m, S8.5-2100). The seagrass reconstruction also yields excellent results, with a 67%

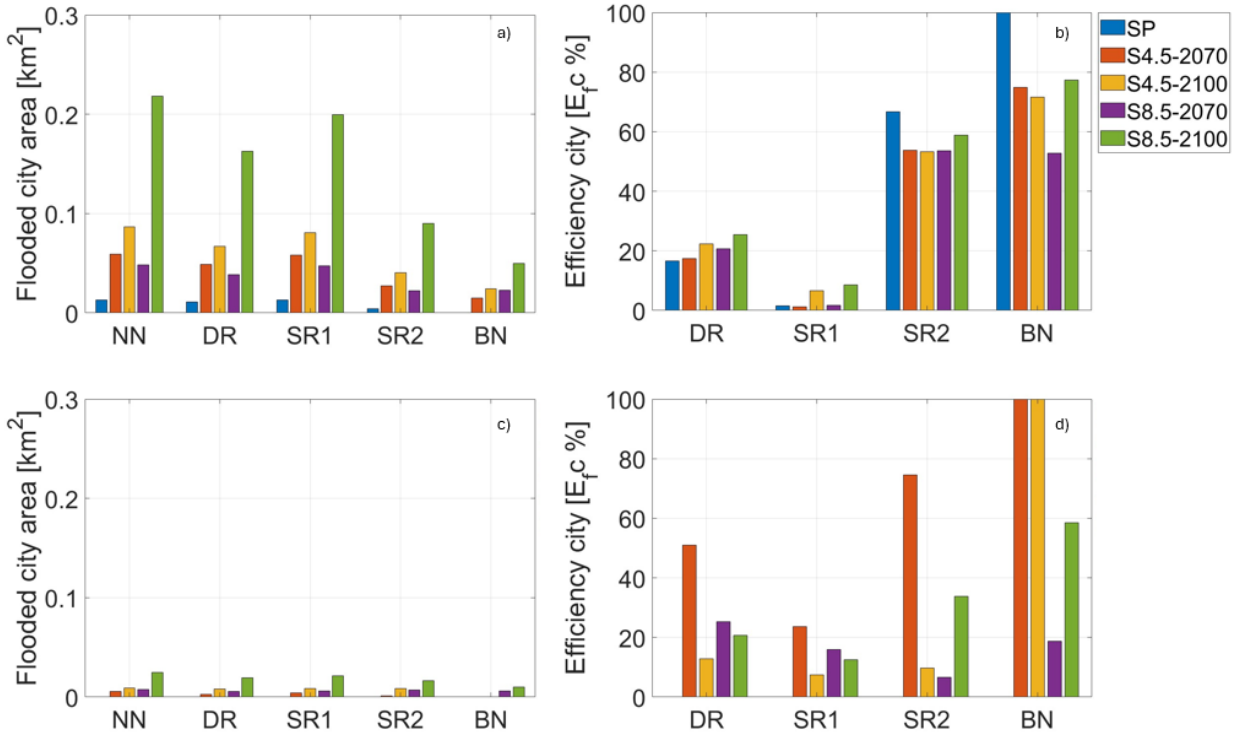

Figure 9-8 Flooded areas due to inundation in the city, for a 100-years return period (a), 5-years return period (c). Flooding reduction efficiency in the city [EfC] due to proposed NbSs , for a 100-years return period (b),5-years return period (d)

reduction in flooded urban areas for the SP scenario; 53% reductions for three projection scenarios (S4.5-2070, S4.5-2100, S8.5-2070), and a 59% reduction for S8.5-2100. The dune revegetation intervention provides a consistent reduction in flooded areas, ranging from 17% (SP) to 25% (S8.5-2100). Finally, the seagrass revegetation intervention covering 87 hectares results in limited percentage reductions, from 1% to 8.6% (S8.5-2100).

The results demonstrate that the presence of NbS plays a crucial role, ensuring a significant reduction in flooded areas and volumes in the urban centre and in the area adjacent to the estuary. Considering a shorter return period, such as 5 years, in the NN scenario, the flooded urban areas are naturally smaller, ranging from 0 km² (SP) to 0.025 km² (S8.5-2100). Adding the various NbS interventions to the model reduces the flooded areas, going from 0 km² (SP) to 0.019 km² (S8.5-2100) for dune revegetation, from 0 km² (SP) to 0.021 km² (S8.5-2100) for seagrass revegetation, from 0 km² (SP) to 0.016 km² (S8.5-2100) for the seagrass upscale, and from 0 km² (SP, S4.5-2070, S4.5-2100) to 0.010 km² (S8.5-2100) for the sand nourishment intervention. It should be noted that, regardless of the type of intervention chosen, for each scenario examined, with a short return time, the flooded urban areas are 0 km² in the present scenario (SP).

Analysing the reduction efficiency chart for this return period (Figure 9-8d), there is a significant decrease in flooded urban areas due to the sand nourishment intervention, ensuring a 100% reduction for the S4.5-2070 and S4.5-2100 scenarios, and 58% for the most critical scenario (S8.5-2100). The seagrass upscale intervention also delivers excellent results, with a reduction efficiency of 34% for the highest sea-level rise scenario (S8.5-2100) and 75% for the highest wave height scenario (S4.5-2070). The dune revegetation also contributes positively, showing a reduction ranging from 12-20% up to 51% for the S4.5-2070 scenario. It is important to emphasise that since there are no flooded urban areas in the current scenario (SP), no percentage reduction efficiency can be calculated.

Once again, the proposed NbS interventions produce excellent results, with percentage reductions for the seagrass expansion ranging from 7% for S8.5-2070 to 34% for S8.5-2100 and up to 74.5% for S8.5-2070.
It's also important to consider the role of sea-level rise (SLR). Comparing some flooded urban area values obtained from two simulations for the current state, both with a 100-year return period: in the S4.5-2070 scenario (Hs = 8.70 m, SLR = 0.37 m), the flooded urban area is 0.059 km², while in the S4.5-2100 scenario (Hs = 7.75 m, SLR = 0.57 m), the flooded area is 0.086 km². This highlights the close correlation between flooding and sea-level rise.

Therefore, from these results, the NbS interventions implemented significantly contribute to the reduction of flooded areas, with reduction efficiencies reaching up to 100% for interventions such as sand nourishment and seagrass meadow upscale in current scenarios (SP). Specifically, the sand nourishment intervention shows significant reductions in flooded areas, especially near the urban centre, helping to protect these vulnerable zones.

9.3.2. Evaluation of NbS erosion reduction efficacy

Figure 9-9 shows the pre- and (modelled) post-storm beach profiles computed along three selected transects. The three transects were chosen to be representative of three portions of the beach, i.e. western, central and eastern parts. Position of the three transects are shown in Figure 9-11a, alongside the shoreline position (grey line). Specifically, Figure 9-11b, c and d show pre-storm (dashed line), NN (black continuous line), DR (orange dotted line), SR1 (purple dashed) and line SR2 (green line) post-storm beach profiles for S4.5-2070 hydrodynamic scenario (H_s = 8.70 m, T_p = 11.77 s, SLR = 0.37 m) at transects T5, T12 and T22 respectively.

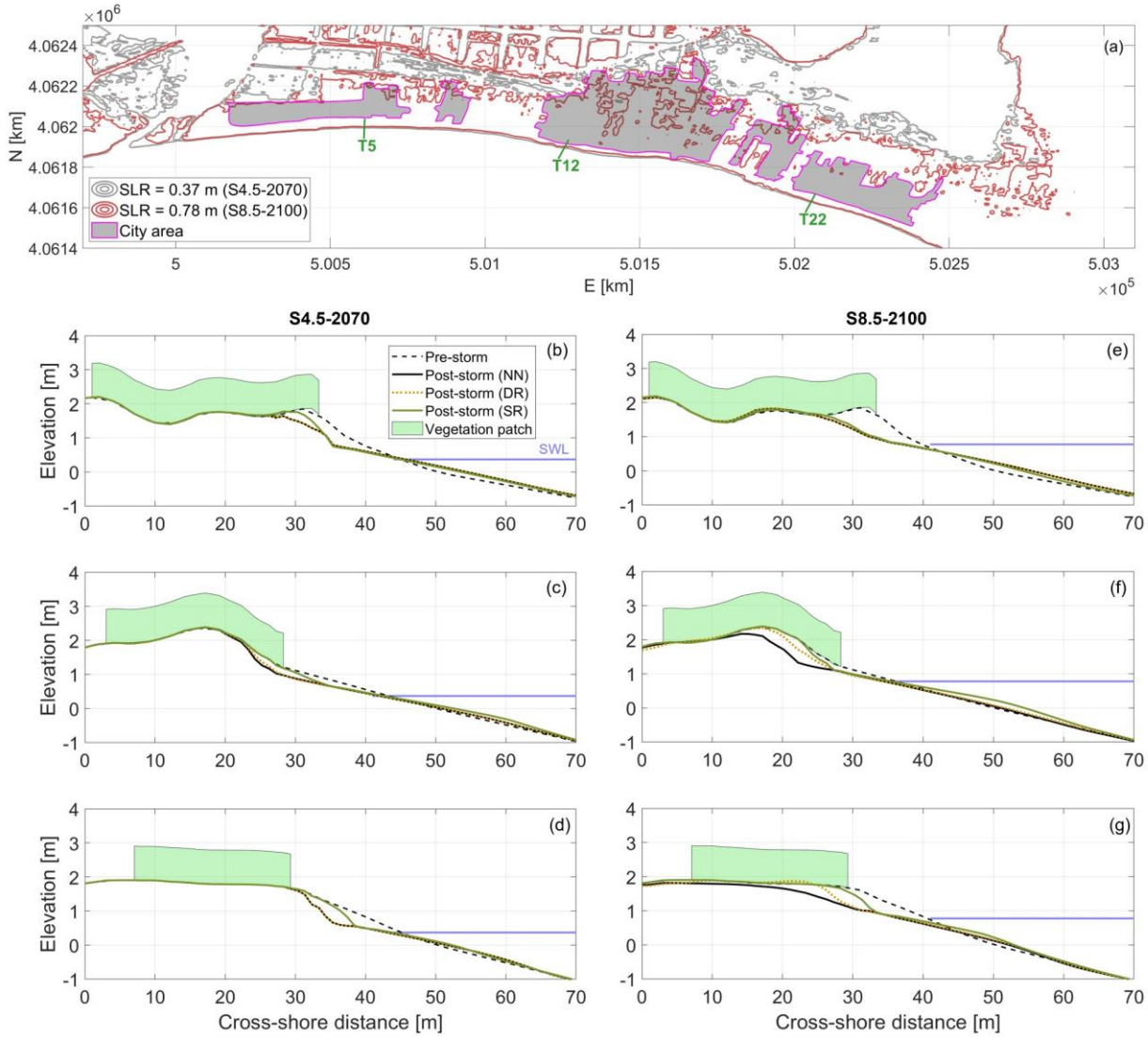

Figure 9-9 Pre- and post-storm (modelled) beach profiles. Planimetric view of the coastal area and beach profile transects (a); beach profiles: pre-storm (black dashed line), no-NbS (NN, black continuos line), dune revegetation (DR, orange dotted line) and seagrass meadow reconstruction (SR, green continuous line) at transects T5, T12 and T22, for S4.5-2070 (b, c and d) and S8.5-2100 (e, f and g). The beach profile plots show also the position and height of the dune vegetation (Ammophila arenaria, light green patch)

Figure 9-9b shows the beach profile at transect T5, i.e., in the western part of the Granelli coastline. The simulated storm induces erosion of the foreshore dune profile, with an estimated eroded volume for the NN scenario of $V_{e,\ NN}$ = 9.40 m³/m. The SR1 intervention do not make any significant effect, with an eroded volume of $V_{e,\ SR1}$ = 9.42 m³/m (E_{eV} = 0.2%) The SR2 instead provides a larger contribution to erosion protection, with an eroded volume of $V_{e,\ SR2}$ = 7.67 m³/m, i.e., corresponding to a E_{eV} of 16%. Given that the wave direction is primarily SSW (205°N at the XBeach offshore boundary), the SR1 and SR2 interventions help attenuate energy from refracted waves that were initially propagating over the restored meadow. In this area of the domain, the DR intervention is absent as the dune retains its natural vegetation. Consequently, no difference is observed between the NN and DR simulations.

Moving closer to the central part of the beach (transect T12, Figure 9-9c), again the SR1 intervention do not contribute significantly in reducing eroded volumes, going from 7.83 m³/m (NN) to 7.90 m³/m corresponding

to an eroded volume reduction of E_{eV} = 0.7%. SR2 instead contribute to volume erosion reduction to 3.17 m³/m, corresponding to a E_{eV} of 42%. The contribution of the DR intervention is limited, with an estimated eroded volume reduction of E_{eV} = 8%.

Given the SSW wave direction, the eastern part of the domain (Figure 9-9d) is expected to be the most heavily affected by the storm. At the same time, it benefits the most from the sheltering effect of the existing seagrass meadow and from the SR1 and SR2 interventions. At transect T22, the NN scenario results in an eroded volume of 9.11 m³/m. The SR1 intervention reduces this to 7.31 m³/m (E_{eV} = 16.34% while SR2 further reduces it to 4.29 m³/m (E_{eV} = 44%). The zone of the DR intervention is not even reached by waves during this simulated storm event; therefore, it does not contribute to erosion reduction in this hydrodynamic scenario.

Figure 9-9e, Figure 9-9f, and Figure 9-9g illustrate the pre- and post-storm beach profiles for the S8.5-2100 scenario, representing the most severe investigated condition (H_s = 9.18 m, T_p = 12.00 s, and SLR = 0.78 m). At the western section of the coast (Figure 9e), the increase in wave height and sea level rise induces larger eroded volumes for the NN case compared to the S4.5-2070 scenario at the same transect ($V_{e,NN}$ = 12.82 m³/m). Compared to Figure 9b, the SR1 and SR2 interventions show diminished effectiveness due to the increase in water depth caused by SLR, being 12.81 m³/m for SR1 (E_{eV} <0.1%) and 11.15 m³/m for SR2 (E_{eV} = 7%). At transects T12 and T22 (Figures 9f and g), eroded volumes for the NN scenario are 13.29 m³/m and 18.70 m³/m, respectively. As waves reach the revegetated dune patch, the DR intervention contributes to the erosion reduction, with $V_{e,DR}$ = 7.19 m³/m and 12.70 m³/m (both E_{eV} = 27%) for T12 and T22, respectively. SR1 reduces erosion significantly only on T22 (11.70 m³/m, E_{eV} = 31%) for T22, whereas SR2 achieves reductions to $V_{e,SR2}$ = 2.74 m³/m (E_{eV} = 47%) for T12 and $V_{e,SR2}$ = 6.49 m³/m (E_{eV} = 55%) for T22.

Figure 9-10 (a, b and c) shows the beach profiles before and after the storm for the S4.5-2070 scenario. Specifically, it depicts the beach profiles before the storm (dashed line), the NN profile after the storm (black solid line), and the profile with the BN intervention (orange line). Figure 9-10 (d, e and f) display the beach profiles before and after the storm for the more severe S8.5-2100 scenario.

From the results for the S4.5-2070 scenario, it is observed that the nourishment intervention in the western part of the area (transect T5, figure 10a) generates a growth volume of 1.48 m³/m and an eroded volume of 4.42 m³/m (Ve,BN), which is much lower than the eroded volume of 9.41 m³/m observed in the case without intervention (EeV = 47%). Moving towards the central part of the beach (transect T12, Figure 9-10b), the protective effect of nourishment induces a slight reduction in eroded volumes, with an eroded volume of 4.16 m³/m and a growth volume of 1.18 m³/m. In the eastern part of the domain (transect T22, Figure 9-10c), the most affected by the storm, the intervention results in an eroded volume of 5.13 m³/m and a growth volume of 0.65 m³/m.

Moving to the more critical scenario, S8.5-2100, characterized by a higher sea level rise (SLR) but a lower wave height compared to the previous scenario, the erosion volumes are lower. In the western part of the domain (transect T5, Figure 9-10d), the nourishment intervention produces an eroded volume of 2.11 m³/m, a growth volume of 1.17 m³/m, and a deposited volume of 1.79 m³/m.

In the central part of the site (transect T12, figure 10e), the intervention yields a growth of sediment volume of 0.43 m³/m, a lower eroded volume of 0.89 m³/m, and a deposited volume of 2.26 m³/m. Finally, in the eastern part (transect T22, figure 10f), an eroded volume of 1.11 m³/m is observed, slightly higher than in other areas of the same scenario due to the greater exposure to wave action, with a growth volume of 0.26 m³/m and a deposited volume of 1.49 m³/m.

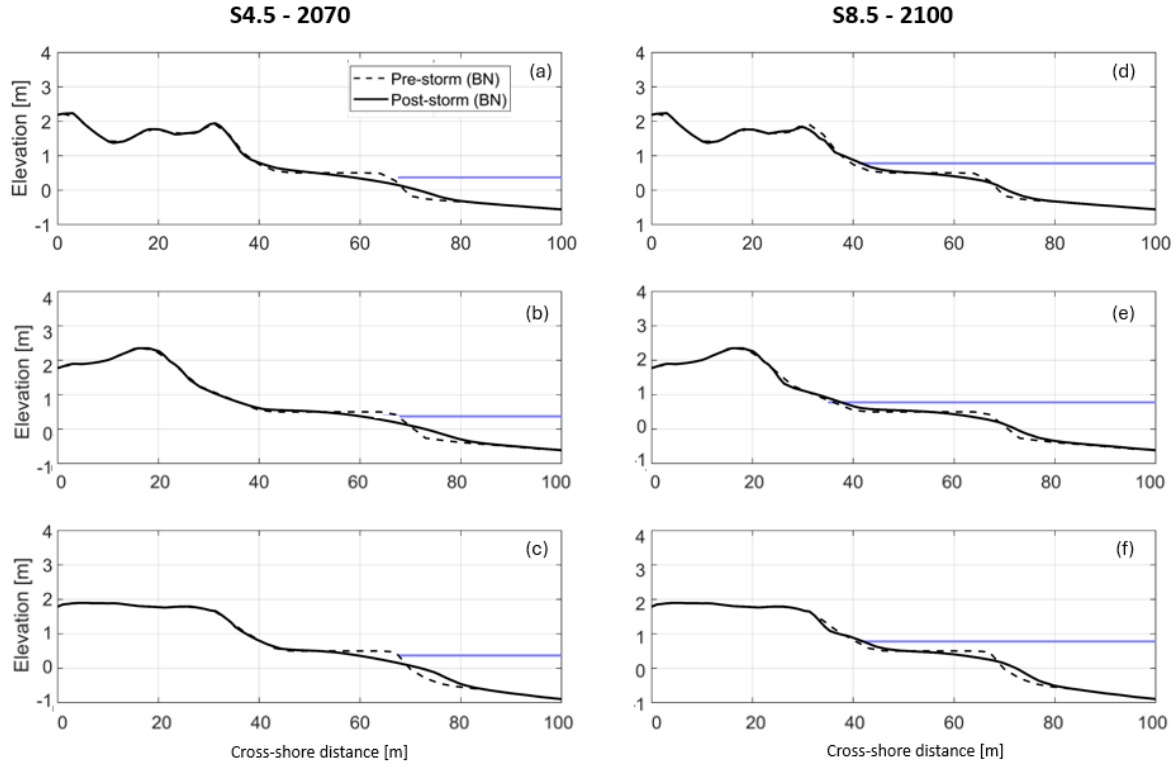

Figure 9-10 Pre- and post-storm (modelled) beach profiles. Beach profiles: pre-storm (black dashed line), no-NbS (NN, black continuos line), beach nourishment (BN, orange dotted line) at transects T5 (a, d), T12 (b, e) and T22 (c, f), for S4.5-2070 (a, b and c) and S8.5-2100 (d, e and f). [100-years return time]

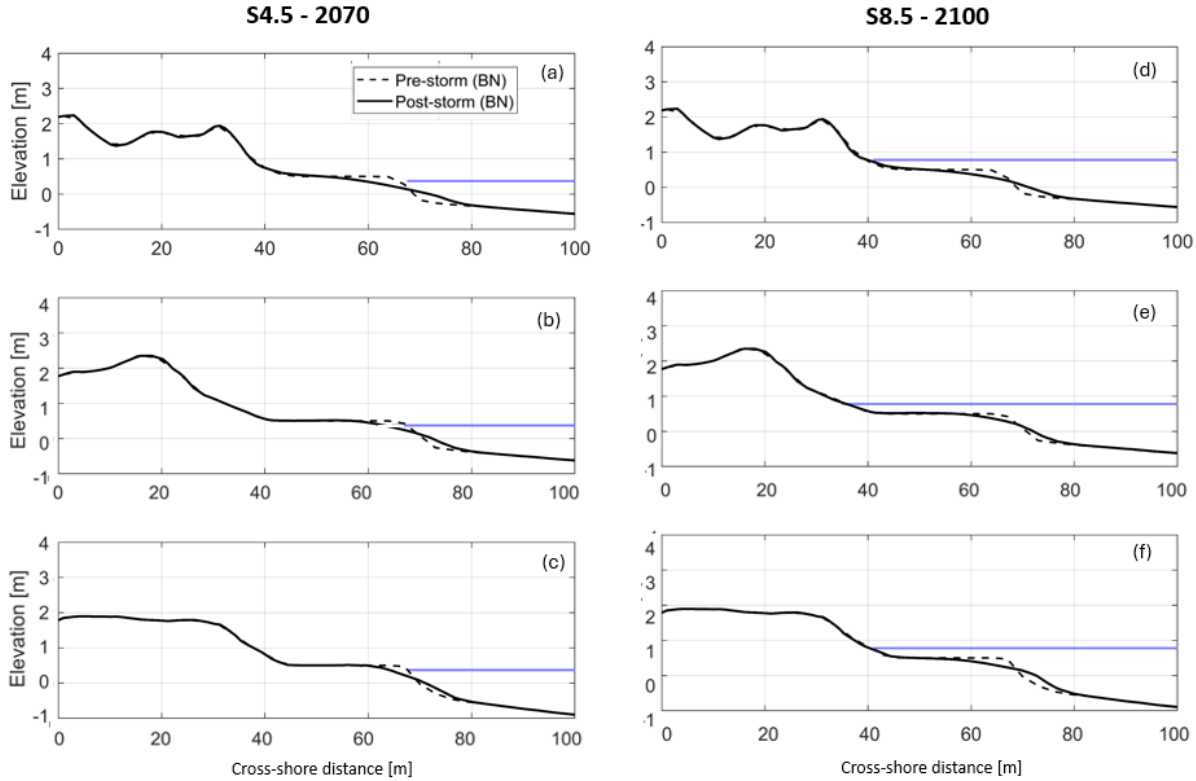

Figure 9-11 Pre- and post-storm (modelled) beach profiles. Beach profiles: pre-storm (black dashed line), no-NbS (NN, black continuos line), beach nourishment (BN, orange dotted line) at transects T5 (a, d), T12 (b, e) and T22 (c, f), for S4.5-2070 (a, b and c) and S8.5-2100 (d, e and f). [5-years return time]

Considering a 5-year return period, shown in Figure 9-11, it can be observed that the erosion results will be lower. Specifically, for the S4.5-2070 scenario, the nourishment intervention in the western part of the area (transect T5, Figure 9-11a) determines a growth volume of 0.69 m^3/m and an eroded volume of 3.38 m^3/m. In the central part of the beach (transect T12, Figure 9-11b), the protective effect of the nourishment determines a slight reduction of the eroded volumes, with an eroded volume of 2.27 m^3/m and a growth volume of 0.35 m^3/m. In the eastern part of the domain (transect T22, Figure 9-11c), the intervention determines an eroded volume of 2.17 m^3/m and a growth volume of 0.17 m^3/m. Moving to the most critical scenario, S8.5-2100, the erosion volumes are even lower. In the western part (transect T5, Figure 9-11d), the nourishment intervention generates an eroded volume of 0.51 m^3/m, a growth volume of 0.07 m^3/m and a deposited volume of 0.88 m^3/m.

In the central part of the site (transect T12, Figure 9-11e), a growth volume of 0.31 m^3/m is recorded, with a lower eroded volume of 0.03 m^3/m and a deposit of 0.52 m^3/m. Finally, in the eastern part (transect T22, Figure 9-11f), an eroded volume of 0.30 m^3/m is observed, with zero growth and a deposited volume of 0.45 m^3/m.

9.3.3. Evaluation of ESS relative change

In this section, we present the findings of the assessment of ecosystem service (ESS) alterations resulting from sea-level rise (SLR) and nature-based solutions (NbS). The methodology delineated in Section 9.2.7 facilitated the evaluation of relative changes in ESS and enabled the classification of ESS provisioning improvements or degradations on a scale from -5 to +5. This analysis focused on three primary ecosystem services: water purification (WP), flood risk reduction (FR), and erosion risk reduction (ER).

Figure 9-12 illustrates the habitat maps generated through the integration of local survey data with the Carta Natura database. Each habitat, as explained in Section 9.2.7, is assigned scores for the three pertinent ESS, which contribute to the calculation of the total ecosystem service score (ESS_{tot}). Figure 9-12a shows the habitat maps for SP, whereas Figure 9-12b show the habitat map in the case of the hydrodynamic scenario S4.5-2070, i.e. with a estimated sea level rise of 0.37 m. The increase of sea level determines a squeezing of the already narrow beach strip. Moreover, the increase in sea level determines the opening of a channel in the estuary region of the Longarini lagoon, inducing a permanent connection with the sea. This connection not only equalizes the salinity levels between the sea and the lagoon but also regulates the lagoon's water level according to sea levels, transitioning the habitat from a saline lagoon to Mediterranean infralittoral sand. Such alterations detrimentally impact the lagoon's natural flood mitigation capacity, as it can no longer function as an expansion reservoir. Consequently, this leads to a significant reduction in the flood risk reduction score from 4 to 1, as depicted in Figure 9-12c for the scenario S4.5-2070, the most severe SLR scenario examined.

Table 9-5 and Table 9-6 shows the ESS sigma score for the comparison case between SP, NN and S4.5-2100, NN, i.e. the present scenario with no NbS compared with an S4.5-2100 hydrodynamic scenario with NN. The decrease of ESS provisining induced by the salinization and permanent connection of the lagoon with the sea determines is in the range of 26-30%, resulting in a sigma score equal to -5 for all ESS. Similar results are obtained, in terms of sigma score, for the comparison between the SP, NN with the S8.5-2100, NN, with relative change ESS_{rel} between 0.43 and 0.52, and a sigma score equal to -5 far all ESS.

Table 9-7 presents the relative ecosystem service change and sigma scores for comparing the SP, NN scenario with the SP, SR1 scenario. The SR1 intervention shows a minimal contribution to maintaining ecosystem service provisioning, with an increase limited to 2%. On the other hand, upscaling significantly enhances ecosystem service provisioning by as much as 16%, as shown by Table 9-8, with details of the computation

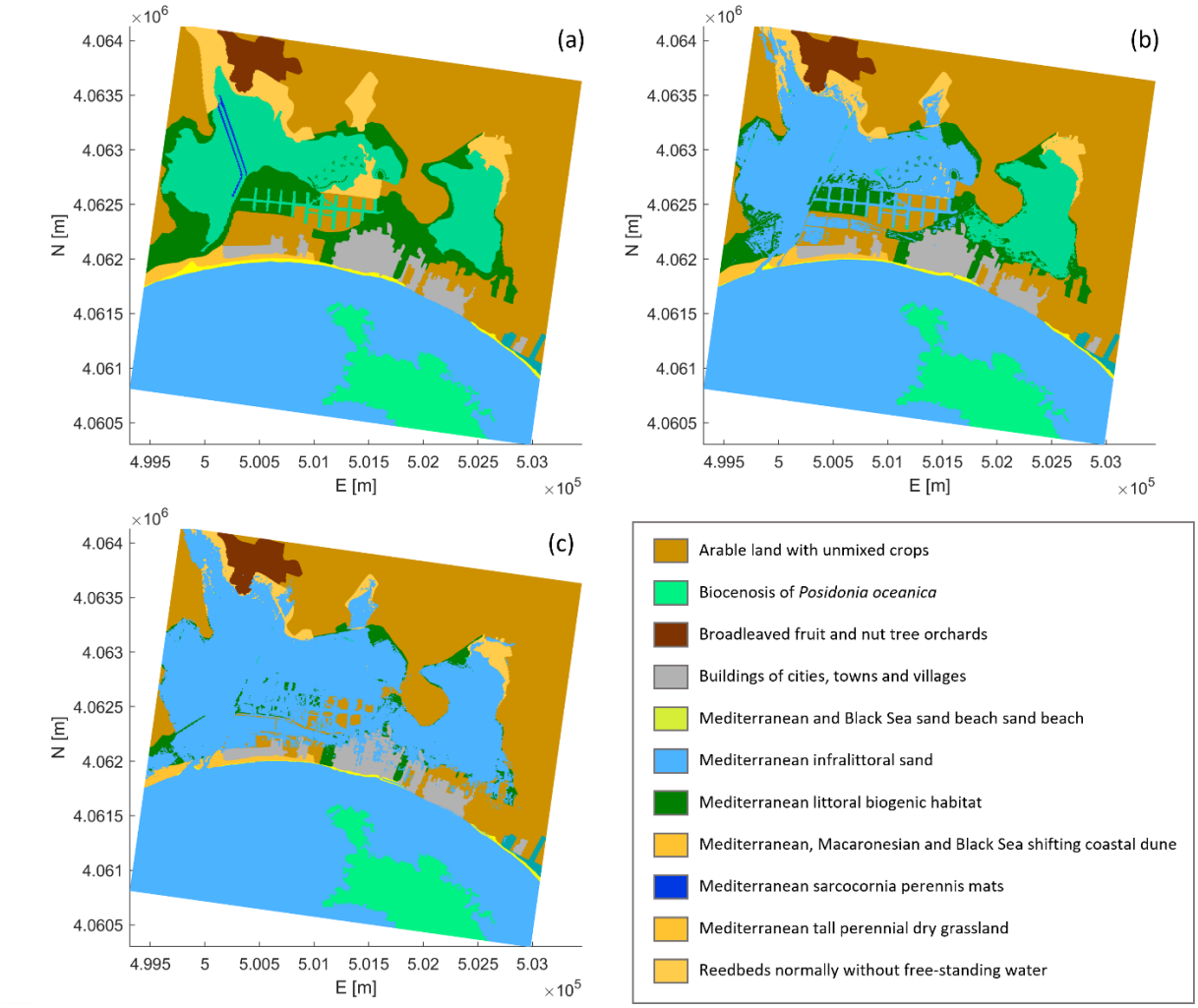

Figure 9-12 Habitat maps for SP (a), S4.5-2070 (b) and (c) S8.5-2100 for the no-NbS scenarios.

Table 9-5 Computation of the sigma score for the comparison between SP, NN scenario with the S4.5-2070, NN scenario

ESS	$ESS_{tot,1}$	$ESS_{tot,2}$	ESS_{rel}	σ_x
WP	2.3070e+07	1.7011e+07	-0.26	-5
RF	2.3231e+07	1.6237e+07	-0.30	-5
RE	2.3712e+07	1.7126e+07	-0.28	-5

Table 9-6 Computation of the sigma score for the comparison between SP, NN scenario with the S8.5-2100, NN scenario

ESS	$ESS_{tot,1}$	$ESS_{tot,2}$	ESS_{rel}	σ_x
WP	2.3070e+07	1.3211e+07	-0.43	-5
RF	2.3231e+07	1.2397e+07	-0.46	-5
RE	2.3712e+07	1.1472e+07	-0.52	-5

of the sigma score for comparing the SP, NN scenario with the SP, SR2 scenario. Finally, Table 9-9 demonstrates the substantial contribution of upscaling within the S8.5-2100 scenario, which enhances ecosystem service provisioning by as much as 28%.

Table 9-7 Computation of the sigma score for the comparison between SP, NN scenario with the SP, SR1 scenario

ESS	$ESS_{tot,1}$	$ESS_{tot,2}$	ESS_{rel}	σ_x
WP	2.3070e+07	2.3530e+07	0.02	1
RF	2.3231e+07	2.3576e+07	0.01	1
RE	2.3712e+07	2.3827e+07	0.01	1

Table 9-8 Computation of the sigma score for the comparison between SP, NN scenario with the SP, SR2 scenario

ESS	$ESS_{tot,1}$	$ESS_{tot,2}$	ESS_{rel}	σ_x
WP	2.3070e+07	2.6810e+07	0.16	4
RF	2.3231e+07	2.6019e+07	0.12	3
RE	2.3712e+07	2.4642e+07	0.04	1

Table 9-9 Computation of the sigma score for the comparison between SP, NN scenario with the SP, SR2 scenario

ESS	$ESS_{tot,1}$	$ESS_{tot,2}$	ESS_{rel}	σ_x
WP	1.6950e+07	2.6810e+07	0.28	5
RF	1.5185e+07	2.6019e+07	0.22	5
RE	1.2402e+07	2.4642e+07	0.08	2

9.4. Conclusions

This study demonstrates the effectiveness of Nature-based Solutions (NbS) in reducing coastal flooding and erosion in the "Pantani della Sicilia Sud-Orientale" region. The interventions, including dune revegetation, seagrass restoration, and beach nourishment, significantly mitigate risks under both present and future climate scenarios.

Beach nourishment showed the highest flood reduction potential, with up to 100% reduction under current conditions and substantial decreases in future scenarios. Seagrass enlargement and dune revegetation also contributed significantly, particularly in reducing erosion. However, future sea-level rise poses challenges, potentially altering lagoon habitats and increasing the risk of saltwater intrusion. Continued monitoring and adaptive strategies are essential to ensure the long-term success of these interventions in the face of climate change.

In addition to flood risk mitigation, NbS substantially contribute to ecosystem service provisioning. Restoration measures not only protect the built environment but also enhance water purification and erosion risk reduction, supporting the long-term sustainability of the lagoon and coastal habitats.

9.5. References

Baptist, M., Marijnissen, R., Różyński, G., Musumeci, R. E., Marino, M., Borzi, L., ... & Cognat, M. (2024). D4. 1 Scorecard methodology (tool) for coastal system restoration effects on ESS and BDV. *ARPHA Preprints*, *5*, e128550.

Barbier E.B., Georgiou I.Y., Enchelmeyer B. and Reed D.J. (2013). The Value of Wetlands in Protecting Southeast Louisiana from Hurricane Storm Surges. *PLoS ONE*, 8(3): 1–6. doi: 10.1371/journal.pone.0058715

Barbier E.B., Hacker S.D., Kennedy C., Koch E.W., Stier A.C. and Silliman B.R. (2011). The value of estuarine and coastal ecosystem services. *Ecological Monographs*, 81(2): 169–193. doi: 10.1890/10-1510.1

Bryant D.B., Bryant M.A., Sharp J.A. and Bell G.L. (2019). US

Bruun, P. (1954). *Coast erosion and the development of beach profiles* (Vol. 44). US Beach Erosion Board.

Boccotti ,P.,2004. Idraulica marittima.UTET Università

Chen W., Staneva J., Jacob B., Sánchez-Artús X. and Wurpts A. (2024). What-if nature-based storm buffers on mitigating coastal erosion. *Science of the Total Environment*, 928(May 2023): doi: 10.1016/j.scitotenv.2024.172247

Caires,S.,Yan,K.,2020.Ocean surface wave time series for the european coast from 1976 to2100 derived from climate projections . Copernicus 595 Climate Change Service (C3S) Climate Data Store (CDS).

Chytrý M., Tichý L., Hennekens S.M., … Schaminée J.H.J. (2020). EUNIS Habitat Classification: Expert system, characteristic species combinations and distribution maps of European habitats. *Applied Vegetation Science*, 23(4): 648–675. doi: 10.1111/avsc.12519

Feagin R.A., Furman M., Salgado K., Martinez M.L., Innocenti R.A., Eubanks K., Figlus J., Huff T.P., Sigren J. and Silva R. (2019). The role of beach and sand dune vegetation in mediating wave run up erosion. *Estuarine, Coastal and Shelf Science*, 219(September 2018): 97–106. Elsevier. doi: 10.1016/j.ecss.2019.01.018

Fernández-Montblanc T., Duo E. and Ciavola P. (2020). Dune reconstruction and revegetation as a potential measure to decrease coastal erosion and flooding under extreme storm conditions. *Ocean and Coastal Management*, 188(February): doi: 10.1016/j.ocecoaman.2019.105075

Forrester J., Leonardi N., Cooper J.R. and Kumar P. (2024). Seagrass as a nature-based solution for coastal protection. *Ecological Engineering*, 206(May): 107316. Elsevier B.V. doi: 10.1016/j.ecoleng.2024.107316

Garzon J.L., Maza M., Ferreira C.M., Lara J.L. and Losada I.J. (2019). Wave Attenuation by Spartina Saltmarshes in the Chesapeake Bay Under Storm Surge Conditions. *Journal of Geophysical Research: Oceans*, 124(7): 5220–5243. doi: 10.1029/2018JC014865

Geijzendorffer, Ilse. Chazée L. and Gaget, Elie. Galewski, Thomas. Guelmami, Anis. Perennou C. (2018). Mediterranean Wetlands Outlook 2: solutions for sustainable Mediterranean wetlands. *Journal of Materials Processing Technology*, 1(1): 1–8.

Grases A., Gracia V., García-León M., Lin-Ye J. and Sierra J.P. (2020). Coastal flooding and erosion under a changing climate: Implications at a low-lying coast (ebro delta). *Water (Switzerland)*, 12(2):. doi: 10.3390/w12020346

Guannel G., Arkema K., Ruggiero P. and Verutes G. (2016). The power of three: Coral reefs, seagrasses and mangroves protect coastal regions and increase their resilience. *PLoS ONE*, 11(7): 1–22. doi: 10.1371/journal.pone.0158094

Jacob B., Dolch T., Wurpts A. and Staneva J. (2023). Evaluation of seagrass as a nature-based solution for coastal protection in the German Wadden Sea. *Ocean Dynamics*, 73(11): 699–727. doi: 10.1007/s10236-023-01577-5

James R.K., Lynch A., Herman P.M.J., van Katwijk M.M., van Tussenbroek B.I., Dijkstra H.A., van Westen R.M., van der Boog C.G., Klees R., Pietrzak J.D., Slobbe C. and Bouma T.J. (2021). Tropical Biogeomorphic Seagrass Landscapes for Coastal Protection: Persistence and Wave Attenuation During Major Storms Events. *Ecosystems*, 24(2): 301–318. Springer US. doi: 10.1007/s10021-020-00519-2

Knutson P.L., Brochu R.A., Seelig W.N. and Inskeep M. (1982). Wave damping in Spartinaalterniflora marshes. *Wetlands*, 2(1): 87–104. doi: 10.1007/BF03160548

Korres,G.,Ravdas,M., Zacharioudaki,A., Denaxa,D., Sotiropoulou,M.,2021.Mediterranean sea waves analysis and forecast (cmems med-waves, 637 med wam3 system)(version1)set.Copernicus Monitoring Environment Marine Service(cmems).

Kulp S.A. and Strauss B.H. (2019). New elevation data triple estimates of global vulnerability to sea-level rise and coastal flooding. *Nature Communications*, 10(1):. Springer US. doi: 10.1038/s41467-019-12808-z

Leonardi N., Carnacina I., Donatelli C., Ganju N.K., Plater A.J., Schuerch M. and Temmerman S. (2018). Dynamic interactions between coastal storms and salt marshes: A review. *Geomorphology*, 301: 92–107. Elsevier B.V. doi: 10.1016/j.geomorph.2017.11.001

Van Loon-Steensma J.M., Hu Z. and Slim P.A. (2016). Modelled Impact of Vegetation Heterogeneity and Salt-Marsh Zonation on Wave Damping. *Journal of Coastal Research*, 32(2): 241–252. doi: 10.2112/JCOASTRES-D-15-00095.1

Maza M., Temmerman S., van Wesenbeeck B.K., Ghisalberti M., Tinoco R.O. and Hu Z. (2022). Editorial: Coastal protection provided by ecosystems: Observations and modeling across scales. *Frontiers in Marine Science*, 9(August): 1–3. doi: 10.3389/fmars.2022.998923

Michael Oppenheimer (USA) B.G. (New Z. (2019). 4Sm Spm. *Supplementary Material*, Chapter 4: 1–26. Retrieved from https://www.ipcc.ch/site/assets/uploads/sites/3/2019/11/SROCC_Ch04-SM_FINAL.pdf

Möller I., Kudella M., Rupprecht F., Spencer T., Paul M., Van Wesenbeeck B.K., Wolters G., Jensen K., Bouma T.J., Miranda-Lange M. and Schimmels S. (2014). Wave attenuation over coastal salt marshes under storm surge conditions. *Nature Geoscience*, 7(10): 727–731. doi: 10.1038/NGEO2251

Morris R.L., Konlechner T.M., Ghisalberti M. and Swearer S.E. (2018). From grey to green: Efficacy of eco-engineering solutions for nature-based coastal defence. *Global Change Biology*, 24(5): 1827–1842. doi: 10.1111/gcb.14063

Mossman H.L., Pontee N., Born K., Hill C., Lawrence P.J., Rae S., Scott J., Serato B., Sparkes R.B., Sullivan M.J.P. and Dunk R.M. (2022). Rapid carbon accumulation at a saltmarsh restored by managed realignment exceeded carbon emitted in direct site construction. *PLoS ONE*, 17(11 November): 1–24. doi: 10.1371/journal.pone.0259033

Neumann B., Vafeidis A.T., Zimmermann J. and Nicholls R.J. (2015). Future coastal population growth and exposure to sea-level rise and coastal flooding - A global assessment. *PLoS ONE*, 10(3):. doi: 10.1371/journal.pone.0118571

Nicholls R.J., Hinkel J., Lincke D. and van der Pol T. (2019). Global Investment Costs for Coastal Defense through the 21 st Century. *Global Investment Costs for Coastal Defense through the 21 st Century*, (February): doi: 10.1596/1813-9450-8745

Ondiviela B., Losada I.J., Lara J.L., Maza M., Galván C., Bouma T.J. and van Belzen J. (2014). The role of seagrasses in coastal protection in a changing climate. *Coastal Engineering*, 87: 158–168. Elsevier B.V. doi: 10.1016/j.coastaleng.2013.11.005

Pillai U.P.A., Pinardi N., Alessandri J., Federico I., Causio S., Unguendoli S., Valentini A. and Staneva J. (2022). A Digital Twin modelling framework for the assessment of seagrass Nature Based Solutions against storm surges. *Science of the Total Environment*, 847(September): 157603. Elsevier B.V. doi: 10.1016/j.scitotenv.2022.157603

Potts, T., Burdon, D., Jackson, E., Atkins, J., Saunders, J., Hastings, E., & Langmead, O. (2014). Do marine protected areas deliver flows of ecosystem services to support human welfare?. *Marine Policy*, *44*, 139-148.

Reguero B.G., Beck M.W., Bresch D.N., Calil J. and Meliane I. (2018). Comparing the cost effectiveness of nature-based and coastal adaptation: A case study from the Gulf Coast of the United States. *PLoS ONE*, 13(4): 1–24. doi: 10.1371/journal.pone.0192132

Reimann L., Vafeidis A.T. and Honsel L.E. (2023). Population development as a driver of coastal risk: Current trends and future pathways. *Cambridge Prisms: Coastal Futures*, 1:. doi: 10.1017/cft.2023.3

Salinas D., Flunkert V., Gasthaus J. and Januschowski T. (2020). DeepAR: Probabilistic forecasting with autoregressive recurrent networks. *International Journal of Forecasting*, 36(3): 1181–1191. Elsevier B.V. doi: 10.1016/j.ijforecast.2019.07.001

Sánchez-Arcilla A., Cáceres I., Roux X. Le, Hinkel J., Schuerch M., Nicholls R.J., Otero del M., Staneva J., de Vries M., Pernice U., Briere C., Caiola N., Gracia V., Ibáñez C. and Torresan S. (2022). Barriers and enablers for upscaling coastal restoration. *Nature-Based Solutions*, 2(September): 100032. doi: 10.1016/j.nbsj.2022.100032

Seddon N., Chausson A., Berry P., Girardin C.A.J., Smith A. and Turner B. (2020). Understanding the value and limits of nature-based solutions to climate change and other global challenges. *Philosophical Transactions of the Royal Society B: Biological Sciences*, 375(1794):. doi: 10.1098/rstb.2019.0120

van Slobbe E., de Vriend H.J., Aarninkhof S., Lulofs K., de Vries M. and Dircke P. (2013). Building with Nature: In search of resilient storm surge protection strategies. *Natural Hazards*, 65(1): 947–966. doi: 10.1007/s11069-012-0342-y

Small C. and Nicholls R.J. (2003). A global analysis of human settlement in coastal zones. *Journal of Coastal Research*, 19(3): 584–599. doi: 10.2307/4299200

Sousa A.I., Lillebø A.I., Pardal M.A. and Caçador I. (2010). Productivity and nutrient cycling in salt marshes: Contribution to ecosystem health. *Estuarine, Coastal and Shelf Science*, 87(4): 640–646. doi: 10.1016/j.ecss.2010.03.007

Sutton-Grier A.E., Wowk K. and Bamford H. (2015). Future of our coasts: The potential for natural and hybrid infrastructure to enhance the resilience of our coastal communities, economies and ecosystems. *Environmental Science and Policy*, 51(July): 137–148. Elsevier Ltd. doi: 10.1016/j.envsci.2015.04.006

Unguendoli S., Biolchi L.G., Aguzzi M., Pillai U.P.A., Alessandri J. and Valentini A. (2023). A modeling application of integrated nature based solutions (NbS) for coastal erosion and flooding mitigation in the Emilia-Romagna coastline (Northeast Italy). *Science of the Total Environment*, 867(December 2022): 161357. The Authors. doi: 10.1016/j.scitotenv.2022.161357

de Vriend H.J., van Koningsveld M., Aarninkhof S.G.J., de Vries M.B. and Baptist M.J. (2015). Sustainable hydraulic engineering through building with nature. *Journal of Hydro-Environment Research*, 9(2): 159–171. Elsevier B.V. doi: 10.1016/j.jher.2014.06.004

Vuik V., Jonkman S.N., Borsje B.W. and Suzuki T. (2016). Nature-based flood protection: The efficiency of vegetated foreshores for reducing wave loads on coastal dikes. *Coastal Engineering*, 116: 42–56. Elsevier B.V. doi: 10.1016/j.coastaleng.2016.06.001

Waltham N.J., Elliott M., Lee S.Y., Lovelock C., Duarte C.M., Buelow C., Simenstad C., Nagelkerken I., Claassens L., Wen C.K.C., Barletta M., Connolly R.M., Gillies C., Mitsch W.J., Ogburn M.B., Purandare J., Possingham H. and Sheaves M. (2020). UN Decade on Ecosystem Restoration 2021–2030—What Chance for Success in Restoring Coastal Ecosystems? *Frontiers in Marine Science*, 7(February 2020): doi: 10.3389/fmars.2020.00071

Werners S.E., Wise R.M., Butler J.R.A., Totin E. and Vincent K. (2021). Adaptation pathways: A review of approaches and a learning framework. *Environmental Science and Policy*, 116(January): 266–275. Elsevier Ltd. doi: 10.1016/j.envsci.2020.11.003

van Zelst V.T.M., Dijkstra J.T., van Wesenbeeck B.K., Eilander D., Morris E.P., Winsemius H.C., Ward P.J. and de Vries M.B. (2021). Cutting the costs of coastal protection by integrating vegetation in flood defences. *Nature Communications*, 12(1): 1–11. Springer US. doi: 10.1038/s41467-021-26887-4

10. Seagrass restoration as a nature-based solution for climate change adaptation in the Foros Bay

Valchev, N.[1], Eftimova, P.[1], Hineva, E.[1], Andreeva, N.[1]
[1]*Institute of Oceanology – Bulgarian Academy of Sciences*

ABSTRACT: The Foros Bay is a part of complex coastal system located in the innermost part of the large Burgas Bay. The area is centrepiece for both unique natural diversity and human uses, which makes it vulnerable to multiple risks such as significant eutrophication and contaminant inflow resulting in water quality deterioration, increased turbidity, and poor light conditions. The accelerated climate change aggravates these risks especially those related to flooding and erosion and will contribute to the ecotopes shift. Therefore, this study aims to assess the ESS provided by seagrass in reduction of coastal hazards such as flooding and erosion in both present conditions and climate change perspective. It also attempts to predict ecotopes shift resulting from sea level rise through D-Eco Impact tool application. Results suggest that the most valuable ESS is reduction of coastal erosion while the effect of seagrass on reduction of flooding is negligible. Sea level rise scenarios indicate a potential expansion of infralittoral sand habitat towards the coast and subsequent loss of tall-helophyte bed due to the anticipated shift.

10.1. Introduction

The Foros Bay is a part of the Burgas Bay located on the western Black Sea coast. Together with adjacent low-laying area, it represents an important biodiversity hotspot. The area is one of the less exposed to wave action along the Bulgarian coast and is a centrepiece for both unique natural diversity (landscape, habitat, and species) and human uses expressed in overlapping economic, social and cultural interests. The area is protected under the NATURA 2000 network (both Birds and Habitat) – BG0000271 Mandra-Poda. Poda was declared a Wetland of international importance according to the Ramsar Convention. The Foros Bay is a part of an important place from ornithological point of view ("Mandra-Poda Complex") and lays on the Via Pontica

Figure 10-1 Map of the study area

bird migratory route. The Foros Bay accommodates soft-bottom vegetation with a total area of 39 ha as the dominant species is the seagrass *Zostera noltei, Hornemann*, which are in focus of the restoration intervention (Figure 10-1).

10.1.1. Description of problems requiring restoration

Several dramatic changes have occurred on the study area and its watershed area since 1920, which nowadays require restoration. Previously, the coastal area bordering the bay was a wetland almost completely covered with hygrophytes. Subsequently, due to city expansion, a part of the swamp was dried out and altered to settling (stabilization) basins. Mandra reservoir is a main source of industrial waters for the Neftochim Petrolium Refinery. The area is under strong anthropogenic pressure due the proximity to Burgas and the large industrial utilities and complexes. Moreover, the international road E87 crosses the eastern part of the pilot thus contributing to pollution with emissions and wastes.

The presence of heavy industries combined with the significant catchment area of both Foros Bay and Poda wetland contributes to significant eutrophication and contaminant inflow resulting in water quality deterioration, increased turbidity, and poor light conditions. These stressors limit the natural spread of seagrass. Furthermore, the increase of coastal flood and erosion hazards add to the multiple risks, which should be considered from the biodiversity protection perspective.

The accelerated climate change aggravates above-mentioned risks especially those related to flooding and erosion as well as the ecotopes shift. Although various dynamic properties have been considered, such as winds, surges, flow and waves, the main climate change impact considered is the sea level rise. The future conditions were addressed by making use of existing climate scenarios, more specifically middle and high-end ones RCP4.5 (SSP2-4.5) and RCP8.5 (SSP5-8.5). Considered projections were 2070 and 2100. According to IPCC AR6 (2023) sea level rise for Burgas would vary between 0.31 and 0.66 cm. Supposed effects can be an increased flooding and erosion of both infralittoral and littoral, resulting in larger inundated area causing changes in ecotopes.

10.1.2. Description of restoration efforts

Within the REST-COAST, efforts have been undertaken to apply a method for seagrass restoration in situ, which is supposed to promote adaptation to climate change impacts through increased water quality, blue carbon sequestration, reduction of flooding and erosion risk and thus enriching the biodiversity. A field experiment was carried out to test the possibility to support seagrass recolonization in highly eutrophic environment by removing one of the potential stressors at the site that probably contributes to seagrass decline and acts as a barrier for natural recolonization, namely macrolagae coverage (mat algae). The experimental set-up consists of three test plots. Within the plots, sods of seagrass of *Z. noltei* species have been transplanted to test the ability of the species to recolonize area.

An upscaling of the above measure would represent a likely recolonization of the area down to 6 m depth, which is the maximum community spread (in Bulgarian Black Sea waters) providing that measures to improve the light conditions would be taken. Therefore, the modelling studies about the effect of restoration were conducted considering the upscaling (Figure 10-2).

The scientific problem to be solved consists in estimation of the effect of seagrass restoration as a climate adaptation measure. Therefore, ecosystem services contributing to the reduction of flooding and erosion risks were assessed through numerical modelling and use of D-Eco Impact tool.

Figure 10-2 Location of the seagrass meadow present in Foros Bay (light green polygon A) and the possible areas of seagrass recolonisation (dark green polygons B and C)

10.2. Methods

10.2.1. Short description of the models

The methodology in use intents to reveal the impact of extreme events on the pilot for present and future climate, and to assess the effect of the restoration. The event approach was employed by taking into account three design events with return periods of 20, 50 and 100 years for present and climate change conditions.

The modelling system depicted in Figure 10-3 consists of two coupled Delft3D-FM domains – Burgas Bay and Foros Bay – as well as the XBeach model implemented on a domain comprising a low-laying coastal stretch in the Foros bay. A more detailed description of modelling efforts is available in REST-COAST Deliverable 2.2.

The Burgas Bay Delft3D-FM domain was implemented by online coupling of 2D flow and wave processes (Deltares, 2021). The flow module uses unstructured grid with spatial resolution varying from 500 m at the offshore boundary to 20 m for depths shallower than 20 m. The wave module uses regular grid with horizontal resolution of 100 m. The Foros Bay Delft3D-FM domain is of higher spatial resolution and covers Poda protected area and Uzungeren Lake as well as surrounding wetland and the located nearby Port of Burgas. The flow module is set on unstructured grid with cell sizes varying from 50 m at the offshore boundary to 20 m in the nearshore part of the grid. The wave grid is regular with spatial resolution of 20 m. The model resolution is considered high enough to allow for a very good representation of flow and wave dynamics within the coastal area of complex bathymetry. The presence of seagrasses into the model domain was

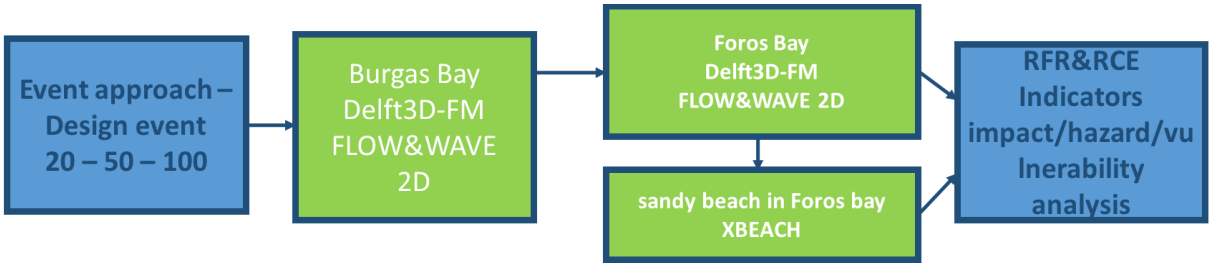

Figure 10-3 Schematization of the modelling and ESS assessment framework

implemented into the model as area trachytopes, using the formula proposed in Baptist (2005). The following input parameters were used: vegetation height (hv) – 0.3 m, density (n) – 6.5, drag coefficient (C_D) – 1.8, and alluvial bed roughness (C_b) – 62.

The 2DH morphodynamic model XBeach (Roelvink et al., 2009) is implemented at the south-western part of the Foros Bay. The domain is limited landward by the international road E87 and covers a costal stretch presented by Poda wetland. It also includes a narrow beach and bottom slope up to 7 m depth. The grid is regular non-equidistant with varying cross-shore cell sizes – from 14 m to 2 m – and regular 5m-resolution along-shore. The model is fed by hourly wave parameters and water levels at the offshore boundary coming from the Foros Bay Delft3D-FM model output. The present and restored seagrass meadows are incorporated into the model using the XBeach vegetation module (Van Rooijen et al., 2015).

D-Eco Impact (Weeber et al., 2024) was used to predict the shift of infralittoral and littoral ecotopes as a consequence of climate change driven sea level rise. This effort represents a first iteration since it is based on change in depths due to sea level rise solely. Twelve EUNIS habitats were identified within the Foros Bay, which are equally distributed between the littoral and infralittoral. Two depth threshold are posed in order to run the D-Eco Impact tool: the first one 0.5 m refers to the EUNIS habitat MA54 Black sea littoral biogenic habitat, Q51 Tall-helophyte bed, dominated by *Phragmites australis*; the second one 6 m – to MB54 Black Sea infralittoral sand dominated by *Z. noltei*. The former relates to the species tolerance to change in depth relative to salinity fluctuations (by expert judgement), while the latter is in accordance with the depth limitation imposed on the spread of seagrass meadows due to the light conditions.

10.2.2. Quantification of ecosystem services

The contribution of two ecosystem services (ESS) – Reduction of Flood Risk (RFR) and Reduction of Coastal Erosion (RCE) – was assessed for both present and future conditions. The indicators are based on result of the hydrodynamic and morphodynamic modelling. The RFR assessment is using model results of Foros Bay Delft3D-FM FLOW&WAVE model, while the RCE assessment is based on the XBeach model results.

The indicator used for assessment of RFR is flooded area (sq.km) calculated for the Foros Bay and the surrounding wetland solely, with a threshold of 1cm of water layer thickness. D-Eco Impact tool was used to extract the of water depth maxima at each grid cell during storm event in order to define the flood extent and to calculate the flooded area. The tool was used to obtain the average of H_{rms} for additional analysis. Two indicators are employed to assess the RCE – eroded volumes and eroded areas – calculated for the entire model domain. The erosion area are outlined using a threshold of 1 cm sediment layer thickness.

With respect to effect on habitats, the indicator is change of area of above-mentioned ecotopes based on depth difference resulting from the sea level rise.

Another ESS under consideration is the carbon sequestration (sediment C-content, bulk density, accretion rate). In order to assess it, carbon content in sediments will be determined following the wet combustion method (sample digestion with $K_2Cr_2O_7$ in H_2SO_4) and colorimetric determination. The upper 0.3 m sediment layer will be analyzed for C-content. Accretion rate is going to be monitored following the pole method described in Erftemeijer and Koch (2001). The assessment of this ESS is ongoing.

10.3. Results and discussion

10.3.1. Reduction of Flood Risk

Flood areas concerning present conditions and two horizons of RCP4.5 and RCP8.5 for all design events are presented in Figure 10-4. The result implies that the seagrass presence has insignificant effect on reduction of flooding risk. Hence, this ESS is not relevant for the case of Foros pilot since the rising level is the main source of flooding, which seagrasses could not influence. The differences due to the direct wave impact and surges are similar and vary within a small range of 3-8% of the flood area as the difference decreases with sea level growth for future scenarios. Moreover, this behaviour is reproduced for all climate change conditions into consideration.

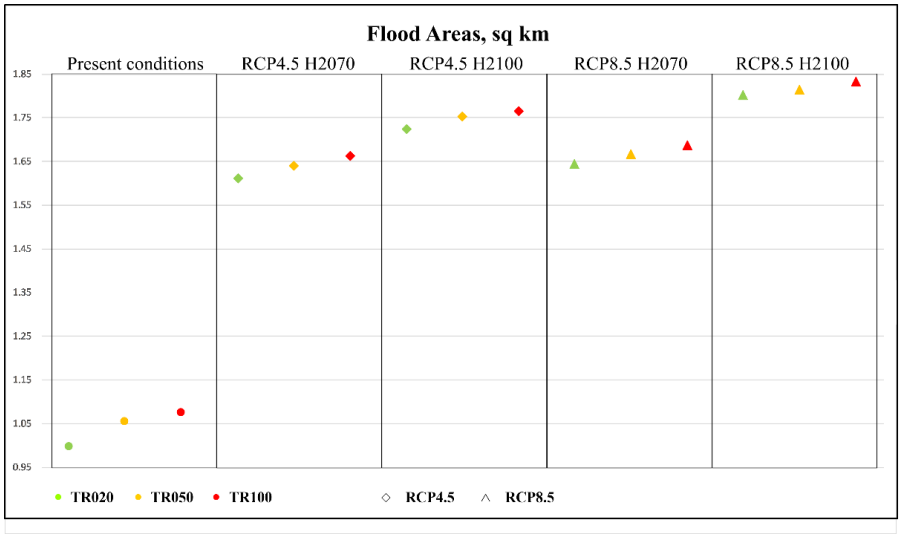

Figure 10-4 Flood areas concerning present conditions and two considered horizons of RCP4.5 and RCP8.5 calculated for all design events

Table 10-1 Flood areas [sq. km] for all design events concerning present conditions and two considered horizons of RCP4.5 and RCP8.5. Right panel presents the percentage of flood increase due to climate change with respect to present conditions

Return period	Percentage of flood increase with respect to TR020 present conditions				
	Present climate conditions	RCP4.5 H2070	RCP4.5 H2100	RCP8.5 H2070	RCP8.5 H2100
TR020	Reference	62	73	65	81
TR050	6	65	76	67	82
TR100	8	67	77	69	84

Table 10-1 shows the percentage of flood increase with respect to TR020 present conditions. The increase for higher return period events due to the surge and wave action is in the range 6-8%. Considering selected climate scenarios and projections, the flood area increase varies between 62% (RCP4.5 H2070) and 84% (RCP8.5 H2100) due to the sea level rise.

The model results show a decrease of wave height over the area occupied by seagrass meadow, which is more pronounced for lower energy conditions (Figure 10-5, left). However, this effect decays with the increase of energy input into the system.

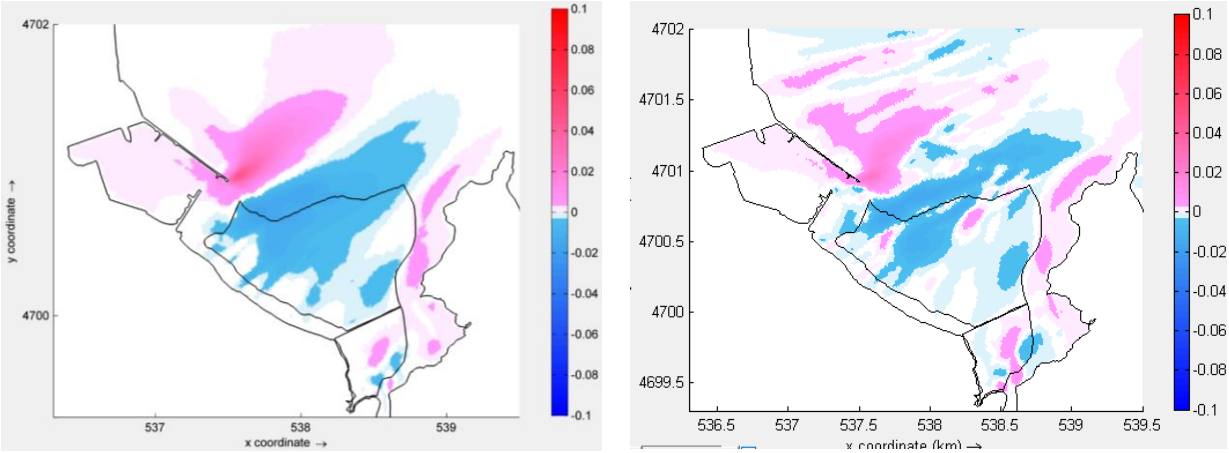

Figure 10-5 RMS wave height difference between presence and absence of vegetation for present conditions with TR020 (left) and TR100 (right)

10.3.2. Reduction of Coastal Erosion

Considering the results of all simulations, it can be stated that the presence of seagrasses has a significant effect on the erosion-accumulation pattern. The most considerable erosion is observed along the coastline while within the surf zone and wetland the intensity of erosion process is less pronounced. It is noted that breaching and subsequent formation of accumulation fans occur at coastline and wetland, while in the surf zone, the morphodynamic pattern is marked by alternation of erosion-accumulation strips of a small layer thickness up to 5 cm expanding to 3 m depth. Erosion processes become more intense with the sea level rise as the area of interaction shifts towards the wetland.

The protection effect of seagrasses on the bottom is substantial for both present and future conditions, whereas concerning the coastline and wetland this effect is notable only for lower sea level. Concerning design event TR020, breaching takes place in case of sea levels 0.49m (RCP4.5 H2100) and 0.66m (RCP8.5 H2100). In former case, the seagrass manages to prevent occurrence of coastline breaching located in the middle of modelled area in case of (Figure 10-6), which is not observed in the latter. Concerning design event TR050, the situation is similar but in both cases the seagrasses cannot cope with erosion reduction. Concerning design event TR100, the breaching of the coastline occurs already in H2070 (sea level 0.31 m) for both climate change scenarios. In presence of seagrasses, the erosion subsides for above-mentioned cases but the effect fails for H2100. The effect of the restored seagrass meadow is noticeable only on the bottom slope reducing considerably the erosion area.

Erosion volumes and areac for cases of no vegetation and upscale recolonization concerning present conditions and two considered horizons of RCP4.5 and RCP8.5 calculated for all design events are presented in Figure 10-7 and Figure 10-8, respectively. In case of no vegetation, the erosion volumes are in the range 2000 – 6000 m3. In presence of seagrasses, the erosion volumes decrease substantially by 1.7 to 7.9 times, as they are below 1000 m3 for all cases except for RCP4.5 H100 (TR050 and TR100) and RCP8.5 H100. The contribution of the restored seagrass meadow over the present vegetation is estimated to be 5% on the average as the maximum one 11.4% is calculated for case of TR020 RCP4.5 H2100 (Figure 10-7).

The behaviour of erosion area indicator shows slightly different trend. It displays the increasing contribution of seagrasses, as the ecosystem service is most valued considering the impact of restored vegetation (Figure

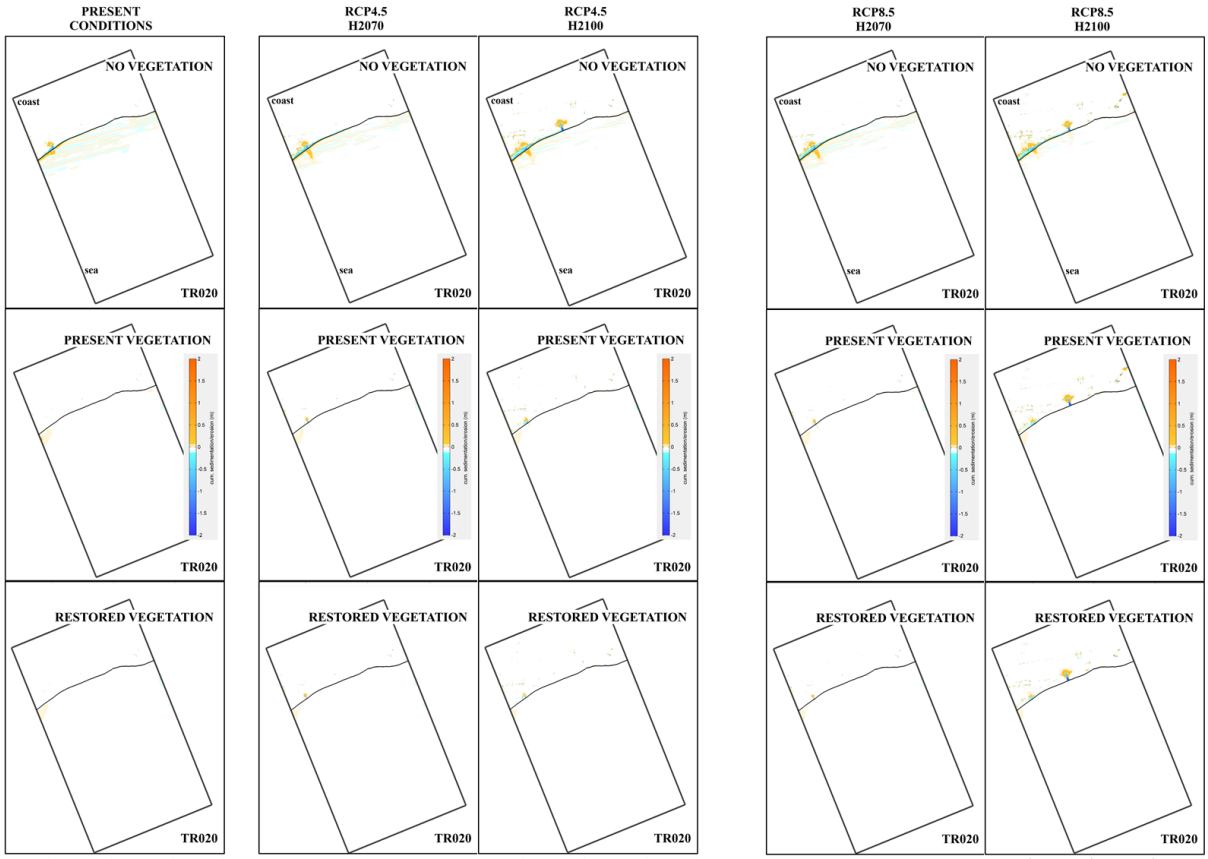

Figure 10-6 Sedimentation-erosion pattern calculated for TR020 storm event for present climate conditions and future climate change under RCP4.5 and RCP8.5, horizons 2070 and 2100

10-8). It should be noted that the indicator takes into account also for small morphological changes since the threshold is set to 1cm sediment layer thickness.

In absence of vegetation, the areas affected by erosion vary between 0.16 and 0.40 sq. km. The existing vegetation contributes to the erosion mitigation by decreasing of the affected area by 1.7 – 7.4 times, whilst the contribution of restored meadows appears to be even more impacting – effected areas decrease by 4.8 – 21.6 times. The contribution of restored seagrass compared to the present vegetation is estimated to be 72% on the average as the maximum one 90% is calculated for case of TR050 RCP4.5 H2070.

The overall results suggest that the tipping point for contribution of ecosystem services towards reduction of erosion lies between climate change scenarios RCP8.5 H2070 and RCP4.5 H2100 with the major role of sea level rise within the range 0.35-0.49 m.

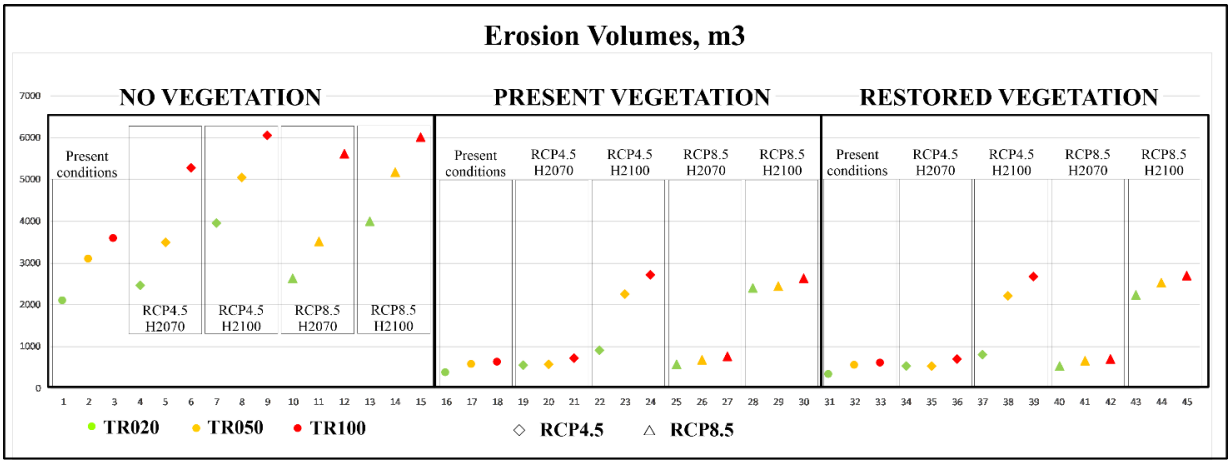

Figure 10-7 Erosion volumes for cases of no vegetation, present and upscale restoration for present conditions and climate change scenarios

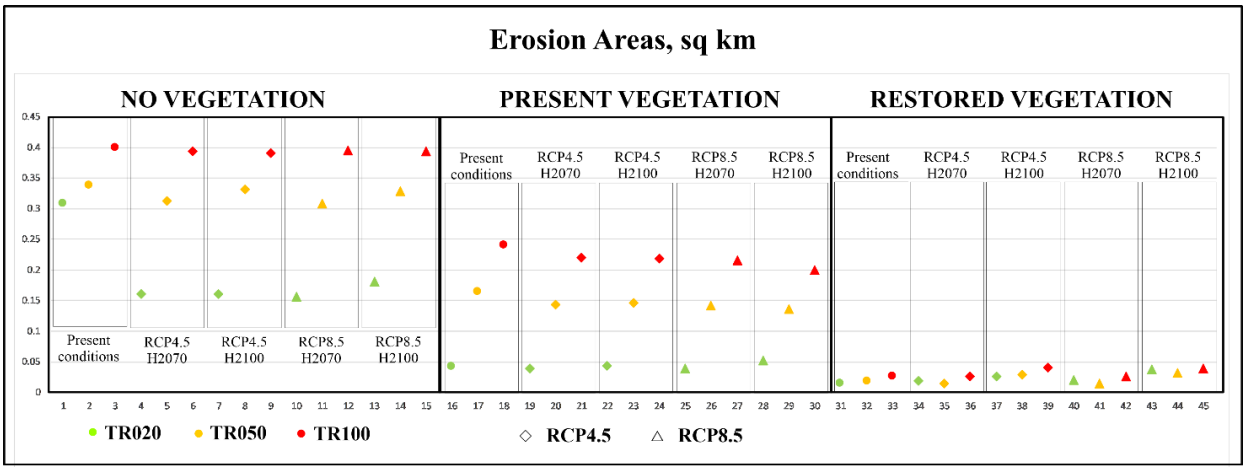

Figure 10-8 Erosion area for cases of no vegetation, present and upscale restoration for present conditions and climate change scenarios

10.3.3. Effect on ecotopes

The effect on ecotopes is estimated based on the increase of water depth due to sea level rise. The storm-driven effects such as surges was neglected since their role is episodic and do not contribute measurably to the long-term ecotopes shift. The thresholds posed are based on observations and expert judgement thus taking into account other variables such as salinity, water quality and light conditions. Overall, three ecotopes were considered of which the most important are those dominated by *Z. noltei* within the near-shore zone and *Phragmites australis* within the Poda wetland. Results of D-Eco Impact tool implementation are shown in Figure 10-9.

Sea level rise scenarios indicate a potential expansion of infralittoral sand habitat towards the coast and subsequent loss of tall-helophyte bed due to the anticipated shift. In the same time, the area suitable for seagrass does not change since the lower limit also tend to shift shoreward. The experimental restoration is not expected to change noticeably the ESS gain but the assisted upscale through natural recolonization would score higher with respect to RCE, carbon sequestration, water quality (purification) and biodiversity (food provisioning) as indicated in the Deliverable 1.4. The loss of wetland area on the other hand would increase the flooding risk. Potential increase of water quality and light regime improvement would benefit the

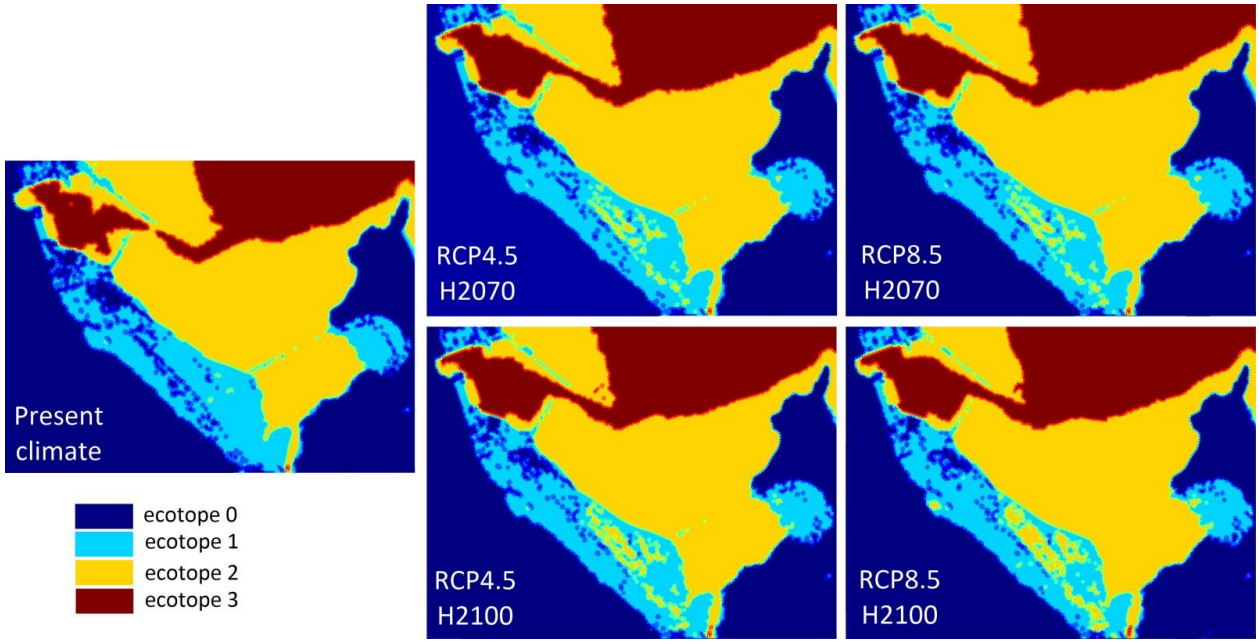

Figure 10-9 Results of D-Eco Impact tool application. Ecotope codes: 0 – surrounding area not considered in the analysis, 1 – MA54 Black sea littoral biogenic habitat, Q51 Tall-helophyte bed, dominated by Phragmites australis, 2 – MB54 Black Sea infralittoral sand dominated by Z. noltei, 3 – sea bottom below 6 m depth

expansion of seagrass meadow towards deeper areas to about 9 m depth, which represents the maximum depth of observed seagrass spread along the Bulgarian coast.

10.4. Conclusions

The presented study dealt with an assessment of ESS provided by seagrass in reduction of coastal flooding and erosion in both present conditions and climate change scenarios for sea level rise in the Foros Bay. The future conditions were addressed by making use of existing climate scenarios, more specifically middle and high-end ones RCP4.5 (SSP2-4.5) and RCP8.5 (SSP5-8.5). Considered projections were 2070 and 2100. It is based on the results of hydrodynamic and morphodynamic modelling performed using Delft3D-FM FLOW&WAVE and XBeach models. Two ecosystem services were assessed – Reduction of Flood Risk (RFR) and Reduction of Coastal Erosion (RCE).

Overall, the restoration intervention does have contributes to reduction of energy input into the system as revealed by the decrease of wave height over the seagrass meadow. The RFR indicator is flooded area (sq.km) while two indicators employed for RCE analysis were the eroded volumes and eroded areas. With respect to the RCE, it can be concluded that the presence of seagrasses affect significantly the erosion-accumulation pattern. In presence of seagrass, the erosion volumes decrease substantially by 1.7 to 7.9 times. The contribution of the restored seagrass meadow over the present vegetation is estimated to be 5% on the average as the maximum one 11.4% is calculated for case of RCP4.5 H2100 TR020. Results suggest that the effect of seagrass on reduction of flooding is insignificant partly due to the modelling approach, which does not account for the sediment dynamics. Nevertheless, we expect that the consideration of morphological changes would increase the role of vegetation in particular by preventing of breaching events.

Furthermore, the ecotopes shift resulting from sea level rise was predicted through application of D-Eco Impact tool by posing depth threshold on the distribution of two important ecotopes. Sea level rise scenarios indicate a potential expansion of infralittoral sand habitat towards the coast and subsequent loss of tall-helophyte bed due to the anticipated shift. The experimental restoration is not expected to change

noticeably the ESS gain but the assisted upscale through natural recolonization would score higher with respect to RCE, carbon sequestration, water quality (purification) and biodiversity (food provisioning).

10.5. References

Baptist, M. J. (2005). Modelling floodplain biogeomorphology. Ph.D. thesis, Delft University of Technology

Delft3D FM Suite (2021). User Manual, 572 p. Deltares (deltares.nl)

Erftemeijer, P.L.A., Koch, E.W. (2001). Sediment geology methods for seagrass habitat. In: Short, F.T., Coles, R.G. (Eds.), Global seagrass research methods. Elsevier Science B.V., Amsterdam, NL, pp. 345-367

IPCC sixth assessment report (AR6) (2023). CLIMATE CHANGE 2023, Sea level rise, 25 p.

REST-COAST Deliverable 2.2: Good practice criteria for multi-variable risk reduction from restoration/ESS at the Pilots, as a function of projection horizon and domain scale, as enablers to introduce risk products in coastal governance

Roelvink J. A., A. J. H. M Reniers, A. R. van Dongeren, J. S. M. van Thiel de Vries, R. T. Mc-Call, and J. Lescinski (2009). Modelling storm impacts on beaches, dunes and barrier islands. Coastal Engineering, 56(11-12):1133–1152, doi:10.1016/j.coastaleng.2009.08.006

Van Rooijen A.A., J. S. M. Van Thiel de Vries, R. T. McCall, A. R. van Dongeren, J. A. Roelvink, and A. J. H. M. Reniers (2015). Modeling of wave attenuation by vegetation with XBeach. E-proceedings of the 36th IAHR World Congress 28 June – 3 July, 2015, The Hague, The Netherlands

Weeber, M., Elzinga, H., Schoonveld, W., van de Vries, C., Klapwijk, M., Mischa, I., Rodriguez Aguilera, D., Farrag, M., Ye, Q., van Oorschot, M., Sager, P., & Icke, J. (2024). *D-Eco Impact (v0.3.0)*. Stichting Deltares. https://doi.org/10.5281/zenodo.10941913

11. Vistula Lagoon

Różyński, G.[1]

[1] *Institute of Hydro-Engineering, Polish Academy of Sciences, Gdańsk, Poland*

ABSTRACT: The Vistula Lagoon, the second largest lagoon in the Baltic Sea, has conducted a pilot in conjunction with the construction of artificial passage to the Polish part of the Lagoon with the construction of an artificial island to store sediment dredged during construction of the new navigational route as a refuge for birds. The Vistula Lagoon pilot provided two major lessons: 1) thick layers of muddy sediments are a serious impediment for implementation of NbS due to their very low strength parameters and 2) due to the main ecosystem service delivered by the island. i.e. provision of safe habitats for birds hatching on meadows, it is fully independent of sea level rise effects. The Vistula Lagoon pilot site has an obvious up- and out-scaling potential in all situations, where formation of grasslands as a safe haven for birds is desired. Potential costs can be reduced in milder environments, where ice action is very rare or does not exist.

11.1. Introduction

11.1.1. The Vistula Lagoon pilot site

The Vistula Lagoon, Figure 11-1, is the second largest lagoon in the Baltic Sea. It covers an area of 838 km2 and has a drainage basin of 23,870 km2. It is shared between Poland - 365 km2, and Russian Kaliningrad Region - 473 km2, Ed. Lillebø et al. (2015). The main inlet - the Baltiysk Strait, is located in the Russian part of the lagoon; in 2022 a new inlet was completed in the Polish part to ensure independent access to it. Vistula Lagoon has an elongated shape along the SW-NE axis with total length of 91 km. The average width is about 9 km; the widest distance measures 13 km. The lagoon's coastline is about 270 km long and the volume of water is only about 2.3 km3, due to general shallowness of Vistula Lagoon basin. The average depth in the

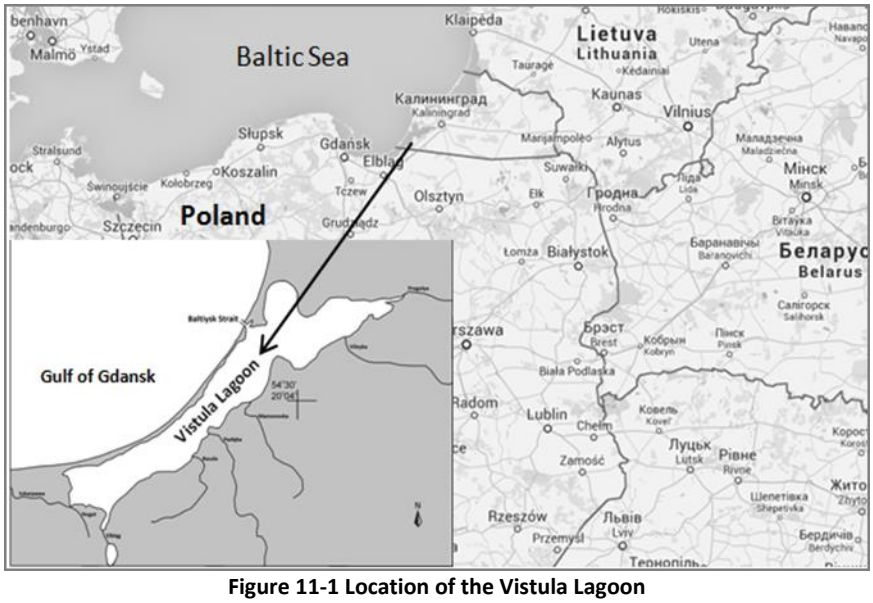

Figure 11-1 Location of the Vistula Lagoon

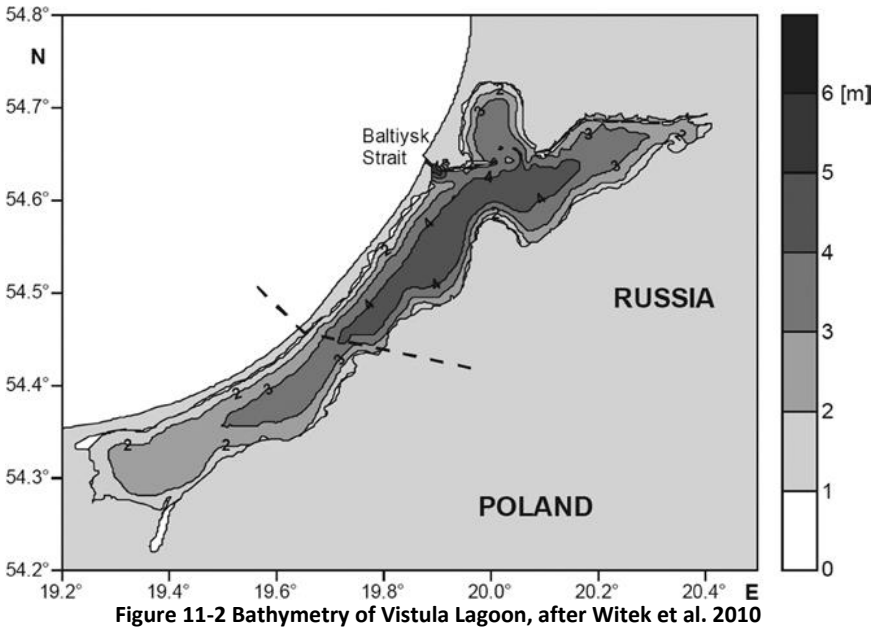

Figure 11-2 Bathymetry of Vistula Lagoon, after Witek et al. 2010

lagoon is only 2.7 m with the deepest area of ca. 5.2 m, located in vicinity of the Baltiysk Strait in the Russian part, Ed. Lillebø et al. (2015), cf. Figure 11-2.

11.1.2. Present-day challenges and expected impacts of climate change requiring restoration

The lagoon is very fragile from an ecological point of view, mainly due to nutrient input sensitivity. Nutrient loads from the large drainage basin and a shallow bathymetry result in very intensive biological processes, which lead to widespread algae blooms in summertime. Considering its depth, the large surface of the lagoon allows for a rapid mixing of the entire water column, even in the case of moderate winds, Ed. Lillebø et al. (2015). With regards to the transboundary character of the lagoon, the sustainable management of nutrient inputs appears to be the most challenging task, despite noticeable improvement of water quality in most rivers discharging to the lagoon. One of possible but very expensive solutions could consist in the placement of artificial floating islands intended to harvest vegetation developing during each summer season to permanently remove nutrient-rich substances in the autumn. This issue if entirely beyond the REST-COAST project, but it appears that meeting the WFD targets will require such type of actions. This however can only be possible when the cooperation with Russia is re-established. Moreover, eutrophication has no direct connection to climate change.

Another reason of concern is the flood risk in the SW corner of the lagoon in the Polish part, Ed. Lillebø et al. (2015). During N and NE winds, large storm surges can develop that attack (dilapidated) flood prevention infrastructures in the low lying areas of the Vistula River delta in the Polish part. This issue resulted in the currently running, long-term program of rehabilitation and refurbishment of hydraulic structures in the SW corner of the Lagoon, known as Żuławy 2030 (Vistula River Delta 2030). This program has a time horizon of 2030 and is entirely beyond the REST-COAST project, although rapid wind-driven surges can be investigated in terms of climate change.

Practical isolation of Vistula Lagoon from the Baltic Sea through Vistula Spit, being one of the most robust features of the Polish coast, results in the prediction of negligible effects of sea lever rise in the lagoon, whose possible outcomes were incorporated into the design of structures under Żuławy 2030. Moreover, the isolation will not produce enhanced erosion risks in a very shallow basin. More information is provided below.

11.1.3. Description of restoration efforts

The Vistula Lagoon pilot site is related to the construction of artificial passage to the Polish part of the Lagoon to provide an independent access to it. The whole Polish part of the Lagoon is a NATURA 2000 site for both birds (PLB280010) and habitats (PLH280007). This investment required a comprehensive EIA assessment which concluded that the project did not produce noticeable negative impacts on the Lagoon's environment. Simultaneously, it was found that the transformation to market economy resulted in a fairly severe depletion of pastures operated by both large state own farms and small farming households. Their bankruptcies resulted in apparent diminishing of birds hatching on meadows, such as **snipes, redshanks, lapwings and shelducks**. On the other hand, the project included construction of an artificial island to store sediment dredged during construction of the new navigational route from the cross-cut through the Spit to the harbor in Elbląg town (the largest municipality on the Polish part of the Lagoon with the [diminishing] population of slightly above 100,000), cf. Figure 11-3.

Hence, the Maritime Office in Gdynia (coastal management agency of the Government with extensive jurisdictional powers in the Lagoon area), after comprehensive consultations with ornithologists, decided to manage the island's vegetation as grassland. This solution was intended to provide new hatching grounds for birds who have been losing habitats in recent decades due to (unexpected) land use change. The maintenance of grassland meant that natural vegetation succession will be inhabited by either periodic annual mowing of the area using mechanical tools, or by much less likely temporary installation of sheep in late July – early August for pasture purposes. The inhibition of natural vegetation succession was also dictated to discourage cormorants – whose largest colony (ca. 12,000 specimen) has been observed in the Lagoon area in recent decades. Apart from the main target – restoration of birds hatching on meadows, the island is also intended to house many water birds – geese and ducks, who do not require urgent restoration efforts, but vastly enrich biodiversity in the area.

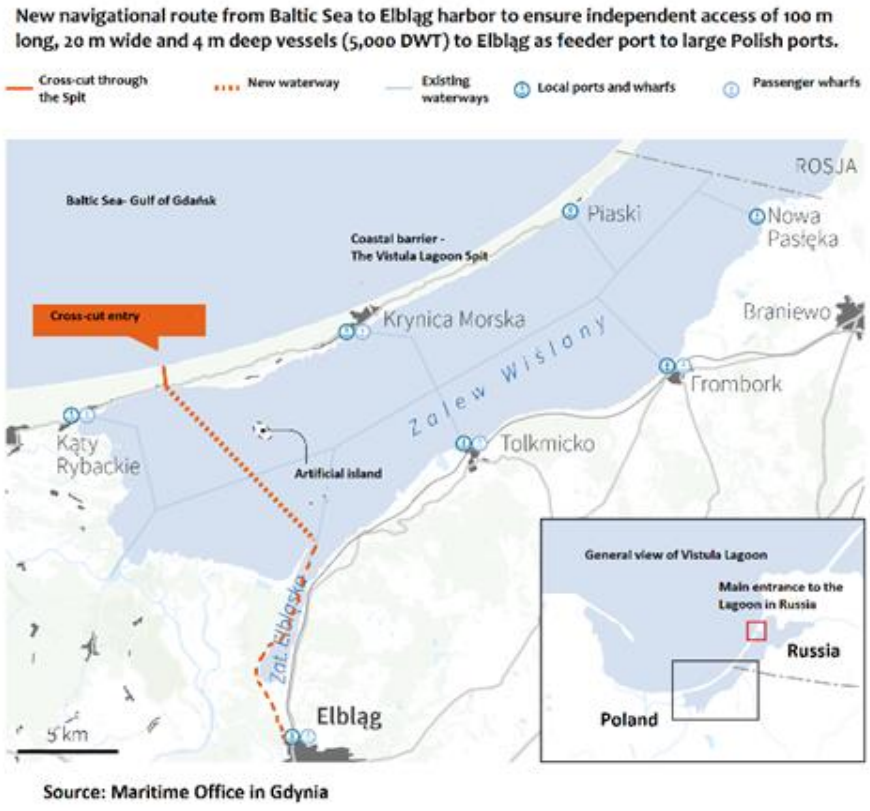

Figure 11-3 Schematic of independent passage to Elbląg harbor on Polish part of Vistula Lagoon

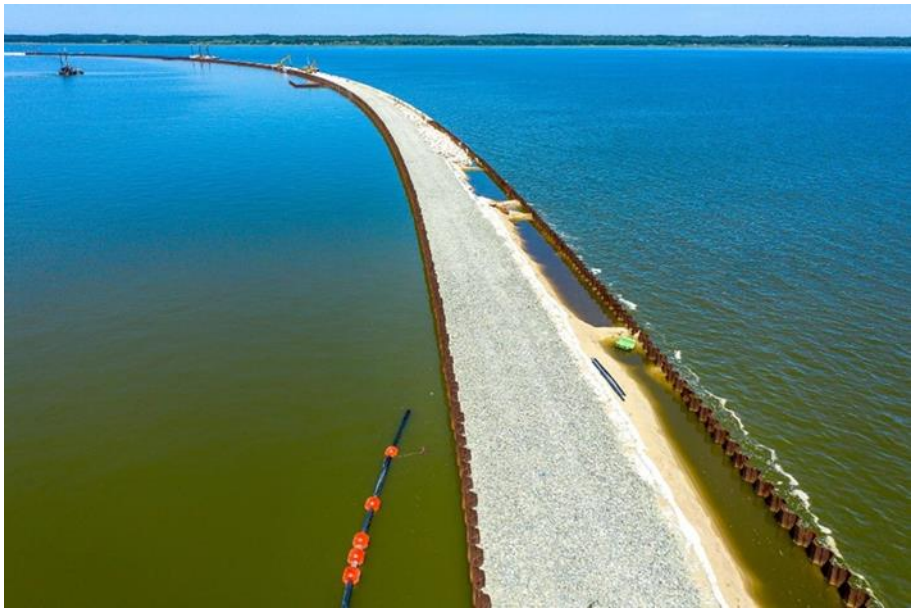

Figure 11-4 Low strength parameters of lagoon bed necessitated the rim made of two rows of sheet piles braced on top and filled with stones to resist ice phenomena

First observation of restoration results (at the island being still under construction) that it also attracted wading birds that feed on organisms living in muds, predominantly the **dunlins** who have become ubiquitous populating the drying silt in great numbers. The most precious new inhabitants are the **Kentish plovers**. Only some 90 pairs are normally observed in the Polish coastal areas, and hatchings are even more rare. The presence of those rare birds should be retained on the island, so it appears that the general strategy of the management of the island should include the maintenance of part of it as a mudflat. Other, rather unexpected but very positive sightings included several pairs of **herons**, who are known to be present in the area, but were not targeted for restoration. Even more surprising are the observations of several pairs of **white-tailed eagles** on the island. They are known to be present in the area in small numbers, but in the absence of high trees they will be neither hatching nor nesting on the island and their visits are probably driven by easy access to prey.

11.1.4. Scientific problem to be solved

The reduction of coastal risks was not a primary concern during realization of the artificial island concept. It basically resulted from very shallow character of the entire Vistula Lagoon basin, where wave climates are usually mild. The first problem was related to the placement of the island so as to minimize alterations in the local wave and current fields, while simultaneously keep sediment deposition costs at minimum. Details are provided below in the next section. The second problem was associated with the selection of optimum type of island's rim so that it can resist the action of ice fields in wintertime. Initially, geo-tubes were planned to be placed directly on the lagoon bed, which turned out to be unrealistic due to the very low strength parameters of that bed (very low angle of repose and cohesion of very soft muddy and silty sediments). Such solution risked very large and uneven settlement of the rim. Therefore, traditional rim in the form of two rows of Larsen sheet piles, braced on top and armored with stones was adopted, see Figure 11-4, indicating the limit of nature base solutions at the basin, where the strength parameters of bed sediments are critically low. Details are provided below in the next section.

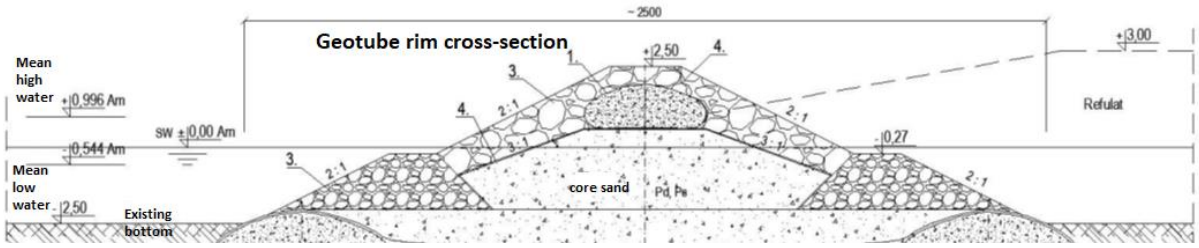

Figure 11-6 Concept of rim made of geo-tubes, courtesy of the Maritime Office in Gdynia

11.2. Methods

11.2.1. Model description

Determination of the location of artificial island was done using computer modeling of wave and current fields, driven by winds running from NE, along the longer axis of Vistula Lagoon. Exemplary results for the wind blowing with the speed of 10 m/s from NE are presented in Figure 11-5; we can see that the increase of the wave height on the up-drift side do not exceed 0.05 m and the decrease on the down-drift side remains below 0.15 m. Furthermore, results of the calculations of waves and currents in the presence of artificial island were used for the modeling of shoreline change on the bay-ward side of the Spit (not shown). The resulting changes were found to be negligible. Thus, construction of the island does not produce any enhanced erosion risks.

The exact location of the island was established upon trial and error simulations, as shown in Figure 11-5. Importantly, this location was determined in as close proximity as possible to the new navigation route, cf. Figure 11-3 with the general aim of minimizing the costs related to transportation of sediments from that route to the island.

The second major issue was the construction of the rim of the island. Initially, it was envisaged to apply geo-tubes as its core in order to minimize the use non-natural materials, see Figure 11-6. Unfortunately, the Lagoon's bed is composed of thick layers of ultra-weak sediments so that very high instances of local subsidence of the rim were imminent. Therefore, traditional engineering solution (Larsen sheet piles) was

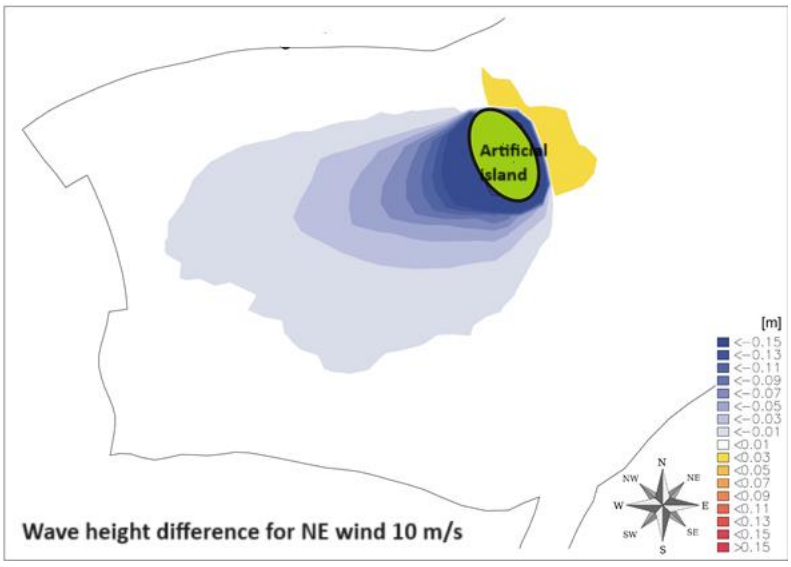

Figure 11-5 Exemplary impact of artificial island on wave field, after Szmytkiewicz et al.(2018)

adopted, see Figure 11-4 demonstrating the limitations of NbS in an environment, where bed strength parameters play a crucial role.

The rim is capable of resisting huge forces resulting from the action of ice in the Lagoon, which is still experiencing formation of thick ice, despite climate change. Simultaneously, it is sufficiently high to resist the impacts of storms surges (which may reach well over 1.5 m), also in the presence of SLR in the range of ca. 1 m. It should be added here that occasional inundations of meadows should occur in normal conditions, so from the point of view of the island as safe haven for birds such events are not a problem.

11.2.2. Quantification of ecosystem services

In general, lagoons isolated from sea by robust barriers, like the Vistula Lagoon, should not face substantial issues related to undesired coastal evolution, driven by changes in hydrodynamic regimes, which are in turn driven by climate change. From the morpho-dynamic point of view of the main task was related to minimization of impacts of the placement of artificial island inside the lagoon on the local hydrodynamic fields, namely waves and currents. These fields are basically wind driven, although high susceptibility of the lagoon to rapid formation of substantial storm surges generates gravity flows when storms recede. The ultimate location of the island guarantees that the impacts on coastal evolution are minimized. Simultaneously, there is no added value in terms of increasing resilience of the Lagoon's banks against sea level rise, since the restoration efforts are almost entirely focused on creation of safe haven for birds hatching on meadows. Short-term inundations of meadows are not deemed problematic for such functions.

We should not forget that creation of the island is expected to yield some additional ecosystem services that can be treated as positive by-products of our pilot site. First, the area near the rim should (slowly) transform into reed fields serving both as spawning areas for fishes in the lagoon ad habitats for many water birds. In addition, creation of reed fields will generate habitats for many insects on which both the fish and birds feed. Second, water, delivered to the island during sediment deposition operations is returning to the lagoon through chambers, where special vegetation is planted to remove nutrients from the effluent. As mentioned in the introduction, eutrophication is by far the main long-term ecological issue Vistula Lagoon faces in the process of meeting the WFD targets, so this water purification scheme yields a tiny step towards improvement of water quality in the Lagoon.

The second issue tackled in this report, i.e. construction of the rim of the island, has no direct bearing on ecosystem services, related to coastal evolution and resilience. Our major discovery is linked to limitations of NbS in basins, whose bed is composed of thick layers of very soft sediments with high proportion of organic elements. We learnt that such sediments practically prevent the use of geo-tubes as barriers for sediment deposition. It is caused by very uneven subsidence of such structures that make such concept inoperable.

11.3. Results

The study on optimum placement of the island required tedious numerical computations. Figure 11-7 demonstrates a computational grid that was used in the simulations of the impact of artificial islands on local hydrodynamic regimes. Although the area of potential location of the island was restricted to the northern region of its SW corner (near the barrier), expert engineering experience was needed to select the location minimizing both the environmental impact and costs of delivery of sediments to the island. It should be noted that there is no added value in terms of coastal resilience – morpho-dynamic processes on the inner side of the barrier are of low intensity in general and the island triggered no visible alterations. Hence, minimization of the environmental impact of the island was achieved.

The initial intention of building the rim using large volumes of local sediments contained in geo-tubes had to be discarded after execution of multiple analyses of lagoon bed samples. They determined high organic matter contents of 2.35% - 5.3% and very high natural moistures varying from 52.6% to 140.6%., which is typical for highly organic soils. The concomitant edometric tests allowed for determination of consolidation times of the samples: roughly speaking 90% of consolidation will require at least 10 years, corresponding to very long, irregular and substantial subsidence of the rim. This is prohibitive in terms of structural safety, hence poor structural characteristics of the Lagoon's bed turned out to be the main factor severely restricting NbS in the construction of the rim. This is the key takeaway message from Vistula Lagoon pilot site.

The role of sea level rise on the delivery of ecosystem services by the artificial island is negligible for at least a century. First, the barrier separating Vistula Lagoon from the Baltic Sea is one of the most resilient coastal segments on the Polish Baltic Sea coast. Therefore, there is no risk of breaching the barrier even in case of SLR reaching a meter or so. Second, delivery of the main function, i.e. creation of safe haven for birds hatching on the meadows, will not be impaired, as occasional inundations of the meadows, either due to heavy rainfalls, or high surges – exacerbated by SLR, normally occur at such biotopes. Third, the island will remain uninhabited upon the decision of the Maritime Office – local coastal management agency with full jurisdiction on the island, which means that no sensitive infrastructures to be used by humans are planned to be built there. Thus, the key aim of restoration efforts was found to be practically independent of sea level rise.

Virtual independence of the restoration efforts on sea level rise is an important premise for up- and out-scaling of this type of actions. Shallow basins like the Vistula Lagoon are particularly fit for such interventions. First, hydrodynamic regimes there are usually mild, so potential alteration of coastal morphologies due to construction of such large objects are usually low. Second, the impacts of sea level rise will be constrained to mostly the 'static' component, since the rims of artificial islands must be robust enough to resist ice phenomena but can be low enough to be insensitive to occasional inundations (inundations can be viewed positively as being a natural phenomenon on lowland meadows). On the other hand, bottom sediments should be thoroughly mapped and examined in the investigations of locations of artificial islands. Optimum locations should be placed on sandy bottoms to build NbS friendly rims, e.g. made of geo-tubes. It should also be remembered that artificial maintenance of grassland on artificial islands is only needed when it is

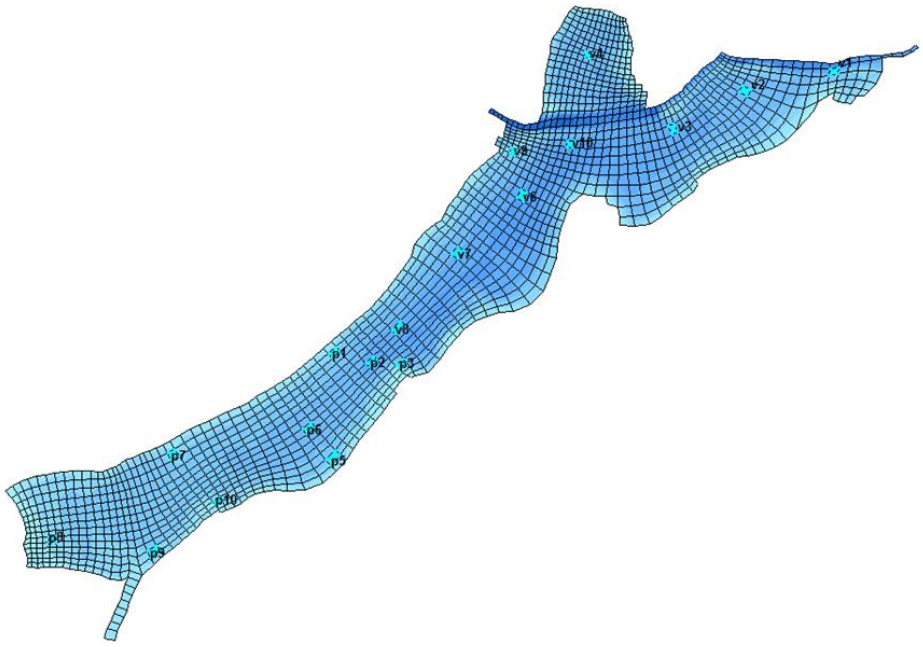

Figure 11-7 Computational grid for hydrodynamic simulations in Vistula Lagoon, Szmytkiewicz et al. (2018)

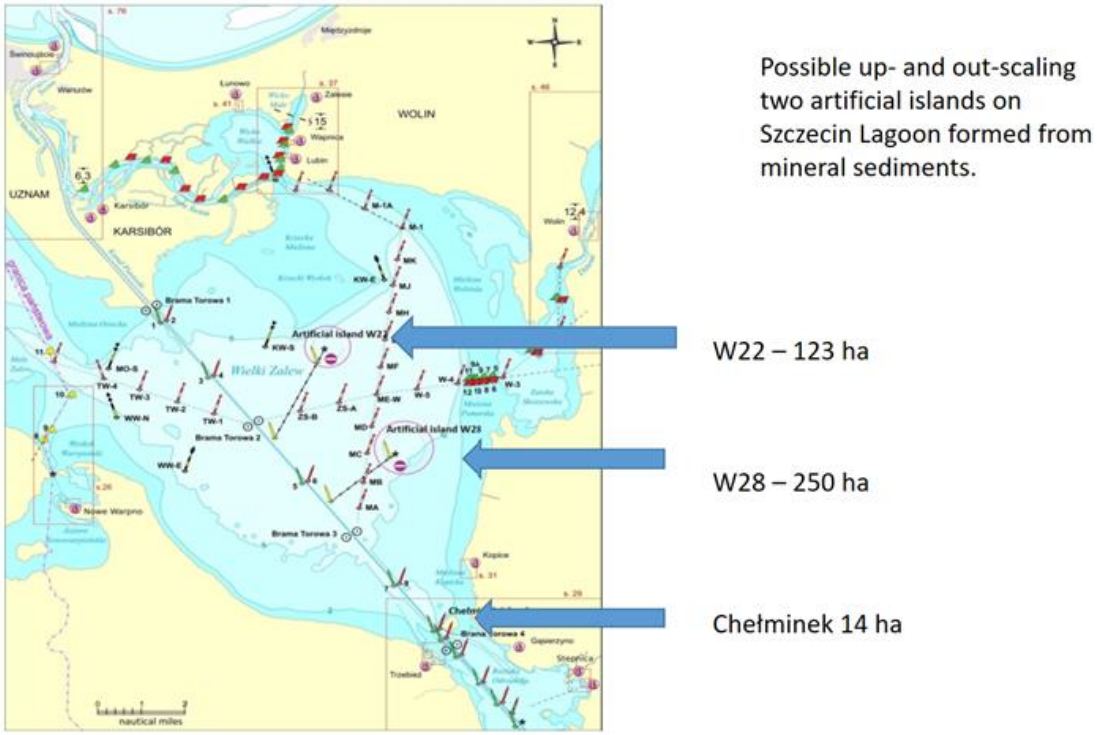

Figure 11-8 Possible out-scaling location: two artificial islands on Szczecin (Oder) Lagoon – shared with Germany

intended to limit the presence of undesired species – cormorants in the case of Vistula Lagoon; when such species are absent natural succession of vegetation should be preferred to exploit the carbon sequestration potential of young forests.

Figure 11-8 presents a possible out-scaling site – the Polish part of Szczecin (Odra) Lagoon, where Odra river – 2nd largest river in Poland forming a boundary with Germany discharges. Recently, two fairly large artificial islands (referred to as W22 and W28) were erected there to accommodate sediments dredged during expansion of the main navigation channel from the Baltic Sea to Szczecin harbour (seen in Figure 11-8 as a straight line running from NW to SE). In case grasslands on those islands are desirable, the Vistula Lagoon pilot can serve as a blueprint. Grasslands may become more feasible if the local colony of cormorants is found to be too much disturbing the local biodiversity. Currently though, natural vegetation succession is preferred, e.g. on the island of Chełminek, also plotted in Figure 11-8, which is the 1st artificial island on the Szczecin Lagoon, dating back to the turn of 20th century.

11.4. Conclusions

The Vistula Lagoon pilot provided two major lessons:

(i) Thick layers of muddy sediments are a serious impediment for implementation of NbS due to their very low strength parameters. Hence, there are severe limitations related to direct founding of engineering structures on weak soils. The associated risks of very high, uneven and long-lasting subsidence of such structures reduce a palette of possible solutions mostly to classical 'grey' solutions. That is why the rim of artificial island had to be constructed in this way in the form of two rows of Larsen sheet piles (each unit length 13 m) enclosing an ellipsoidal area of 180 hectares. Both rows were braced on top with cross-beams and filled with very robust stone armor. Such robustness was dictated by forces generated by ice fields, which are still occurring

in Vistula Lagoon, despite climate change. Probably, replication of the project in milder environments could be executed using less bulky structures.

(ii) Due to the main ecosystem service delivered by the island. i.e. provision of safe habitats for birds hatching on meadows, it is fully independent of sea level rise effects; occasional inundations either by heavy downpours or by storm surges can be rather viewed as an asset, since such events are not uncommon in lowland meadows. This insensitivity was possible, because of very strong jurisdiction of coastal authorities (the Maritime Office in Gdynia), who laid total restriction on human activities on the island: it should remain as safe haven for birds, which will not be disturbed by humans as well as by predatory mammals (due to isolation of the island from the mainland).

(iii) Current observations show that the island, despite being still under construction, already attracts thousands of birds, which were not targeted for restoration. It particularly concerns the wading birds, particularly Kentish plovers. This species is rare along the Polish coast and their presence is unexpected but very clear added value in terms of biodiversity restoration. Therefore, regular maintenance dredging operations on the navigation channel are a favorable circumstance for the presence of waders on part of the island, not intended for grassland.

(iv) The Vistula Lagoon pilot site has an obvious up- and out-scaling potential in all situations, where formation of grasslands as safe haven for birds is desired. Potential costs can be reduced in milder environments, where ice action is very rare or does not exist.

11.5. References

Ed. Lillebø, A.I., Stålnacke, P., and Gooch, G.D. (2015). Coastal Lagoon in Europe, IWA Publishing Alliance House 12 Caxton Street London SW1H 0QS, UK, DOI: 10.2166/9781780406299, 252 pp.

Szmytkiewicz, M., Ostrowski R., Schönhofer J., Skaja M., Szmytkiewicz P., (2018). Wpływ konstrukcji hydrotechnicznych, w tym sztucznej wyspy na kształtowanie się brzegu oraz plaż od strony Zalewu Wiślanego na Mierzei Wiślanej dla inwestycji pod nazwą „Budowa drogi wodnej łączącej Zalew Wiślany z Zatoką Gdańską" (*Impact of hydraulic structures, incl. artificial island, on coastal evolution of the inner side of Vistula Spit for the project 'Construction of navigation route from the Gulf of Gdańsk to Vistula Lagoon'*), IBW PAN report, ref. no. C2-21, commissioned by the Maritime Office in Gdynia.

Witek Z., Zalewski M., Wielgat-Rychert M. (2010). Nutrient Stocks and Fluxes in the Vistula Lagoon at the End of the Twentieth Century. SFI Publishers, 160 pp.

12. Modelling the Impact of Large-Scale Laguna Complex Restoration on Ecosystem Services with Climate Resilience: A Case Study of the Rhône Delta

Jolivet, M.[1], Cathala, M.[1], Faraon, T.[1] & Boutron, O.[1]

[1] *Fondation Tour du Valat, 13200, Le Sambuc, Arles, France.*

ABSTRACT: The Rhône Delta Pilot Site, as part of the EU Horizon 2020 REST-COAST project, represents a critical initiative in large-scale coastal ecosystem restoration aimed at enhancing ecosystem services (ESS) while mitigating coastal risks. This restoration effort focuses on re-establishing natural coastal dynamics by abandoning the maintenance of historic sea dikes and implementing an integrated water management system. The project targets the restoration of key habitats across a newly designated 4600-hectare buffer zone, aiming to improve water quality, reduce coastal flooding and erosion risks, and enhance biodiversity and food provisioning services. To assess the effectiveness of these interventions, hydrodynamic and morphodynamic models were developed and calibrated using in-situ data to simulate the site's hydro-saline and morphodynamic dynamics under current and projected future climate conditions. The models reveal that the restoration efforts have led to improved water circulation, re-established habitat connectivity, and enhanced biodiversity, particularly in coastal lagoons and salt marshes. These improvements are crucial for the recovery of fish populations and the overall ecological health of the Rhône Delta. However, the study also highlights significant challenges. The balancing of various ESS, such as water quality regulation and habitat restoration, poses difficulties due to potential feedback loops and trade-offs. Moreover, future climate scenarios predict rising sea levels, which could lead to increased lagoon water levels and heightened flood risks, particularly if the internal dikes are not reinforced. The models suggest that while current restoration measures are effective, ongoing adaptation will be necessary to maintain these gains in the face of accelerating climate change. Overall, the Rhône Delta restoration project demonstrates the potential of adaptive management strategies in coastal ecosystems to improve resilience and ESS delivery. However, it underscores the need for continuous monitoring and adaptive responses to emerging climate threats to ensure the long-term sustainability of these interventions.

12.1. Introduction

12.1.1. Pilot site

The site of the Former Saltworks, located in the south-eastern part of the Rhone delta (Figure 12-1), is an area of about 6500 ha which was acquired by the French Coastal Protection Agency (Conservatoire du Littoral) between 2008 and 2012. Until 2008, and during about 50 years, this site was devoted to industrial salt production, operated by a private company.

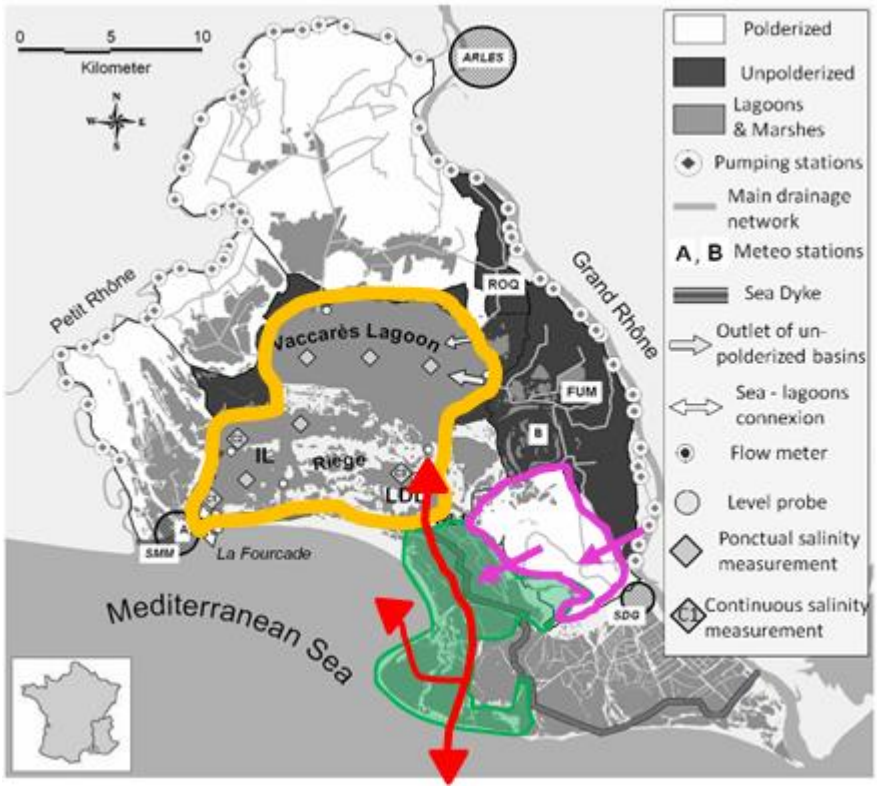

Figure 12-1 Location of the "Former Salt Works" (in green).

12.1.2. Problem description

The acquisition of this site by the French Coastal Protection Agency involved changes in management, compared to that implemented in an industrial salt production model. Water management by means of hydraulic pumps, as well as continuous maintenance of the dikes of the former salt production site in the context of sea level rise, was in particular no longer economically sustainable without the financial benefits of salt production. In addition, with the existing dikes of the former salt production site, and without the use of hydraulic pumps to generate water flows, the Former Salt Works site would have been with no change in management a very confined site with long renewal times. Due to the high evaporation rates in Mediterranean areas, this site would have been exposed to very high salinity and an absence of water for several months of the year, which would have been problematic for several plant species, birds and fish.

12.1.3. Description of restoration efforts

It was therefore decided since 2010 to implement a realignment strategy on the site (Figure 1): the sea-dikes protection of the former salt production site is no longer maintained, and the protection effort is now focused on a government owned dike which is located about 7 km inland, resulting in a new 4600 ha "Climate change buffer area" between the former and the inland dikes. Several works have been carried out (opening of dikes, dredging works, etc.) to create connections between the various former salt production basins (North-South red arrow in Fig.1). Hydraulic works have reconnected the site to a nearby agricultural catchment, itself irrigated from the Rhone river, allowing new fresh water flows in the site (purple arrows in Figure 12-1).

The restoration measures implemented as part of REST-COAST for the Rhone delta pilot site aim to:

1. Improve the connection of the site to the sea, and restore the natural coastal dynamics, by continuing not to maintain the historic sea walls of the site. (Passive restoration: elimination of the "historic" seawalls by their non-maintenance (Figure 12-1).
2. Implementing a new integrated water management:

a. Fostering the restoration of targeted habitats within REST-COAST: Coastal lagoons (N 1150), Beach areas (N 1140), Mediterranean and thermo-Atlantic halophilous scrubs (N 1420), and Salicornia and other annuals colonizing mud and sand (N 1310).
b. Enhancing the following Ecosystem Services targeted by REST-COAST: Water quality purification (through hydro-saline regulation), Reduction of coastal flooding and erosion risks, Food (fish) provisioning, and Climate change regulation.

12.1.4. Scientific problem

The main challenge of the restoration project for the Rhone delta Pilote Site is to determine whether it is possible to restore and improve all the targeted habitats and ecosystem services at the same time, or whether feedback loops, causal chains and side effects exist in the system that would lead to the deterioration of one of the ecosystem service as a result of the improvement of one of the other services, or if obtaining the hydro-saline conditions necessary for the restoration of one of the habitat types in one part of the site will lead to unfavorable hydro-saline conditions for other habitats in other parts of the site. Another challenge is to estimate the future of the restoration work carried out and the ecosystem services targeted in the context of climate change, considering rising sea levels and changes in rainfall and temperature. To address these challenges, modelling tools have been developed as part of REST-COAST.

12.2. Method

12.2.1. Models

The hydro-saline and morphodynamic dynamics of the site determine the ESS and restoration trajectories of the habitats targeted by REST-COAST. Models have therefore been developed within REST-COAST to simulate the hydrosaline dynamics of the entire site and the morphodynamics of the southern part of the site, to estimate the consequences of the project on i) the achievement of the hydro-saline conditions required for the restoration of the targeted habitats and the recolonisation of the site by fish (ESS food provisioning), ii) the ESS hydro-saline regulation and reduction of erosion and flooding risks.

Hydro-saline modelling

The summary of the hydro-saline modelling chain for the Rhone Delta Fellow Pilot is shown in Figure 12-2. Two hydrodynamic models (Sea model and Lagoons/marshes model) have been developed (Figure 12-3). The first TELEMAC-2D / TOMAWAC model covers the sea area and propagates the waves, the sea level and the salinity to the coast.

The mesh of the marine model consists of 30,760 nodes and 56,788 triangular elements, with a size ranging from 500 meters at the offshore boundary to 10 meters along the coastline. The boundaries to the south, west and east are liquid boundaries, forced with water level, wave and salinity data from the two regional Copernicus numerical models “MEDSEA_ANALYSISFORECAST_PHY_006_013” and “MEDSEA_ANALYSISFORECAST_WAV_006_017”, extracted at the red squares and triangles indicated in Figure 3. The boundary to the north is a rigid one with slip conditions. The marine model accounts for meteorological forcing such as atmospheric pressure, rainfall, and wind, provided by ERA5.

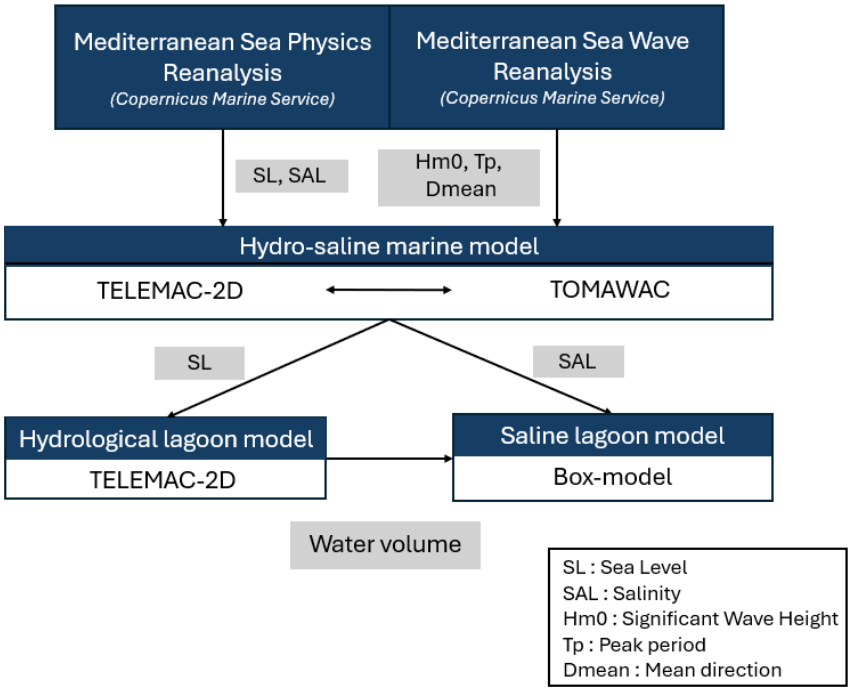

Figure 12-2 Modelling chain. "Water volume" refers to both volume of water in the different lagoons/marshes, and volumes exchanged through the different lagoons/marshes.

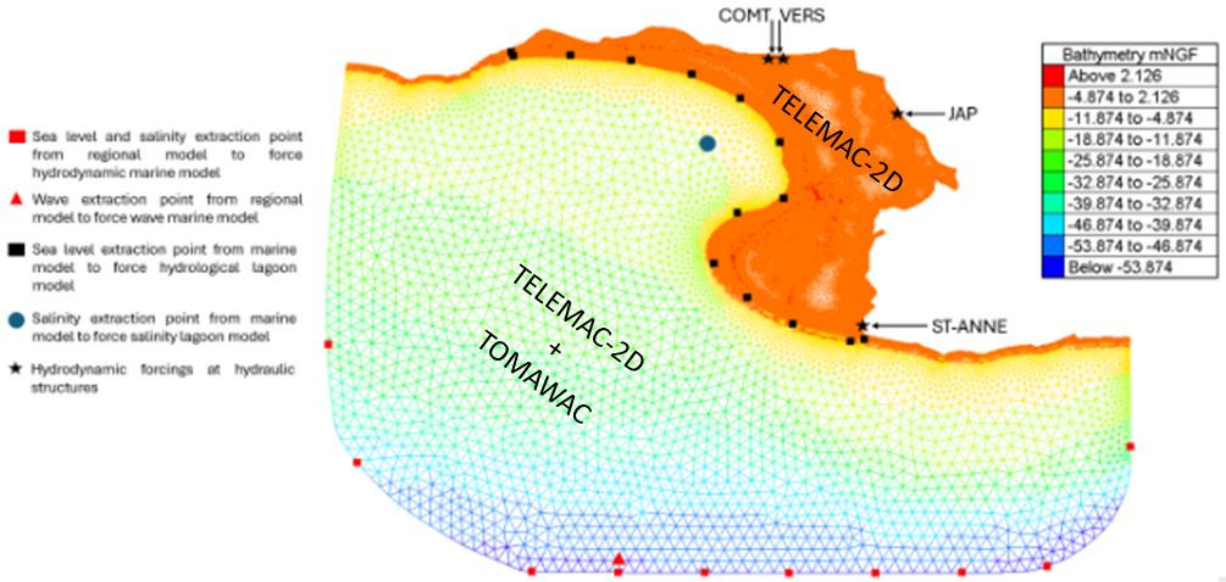

Figure 12-3 Unstructured meshes of the marine TELEMAC-2D / TOMAWAC and TELEMAC-2D lagoons/marshes model and resulting bathymetry. COMT, VERS, JAP and ST-ANNE are respectively the hydraulic liquid boundaries of the lagoons/marshes model at locations "Comtesse" (connection trough sluice gates with another complex of lagoons), "Versadou" (outlet of an agricultural drainage channel), "Japon" (outlet of an irrigation agricultural channel) and "Saint-Anne" (connection through sluice gates to an area of industrial salt production).

The mesh of the lagoons/marshes model contains 209,415 nodes and 416,102 triangular elements with a size ranging from 200 meters in the central part of major lagoons to 3 meters in channels. The boundary to the south is a liquid boundary forced with water levels extracted from the marine model at the black squares indicated in Figure 12-3. Other boundaries are rigid with slip conditions, except for four locations defined

with liquid boundaries: “Comtesse” (“COMT” in Figure 12-4, connection trough sluice gates with another complex of lagoons), “Versadou” (“VERS” in Figure Figure 12-4, outlet of an agricultural drainage channel), “Japon“ (“JAP” in Figure 12-4, outlet of an irrigation agricultural channel) and “Saint-Anne” (“ST-ANNE” in Figure 4, connection through sluice gates to an area of industrial salt production). The volumes exchanged at these locations are calculated using hydraulic laws, based on data from pressure probes upstream and downstream of the structures. The lagoons/marshes model accounts for meteorological forcing such as atmospheric pressure, rainfall, evaporation and wind. Atmospheric pressure is provided by ERA5-LAND. Rainfall and wind are supplied by Meteo France, collected from a local weather station. Daily evaporation is estimated using the Penman method (Penman, 1948). The daily evaporation rate is then divided by 24 to approximate hourly evaporation (Boutron, 2015).

Volumes of water in each lagoons/marshes and volumes exchanges between the different lagoons/marshes simulated with the TELEMAC-2D lagoons/marshes model are used as input variables in the salinity box model of the site (Figure 12-2 and Figure 12-4).

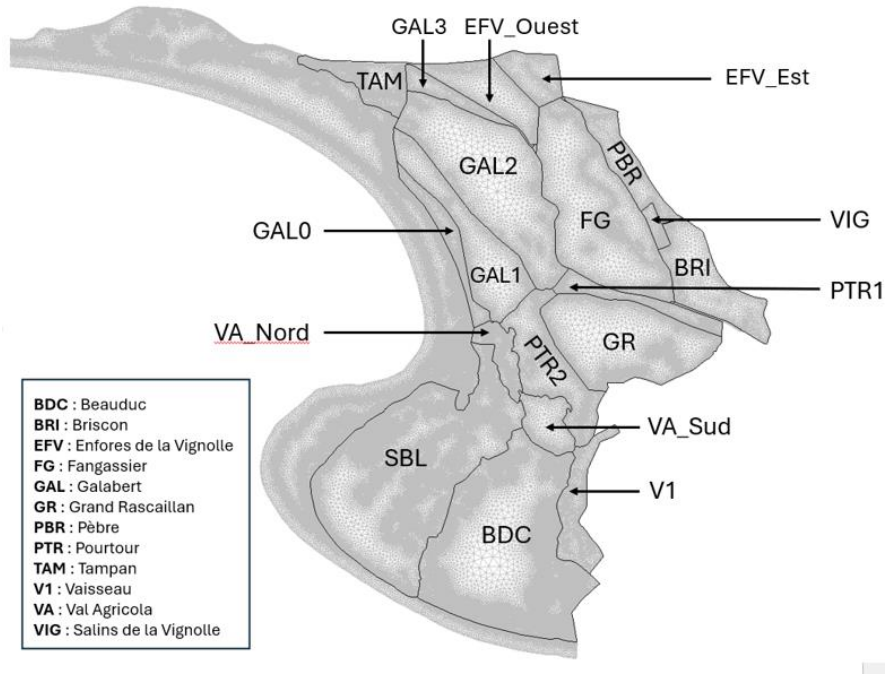

Figure 12-4 Location of the boxes modelled in the saline model. The names of the boxes are the names of the lagoons/marshes of the Rhone delta pilot site.

More specifically, the TELEMAC-2D lagoons/marshes model provides to the salinity box model:

- The flow passing through each hydraulic section (Appendices Figure D-1) at each time step and the positive and negative cumulative flow passing through each section since the beginning of the computation.
- The flow passing through each hydraulic structure (Appendices Figure D-2) at each time step and the positive and negative cumulative flow passing through each structure since the beginning of the computation.

Based on knowledge of these volumes, and the relationships linking water levels to water surface area and volume for each lagoon/pond, the salinity model solves a system of ordinary differential equations at daily time steps to calculate for each lagoon/marsh ("each box", see Figure 12-4) changes over time in the mass of salt in water, the salinity and the mass of salt in sediment. The phenomena of salt crystallization and dissolution are simulated. Salinity at sea is calculated from the marine model (Figure 12-2 and Figure 12-3). Salinities at locations "Comtesse" ("COMT" in Figure 12-4 connection trough sluice gates with another complex of lagoons), "Versadou" ("VERS" in Figure 12-4, outlet of an agricultural drainage channel), "Japon" ("JAP" in Figure 12-4, outlet of an irrigation agricultural channel) and "Saint-Anne" ("ST-ANNE" in Figure 12-4, connection through sluice gates to an area of industrial salt production) are provided by conductivity probes.

Morphodynamic modeling

To model the evolution and dynamics of the coastline studied, the choice was made to use the XBeach model (Deltares, 2023) in 2D Surfbeat mode to resolve short and long waves. XBeach is an open-source model developed by a consortium of researchers from UNESCO-IHE, Deltares, Delft University of Technology and the University of Miami. Designed to resolve the morphodynamic response of the coastline to hydrodynamic forcing during extreme events and used in case of overwash processes.

We set-up a mesh using an airborne topo-bathymetric LIDAR survey carried out by GEOFIT (https://geofit.fr/) on 14/10/2022 for the ResCoast project, supplemented offshore by the SHOM's Litto3D 2022 to prevent a thin zone without data. Both DEM are 1m of resolution. The grid extends 3.6km along shore and 1.6km from the laguna to offshore. A varying grid was built up, depending on depth, with reduce size (5m) on shallow bathymetry, to benefit better resolution of fine processus, and a wider grid size (15m) on deeper area. The

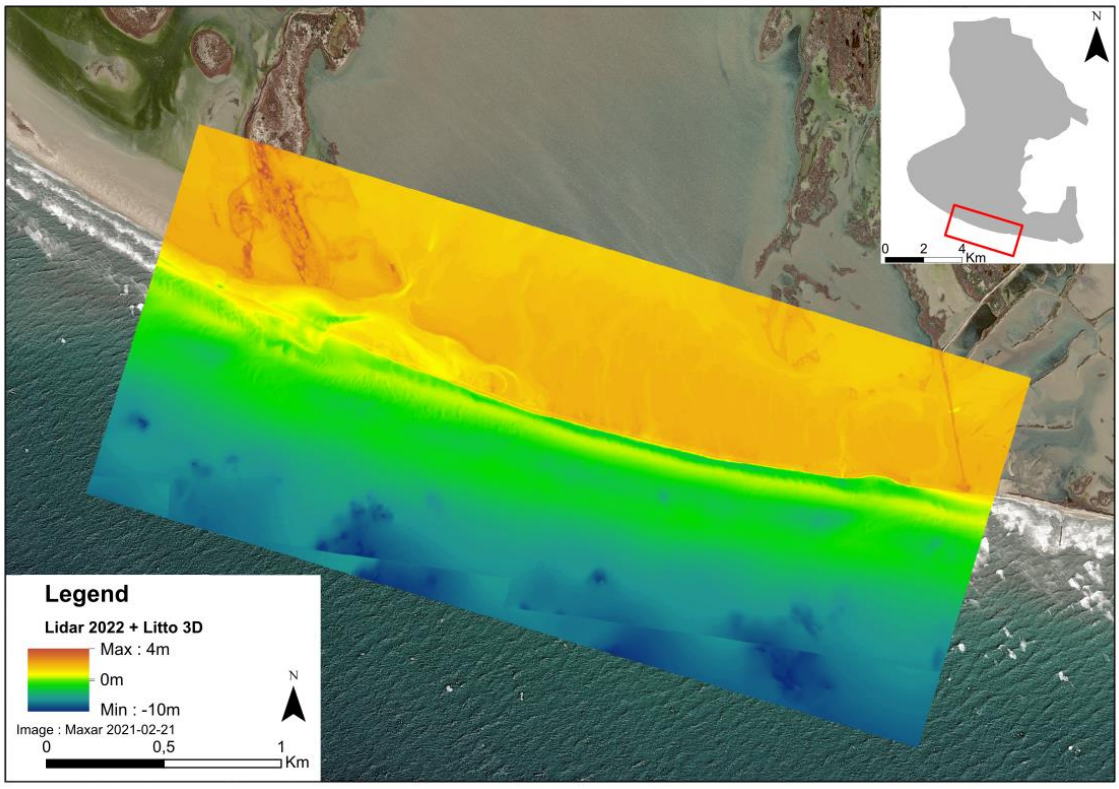

Figure 12-5 Domain of the Xbeach simulation with lidar DEM 2022 and Litto3D offshore

grid size is homogenous on the longshore axe, with 5m size (Figure 12-5). The dyke was represented by non-erodible, non-transmissive grid cells, with elevation based on the DEM.

The boundaries conditions waves data comes from the Copernicus Med-WAV model, which has been validated compared to buoy data. They are sampled at hourly intervals over a period running. Water level data were extracted from the Fos-sur-mer tide gauge, the nearest tide gauge, at an hourly frequency on national topographic geode reference (0 NGF). An initial water level data in the lagoon (NGF height) was input in landward domain, taken from measuring devices installed in Beaduc pond. Details about data are presented in Appendices Figure D-3.

Definition of scenarios

To simulate hydro-saline and morphodynamic dynamics without and with restoration, we have adapted the modelling tools developed.

For the marine and lagoons/marshes hydrodynamic models, as well as for the salinity box model, we have adapted the topo-bathymetry using different datasets:

- Bathymetry before restoration: This bathymetry incorporates data from four datasets combined to cover the entire area. Within the former saltworks, two DTMs acquired by LIDAR in 2016 and in October 2022 are used. The missing terrestrial and coastal areas are supplemented by LITTO3D (2015) which is a continuous land-sea digital model covering the backshore, foreshore and foreshore with a resolution of 5 meters or 1 meter. Additionally, EMODnet Bathymetry's DTM (115x115 meter resolution) is used for areas not covered by previous data. Most recent and highest-resolution datasets are prioritized over the others.
- Bathymetry after restoration: two datasets has been combined to cover the former saltwork site: the topogaphic database of the Rhone (later name BDT Rhone), acquired in 2011 by from LIDAR acquisition (IGN), and bathymetric data of lagoons from the saltwork society, later called Saltworks bathymetry. As the BDT Rhône has no data on aquatic areas, a fusion of the 2 datasets is made to combine the terrestrial areas from the BDT Rhone with the aquatic areas from the Saltworks bathymetry. When the 2 datasets overlap, the data with the maximum value is prioritized. Finally, because the "no-restauration bathymetry" doesn't cover the entire area, a fusion with the "Bathymetry before restauration" is made with a priorization of the latter.

After discussion with the co-managers of the site, we defined the scenario as representative of the site "without restoration": it consists of a site with a continuous maintenance of the dikes, no creation of hydraulic connections and no use of hydraulic pumps to generate water flows. The resulting hydro-saline dynamics in this hypothetical site, for both current and future conditions, are presented and linked to target Ecosystems Services and habitats of interest (see section 12.2.2).

For the coastal morpho dynamic model (Xbeach), we have adapted the topo-bathymetry using different dataset:

- Bathymetry before restauration: This bathymetry combined three datasets. Landward, in the laguna, we used bathymetric measurements made by the saline company during exploitation (1972). The terrestrial part of the coastline was extracted from a Litto 3D DEM, in 2009 corresponding to the transition between the saltworks and the actual natural area, but before restauration. The seaside bathymetry was extracted from a bathymetric single beam campaign (SEMANTIC) in 2006 and interpolate at 5m. The grid extends 3.6km along shore and 1.6km from the laguna to offshore with a variation size depending on bathymetry (from 5 to 15m).

- Bathymetry after restauration: It correspond to the actual state under restauration with abandonment of the dike. We extracted the Lidar topo bathymetric DEM of 2022 completed offshore by Litto 3D of 2016, shown in Figure 12-5.

Climate scenarios

For the hydrosaline modelling, to consistently forecast the effects of restoration on ESS delivery, five climatic scenarios are defined and tested (Figure 12-6): a present scenario with current conditions and four climate change scenarios by 2050 and 2100, with radiative forcing of +4.5 W/m^2 (RCP4.5) and +8.5 W/m^2 (RCP8.5), respectively. Each simulation is carried out on 1 year.

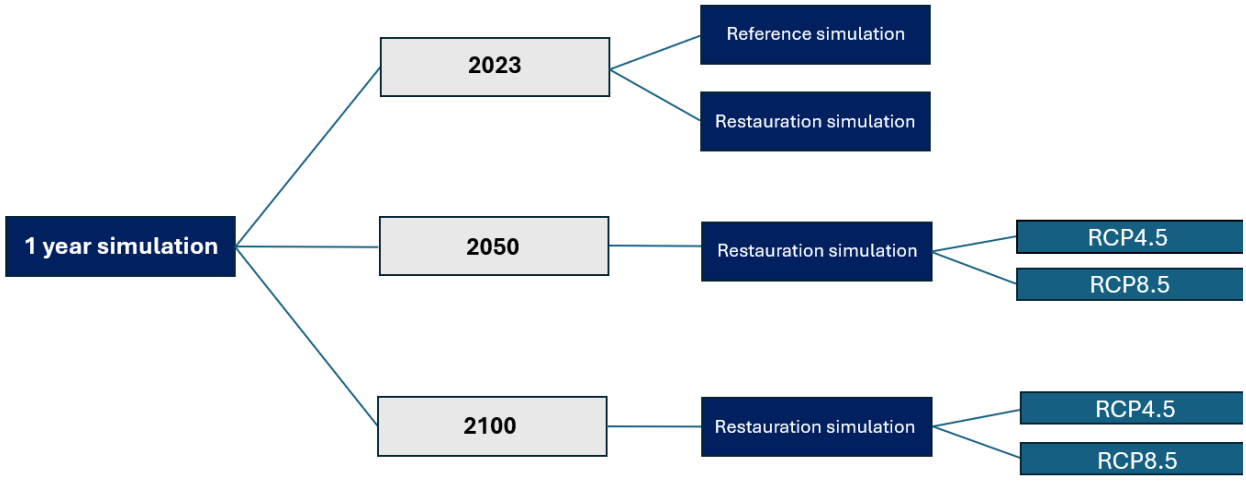

Figure 12-6 Flowchart of model scenarios

For the morphodynamics, we developed a modelling strategy based on assessment of effects of storms and SLR and storm conjugated to SLR. Return period of storms were calculated from Copernicus dataset "Mediterranean Sea Physics/Wave Reanalysis", with a historical extend from January 1993 to May 2021. Return period of 5, 10 and 50 years were calculated for waves heights (Hs), waves periods (Tp) and sea water level (SWL). Most stormy conditions occurred from direction South-South-East, 170°-degree direction. To transpose this statistical analysis to storm simulation on our site, we selected one of the most relevant storms from the last years, occurred in March 2018, to transpose our return period parameters to this storm "shape". Return period of storms are presented in Appendices Figure D-6.

To model the response of the area to climate change, projection of SLR, scenarios RCP4.5 (SSP2-4.5) and RCP7(SSP5-7) are selected by 2050 and 2100. We selected RCP7 instead of RCP8, because a high pessimistic scenario would have totally flooded the overwash plateform. These projections forecast a sea level rise between +0.21 cm and +0.66 cm relative to the 1995-2014 period, the specific sea level rise to apply is indicated on the Table 12-1. Furthermore, no changes are accounted for in wave forcings. By using this method, it is considered that the wave climate, storm frequencies and intensities will remain unchanged in the future. This modelling strategy result in application of twelve climatic scenarios on three morphological scenarios presented before (non restauration/restauration), and in Figure 12-7.

Table 12-1 Sea level rise in Camargue according to predictions of IPCC AR6 (2023) relative to the 1995-2014 and 2023 period.

	RCP4.5 (limited attenuation of the Climate Change) relative to 1995-2014 period	RCP7 (no attenuation of the Climate Change) relative to 1995-2014 period
2050	+0.21 cm	+0.22 cm
2100	+0.56 cm	+0.66 cm

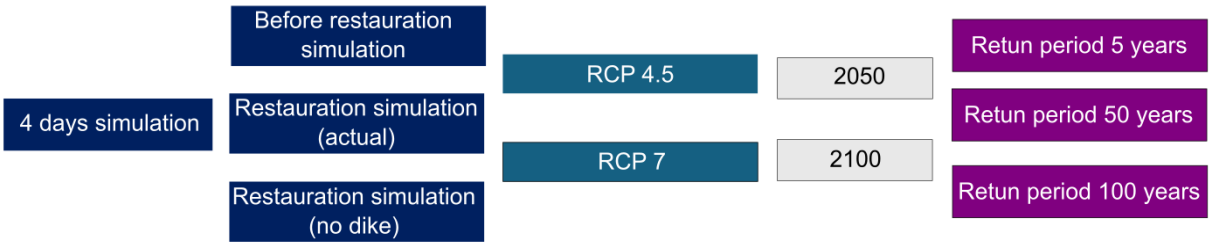

Figure 12-7 Flowchart of model scenarios

12.2.2. Quantification of ESS

The models developed for the Rhone Delta Pilot Site provide interesting information on the consequences of the restoration project on the restoration of the habitats and ESS targeted by the project, and the future of this restoration in the context of climate change.

ESS hydro-saline regulation and food provisioning (fish)

As part of the process of drawing up a management plan for the Pilot site, a number of hydro-saline criteria were defined by the site managers (Regional Natural Park of Camargue et al., 2022). These criteria define the hydro-saline conditions to be achieved for different periods and areas of the site (detailed in Appendices Figure D-7 and Appendices Figure D-8), in order to promote:

- The restoration of Coastal lagoons, Mediterranean and thermo-Atlantic halophilous scrubs, and Salicornia and other annuals colonising mud and sand.
- The preservation of ecological continuity for fish migration on the site.
- The creation of a nursery area for fish in the lagoons to the south of the site.
- Bird nesting on the site, in particular for the Greater Flamingo , and Terns in the Salins de la Vignolle lagoon (“VIG” on Figure 12-4).
- The welcoming of migratory birds (all the lagoons and marshes).

The hydro-saline indicator defined by the management plan are based on water level and salinity thresholds or average values over different periods, or on the flooding characteristics of the various areas, which can be simulated using the modelling tools developed within REST-COAST.

ESS reduction of coastal flooding

With the restoration project, the site is no longer protected from the risk of flooding by a system of dykes directly facing the sea to the south of the site, but by the dyke located 7 km inland, with 4600 ha of natural environment restored between this inner dyke and the sea. The historic protective dyke was subject to strong waves and rip currents. The dyke located inland is only subject to moderate wind waves limiting its erosion. Water flows at the bottom of this dyke are also more limited than that to which the historic protection dyke is subject, requiring less maintenance. To limit the hydraulic stress on the internal dyke, the management

plan for the Pilot site defines water level objectives for different periods of the year (Regional Natural Park of Camargue et al., 2022).

ESS reduction of coastal erosion and inundation (submersion)

With the abandonment of the sea-front dike, the goal is not simply to prevent shoreline retreat and erosion but to assess the capacity of the restored coastal dynamics to trap and accumulate sediments. The recreated barrier-lagoon system is intended to mitigate the impacts of sea level rise (SLR) and storm surges by increasing coastal mobility. The criteria to assess submersion will be the sea-water level at the dike with overtopping. Criteria to estimate the sediment mobility will be the final sediment budget on the land and sea side of the dike.

12.3. Results

12.3.1. Calibration and Validation

Marine and lagoons/marshes hydrodynamic models

A sensitivity analysis and parameter calibration have been deployed and more details are listed in Appendix D-1. The marine and lagoon models have been validated with data from 17 November 2022 to 1st December 2022. The marine model has been validated using *in-situ* data from the La Fourcade gauge (Figure 12-8) and modelled data from MEDSEA_ANALYSISFORECAST_PHY_006_013 and MEDSEA_ANALYSISFORECAST_WAV_006_017. On the other hand, the lagoons/marshes model has been validated using in-situ data from eleven tide gauge stations located throughout the Pilot site area (Figure 12-8).

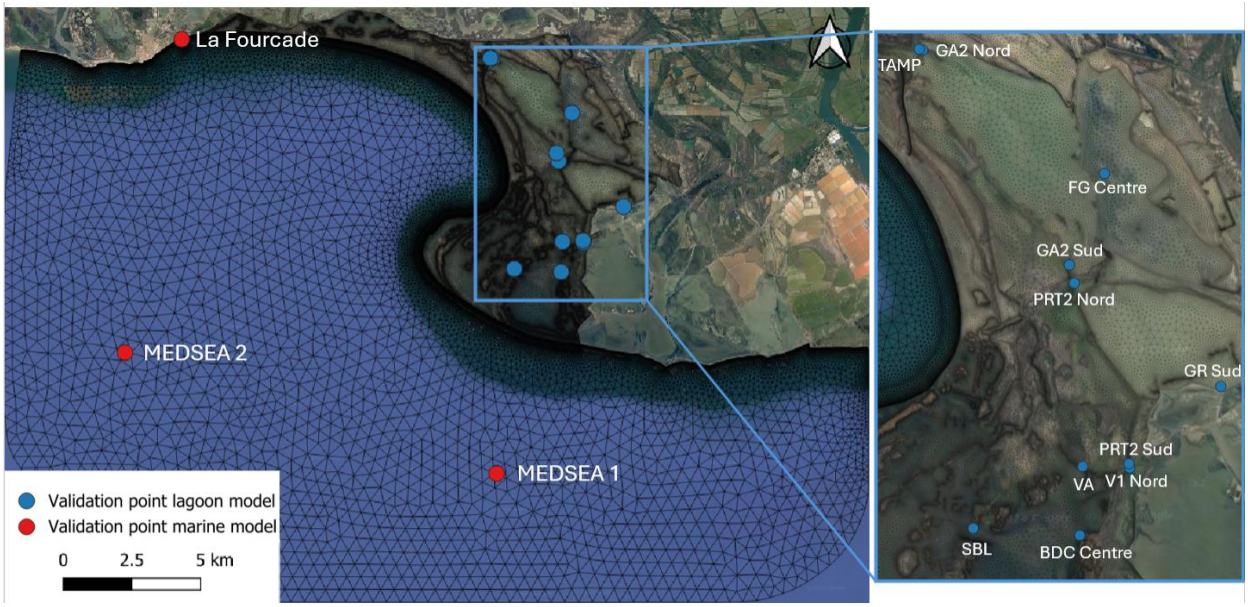

Figure 12-8 Model validation positions of modelled points issued of MEDSEA model for wave parameters and surface elevation and La Fourcade in-situ gauge for surface elevation, for the marine model (red circles); Model validation positions of water levels gauge stations for the lagoons/marshes model (blue circles).

The main results of this validation are:

1. Wave marine model
    a. The mean waves period is slightly underestimated throughout most of the simulation period.

   b. The spectral significant wave height is generally well represented but is underestimated during energetic periods, with discrepancies of up to 40 cm. Error ranges from 0.126 m to 0.185 m according to the MAE (Mean Absolute Error) and RMSE (Root Mean Square Error).
   c. The mean direction is effectively calculated by the model, with an average NRMSE (Normalized Root Mean Square Error) of 9.9 %.

2. Hydrodynamic marine model
   a. Good agreement between predicted and modelled data in MEDSEA 1 and 2 (MAE: 0.007 m to 0.012 m; RMSE: 0.01 m to 0.015 m; NRMSE: 2.2% to 2.3%).
   b. Good agreement between in-situ and simulated water levels at "La Fourcade" location (MAE: 0.021 m; RMSE: 0.027 m; NRSME: 0.063).
   c. The model tends to underestimate the water levels during low-water periods and overestimate it during high-water periods, even though these deviations remain within the order of a centimeter.

3. Hydrodynamic lagoon model
   a. The modelled data capture the wide variations of in-situ water level with nevertheless an error that can reach up to 10 cm.
   b. NRMSE, ranging from 13.4% to 38.2%, shows that the error increases with distance from marine connections, in accordance with MAE and RMSE.

Salinity box model

To calibrate the salinity model, we were faced with several difficulties. Due to the pronounced sediment dynamics in the south of the site, the areas of connection with the sea change very regularly, over a period of a few weeks: it was therefore not possible to calibrate the model over a full year, the time scale conventionally adopted for validating salinity models. In addition, a reduction in the accuracy of the hydrodynamic model is observed from February 2023 onwards, due in part to the assumptions made about the handling of hydraulic structures. To ensure satisfactory results of the hydrodynamic model in terms of flows and water levels, detailed in Appendices Table D-1, and using available experimental data (map in Appendices Figure D-4), the salinity model has been calibrated for the period from 23 November 2022 to 18 January 2023.

The variables used for calibration are the coefficients of the crystallization/dissolution kinetics of salt in water. MAE, RMSE and RMSE are detailed in in Appendices Table D-2 for this period. Here NRMSE is calculated as the division of RMSE by the average salinity measured over the period.

For all the lagoons, with the exception of the Fangassier "FG" lagoon:
- MAEs range from 2.5 to 24.2 $gk.m^{-3}$.
- RMSEs range from 2.8 to 24.3 $gk.m^{-3}$.
- NRMSEs range from 4% to 46%.

The Fangassier "FG" lagoon is a special case. During the first year of REST-COAST, the owner of the site (coastal protection agency) agreed to allow the saline company located to the east of the site to pump water into the Fangassier to extract salt for industrial production. As we did not have access to these volumes of pumped water, they were not considered in the modelling, which therefore logically overestimates the salinities in the Fangassier lagoon (this lagoon was not considered when calibrating the model). It should be noted that determining salinity from conductivity measurements, the most commonly used method, involves uncertainties for high salinity levels (Anati, 1999; Mor et al., 2021, Le Menn et al. 2022). Model results for in-situ salinities in excess of 80 $kg.m^{-3}$ should therefore be treated with a degree of caution.

Xbeach model

We configured the model with a morphologic calibration, based on method from Sánchez-Artús et al (2024). This method is based on comparison of in situ morphology deduced from satellite imagery and output from the model.

We conducted the calibration for an event close to our 2022's Lidar campaign for bathymetry to fit closer to the pre-event stage, from 16/10/2022 to 24/10/2022. We extracted hourly data from wave model of Copernicus Med-WAV model, tide gauge from SHOM (measurement point of Fos-sur-mer) and water level from measuring devices in laguna.

The chosen criterion for assessing model quality and the influence of different parameters is the Goodness Of Fit (GOF) based on the method presented by Hargrove et al. (2006) and used by Sánchez-Artús et al. (2024). It is used to represent the percentage of overlap between two map features made up of multiple polygons. Vectorisation from the satellite imagery were compared to model outputs for each simulation (map in Appendices Figure D-5). The optimal parametrisation is detailed in Appendices Table D-3, with values of parameters and final satisfying GOF score of 0.747.

12.3.2. Effect of non-restoration on ESS under current and future conditions

Hydro-saline regulation, flooding risk and biodiversity

This section presents the results from hydrosaline simulations for the non-restoration scenario under current and future conditions, through the assessment of ESSs of Water quality purification (through hydro-saline regulation), reduction of coastal flooding and restoration of targeted habitats.

The seasonal mean water height of 2023 for the non-restoration scenario is indicated in Figure 12-9. The results illustrate a progressive draining of the lagoons from spring to autumn, with most of the domain remaining dry. Water heights are the lowest during spring and autumn with values not exceeding 30 centimeters. In winter, the water height increases in some lagoons such as Beauduc, Grand Rascaillan, Galabert 2 and Fangassier, where water heights can reach up to 1 meter (see Figure 12-4 for the names of the different locations).

Ax explained in section 12.2.2, Briscon is a nesting area for colonial birds that requires permanent flooding. However, the results indicate that this condition is not respected, as the area remains dry throughout the year. Galabert 3, Pebre and Enfore de la Vignolle need to be dry during summer and flooded during the rest of the year to support the reconquest of saltmarshes. But it clearly appears that these areas remain dry throughout the year which does not guarantee ideal conditions for the development of Mediterranean and thermo-Atlantic halophilous scrubs, Salicornia and other annuals colonising mud and sand.

The predicted seasonal mean water height evolution of the non-restoration site in 2050 and 2100 according to RCP4.5 and RCP8.5 scenarios is illustrated in Figure 12-10. These results show sub-annual and inter-annual dynamics. As in 2023, the lagoons are drained during spring and summer. However, unlike 2023, where filling occurs only in winter, they are also filled in autumn in 2050 and 2100. These results also show that water levels increase over the years (whatever the scenario) in accordance with the sea level rise. This means that the flooded area increases over the years. But values do not exceed 2.5 meters in the deepest lagoons (2100 RCP8.5).

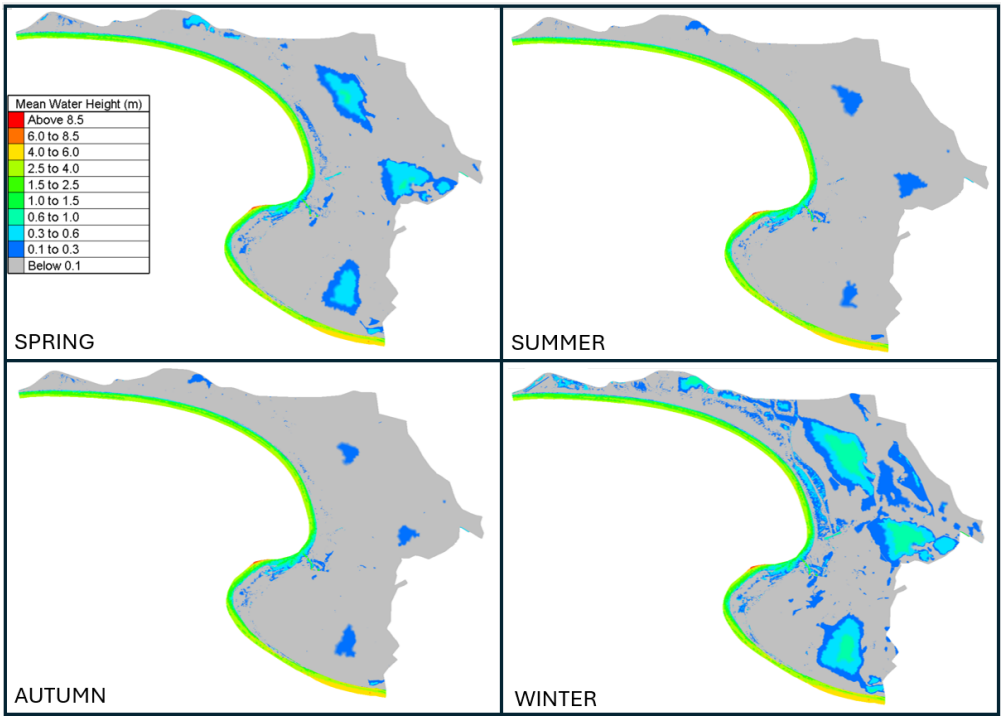

Figure 12-9 Seasonal mean water height (m) for 2023 without restoration. Spring is considered from 1 Marsh to 31 May, Summer from 1 June to 31 August, Autumn from 1 September to 30 November and Winter from 1 December to 28 September.

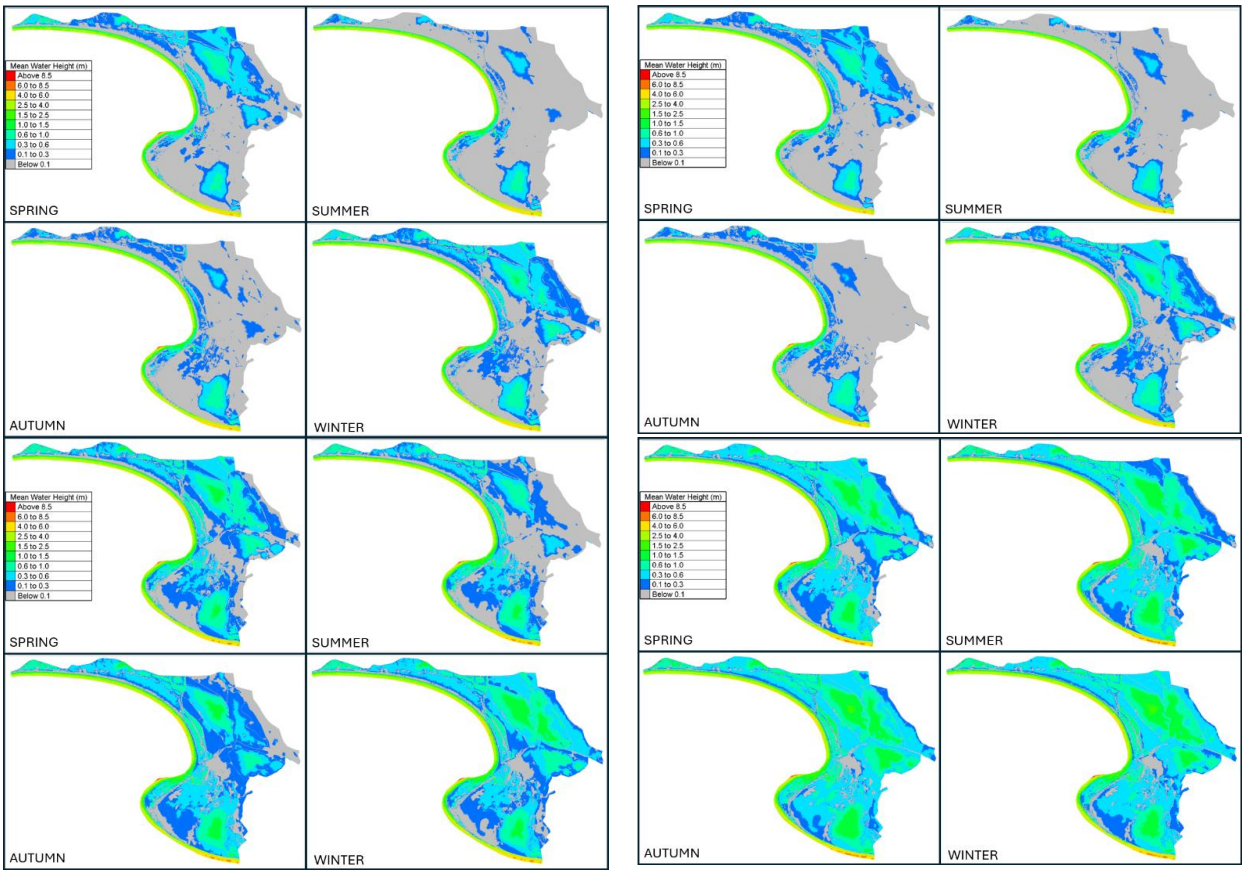

Figure 12-10 Seasonal mean water height (m) for 2050 and 2100, with RCP4.5 and RCP8.5, without restoration. Spring is considered from 1 Marsh to 31 May, Summer from 1 June to 31 August, Autumn from 1 September to 30 November and Winter from 1 December to 28 September.

According to Figure 12-10, Briscon is annually flooded only in 2100 considering RCP8.5. In 2050 (under both scenarios) and in 2100 (RCP4.5), a drought is observed during summer and autumn. Regarding Galabert 3, Pebre and Enfore de la Vignolle, the results for both RCP4.5 and RCP8.5 indicate a long summer drought in 2050, which can be beneficial for the development of saltmarshes. However, the outlook for 2100 is less encouraging: only Pebre experiences a summer drought under RCP4.5, and there are no longer any summer droughts in any of the lagoons according to RCP8.5.

Figure 12-11 displays the water height at four points located on the crest of the inland dike, for both current and future conditions, to evaluate the overflow flooding, defined as an increase of the static water level of 0.1m (arbitrary threshold) above the dike level. This figure indicates that the risk of flooding by overflow is zero, except for the point 1 and 2100 RCP8.5 scenario where a 5% risk is calculated. Comparing these results with those observed in Figure 12-10 and Figure 12-11 suggests that the flooding produced behind the sea dike in 2050 and 2100 (whatever the scenario) is only induced by an opening of the hydraulic structures (PRT1.1 and FG2.1, in Appendices Figure D-2) during the simulation. These results do not account for overwash flooding, generated on this site by wind waves, which can amplify flooding. Moreover, the dike, originally built as an internal dyke for a salt production site, isn't adapted to higher water levels in the lagoons generated by the sea level rise. Thus, overflow and the action of the waves could create breaches that might lead significant flooding.

These results imply that the increase water levels in the lagoons will have no effect on the flooding risk, on the other side of the inland dike. However, without accounting for waves, these results may underestimate the potential flooding.

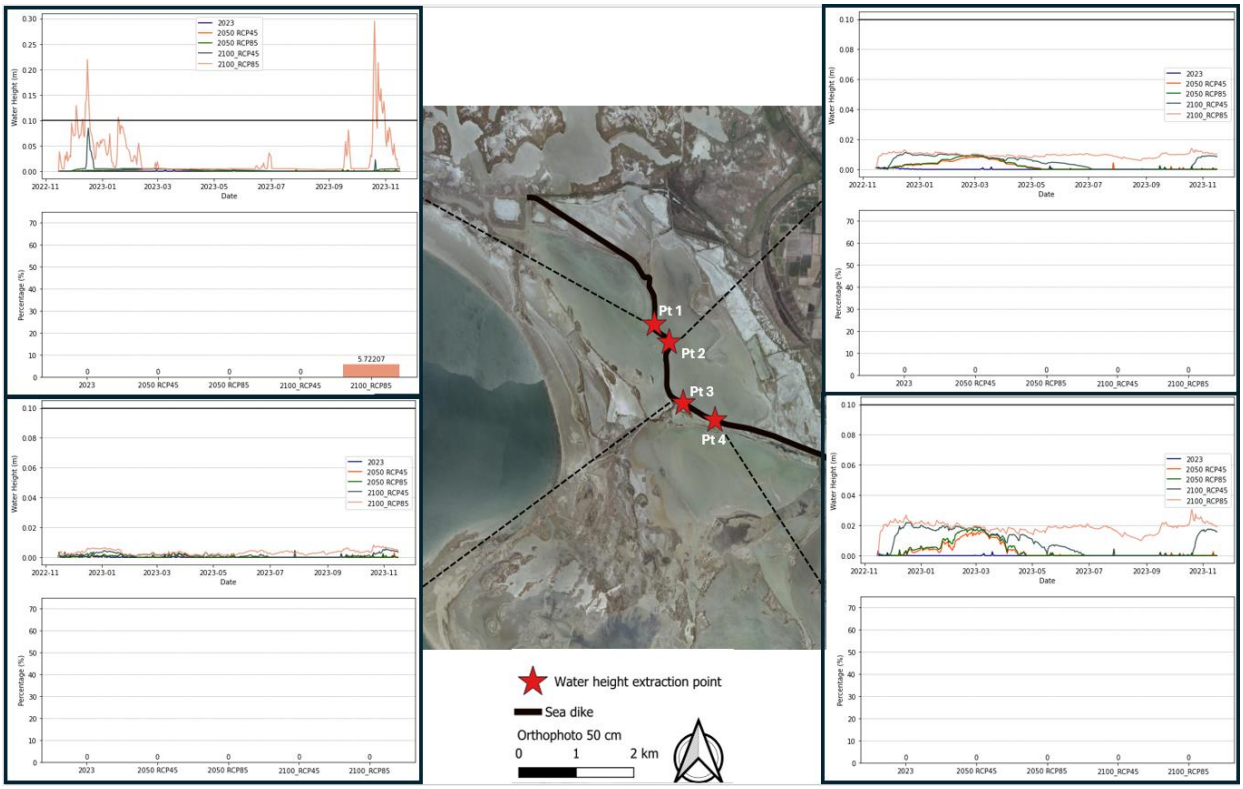

Figure 12-11 Timeseries of the water height in 4 points for both present and future conditions, and histograms showing the percentage of time for which the water height is superior at 0.1 m at these points. The latter are located on the lowest areas of the sea dike. 2023 results are shown with blue lines, 2050 RCP4.5 with orange lines, 2050 RCP8.5 with green lines, 2100 RCP4.5 with green lines and 2100 RCP8.5 with salmon lines.

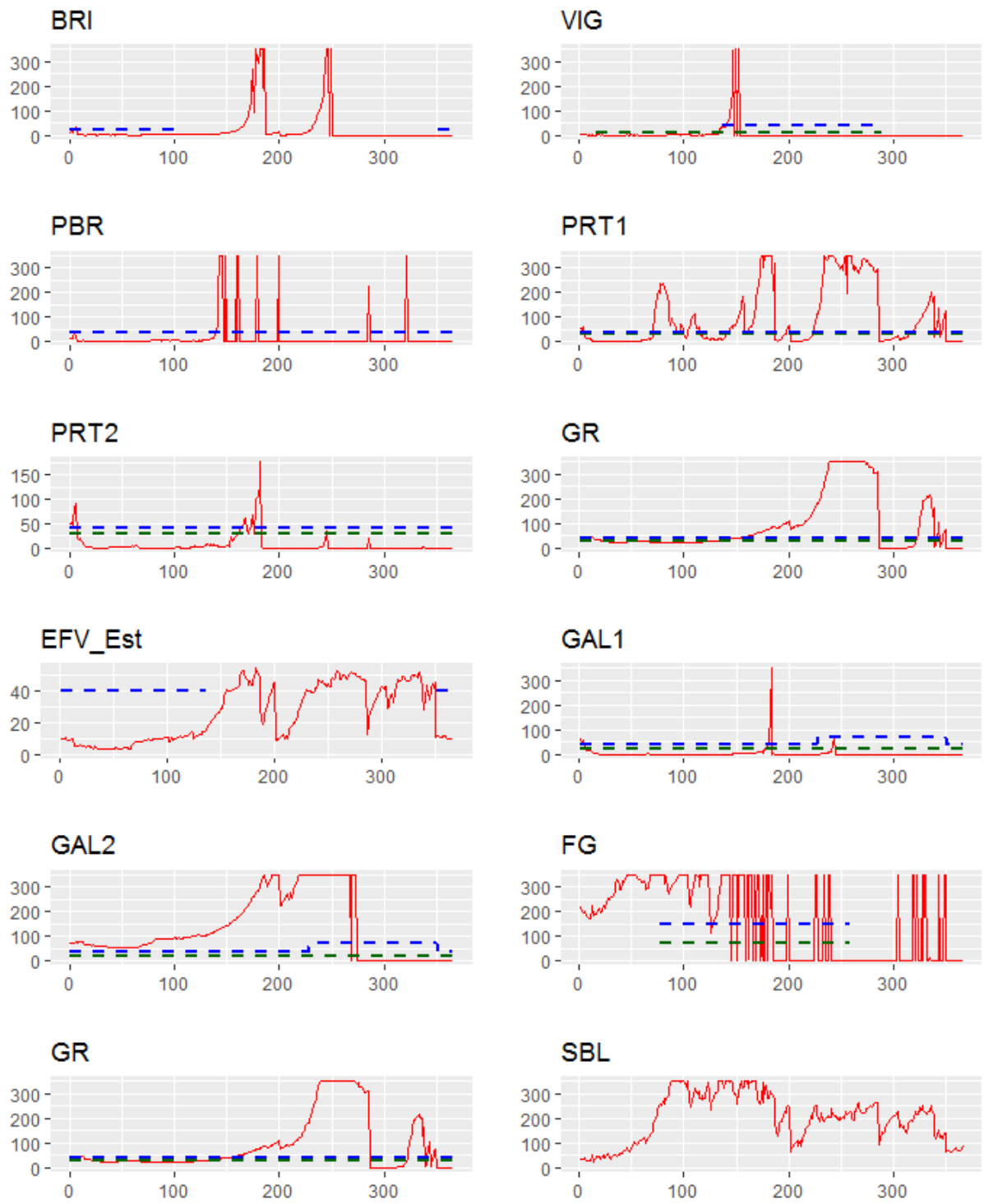

Figure 12-12 Daily average simulated salinity (red line) in 2023 for the non-restoration scenario, in combination with the maximum (in blue) and minimum (in dark green) salinity thresholds defined for certain periods of the year as part of the site's management plan, in order to respect the objectives of habitat restoration, the presence of fish and birds, and the sustainability of the site's internal dykes (See section12.2.2).

Concerning the consequences of not carrying out a restoration project on the site, the daily average simulated salinity (red line) in 2023 for the non-restoration scenario is indicated in Figure 12-12, in combination with the maximum (in blue) and minimum (in dark green) salinity thresholds defined for certain periods of the year as part of the site's management plan, in order to respect the objectives of habitat restoration, the presence of fish and birds, and the sustainability of the site's internal dykes (see section 12.2.2).

The simulation results clearly indicate that, in the absence of the restoration project, it would not have been possible to meet the objectives of the site management plan in terms of salinity, especially for the objectives of restoring coastal lagoons (N 1150), Mediterranean and thermo-Atlantic halophilous scrubs (N 1420), Salicornia and other annuals colonising mud and sand (N 1310), and stakes related to fish and birds. Note that the nil salinities on the graphs correspond to an absence of water, which is not in line with the objectives of the management plan for the periods concerned.

Food (fish) provisioning

This section presents the hydrodynamic results for the non-restoration scenario under current and future conditions, relative to the ESS food provisioning whose ideal state is a permanent connection between the lagoons and the sea to allow fish migration.

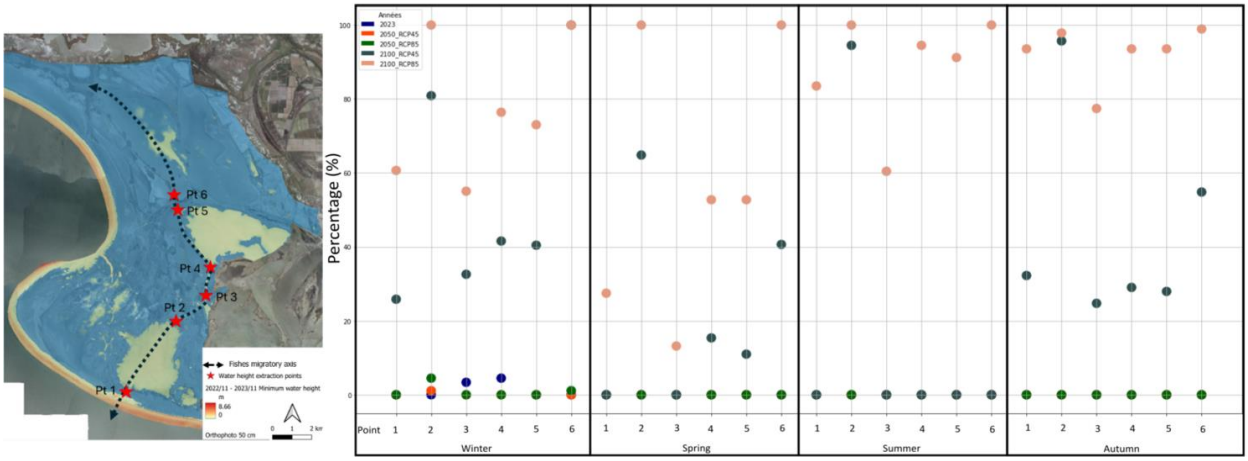

Figure 12-13 Diagram showing the seasonal percentage of time for which the water height is superior at 0.3 m for both current and futures conditions at 6 points located on the fish migratory axis. It is in these points that the water height is the lowest on migratory axis during all of 2023. These calculations are made from seasonal mean water height of each scenario. 2023 results are shown with blue points, 2050 RCP4.5 with orange points, 2050 RCP8.5 with green points, 2100 RCP4.5 with green lines and 2100 RCP8.5 with salmon points.

Figure 12-13 indicates that in 2023 and 2050 (for both RCP4.5 and RCP8.5), the water height rarely exceeds 0.3 meter, whatever the point and the season considered, which does not allow the fish migratory between the sea and the lagoons. In 2100, in accordance with an increase of the sea level, the water height is higher along the migratory axis. With RCP4.5, the water height is still inferior to 0.3 m in summer, except for the point 2. In autumn and winter, the threshold of 0.3 m is exceeded 20-30% of the time, and in spring about 10%. With RCP8.5, points 2 and 6 are always flooded by more than 0.3 m whatever the season. For other points, the threshold is exceeded in average 70 % during winter, 50% during spring, 80% during summer and 95% during autumn.

These results illustrate well the necessity to have undertaken restoration work to restore the fish dynamic reduced by the construction of dykes during the industrial salt production period.

Coastal erosion and flooding risk (submersion)

This section presents the results from morphodynamic modelling of the overwash platform south of Beauduc Pond. Figure 12-14 displays the morphological evolution at the end of a 4-day storm simulation using XBeach, for each scenario (Sea Level Rise (SLR) + storms). The differential analysis highlights areas of erosion (in blue) and accretion (in red). Storm conditions are illustrated in Figure 12-15, showing locally on a point (a) the water level in front of the dike, and (b) the incident significant wave height.

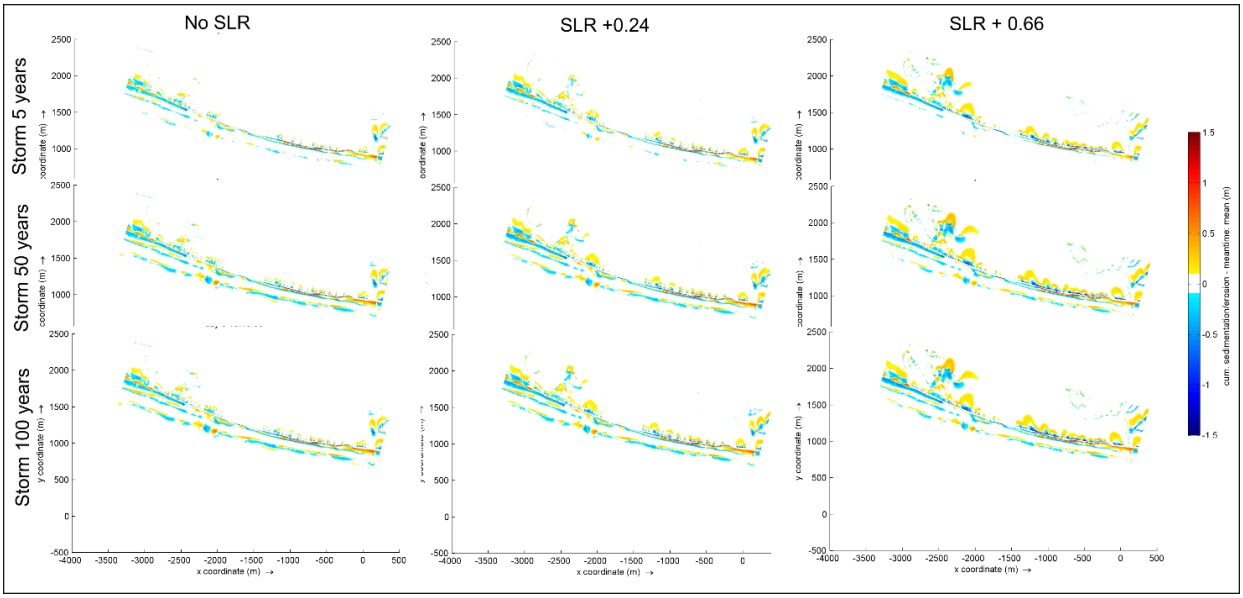

Figure 12-14 Differential of DEM for scenarios of SLR and storms, with management scenario corresponding to the former saltworks and dike management (2005).

In scenarios without SLR, the most significant changes occurred on the seaside. Maximum erosion is observed on the eastern part, at the base of the dike, accompanied by sediment accumulation further offshore. This erosion pattern is characteristic of wave reflection off the dike, leading to scouring at the base of the structure. Figure 12-15 shows the topobathymetric variation during the storm along a profile from the eastern part. In front of the dike, the profile tends to steepen throughout the storm due to erosion.

The differential DEM analysis also illustrates the movement of sandbars, which migrate onshore due to the storm. The morphological patterns are similar across all storm scenarios, with variations in the magnitude of erosion and accretion. Onshore, behind the dike, a channel is dredged along the dike, and small deposition cones are observed. In the scenario with a +0.24m SLR, the storm with a 5-year return period shows similar behavior to the no-SLR scenario. However, significant changes occur in storms with 50- and 100-year return periods, where larger cones of erosion form along the dike. In the climatic scenario SSP7, with a +0.66m SLR, larger cones of deposition appear, indicating that the storm has overtopped the dike.

Figure 12-15 presents profiles at different time steps during the storm, including the initial condition, peak storm condition, and post-storm condition. At the storm's peak, the 1m-high dike is overtopped by waves (1.16m at the shore). Overtopping is very localized, as shown by the differential DEM, with small cones forming and no significant overwash process observed.

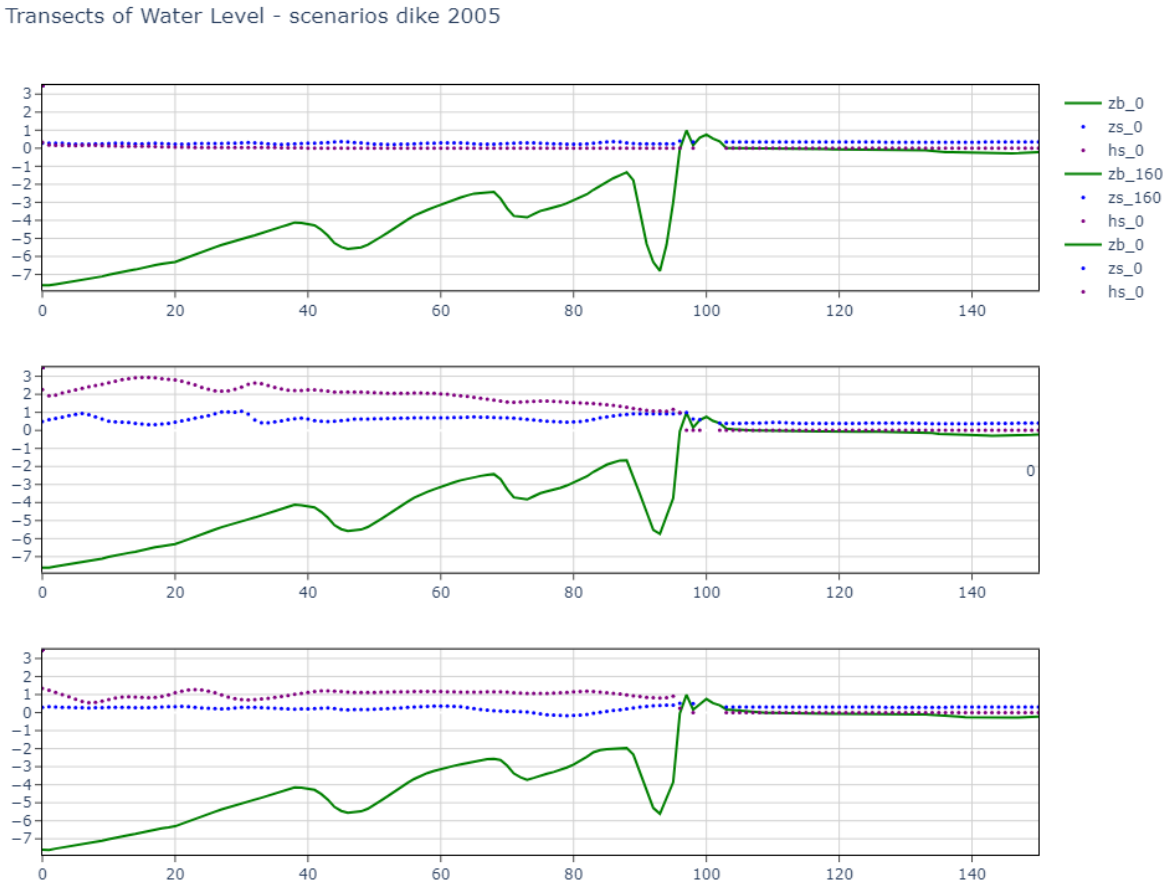

Figure 12-15 Water level and Hs along one profile of scenarios 2005 with dike, at different time steps, (a) initial stage, (b) during storm with Hs=3m offshore, (c) post-storm conditions.

12.3.3. Effect of restoration on ESS under current and future conditions

The restoration project aims to enhance water circulation (ESS water quality purification and biodiversity) to improve hydro-biological exchange between the lagoons and the sea (ESS food provisioning i.e fishery) and to restore coastal dynamics to adapt the site to coastal erosion (ESS reduction of coastal erosion risk) and sea level rise (ESS reduction of coastal flooding risk). For both present and future conditions, these ESS are evaluated according to the result of morpho-hydro-saline-dynamic modelling.

Flooding risk and biodiversity

One of the objectives of the restauration project is to reduce the damage risk of main dykes, especially the sea dike (Figure 12-1). In terms of ecosystem services, the purpose is to reduce the coastal flooding risk by dampening wave energy up-stream of the inland dike.

The seasonal mean water height (m) at the site for 2023 is represented in Figure 12-16. The results show that the lower water heights are simulated in summer (maximum of 1.5 meters in Grand Rascaillan lagoon), while higher water heights occur in winter with values which can reach 2.5 meters (in Grand Rascaillan lagoon). Several areas such as Sablon, Beauduc, Grand Rascaillan and Galabert 2 (see Figure 12-4 for the location of these lagoons) are always flooded, while others, like Pourtour 2 and Fangassier, are dry only in summer.

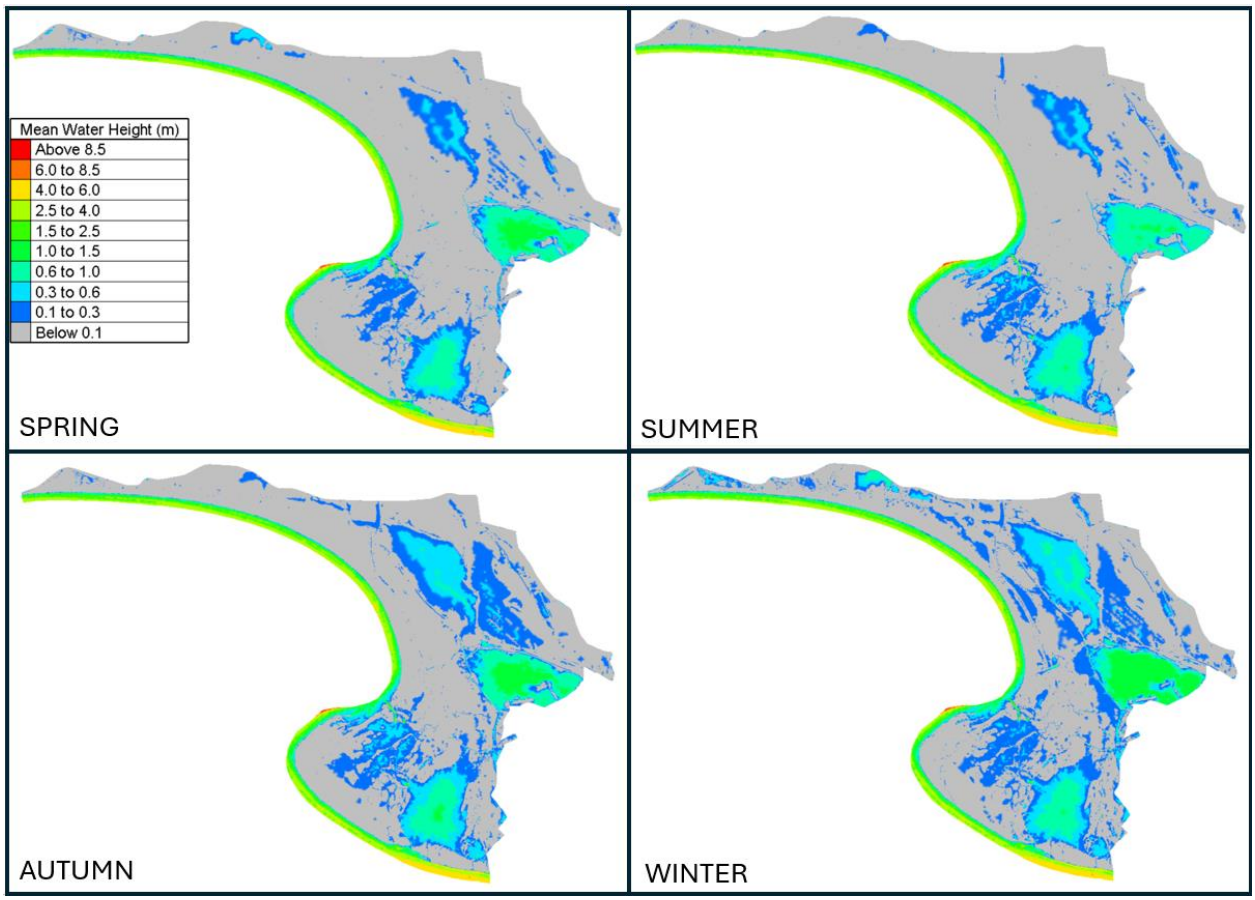

Figure 12-16 Seasonal mean water height (m) for 2023 with restoration. Spring is considered from 1 Marsh to 31 May, Summer from 1 June to 31 august, Autumn from 1 September to 30 November and Winter from 1 December to 28 September.

On the contrary, some locations remain dry throughout the year, such as Enfore de la Vignolle Ouest and Est, while other are flooded only during the winter (Galabert 0, Galabert 1, Galabert 3 Figure 12-4).

Figure 12-17 illustrate the seasonal mean water height (m) for 2050 and 2100 according to RCP4.5 and RCP8.5 scenarios. As observed in Figure 19, water heights are higher in winter than in summer. However, their values are higher than 2023, regardless of the scenario. For example, water heights are between 0.1 m and 1 m in summer 2023 in Beauduc, between 0.3 m and 1.5 m in summer 2050 (RCP4.5) and until 2.5 m in summer 2100 (RCP8.5). This global increase in water heights is linked with the increase of flooded areas across different years and scenarios, as illustrated in Figure 12-17. A general trend is also observed with a decrease of annual/seasonal dry zone.

Concerning the sea-lagoon connections, Figure 12-16 shows one channel that remains flooded throughout 2023. In 2050, assuming the bathymetry remains identical to 2023, new channels are observed between the sea and the lagoons (Figure 12-17). In 2100, the overwash zone remains completely flooded throughout the year (Fig.17). Sea level rise generates an increase in the number of sea-lagoon connections and their sustainability, enhancing the volume of water transiting on the site to the inland dike.

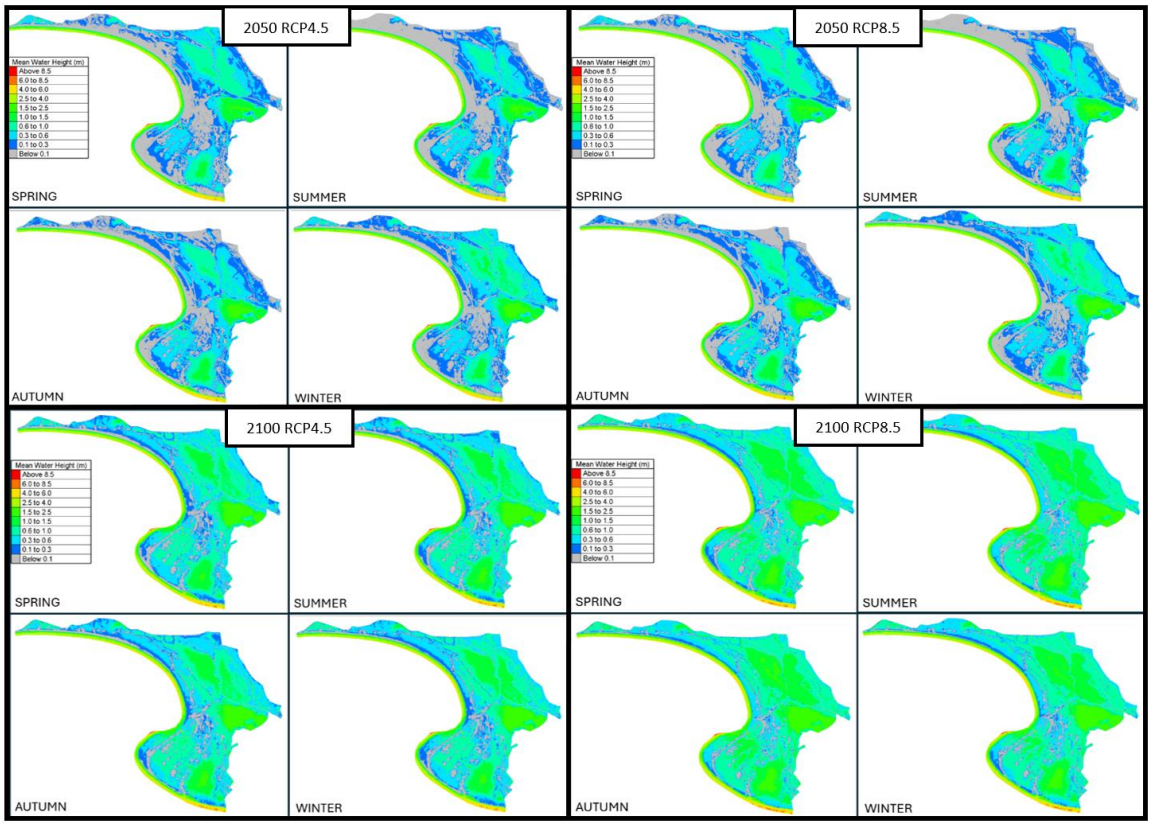

Figure 12-17 Seasonal mean water height (m) for 2050 and 2100, with RCP4.5 and RCP8.5 scenarios, with restoration. Spring is considered from 1 Marsh to 31 May, Summer from 1 June to 31 1ugust, Autumn from 1 September to 30 November and Winter from 1 December to 28 September.

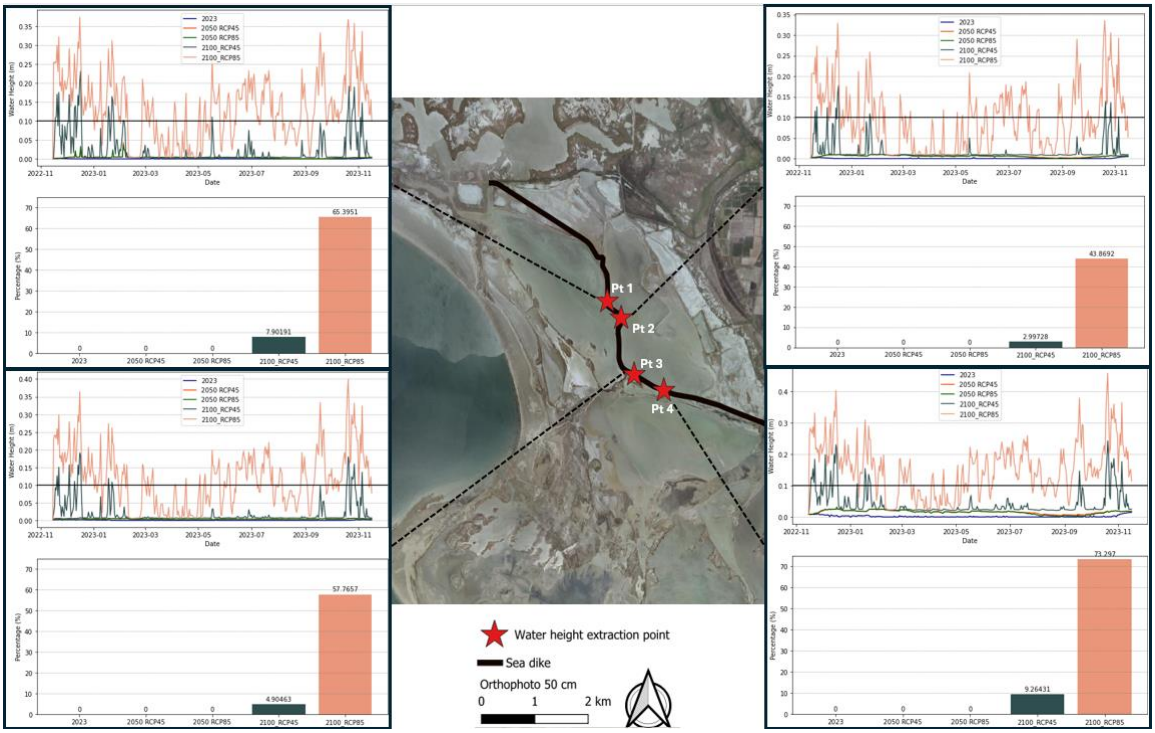

Figure 12-18 Timeseries of the water height in 4 points for both present and future conditions, and histograms showing the percentage of time for which the water height is superior at 0.1 m at these points. The latter are located on the lowest areas of the sea dike. 2023 results are shown with blue lines, 2050 RCP4.5 with orange lines, 2050 RCP8.5 with green lines,

Figure 12-18 displays the water height in 4 points located on the crest of the sea dike, for both current and future conditions, to evaluate the overflow flooding, i.e. an increase of the static water level of 0.1m (arbitrary threshold) above the dike level. Whatever the point, results indicate no overflow simulated in 2023 and 2050. However, by 2100, the dike will be submerged between 3% (point 2) and 9.2% (point 4) of the time under RCP4.5 and 43.9% (point 2) and 73.3% (point 4) under RCP8.5. In 2100, there is an increase from 8% (point 1 and 4) to 15% of submersion episodes depending on the scenarios, despite a sea level rise of only 0.18 m. Comparing these results with those observed in Figure 12-16 and Figure 12-17 suggests that the flooding produced behind the sea dike in 2050 (whatever the scenario) is only induced by an opening of the hydraulic structures (PRT1.1, FG2.1, FG1.1, GA2.2 North and South, see Figure 12-4) during the simulation.

To conclude, these results imply that sea level rise in the future will increase water levels in the lagoons, regardless of the season, thereby increasing the risk of inundation behind the inland dike. Without accounting for waves, these results may underestimate the potential flooding. So, it seems necessary to raise and reinforce the dike to prevent more frequent flooding episodes.

Regarding salinity, it can be observed that the restoration project implemented on the Rhône delta pilot site has resulted in salinity variations that are smoother (ESS Hydro-saline regulation) over the year than those that would have been observed without restoration (Figure 12-19). It is important, however, that there are always significant variations in salinity on the site, which is one of the objectives of the management plan, as salinity levels must respect the variations typically observed in Mediterranean habitats. This is the case with the salinities obtained with the restoration project.

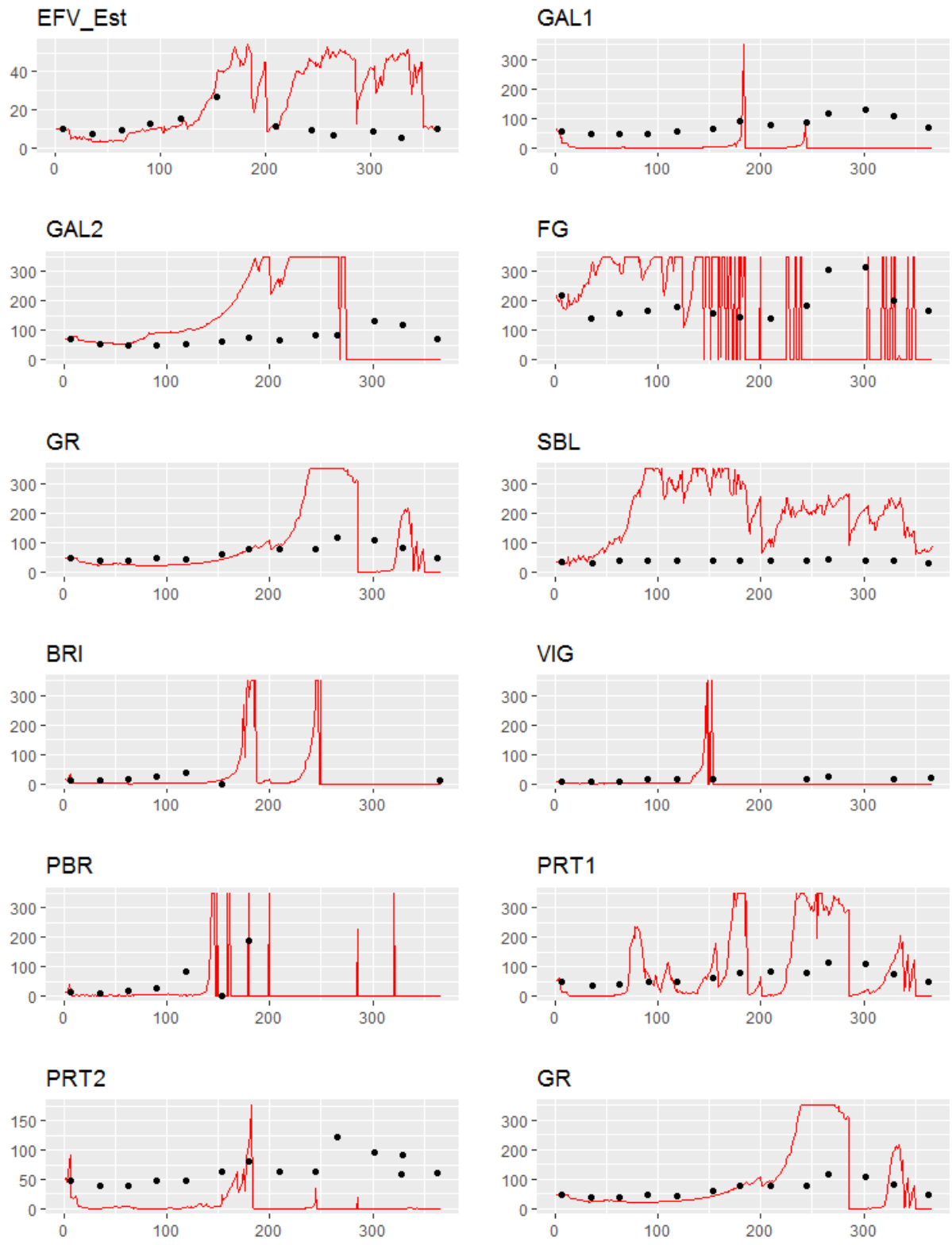

Figure 12-19 Daily average simulated salinity (red line) in 2023 for the non-restoration scenario, in combination with the field data of 2023 (black dots), corresponding to the situation with the restoration project implemented. A salinity of zero indicates an absence of water.

Food (fish) provisioning

One of the objectives of the restauration project is to reduce the damage risk of main dykes, especially the sea dike (Figure 12-1). In terms of ecosystem services, the purpose is to reduce the coastal flooding risk by dampening wave energy up-stream of the inland dike.

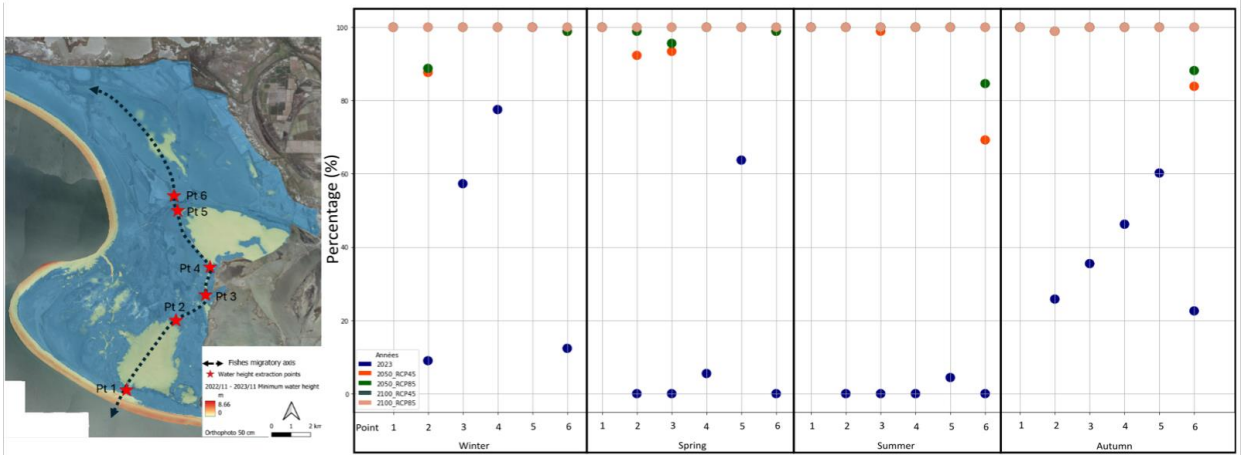

Figure 12-20 Diagram showing the seasonal percentage of time for which the water height is higher than 0.3 m for both current and futures conditions at 6 points located on the fish migratory axis. It is for these points that the water height is the lowest on migratory axis during all of 2023. These calculations are made from seasonal mean water height of each scenario. 2023 results are shown with blue points, 2050 RCP4.5 with orange points, 2050 RCP8.5 with green points, 2100 RCP4.5 with green lines and 2100 RCP8.5 with salmon points.

The seasonal mean water height (m) at the site for 2023 is represented in Figure 12-16. The results show that the lower water heights are simulated in summer (maximum of 1.5 meters in Grand Rascaillan lagoon), while higher water heights occur in winter with values which can reach 2.5 meters (in Grand Rascaillan lagoon). Several areas such as Sablon, Beauduc, Grand Rascaillan and Galabert 2 (see Figure 12-4 for the location of these lagoons) are always flooded, while others, like Pourtour 2 and Fangassier, are dry only in summer.

On the contrary, some locations remain dry throughout the year, such as Enfore de la Vignolle Ouest and Est, while other are flooded only during the winter (Galabert 0, Galabert 1, Galabert 3, Figure 12-4).

Figure 12-20 illustrates a significant increase in the percentage of time flooded for selected climate scenarios regardless the specific point or season. In fact, while the migratory axis is more often dry than flooded in 2023 for most points and seasons, the simulations indicate a rise of the flooding duration that can reach 100% for all points in 2100 with RCP8.5. For instance, point 3 is dry 42% of time in winter and around 100% in summer. Simulations suggest that this area will be consistently flooded in both seasons by 2050 and 2100 under the selected scenarios. At point 1, the results show that the area will be consistently flooded year-round regardless of the season and scenario.

These results suggest that the frontal sea dike maintenance shutdown have a good impact on hydro-biological connexion between the sea and the site. But the restauration works which consisted of creating openings between the lagoons prove to be insufficient in current conditions. So, the positive impact is currently limited but tend to be improve in the future, regardless the scenario.

Coastal erosion and flooding risk (submersion)

This section presents the results from morphodynamic modeling of the overwash platform south of Beauduc Pond in the context of restoration. Figure 12-21 illustrates the morphological evolution at the end of a 4-days storm simulation using XBeach, for each scenario (SLR + storms). The differential analysis highlights areas of erosion (in blue) and accretion (in red).

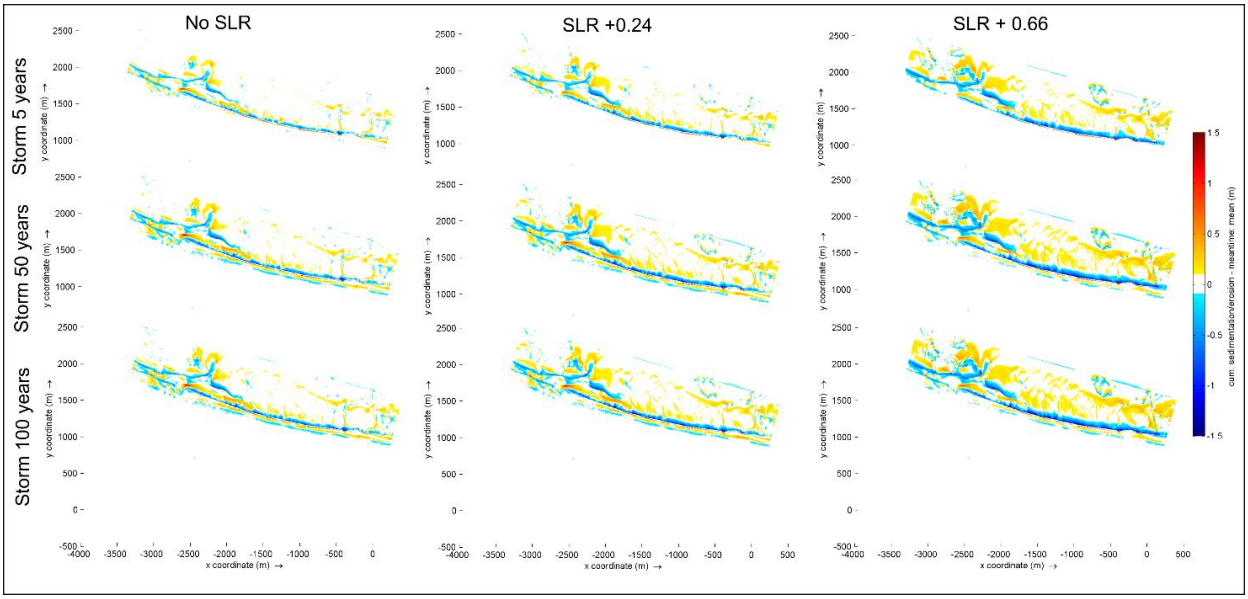

Figure 12-21 Differential of DEM for scenarios of SLR and storms, with restoration scenario corresponding to the actual morphology (2022).

Across all simulations, significant changes occur in the inlet, west of the beach. The dynamics of the inlet tend to retreat landward, characterized by frontal erosion and backward deposition. A longshore bar forms at the inlet entrance, behind the dike, due to reduced flow as a result of dike protection. A channel is incised, marked by erosion from the sea to the lagoon. Sediments are deposited in the lagoon, forming a flood delta. This indicates a flood-dominated inlet, with strong flows from the sea due to storm conditions and an increase in onshore water levels. In this case, there is no surge from the lagoon during storm events because most of the water input comes from sea flooding into the lagoons.

Changes on the overwash platform begin to occur with no SLR and a 50- to 100-year return period of storms, with deposition at the landward limit of the overwash platform. However, more significant changes occur at a storm scale in scenarios with 0.66 m SLR (Figure 12-21). Notable depositions are observed across the entire platform surface, with two main accumulation areas: surrounding the inlet and at the limit of the platform. This results in a total volume of sediment of 270k m^3. This indicates aggradation of the overwash platform. The main driver is the water level (due to storm or SLR) that allows possibility of sediment transport.

The magnitude of overwash platform deposition is also associated with erosion occurring along the shore, on the landside of the dike. Due to wave overtopping of the dike (Figure 12-22), an erosion channel forms behind the dike, leading to the progressive disconnection of the overwash platform from the dike.

In the transects shown in Figure 12-22, the +0.66 m SLR scenario combined with a 100-year return period storm results in the complete flooding of the overwash platform. This significantly increase the storm impacts, as the combination of higher sea level and wave energy, reducing the wave damping effect provided

Figure 12-22 Water level and Hs along one profil of scenarios with restoration (2022), for a return period storm of 100years, at different time steps of initial stage and during storm, with case of no SLR and SLR of 0.66 cm increase.

by the dike and the sandy barrier. This explains the magnitude of erosion observed at the dike, as well as the increased capacity to transport sediments landward.

12.3.4. Effect of upscaling on effectiveness of interventions (on ESS)

The restoration project implemented on the Rhône delta pilot site has resulted in the establishment of hydro-saline conditions favourable to fish migration, with the maintenance of hydrobiological continuity at key periods of the year for several species of fish. Through concerted management of a hydraulic structure linking the REST-COAST pilot site to a system of lagoons in the centre of the Rhône delta ("the Vaccarès lagoon System, in yellow on Figure 12-1), it will be possible to extend the benefits of the REST-COAST restoration project to these lagoons.

In addition, the Vaccarès Lagoon System is subject to major problems of hypersalinity (Boutron et al., 2021). The new hydro-saline conditions at the REST-COAST pilot site, made possible by the restoration project, are

a new possibility to solve this problem of hypersalinity, and will have to be concerted locally through the management of the structure linking these two systems, or through the creation of new connections between them.

12.4. Discussion

The modelling tools developed for the Rhône delta pilot site as part of REST-COAST show that the site restoration project is positive overall for the following ecosystem services targeted by REST-COAST: Water quality purification (through hydro-saline regulation), Reduction of coastal flooding and erosion risks and Food (fish) provisioning. The restoration of natural hydro-sedimentary dynamics to the south of the site has created beach areas and water exchange, through inlets creation, between the site and the sea, enhancing the restoration of lagoon systems. Hydraulic connections, via topographically low points, exist on a south-north axis of the site, favoring fish migration. One fear that might have existed with the creation of this hydro-biological connection axis and the restoration of the lagoon system was an increase in the risk of flooding. The modelling results show that this is not the case at present time. With regard to climate projections, flood simulation results indicate that the site's internal dyke should be raised to take account of sea level rise. The raising of this dyke is currently being studied as part of a study by the French government into the adaptation of the coastline of the entire Rhone delta. The simulation results also show that the salinities obtained thanks to the restoration project now respect the variations typically observed in Mediterranean habitats, favoring their restauration and the dynamic of fish.

The successful assessment of inundation and erosion risks along coastlines requires more comprehensive insights and discussions, especially when evaluating long-term strategies. The decision to abandon the seafront dike has introduced greater coastal dynamics, leading to increased shoreline retreat and a negative erosion trend in the sediment budget. Rather than relying solely on quantitative indicators, the situation should be evaluated with a focus on the potential for adaptation and mitigation of climate change and sea level rise impacts. Our modeling results indicate that the new barrier system has the potential to withstand extreme events through constructive processes and sediment mobility, promoting aggradation on the overwash platform. This sediment mobility is a key indicator of resilience. In contrast, the dike scenario showed reduced sediment mobility on the upper shoreface and less immediate erosion, but led to significant scouring and erosion along the nearshore, making it unsustainable in the long term. Given the short-term morphological approach provided by XBeach, the results, particularly for scenarios involving dike removal and rising water levels due to sea level rise, should be interpreted as indicative trends rather than precise quantitative outcomes. In this long-term evolution scenario, the equilibrium profile is not maintained, and our analysis is based on the current static profile.

12.5. On this chapter of the deliverable in relation D2.2.

This deliverable presents the models developed to simulate the morphodynamics and hydro-saline dynamics of the Rhône delta pilot site, and their use to estimate the consequences of the restoration project (present time and climate scenarios) on several ecosystem services targeted by REST-COAST: Water quality purification (through hydro-saline regulation), Reduction of coastal flooding and erosion risks, Food (fish) provisioning.

The models presented were calibrated and validated against in-situ data in a previous REST-COAST phase. However, this information, as well as the detailed presentation of the model equations, was not included in deliverable 2.2 due to the unplanned termination of a PhD during its second year, which caused a delay in the results presented.

In addition to the information required for deliverable 2.3, this chapter for the Rhône delta therefore also summarizes additional information relating to the calibration and validation of the models, such as the performance criteria obtained, shown in Annexes.

12.6. References

Boutron, O., Bertrand, O., Fiandrino, A., Höhener, P., Sandoz, A., Cherain, Y., Coulet, E., & Chauvelon, P. (2015). An Unstructured Numerical Model to Study Wind-Driven Circulation Patterns in a Managed Coastal Mediterranean Wetland: The Vaccarès Lagoon System. Water, 7(11), 5986-6016. https://doi.org/10.3390/w7115986

Boutron, O., Paugam, C., Luna-Laurent, E., Chauvelon, P., Sous, D., Rey, V., Meulé, S., Chérain, Y., Cheiron, A., Migne, E., 2021. Hydro-Saline Dynamics of a Shallow Mediterranean Coastal Lagoon: Complementary Information from Short and Long Term Monitoring. JMSE 9, 701. https://doi.org/10.3390/jmse9070701

DAVID A. ANATI. The salinity of hypersaline brines: Concepts and Misconceptions. International Journal of Salt Lake Research 8: 55-70, 1999.

Deltares. (2023). Xbeach documentation. Delft University of Technology

De Vet, P. (2014). Modelling sediment transport and morphology during overwash and breaching events.

Hargrove, W. W., Hoffman, F. M., & Hessburg, P. F. (2006). Mapcurves: A quantitative method for comparing categorical maps. Journal of Geographical Systems, 8 (2), 187–208. https://doi.org/10.1007/s10109-006-0025-x

Holthuijsen, L., Booij, N., & Herbers, T. (1989). A prediction model for stationary, short-crested waves in shallow water with ambient currents. Coastal Engineering, 13 (1), 23–54. https://doi.org/https://doi.org/10.1016/0378-3839(89)90031-8

Le Menn M., Naïr R., 2022. Review of acoustical and optical techniques to measure absolute salinity of seawater. Frontiers in Marine Science, 9, 1031824.

Mor Z., Lutzky H., Shalev E., Lensky N.G., 2021. Hydrostatic densitometer for monitoring density in freshwater to hypersaline water bodies. Water, 13 (13), 1842.

Parc naturel régional de Camargue, Tour du Valat, Société nationale de protection de la nature & CPIE Rhône Pays d'Arles, 2022. Plan de gestion des Etangs et marais des salins de Camargue 2023 – 2032. Volet 1 : Etat des lieux – diagnostic. Rapport pour le Conservatoire du littoral.

Penman, H. L. (1948). Natural evaporation from open water, bare soil and grass. Proceedings of the Royal Society of London. Series A. Mathematical and Physical Sciences, 193(1032), 120-145.

Unesco. Joint Panel on Oceanographic Tables and Standards. International Oceanographic Tables: Volume 3; Unesco: Paris, France, 1981.

IPCC SIXTH ASSESSMENT REPORT (AR6) "CLIMATE CHANGE 2023" (https://www.ipcc.ch/report/ar1/wg1/sea-level-rise/), 2023

OpenTELEMAC. (2023, 30 décembre). EDF FR. https://www.edf.fr/groupe-edf/inventer-l-avenir-de-l-energie/r-d-un-savoir-faire-mondial/nos-offres/codes-de-calcul/opentelemac

Penman, H. L. (1948). Natural evaporation from open water, bare soil and grass. Proceedings of the Royal Society of London. Series A. Mathematical and Physical Sciences, 193(1032), 120-145.

Phillips, O. M. (1977). The dynamics of the upper ocean.

Roelvink, J. (1993). Dissipation in random wave groups incident on a beach. Coastal Engineering, 19 (1-2), 127–150.

Sanchez-Artus, X., Subbiah, B., Gracia, V., Espino, M., Grifoll, M., Espanya, A., & S´anchez-Arcilla, A.(2024). Evaluating barrier beach protection with numerical modelling. a practical case. Coastal Engineering, 191, 104522.

Smolders, S., Leroy, A., Teles, M. J., & Vanlede, J. (2016). Culverts modelling in TELEMAC-2D and TELEMAC-3D. ResearchGate. https://www.researchgate.net/publication/309136136_Culverts_modelling_in_TELEMAC-2D_and_TELEMAC-3D

Van Rhee, C. (2010). Sediment entrainment at high flow velocity. Journal of hydraulic engineering, 136 (9), 572–582.

Winterwerp, J. C., & Van Kesteren, W. G. (2004). Introduction to the physics of cohesive sediment dynamics in the marine environment. Elsevier.

13. A Synthesis of Restoration Strategies

van Maren, D.S.[1,2], Marijnissen, R.J.C.[1]

1 Department of Marine and Coastal Systems, Deltares, Delft, The Netherlands

2 Faculty of Civil Engineering and Geosciences, Delft University of Technology, Delft, The Netherlands

13.1. Introduction

In this portfolio of restoration strategies, we have collected a range of model-based predictions assessing how implementation of Nature-based Solutions (NbS) on a larger scale strengthen Eco System Services (ESS) within a range of coastal systems – now and in the future for a range of Sea Level Rise (SLR) scenarios. This synthesis integrates these findings, focusing on (1) the restoration strategies numerically evaluated as part of the REST-COAST project, (2) how these strategies and implemented and Ecosystem Services evaluated, (3) the predicted present-day effectiveness of NbS on ESS, and (4) the role of NbS in mitigating adverse effects of climate change, notably SLR.

13.2. Portfolio of restoration strategies

Seagrass restoration

The most widely applied restoration strategy is Sea grass restoration (see also Table 1.1), which is implemented in Foros Bay, Arcachon Bay, the Wadden Sea, Venice Lagoon, and Sicily Lagoon. The way the seagrass is restored differs greatly across the pilots. Seagrass in Foros Bay is restored by eliminating its most important stressor (macro algae coverage) and by transplanting seagrass sods. In Arcachon Bay the restoration of seagrass is achieved by attenuating tidal currents by means of a biomimetic device. No actual pilot experiments were done in the Wadden Sea but in several locations in the Wadden Sea spontaneous recovery of seagrass was observed, probably in response to increasing water quality. In Venice Lagoon, feasibility of seagrasses is based on historical seagrass restoration efforts. In the numerical models, seagrass is in all cases 'restored' by adding a numerical representation of seagrass to the model.

Sediment management

The second most widely applied restoration strategy is sediment management. It is implemented in Sicily and Ebro delta in the form of a beach nourishment, aiming to reduce erosion rates and flood risks. In the Ebro delta also alternating dunes were digitally experimented with as a potential restoration strategy. In the Ebro River, strategies have been explored to revitalise the sediment supply through the various reservoirs to nourish the sediment-depleted Ebro River delta. A completely different type of sediment management is sediment extraction (bringing sediment dredged from harbours on land) – this is practiced in the Ems estuary in order to reduce the turbidity in the estuary. Sediment extraction is already being implemented, and REST-COAST is especially concerned with scaling up extraction through numerical experiments

Salt marsh restoration

Salt marsh restoration was investigated in the Ems Estuary (Ley Bay in Chapter 5 and Dollard Bay in Chapter 6). The Dollard Bay restoration aligns with ongoing efforts, with construction of wave damping structures in an advanced stage of planning. Salt marsh restoration is discussed as part of the Venice lagoon pilot as a sink of nutrients, reducing hypoxia events.

Restoring hydraulic connectivity

The Rhone delta is a former salt pond which is restored by managed realignment in combination with restoration of hydraulic connectivity (opening of dikes, dredging of channels). In Venice lagoon the restoration of hydraulic connectivity is especially targeting more riparian vegetation to take up nutrients.

Other
Several restoration options are only implemented in one specific pilot area, which are briefly discussed here. These solutions include

- Revegetation of dunes (Sicily) in order to reduce erosion rates of the dunes during storms.
- Creation of a bird island for biodiversity gains (Vistula lagoon): an island was created using dredge spoil from nearby capital dredging. The ESS served with this restoration is to provide hatching grounds for birds.
- Converting polders to wetland (Ems estuary) in order to reduce turbidity in the estuary while at the same time raising low-lying land adjacent to the estuary.

13.3. Implementation of restoration strategies

13.3.1. Numerical approach

The most commonly used platform to implement restoration strategies are X-Beach (Jade Bay, Ebro Delta, Sicily pilot, Foros Bay, Rhone Delta) and Delft3D (Ems Estuary, Ley Bay, Foros Bay, Arcachon Bay). Other model platforms include Telemac (Rhone Delta), Schism (Jade Bay) and Shyfem (Venice Lagoon). Herein X-Beach is typically used to compute erosion rates during storm conditions, sometimes also to assess flood safety as well. Delft3D and Schism are used for longer-term sediment dynamics influenced by tides and storms; Telemac and Shyfem have mainly been applied to analyse hydrodynamics.

Vegetation effects are modelled in the Ems Estuary (Dollard and Ley Bay) and Arcachon Bay following the method of Baptist (2005) jointly increasing the flow resistance and bed roughness – this approach was specifically developed to combined vegetation patches with morphodynamic changes. All three pilots use Delft3D as modelling platform. The various X-beach applications (Sicily, Foros) do not specify which vegetation model was applied. In the Wadden Sea (Jade Bay) seagrasses are modelled with SCHISM, using an additional drag term in the Navier-Stokes equation as well as an additional source of turbulent kinetic energy (Zhang et al., 2020). Hydrodynamic modelling in the Rhone delta is done using Telemac to provide salinity changes and with X-beach to compute erosion and flooding.

Most modelling approaches specify an area in which a certain vegetation type exists as part of the numerical restoration. In Sicily, an existing patch of seagrass was numerically enlarged as part of a limited seagrass restoration effort and strongly extended as part of an upscaling plan. Large parts of the intertidal zone are converted to Seagrass in the Jade Bay study, while large areas are numerically converted to salt marsh in the Ley Bay pilot. In contrast, vegetation characteristics were modelled dynamically in the Dollard Bay application of the Ems Estuary. Whether vegetation occurs in an area is based on the inundation frequency, calibrated against the present distribution of salt marsh and present-day inundation frequency. The inundation frequency changes as sediment deposits and sealevels rise. Based on the change in inundation frequency, the distribution of salt marshes changes over time. Salt marsh restoration was implemented in the Dollard Bay by numerically implementing structures which reduce wave heights, thereby promote sedimentation, hence resulting in the development of salt marshes.

In the Venice lagoon a hydrodynamic model coupled with a water quality model (SHYFEM-BFM) is used to compute various water quality scenarios (with / without SLR). A hybrid bio-chemical machine-learning (ML) technique is applied to relate hypoxia events to hydrodynamic forcing, and through this predict the occurrence of hypoxia under climate change (sealevels, temperature) conditions.

The sediment transport regimes in the Ebro River were explored by prescribing a rating curve (relating sediment transport to river discharge) based on 19th century observations to a fluvial morphodynamic model of the Ebro River.

13.3.2. Definition of Ecosystem Services

A range of Eco System Services (ESS) were evaluated for the various numerical models. With the large variation in pilots (hence processes and restoration purposes) the variability of ESS is large as well. On a high aggregation level the computed ecosystem services are fairly similar across the various pilots (improving water quality' or 'reduce flooding') but on a more detailed level the definition of relevant ESS was more variable.

Water quality improvement

Water quality improvement as an ESS focused on residence times (Arcachon Bay), Hypoxia (Venice), or turbidity (Ems Estuary, Arcachon Bay). Especially in the Ems Estuary the high turbidity is the main reason for which mitigating measures are being developed. In Arcachon Bay dredging volumes were considered to negatively influencing water quality through contaminants which adhere to the dredge spoil being released in the water column during dredging. As such, reduction of sedimentation in channels is evaluated as an ESS influencing water quality. In the Rhone delta, water purification is the main ESS to restore, aiming at reducing the salinity in a previously hypersaline salt pond.

Flood risk reduction

Flood risk was assessed for conditions during extreme storms in the Wadden Sea. The Schism-based model study in Jade Bay computed the maximum, mean and 95 quantile of extreme water level setup and wave height whereas the Delft3D-based model study in the Ems Estuary evaluated the change in significant wave height H_s during two selected storms. Storm surge levels and maximum wave height (changes) were evaluated for Arcachon Bay. The X-beach model developed for the Rhone delta evaluates (changes in) seasonally average wave heights in combination with the fraction of time a certain critical water level is exceeded. Only for the Sicily pilot the actual areas of flooded land was computed using an X-BEACH model including flood-prone areas. A flood reduction efficiency (by restoration) was defined for the entire coastal zone, but also for urban areas only.

Reduction of Erosion

Bed level changes were evaluated as shoreline changes (Sicily pilot), channel infill volumes (Arcachon Bay), erosion volumes / areas (Foros Bay, Ebro Delta, Ley Bay, Ems Estuary), erosion – sedimentation maps (Rhone delta, Arcachon Bay, Ley Bay), and changing Ecotope maps (Jade Bay, Ems Estuary, Sicily pilot). However, the changes in bed level controlled many other ESS such as carbon sequestration (Ems Estuary), Flood risk reduction (all), water quality improvement (Arcachon Bay).

Climate change regulation

Only the Ems Estuary pilot site assesses climate change regulation in the form of Carbon Sequestration. Based on field data a relationship was established between Carbon content and sedimentation rates, allowing modelled sedimentation rates to be converted to Carbon sequestration.

Food (fish) provisioning

The Rhone delta pilot included food provisioning by improving migratory fish routes through excavation of channels and removal of dikes, and evaluated their effectiveness by computing the percentage of time these migratory routes are inundated. The turbidity is grouped under water quality in the Ems Estuary case, but it should be noted that the main reason underlying the restoration efforts to reduce turbidity is the negative ecological impact of the high turbidity on algae growth and therefore food production.

Ecotope maps

Ecotope maps convert model output into a representation of current and/or future ecotopes. Interpretation of such maps (or its results in tabulated form) yield information of ecological impact of NbS and climate change. Such an approach was followed in various Wadden Sea cases (Jade Bay, Ems Estuary).

13.4. Demonstration of the effectiveness of NbS in improving ESS

Ebro River and delta (chapters 2, 3)
The restoration strategies in the Ebro River and delta strongly reflect the area's prolonged sediment starvation resulting from upstream dams in the Ebro River. Sediment transport regime in the Ebro river was numerically restored to pre-damming conditions, by definition bringing sediment back to the Ebro delta in large quantities. The two sediment management strategies in the delta (nourishing sediment underwater or creation of dunes above water) successfully mitigating flooding and erosion.

Jade Bay (Wadden Sea, chapter 4)
An upper range of the effect of seagrass on hydrodynamics was assessed for the Jade Bay, by prescribing seagrass throughout the intertidal area of the German Bight and most of Jade Bay. For such conditions, seagrass restoration greatly reduced the bed shear stress (45%), erosion flux (80%), and significant wave height (50%).

Ems Estuary (Wadden Sea, chapters 5, 6)
The most straightforward impact of restoration measures in the Ems Estuary is sediment extraction – this led to a clear reduction in turbidity and hence improvement of water quality. This solution is limitedly influenced by sea level rise. Measures aiming at promoting salt marsh growth reduce flood risks (Dollard Bay and Ley Bay). The Ley Bay pilot demonstrates that restoration of salt marshes stabilizes the bed (less erosion and less deposition), and that this dampening effect becomes more pronounced as sea levels rise. The ESS of other restoration strategies are more subtle. Typically, measures that improve water quality (extraction, but also wetland creation) reduce coastal flooding (because the sediment is stored elsewhere). At the same time, sediment that is extracted may be used for constructing dikes or raise land landward of the dikes (which is essentially also what happens with the wetland conversion scenario). Over longer timescales such developments contribute to flood protection, but as part of the current safety evaluation method extraction and wetland construction reduce flood safety.

Venice lagoon (chapter 7)
Restoration efforts aiming at minimizing hypoxia focus on uptake of nutrients in riparian buffers (transition between the fluvial and marine environment), seagrass meadows and salt marshes. These restoration efforts have not been explicitly modelled but its relationships with nutrient uptake are well known.

Arcachon Bay (chapter 8)
Seagrass restoration reduces the turbidity over the tidal flats of Arcachon Bay but also sedimentation rates in the tidal channels resulting from higher flow velocities. Sedimentation rates over some of the flat areas reduce, possibly because there is less tidal transport while in others it increases (more efficient trapping). Lower channel sedimentation reduces maintenance dredging rates, which also leads to lower turbidity levels. Restoration also strengthens refresh rates of water, which is important for tourism in the area.

Sicily pilot (chapter 9)
Using an X-beach model, the Sicily pilot was the only case explicitly computing flooding of land during storms. The effectiveness of seagrass restoration depends on the scale, with minor seagrass restoration only limitedly mitigating flooding, but upscaling of restoration proving more effective. Dune revegetation is more efficient

in preventing flooding than the limited seagrass restoration, but less than upscaled seagrass restoration. Most efficient in preventing flooding, however, was a beach nourishment.

Foros Bay (chapter Error! Reference source not found.**)**
Seagrass does not influence flood risk but does reduce erosion rates in Foros Bay. Most of the erosion rate reduction results from seagrass meadows already present. Restoring seagrass (extending the existing meadows) leads to a reduction in erosional areas. However, the total erosion volume is only slightly influenced because in the existing situation only a thin layer of sediment was eroded from the restored areas.

Vistula lagoon (chapter 11)
An island was created using dredge spoil from nearby capital dredging. The ESS served with this restoration is to provide hatching grounds for birds.

Rhone Delta (chapter12)
Restoration of hydraulic connectivity resulted in a much smoother salinity distribution in the Rhone delta pilot, with a sharp decrease in extreme salinity values. This improved the ESS food provisioning. Managed realignment reduced flood risks and coastline erosion rates, with restoration of connectivity not negatively influencing coastal safety (as was originally feared).

13.5. Role of restoration in mitigating climate change

The various pilots have implemented climate change effects. Most pilots primarily focus on sea level rise while Venice Lagoon additionally evaluates the change in temperature and the Ebro River is focused on precipitation changes. Adaptation to SLR was computed with the shared social-economic pathways 2-4.5 and 5-8.5 (Table 13-1). The exact rate of SLR mentioned by the various pilots may slightly differ because of the reference year (2020 in Table 13-1, others may use other reference years) and spatial variability in SLR. But overall, sea levels in the year 2100 are around 60 cm higher than in 2020 for ssp245 and 80 cm higher for ssp585.

Table 13-1 Median Sea-Level Rise Projections per shared social-economic pathway from Garner et al. (2021) for the location of Delfzijl (Ems Estuary), with 2020 as the year of reference and excluding vertical land motion.

Year	Sea-level rise scenario	
	SSP2-4.5	**SSP5-8.5**
2030	+0.12 m	+0.12 m
2050	+0.24 m	+0.26 m
2100	+0.58 m	+0.78 m

Seagrass restoration
Seagrass restoration strongly mitigated the adverse effects of climate change in the Wadden Sea. This positive outcome follows from the large-scale implementation of the seagrass. Although such large-scale restoration was motivated by observations of natural return of seagrass, it has not been verified to what extent such an extensive restoration effort is realistic in the Jade Bay and adjacent Wadden Sea. The importance of the scale of restoration is further illustrated with the Sicily pilot, showing that a small-scale restoration only limitedly reduces the adverse effects of SLR while larger-scale restoration efforts substantially reduce flood risks. A range of seagrass scenarios implemented in Arcachon Bay suggest that the degree of restoration influences the spatial distribution of the effectiveness of various ESS.

In Foros Bay the seagrass has a major influence in preventing erosion, also in case of SLR. SLR is predicted to strengthen erosion rates, but this erosion is much less when seagrass meadows are present. Restoring seagrass further reduced the erosion rates, especially in erosional areas but only slightly in terms of eroded volumes. These results suggest that the existing seagrass meadows should be carefully protected and possibly expanded. In the Sicily case, however, the restoration of seagrass has a limited impact on erosion mitigation (while it did reduced flooding, as discussed above).

SLR leads to more sedimentation and lower turbidity over the flats in Arcachon Bay. More sedimentation in the channels is unfavourable, as this requires more maintenance dredging which negatively influences the water quality. The negative effects on siltation in channels are partly mitigated by restoration of seagrass. Both seagrass and SLR reduce turbidity. SLR further decreases the refresh rate of water in some parts the bay while it may improve in other parts. With seagrass restoration typically improving the refresh rates, it provides a mitigating measure for SLR in some sections of Arcachon Bay.

Other restoration strategies
Nourishing sediment proved effective for reducing flooding and erosion (Ebro Delta, Sicily pilot), especially under current conditions. However, under sea level rise also the restored sand dunes and the beach nourishment failed to effectively reduce flooding or erosion rates in the Ebro Delta. For SLR exceeding 60 cm larger interventions are needed that experimented with in the pilot.

Climate change will lead to a strong deterioration of water quality in the form of more hypoxia in Venice Lagoon, mostly under influence of rising temperatures. Mitigating measures in the form of more nutrient uptake in seagrasses, salt marshes or riparian vegetation are therefore crucial.

A counterintuitive response to sea level rise was predicted for the Ems Estuary. The increasing tidal prism resulting from drowning of intertidal areas strongly increased the landward sediment transport capacity, resulting in accelerated sedimentation as sea levels exceed a critical limit. Such a behaviour is not realistic, since the amount of available sediment is limited. It does indicate however, how SLR may influence the future up-estuary sediment transport capacity and illustrates how important sediment budgets will become in the future.

The managed realignment implemented in the Rhone delta provide a large amount of mobile sand. This mobile sand is re-arranged into a sandy barrier seaward of the current dike which offers protection against rising sea levels; especially during storms. There is no protection against the increase of average water levels though, resulting in an increase in time that critical water levels are exceeded.

13.6. Concluding remarks

The effect of implementation of NbS depends quite strongly per pilot, which is partly resulting from numerical implementation, but especially because of scenario definition. Jade Bay, for example, computes the effect of a very large-scale restoration effort which, obviously, has a larger impact than smaller-scale restoration efforts adding to existing seagrass meadows (Foros Bay). This effect of size was explicitly addressed in the Sicily pilot and Arcachon Bay, showing that the size of the restoration (of seagrass) is indeed important. Interestingly, seagrass mainly reduced flooding in Sicily (while limitedly reducing erosion) while the exact opposite was found for Foros Bay.

Also the way morphodynamics is handled throughout the various pilots differs. In most pilots the sediment is primarily locally redistributed, which does not necessarily mean bed level adaptation to SLR is correctly

taken into account. Such long-term bed level adaptation mechanisms were a key effort for the Ems Estuary modelling.

13.7. References

Baptist, M., 2005. Modelling floodplain biogeomorphology, PhD Dissertation, TU Delft library, http://resolver.tudelft.nl/uuid:b2739720-e2f6-40e2-b55f-1560f434cbee.

Zhang, Y. J., Gerdts, N., Ateljevich, E., & Nam, K. (2020). Simulating vegetation effects on flows in 3D using an unstructured grid model: Model development and validation. Ocean Dynamics, 70, 213-230. https://doi.org/10.1007/s10236-019-01333-8

Appendix A. Appendices belonging to Chapter 3: Barrier beach management under climate change scenarios. The Ebro Delta study case

Appendix A-I - Bed level impacts in +0.27 m SLR conditions

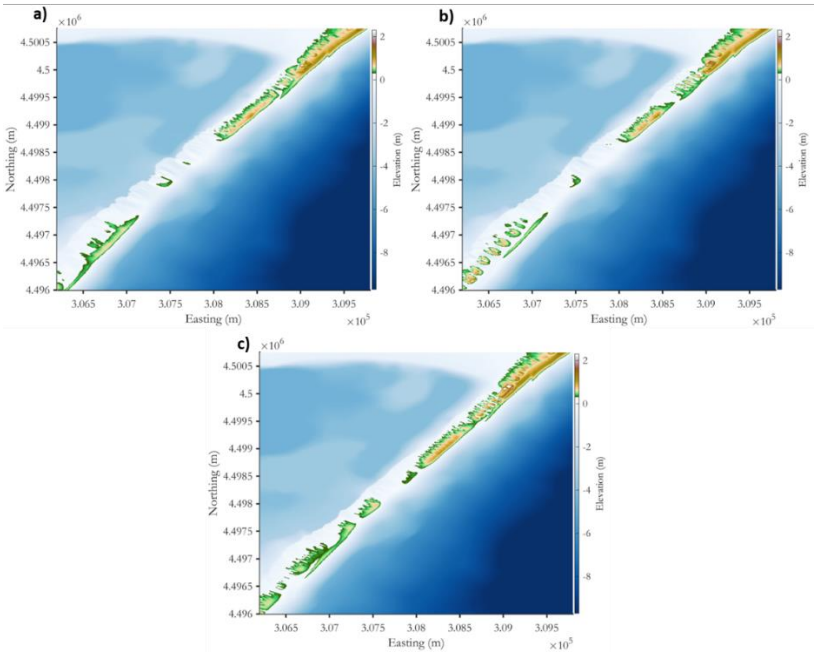

Appendices Figure A-1 Final bed level after storm Filomena in +0.27m SLR condition. a) No protection, b) Alternating dunes, and c) Classical nourishment

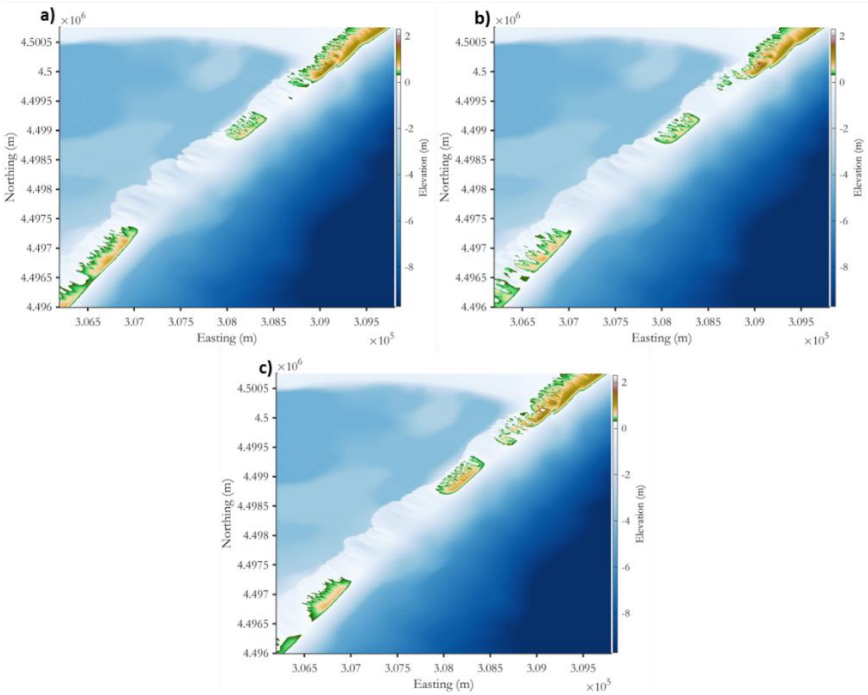

Appendices Figure A-2 Final bed level after storm Gloria in +0.27m SLR condition. a) No protection, b) Alternating dunes, and c) Classical nourishment

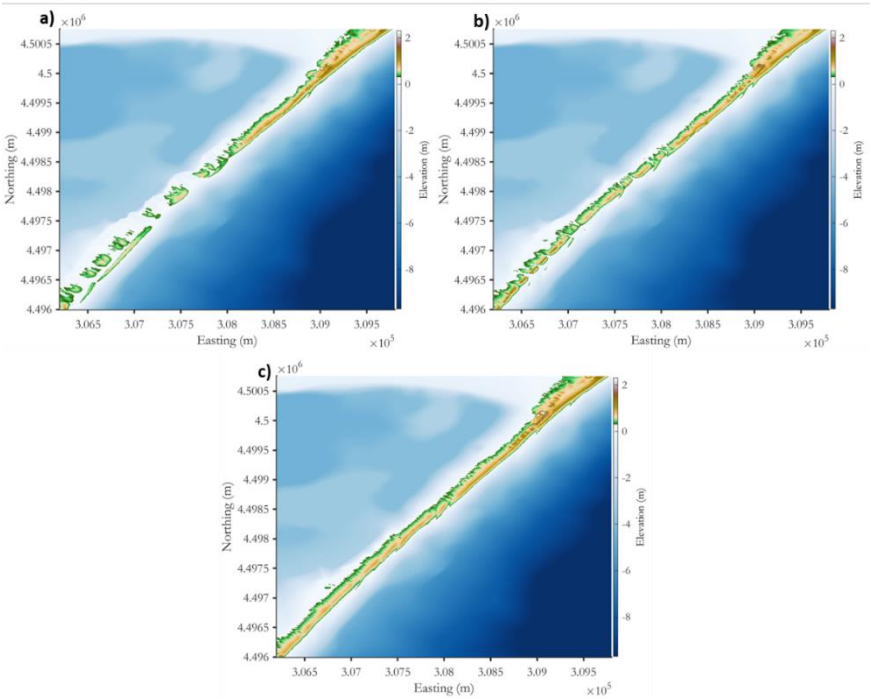

Appendices Figure A-3 Final bed level after storm Isaak in +0.27m SLR condition. a) No protection, b) Alternating dunes, and c) Classical nourishment

Appendix A-II - Bed level impacts in +0.57 m SLR conditions

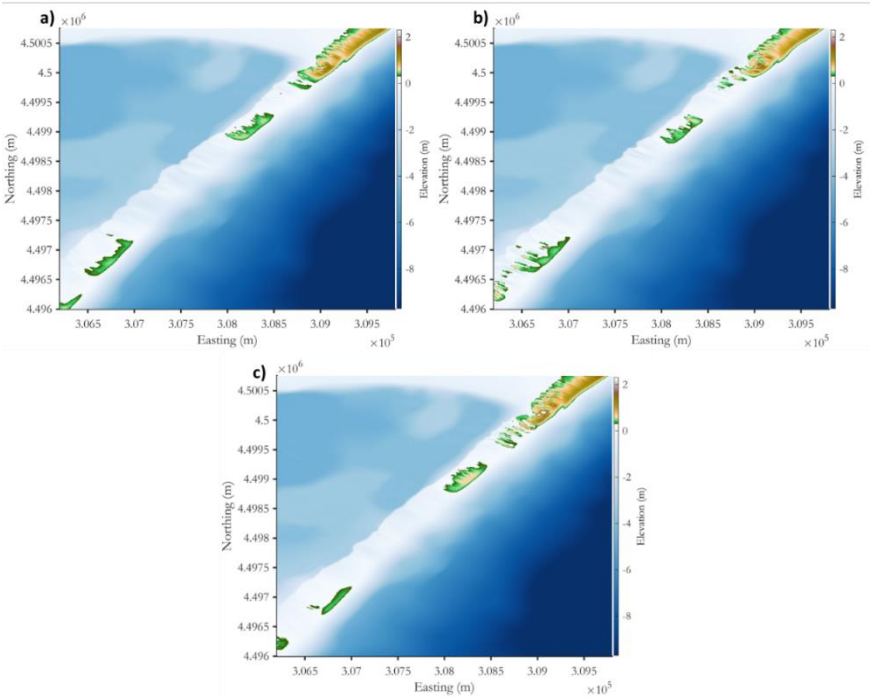

Appendices Figure A-4 Final bed level after storm Filomena in +0.57m SLR condition a) No protection, b) Alternating dunes, and c) Classical nourishment

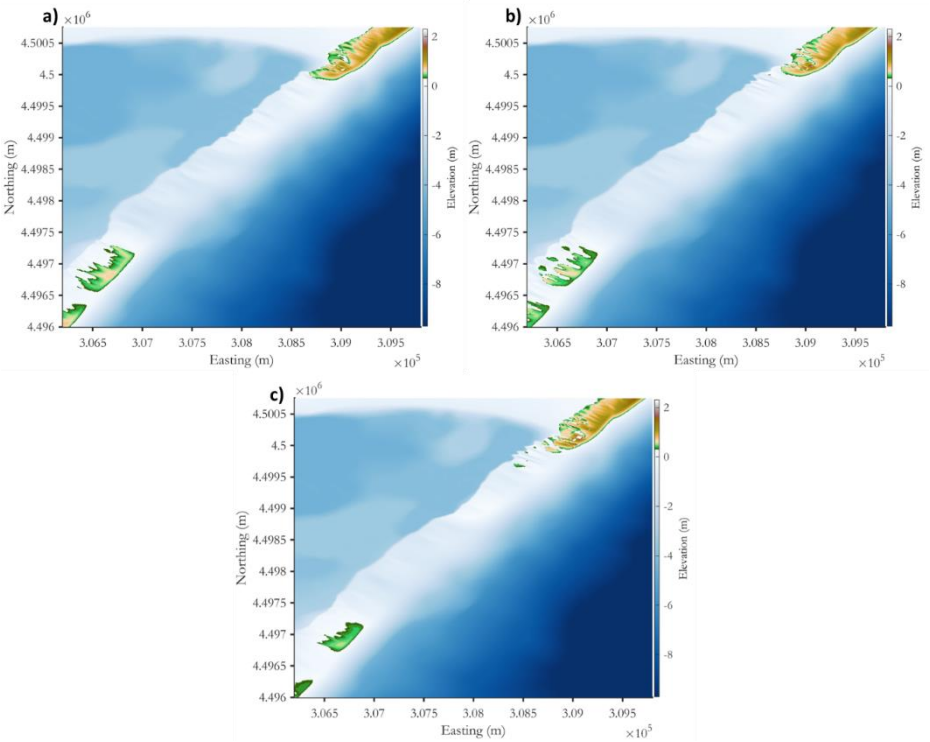

Appendices Figure A-5 Final bed level after storm Filomena in +0.57m SLR condition a) No protection, b) Alternating dunes, and c) Classical nourishment

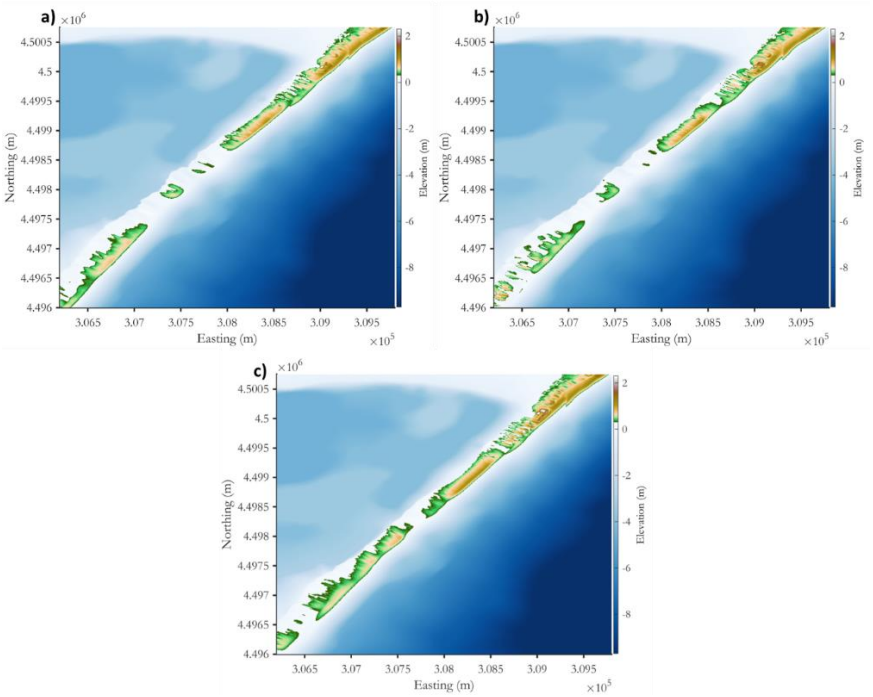

Appendices Figure A-6 Final bed level after storm Isaak in +0.57m SLR condition. a) No protection, b) Alternating dunes, and c) Classical nourishment

Appendix A-III - Bed level impacts in +0.75 m SLR conditions

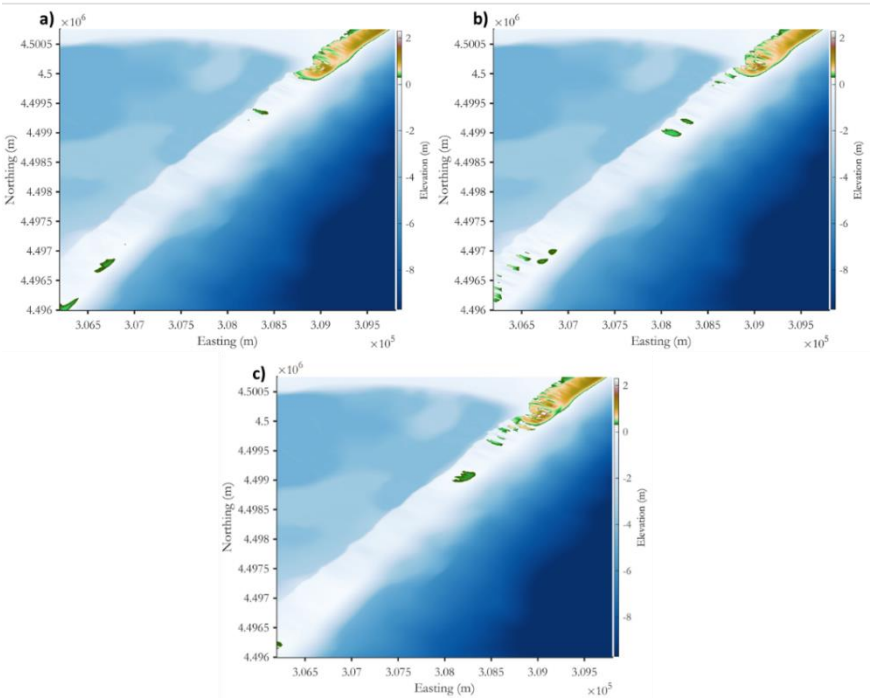

Appendices Figure A-7 Final bed level after storm Filomena in +0.75 m SLR condition. a) No protection, b) Alternating dunes, and c) Classical nourishment

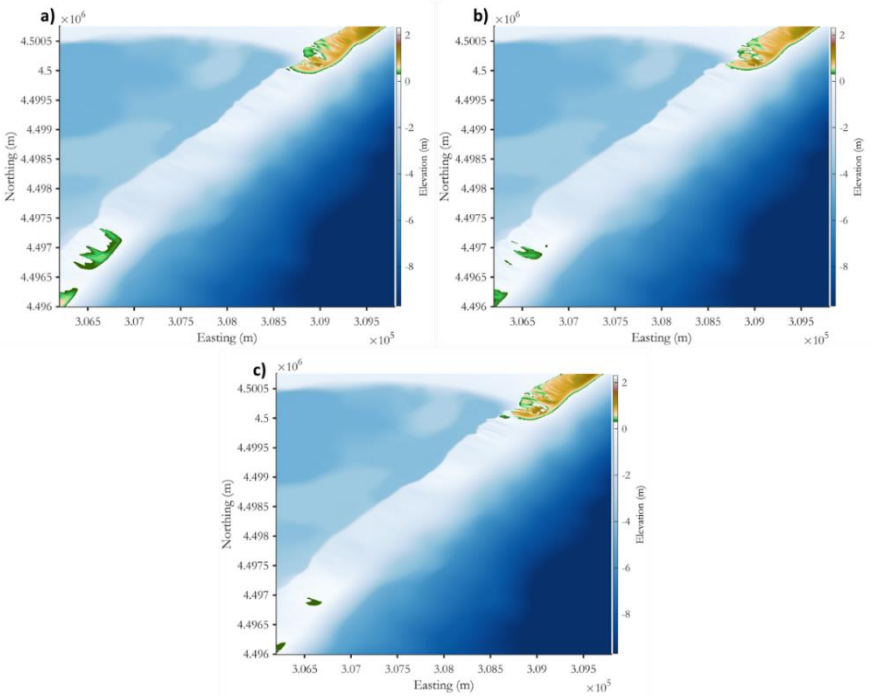

Appendices Figure A-8 Final bed level after storm Gloria in +0.75m SLR condition. a) No protection, b) Alternating dunes, and c) Classical nourishment

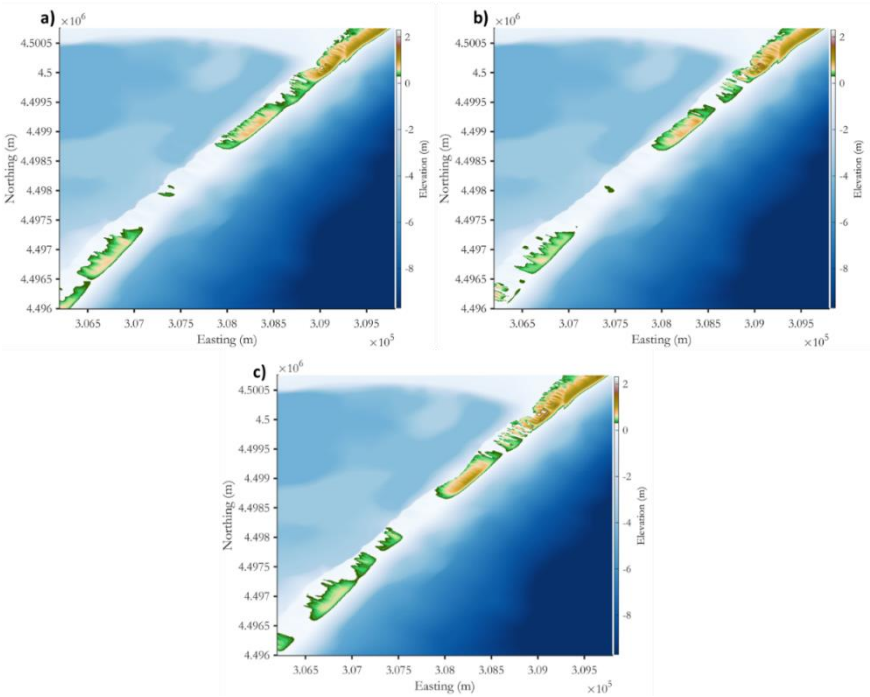

Appendices Figure A-9 . Final bed level after storm Isaak in +0.75m SLR condition. a) No protection, b) Alternating dunes, and c) Classical nourishment

Appendix B. Appendices belonging to Chapter 7: Matching restoration interventions with NbS upscaling for climate adaptation in the Venice lagoon based on hypoxia risk under present and future climate scenarios

Appendix B-I - Feature selection: Processes driving hypoxia

The oxygen cycle is driven by a network of biological, physical, and meteorological processes, whose imbalances may lead to hypoxic conditions, causing large-scale damage to aquatic life (Pena et al., 2010; Oschlies et al., 2018). In particular: i) surface water oxygen concentrations are substantially influenced by air-sea gas exchange, dependent on the gas saturation levels and water turbulence, both affected by temperature, as well as ii) oxygen production through photosynthesis by phytoplankton macroalgae, and macrophytes, and iii) oxygen sinks through the collective respiration by all the living marine species. In the deeper part of the water column, oxygen concentrations are impacted by iv) vertical transport, which depends on the levels of vertical mixing and the pycnocline, and v) respiration, especially by microbes remineralizing non-living organic matter at the bottom, or in the sediments. Finally, as most biogeochemical tracers, oxygen is also influenced by vi) water advection, and vii) diffusion processes.

Its occurrence is common in wetlands and estuaries driven by the interaction between variable rates of primary production and consistently high respiration-induced oxygen demand (Cheek et al., 2009). During the day, high levels of photosynthesis effectively compensate for the oxygen consumed through respiration. However, as photosynthesis ceases at night, the high biological oxygen demand rapidly reduces DO concentrations to low levels, and atmospheric diffusion cannot adequately keep pace with demand. DO levels are subsequently restored the following day when photosynthesis resumes. The warm temperatures experienced in shallow waters limit oxygen solubility and favour seasonal stratification, enhancing deoxygenation. The rates of oxygen consumption and renewal in these shallow, isolated systems are in such a delicate balance that the nocturnal cessation of photosynthesis results in decreased DO within hours of sunset (Cornell and Klarer, 2008).

Appendix B-II - Future water quality and climate projections: Models

Hydrodynamical-biogeochemical model

The BGC model SHYFEM-BFM has been recently developed and applied to the Venice Lagoon (Canu et al., 2023), compared with field data, and used to perform simulations under climate scenarios. The coupled model is based on the open-source models SHYFEM for the hydrodynamic (Umgiesser et al., 2004), and on BFM for the biogeochemistry (Vichi et al, 2020). The Biogeochemical Flux Model (BFM) is a biomass-based numerical model designed to simulate key biogeochemical processes in marine ecosystem. It tracks the cycles of nutrients, carbon, oxygen, a pool of phytoplankton, zooplankton and bacteria across the modeled system.

The SHYFEM-BFM model is implemented using an unstructured mesh of over 10000 elements and 6000 node that allows for a good representation of the lagoon properties and variability. It takes into account time variable inputs, boundary conditions and meteorological forcing such as river inputs of water and nutrients, exchange of water and biogeochemical variables with the sea, and meteorological forcing. The SHYFEM-BFM model is forced using the best available and coherent information to perform the Venice Lagoon biogeochemical climate scenario. The meteorological conditions are provided by the CCLM model (COSMO-CLM) covering the Venice Lagoon with a spatial resolution of 8 km (Bucchignani et al., 2016; Zollo et al.,

2016), and the marine biogeochemical boundary conditions are provided by the climate simulations for the years 2005-2100 performed for the whole Mediterranean Sea with the OGSTM-BFM biogeochemical model (Reale et al., 2022) which dynamically simulates the Mediterranean Sea biogeochemistry at 1/16° spatial resolution, ~ 6.5 km, with 72 unevenly spaced vertical levels (ranging from 3 m at the surface down to 600 m in the deeper layers; see Lovato et al., 2013). Marine water levels at the inlets were estimated from (Zanchettin et al., 2021), applying a linear trend up to the projected value of 0.71 m at the end of the century (for the 8.5 RCP scenario, using the 50◦ percentile of the ensemble model projections). The model simulates heat transport, water temperature, and oxygen concentration, and all the biogeochemical variables, including Chlorophyll, at each node of the high-resolution domain, at each day of simulation, in response of the changing meteorological forcing and boundary conditions.

Atmospheric model

COSMO Climate Change (COSMO-CLM) model (Rockel and Geyer, 2008) provides projections of future precipitation, relative humidity, and solar radiation at the regional level. It is the climate version of the COSMO LM model (Steppeler et al., 2003), which is the operational non-hydrostatic mesoscale weather forecast model developed initially by the German Weather Service (DWD) and then by the European Consortium COSMO. COSMO-CLM is currently used to perform dynamical downscaling of global climate simulations. For the case study scale, the COSMO-CLM model reports the predictions for the time period 2006-2100 covering the Venice Lagoon with a spatial resolution of 8 km for the RCP 8.5 scenario (Bucchignani et al., 2016; Zollo et al., 2016).

Recalculation DO

In order to align the mid and far future time series with the historical ones, a three-step process is implemented to recalculate DO: first, for each station (1-10) and for each calendar day the 20° percentile in the historical timeframe (2008-2019) is extracted. The 20° percentile has been selected as it is the indicator that best represents the historical percentage of hypoxia events (3.13%) among a set of other indicators tested (e.g. mean, minimum, 10° and 30° percentiles). Thus, 10 vectors of 365 elements are calculated, each corresponding to the daily 20° percentile for each station in the historical period, named here reference. Secondly, the model anomalies are computed from output of the SHYFEM-BFM simulations as the difference of the DO values between the years 2050 and 2019 (mid future anomalies) and between 2100 and 2019 (far future anomalies) for each station and calendar day. Finally, the mid future anomalies and the far future anomalies are summed up to the reference to obtain the corrected DO data for the mid and far future scenarios.

Appendix B-III - ML Model Performance

The binary classification of *hypoxia events* or *normal conditions* are performed by six separate ML models, i.e., RF, AdaBoost, LR, Weighted SVM, XG Boost, and MLP, and a Staking ensemble model. The models are trained, validated and tested with daily water quality and meteorological data monitored in the Venice Lagoon during the period 2008-2019. Their accuracy, ROC-AUC score, precision, recall, and F1 score metrics calculated on the two classes, are presented in Appendices Table B-1.

The results indicate that RF, AdaBoost, MLP, and the Stacking ensemble models achieve the highest accuracy (0.99). Among them, RF, AdaBoost, and the Stacking ensemble also demonstrate the highest F1 score for class 0 (i.e. *hypoxia event* occurrence), while MLP exhibit a lower F1 score for this class, as indicated by its very high precision (0.94) but lower recall (0.61), suggesting that it may miss various positive cases.

When comparing the AUC-ROC scores, Weighted SVM and XG Boost score the highest. Nevertheless, their precision and accuracy scores in class 0 are weak (e.g., 0.34 and 0.67 for precision, respectively), indicating that these algorithms are not suitable for describing this particular problem of an unbalanced dataset.

Appendices Table B-1 Performances on the test set of the ML models implemented in the methodology

Algorithm	Accuracy	ROC AUC score	Class	Precision	Recall	F1 score
RF	0.99	0.89	0	0.88	0.78	0.83
			1	0.99	1.00	0.99
AdaBoost	0.99	0.89	0	0.87	0.79	0.83
			1	0.99	1.00	0.99
LR	0.93	0.93	0	0.29	0.92	0.45
			1	1.00	0.93	0.96
Weighted SVM	0.94	0.94	0	0.34	0.95	0.50
			1	1.00	0.94	0.97
XG Boost	0.98	0.94	0	0.67	0.89	0.76
			1	1.00	0.99	0.99
MLP	0.99	0.80	0	0.94	0.61	0.74
			1	0.99	1.00	0.99
Staking ensemble	0.99	0.89	0	0.91	0.78	0.84
			1	0.99	1.00	1.00

Based on these results, RF, AdaBoost and the Stacking ensemble are identified as the models with the strongest predictive power. Therefore, they have been selected as the most suitable for predicting climate change scenarios by composing the *multiple selected ML models*. Appendices Figure B-1 shows the confusion matrices for these three selected models. From these plots, it can be seen that the hypoxia class (i.e. true positive) is correctly predicted by the three models with a very similar number of times: 206 times with AdaBoost and 204 times with RF and Staking ensemble. The main difference between the three models is in the number of false positives, i.e. cases predicted in class 0 instead of class 1. The best model in this case is the Staking ensemble with 20 errors, followed by FR with 27 and AdaBoost with 31.

Moreover, sensitivity analysis shows how variations in the input data affect the predictions of the model. This type of analysis is useful for identifying the most influential features and providing a greater explainability of the results evaluating the robustness and precision of the models and analyzing the contributions of the considered variables to the outcomes. Results concerning the sensitivity analysis are reported in Appendices Figure B-2 (a, b, c). It can be seen from the figures that the three models behave differently in terms of feature importance. All the models assign significant importance to the daily mean DO concentrations. However, the RF model distributes relative importance more evenly across all the other

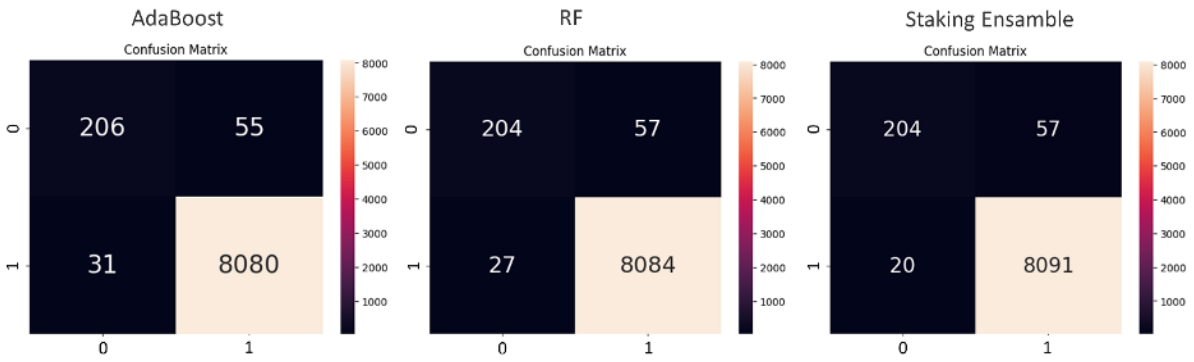

Appendices Figure B-1 Confusion matrix of the selected ML models (Adaboost, RF and Staking ensemble).

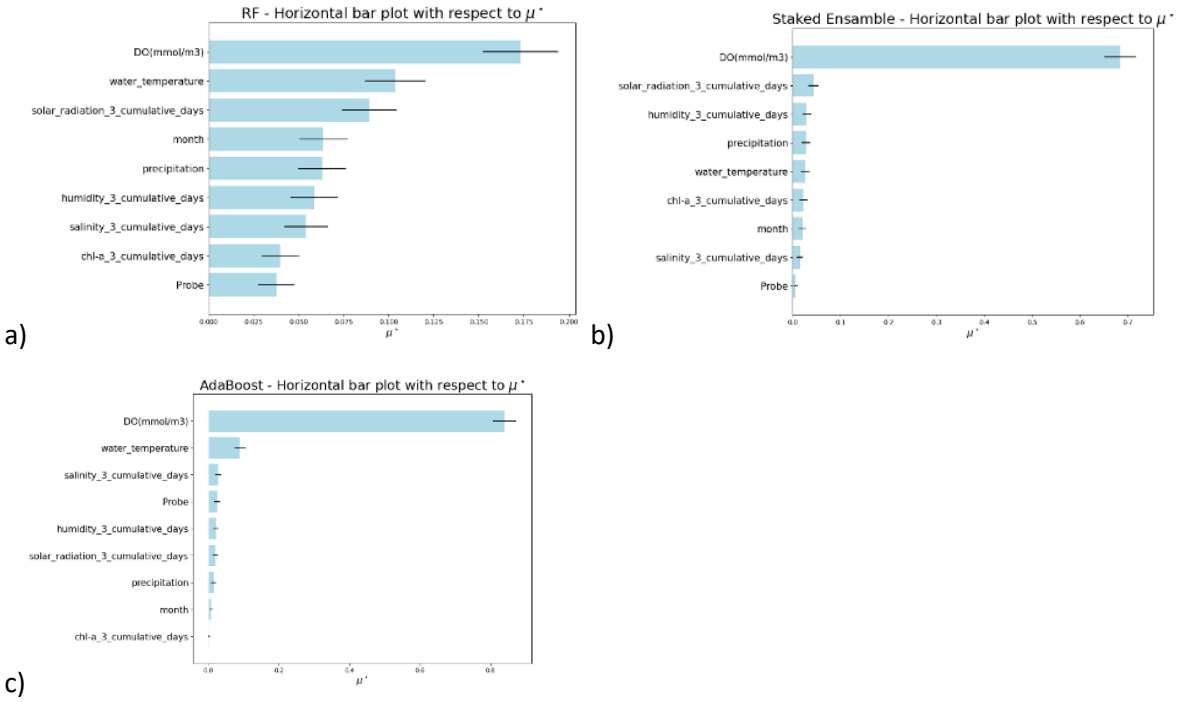

Appendices Figure B-2 Sensitivity analysis results using the Morris method for the RF (a), Staked ensemble (b), and AdaBoost (c) models.

variables. Specifically, it assigns considerable importance to water temperature and solar radiation, as well as to monthly information, humidity, and salinity (in this order). The Adaboost model places the most weight on DO, with some importance given to water temperature, while all other variables have negligible relevance. Similarly, the Stacking ensemble also prioritizes DO, but ranks solar radiation second in importance.

Appendix C. Appendices belonging to Chapter 9: Catalogue of Nature-based Solutions to reduce storm-driven coastal flooding and erosion along the Sicily coast

Appendix C-I - Plan of simulations

Appendices Table C-1 Plan of simulations for return period of 5 years

id	Nbs scenario	Hydrodaynamic scenario	H_S [m]	T_P [s]	SLR [m]
1	NN	Present (SP)	4.26	9.65	0.00
2		S4.5-2070	5.68	10.42	0.37
3		S4.5-2100	5.16	10.14	0.57
4		S8.5-2070	5.22	10.20	0.48
5		S8.5-2100	5.48	10.34	0.78
6	DR	Present (SP)	4.26	9.65	0.00
7		S4.5-2070	5.68	10.42	0.37
8		S4.5-2100	5.16	10.14	0.57
9		S8.5-2070	5.22	10.20	0.48
10		S8.5-2100	5.48	10.34	0.78
11	SR1	Present (SP)	4.26	9.65	0.00
12		S4.5-2070	5.68	10.42	0.37
13		S4.5-2100	5.16	10.14	0.57
14		S8.5-2070	5.22	10.20	0.48
15		S8.5-2100	5.48	10.34	0.78
16	SR2	Present (SP)	4.26	9.65	0.00
17		S4.5-2070	5.68	10.42	0.37
18		S4.5-2100	5.16	10.14	0.57
19		S8.5-2070	5.22	10.20	0.48
20		S8.5-2100	5.48	10.34	0.78
21	BN	Present (SP)	4.26	9.65	0.00
22		S4.5-2070	5.68	10.42	0.37
23		S4.5-2100	5.16	10.14	0.57
24		S8.5-2070	5.22	10.20	0.48
25		S8.5-2100	5.48	10.34	0.78

Appendices Table C-2 Plan of simulations for return period of 50 years

id	NbS scenario	Hydrodynamic scenario	H_s [m]	T_p [s]	SLR
26	NN	Present (SP)	5.61	10.37	0.00
27		S4.5-2070	8.06	11.52	0.37
28		S4.5-2100	7.21	11.16	0.57
29		S8.5-2070	6.67	10.95	0.48
30		S8.5-2100	8.36	11.68	0.78
31	DR	Present (SP)	5.61	10.37	0.00
32		S4.5-2070	8.06	11.52	0.37
33		S4.5-2100	7.21	11.16	0.57
34		S8.5-2070	6.67	10.95	0.48
35		S8.5-2100	8.36	11.68	0.78
36	SR	Present (SP)	5.61	10.37	0.00
37		S4.5-2070	8.06	11.52	0.37
38		S4.5-2100	7.21	11.16	0.57
39		S8.5-2070	6.67	10.95	0.48
40		S8.5-2100	8.36	11.68	0.78
41	SR1	Present (SP)	5.61	10.37	0.00
42		S4.5-2070	8.06	11.52	0.37
43		S4.5-2100	7.21	11.16	0.57
44		S8.5-2070	6.67	10.95	0.48
45		S8.5-2100	8.36	11.68	0.78
46	BN	Present (SP)	5.61	10.37	0.00
47		S4.5-2070	8.06	11.52	0.37
48		S4.5-2100	7.21	11.16	0.57
49		S8.5-2070	6.67	10.95	0.48
50		S8.5-2100	8.36	11.68	0.78

Appendices Table C-3 Plan of simulations for return period of 100 years

id	NbS scenario	Hydrodynamic scenario	H_s [m]	T_p [s]	SLR
51	NN	Present (SP)	6.01	10.56	0.00
52		S4.5-2070	8.70	11.77	0.37
53		S4.5-2100	7.75	11.39	0.57
54		S8.5-2070	6.97	11.09	0.48
55		S8.5-2100	9.18	12.00	0.78
56	DR	Present (SP)	6.01	10.56	0.00
57		S4.5-2070	8.70	11.77	0.37
58		S4.5-2100	7.75	11.39	0.57
59		S8.5-2070	6.97	11.09	0.48
60		S8.5-2100	9.18	12.00	0.78
61	SR1	Present (SP)	6.01	10.56	0.00
62		S4.5-2070	8.70	11.77	0.37
63		S4.5-2100	7.75	11.39	0.57
64		S8.5-2070	6.97	11.09	0.48
65		S8.5-2100	9.18	12.00	0.78
66	SR2	Present (SP)	6.01	10.56	0.00
67		S4.5-2070	8.70	11.77	0.37
68		S4.5-2100	7.75	11.39	0.57
69		S8.5-2070	6.97	11.09	0.48
70		S8.5-2100	9.18	12.00	0.78
71	BN	Present (SP)	6.01	10.56	0.00
72		S4.5-2070	8.70	11.77	0.37
73		S4.5-2100	7.75	11.39	0.57
74		S8.5-2070	6.97	11.09	0.48
75		S8.5-2100	9.18	12.00	0.78

Appendix D. Appendices belonging to Chapter 12: Modelling the Impact of Large-Scale Laguna Complex Restoration on Ecosystem Services with Climate Resilience: A Case Study of the Rhône Delta

Appendix D-I - Methods and Calibration complements

Regarding the marine and lagoons/marshes models, a sensitivity analysis and parameter calibration have been carried out to determine their impacts on model performance and determine optimal values with the following results:

- A timestep of 5 seconds for TELEMAC2D is required to achieve a steady model.
- The optimal coupling period between TELEMAC2D and TOMAWAC is 5 seconds.
- The consideration of the wind improves model accuracy.
- There is no influence of the wind coefficient on TOMAWAC.
- In TELEMAC2D, the optimal value for the wind coefficient is equal to 10^{-6}.
- Results are better when the linear growth is not considered.
- Including dissipation due to breaking waves, strong currents and whitecapping gives the best results for significant wave heights.

For parametrization, Xbeach parameters were selected for their relevance and their influence on morpho dynamics and sediment transport in overwash dynamic as fall velocity (FallVelRed), dilatancy, critical bottom for avalanching (WetSlp/DrySlp) and wave shape (Facua). A sensitivity parametrization was investigated. Each parameter was tested independently, keeping the default values of the other parameters, with a total of 27 simulation. Moreover, the morphological acceleration parameter was set to 10, in order to save calculation time, after checking the possible impact of this acceleration on the accuracy of the results. The standard error was evaluated on transects with different morphologies and over the entire domain. The mean error is 4.8%.

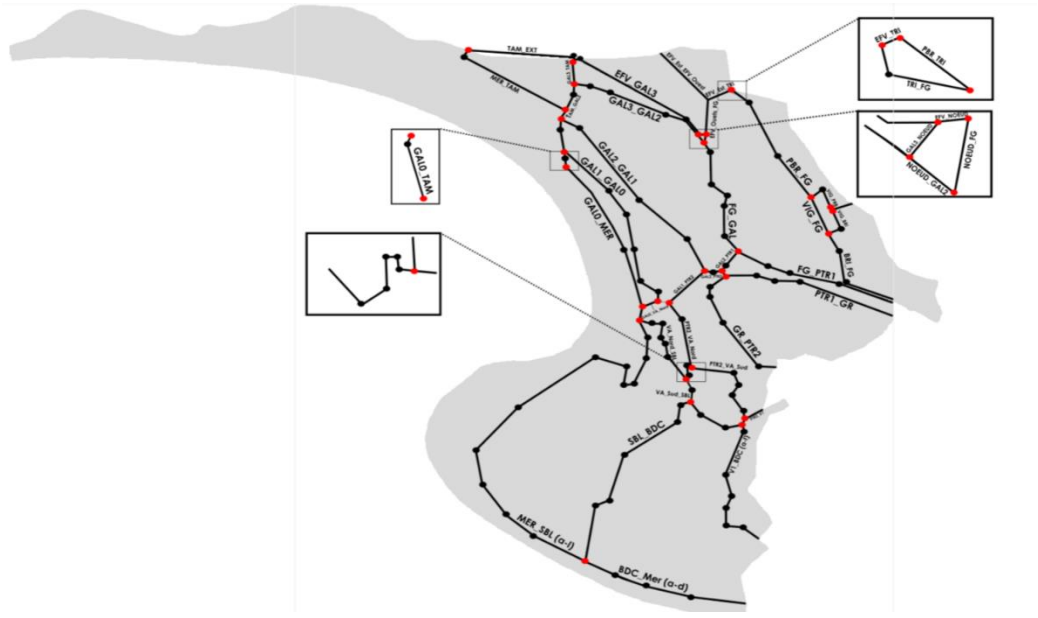

Appendices Figure D-1 Hydraulic sections

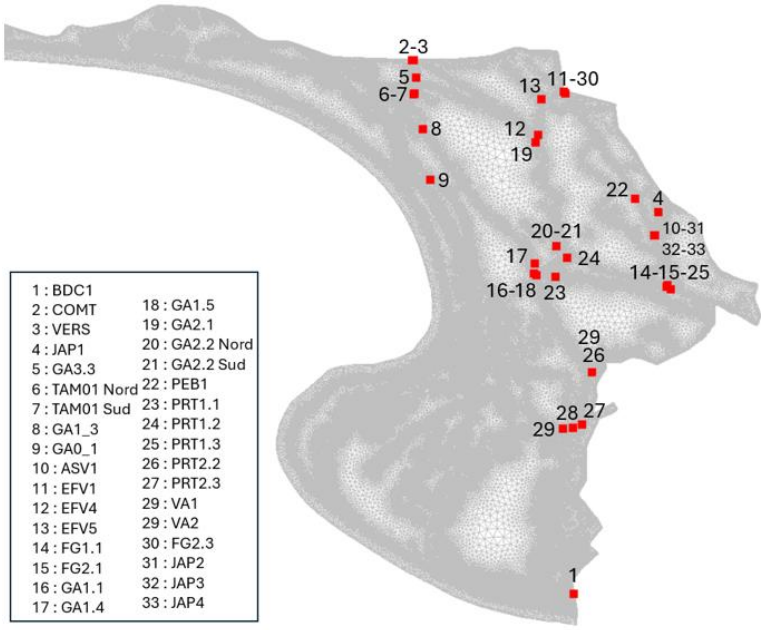

Appendices Figure D-2 Hydraulic structures

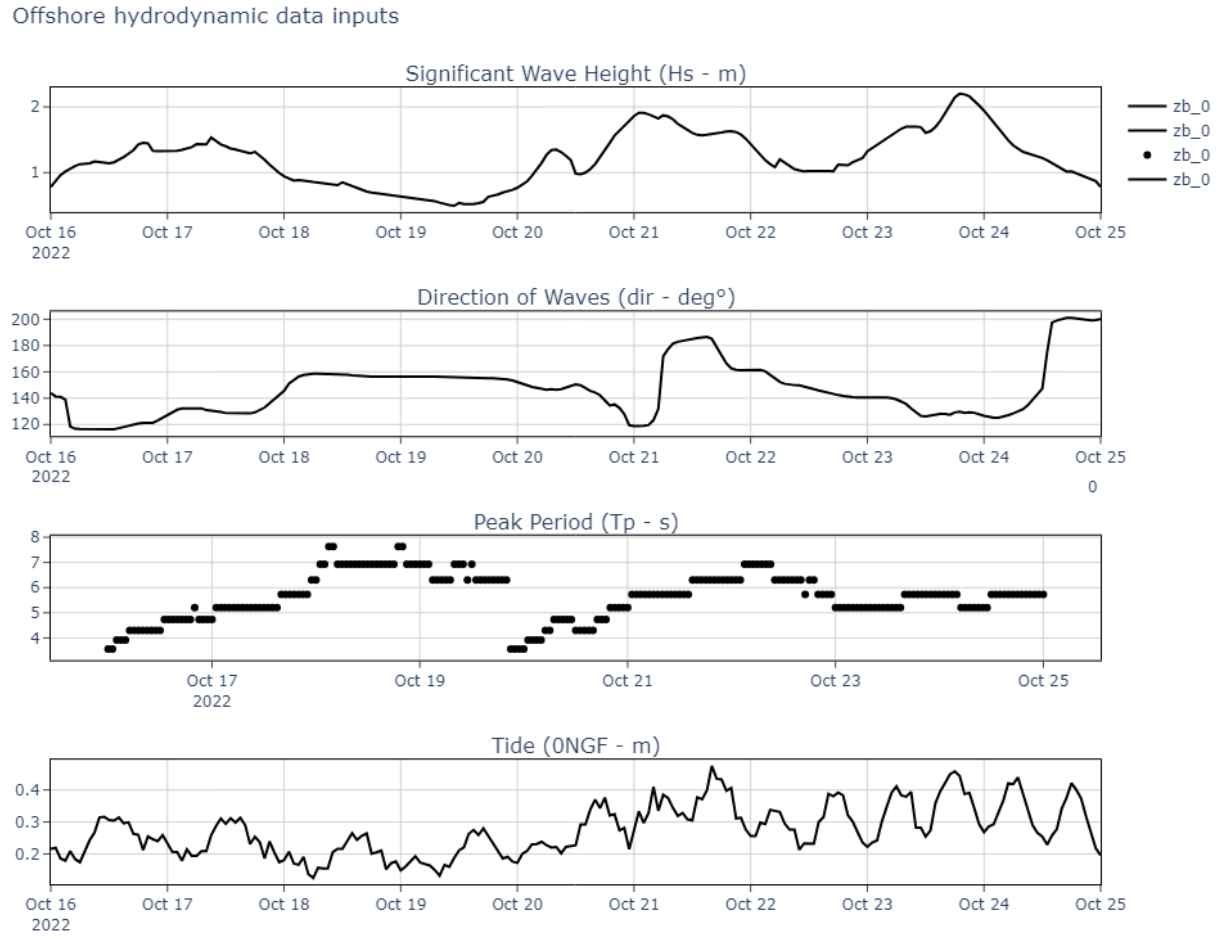

Appendices Figure D-3 Offshore hydrodynamic data from the Copernicus Med-WAV model and tide gauge record (SHOM - REFMAR) for the morphodynamic calibration period from 16/10/2022 to 04/10/2022.

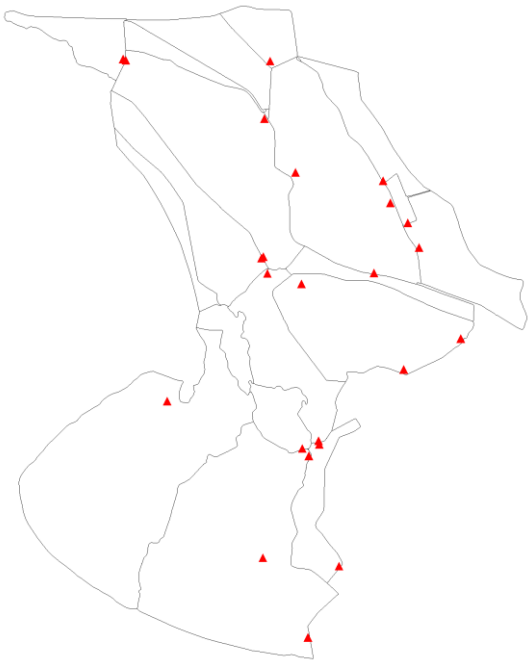

Appendices Figure D-4 Locations of monthly salinity measurements used to calibrate the salinity model. Conductivity is measured with a WTW TetraCon 325 conductivity meter and converted to salinity using the international oceanographic table (Unesco 1981). For conductivities exceeding 60,000 µS/cm, one or several successive dilutions were performed with distilled water to fall within the validity range of the equation to derive salinity from conductivity.

Appendices Table D-1 TELEMAC-2D lagoons/marches model: MAE, RMSE and NRMSE at several locations for simulated versus monitored water levels from 23 November 2022 to 18 January 2023

Lagoon	MAE (m)	RMSE (m)	NRMSE (-)
SBL	0.077	0.102	0.227
BDC Center	0.075	0.103	0.195
VA	0.093	0.110	0.239
V1 North	0.072	0.092	0.210
PRT2 South	0.042	0.057	0.152
PRT2 North	0.055	0.068	0.214
GR South	0.041	0.050	0.162
GA2 South	0.063	0.085	0.305
GA2 North	0.089	0.102	0.343
TAMP	0.089	0.103	0.231
FG Center	0.228	0.250	1.143
Mean	**0.084**	**0.102**	**0.311**

Appendices Table D-2 Salinity box model: MAE, RMSE and NRMSE at several locations for simulated versus monitored spatially averaged salinities for each lagoon/marsh from 23 November 2022 to 18 January 2023.

Lagoon	MAE ($gk.m^{-3}$)	RMSE ($gk.m^{-3}$)	NRMSE (-)
BRI	3.5	4.4	0.28
VIG	2.7	2.8	0.2
PBR	14.9	15.5	0.32
PRT1	24.2	24.3	0.36
PRT2	7.3	9.9	0.15
GR	4.5	4.6	0.07
EFV_Est	3.7	3.8	0.35
GAL1	2.5	3.2	0.04
GAL2	13	13	0.18
FG	161.7	168.7	0.89
BDC	12.1	15.7	0.34
SBL	16.9	17	0.46

Appendices Table D-3 Xbeach model : optimal parametrisation of the model after calibration and final GOF

γx	FallVelRed	Dilatancy	WetSlp	DrySlp	Facua	GOF
1	1	1	0.2	1.1	0	**0.747**

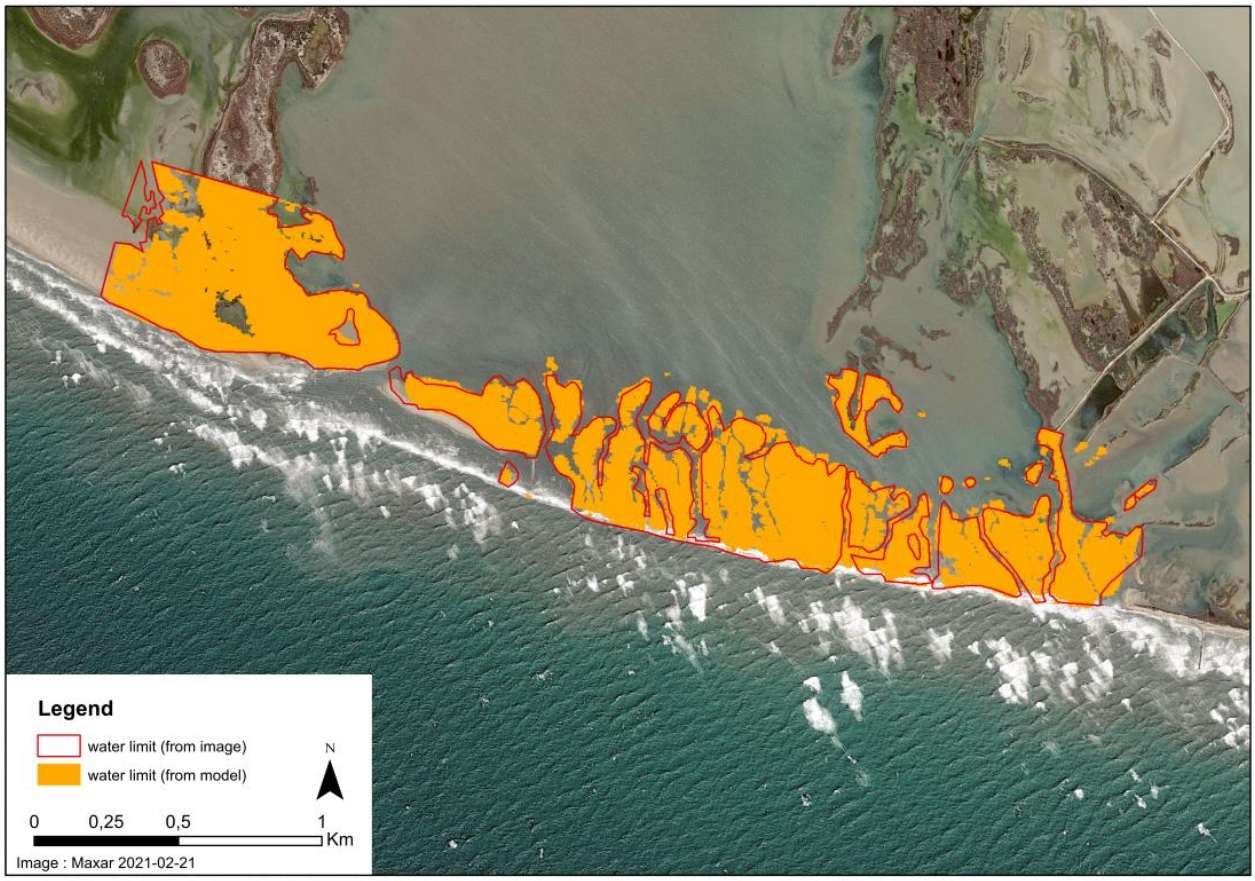

Appendices Figure D-5 Morphological results from calibration, with vectorization of water level from the satellite imagery compared to final water level extracted from modelled results

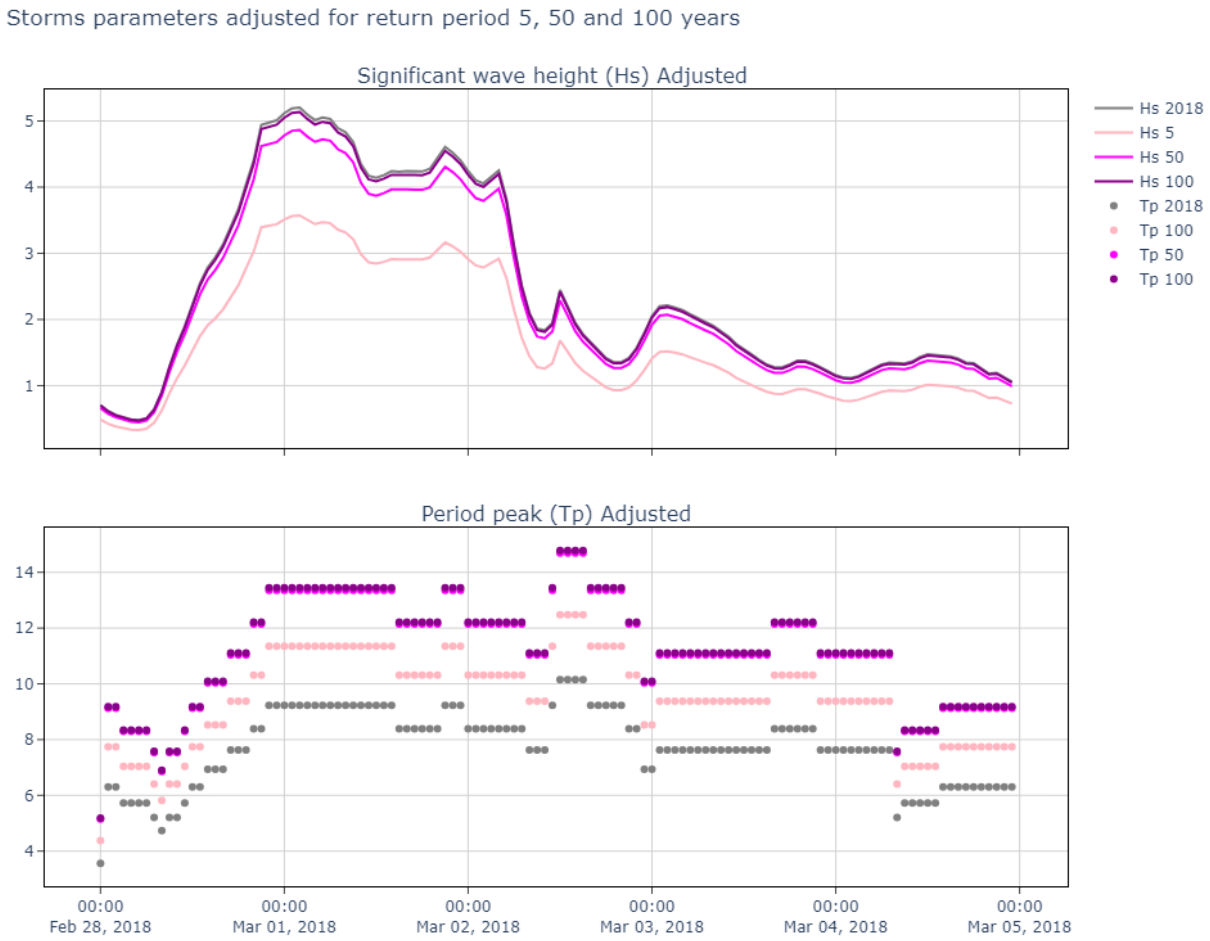

Appendices Figure D-6 Significant wave height and peak period adapted from 2018's storm to the return periods 5, 50, 100 years.

Appendix D-II - Quantification of ESS services relate to management plan

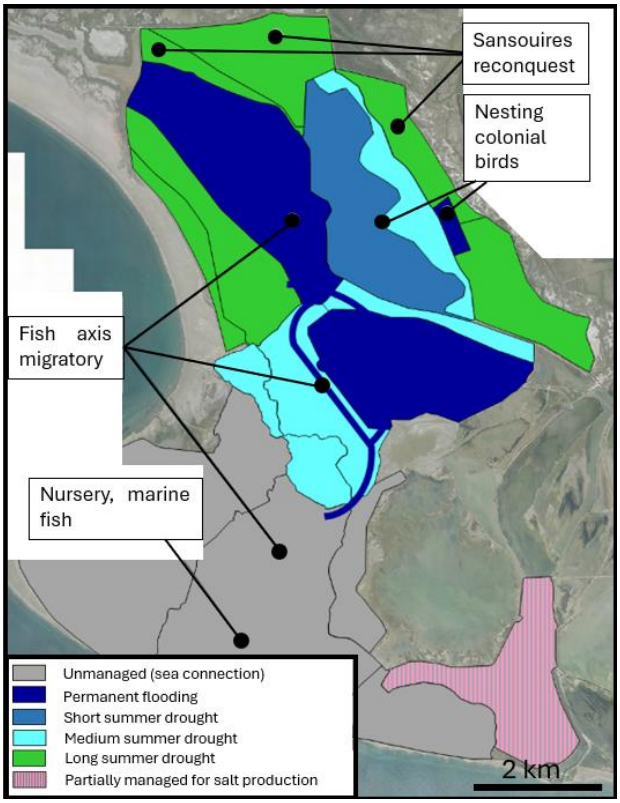

Appendices Figure D-7 Management objectives for the different areas of the pilot site

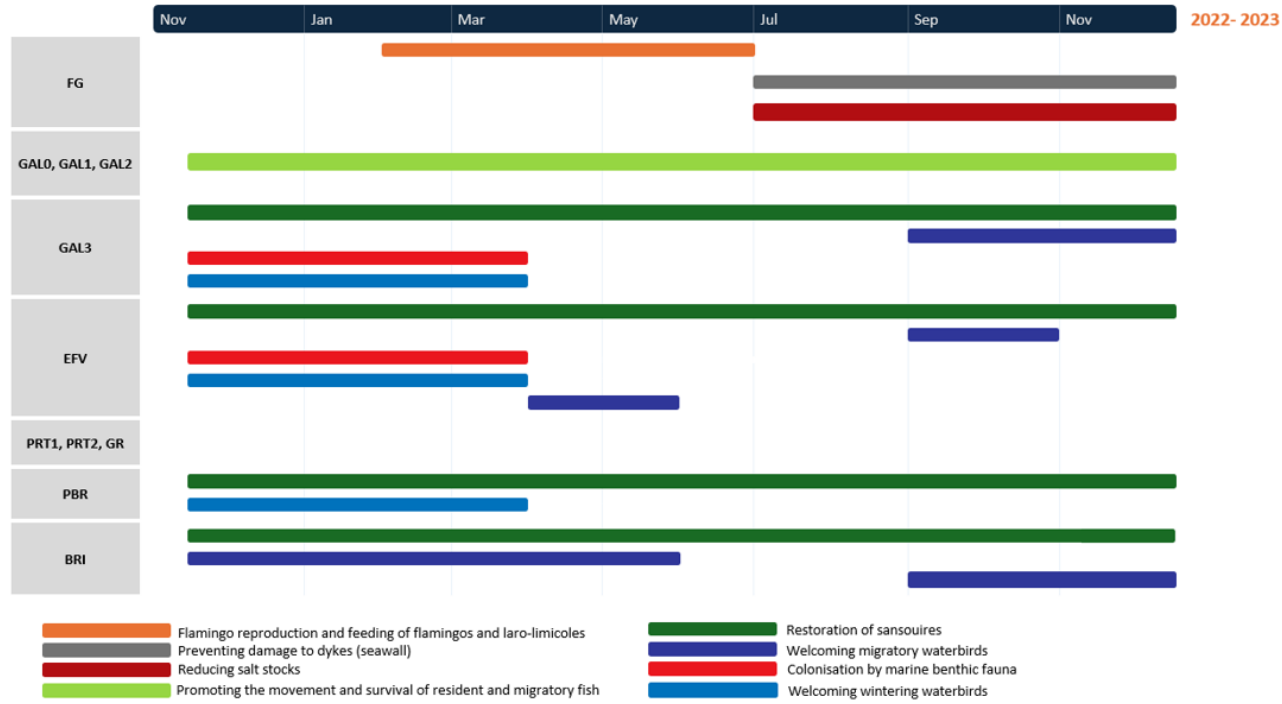

Appendices Figure D-8 Timeframes over the year for different stakes of the management plan of the Pilot site